
CONTRIBUTION TO REDUCE DEFECTS IN PRODUCTION OF PLAIN BEARINGS

Darko SKUPNJAK

Daido Metal Kotor Ad, Faculty of Mechanical Engineering, University of Montenegro,
MONTENEGRO

Abstract:

DAIDO METAL KOTOR AD (DMK) is a Japanese company dealing with production of plain bearings for vehicle engines. There are four highly productive automatized machining lines in DMK for bearings production. During production, some measures can deviate from the required ones. For this purpose, I have made a resolving concept, designed, had it made and tested a device-machine for checking bearings production and reached excellent results. The device is installed on the line consisting of: machine construction, electro-pneumatics, optical sensors, other sensors, PLC operation. After treatment, the bearing comes into device, it is checked, and if defected, it is rejected, the line is stopped and the operator searches the cause. This ensures quality of production, eliminates defected bearings, reduces costs, making customers more satisfied. Some of many high rating customers are: Honda, Volvo, Mercedes,..

Keywords:

Plain bearing, sensors, electro-pneumatics, PLC operating

1. INTRODUCTION

DAIDO METAL KOTOR AD (DMK) located in Kotor, Montenegro is one of the affiliated companies of DAIDO METAL Ltd. Co, which is the head company located in Nagoya – Japan, dealing with the production of plain bearings for vehicles engines. There are four automatized highly productive machining lines and two lines of presses in DMK, for OEM (Original Engine Manufacturing) mass production of plain (slide) bearings.



Figure 1 Typical example of plain bearing

DMK supplies top world companies with its products, such as: Volvo, Honda, Mercedes, Ford, etc. Figure 1 shows typical example of plain bearing. Products, that are made for the famous customers on the machining lines herein noted, are connrod and main bearings.

This production, as much as any other, is followed by appearance of defected products, which has to be identified, located, controlled, reduced or, if possible, to be completely eliminated.

2. DEVELOPMENT OF DEVICE FOR CHECKING PLAIN BEARINGS

Plain bearing, as a mechanical element, appears simple, on the first sight. However, this is a very important, precise product for vehicles engines, which has specific characteristics of materials made of. Figure 2 shows location of plain elements-bearings.

Materials used for making plain bearings for vehicles engines of bimetal strip, are mostly alloys of aluminium, bronze and tin. Figure 3 shows bimetal strip- material for production of plain bearings.

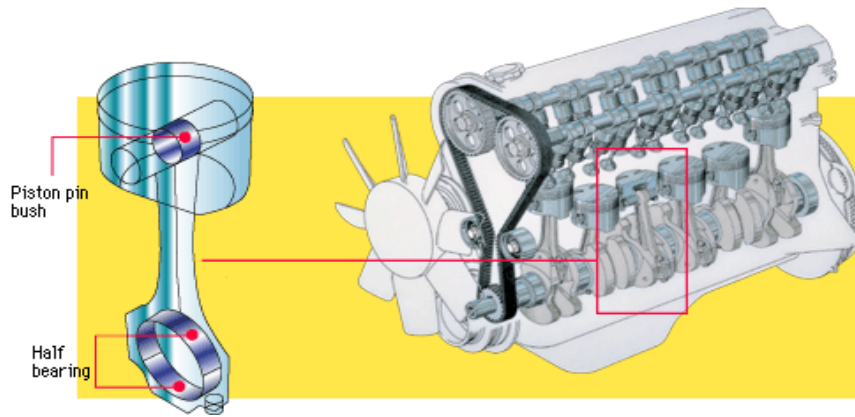


Figure 2. Plain elements as parts of vehicles engines



Figure 3 Bimetal strip

Elements characteristic for plain bearings are: wall thickness, height of half bearing, including its height crush, nick, oil groove, lubrication holes, free spread, relief, etc.

Technology of manufacturing plain bearings from bimetal strip involves the operations on the pressing machines and the machining lines.

There are four operations carried out on the pressing machines: stamping the blanks, cutting the blanks off the bimetal strip which is coiled, then operations of bending and forming.

There are 11 operations carried out on the machining lines: face and chamfering, corner chamfering, piercing the lubrication holes, nick milling, nicking, grooving, counter sinking, back side brushing, height crush finishing, auto checking and wall thickness finishing.

On the operations carried out on the lines of presses and the machining lines, from different reasons there comes to production of defected bearings. A list defining the causes of defected (rejected) bearings was made, according to the records and analysis of defected bearings.

The reject causes are: indents on back steel, set - up pieces, thickness, length, height crush, corrosion of back steel, indents on inner surface, mechanical damages of back steel on bm – strip, roundness, inside chamfering, position of nick, damage of inner surface, position of lubrication holes, position of oil grooves, outside chamfering, countersinking, free spread, bad blue contact, twisting, bad nick shape, bad stamp, etc.

Control of some elements (dimensions) of each bearing is carried out during the machining process. Former control refers to the elements of bearings that are checked on Autochecker machine: height, nick protrudence (if the bearing has nick, according to drawing), detection of lubrication holes, but not the position (if the bearing has any, according to drawing), and wall thickness which is controlled on the boring machine.

According to the analysis of plain bearings, proposals for improving production process and reducing reject, aiming to cut down expenses, upgrade satisfaction of customers and employees, in conformity with ISO standards, the Device for checking plain elements which is installed into the machining line Y-01 has been developed.

According to my conception and project, the Device for checking plain bearings working *in-line* and controlling certain elements of each bearing being machined on the line Y-01, has been developed within the company DAIDO METAL KOTOR AD.

The elements that have to be checked are the following: length of plain bearings (Figure 4a), position of lubrication holes in respect to the angle and length of bearings (Figure 4a) and free spread of plain bearings (Figure 4b).

The elements noted have not been so far controlled on every bearing made, having as a consequence considerable amount of rejected-bad bearings. Figure 4 shows the elements of plain bearings which have to be controlled.

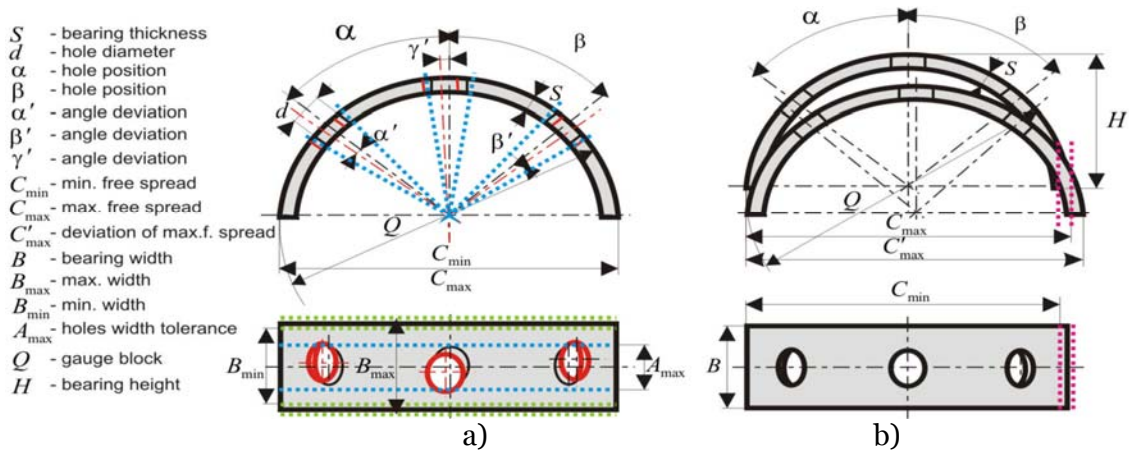


Figure 4 Elements of plain bearing which is checked

Deviation of position of lubrication holes, length and free spread of bearings from the dimensions required by the drawing, can be caused by the following: bad set up of machines and tools, mishap of tool, change delay, etc.

Projected and made device (Figure 7) for checking three elements of plain bearings (holes, width and free spread), will be installed on the most suitable location in the line Y-01 and it will be working in-line. When projecting, the following parameters were used: velocity (cycle) of Y-01 operation, 1.8 sec. , diameter of bearing which can be reached on the line, and which is 30-80 mm, length of bearing which is to be checked, 13-30 mm, number of holes for checking, 0-3, positioning is after Autochecker machine.

Construction

Construction is made of steel consisting of: control assembly (Figure 7), conveyor belt, support and stand, energetic-driving box, operating-commanding box, pneumatics and electropneumatics, and technique of sensors.



Figure 5 Device for checking plain bearings

Driving

Driving is microcontrolling-PLC MITSUBISHI Fxon-60MR , shown in Figure 6.



Figure 6. PLC of device for checking plain bearings

Description of operation

Before activating the Device for checking bearings to automatic operation, the option for checking plain bearings, ie., bearing with a hole, number of holes, is chosen by switches. Of course, before starting automatic operation, the Device for checking bearings is set up manually.

After having been checked in autochecker machine in the line Y-01, plain bearings (one by one) are driven by a conveyor belt to the separator (assembly activated by a pneumatic cylinder) which stops them making „magazine“ (row of 2-8 bearings). Receiving the command from PLC (Programabil Logic Controler), the separator passes one by one bearing into Device for checking where the check is carried out in the control assembly (Figure 7a). When the bearing is let through by the separator, the conveyor belt takes it to the entry of the Device for checking, goes down the ramp between the guides (one guide is fixed, and the other one is movable depending on the length of the plain bearing being machined) and gets stopped by a stopper to the checking position.

When the bearing is stopped, its presence is detected by an inductive proximity sensor, and according to the program, PLC provides an instruction ie. an outgoing signal which activates a pneumatic valve 5/2 of a clumper. The clumper is a plate linked to the pneumatic cylinder and clamps the bearing to the plate which makes it fixed and ready for control.

In the same time, checking is performed, ie., comparing the values with input tolerances on amplifiers for lubrication holes, width and free spread.

After checking, which lasts for 0.4 ms, the bearing is released by the clumper and the stopper, and if any of checked values is not good ie., is not in conformity with the input tolerances, a lamp switches on through PLC, giving a signal to the pneumatic valve of the pusher, that after the bearing goes under the second inductive proximity sensor, it is detected and pushed to the box for bad-rejected bearings. However, if the bearing is good, it goes freely down the ramp to the conveyor which is horizontal. The conveyor then takes it towards the machine for the final treatment (wall thickness finishing).

The Device contains the following electro-pneumatic and pneumatic elements: Electro-pneumatic valve, type SMC SY7120-1MZ-02, SMC VS3115-021DBL, noise bumper SMC ANA 1-02, clamping switch NISCON BN-121B-10, pneumatic cylinder KOGANEI DA 20x15-12, pneumatic cylinder SMC MGPM-20-20-Z7BW, pneumatic cylinder KOGANEI DA 20x50-12, pneumatic cylinder SMC CM2RK-A20-25, bumping irretrievable valve SMC AS 2201 F 1/8.

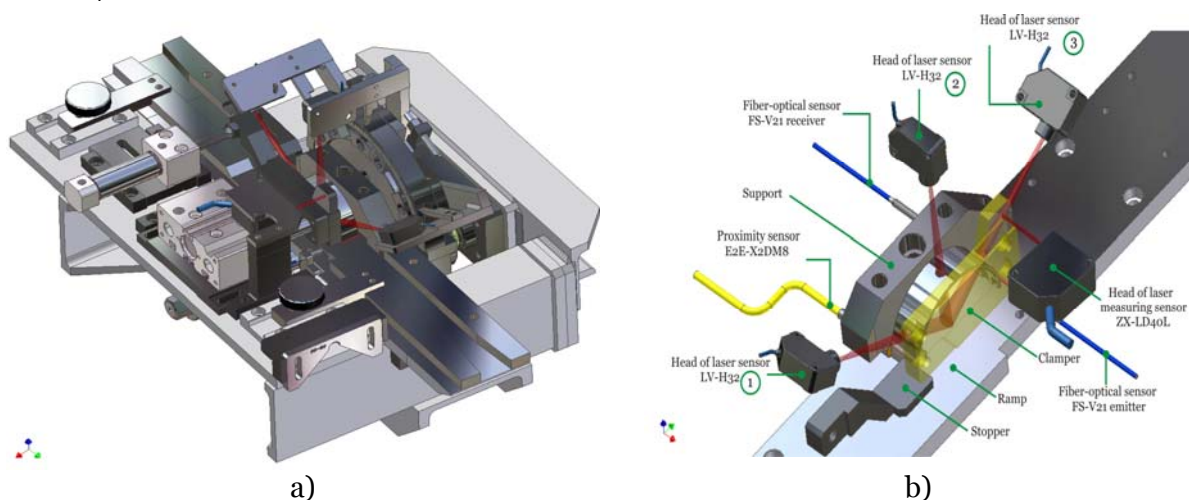


Figure 7. Control assembly

Figure 7a – Control assembly of device for checking plain bearings

Figure 7b – Sensor control of plain bearings elements

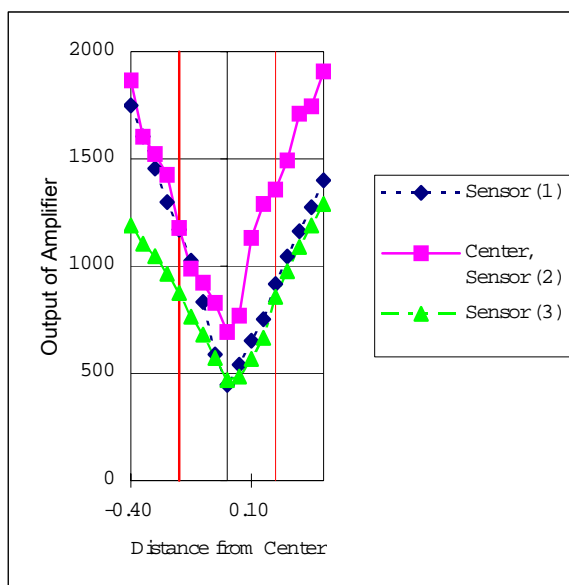
The following checks are done by selecting the sensors shown in Figure 7b: checking position of lubrication holes in relation to the angle and width KEYENCE LV-H32, checking the plain bearing width OMRON ZX-LD40L and checking free spread of plain bearing KEYENCE FS-V21.

2.1 Testing device for checking plain bearings

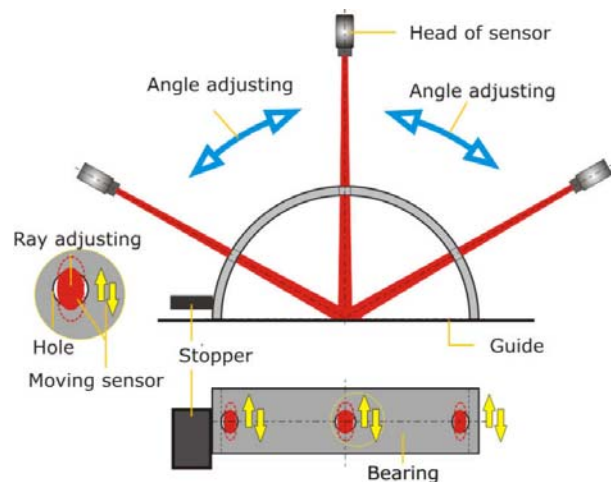
Testing the head of the laser optical sensors LV-H32 (1), (2), (3) and amplifiers LV-21A. Sensitivity and sensing the amplifier to the change of positions of the holes for lubricating bearings. Sensing the amplifier LV-21 A

Table 1 Sensing the amplifier for different holes out of position

Distance from hole centre	Sensing the amplifier			Note
	Sensor (1)	Centre, sensor (2)	Sensor (3)	
0,40	1400	1908	1290	Forward
-	-	-	-	
0,05	540	768	485	
0,00	446	692	469	Centre
-0,05	588	828	572	Backward
-	-	-	-	
-0,40	1750	1865	1190	



a)



b)

Figure 8 Testing sensitivity of laser optical sensor LV-H32 and amplifier LV-21A

Figure 8a shows a diagram of results reached by testing sensitivity of sensing the amplifier KEYENCE LV-21A, to the changes of positions of holes related to width. Figure 8b shows set up of the control assembly for this testing and laser light beam previously adjusted, holes deviation rating $0.0 \text{ do } \pm 0.4 \text{ mm}$ by step of 0.05 mm in direction of bearing axis, on the diagram, sensing the amplifier is shown (with enough accuracy) by linear dependence.

2.2 Testing device for checking – Position of holes for lubricating plain bearings

Testing Device for checking plain bearings, regarding the position of holes for lubrication, was done using forty plain bearings with three holes, prepared in advance. Also, all measuring pieces were measured, marked, and all required measures were entered into the diagram (Figure 10).

After setting Device for checking plain bearings, all measuring pieces-bearings are let through device where sensing the amplifier is done and data are entered into the table 2 and diagram in figure. These data are taken for all measuring pieces for different adjustments (size of laser beam) of head of laser sensor LV-H32.

After having these data, the diagrams for every sensor (1,2,3) were made, which resulted with a final analysis.

Table 2 Sensing the amplifier for beam adjusted as in Figure 9

r/b	Head 1, amplifier 1	Head 2, amplifier 2	Head 3, amplifier 3
No.1	163	177	147
No.2	197	181	156
-	-	-	-
No.40	787	442	739

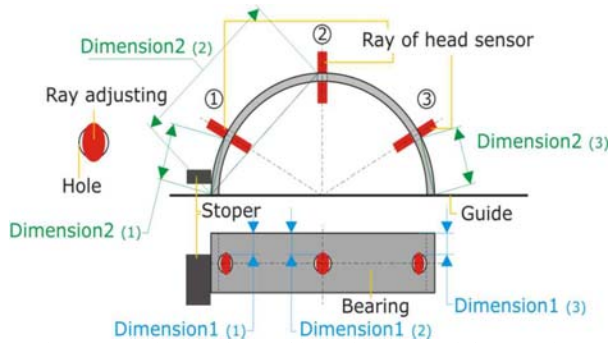


Figure 9 Dimension of bearings used for testing

Figure 10 shows the diagram of testing the device for the hole 1, all 40 bearings, for adjusted beam of laser light of sensor head LV-H32, as in Figure 9. Also, this diagram presents sensing the amplifier and measured Dimension 1 and Dimension 2, as well as rejected pieces marked with x, for 40 measuring pieces.

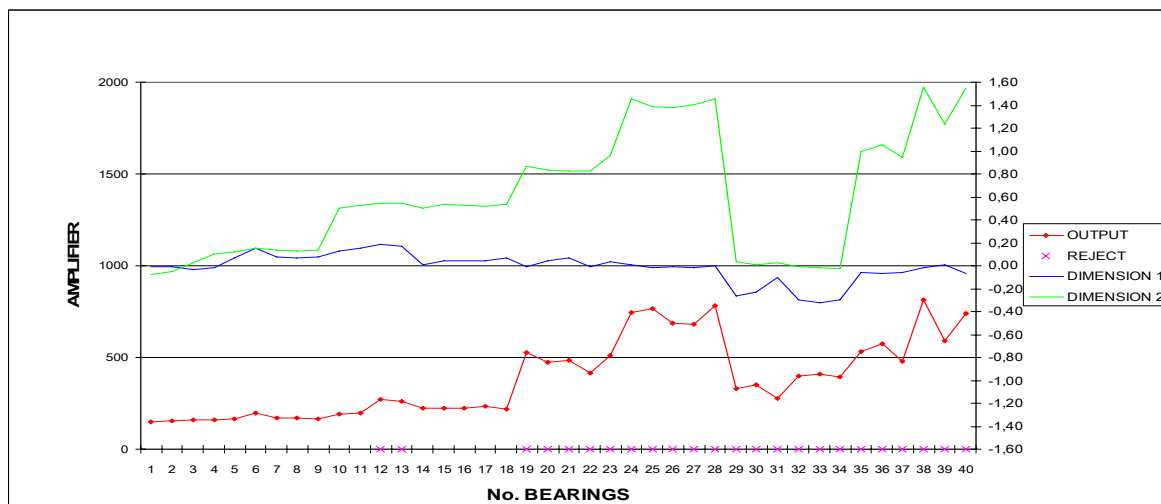


Figure 10 Diagram of results got by testing device regarding the position of holes for lubricating bearings

Figure 10 shows that changes of Dimension 1, Dimension 2 cause changes in sensing the amplifier. If you input the sensing limit corresponding the values of amplifier sensing good pieces or if it is greater enough, the rejected bearings (x) will be detected (value of sensing the amplifier exceeds the limits) and device for checking will eliminate them, according to the program defined in PLC.

2.3 Testing device for checking – Width of plain bearings

For testing the device regarding width of bearings, 10 measuring pieces were prepared.

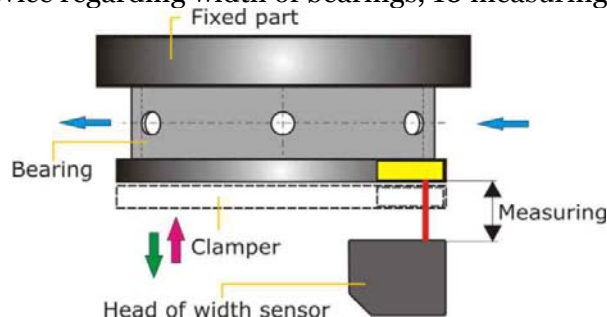


Figure 11 Layout of checking width of bearings in device

Table 3 Dimensions and results of testing with measuring pieces for checking width of bearings

Measuring pieces	Mark	Measured values	Sensing the amplifier	Bottom value, by drawing	Peak value by drawing	Bottom value of amplifier	Peak value of amplifier
No.1	1	19,00	19,03	19,10	19,60	19,15	19,55
-	-	-	-	-	-	-	-
No.10	10	19,70	19,689	19,10	19,60	19,15	19,55

Figure 12 shows the diagram of results got by testing for 10 bearings prepared in advance whose dimensions were measured and shown in table 3.

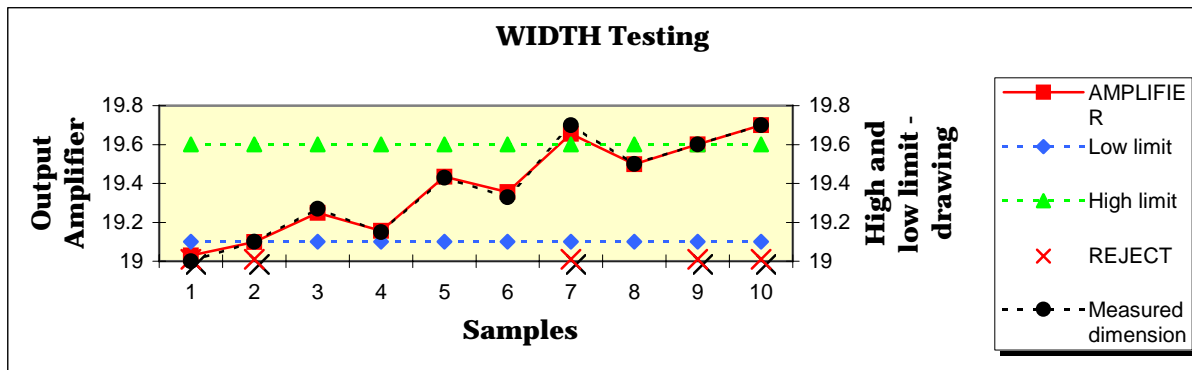


Figure 12 Diagram of results got by testing device regarding bearing width

Highly precise optical OMRON laser sensor ZX-LD40L and amplifier OMRON ZX-LDA 11-N, were previously adjusted to the device and the bearings drawing, sensing the width values of measuring pieces (Figure 11) which were later on entered into the diagram. Bottom and peak values set on the amplifier, correspond to the tolerance field being a little bit more narrow in respect to the tolerance field defined by the drawing, because of those bearings whose values are on the limit of tolerance field – for sake of assurance. The amplifier detects those bearings whose width is out of tolerance field and according to PLC program, the elements of device eject them as defected.

2.4 Testing device for checking – Free spread of plain bearings

For testing the device in respect to the bearing free spread, 10 measuring pieces were prepared.

Firstly, the Control assembly of device (figure 7a) is set for a certain product ie., measuring pieces, according to Figure 13, as well as the position of a fiber optical sensor KEYENCE FS-V21 (emitter and receiver). Measuring pieces are let through device and the amplifier reads the values for every part. Values got are shown in Table 4 and on diagram. Diagram also shows that dimensions which were previously measured (given in Table 4) follow the values read on the amplifier. If you set peak value of the amplifier sensing, in accordance with the initial value on the amplifier and the bearing drawing, measuring parts exceeding the limit set on the amplifier, are ejected from device. Dependence of values of sensing the amplifier and changes of free spread dimensions is linear.

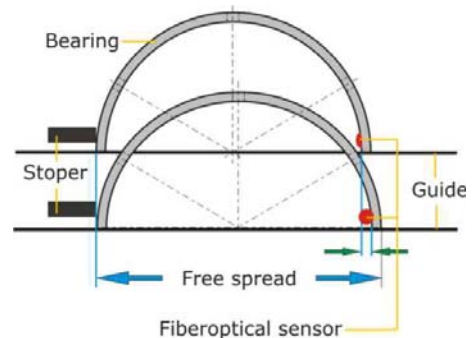


Figure 13 Layout of checking free spread in the device for checking

Table 4 Dimensions and results of testing with measuring pieces for checking free spread of bearing

Measuring pieces	Mark	Measured values	The amplifier sensing	Bottom value by drawing	Peak value by drawing	Peak value of amplifier
No.1	1	71,00	445	69,5	71	430
-	-	-	-	-	-	-
No.10	10	70,75	367	69,5	71	430

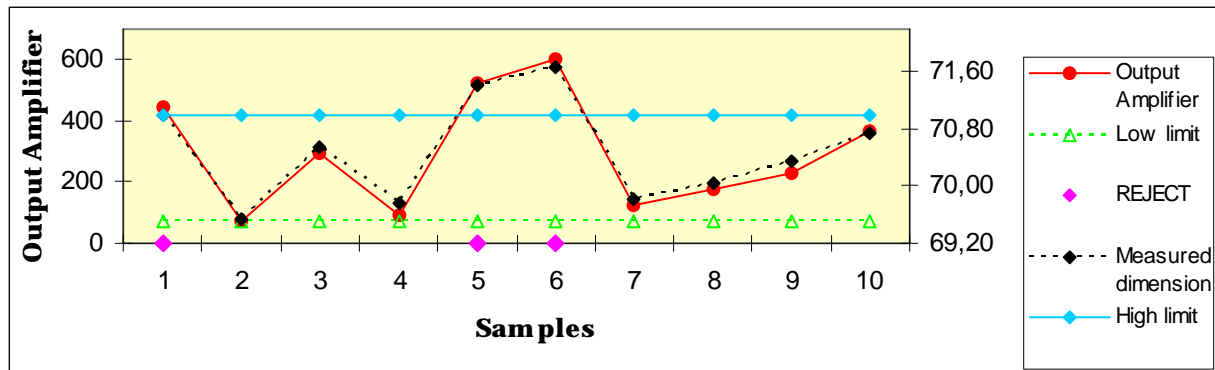


Figure 14 Diagram of results got by testing device in respect to free spread of bearings

3. ANALYSIS

Using the most modern laser technique and constructive design of the device – adjusted to the selected sensors, PLC driving, has contributed to control of products elements in this type of industry. Testing results, previously described, confirm possibility of checking the elements of bearings with selected sensors (wide range of adjustments) and assurance that a rejected bearing, caused by these three elements being controlled, will be detected.

After individual testing, testing of operation stability of Device for checking was also performed, including coexistence of results got by individual testing. All measuring parts were mixed and let through device, which exactly selected and ejected all defected parts into the reject box. Process of testing was repeated for 10 times.

4. CONCLUSION

This paper describes the device which was projected with intention to work in-line and to check three parameters of each bearing during the production process. In case of detecting defected parts, it stops the process of bearings production on the machining line Y-01. The device for checking incorporates: electro-pneumatics, the most modern sensor technique and its application in industry, including complete driving by PLC.

Reduction of rejects, based on three elements noted in total reject amount, is also reflected in cutting down production costs, price of manufacturing, final price of product. This also results in providing profit for the company, therefore affecting the employees' salaries and their satisfaction, as well.

This project is important, not only for reducing defects in production, but also to assure that the final customer will get well controlled and high quality product.

REFERENCES

- [1] G. Vogel and E. Mühlberger: *The Amazing World of Pneumatics*, 2002.
- [2] Hohn: *Bearings for Steam Turbopumps*, BBC – No 3, 1975.
- [3] Nebojša Matić: *PLC mikrokontroleri 4 izdanje*, MikroElektronika, Beograd, 2003.
- [4] S. Hesse: *Sensors in Production Engineering*, Festo AG&Co, 2001.
- [5] S. Hesse: *Compressed Air as an Energy Carrier*, Festo AG&Co, 2002.
- [6] Zoran B. Ribar: *Pneumoelektrični upravljački sistemi*, Beograd, 1997.



SLIDING MODE CONTROL OF A ROBOT ARM DRIVEN BY PNEUMATIC MUSCLE ACTUATORS

Péter TOMAN¹, János GYEVIKI², Tamás ENDRÓDY²,
József SÁROSI², Antal VÉHA², Zénó SZABÓ²

¹Alfa Busz Kft, Székesfehérvár, HUNGARY

²Department of Technical and Process Engineering, Faculty of Engineering,
University of Szeged, H-6724, Szeged, Mars tér 7, HUNGARY

Abstract:

As an important driver element, the pneumatic artificial muscle (PAM) is widely used in industrial applications for many automation purposes thanks to their variety of advantages. The design of a stable robust position controller for PAM is difficult since it is a very nonlinear time-variant controlled plant because of the compressibility of air, air mass flow rate through the valve, etc. The main contribution of this paper is a robust position control method based on sliding mode for a robot arm, driven by pneumatic muscle actuator. Finally, it presents experimental results.

Keywords:

Pneumatic artificial muscles, PAMs, sliding mode control

1. INTRODUCTION

This work is the first fundamental step of a wider project, aimed at studying the humanoid robot. Muscles only generate a force via contraction, i.e. a muscle can only “pull” and does not “push.” One muscle (agonist) contracts and simultaneously the other muscle relaxes (antagonist, which increases in length), thus producing a force and motion on the mass. The same effect can be realized in a rotational sense by generating a rotation or torque on the robotic joint through the contraction of the agonist and relaxation of the antagonist muscle.

Many researchers have investigated the precise position control of pneumatic muscles during the past several years. Most of them dealt with the control of single or antagonistic pneumatic muscles.

Due to the fact that the results obtained with a classical PI controller were not good, robust control techniques were considered. For pneumatic muscles, the application of different control techniques is found in the literature, but a good performance requires the use of robust or non-linear control techniques. A variety of approaches, with varying success, have been attempted. PID control, neural networks, and adaptive control, among others, have been utilized [1, 2, 3, 4]. While PID control is well known, the results are particularly sensitive to errors in the feedforward term. Adaptive and neural network control may be more robust, but suffer from slow convergence and long training sessions respectively. Thus, adaptive control is not well suited for the fast movements required of an orthotic actuator. Analogously, neural control, with its training workspace, does not handle unique or unexpected situations well.

Therefore, a non-linear robust control technique, sliding-mode, was applied to design a position controller.

2. MATERIALS AND METHODS

The pneumatic valve is the key element in the system. There are two types of valves used in the pneumatic positioning, servo-valves and on-off valves. With conventional on-off valves accurate position control is difficult to achieve because of the limitation of the valve

response time. In the past few years there has been a wide interest in the use of cheap high speed solenoid valves [7]. The most of applications are on pulse with modulation (PWM). By the advent of DSPs with high computation power, the precise and robust control of pneumatic actuators has become possible.

Sliding mode control was introduced in the late 1970's [8] as a control design approach for the control of robotic manipulators. Among experimental studies, a few succeeded in showing closed-loop system behaviour which was predicted by the theory [9].

Another solution is to employ the advanced nonlinear control strategies developed in recent years (soft computing) [10].

The design of a sliding mode controller consists of three main steps. One is the design of the sliding surface, the second step is the design of the control which holds the system trajectory on the sliding surface, and the third and key step is the chattering-free implementation. The purpose of the switching control law is to force the nonlinear plant's state trajectory to this surface and keep on it. When the plant state trajectory is „above” the surface, a feedback path has one gain and a different gain if the trajectory drops „below” the surface.

Consider a single-input, single-output second-order nonlinear dynamic system:

$$\ddot{x} = f(x, \dot{x}, u). \quad (1)$$

Where x is the output signal (position) of the controlled plant, u is the control signal. If x_d denotes the desired value, then the error between the reference and system states may be defined as

$$e = x_d - x. \quad (2)$$

2.1. Sliding surface design

Classically, a scalar variable s is calculated as a linear combination of the error and its derivative.

$$s = e + \lambda \cdot \dot{e}. \quad (3)$$

Let $s(\dot{e}, e) = 0$ define the „sliding surface” in the space of the error state. The purpose of sliding mode control law is to force the state trajectory of the error to approach the sliding surface and then move along the sliding surface to the origin (Fig.1.).

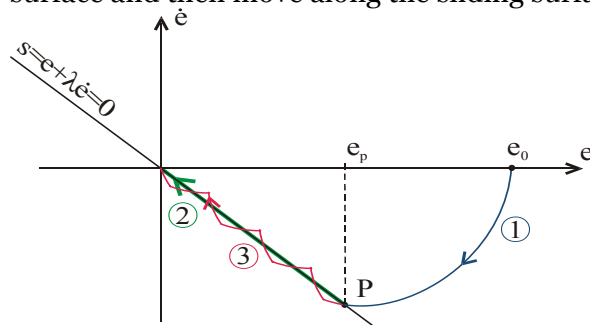


Figure 1. Sliding motion in the state space

The process of sliding mode control can be divided into two phases, that is, the approaching phase with $s(\dot{e}, e) \neq 0$ and the sliding phase with $s(\dot{e}, e) = 0$. If the system is in sliding mode the error is decreasing exponentially, where λ is a time constant type parameter. If λ is big than the system response is slow but accurate. If it is small than the system response is fast but the system might chatter.

2.2. Selection of the control law

In order to guarantee that the trajectory of the error vector e will translate from approaching phase to sliding phase, the control strategy must satisfy the sliding condition

$$s(\dot{e}, e) \cdot \dot{s}(\ddot{e}, \dot{e}) < 0. \quad (4)$$

This means that e will always go toward the sliding surface. A proper control should be selected to satisfy the condition (4) in any time instant. The simplest control law that might lead to sliding mode is the relay.

$$u = \delta \cdot \text{sign}(s). \quad (5)$$

2.3. Chattering free implementation

Chattering is the main problem of sliding mode control and chattering free implementation is the key step in design of a sliding mode controller. A quite general solution is that the relay (which changes its output value suddenly) is replaced by a saturation

function. There is a boundary layer around the sliding surface where the control signal is changing continuously. If the system trajectory is close to the sliding surface and the control signal is small, than the system might stick before the goal.

To avoid it a modified saturation function shown in Table 1. is proposed. When the limitation of the position is satisfied, all high-speed on-off solenoid valves are ON to stop the overshoot. The control will be finished when $|e_s|$ is smaller than ϵ .

3. THE SERVOPNEUMATIC POSITIONING SYSTEM

The experimental set-up, is shown in Fig.2. and Fig.3. consists of a slider mechanism. One side of the muscle is fixed to a load cell, while the other side is attached to the movable frame. The load cell (7923 type from MOM) is a 4 bridge element of strain gauges. It is mounted inline to the PAM on the fixed surface. The load cell measures the force exerted by the PAM. The linear displacement of the actuator is measured using a LINIMIK MSA 320 type linear incremental encoder. Velocity and acceleration are obtained by numerical derivation. During each test, slider position, muscle force and applied gauge pressure are recorded. Since PAMs are one-way acting, two are needed to generate bidirectional motion: as one of them moves the load, the other one will act as a brake to stop the load at its desired position. To move the load in the opposite direction the muscles change function. The PAMs were installed horizontally such that the only force present during activation was the small friction force of the slider mechanism. In the test-bed, two DMSF-20-200N-RM-RM type fluidic muscle (from FESTO) can controlled by tree-way and two-way solenoid valves (MATRIX HX 751.102 C 324 3/2 NC and PX 861.9E4C2KK fast switching types).

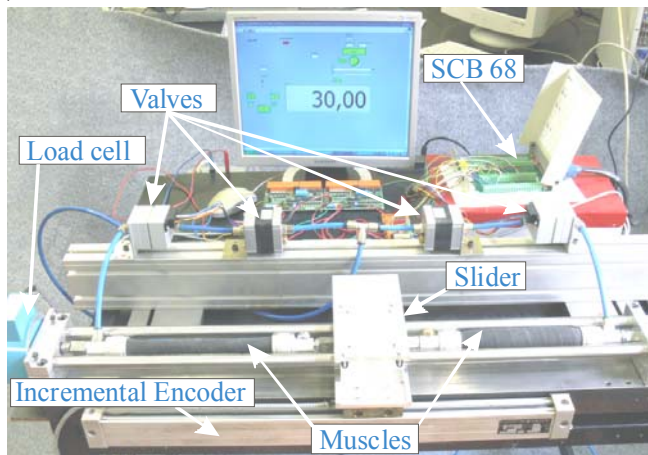


Figure 2. The photo of the experimental setup

We repeated experiments for several levels of pressures in the range from 0 to 5 bar. To measure the air pressure, two Motorola MPX5999D pressure sensors were plumbed into the pneumatic circuit. A National Instruments data acquisition card (NI 6251/M) reads the signal of force, pressure sensors and incremental encoder into the PC. National Instruments LabVIEW will be used to monitor and collect the data imported through the DAQ card. It will also dispatch the control profiles for the PAMs. (Fig. 4 and Fig. 5)

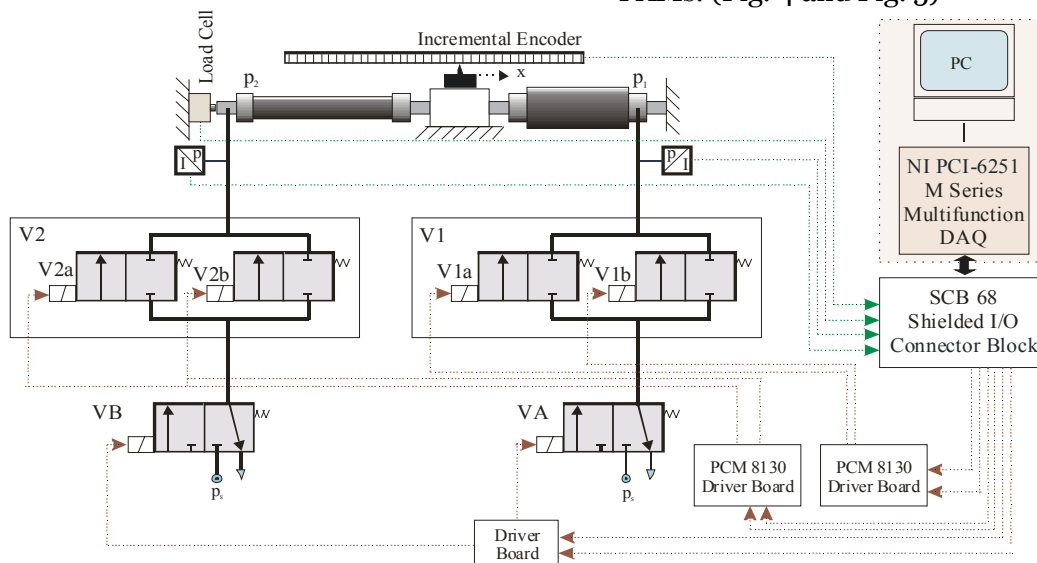


Figure 3. Configuration of pneumatic positioning system

Table 1.

		Fast Forward	Slow Forward	In Position	Slow Backward	Fast Backward
VA		1	1	1	0	0
VB		0	0	1	1	1
V1	V1a	1	1	0	1	1
	V1b	1	0	0	0	1
V2	V2a	1	1	0	1	1
	V2b	1	0	0	0	1

The system pressure is set to be 6 bar, the sampling time is 10 ms. In order to analyze the positioning methods a real-time data acquisition program was designed. The control program is based on Table1.



Figure 4. Front Panel of the LabVIEW program

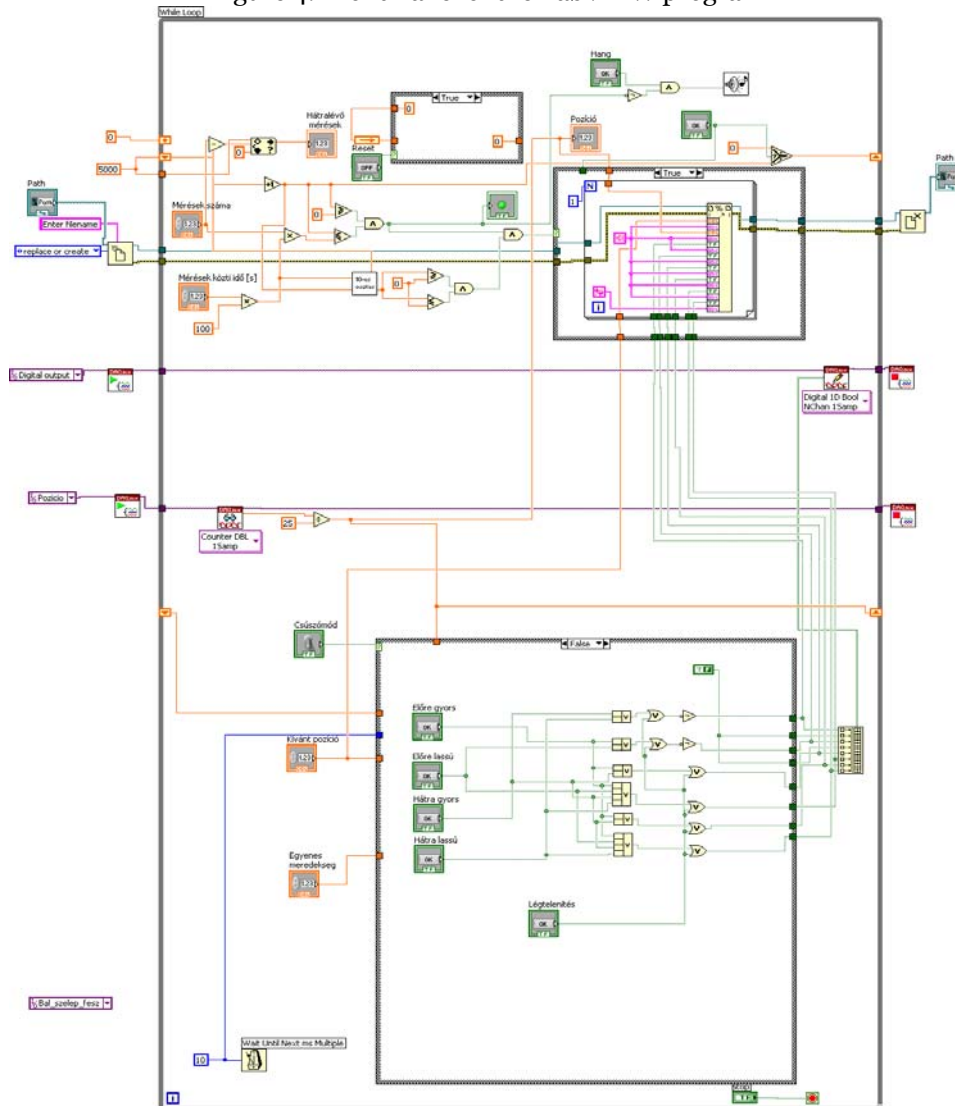


Figure 5. Block Diagram of the LabVIEW program

4. EXPERIMENTAL RESULT

The conventional, single stage solenoid operated on-off valves are very bulky and their dynamic performances are low. With these valves fine motion control is difficult to achieve because of the limitation of the valve response time. With on-off control the system will never reach a steady state value.

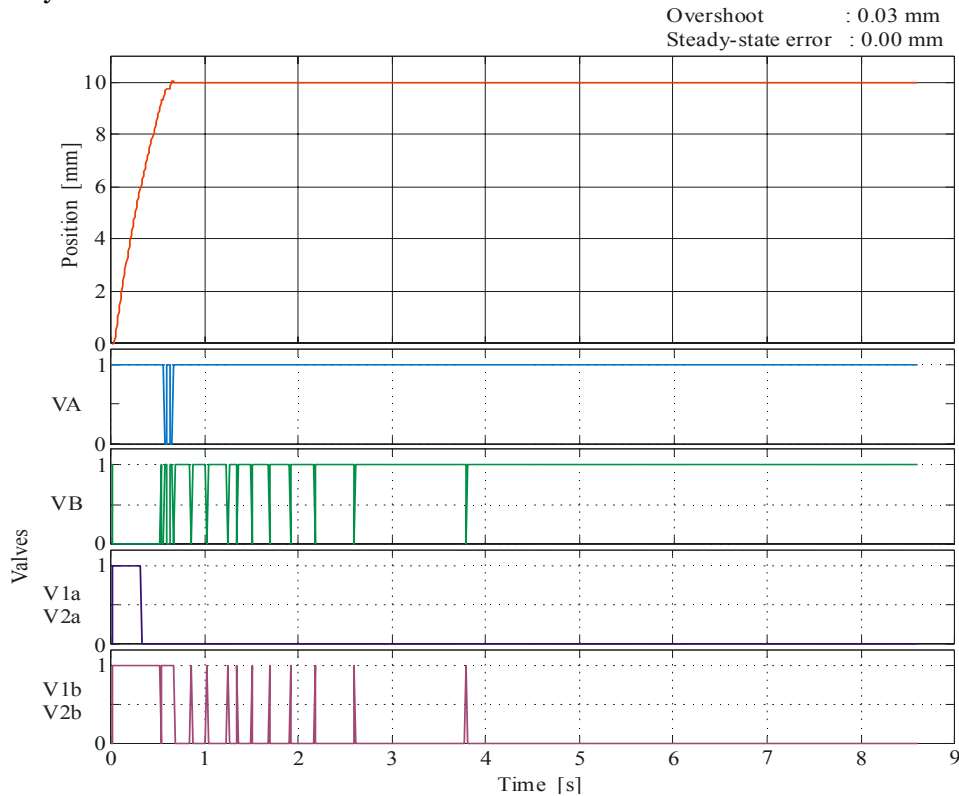


Figure 6. The time functions of the position and control signal

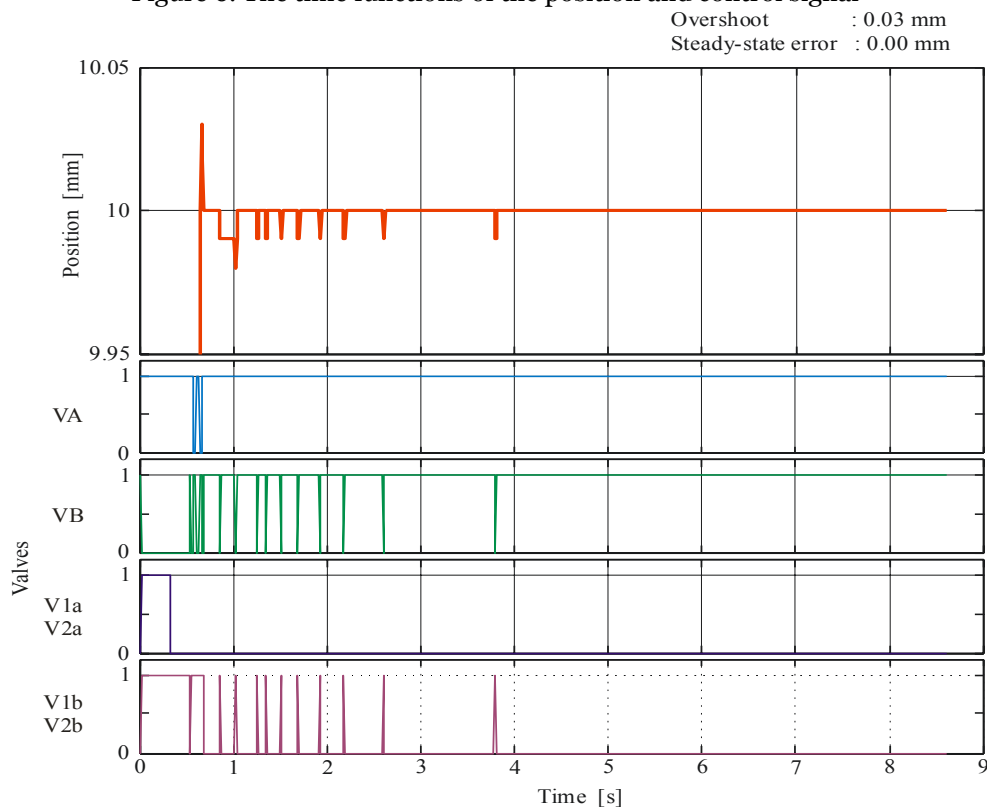


Figure 7. The time functions of the position and control signal (enlarged)

The actual position will tend to oscillate around the desired position. The second measurement is a positioning with high-speed on-off solenoid valves. The time functions of the position, and control signal is shown Fig.6. and Fig.7. The position error of the LabVIEW-based relay type sliding mode control is within ± 0.02 mm.

The experimental results show an excellent control performance and that the sliding mode control is an effective methods to develop a practically available human-friendly robot by using the PAM manipulator.

This behavior is in absolute contrast to that of a pneumatic cylinder: a cylinder develops a force which depends only on the pressure and the piston surface area so that at a constant pressure, it will be constant regardless of the displacement.

5. CONCLUSIONS AND FUTURE WORKS

This work is the first fundamental step of a wider project aimed at studying the PAMs. With the help of this test-bed we can carried out several static and dynamic investigations and control methods. Based on the laboratory measurements we can conclude that the pneumatic servo-systems can be used for precise robust position control. The sliding mode control is a promising tool for controlling such systems. The proposed modified saturation function can eliminate the chattering, which is the main problem in case of sliding mode control.

Further works we have done with applying the input shaping method. Once the system has reached the setpoint, the residual oscillation will degrade positioning accuracy and may cause a delay in task completion. Input Shaping is a feedforward control technique for reducing vibrations in computer controlled machines. The method works by creating a command signal that cancels its own vibration. That is, vibration caused by the first part of the command signal is canceled by vibration caused by the second part of the command. Input shaping is a command generation technique that is used to reduce command-induced vibration (as opposed to disturbance-induced vibration) [11]. Input shaping is implemented by convolving a sequence of impulses, called an input shaper.

REFERENCES

- [1] T. Hesselroth, K. Sarkar, and K. S. Patrik van der Smagt, \Neural network control of a pneumatic robot arm," *IEEE Transactions on Systems, Man, and Cybernetics*, vol. 24, no. 1, pp. 28{38, Jan. 1994.
- [2] D. Caldwell, G. Medrano-Cerda, and M. Goodwin, \Braided pneumatic actuator control of a multi-jointed manipulator," in *Proceedings of the 1993 International Conference on Systems, Man, and Cybernetics*, vol. 1, Oct. 1993, pp. 423{428.
- [3] Caldwell, D.G et al., Control of Pneumatic Muscle Actuator, *IEEE Control Systems Mag.* Feb. 1995, pp. 40-48.
- [4] G. Medrano-Cerda, C. Bowler, and D. Caldwell, \Adaptive position control of antagonistic pneumatic muscle actuators," in *IEEE/RSJ International Conference on Intelligent Robots and Systems*, vol. 1, Aug. 1995, pp. 378{383.
- [5] B. Tondy and P. Lopez, \Modeling and control of McKibben artificial muscle robot actuators," *IEEE Control Systems Magazine*, vol. 20, no. 2, pp. 15{38, Apr. 2000.
- [6] Frank Daerden (1999): Conception and Realization of Pleated Pneumatic Artificial Muscles and their Use as Compliant Actuation Elements. Dissertation Vrije Universiteit Brussel
- [7] M.C.Shih, M.A.Ma, "Position Control of a Pneumatic Rodless Cylinder Using Sliding Mode M-D-PWM Control the High Speed Solenoid Valves" *JSME International Journal Series C*, Vol. 41, No.2,1998 pp.236-241
- [8] V.Utkin, "Variable Structure Systems with Sliding Mode" *IEEE Trans.* vol. AC-22, No.2, 1977. pp. 212-222.
- [9] P.Korondi, H.Hashimoto, "Sliding Mode Design for Motion Control" (12 pages) *Studies in Applied Electromagnetics and Mechanics* vol. 16. ISBN 90 5199 487 7, IOS Press 2000.
- [10] GY. MESTER: "Neuro-Fuzzy-Genetic Controller Design for Robot Manipulators." Proc. IECON'95, IEEE,Orlando,Florida,USA,Vol.1.pp.87-92,1995.
- [11] William Singhose, Erika Biediger, Ye-Hwa Chen,and Bart Mills. "Reference command shaping using specified-negative-amplitude input shapers for vibration reduction." *ASME J. of Dynamic Systems, Measurement, and Controls*, 2004.



DESIGN AND FABRICATION OF A TEST-BED AIMED FOR EXPERIMENT WITH PNEUMATIC ARTIFICIAL MUSCLE

Péter TOMAN¹, János GYEVIKI², Tamás ENDRÓDY²,
József SÁROSI², Antal VÉHA²

¹Alfa Busz Kft, Székesfehérvár, HUNGARY

²Department of Technical and Process Engineering, Faculty of Engineering, University of Szeged, H-6724, Szeged, Mars tér 7, HUNGARY

Abstract:

Pneumatic artificial muscles (PAMs) are contractile or extensional devices operated by pressurized air. Similarly to human muscles, PAMs are usually coupled antagonistically. PAMs were first developed (under the name of *McKibben Artificial Muscles*) in the 1950s for use in artificial limbs. There is growing interest in the use of pneumatic artificial muscles for robotic applications due to their high power to weight ratio and the adaptable compliance. To control the actuator, we have to know its properties. The objective of this project was to design an apparatus which would enable experimental investigation of PAMs.

Keywords:

Pneumatic artificial muscles, PAMs, test-bed

1. INTRODUCTION

The stand described in this paper is a didactic laboratory stand, which task is to enable investigations and gather knowledge of construction and the way of working such elements as: a Fluidic Muscle, a PLC controller, DSP systems as well as proportional pressure control techniques. It offers many didactic and investigative possibilities and thanks to applied solutions its development is easily available. The module structure of the research stand gives possibility to make its further development by adding extra modules that can be easily mounted on plates.

2. MATERIALS AND METHODS

The stand was designed and visualised by utilisation of professional CAD software – Autodesk Inventor. Figure 1 shows a schematic representation of the experimental set-up that was used to carry on the research presented in this paper.

The experimental set-up consists of a slider mechanism. One side of the muscle is fixed to a load cell, while the other side is attached to the movable frame. The load cell (7923 type from MOM) is a 4 bridge element of strain gauges. It is mounted inline to the PAM on the fixed surface. The load cell measures the force exerted by the PAM. The tests are performed by changing the displacement of this slider. The linear displacement of the actuator is measured using a LINIMIK MSA 320 type linear incremental encoder. During each test, frame position, muscle force and applied gauge pressure are recorded. Since PAMs are one-way acting, two are needed to generate bidirectional motion: as one of them moves the load, the other one will act as a brake to stop the load at its desired position. To move the load in the opposite direction the muscles change function. This opposite connection of the muscles to the load is generally referred to as an antagonistic set-up: the driving muscle is called the flexor or agonist, while the brake muscle is referred to as the extensor or antagonist. The antagonistic coupling can be used for either linear or rotational motion. The PAMs were installed horizontally such that the only force present during activation was the small friction

force of the slider mechanism. In the test-bed, two DMSP-20-200N-RM-RM type or two DMSP-10-250N-RM-RM type fluidic muscle (from FESTO) can mounted, with a pre-tension of about 15% (half of the maximum contraction ratio which is 30%). This work is the first fundamental step of a wider project, aimed at studying the humanoid robot.

Instead of second PAM a bias spring or an external load can attached with a flexible steel cables, producing the necessary counter force to pull the actuator back when it is not activated. In a spring, the stiffness is constant within a definite field.

We repeated experiments for several levels of pressures in the range from 0 to 5 bar. The air pressure applied to the actuators can regulated with two adjustable regulator type Festo VPPM-6L-L-1-G1/8-0L6H-V1N-S1C1. The proportional pressure regulators (PPRs) are controlled by voltage inputs. The main purpose of the PPR is to regulate the pressure entering the PMA. To measure the air pressure, two Motorola MPX5999D pressure sensors were plumbed into the pneumatic circuit. A National Instruments multi-IO card (Lab PC 1200) reads the signal of force, pressure sensors and incremental encoder into the PC. National Instruments LabVIEW will be used to monitor and collect the data imported through the DAQ card. It will also dispatch the control profiles for the PPRs. LabVIEW allows for the dynamic collection of data.

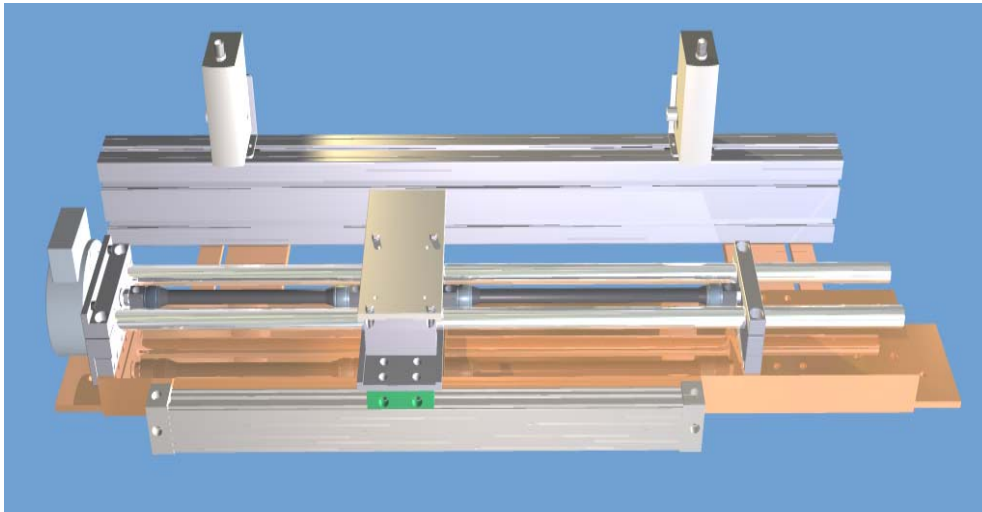


Figure 1. The view of the stand for Fluidic Muscle investigations

With the specially constructed dynamic testing machine, we are able to measure the static and dynamic characteristics of several versions of these actuators. The photos of the set up are shown in Fig. 2-5.

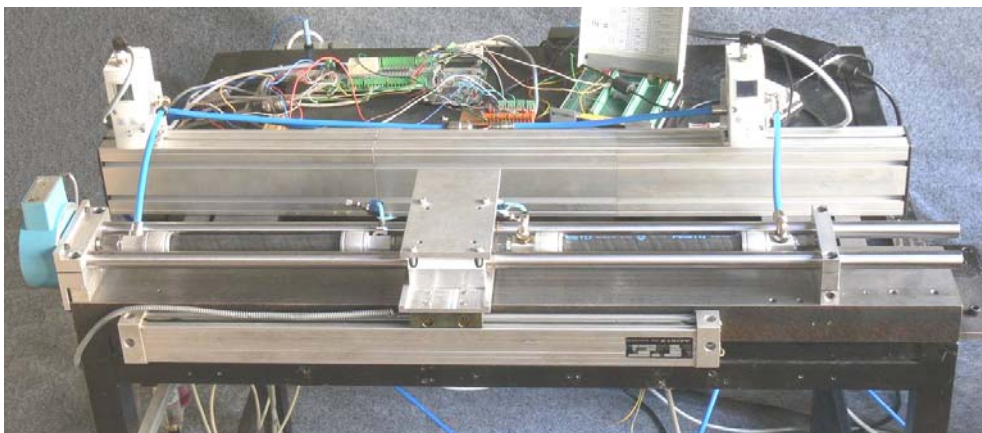


Figure 2. The photo of the stand for Fluidic Muscle investigations (two antagonistic muscle)

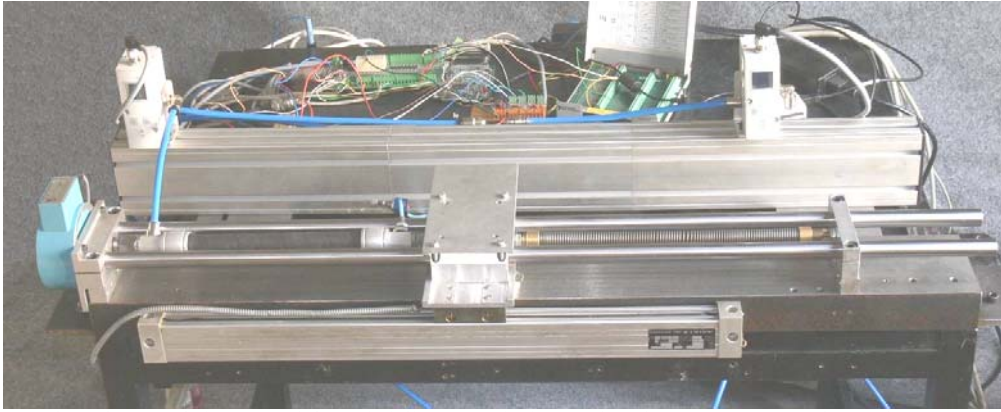


Figure 3. The photo of the stand for Fluidic Muscle investigations (one muscle and one spring pair)

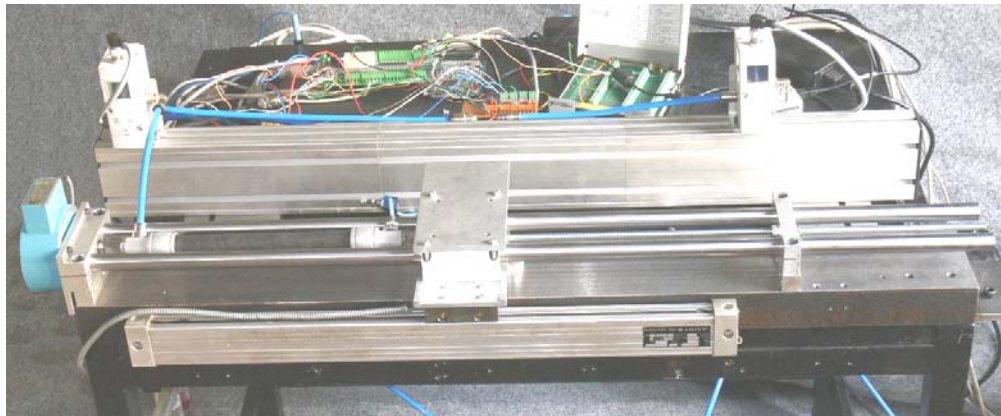


Figure 4. The photo of the stand for Fluidic Muscle investigations in fixed slider position

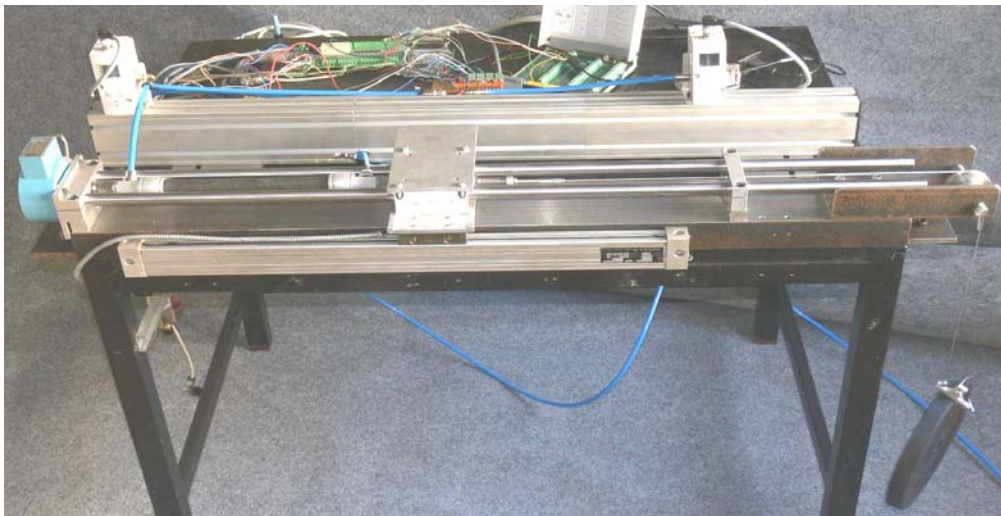


Figure 5. The photo of the stand for Fluidic Muscle investigations with external load

The fluidic muscle can be used as an actuator or a spring. If internal pressure is changed, the muscle can set an external load into motion like an actuator (Figure 6). If the external load is changed, the fluidic muscle reacts like a spring by changing its length. Contraction of the fluidic muscle is thus dependent upon internal pressure as well as external load (Fig. 7).

To see how the device operates, two basic experiments can be considered. In both cases a PAM of an arbitrary type is fixed at one end and has a mass hanging from the other. In the first experiment, shown in Figure 6, the mass M is constant and the pressure difference across the membrane, i.e. its gauge pressure, is increased from an initial value of zero. At zero gauge pressure the volume enclosed by the membrane is minimal, V_{min} , and its length maximal, l_{max} . If the muscle is pressurized to some gauge pressure p_1 , it will start to bulge

and at the same time develop a pulling force. The mass will thus be lifted until the generated force equals Mg . The membrane's volume will then have grown to V_1 and its length contracted to h . Increasing the pressure further to p_2 will continue this process. From this experiment two basic actuator behavior rules can be deduced: a PAM shortens by increasing its enclosed volume, and it will contract against a constant load if the pneumatic pressure is increased.

The other rules can be derived from the second experiment, shown in Figure 7. The gauge pressure is now kept at a constant value p , while the mass is diminished. In this case the muscle will inflate and shorten. If the load is completely removed, as depicted by Figure 7 (c), the swelling goes to its full extent, at which point the volume will reach its maximum value, V_{max} , the length its minimal value, h_{min} , and the pulling force will drop to zero. The PAM cannot contract beyond this point, it will operate as a bellows at shorter lengths, generating a pushing instead of pulling force. This means that a PAM will shorten at a constant pressure if its load is decreased and its contraction has an upper limit at which it develops no force and its enclosed volume is maximal. Concluding from both experiments a fifth rule can be added: for each pair of pressure and load a PAM has an equilibrium length.

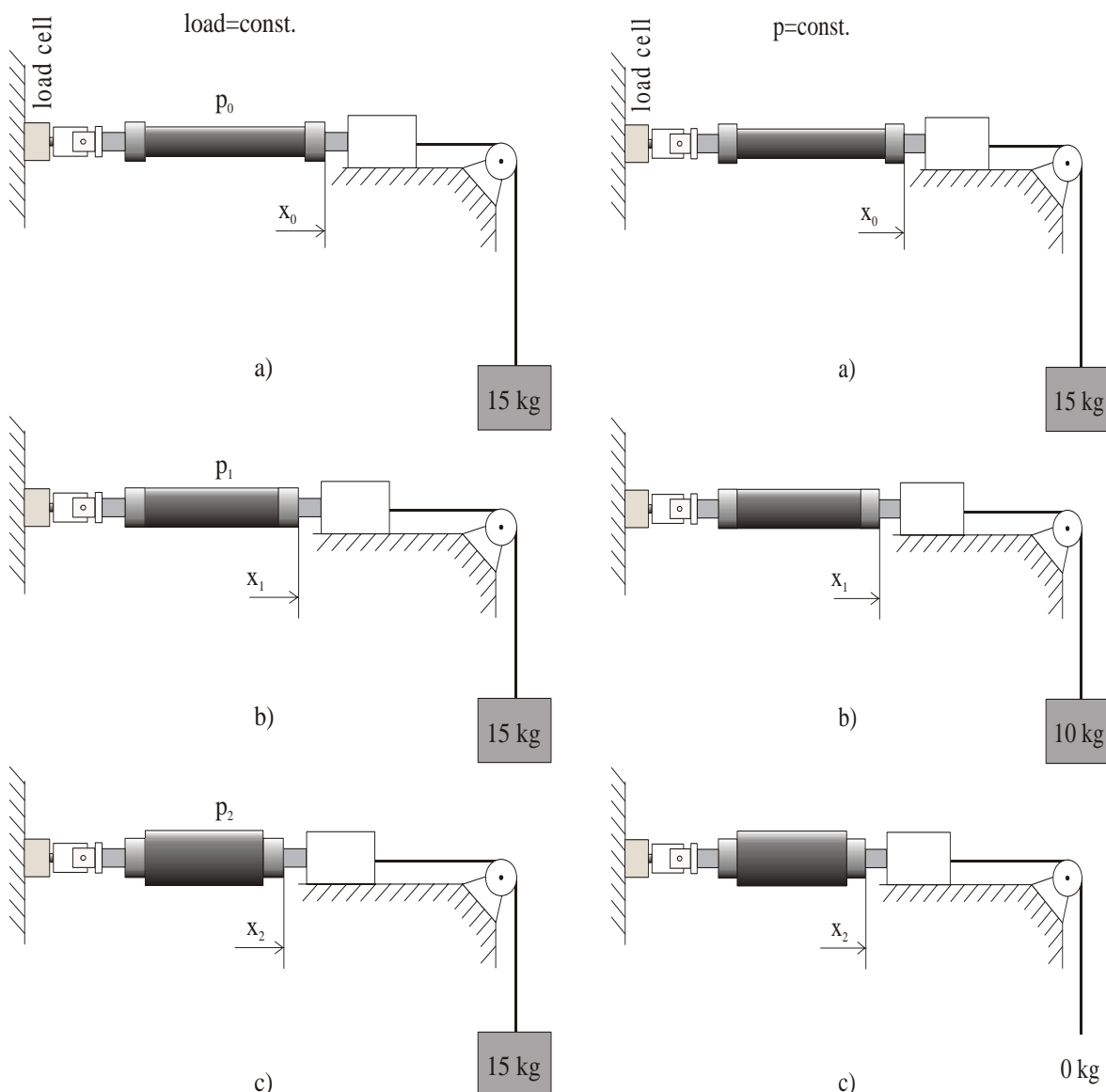


Figure 6. PAM at constant load

Figure 7. PAM at constant pressure

This behavior is in absolute contrast to that of a pneumatic cylinder: a cylinder develops a force which depends only on the pressure and the piston surface area so that at a constant pressure, it will be constant regardless of the displacement.

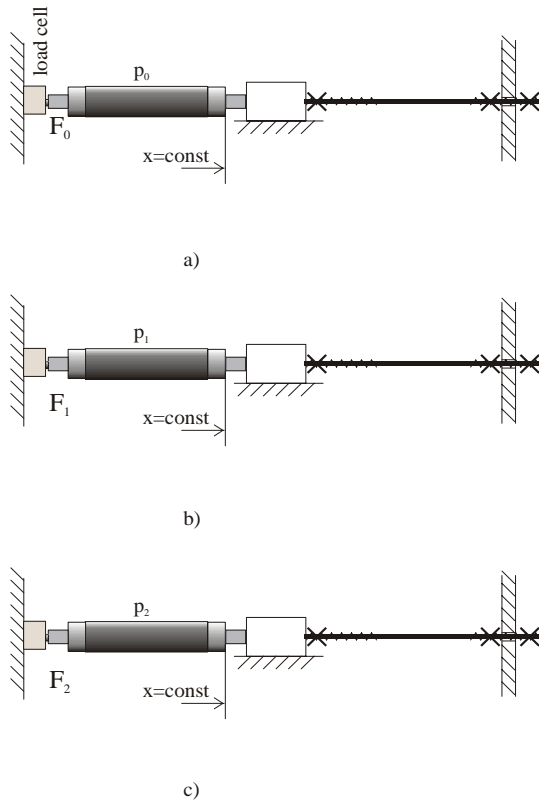


Figure 8. PAM at fixed position

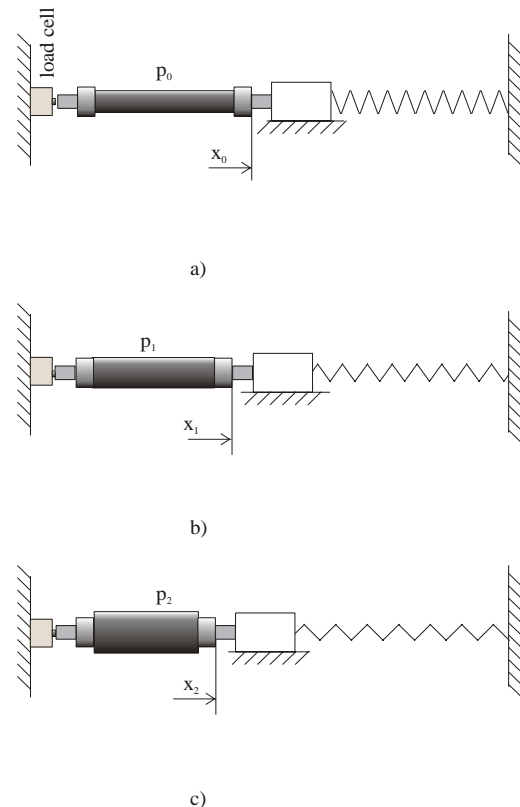


Figure 9. PAM with bias spring

3. RESULTS AND DISCUSSION

A pneumatic artificial muscle (PAM) is essentially a volume, enclosed by a reinforced membrane, that expands radially and contracts axially when inflated with pressurized air. Thereby, the muscle generates a unidirectional pulling force along the longitudinal axis. When neglecting the membrane's material deformation and the low inertial muscle properties, the generated force is expressed as:

$$F = -p \frac{dV}{dl} \quad (1)$$

with p the gauge pressure inside the muscle, dV the enclosed muscle volume changes and dl the actuator length changes. The volume of the actuator increases with decreasing length until a maximum volume is reached. At maximum contraction these forces become zero; at low contraction these forces can be very high. Depending on the geometry and type of membrane, the specific force characteristic alters. Several concepts of PAM have been developed over time.

This work is the first fundamental step of a wider project aimed at studying the PAMs. With the help of this test-bed we can carry out several static and dynamic investigations (Figure 8-9).

REFERENCES

- [1] Frank Daerden (1999): Conception and Realization of Pleated Pneumatic Artificial Muscles and their Use as Compliant Actuation Elements. Dissertation Vrije Universiteit Brussel
- [2] Masanori Sugisaka · Huailin Zhao (2007): The characteristics of McKibben muscle based on the pneumatic experiment system. *Artif Life Robotics* (2007) 11:223–226 p.
- [3] G. Wszolek, G. Stawarz, P. Zub, (2007): The laboratory stand for didactic and research of a Fluidic Muscle. *Journal of Achievements in Materials and Manufacturing Engineering* 77-80 p.

- [4] T. Hesselroth, K. Sarkar, and K. S. Patrik van der Smagt, \Neural network control of a pneumatic robot arm," *IEEE Transactions on Systems, Man, and Cybernetics*, vol. 24, no. 1, pp. 28{38, Jan. 1994.
- [5] D. Caldwell, G. Medrano-Cerda, and M. Goodwin, \Braided pneumatic actuator control of a multi-jointed manipulator," in *Proceedings of the 1993 International Conference on Systems, Man, and Cybernetics*, vol. 1, Oct. 1993, pp. 423{428.
- [6] Caldwell, D.G et al., Control of Pneumatic Muscle Actuator, *IEEE Control Systems Mag.* Feb. 1995, pp. 40-48.
- [7] G. Medrano-Cerda, C. Bowler, and D. Caldwell, \Adaptive position control of antagonistic pneumatic muscle actuators," in *IEEE/RSJ International Conference on Intelligent Robots and Systems*, vol. 1, Aug. 1995, pp. 378{383.
- [8] B. Tondu and P. Lopez, \Modeling and control of McKibben artificial muscle robot actuators," *IEEE Control Systems Magazine*, vol. 20, no. 2, pp. 15{38, Apr. 2000.



EXAMINATION OF THE EFFECT OF MICROWAVE HEATING ON THE BIODEGRADABLE AND SOLUBLE FRACTION OF ORGANIC MATTER OF SLUDGE

Sándor BESZÉDES, Zsuzsanna LÁSZLÓ, Gábor SZABÓ, Cecilia HODÚR

University of Szeged, Faculty of Engineering, Department of Technical and Process
Engineering, H-6725, Szeged, Moszkvai krt. 5-7, HUNGARY

Abstract

Because of the high industrial wastewater output the quantity of sludge has been increased. The efficiency of biological sludge handling process was limited by the non-soluble and non-degradable component. Among sludge handling processes the thermal treatments are known as more utilizable methods because of pathogen destruction and digestion effect. In the case of microwave treatment the biodegradability is increased. In our work the effect of microwave irradiation on biodegradability and anaerobic digestionability of dairy originated sewage sludge was investigated. Our results showed that microwave pretreatment is appropriate to enhance solubility of organic compounds thus the biodegradability and biogas product increased.

Keywords:

sludge, microwave pre-treatment, solubility, biodegradability, biogas

1. INTRODUCTION

The drinking water supply has been turned into the most urgent problem for assuring healthy human being in the world. A large scale development was experienced in the drinking water and waste water management technology and hereby the cleaning efficiency could be in a large measure improved, but simultaneously the quantity and the environmental risk of emitted sewage sludge increased. Generally, the solid phase of waste water is named sewage sludge.

Depending on the processed raw material the sludge may be rich in carbohydrates, lipids or proteins. In most cases the sludge handling system has become the bottleneck of capacity of waste water treatment plants. The most common alternatives of sewage sludge handling are landfill, cropland application, incineration and in the last resort conditioned dumping as hazardous waste.

Waste management has become an acute problem in many countries. Management options require extensive waste characterization since many of them may contain compounds deleterious for the ecosystem, such as heavy metals, organic micropollutants and other persistent and less biodegradable compound. Beside the general characterization and testing of waste sludge the digestion and biodegradability testing give more utilizable information for planning of composting and biogas producing. The main structure of municipal and food industrial sewage sludge consists of extracellular polymeric substance (polysaccharides, proteins, lipids, nucleic acids), multivalent cations, other organic and inorganic matter and microbial cells which compose a special flock structure [1]. This agglomerated complex flock structure is resistance to a direct anaerobic degradation since cell walls and polymeric conformation present physical and chemical barriers for microbial and enzymatic degradation.

Extracellular polymeric substance are present in varying quantities in sewage sludge, occurring as highly hydrated capsule surrounding the cell wall and loose in solution as slimy polymers and it is able to retain a large volume of water within the sludge matrix by electrostatic interactions and hydrogen bounds. The non-biodegradable polymeric structure does not only originate from cell autolysis and sludge bacterial cell but also originates from the compounds of raw wastewater. So besides the cationic content of dosed chemical and organic content, the efficiency and specific removal capacity of applied waste water treatment technology (chemical, biological or combined) have effect on biodegradability of sludge [2].

There are many possibilities to improve the digestibility and aerobic biodegradability of sludge. Mechanical, thermal, ultrasound, chemical, thermo-chemical and enzymatic pre-treatment methods can enhance the extent and the rate of biological degradation [3, 4]. It is verified the thermal pretreatments improve pathogen destruction and dewaterability process of sludge, too [5].

Microwave heating is used as a popular alternative to conventional heating mainly due to considerable reaction time reducing effect. The microwave equipment generally uses 2450 MHz frequency with a 12,24 cm operating wavelength. The microwave magnetron with 900 MHz operating frequency is used for industrial scale heating and drying of solid and low water content matter on the ground of larger penetration ability. Applications of microwave-assisted techniques in many fields of analytical methods, such as sample drying, moisture measurements and extraction processes are used [6].

The microwave irradiation has thermal and athermal effect. The thermal effect can be attributed heat generation in the matter due to rotation of dipole molecules or ionic conduction. Ionic conduction is the electrophoretic migration of ions when an electromagnetic field is applied. Dipole rotation means realignment of dipoles with the applied fields, for example at 2450 MHz the dipoles align and randomized $4,9 \times 10^9$ times per second and this forced molecular motion results heat. In many applications these two mechanisms have been applied simultaneously.

Due to high water content the sewage sludge can absorb microwave energy efficiency. Although the quantum energy of microwave radiation is too low ($1,05 \times 10^{-5}$ eV) to break the chemical bounds but some structures can be altered by the energies carried by microwaves. For example the athermal effect of microwave radiation is caused by polarized parts of macromolecules, it results breakage of hydrogen bound. The intensive microwave heat generation and the different dielectric properties of compounds of cell wall lead to a rapid disruption of extracellular polymer network and residue cells of sludge [7, 8]. However the cell liquor and extracellular organic matter within polymeric network can release into the soluble phase, hereby increase the ratio of accessible and biodegradable component [9, 10].

2. MATERIALS AND METHODS

The sewage sludge was originated from a industrial waste water treatment plant of a local dairy works (Sole-Mizo Ltd., Szeged, Hungary). In the case of dairy industrial sewage sludge a physico-chemical waste water technology was applied and the final water content of sludge was 58,2 w/w%.

The microwave pre-treatments were performed in a self-developed monomode microwave treating and measuring unit, at 2,45 GHz frequency, at 50 to 700 W microwave power. The microwave irradiation time was 10 to 40 minutes. The applied specific microwave power level was 1, 2 and 5 W/g, which was adjusted by the ratio of magnetron power and the quantity of treated sludge. The sludge samples were placed invariably in 2 cm layer because of penetration depth of microwave radiation. Poly-tetrafluor-ethylene (PTFE) vessels were used on account of efficient microwave penetration and absorption. Cover was applied to prevent the evaporation during the irradiation. The surface temperature of sludge an Infracam (FLIR InfraCAM-SD, Sweden) was determined after microwave irradiation

As comparing method convective heat-treatments were performed. The convective heat-treatment was performed in automatic temperature controlled laboratory heater equipment (Medline CM 307, UK) at 95 °C.

The value of biodegradability (BD) is commonly characterized by the BOD/COD ratio. COD is the chemical oxygen demand; the quantity of oxygen required oxidation by chemical oxidant. The soluble COD (sCOD) indicate the water soluble part of COD. BOD is the biochemical oxygen demand, the quantity of oxygen consumed by aerobic microorganisms due to carbonaceous oxidation at a standard temperature (20°C).

COD was measured according to the dichromate standard method in COD test tubes with an ET 108 digester and a Lovibond PC Checkit photometer. Before sCOD determination the samples were centrifuged for 20 minutes at 6000 RCF. The separation of water soluble phase a 0,45 µm pore size disc filter (Millipore) was used. The biochemical oxygen demand measurements were carried out in a respirometric BOD meter (BOD Oxidirect, Lovibond, Germany), at 20°C. To ensure the consistency of the results BOD microbe capsules (Cole Parmer, USA) were used for measurements. Biodegradability during 5 days (BD₅%) was characterized by the (1) expression:

$$BD_5\% = \frac{BOD_5}{COD} \times 100\% \quad (1)$$

The anaerobic degradability batch mesophilic biochemical methane potential (BMP) tests are used with applying of acclimated inoculums of methanogenic bacteria at mesophilic temperature range (25-45 °C). By our measurements the cumulative biogas production tests were performed in batch mode under mesophilic conditions, at 40°C for 30 day, in a temperature controlled anaerobic digester with Oxitop Control type pressure mode measuring system (WTW Gmbh, Germany). The digesters were inoculated with an acclimated anaerobic sludge from a biogas reactor of municipal wastewater treatment plant (Hódmezővásárhely, Hungary) in order to eliminate the possible lag-phase of biological degradation process. After inoculation nitrogen gas was flowed through the reactor to prevent exposure to air.

3. RESULTS AND DISCUSSION

The surface temperature of samples was measured by infracam, and the average temperature and standard deviation were represented in the following table.

Table 1: The surface temperature of microwave irradiated sludge after treatments

MW Power level	Surface temperature [°C]			
	10 min.	20 min.	30 min.	40 min.
1 W/g	75,7 ± 2,9	83,5 ± 1,8	89,2 ± 1,6	90,2 ± 1,3
2 W/g	79,3 ± 2,2	86,7 ± 1,4	89,6 ± 1,1	91,7 ± 0,7
5 W/g	83,6 ± 0,8	89,1 ± 0,9	90,8 ± 0,3	92,8 ± 0,4

In the first series of our experiments the effect of microwave irradiation on biodegradability of sewage sludge was investigated at different specific microwave power level. Besides the specific power level the effect of irradiation time was studied too. It was found that without pre-treatment the dairy industrial sludge was less biodegradable because the biodegradability of untreated dairy sludge was 8%.

The biodegradability of dairy sewage sludge was 8% and however it was find that without pre-treatment the sludge was in a large measur resistant to aerobical biological degradation. The structure of dairy sludge, formed by interaction of extracellular polymeric substance and applied chemicals, caused less accesible property for biological decomposition.

Microwave irradiation at low power level (1 W/g) had slightly effect on biodegradability, but the higher microwave power level and enhanced irradiataion time seemed to be more efficiently. By higher applied power level (5-10 W/g) a saturation value of biodegradability was observed. The ratio of biodegradable component of dairy originated sludge was enhanced from 8 % to 40 % after 30 minutes microwave irradiation at 5 and 10 W/g (Fig. 1).

The following measurements the effect of microwave irradiation on solubility of organic matter content of dairy originated sewage sludge were examined. The water-solubilization of organic component was characterized by the ratio of soluble COD (sCOD) and total COD.

It was found that the microwave pre-treatment could increase the quantity of water-soluble part of organic matter. Similar to biodegradability in the case of solubility of organic matter content saturation values were observed at 5 and 10 W/g specific microwave treatment level, but the differences in values of solubilisation were more considerable (from 10% to 50%) than values of biodegradability (Fig. 2). But the efficiency of increased microwave power level was slighter than the difference by biodegradability. Enhancing of biodegradability may be linked to solubilization of organic matter which was indicated by the increased sCOD/COD ratio.

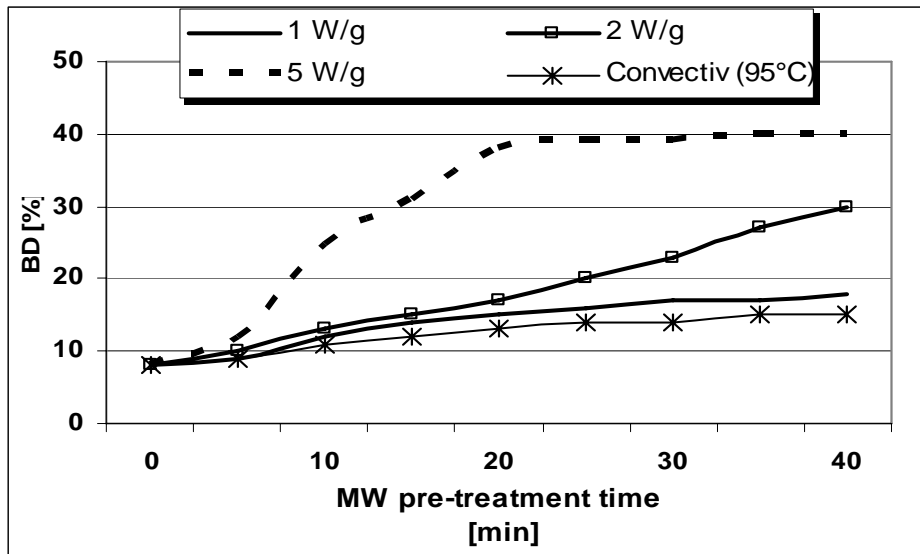


Fig. 1. Biodegradability (BD%) of dairy sewage sludge after microwave and convective pre-treatments

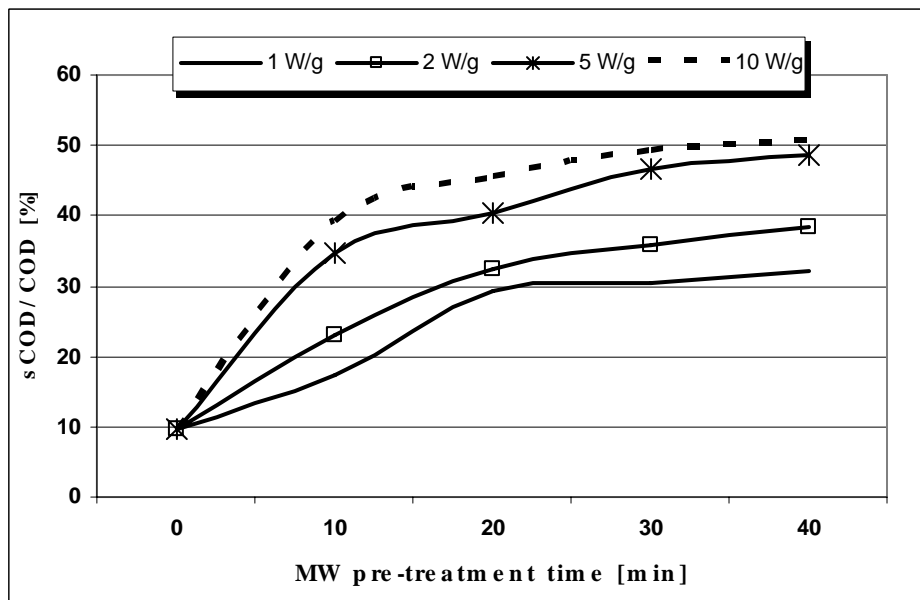


Fig. 2. The effect of microwave pre-treatments on solubilization (sCOD/COD ratio) of organic matter content of sludge

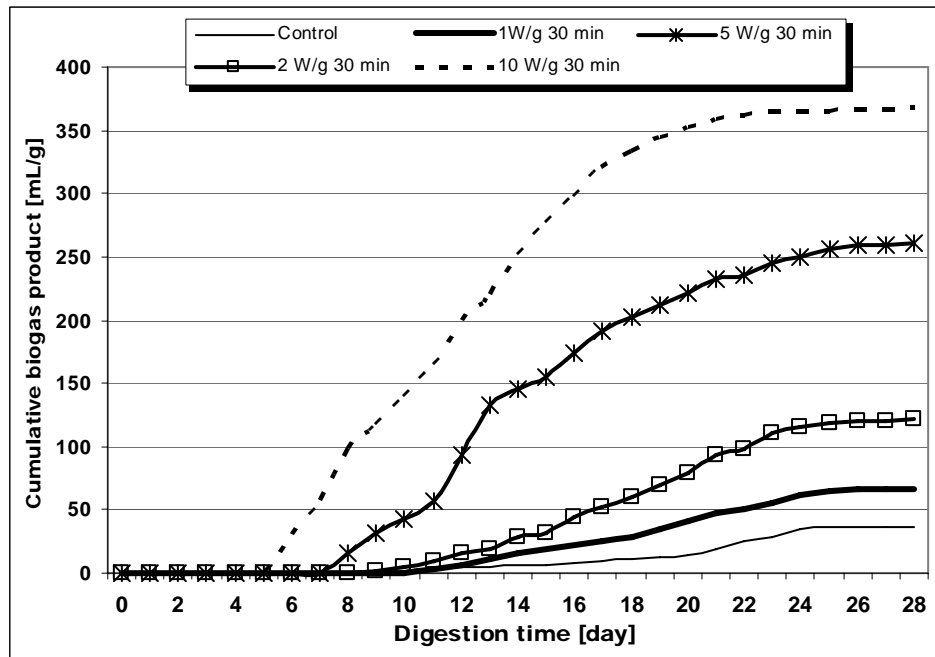


Fig. 3. Cumulative biogas product of microwave pre-treated sludge

Besides the change of biodegradability and solubilization the effect of microwave irradiation on anaerobic digestion was investigated also. The digestionability was characterized by cumulative biogas production. Similar to aerobical biodegradation the microwave pre-treatment improved the efficiency of the anaerobical decomposition. The untreated control sample had a small (40 cm³/g) biogas production, and after a pre-treatment at 2 W/g for 30 minutes enhanced the methane product up to 120 cm³/g and by 10 W/g microwave treatment the biogas product could reach the 350 cm³/g value. The applied microwave treatment could decreased the lag-phase period of anaerobic digesting process. The higher specific microwave power caused higher increasing in biogas production and however higher decreasing could have measured in period of lag-phase. Increasing power level of microwave treatment from 5 to 10 W/g caused a great enhancing in biogas product but not in the solubilization or aerobical biodegradability (Fig. 2, 3).

4. CONCLUSION

Our results showed that the microwave irradiation is successfully adjustable and utilizable technique in sewage sludge handling. Applying of microwave pre-treatment the solubility of organic matter content increased and it enhance more efficiently the aerobical biodegradability and biogas yield than the convective heat pre-treatments.

REFERENCES

- [1] Neyens E., Baeyens J., Dewil R., DeHeyder, B.: Advanced sludge treatment affects extracellular polymeric substances to improve activated sludge dewatering. . *Journal of Hazardous Materials, Vol. 106B*, pp. 83-92. (2004)
- [2] Eskicioglu, C., Kennedy K., J., Droste R. L.: Characterization os soluble organic matter of waste activated sludge before and after thermal pretreatment. *Water research*, Vol. 40, pp. 3725-3736. (2006)
- [3] Stasta, P., Boran, J., Bebar, L., Stehlik, P., Oral, J.: Thermal processing of sewage sludge. *Applied Thermal Engineering*, Vol. 26, pp. 1420-1426. (2006)

- [4] Bougrier, C., Delgenes J. P., Carrere H.: Effects of thermal treatments on five different waste activated sludge samples solubilisation, physical properties and anaerobic digestion. *Chemical Engineering Journal*, Vol. 139, pp. 236-244. (2007)
- [5] Wojciechowska, E.: Application of microwaves for sewage sludge conditioning. *Water Research*, Vol. 39, pp. 4749-4754. (2005)
- [6] Jones, D. A., Lelyveld, T. P., Mavrofidis, S. D., Kingman, S. W., Miles, N. J.: Microwave heating applications in environmental engineering. *Resources, Conservation and Recycling*, pp. 75-90. (2002)
- [7] Eskicioglu, C., Terzian N., Kennedy K., J., Droste, R., L., Hamoda M.: Athermal microwave effects for enhancing digestibility of waste activated sludge. *Water Research*, Vol. 41, pp. 2457-2466. (2007)
- [8] Beszédes S., Kertész Sz., László Zs., Géczy G., Hodúr C., Szabó G.: Sewage sludge treatment by microwave energy. *Proceedings of 5th International Congress on Food Technology*, Thessaloniki, Volume 3. pp. 441-446. (2007)
- [9] Climent, L., Ferrer, I., Baeza M., Artola A., Vázquez F., Font X.: Effect of thermal and mechanical pretreatments of secondary sludge on biogas production under thermophilic conditions *Chemical Engineering Journal* pp. 273-278. (2007)
- [10] Sándor Beszédes, Szabolcs Kertész, Zsuzsanna László, Zsuzsanna, Gábor Szabó, Cecilia Hodúr: Biogas production of ozone and/or microwave-pretreated canned maize production sludge. *Ozone Science & Engineering Journal* (in press) (2008)



THE EFFECT OF MICROPARTICLES FOR THE MEMBRANE RESISTANCE

Angéla SZÉP, Szabolcs KERTÉSZ, Zsuzsanna LÁSZLÓ, Cecilia HODÚR

Department Of Mechanical And Process Engineering,
University Of Szeged, H-6725 Szeged, Moszkvai Krt 5-7, HUNGARY

Abstract

The aim of this study was to examine the applicability of bakelite particles for the reduced of the cake layer. Formation of a cake layer on the membrane surface has a decreasing effect on the long-term behaviour of the system. A typical cake layer shows compaction, which causes decrease in the porosity of the cake layer. One alternative approach to reduce fouling is to enhance the local shearing near the membrane surface, thereby increasing mass transfer of accumulated compounds back into the feed bulk. Ways of increasing the local shear rate near the membrane surface is use of scouring particles.

Keywords:

microfiltration, microparticles, shearing

1. INTRODUCTION

Pressure-driven membrane separation processes (microfiltration, ultrafiltration, nanofiltration and reverse osmosis) are important and attractive alternative candidates to conventional wastewater treatments for purification of wastewater and surface water [1], because of their high removal efficiencies and also because it allows reuse of the treated water or some of the valuable waste constituents [2]. The pressure-driven membrane techniques present several advantages: the permeate purified usually has a great quality, the processes are easy to operate with moderate temperatures and low energy requirements in general, no chemicals are needed, and combination with other separation processes is easy due to modular construction. In these processes, the water passes through the membrane and contaminants are removed by various mechanisms mainly depending on the pore size. Generally, microfiltration membranes have pores ranging from 0.1 to 10 μm and operate at pressures below 5 bar [3]. They are useful for the removal of suspended solids, emulsified components and microorganisms larger than the pore size. Crossflow microfiltration is widely used in concentrating, purifying or separating macromolecules, colloids and suspended particles from solution.

Among the numerous applications of cross-flow microfiltration in the food processing industry. However, industrial applications of this technology meet two main problems. Permeate flux in microfiltration processes decreases with time as the retained particles accumulate on the membrane [4].

Membrane fouling is a very complicated phenomenon mainly caused by adsorption of particles, pore shrinkage and blockage, deposition of particles on the membrane surface and concentration polarization [5], and it is the irreversible alteration in the membrane caused by specific physical and/or chemical interactions between the membrane and various components [6].

The build-up of the filter cake increases the cake-layer resistance to flow, thereby it reduces the filtration flux rate, decreases the longevity of the membrane modules and increases the cost of production and limits the further industrial application to membrane microfiltration technology. Hence, how to alleviate the thickness of filter cake on the membrane surface is still a focus and key technology in membrane field and many various techniques have been suggested, such as turbulence promoting inserts, rotating. [7]. One alternative approaches to reduce fouling are discussed here. The local shear increase near the

membrane surface, thereby increasing mass transfer of accumulated compounds back into the feed bulk. Ways of increasing the local shear rate near the membrane surface is use of scouring particles (bakelite) [8].

2. MATERIALS AND METHODS

Solution preparation

40 g bakelit particles were added into the 20l chulk-dust solution to prepare suspensions. We were added 125-160 μm , 160-200 μm and a 200-400 μm size bakelite. The prepared suspension was well mixed and was pumped into the cross-flow system by using a circulation pump. The suspension concentrations are 0.2, wt%.

Microfiltration experiments

The cross-flow microfiltration (MF/K1) unit used is represented in Fig. 1. It featured a tubular ceramic membrane, with the following attributes: 19 channels with an internal diameter ($d=2.5$ mm), average pore size diameter (0.45 μm), and a total effective filtration area ($A = 0.125$ m²). Temperature was controlled, using cold water circulating through a tubular heat exchanger (H). Operating temperature was adjusted to 25 ± 2 °C. The cross-flow velocity was adjusted and measured by a rotameter (R). The filtration pressure was adjusted by the control valves (14,17) and was measured using the pressure indicators (PI/1, PI/2). TMPs were varied at 100, 150, 200, 250, 300 kPa to determine TMP-dependent changes in

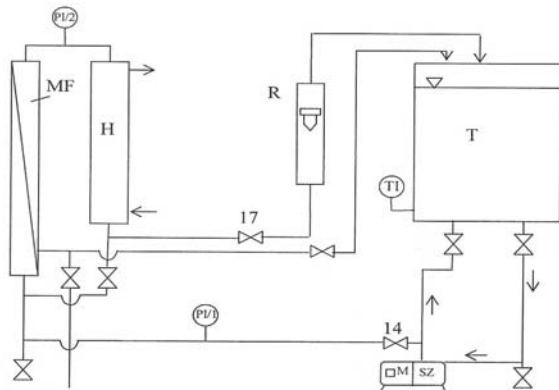


Figure 1. MF/K1 microfiltration equipment [9]

permeate recycle of cross-flow filtration. The crossflow velocities are 2, 4, 6, 8, 10, 12 in this study. The Reynolds number is about 1500–5500. The concentrated chalk-dust solutions were recycled back into the suspension tank.

Before each experiment, the water flux was measured with distilled water at 20 °C. Membrane regeneration was achieved by washing in a 10gL^{-1} NaOH solution and rinsing with distilled water under flux. A classic industrial cleaning procedure is carried out and followed by another determination of the clean membrane resistance:

$$J_w = \frac{\Delta p_{TM}}{\eta_w \cdot R_M} \quad (1)$$

where J is the permeate flux rate (m s^{-1}) and Δp_{TM} is the transmembrane pressure (Pa). The resistance (R_M) of the membrane was calculated from the flux using:

$$R_M = \frac{TMP}{\eta_w \cdot J_w} \quad (2)$$

where η_w is the dynamic viscosity of water (Pa s). The membrane resistance at a TMP of 100 kPa was $1.16 \pm 0.21 \times 10^{11} \text{ m}^{-1}$.

The total resistance (R_T) is calculated as:

$$R_T = R_M + R_{\text{cake}} \quad (3)$$

where R_M is the membrane resistance and R_{cake} the cake-layer resistance [10].

For the Re numbers, the following equation is used:

$$\text{Re} = \frac{d_e \cdot v \cdot \rho}{\eta} \quad (4)$$

where d_e is the equivalent pipe diameter, the v is the velocity, the ρ is the density and the η is the viscosity [11].

3. RESULTS AND DISCUSSION

The relation between flux and TMP was measured for the different particles used in chulk-dust solution. The results are presented in Fig. 2.

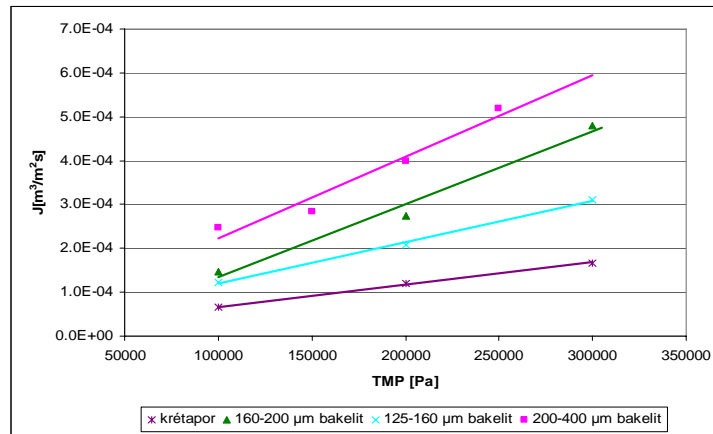


Figure 2. Flux change on the different TMP

There is a linear relationship between the flux and the transmembrane pressure difference at each case. The fluxes of the culk-dust solution are always lower than the bakelite solution because of the bakelite particles cause turbulence on the surface of the membrane. Due to the greater shearing on the membrane surface the cake layer resistance reduced and the molecules of the solvent can go easier through the membrane pores. I measured the lowest fluxes with the 125-160 µm size bakelite. The increasing of the diameter of particles caused increasing in the flux. I received the best fluxes with the 200-400 µm size bakelite, so here was the largest the shearing force.

We examined the hydrodynamic effect and we calculated the Re numbers. Increasing of Re numbers caused increasing of the permeate flux as well (Figure 3.).

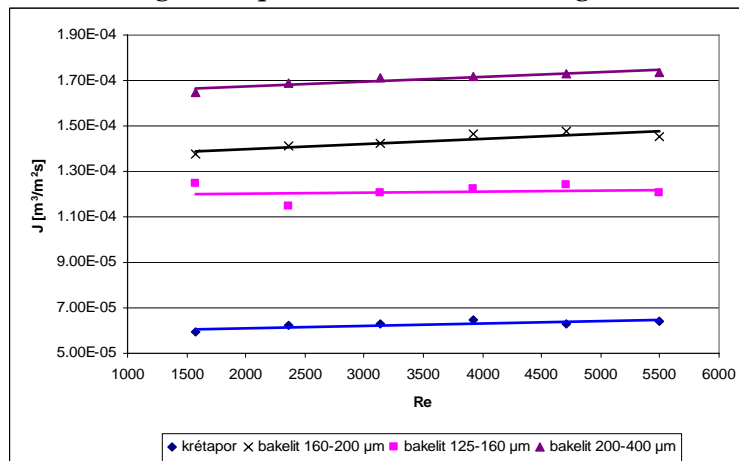


Figure 3. The measured fluxes vs. Re numbers

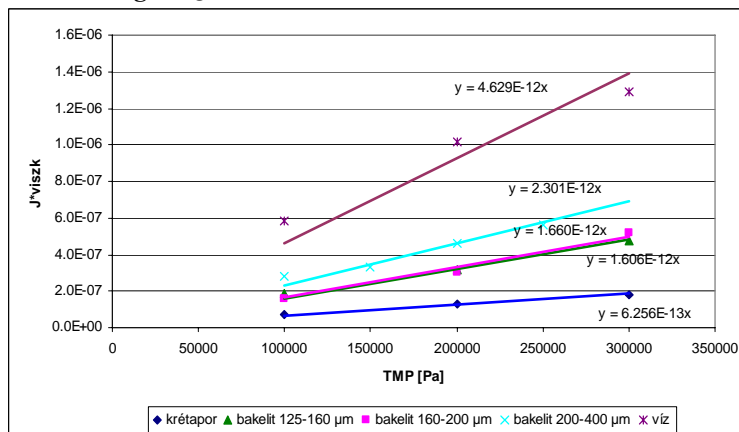


Figure 4. The total resistance (R_T) determination by fitted lines

The fluxes of the chulk-dust solution are the lowest. The Re number values are into the laminar and transitional range, but the bakelite particles caused local turbulence on the surface of the membrane, that show the higher flux values. From the slopes of the lines according to Eqs. (5) the total resistance (R_T) at the end of the process can be calculated (Figure 4.).

$$J \cdot \eta = \frac{1}{R_T} \cdot \Delta p_{TM} \quad (5)$$

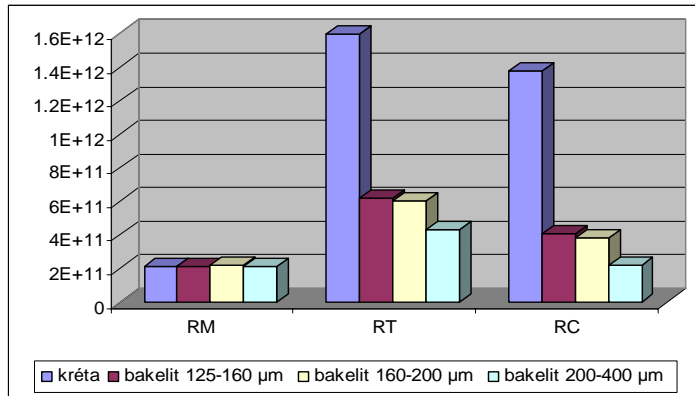


Figure 5. The comparison of resistance values

In the Figure 5 we can see, that the total resistance and the cake resistance are significant higher with the chulk-dust solution. The total resistance is the lowest with the 200-400 µm size bakelite, so these particles made the highest shearing force on the membrane surface, so decreased the thickness of the cake. The membrane resistance values are similar in all cases, because the membrane purification was efficient.

4. CONCLUSIONS

This work reports new results in the alternative approach to reduce of fouling. The use of bakelite can improve the performance of membrane processes. Introducing scouring particles seems very beneficial some microfiltration processes using conventional equipment. The bakelite enhances the local shear near the membrane surface. This approach has been successful in increasing fluxes of microfiltration. The larger particles induce much higher shear-induced diffusion and therefore dramatically improve mass transfer. The shear force is dependent on the square of the particle radius. Increasing size of bakelite was associated with an increasing flux. The total and the cake resistance were significant higher with the chulk-dust solution than with the bakelite. So the bakelite particles decreased the resistance of the filtration.

REFERENCES

- [1] R. W. Baker, Membrane Separation Systems-Recent Development, Future Direction, Noyes Data Corporation, New York, 1991
- [2] W. Scholz, M. Lucas, Techno-economic evaluation of membrane filtration for the recovery and re-use of tanning chemicals, *Water Res.* 37 (2003) 1859–1867.]
- [3] M.R. Wiesner, P. Aptel, Mass transport and permeate flux and fouling in pressure-driven processes, *Water Treatment Membrane Processes*, McGraw-Hill, NewYork, 1996 (Chapter4).
- [4] L. Fillaudeau, M. Lalande, A partial method to predict steady-state flux and fouling in the crossflow microfiltration of rough beer with 1.40 µm tubular ceramic membranes, *Trans IChem*, Vol 76, (1998), 217-223
- [5] G. Belfort, R.H. Davis and A.L. Zydney, The behavior of suspensions and macromolecular solutions in cross-flow microfiltration, *Journal of Membrane Science*, 96 (1994) 1–58.
- [6] A. A. Makardij, M.M. Farid and X.D. Chen, A simple and effective model for cross-flow microfiltration and ultrafiltration, *Can. J. Chem. Eng.*, 80 (2002) 28–36.
- [7] Zhan Wanga*, Jin-shu Chua, Wen-juan Wub, Jin-miao Yaoa, Study of unsteady-state flux prediction in cross-flow microfiltration, *Desalination* 238 (2009) 290–301
- [8] Rino Rappuoli, Derya Unutmaz, Improving membrane filtration processes, *Trends in Biotechnology*, Vol. 13., (1995), 129-131
- [9] MF/K1 Microfiltration Unit Operating and Maintenance Instructions, MEVATECH Kft, Budapest
- [10] Román A., Jianming Wang, Csanádi J., Hodúr C., Vatai Gy., Concentration of sweet whey with nanofiltration. CIGR Section VI International Symposium on Food and Agricultural Products: Processing and Innovations. Nápoly, Italy, (2007).
- [11] R. Paul Singh, Dennis R. Heldman, Introduction to Food Engineering 3rd Edition, Academic Press, (2001), 81-82



CALCULUS METHOD OF THE TECHNOLOGICAL LOADS TRANSMITTED TO THE EXTRACTING TOWERS WITH THE HOISTING INSTALLATIONS OF WINDING MACHINES WITH MULTICABLE DRIVING WHEELS ON

ITU Vilhelm, DUMITRESCU Iosif, COZMA Bogdan-Zeno

University of Petroșani, ROMANIA

Abstract:

In the paper there are presented certain aspects concerning the calculus of technological loads transmitted through the bearings of the extracting pulleys of the structure of the towers of the extracting installations in the case of functioning loads.

In the case of the extracting installations which have the extracting machine on the ground, having as a wrapping organ of the cables friction driving wheels, or a moving wheel the variation of the loads is determined not only by the kinematics of the installation (kinematics parameters), the dynamic (friction and inertia forces), but also by certain geometrical elements which define the position of the extracting machine towards the well geometrical elements that refer only to these type of installations. These geometrical elements are the incline angles of the extracting cable chords. These aspects were showed on the installation „Skip Shaft“ belonging to Mining Plant Lonea.

Keywords:

calculus method, technological loads, extracting tower

1. INTRODUCTION

In the case of the extracting installations which have the extracting machine on the ground, having as a wrapping organ of the cables double cylindrical wheels, or a moving wheel the variation of the loads is determined not only by the kinematics of the installation (kinematics parameters), their dynamic (friction and inertia forces), but also by certain geometrical elements which define the position of the extracting machine towards the well geometrical elements that refer only to these type of installations.

These aspects were showed on the installation „ Skip well “ Lonea Mining Plant (Fig.1). The installation taken into study has been described as follows.

2. THE INSTALLATION TAKEN INTO STUDY

The extracting installation that operates on the new skip well from Lonea Mining Plant, is destined [7] for the extraction from the underground of minerals. The extraction is done from the horizons +169,40; +203,3 and 403,45 to the surface (the surface level is +704,5m; and the skip unloading level is +715,5m).

The installation (Fig.1) is balanced and has an extracting machine type MK 5x2 (Fig.2) equipped with two motors type M2M-1000-213-4YXP/1986, of 1000 kW power and a nominal rpm of 54 rot/min (Fig.3).

The cables are wrapped around a moving wheel of ϕ 5000 mm (Fig.4).

The extracting cables with diameters of ϕ 46,5 mm and a mass (on a linear meter) of 8,049 kg/m are wrapped around the two extracting pulleys of ϕ 5000 mm with a mass (the pulley, the axle of the pulley and the bearing of the axle) of 12.108,83 kg (Fig.5), laying on the tower at a height of 51 m (pulley axle) The balanced cables have a section of 135x20 mm and a mass (on a linear meter) of 9,062 kg. The extracting vessels are skips having a mass (own mass, plus D.L.C., plus D.E.C. and supplementary mass) of 21600 kg and the effective load is 7000-8000 kg/skip. Another main component of the extracting installation is the metallic

tower (fig.6) with a height until the pulley axel of 51 m. The structure of the tower is composed of the extracting pulley platform sustained by the leading component and the one abutment set up as a frustum pyramid. The extracting machine lies on the ground (at a height of 7,5 m to the 0 level of the well (well collar), sideways from the tower (well tower), at a distance (of the wheel axel), towards the vertical portion of the extracting cables which enter the well of 44m. The length of the cable chord (the distance between the tangent points of the cable to the deviating pulley from the tower and the wheel of the extracting machine, in the central position of the chord (perpendicular on the wheel axel)), is for the bottom branch $L_{ci}=52,78253595m$, and $L_{cs}=58,78482883m$ for the top branch. The incline angles of the cables chords are $\beta_i = 48^\circ 43' 37''$ for the bottom branch and $\beta_s = 44^\circ 37' 07''$, for the top branch [7].



Figure 1. Extracting installation

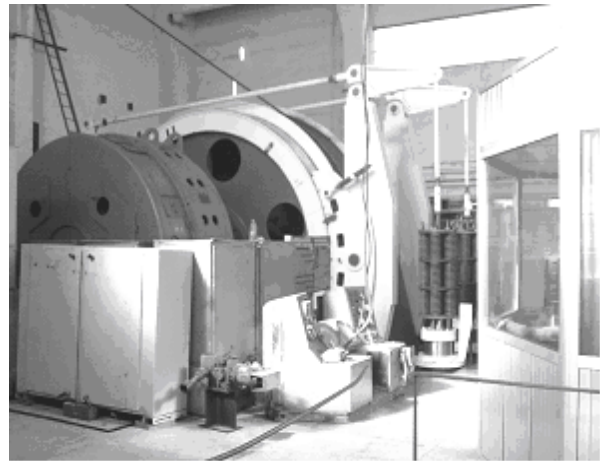


Figure 2. Extracting machine

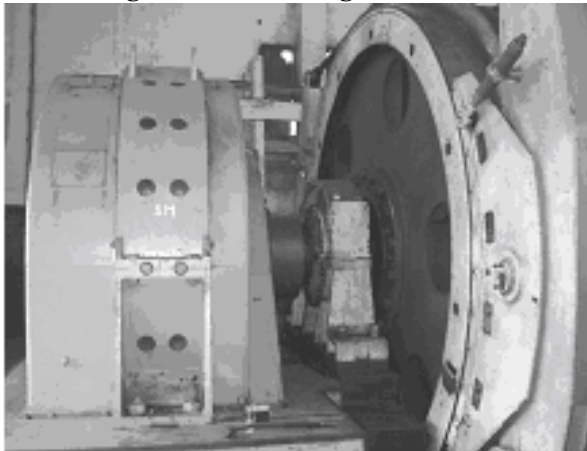


Figure 3. The motor

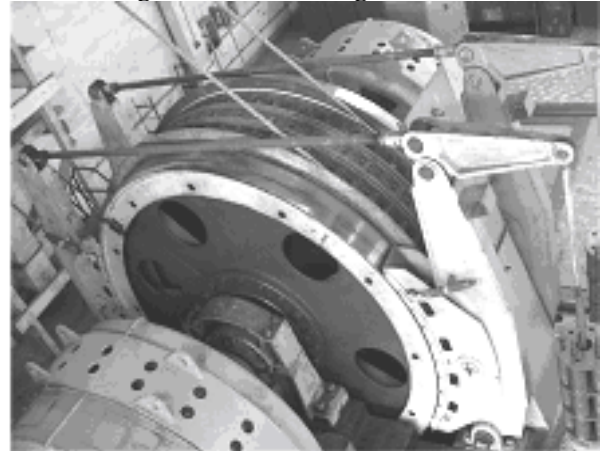


Figure 4. Wrapping organ



Figure 5. Extracting pulleys

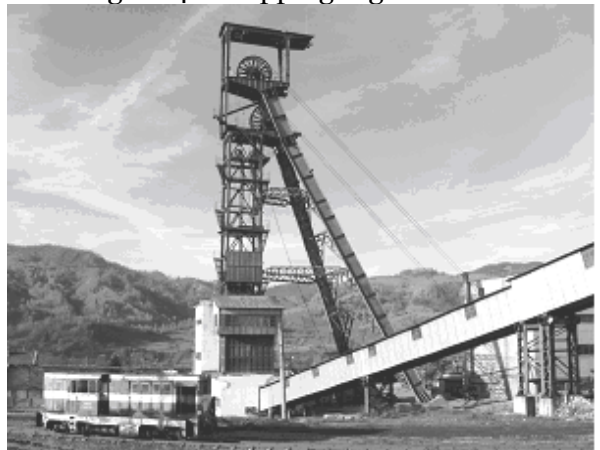


Figure 6. Metallic tower

3. LOADS TRANSMITTED TO THE TOWER

For the determination of the loads (efforts) which act upon the installation taken into consideration it has been taken into study the case when one of the skips is descending (ascending) on one of the branches.

On the calculation of loads it has been considered the fact that their variation is determined not only by the kinematics of the installation (kinematical parameters) but also by certain geometrical elements which define the position of the extracting machine towards the well geometrical elements regarding only the installations where the extracting machine lies on the ground. ([1],[3],[4],[5],[6]).

For this purpose it has been taken into analysis the case when the skip is descending on the top branch (case 1, the skip of the bottom branch is climbing and the top one is descending) and the case when the skip is descending on the bottom branch (case 2, the skip of the bottom branch is descending and the top one is climbing). The diagrams for the space, speed, and acceleration for the two cases taken into analysis are presented into Fig 7 case 1 and in Fig 8 case 2. The variations of acceleration and space have been used for the calculation of the loads applied to the tower. The determination of the loads acting upon the tower through the deviating pulleys has been done using the d’Alembert principle (the kinetics-static method [2]) taking into consideration the static forces (the weight of the extracting cable, the cage the trolley the pulley and the load), the friction forces (multiple friction and aero-dynamic resistances which for installations with cages is approximated with a coefficient of $k'=0,2$ from the useful load [1]) and the dynamic forces (which intervene only in the acceleration and deceleration periods, Fig. 7 and Fig. 8).

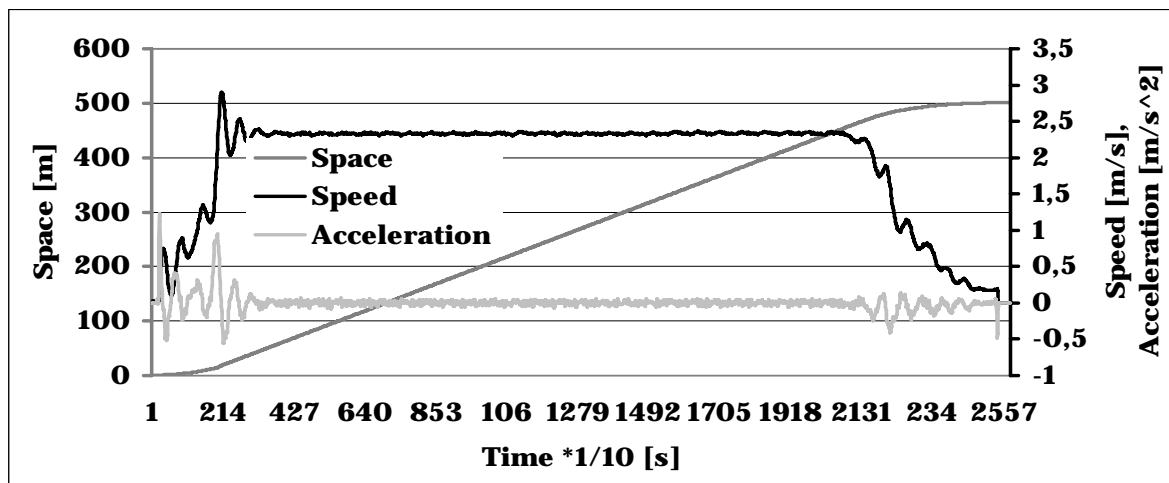


Figure 7. Speed acceleration and space for case 1

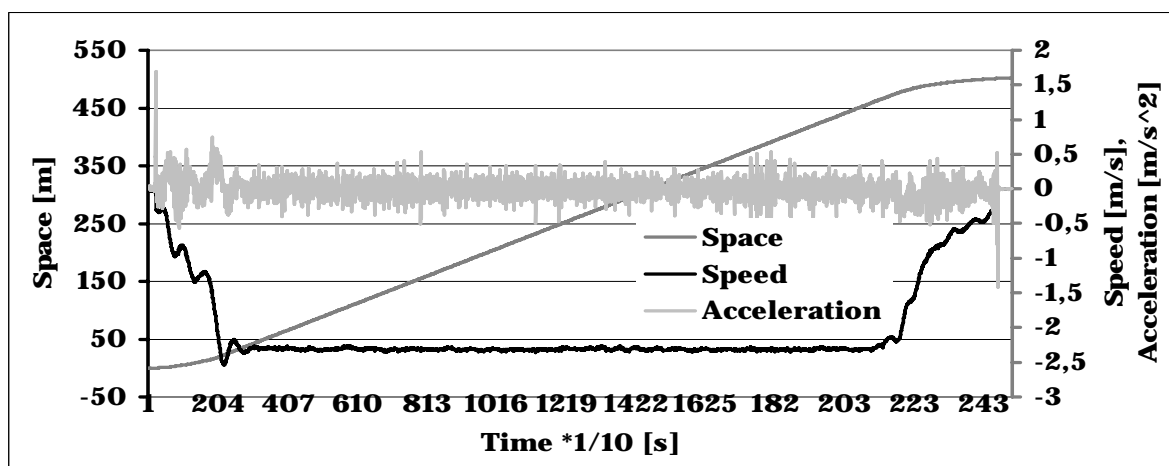


Figure 8. Speed acceleration and space for case 2

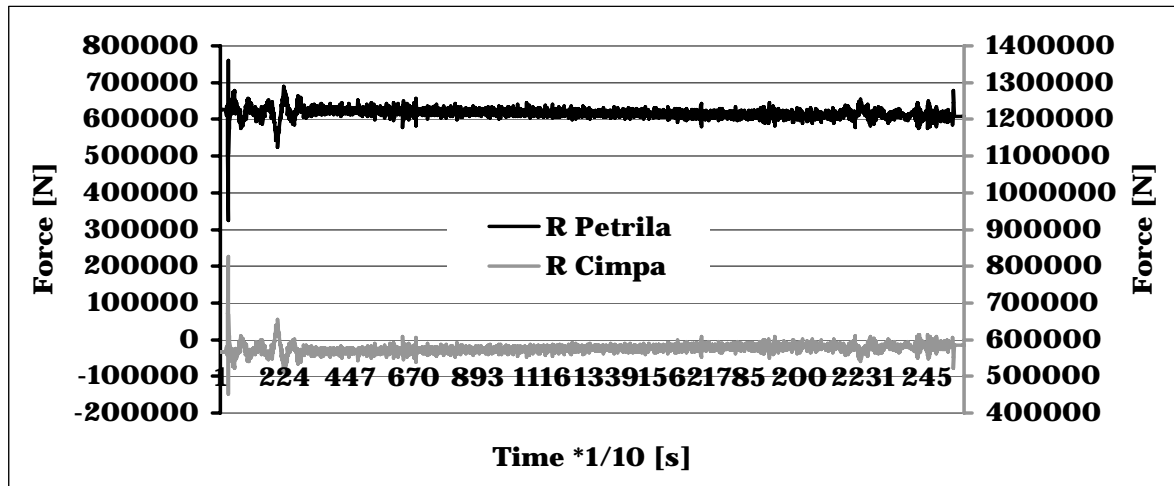


Figure 9. Reactions from the bearing of the top and bottom pulley when the top cage descends and the bottom one climbs, case 1

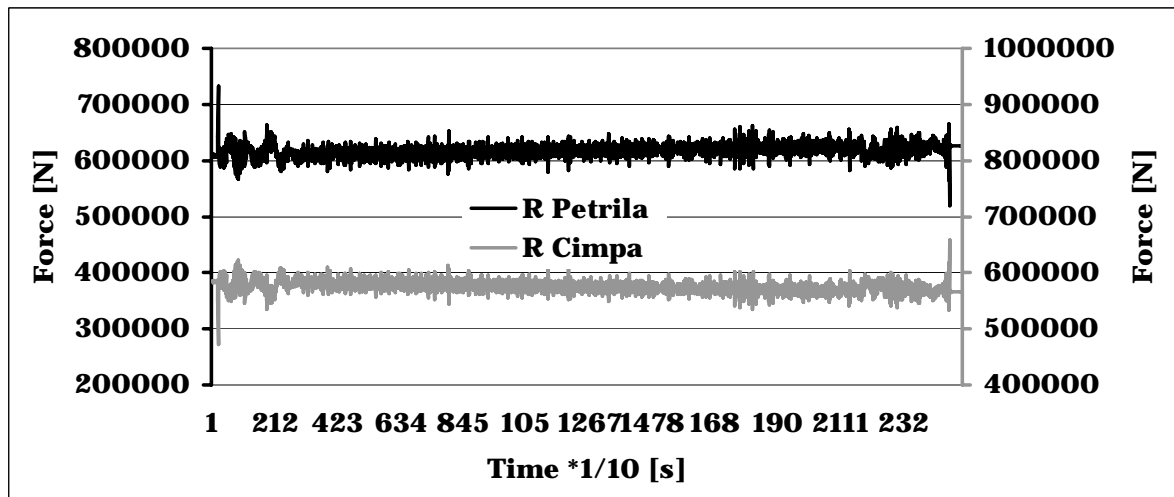


Figure 10. Reactions from the bearing of the top and bottom pulley when the top cage climbs and the bottom one descends, case 2

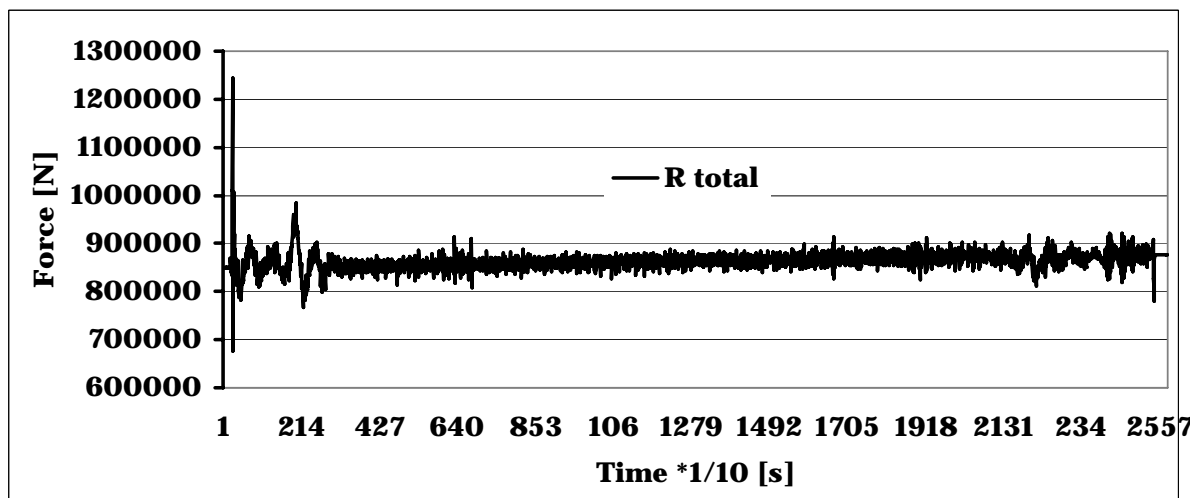


Figure 11. Total loads when the top cage descends and the bottom one climbs case 1

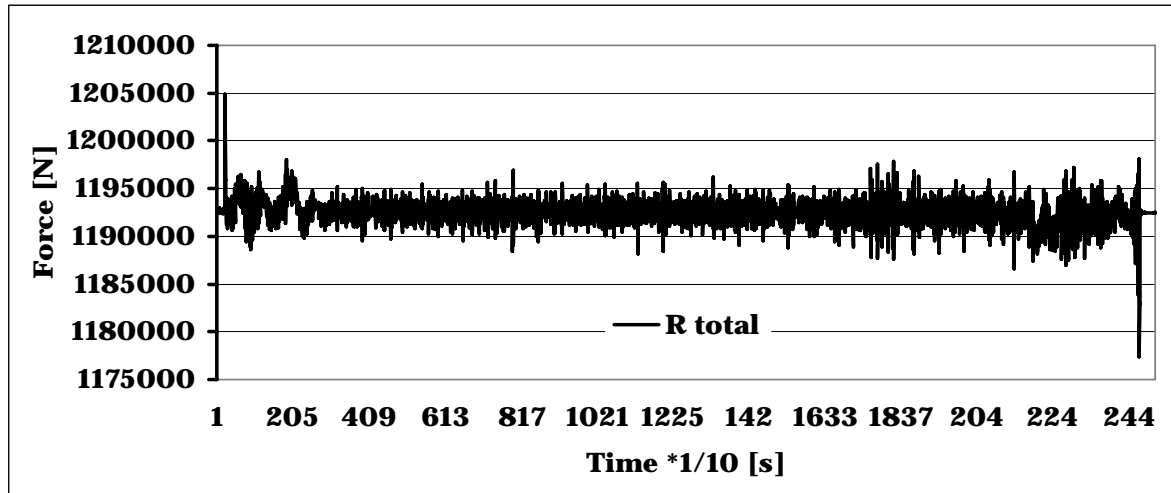


Fig. 12. Total loads when the top cage climbs and the bottom one descends case 2

The variation of the resultant forces from the bearings of the extracting pulleys for the two cases taken into consideration is presented in Fig 9, for case 1, for the top and bottom pulley and Fig 10, for case 2, also for the top and bottom pulley.

4. CONCLUSIONS

The calculation the structure of the mining extracting towers is done taking into consideration all the unfavorable combinations practically possible of the different loads called groups of loads.

Following the classification and grouping of the loads transmitted to the extracting mining towers in the paper there are presented certain aspects concerning the establishing of the exceptional short term loads due to the extracting cycle in the case of the appliance of the safety brake which are transmitted to the structure skip and the wrapping organ of the extracting machine is moving wheel.

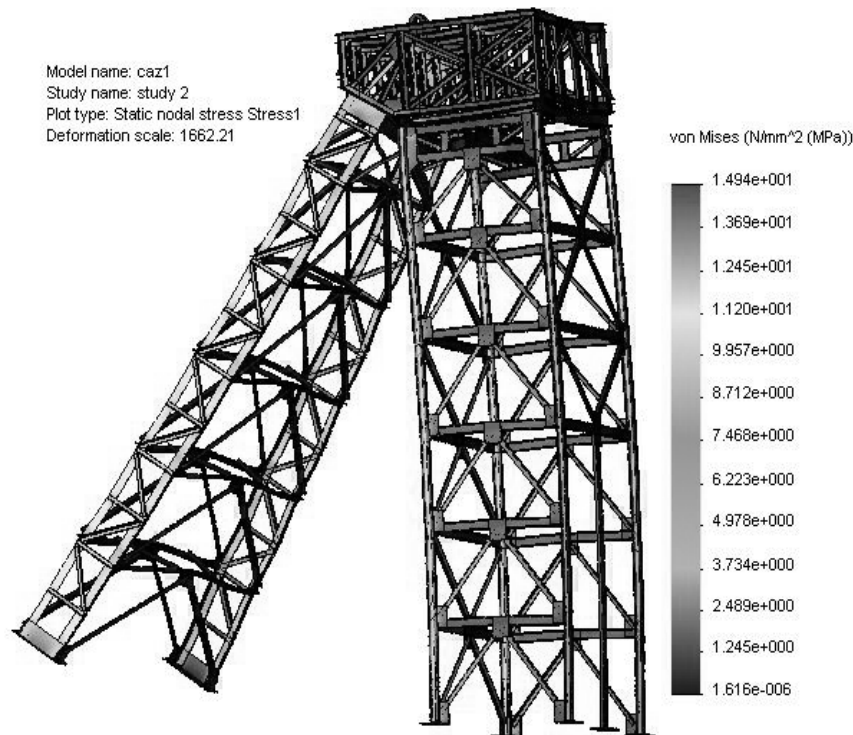


Figure 13. Stress on the tower

The loads transmitted to the tower through the bearings of the extracting pulleys from the tower due to the efforts from the extracting cables have been considered in the case when the emergency brake is applied due to an overcome of the max speed allowed when the skip are climbing and descending on one of the two extracting branches.

The variation of loads is due both for the cinematic parameters as well as for the geometric parameters of the extracting installation.

As noticed from the variation of the total loads which act upon the tower during an extracting cycle the maximum values are in case 1 of the cycle and in case 2 at the beginning of the cycle (Fig 11 and Fig 12).

The maximum values of the loads determined are further used to determine the values of mechanical stress and strain from the elements of the structure of the metallic tower of the installation in order to verify its resistance, like in Valea Arsului tower case, from Lonea Mining Plant. (Fig. 13).

REFERENCES

- [1] Magyari A., Instalații mecanice miniere, Editura tehnică, București, 1990;
- [2] Ripianu A., ș.a. Mecanica tehnica, Editura Didactică și Pedagogică, București, 1982;
- [3] Vlad P. C., Prescripții de calcul pentru instalații de extracție mono și multicablu, Vol. I, O.D.P.T., București, 1972;
- [4] Vlad P. C. Prescripții de calcul pentru instalații de extracție mono și multicablu Vol. II, O.D.P.T., București, 1973;
- [5] Itu, V., Variația sarcinilor ce se transmit în timpul unui ciclu de extracție turnurilor instalațiilor de extracție cu colivii nebasculante și mașină de extracție cu tobă dublă și acționare asincronă, Revista Minelor, vol 168, nr. 6/2005, pag.34-40;
- [6] Itu, V., Influența elementelor geometrice ce definesc poziția mașinii de extracție față de puț asupra sarcinilor de funcționare instalațiilor de extracție transmise structurii turnurilor, Revista Minelor, vol 172, nr. 10/2005, pag.21-31;
- [7] * * * Documentație tehnică, E. M. Lonea.



ELEMENTS OF THE GEOMETRIC CALCULATION FOR STRAUGHT-TOOTHED CYLINDRICAL GEARS IN INCHES AND IN THE METRIC SYSTEM

Vasile ZAMFIR, Gheorghe Bogdan URDEA

University of Petroșani, ROMANIA

Abstract

The paper approaches the calculations of the basic geometrical elements of the cylindrical gear in inches and in metric system.

In the first part of the paper we present standardized reference racks in the main industrial states while in the second part we deal with the main gear equations that are used for diametral pitch inch gears and for metric gears.



MODIFIED DIAGRAM FOR STEAM-WATER INJECTOR MIXING CHAMBER

Maša BUKUROV, Slobodan TAŠIN, Siniša BIKIĆ

University of Novi Sad, Faculty of Technical Sciences, Department of Energy and Process Engineering, Novi Sad, SERBIA

ABSTRACT

The scope of this paper is a thermodynamic process in mixing chamber of supersonic steam-water injector. This injector is actually a simple heat pump due to the fact that it can substitute a pump and heat exchanger. Initial energy source of supersonic steam-water injector is usually a small amount of steam with low thermal properties which could not be used for more demanding utilities.

The aim of wider investigation is to build up a relatively high pressure of hot water at the outlet of mixing chamber during a "forced condensation" of steam which is in the cold water surrounding in mixing chamber. Forced condensation, which is described by modified Mollier diagram of wet steam, reveals clearer picture of this complex flow process.

The paper emphasizes Mach number ($M=v/c$) which, largely, represents flow process in mixing chamber. Sound velocity (c) is a physical property of fluid which is a function of different parameters (T , ρ , η , pipeline elasticity, solid impurities, gas bubbles). Intensity of sound velocity, in the case of steam-water injector, depends mostly on steam wetness. Experiments showed that flow process without shocks is possible and worthwhile because it provides the increase of efficiency rate and reliable operation. In addition, it can be concluded that the flow is without interruption and shocks due to small velocities of sound and fluid, which refers to outlet of mixing chamber where $M=1$. Momentum equation provides a possibility to determine location and intensity of average pressure (p_{ave}) in mixing chamber.

Accepted principles for description and analyses of thermodynamic processes in mixing chamber are based on process continuity, homogeneous flow field and thermodynamic and compressible flow laws. Experimental investigation was done in Laboratory for Fluid Mechanics, at the Faculty of Technical Sciences in Novi Sad, Serbia.

KEYWORDS

Steam-water injector, mixing chamber, forced condensation, modified Mollier diagram, supersonic mixing chamber

1. INTRODUCTION

A possibility to gain pressure and rise temperature of mixture of cold water and steam was registered more than 120 years ago. Injector was instantaneously applied in feeding steam boiler with water. However, until today, reasonable and acceptable explanation of what really happens in mixing chamber has not appeared, although there have been numerous attempts. Many registered patents for different purposes of steam-water injector pointed out the usefulness of this device. Hence, striving to explain thermodynamic flow process through mixing chamber is fully justified. Detailed research of *Deich and Filipov* (1968) provided real basics for further investigations.

Steam and water parameters in experiments are: ratio steam-cold water is 1:5; $p_s=2.5$ bar; $t_s=127.5$ °C; $t_{cw}=10-30$ °C; $t_{hw}=65-85$ °C. In Fig. 1. is presented experimental steam-water injector. Pressure rise in mixture of steam and water, which is an intensive process of forced condensation, obey laws of compressible (supersonic) flow. Supersonic flow of steam at the outlet of Laval's nozzle, due to its dominating volume, transfers into the region of steam-water mixture. Locally formed shock waves, different in origin, are negligible when injector works properly. Conducted experimental research proved a possibility to maintain shock-less flow along injector. Relevant questions, which deserve precise answers, are:

- ✚ Which part of pressure rise in mixing chamber can or cannot be connected directly to enthalpy of initial steam?

- How to define sources and nature of losses in mixing chamber and determine efficiency rate of mixing chamber and total injector.

Mentioned shock-less transition of steam through Laval's nozzle and mixture through outlet throat of mixing chamber, can be explained with diagram of isentropic flow in supersonic regime (Fig. 2). This diagram is valid, to a certain extent, for homogenous mixture flow with considerable participation of steam in volume (Tab. 1, row 6.5).

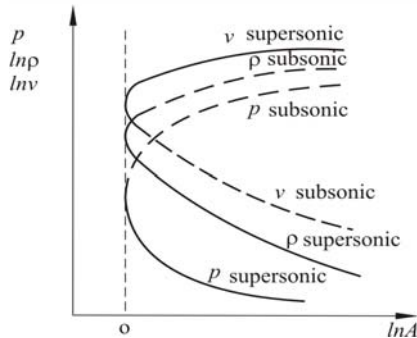
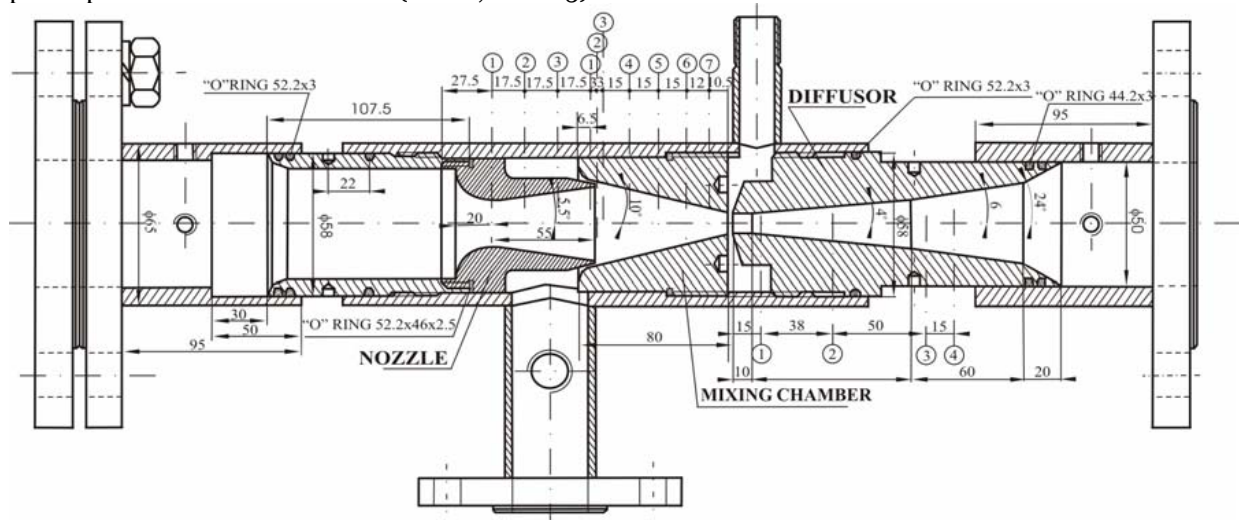


Fig. 1. Configuration of measuring locations and different positions of Laval's nozzle and mixing chambers (Bukurov 2004)

Gradients of compressible properties of mixture (p , ρ) are specially large in very wet mixture at outlet section of mixing chamber, where transition from supersonic to subsonic flow takes place.

Fig. 2. Isentropic changes of flow parameters through supersonic-subsonic transition as function of nozzle geometry

2. MODIFIED ENERGY DIAGRAM

Modified diagram or diagram of forced condensation allows comparing three types of condensation processes:

- natural - free condensation of steam – without flow under $p = \text{const.}$, $T = \text{const.}$ (Mollier diagram)
- free condensation - flow without direct mixing of steam and water under $p \neq \text{const.}$ and $T \neq \text{const.}$ (Mollier diagram)
- forced condensation with direct mixing of steam and water ($\text{grad} p_{\text{forced}} > \text{grad} p_{\text{free}}$).

Range of condensation in modified diagram corresponds to borders of mixing chamber where the whole condensation process takes place. Energy change, no matter if condensation is free or forced, is from 2500 kJ/kg to 0 kJ/kg (Fig. 3).

Graphical presentation of processes during forced condensation in mixing chamber, due to introduced cold water, provides better physical view than applicable analytic equations. Also, there are open possibilities to make conclusions about certain parts of processes as well as data which can help to organize experiments more efficiently.

Diagram $p-h$ is the most convenient way to present the results of investigation.

Forced condensation begins when water is introduced into steam region. It has four basic characteristics:

- Condensation process is faster and lasts shorter;
- Geometry of mixing chamber is changed (central angle of conical mixing chamber increases);
- Gradients of physical, flow and energy characteristics, which are functions of time and distance, are considerably larger;
- Temperature through condensation process is below steam temperature at the inlet of Laval's nozzle (127.5 °C, Fig.3).

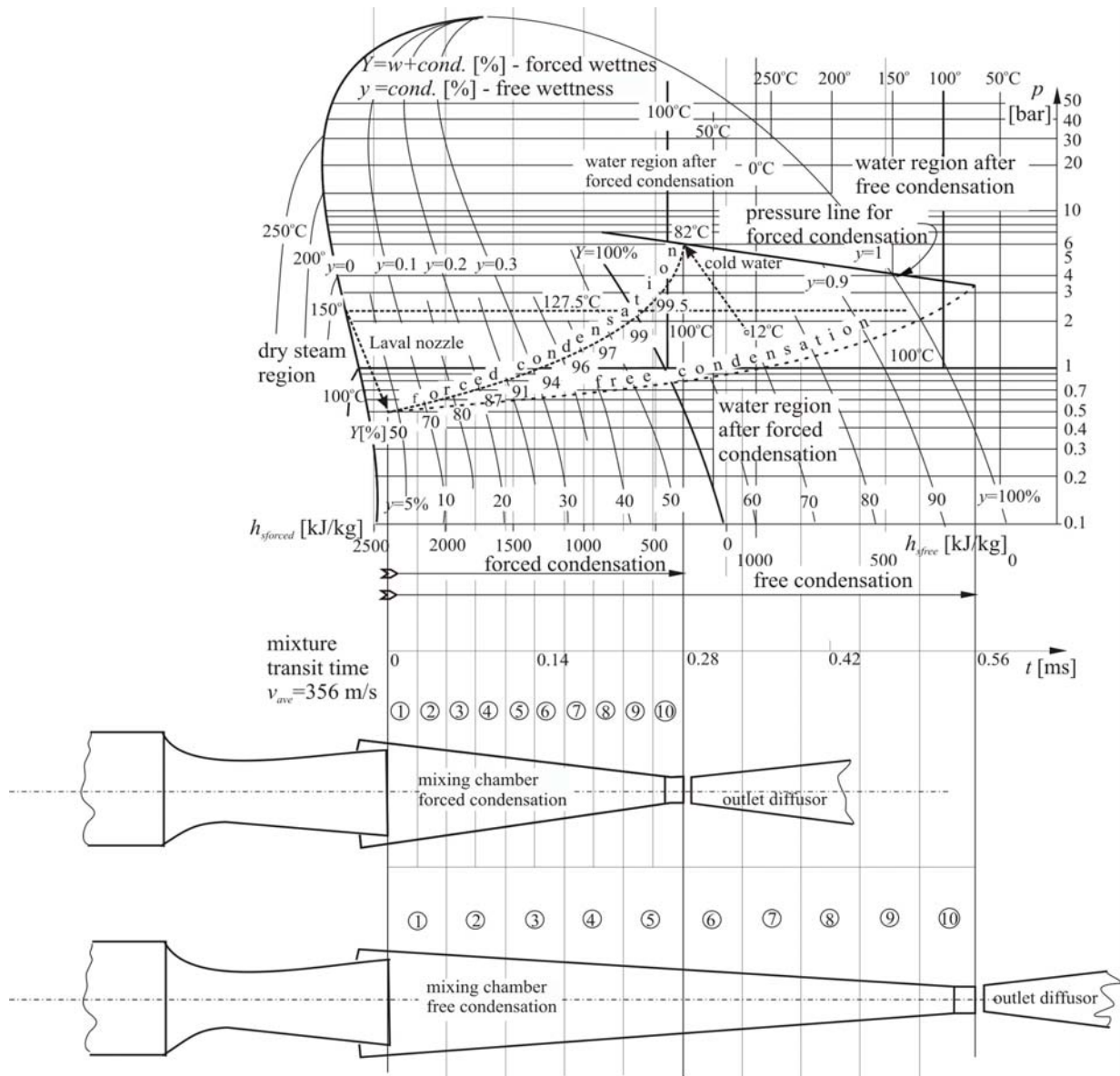


Fig. 3. Energy and geometry change in mixing chamber for forced and free condensation

3. LOCAL CONDENSATION PARAMETERS X, Y

Modified energy diagram is formed by drawing new lines (X, Y) in Mollier diagram (x, y) of wet steam. Steam quality X is a concentration of dry saturated steam ($x=X$). Wetness Y is water fraction which is involved during forced condensation. In Mollier diagram of wet steam, x and y represent mass fractions of dry saturated steam and water under standard (static) conditions. It is possible to reach such conditions during the flow (hypothetically) when every section of mixing chamber is instantaneously separated. Masses of steam and water are calculated for each section (1-10 in Fig.3). This type of concentration of steam and water is called local concentration, i.e. local dryness (steam quality) and wetness.

Although total amount of cold water is introduced at the entrance of mixing chamber, it is considered that cold water is mixing with wet steam along the whole mixing chamber. Mixing occurs in such manner that each 1/10 of inlet water is mixed with steam in every section and thus, mixture (X, Y) is produced. Unmixed part of water flows further. Hence, there are two different kinds of water: water for mixing (w_m) and the rest of water (w_{rest}).

Condensation of steam (y) is conducted continuously and homogeneously along the whole mixing chamber. Definition of free condensation ($p=\text{const.}, T=\text{const.}$) is valid for forced condensation too, although pressure and temperature rise. Volume of steam in mixing chamber corresponds to uniform condensation profile in the mixing nozzle according to *Beithou et al.* (2000).

Mass characteristics of steam and water, i.e. dryness X and wetness Y along the mixing chamber are determined according to velocities of steam (v_s) and water flow through chamber, which are presented in Table 1. Velocity diagram (v_s, v_m) is presented according to experimental results and flow laws.

Table 1. Characteristic values of mixture in sections of mixing chamber

Inlet properties of steam and water: $\dot{m}_s = 0.17 \text{ kg/s}$; $\dot{m}_w = 0.85 \text{ kg/s}$. Assumption: steam condenses equally in each section of mixing chamber; cold water mixes with steam evenly in each section of mixing chamber; the rest of cold water, which does not mix, stays inert.

No. of section i		1	2	3	4	5	6	7	8	9	10
Geometry of sections											
1.1	d_{iave} [cm]	3.28	3.04	2.8	2.56	2.32	2.08	1.84	1.6	1.36	1.12
1.2	A_i [cm ²]	8.44	7.25	6.15	5.14	4.22	3.4	2.66	2.01	1.45	0.98
1.3	V_i [cm ³]	8.44	7.25	6.15	5.14	4.22	3.4	2.66	2.01	1.45	0.98
Characteristics of steam											
2.1	v_s [m/s]	710	680	650	600	530	450	350	250	150	50
2.2	ρ_s [kg/m ³]	0.338	0.395	0.45	0.507	0.646	1.0	1.40	1.7	2.16	3.0
2.3	\dot{m}_s [kg/s]	0.161	0.144	0.127	0.110	0.093	0.08	0.059	0.04	0.02	0.008
2.4	Q_s [l/s]	478	366	283	218	145	76.5	39.2	25	11.2	0.28
2.5	A_s [cm ²]	6.729	5.628	4.358	3.632	2.73	1.7	1.122	1.0	0.79	0.566
Characteristics of condensate in the central part of each section (0.05, 0.15,...0.95)											
3.1	\dot{m}_{con} [kg/s]	0.0085	0.025	0.0425	0.0595	0.0765	0.093	0.11	0.127	0.144	0.15
3.2	Q_{con} [l/s]	0.0085	0.025	0.0425	0.0595	0.0765	0.093	0.11	0.127	0.144	0.15
3.3	A_{con} [cm ²]	0.0001	0.0004	0.0006	0.001	0.0014	0.002	0.0031	0.005	0.009	0.03
Characteristics of water for mixing $v_{wm}=0.5v_s$											
4.1	v_{wm} [m/s]	355	340	325	300	265	225	175	125	75	25
4.2	Q_{wm} [l/s]	0.085	0.17	0.255	0.34	0.425	0.51	0.595	0.68	0.765	0.85
4.3	A_{wm} [cm ²]	0.0024	0.005	0.0078	0.011	0.016	0.023	0.034	0.054	0.102	0.34
Characteristics of rest of water											
5.1	\dot{m}_{wrest} [kg/s]	0.765	0.68	0.595	0.51	0.425	0.34	0.255	0.17	0.085	0
5.2	A_{wrest} [cm ²]	1.708	1.617	1.783	1.496	1.473	1.675	1.501	0.946	0.55	0.044
5.3	v_{wrest} [m/s]	4.479	4.205	3.337	3.409	2.885	2.030	1.699	2.24	1.797	0
Volumes of fluids											
6.1	V_s [cm ³]	6.729	5.628	4.358	3.632	2.73	1.7	1.122	1.0	0.788	0.566
6.2	V_{wm+con} [cm ³]	0.0025	0.0054	0.0084	0.012	0.0174	0.025	0.0371	0.059	0.112	0.37
6.3	$V_{s+wm+con}$ [cm ³]	6.7315	5.6334	4.3664	3.644	2.7474	1.725	1.159	1.059	0.9	0.936
6.4	V_{wrest} [cm ³]	1.708	1.617	1.783	1.496	1.473	1.675	1.501	0.946	0.55	0.044
6.5	$V_s/V_{s+wm+con}$ [-]	2691.6	1042.2	518.8	302.7	157	68	30.2	16.9	7	1.53
6.6	$V_s/(V_{s+wm+con}+V_{wrest})$ [-]	0.8	0.776	0.708	0.706	0.647	0.4	0.421	0.5	0.543	0.604
Masses of fluids											
7.1	m_s [g]	0.0022	0.0022	0.0019	0.0018	0.0018	0.0017	0.0016	0.0017	0.0017	0.0003
7.2	m_{wm+con} [g]	0.0025	0.0054	0.0084	0.012	0.0174	0.025	0.0371	0.059	0.112	0.37
7.3	m_{wrest} [g]	1.708	1.617	1.783	1.496	1.473	1.675	1.501	0.946	0.55	0.044
7.4	m_{total} [g]	1.71	1.622	1.791	1.508	1.49	1.7	1.538	1.005	0.662	0.414
Mixture humidity during forced condensation $Y=(m_{wm+con})/(m_s+m_{wm+con})$ $X=m_s/(m_s+m_{wm+con})$											
8.1	Y [-]	0.527	0.707	0.812	0.867	0.908	0.936	0.959	0.972	0.985	0.999
8.2	X [-]	0.473	0.293	0.188	0.133	0.092	0.064	0.041	0.028	0.015	0.0007
Exponent of polytropic process (Deich, 1968)											
9.1	κ [-]	1.08	1.015	0.95	0.86	0.76	0.67	0.5	0.38	0.25	0.01

where are in Tab 1.

$$2.5 \ A_s = \frac{\dot{m}_s}{\rho_s v_s}; \ 3.1 \ \dot{m}_{con} = \dot{m}_{sin} - \dot{m}_s = 0,17 - \dot{m}_s; \ 3.3 \ A_{con} = \frac{(0.05 \dots 0.95) \dot{m}_s}{\rho_w v_{con}}, \ v_{con} = v_s;$$

$$4.3 \ A_{wm} = \frac{Q_{wm}}{v_{wm}}; \ 5.1 \ A_{wrest} = A_d - (A_s + A_{con} + A_{wm}); \ 5.1 \ \dot{m}_{wrest} = \dot{m}_w - \dot{m}_{wm};$$

$$5.2 \ A_{wrest} = A_i - (A_s + A_{con} + A_{wm}); \ 5.3 \ v_{wrest} = \frac{\dot{m}_{wrest}}{\rho_w A_{wrest}}$$

Mass flow rates of steam and water are determined with their entrance values ($(\dot{m}_s)_{in} = 0.17$ kg/s, $\dot{m}_{cw} = 0.85$ kg/s). It is assumed that mixing and condensation are consistent in each section of the chamber. Volume flow rates of steam are determined according to data given in steam table for density (ρ) as function of pressure and temperature. Density of steam through chamber is changeable from 0.338 to 3.0 kg/m³.

Velocity of water through mixing chamber, as well as its volume in considered section ($i=1,2,\dots,10$), are determined according to geometry of mixing chamber and volume of steam.

Characteristics of water-steam mixture in certain sections of mixing chamber are shown in Table 1. Steam is condensed (*con*) in each section of mixing chamber equally. Cold water (*cw*) is mixed with steam equally in each section of mixing chamber, too. The rest of cold water (*rest*) which is not mixed with steam jet does not participate in steam water mixture formation. Entrance and exit diameters of experimental chamber are 3.4 and 1 cm. Length of chamber is 10 cm, and each section is 1 cm long. Volume of chamber is 41.70 cm³.

4. BASICS FOR ENERGY FLOW ANALYSES

Borders of polytropic flow

Relation between volume of steam (V_s) and volume with active water ($V_{con} + V_{wm}$) is authoritative for estimation to which length of mixing chamber laws of gas dynamics are valid. It could be seen that steam is still present even in the last section of the chamber.

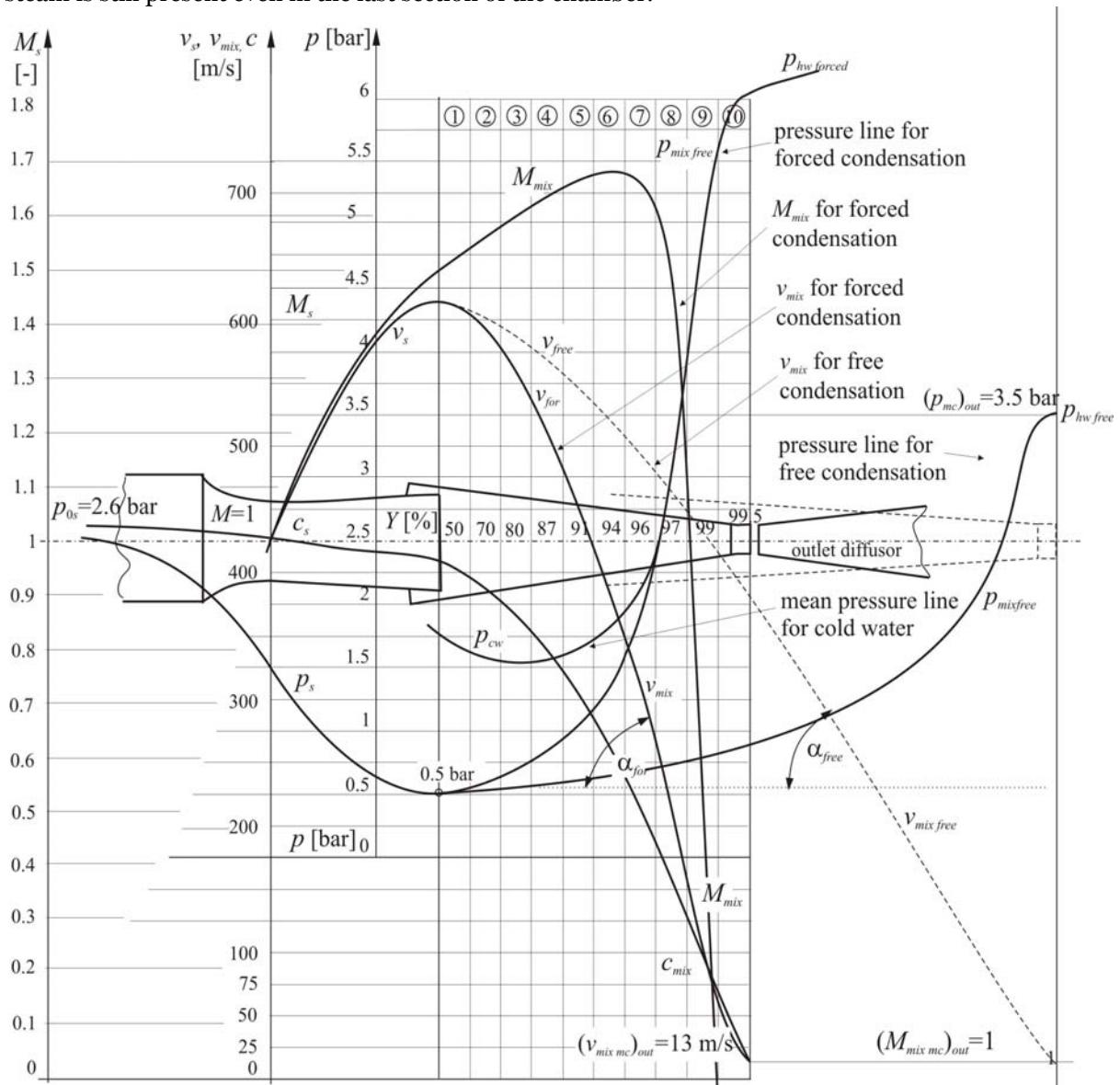


Fig 4. M, v, p comparative diagram for forced and free condensation

High wetness of steam water mixture through the whole mixing chamber causes low sound velocities and high Mach numbers, which confirms the behavior of compressible flow together with the given polytropic exponents κ (Deich and Filipov 1968).

The basic task is to determine a volume of steam and water along the mixing chamber. Steam carries total energy and thus, steam flow laws can be estimated according to thermodynamic relations with certain corrections. The flow is conducted in certain volume, so relation V_s/V_w determines the area of mixing chamber in which these relations are valid. It is considered that this border is within 2/3 of mixing chamber length which is agreeable with Narabayashi et al. (2000).

Basic relations

Basics for analyses of complex energy flow process through mixing chamber are given in:

- ✚ diagram of isentropic changes of flow parameters through supersonic-subsonic transition (Fig 2.)
- ✚ change of sound velocity (c) and polytropic exponent (κ) depending on relevant factors of influence (Deich and Filipov 1968)
- ✚ basic equations (Eq. 1 to 3) for the flow of compressible flow

$$\frac{v^2}{2} + \frac{c^2}{\kappa - 1} = const. \quad (1)$$

$$\frac{p_t}{p} = 1 + \frac{\kappa}{2} M^2 + \frac{\kappa}{8} M^4 + \dots \quad (2)$$

$$\frac{T_t}{T} = 1 + \frac{\kappa - 1}{2} M^2 \quad (3)$$

- ✚ energy equation (Eq. 4)

$$\left[\left(h_s + \frac{v_s^2}{2} + \frac{p_s}{\rho_s} \right) \dot{m}_s \right]_{in_{mc}} + \left[\left(h_{cw} + \frac{v_{cw}^2}{2} + \frac{p_{cw}}{\rho_{cw}} \right) \dot{m}_{cw} \right]_{in_{mc}} = \left[\left(h_m + \frac{v_m^2}{2} + \frac{p_m}{\rho_m} \right) \dot{m}_{hw} \right]_{out_{mc}} + h_l \dot{m}_{hw}. \quad (4)$$

Momentum equation

Momentum equation, as it is known, is without any practical limitation in application on any flow process. It is applied on control volume which represents mixing chamber and takes into account only changes on borders of control volume. Its simplicity and reliability leads to accurate information which, in this case, gives magnitude of average pressure in mixing chamber.

Control volume (Fig. 5) represents two inlet sections (steam and cold water) and one outlet – throat of mixing chamber. It is well known that this law governs only those parameters which prevail on borders of control volume. Inner changes are negligible. This simple relation determines average pressure in mixing chamber. According to Bukurov (2004), it is possible to determine more accurate pressure distribution in mixing chamber with known average pressure p_{ave} .

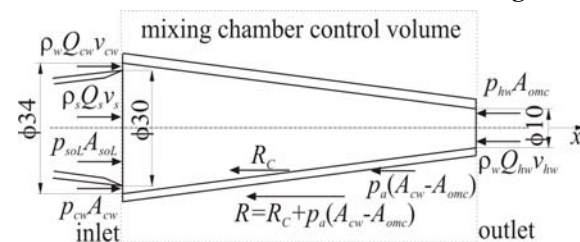


Fig. 5 Momentum equation applied to mixing chamber

pressure in mixing chamber. According to Bukurov (2004), it is possible to determine more accurate pressure distribution in mixing chamber with known average pressure p_{ave} .

If average pressure in mixing chamber increases, pressure at the throat of mixing chamber also increases.

The influence of surrounding to insulated mixing chamber is realized with forces which are presented in Fig. 5. Momentum equation is given as

$$F_{ps} + F_{pcw} - F_{phw} - F_a + F_{cw} + F_s - F_{hw} - R_c = 0 \quad (5)$$

From here, the pure reaction of connection is

$$R_c = F_{ps} + F_{pcw} - F_{phw} - F_a + F_{cw} + F_s - F_{hw} \quad (6)$$

On the other hand, pure reaction R_c can be presented with average pressure in mixing chamber acting on orthogonal projection of mixing chamber:

$$R_c = p_{mave} \left((A_{mc})_{in} - (A_{mc})_{out} \right) \quad (7)$$

where is p_{mave} – is average manometric pressure in mixing chamber. Combination of eq. (6) and (7) leads to average manometric pressure

$$p_{mave} = \frac{F_{ps} + F_{pcw} + F_{cw} + F_s - (F_{phw} + F_a + F_{hw})}{(A_{mc})_{in} - (A_{mc})_{out}} \quad (8)$$

Forces that act on mixing chamber are ($v_{cw}=4.1$ m/s; $v_{hw}=13$ m/s):

$$F_{ps} = p_{sOL} A_{sOL} = 50000 \times 0.03^2 \times p / 4 = 35.34 \text{ N} \quad (9)$$

$$F_{pcw} = p_{cw} A_{cw} = 180000 \times (0.034^2 - 0.03^2) p / 4 = 36.19 \text{ N} \quad (10)$$

$$F_{phw} = p_{hw} (A_{mc})_{out} = 600000 \times 0.01^2 p / 4 = 47.12 \text{ N} \quad (11)$$

$$F_s = r_s Q_s v_s = \dot{m}_s v_s = 0.17 \times 611 = 103.87 \text{ N} \quad (12)$$

$$F_{cw} = r_w Q_{cw} v_{cw} = \dot{m}_{cw} v_{cw} = 0.85 \times 4.1 = 3.48 \text{ N} \quad (13)$$

$$F_{hw} = r_w Q_{hw} v_{hw} = \dot{m}_{hw} v_{hw} = 1.02 \times 13 = 13.26 \text{ N} \quad (14)$$

$$F_a = p_a ((A_{mc})_{in} - (A_{mc})_{out}) = 101325 \cdot (0.034^2 - 0.01^2) \cdot \frac{\pi}{4} = 84.04 \text{ N} \quad (15)$$

All pressures in equations above are absolute.

By substituting eq. (9)-(15) into eq. (8), p_{mave} is determined:

$$p_{mave} = \frac{35.34 + 36.19 + 3.48 + 103.87 - (47.12 + 84.04 + 13.26)}{(0.034^2 - 0.01^2) \pi} = 41670 \text{ Pa} \quad (16)$$

Average pressure p_{mave} rises if known terms in numerator of eq. (8) are greater. Forces acting at the outlet of mixing chamber are considered as given. Average pressure depends to the greatest extent on F_s , since relations of forces are following: $F_s/F_{ps}=3$, $F_s/F_{pcw}=3$, $F_s/F_{cw}=35$. These values are known from experimental investigations. If it is possible to provide higher pressure of cold water at the entrance of mixing chamber, without extra energy, efficiency rate of mixing chamber increases proportionally. But, if cold water is on atmospheric pressure, or even lower, vacuum at the entrance of mixing chamber will suck in cold water what is a valuable technical advantage (pump for cold water is not necessary); and efficiency rate decreases compared to previous case. Force F_{cw} is neglectable. Force F_s is three times greater than force F_{ps} , and from energy point of view, it is more favourable to achieve higher steam velocity at the outlet of Laval nozzle, which requires decrease of pressure p_s at the outlet of Laval nozzle. The limit to which it is possible to decrease outlet steam pressure from Laval nozzle p_{sL} depends on possibility to maintain isentropic steam expansion without shocks. Higher steam pressure at inlet of Laval nozzle provides higher values of F_{ps} and F_s , what should be used if steam of such quality is at disposal.

For experimentally gained inlet and outlet values $D_{oL}=30$ mm, $(D_{mc})_{in}=34$ mm, $(D_{mc})_{out}=10$ mm, $\dot{m}_s = 0.17$ kg/s, $\dot{m}_m = 1.02$ kg/s, $p_{cw}=1.8$ bar, $p_{os}=2.6$ bar, $p_{hw}=6$ bar, $v_{cw}=4.1$ m/s, $v_{hw}=13$ m/s, average absolute pressure in mixing chamber is 1.42 bar.

5. CONCLUSION

Inaccessible and deficient data on what happens in mixing chamber during the flow of supersonic mixture of cold water and steam is one of the reasons for conducting a careful investigation on this complex process of forced condensation. Unstable flow conditions through injector over a longer period of time hinders accurate measuring and its reviewing. Determining relatively accurate pressure change through mixing chamber would lead to more precise analyses of established procedures and conditions in mixing chamber.

Since the general laws are non-existent, analyses of complex energy transformation through injector device demand puzzle like collection of data and filling in reliable details.

Reliable details presented in this paper are:

- ✚ Mach number strongly represents the process. Sound velocity c entirely depends on mixture wetness, and thus, analytic relations of compressible flow can be applied. Dynamic relation of compressible flow consists of inertial and elastic forces (v^2 , κM^2) and can be applied to flow process in mixing chamber, taking into account change of κ .
- ✚ Modified diagram of forced condensation locates energy and flow changes in corresponding cross sections in mixing chamber. Diagram connects energy surrounding (superheated steam and cold water) with flow process, which can be directed into desired course. Diagram of forced condensation indicates that in order to get higher pressures of warm water, shorter condensation process with higher wetness seems to be more appropriate.
- ✚ Determining magnitude of average mixture pressure in mixing chamber (p_{ave}) enables to get a more accurate pressure distribution in mixing chamber and geometry of mixing chamber, according to the inlet parameters. Application of momentum equation provides a clear inside of forces acting in mixing chamber. The influence of some of these forces to pressure change in the

chamber is obvious and thus, there is no need for further investigation. Considerably high deceleration of mixture velocity in front of the mixing chamber throat, during forced condensation, in comparison with free condensation (t_{ga} in Fig. 3), is a measure of outlet pressure increase. Outlet pressure multiplied by cross section area is acting inertial force.

Further investigation predicts:

- ✚ Determining velocity distribution in mixing chamber by using LDA of new generation and its comparison with the research of *Dumaz et. al.* (2005).
- ✚ Investigating central water nozzle and annular steam nozzle and its comparison with the research of *Deberne et. al.* (1999). That investigation could deal with determination of friction losses on the wall with annular introduction of steam in mixing chamber.

NOMENCLATURE

A	[cm ²]	cross section area
h	[J/kg]	enthalpy
\dot{m}	[kg/s]	mass flow rate
p	[Pa]	pressure
Q	[m ³ /s]	flow rate
q	[J/kg]	heat energy
T	[K]	temperature
t	[°C]	temperature
V	[m ³]	volume
v	[m/s]	velocity
X	[%]	dryness during forced condensation
x	[%]	dryness during free condensation
Y	[%]	wetness during forced condensation
y	[%]	wetness during free condensation
ρ	[kg/m ³]	density

Subscripts

o	total
a	atmospheric
ave	average
con	condensed
cw	cold water
d	diffuser
hw	hot water
i	section number ($i=1,2,\dots,10$)
in	inlet
L	Laval's nozzle
l	losses
m	manometric
mc	mixing chamber
mix	mixture
out	outlet
s	steam
w	water
wm	water for mixing
$wrest$	the rest of water

ACKNOWLEDGEMENT

This work was supported by Serbian Ministry of Science in the framework of the project “Quality of Dry Fruits Production” TR.20065.B.

REFERENCES

- [1] Beithou, N., Aybar, H.S., 2000, A mathematical model for steam-driven jet pump, *Int. J. of multiphase Flow* 26, pp. 1609-1619
- [2] Bukurov, M., 2004, Investigation of Supersonic Steam-Water Injector Characteristics, Ph.D. Theses, Faculty of Technical Sciences, Novi Sad, Serbia (in Serbian)
- [3] Deberne, N. et. al., 1999, A model for calculation of steam injector performance, *Int. J. of Multiphase Flow* 25, pp. 841-855
- [4] Deich, M.E., Filipov, G.A., 1968, *Gas Dynamics of Two-Phase Fluids*, Energy, Moscow (in Russian)
- [5] Dumaz, P. et. al., 2005, The DEEPSSI project, design, testing and modelling of steam injectors, *Nuclear Engineering and Design* 235, pp. 233-251
- [6] Malibashev, S.K., 2001, Experimental investigation of transparent models of steam-water injector with convergent nozzle, *Atomic Energy*, Vol. 90, No. 6
- [7] Narabayashi, T., Mori, M., Nakamaru, M., Ohmori, S., 2000, Study on two-phase flow dynamics in steam injectors II. High-pressure tests using scale models, *Nuclear Engineering and Design* 200, pp.261-271



ANALYSIS OF THE MOST COMMON FAILURES OF GEARS IN UNIVERSAL GEAR REDUCERS

Milan RACKOV, Siniša KUZMANOVIĆ

University of Novi Sad, Faculty of Technical Sciences, Serbia

Abstract:

Universal gear reducers are important mechanisms of every machine and production line and they are often used in all branches of mechanical engineering. Regular work and quality of many machines depend on reliability and quality of gear reducers. Thus, the gears, as the most important elements of every gear reducer, have to be properly calculated, dimensioned and designed. However, beside all this precautions, gear failures can happen due to occurring of overloads, manufacturing and material failures of gears and other different unpredicted influences. Failures can occur suddenly or as a gradually teeth wearing off. This paper will give a review of the most common failures of gears in gear reducers and also some measures for their prevention.

Key words:

gear reducers, gears, breakdowns, gear failures

1. INTRODUCTION

Mechanical power transmission units are among the oldest mechanisms that mankind invented and they are certainly the most often used mechanisms in mechanical engineering and machine industry today.

Today, mechanical power transmission devices are produced in large series of millions specimens as special units (for example in the frame of automotive industry, railway machine industry, constructing machines industry, etc.), and as universal units (for all fields of mechanical engineering, usually with electric motor mounted, so called motor gear units or driving units). Application of mechanical power transmission units is certainly wide today, and it can be concluded that there is no industry branch that does not need any type of gear unit. Universal gear units are usually applied in mines, thermo and hydro plants, food industry, constructing materials industry, municipal service companies, etc.).

By their proper operating, mechanical gear units, as an important component of driving system, have significant influence on reliability of overall system. However, breakdowns of gear units can also happen, and thus they could be the cause of unplanned production interrupts. Although all conditions for proper operating are ensured by their construction, their sudden breakdowns yet occur. The reason for that can be failure of one or several elements, which causes irregular operating, or momentary break of gear unit operating.

Because of its function, to transfer mechanical energy from motor to some working machine, breakdown of mechanical gear unit refers to momentary breakdown of overall system, interrupt of its operating and production stop, which can cause large economic losses for users of gear units.

2. BREAKDOWNS OF GEAR REDUCERS AND THEIR CAUSES

In order to provide reliable and quality operating of gear units and systems that contain gear units, during whole projected operating life, it is necessary to analyze in detail all

characteristics of proper operating of gear unit, their operating characteristics with different failures, as well as reasons for occurring of accidental and breakdown situations.

This paper analyses different causes and failures of gears inside of motor gear reducer. Reducing possibility of failures occurrence is also considered by the authors of this paper, using particular example of gear reducer made by Sever-Subotica with axis height 90 mm. Possibility of failures reducing is analyzed prevailing due to constructional malfunctions which are the most usual technical causes of gear units breakdowns. As a result of this analysis, modified design solution is recommended, so it can carry projected loading without breakdowns.

The most of breakdowns of gear reducers do not happen immediately, but gradually, because some period of time is necessary to pass, so that all conditions requisited for breakdown occurrence are created. Failures of gear reducer components usually occur due to design defects, material defects, manufacturing defects and exploitation defects. Failure occurrence, i.e. occurrence of reduced operating capability, can be manifested by different intensity. Increasing failure intensity, in one moment reducer will turn to the breakdown state. Gear reducer breakdowns can be considered from different points of view, so that they can be classified according to several criteria (Fig. 1) [1].

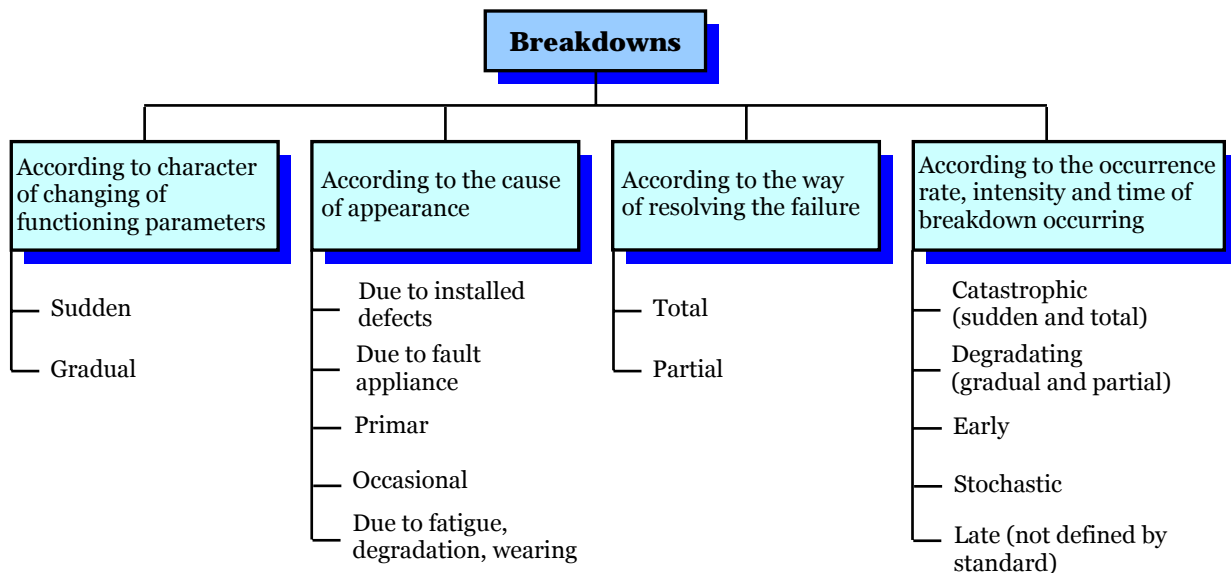


Figure 1. Schematic review of breakdown classification of gear reducer [1]

According to changing of functioning parameters of gear reducers, breakdowns can be sudden or gradual (late). Causes of sudden breakdowns have stochastic, unsteady character and they can not be predicted (for example connection breaking, fractures, processes of concentric wearing, etc.). Gradual breakdowns can be predicted by its intensity and direction (surfaces wearing processes, material degradation, corrosion processes, weakening of connections between reducer components, etc.).

According to cause, breakdowns can occur due to installed defects, due to fault appliance, due to fatigue, degradation or material wearing, and also can be primar and occasional.

According to breakdowns resolving, there are total and partial breakdowns. Total breakdowns result with totally loss of operating capability of reducer and they are resolved by replacing part that has broken down. These breakdowns are usually breakings and fractures, and this kind of breakdown can cause breakdown of other reducer components. Partial breakdowns occur as a result of disturbance in operating process, when only partial operating capability of reducer is lost. This kind of breakdowns can be failures of sealers and washers, oil leaking, higher vibration due to fault mounting or improper installation, and they are resolving by certain maintenance procedures.

According to speed, intensity and time of occurring, breakdowns can be catastrophic, degrading, early, stochastic and late. Catastrophic breakdowns are, in the same time, sudden and total, and their characteristic is large economic and material damage. Degrading breakdowns are gradual and partial in the same time. Early breakdowns of reducer occur in the period of running in. Stochastic breakdowns occur during regular exploitation, and late breakdowns intensively occur after period of projected operating life.

Breakdowns of gear reducers can happen due to technical defects, organizational faults and unsatisfactory competence and personnel training. Nevertheless, gear reducers usually fail due to technical malfunctions, where especially belong design, technological and exploitation causes (Fig. 2). 12% breakdowns, of overall breakdowns amount, are caused by mistakes and defects made during the process of constructing and design [1]. This paper deals with possibility of intensity reducing this kind of design failures to minimum.

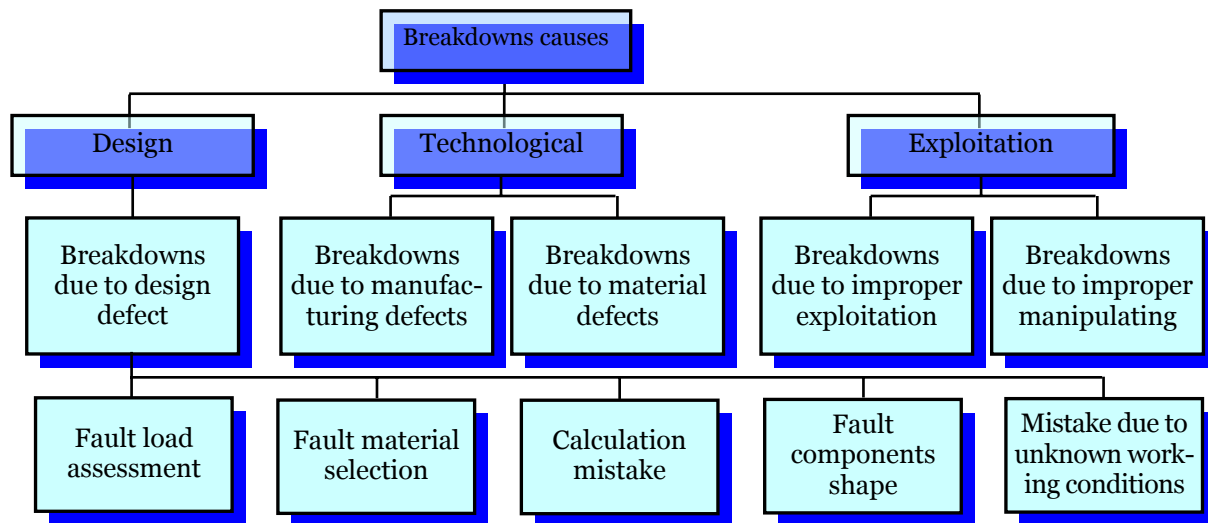


Figure 2. Causes of breakdowns occurrence

Considering breakdowns during exploitation and their causes, three characteristic periods can be noticed. In the beginning of exploitation, early breakdowns occur as a result of latent design and technological malfunctions. In further reducer exploitation, stochastic breakdowns can occur due to overloadings. After long period of exploitation, amplified (late) breakdowns occur as a result of fatigue, corrosion and aging. Causes of breakdowns for all these three domains are different, so that measures for their reducing (increasing reducer reliability) are different for all of these three time range. Frequency of all these breakdowns is directly proportional to undertaken activities for resolving design and technological causes of breakdowns during period of reducer development. Therefore, it is important to detect and remove as much causes as possible in this period, especially those latent defects and causes which could cause later, during exploitation, premature breakdowns and reducing projected operating life of gear reducer.

3. GEAR FAILURES

60% of gear reducer breakdowns happen due to gear failures [2], which means that quality and reliability of gears are very important for proper operating of reducer. When transfer load from pinion to gear wheel, teeth flanks relatively move between each other by sliding and rolling. Thus, depending on torque value, teeth flanks are exposed to smaller or bigger contact pressures with sliding at the same time, and tooth dedendum is exposed to flexion, too. In these conditions, depending on torque and operating regime, different failures of gears can occur, i.e. breakdowns can be manifested in different ways. Failures that occur on gear teeth, are various and can be, according to ISO 10825, classified as: surface disturbances, scuffing, permanent deformations, surface fatigue phenomena, fissures and cracks and tooth breakage (Fig. 3).

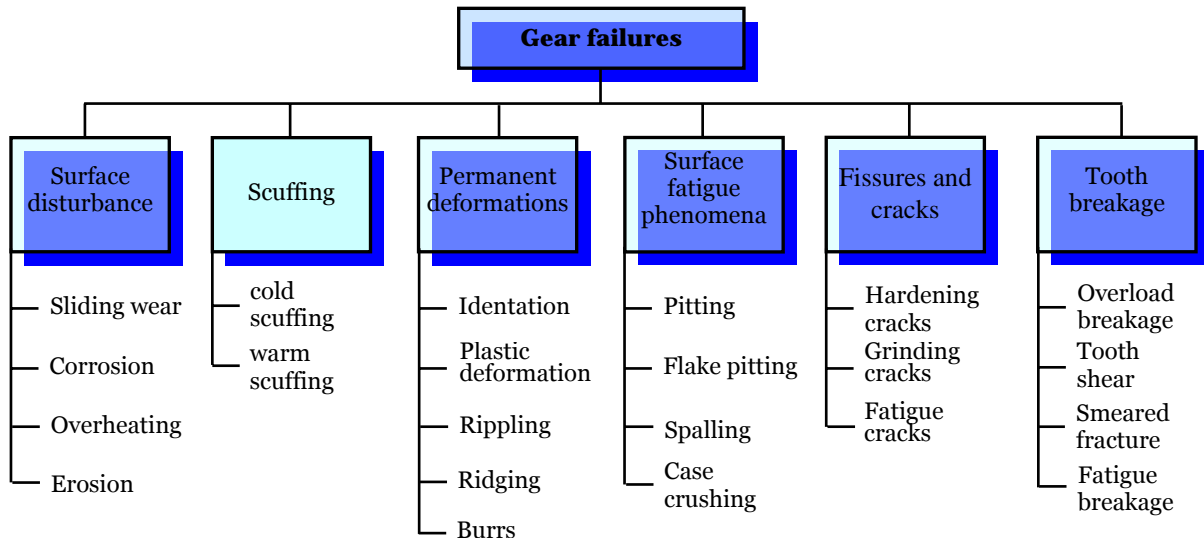


Figure 3. Classification of gear failures according to ISO 10825 [5]

Indications of surface disturbances comprise failures of gear teeth, such as: sliding wear (Fig. 4-a), corrosion (Fig. 4-b), overheating (Fig. 4-c), as well as some types of erosion, but they are not result of fatigue process.

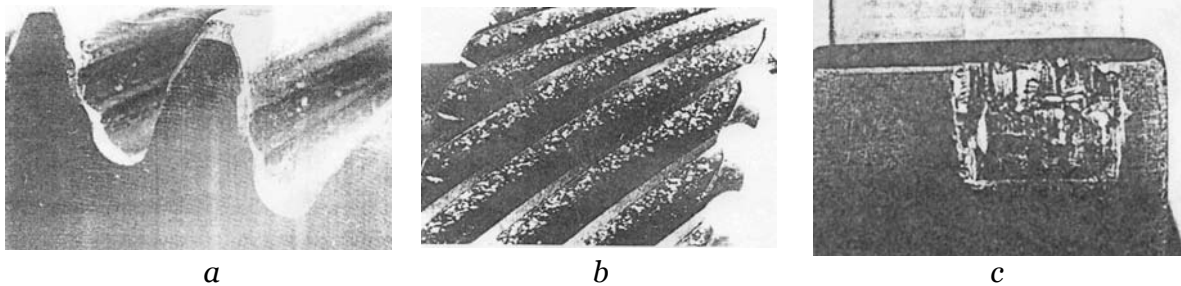


Figure 4. Types of surface failures of gear teeth (a- sliding wear; b - corrosion; c - overheating)

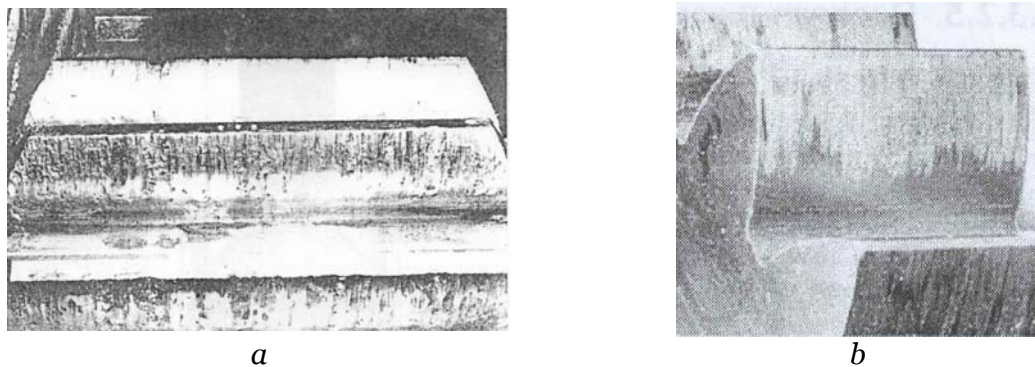


Figure 5. Scuffing of gear teeth (a- cold scuffing; b - warm scuffing)

Scuffing of gear teeth (Fig. 5) occurs due to great pressure loads and high sliding velocities. It represents drastic kind of teeth failure. Scuffing occurs suddenly, when lubricant film between the tooth flanks is disrupted. This can lead to localized welding of the tooth flanks with transfer of material.

Permanent deformations of gear teeth are failures of tooth profile. They occur due to great torques, when material of gear or heat treatment of gear are not properly matched with working conditions, or some filthiness or foreign bodies are present in lubricant. This kind of failure usually comprises: indentation (Fig. 6-a), plastic deformations (Fig. 6-b) and rippling (Fig. 6-c).

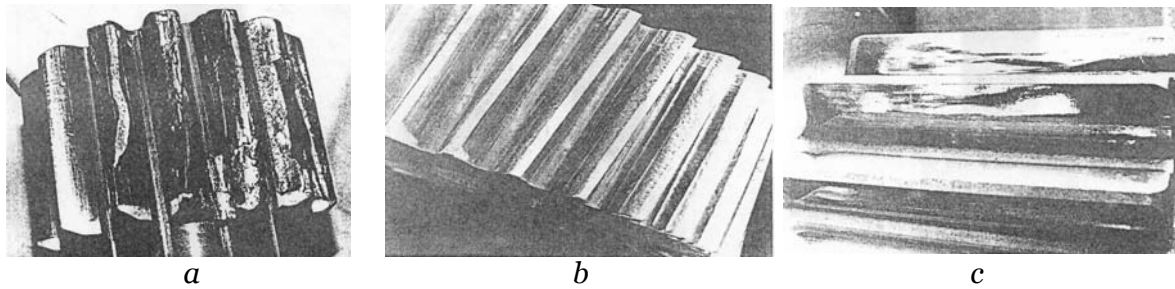


Figure 6. Permanent deformations of gear teeth
(a - indentation; b - plastic deformations; c - rippling)

Surface fatigue phenomena occur because of material damage due to surface and subsurface stresses produced by the repeated application of forces. It is characterized by removal of metal and the formation of cavities. Pitting is one of the most usual fatigue surface failures. It occurs in the presence of rolling or mixed rolling and sliding contacts. Particles break out of affected areas leaving surfaces pock-marked with scattered holes. There are several kinds of pitting: initial pitting (Fig. 7-a), progressive pitting (Fig. 7-b), micropitting (Fig. 7-c), flake pitting (Fig. 7-d) and progressive macropitting, called spalling (Fig. 7-e).

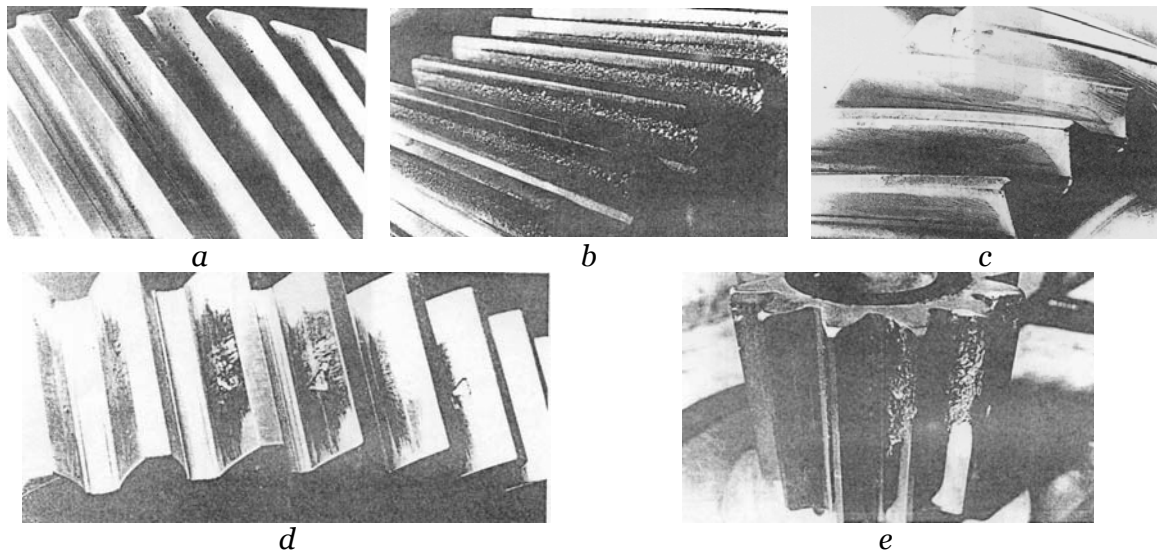


Figure 7. Surface fatigue failures of gear teeth
(a - initial pitting ; b - progressive pitting; c - micropitting; d - flake pitting; e - spalling)

Fissures and cracks of gear (Fig. 8) can occur even before gear start to transfer torque, i.e. in its manufacturing phase. They usually occur as a result of defects, filthiness and gas inclusions in material that gear is made of, and also as a result of improper heat treatment, high internal stresses and defects during grinding operation.

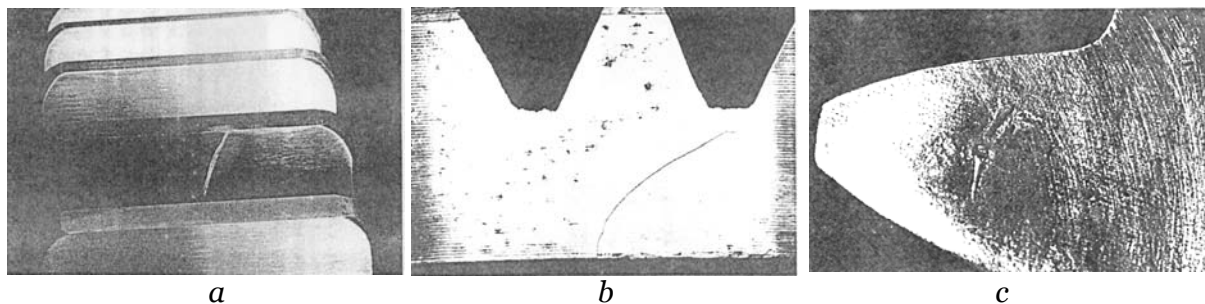


Figure 8. Fissures and cracks of gear teeth
(a - crack caused by a forging defects; b – crack in the rim of a wheel due to inadequate rim thickness; c – fatigue crack which has appeared in the tooth root fillet below the loaded flank)

Tooth breakage usually occurs at the tooth dedendum, where the stresses are higher, especially on flexion tooth flank. It also may occur on the other place when it is a result of pitting process, fault heat treatment or other failures on flanks. These failures are classified as: overload breakage (Fig. 9-a), tooth shear (Fig. 9-b), breakage after plastic deformation, so called smeared fracture (Fig. 9-c) and fatigue breakage (Fig. 9-d). When overload breakage happens, several teeth are damaged, and if it is fatigue breakage, usually one tooth is damaged.

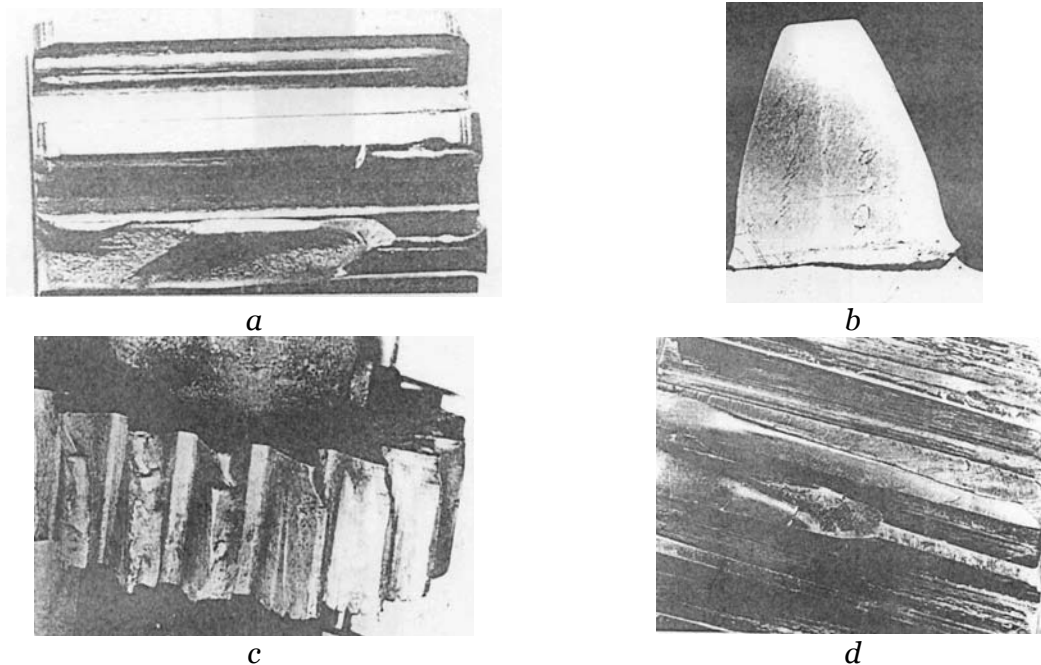


Figure 9. Surface fatigue failures of gear teeth
(a- overload breakage; b - tooth shear; c - smeared fracture; d - fatigue breakage)

4. PROBLEM DESCRIPTION

After testings of new series of gear reducers of axis height 90 mm, it is identified that early failures of some components occur and that reducer rapidly degrades. These early breakdowns of reducer are caused due to constructional faults and design defects. Problem occurs because gear reducer is not adapted to projected load capacity, so that projected output torque can not be achieved, for such defined sets of gears and current reducer construction. Projected output torque value is defined according to new series of reducers of leading manufacturers of gear units. However, because of constructional faults and design defects, Sever's gear reducers are not capable to fulfill established demands. Values of gear ratii are satisfied, but still output torque is not, so that Sever's gear reducers can not be competitive on the market.

Testings are carried out on two stages and three stages gear reducers according to standard program and testing methodology of gear units that is used in Sever factory. After testing with particular torque value, gear reducer is disassembled and every component is being examined and analyzed. If total breakdown of some component occurs, or some failures are noticed, testings are being repeated with smaller torque. The biggest output torque, for which breakdowns and failures do not occur, is adopted as nominal permitted output torque for particular gear ratio.

According to defined testing methodology, testings are carried out for reducer with the smallest overall gear ratio, and at the same time the biggest gear ratio on output gear stage. For this two stages gear reducer, it is gear set with speed ratio 9.73, and for three stages variant, it is gear set with speed ratio 96. After testings of both variants of reducer, besides some failures of shaft and bearing, following failures of gears are also noticed:

% failure of output gear pair, i.e. occurring pitting and uneven loading trace on tooth flanks;
 % uneven loading trace also on the first gear pair, as well as pitting occurrence on pinion of the first pair, due to excessive deformation of input shaft.

5. RESULTS AND CONCLUSION

On the basis of calculated results, following modifications of present reducer design are recommended:

- % modifying of axis distance of output gear stage $a_{5/6}$ from 53 mm to 54 mm;
- % increasing the diameter of fifth gear shaft under the gear z_5 , raising the pinion teeth number for one, from $z_5 = 11$ to $z_5 = 12$, by maintaining approximately same partial speed rati of output gear pair;
- % increasing overhanged diameter of fifth gear shaft, from 15, and 12 mm to 17 mm;
- % choosing stronger cylindrical bearing, instead of NU202 it is chosen NU203.

After increasing axis distance of output gear stage $a_{5/6}$ from 53 mm to 54 mm, position of shaft axes in reducer has been changed and the axis of input shaft comes down from 11.58 mm to 12.9 mm, relating to output shaft (Fig. 10).

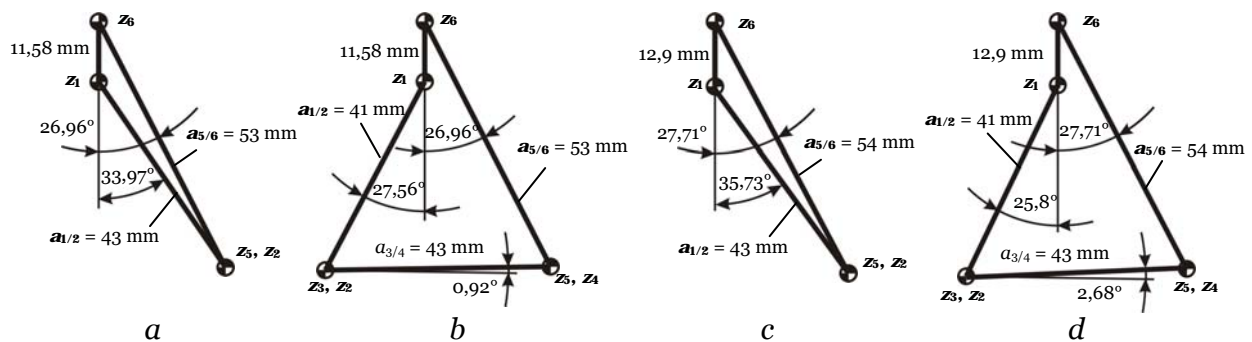


Figure 10. Position of gear axes for present design solution of gear reducer with axis height 90 mm (a - present two stages, b - present three stages) and for proposed design solution (c - proposed two stages, d - proposed three stages)

Increasing axis distance of output gear stage $a_{5/6}$ for only 1 mm enables raising teeth number of fifth gear for one, as well as teeth number of sixth gear, so that approximately same partial speed rati will be maintained. Also, increasing teeth number of fifth gear influenced increasing rigidity and reducing shaft deformations under the gear. This simply increasing of teeth number was possible for partial speed rati 2.94 (teeth number $z_5 = 17$ and $z_6 = 50$ has been increased to $z_5 = 18$ and $z_6 = 53$), 4.08 (teeth number $z_5 = 13$ and $z_6 = 53$ has been increased to $z_5 = 14$ and $z_6 = 57$) and for 4.91 (teeth number $z_5 = 11$ and $z_6 = 54$ has been increased to $z_5 = 12$ and $z_6 = 59$). Thus, loading capability of gear pair z_5/z_6 enabled carrying projected output torque. However, for speed ratio 6.27 (teeth number $z_5 = 11$ and $z_6 = 69$ has been increased to $z_5 = 12$ and $z_6 = 75$), due to insufficient axis distance, loading capability was not satisfied. Because of that, teeth number of sixth gear is reduced to $z_6 = 73$, so that projected output torque could be satisfied, but with negligible reducing of speed ratio, i.e. from 6.25 to 6.08 (Fig. 11).

It is demonstrated that it is possible to reduce breakdown intensity and to prevent failures of gears and thus increase loading capability of two stages and three stages gear reducers by applying certain design modification and avoiding constructing faults.

This paper gives a review of different types of gear failures which can occur due to various kinds of malfunctions and improper working condition. Gear failures usually occur due to design faults, wrong assembling and mounting, poor maintenance and uncaredful manipulating.

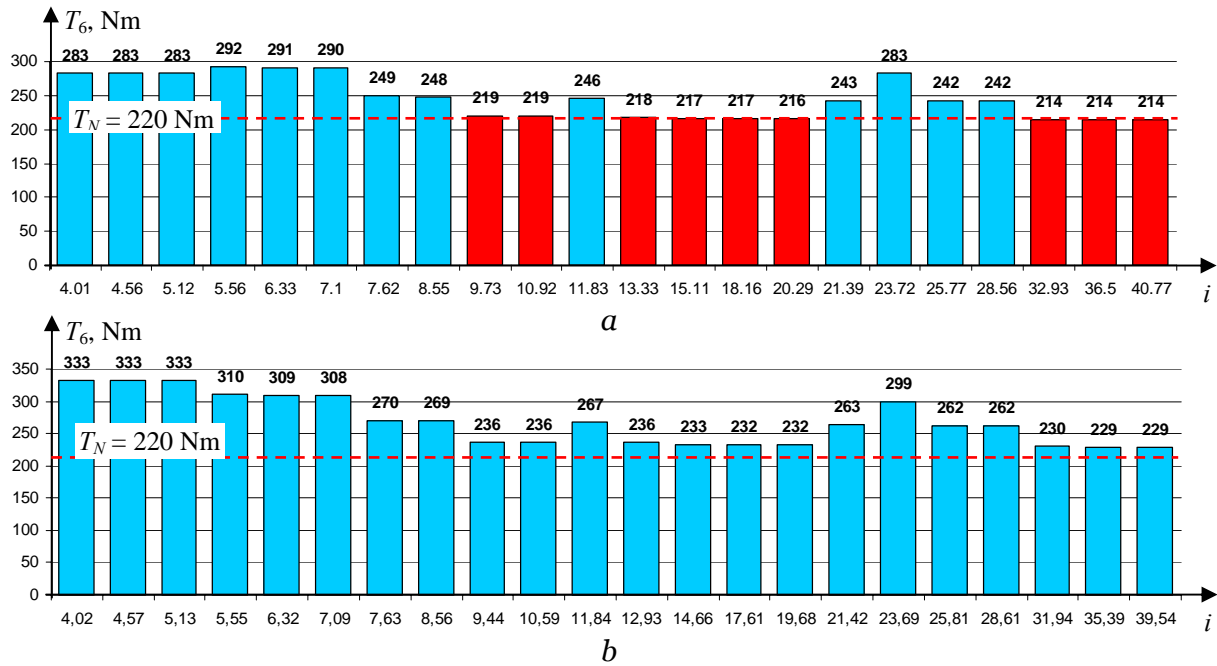


Figure 11. Permissible output torques of present (a) and proposed (b) design solution of two stages gear reducer with axis height 90 mm depending on endurance of teeth flanks of output gear pair z_5/z_6

After recommended design modifications, significant increasing of loading capacity of gear reducer is obtained. After carried out modifications, projected parameters of gear reducer are achieved, so that analyzed construction of Sever's reducer can be competitive with other leading manufacturers of gear units. Proposed modifications should be implemented to all other dimensions of gear reducers' family, which will enable successful access of these reducers to world market.

REFERENCES

- [1] ADAMOVIĆ, Živoslav, *Maintaining Technology*, University of Novi Sad, Technical Faculty "Mihajlo Pupin" in Zrenjanin, 1998
- [2] MILČIĆ, Dragan, *Machine Systems Reliability*, University of Niš, Faculty of Mechanical Engineering, Niš, 2005
- [3] KUZMANOVIĆ, Siniša, *Universal Gear Reducers With Cylindrical Gears*, University of Novi Sad, Faculty of Technical Sciences, Novi Sad, 1998
- [4] RACKOV, Milan, *Researching of Design Solutions of Reducing Failure Rate of Universal Gear Reducers*, Master thesis, Faculty of Technical Sciences, Novi Sad, 2007
- [5] International Standard ISO 10825, *Gears – Wear and damage to gear teeth – Terminology*, First edition 1995-08-01



GENERAL CONCEPTS OF MAINTENANCE

BUZGAU Natalia-Cernica

S.C. Reva S.A. Simeria, ROMANIA

Abstract:

Maintenance involves preventive (planned) and unplanned actions carried out to retain a system at or restore it to an acceptable operating condition. Optimal maintenance policies aim to provide optimum system reliability and safety performance at the lowest possible maintenance costs. Proper maintenance techniques have been emphasized in recent years due to the fact that the safety and reliability requirements of system, increased complexity and costs of material and labor are increasing.

Keywords:

maintenance, reliability, Preventive maintenance (PM),
Corrective Maintenance (CM), Imperfect maintenance

1. INTRODUCTION

Maintenance has evolved from simple model that deals with machinery breakdowns, to time-based preventive maintenance, to today's condition-based maintenance. It is of great importance to avoid the failure of a system during its actual operation especially, when such failure is dangerous or costly. Time-based and condition-based maintenance are two major approaches for maintenance. In contrast, condition based maintenance can be more profitable in order to avoid failure occurrence at the lowest cost and to improve the availability and reliability of the maintained system.

The choices of the inspection schedule and preventive maintenance thresholds obviously have a great influence on the economic performance of the maintenance policy. The inspection dates and the preventive maintenance are main decision variables considered in many researches.

2. MAINTENANCE CLASSIFICATION

Maintenance can be classified by two major categories: corrective and preventive. Corrective Maintenance (CM) is the maintenance that is performed when the system fails. Corrective maintenance means all actions performed as the result of failure, to restore an item to a specified condition.

Preventive maintenance (PM) is the maintenance that happens when the system is operating and it means all actions performed in an attempt to retain an item in specified condition by providing systematic inspections, detection, and prevention on failures. Maintenance can also be classified according to the degree to which the operating condition of an item is restored by maintenance in the following way [1]:

1. Perfect repair: perfect maintenance is maintenance actions which restore a system operating condition to as „good as new”. That is, perfect maintenance and a system has the same lifetime distribution and failure rate function as a new one. Generally, replacement of a failed system by a new one is a perfect repair.
2. Minimal repair: minimal maintenance actions which restore a system to the same failure rate as it had when it failed. Minimal repair was first studied by Barlow [2]. The system operating state after the minimal repair is literally called „as bad as old”.
3. Imperfect repair or imperfect maintenance: maintenance actions which do not make a system not „as good as new” but younger. Usually, it is assumed that imperfect

4. maintenance restores the system operating state to somewhere between „as good as new” and „as bad as old”. Clearly, imperfect repair (maintenance) is a general repair (maintenance) which can include two extreme cases: minimal and perfect repairs (maintenance). Engine tune-up is an example of imperfect maintenance.
5. Worse repair or worse maintenance: maintenance actions which un-deliberately make the system failure rate or actual age increase but the system dose not breakdown. Thus, upon worse repairs a system operating condition became worse than that just prior to its failure.
6. Worst repair or worst maintenance: maintenance actions which un-deliberately make the system fail or break down.

According to the above suggested classification, we can say that a PM can be a minimal, perfect, imperfect, worst or worse one. Similarly, a CM could be a minimal, perfect, imperfect, worst or worse CM. We will refer to imperfect CM and PM as imperfect maintenance later. The type and degree of maintenance used in practice depends on types of systems, their costs as well as reliability and safety requirements.

In the related literature, most studies assume that the system after CM or PM is „as good as new” (perfect maintenance) or „as bad as old” (minimal maintenance). In practice, the perfect maintenance assumption may be acceptable for system with one component which is structurally simple. On the other hand, the minimal repair assumption seems reasonable for failure behavior of systems when one of its components, non-dominating component, is replaced by a new one. However, many maintenance activities may not result in these two extreme situations but in a complicated intermediate one. Therefore, perfect maintenance and minimal maintenance are not practical in many actual instances and realistic imperfect maintenance should be modeled.

Recently, imperfect CM and PM have received more attention in reliability and maintenance literature. In fact, we can say that imperfect maintenance study indicates a significant breakthrough in maintenance and reliability and maintenance theory. In [3] the author mentioned that imperfectness of maintenance is related to the skill of the maintenance personnel, the quality of the maintenance procedure, and the maintainability of the system [3]. Obviously, maintenance expenditure and reliability requirement also have important effects on imperfectness of maintenance. Barlow and Proschan presented some possible causes for imperfect, worse or worst maintenance due to the maintenance performer [4]:

- ✚ Repairing the wrong part.
- ✚ Only partially repairing the faulty part.
- ✚ Repairing (partially or completely) the faulty part.
- ✚ Incorrectly assessing the condition of the inspected units.
- ✚ Performing the maintenance action not when called for but at customer convenience.
- ✚ Nakagawa mentions three reasons causing worse or worst maintenance [5]:
- ✚ Hidden faults and failure which are not detected during maintenance.
- ✚ Human errors such as wrong adjustments and further damage done during maintenance.
- ✚ Replacement with faulty parts.

According to Barlow and Proschan [4], maintenance policies based on planned inspections are „periodic inspection” and „inspection interval dependent on age”. By periodic inspections, a failed unit is identified or it is determined whether the unit is functioning or not. With aging of the unit, the inspection interval may be shorter. These inspection methods are subject to imperfect maintenance caused by randomness in the actual time of inspection, in spite of the schedule, imperfect inspection and cost structure. Therefore, realistic and valid maintenance models must incorporate with random features of the inspection policy. So far only a small portion of literature concerning to the stochastic behavior of the repairable systems and maintenance is involved in imperfect maintenance.

3. MULTI COMPONENT SYSTEM’S MAINTENANCE

Currently, the interest for multi component maintenance models is increasing. In the beginning vast majority of the maintenance models were concerned about a single piece of

equipment operating in a fixed environment, considered as an intrinsic barrier for allocations. Maintenance action of a multi component system differs from that one for a single-unit system; because these depend on some factors. One of the dependencies is economic dependence. Another one is failure dependence, or correlated failures. Economy dependency is a common term in most continuous operating systems. For this type of systems, the cost of system unavailability (one-time shut-down) may be much higher than component maintenance costs. Therefore, there is often great potential cost saving by implementing an opportunistic maintenance policy.

Obviously, the joint maintenance of two or more subsystems tends to spend less money and less time (economy dependency), and the failures of different subsystems in multicomponent system may not be independent (failure dependency). Thus, each subsystem may not be considered as a single-unit system, and to apply the existing optimum maintenance models of a single-unit system to each of such subsystems may not be practical.

Imperfect maintenance exists also in a repairable multi-component system. If one of its subsystems fails, it can be repaired by replacing some of its parts. Clearly, reliability measures of the repaired subsystems are improved after repair but it might not be as good as new (imperfect CM), and consequently the entire system will no longer function as well as a new one.

Realistic imperfect maintenance associated with individual subsystems and accordingly systems have to be modeled. According to [6], systems used in the production of goods and delivery of services constitute the vast majority of most industry's capital. These systems are subject to deterioration with usage and age. System deterioration is often in higher production costs and lower product quality, to keep production costs down while maintaining good quality. PM is often performed on such systems. It is obvious that these kinds of system are often composed by many subsystems whose maintenance is often imperfect or sometimes even worse. It is necessary to point out that considering the entire system as a single unit by a minimal repair model may not be suitable for large-scale systems. Such maintenance modeling is also too rough for complex systems due to the economy and failure dependencies. In practice, some subsystems are inspected and tested separately and their reliability performances are also evaluated individually.

Lifetime distributions of all new subsystems are known through reliability tests and statistical results before they will be used for such systems. As a result, we can evaluate whole system reliability measure and system maintenance cost based on failure information, maintenance costs, and maintenance degree of all subsystems. Therefore, we may say that a realistic method is to treat a system the same as one with many subsystems which are subjects to imperfect maintenance. We are, also able to model imperfect maintenance of the system through imperfect maintenance modeling of all subsystems and at the same time economical model and failure dependency of the system in order to obtain global optimum maintenance policies for the system.

4. CONCLUSIONS

The usual criteria of optimization of maintenance policies are based on maintenance cost measures, same as expected maintenance costs per unit of time and total discounted costs. Hence the optimal maintenance policies are the ones that minimize or maximize a given cost criterion

Reliability is the branch of quality assurance that deals specifically with the ability function upon demand. During the last decades many works have been devoted to the binary-state reliability analysis, where it is assumed that a system may experience only two possible states: one working state and one failure state.

However, in many real world situations a system or a component could experience more than two levels of performance varying from perfect functionality to complete failure; these systems are called multi-state systems. The evaluation of maintenance, testing, and repair policies becomes more and more complex for multi-state systems that contain combinations of revealed and unrevealed failure [7].

BIBLIOGRAPHY

- [1.] Nakagawa T., *Sequential Imperfect Preventive Maintenance Policies*, IEEE, Trans on Reliab., 37, 1988.
- [2.] Barlow R. and Proschan F., *Statistical Theory of Reliability and Life testing*, Holt, Rinehart and Winston Inc, 1975.
- [3.] Helvic B., *Periodic Maintenance on the effect of Imperfectness*. 10th, *Int. Fault-tolerant Computing*, 1980.
- [4.] Barlow R. and Proschan F. *Imperfect Maintenance. IMS lecture Notes-Monograph*. Hayward, California, 1982.
- [5.] Nakagawa T. and Yasui K. *Optimal Policies for a System with Imperfect Maintenance*, IEEE Trans on Reliab., Vol.36, 5, 1987.
- [6.] Valdez-Flores C. and Feldman R., *A Survey of Preventive Maintenance Models for Stochastically Deteriorating Single-Unit System*, Naval Research Logistics, 36, 1989.
- [7.] Lewis E. E. *Introduction to Reliability Engineering*. John Wiley and Sons. Co. 1987.

A STUDY OF THE BOCKER'S OBSERVER IMPLEMENTATION TO ESTIMATE THE INDUCED POWER WITHIN A CAST-IRON CONVEYANCE AND DOSAGE ELECTROMAGNETIC PUMP

Adrian DĂNILĂ

Transylvania University of Braşov, ROMANIA

Abstract:

In this paper the structural elements and applications of the electromagnetic pumps for melted cast iron conveyance and dosage within the metallurgical engineering are presented. The mathematical model in steady-state operation of the electromagnetic pump is deduced within Chapter 2. Based on this model, the physical parameters of the melted metal may be estimated. The vector-matrix representation of the dynamic set of equations of the pump is then used, in Chapter 3 to obtain the Bocker's observer. This observer allows to reconstruct the flux-linkages of the magnetic field. Based on these results an estimate of the induced power is subsequently obtained. At the end of the paper, an implementation of this approach on a given electromagnetic pump is presented

Keywords:

electrothermy, electromagnetic pump, state observers

1. INTRODUCTION

The implementation of the Electro-thermal processes within foundries and forge departments is an important element to improve the products quality and to optimize the energy costs. A modern approach for the conveyance and dosage of melted metals, cast-iron, aluminum, copper and so is the useage of the electromagnetic pumps, Figure 1. The electromagnetic pumps may be used [1] to extract the melted metal directly from the basis of the induction furnace with a not mobile structure and to cast and dose the melted metals from the mobile melting pot. The electromagnetic pumps may be easily inserted into complex plants for continuous casting.

The advantages of the electromagnetic conveyance of melted metals are: (1) the control by electrical means of the liquid's flow-rate if the pump is supplied from controlled three-phased frequency converters, (2) costs reduction due to the elimination of purging the channel with tempered metal scraps, (3) the increase of the metal's pureness because the non-metallic elements aren't drawn by the electromagnetic forces, (4) the melting furnace and the melting pot may be at the same level thus their structure is much simpler, and (5) an improve of the working conditions within the casting departments.

The main disadvantage of the electromagnetic pump is the channel maintenance especially to the channel's basis where the material is highly solicited.



Figure 1. An electromagnetic pump for casting melted cast-iron

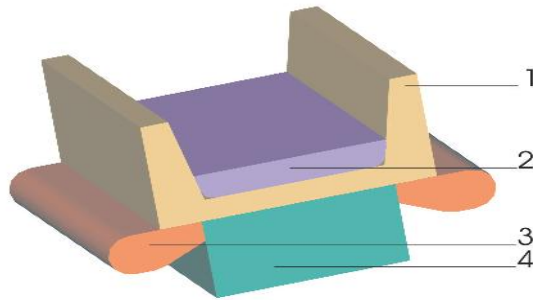


Figure 2. A Simplified cross-section through an electromagnetic pump, single-sided stator.

Table 1
The main features of the electromagnetic pumps

Denomination	Units	Light metals	Heavy metals	Cast-iron
Temperature	°C	650	900	1450
		-	- 1200	-
Flow rate	kg/s	750	-	-
		0,1	0,3	1,3
		-	-	-
Level	mm	10	30	100
		50	80	80
		-	-	-
Length	mm	540	540	930
		1080	1800	1800
		-	-	-
		2600	2600	4200

The induction electromagnetic pump is an induction motor with a two-sided or single-sided stator. The main parts of an induction electromagnetic pump with single-sided stator are, Figure 2. The magnetic circuitry 4 with the three-phased winding 3 are placed below the ascending channel 1, build with refractory cement concrete. The melted metal 2 flows through the channel due to the electromagnetic forces. The main technical characteristics of some widely used electromagnetic pumps are presented in Table 1.

2. THE MATHEMATICAL MODEL OF THE SINGLE-SIDED-STATOR ELECTROMAGNETIC PUMP

The stator winding of the induction electromagnetic pump supplied from a three-phased electric network produces a progressive electromagnetic field, Figure 3. The first harmonic of the resulting electromagnetic field above the single-sided stator is given by the following expression:

$$B_{\delta}(x,t) = B_{\delta m} \cdot \sin\left(\omega_1 \cdot t - \frac{\pi}{\tau} \cdot x\right) \quad (1)$$

where: $B_{\delta m}$ - the magnitude of the magnetic induction, $\omega_1 = 2 \cdot \pi \cdot f_1$ - the angular frequency and the frequency of the voltages at the stator windings, τ - the stator's winding polar step.

The motion speed of the first harmonic of the progressive wave, v_1 is:

$$v_1 = \frac{\Delta x}{\Delta t} = 2 \cdot \tau \cdot f_1 \quad (2)$$

The progressive magnetic field induces into the melted metal electric electrical currents due to the electromagnetic induction phenomenon. From the interaction between the resulting magnetic field and the induced currents, electromagnetic force results. This force acts on the melted metal. The electromagnetic force over a unit volume of melted metal may be computed with the relation:

$$\bar{f} = \bar{J} \times \bar{B} \quad (3)$$

where: \bar{J} - the per-unit induced currents and \bar{B} - the induction of the resulting magnetic field into the melted metal.

The expressions of the physical variables of the progressive field and the electromagnetic force, respectively may be deduced through the Maxwell's equations into the space above the inductor –l the air gap of the electromagnetic pump such as for the classical electric machines. In addition, for the induction electro-magnetic pumps the following phenomena have to be taken into account: the transversal edge effect, and the longitudinal edge effect (static and dynamic).

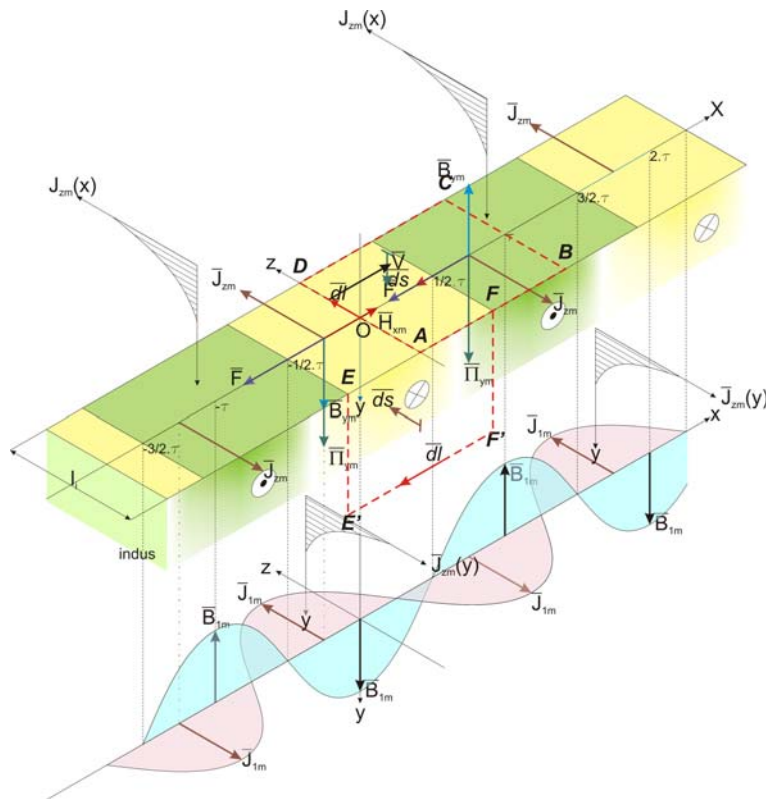


Figure 3. The distribution of the progressive field's first harmonic within the air gap of the electromagnetic pump.

The transversal edge effect consists in the modification of currents distribution through the transversal cross-section of the massive induced because the currents paths freely encircle the magnetic field.

The electro-magnetic force results less than the classical machines provided with windings on both armatures. The decrease of the electromagnetic force depends on the ratio between the polar step and the geometrical dimensions of the induced cross-section within the field, Figure 4.

The transversal edge is taken into account in the electrical equivalent diagram through an additional coefficient that increases the value of the equivalent induced resistance.

The static longitudinal edge effect is because the stator windings aren't balanced – linear stator. The phenomenon

consists in a non-symmetrical currents sequence in the stator's windings.

If the magnitudes of the phase voltages are known through measurements and the electric and magnetic parameters are estimated through computations, than the direct- and inverse phase sequence of the stator currents may be determined with the following set of equations:

$$\begin{cases} (3 \cdot \underline{Z}_d + j \cdot 4 \cdot X_0) \cdot \underline{I}_d + (3 \cdot \underline{Z}_i + j \cdot 4 \cdot X_0) \cdot \underline{I}_i = \underline{U}_{AB} - \underline{U}_{CA} \\ \underline{Z}_d \cdot \underline{I}_d - \underline{Z}_i \cdot \underline{I}_i = \frac{j}{\sqrt{3}} \cdot \underline{U}_{BC} \end{cases} \quad (4)$$

A practical approximation is: $\underline{Z}_d = \underline{Z}_i = \underline{Z}_l$. In the relations (4) the significance of the terms is: $\underline{Z}_d, \underline{Z}_i, \underline{Z}_l$ - the stator direct- and inverse-phase sequence impedances respectively, $\underline{I}_d, \underline{I}_i$ - the symmetrical components of the stator phase currents, X_0 - reactanța totală de dezechilibru și $\underline{U}_{AB}, \underline{U}_{BC}, \underline{U}_{CA}$ the unbalanced total reactance and - the stator phase voltages.

The dynamic longitudinal edge effect consists in the modification of currents distribution along the longitudinal direction.

This is due to the induced motion with respect to the progressive magnetic field.

If the induced reaction is weak then the static longitudinal edge effect on the non-symmetrical system of currents will be preponderant.

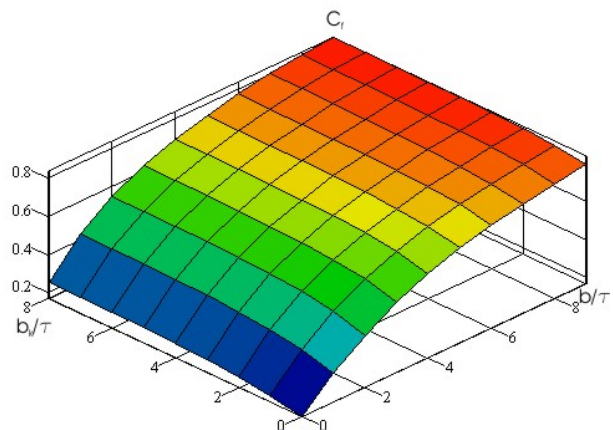


Figure 4. The dependencies of the induced resistance's coefficient.

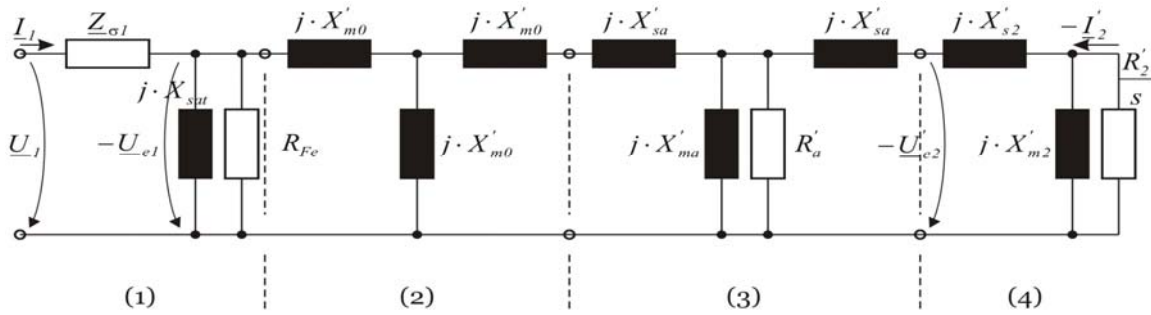


Figure 5. The equivalent electrical diagram of the electromagnetic pump, single-sided stator: (1) – stator, (2) – air, (3) – channel, (4) – melted liquid (induced).

The electrical equivalent diagram on a phase of the induction electromagnetic pump may be deduced by integrate the Maxwell's equations into the space above the single-sided stator.

To perform this operation, the vector magnetic potential, $\underline{\Psi}$ has to be used with the boundary conditions on the surfaces between the layers within the pump's air gap:

$$\frac{d^2 \underline{\Psi}}{dz^2} - \underline{\beta}^2 \cdot \underline{\Psi} = 0, \quad \underline{\beta} = \sqrt{\left(\frac{\pi}{\tau}\right)^2 + j \cdot \frac{s \cdot \omega_l \cdot \mu_0}{k_r \cdot \rho}} \quad (5)$$

where: s – the slip, μ_0 – the vacuum magnetic permeability, ρ – the melted metal resistivity, k_r – the resistance's coefficient due to the transversal edge effect.

An equivalent electric diagram is obtained through cascade connection of equivalent elements corresponding to the air gap layers, Figure 5.

For the on-line computations i.e. adaptive control, the simplified electrical equivalent diagram, Figure 6, is to be used; the significance of the components in Figure 6 is as follows: $Z_{\sigma 1}$ – the leakage inductance with respect to the induced, X_m – the linkage inductance, R_{Fe} , R'_a – the equivalent resistances corresponding to the cast-iron and channel losses respectively R'_2 – the equivalent resistance of the induced and s – the slip. The simplified diagram is only valid for larger polar step inductors at low frequencies.

If the pump is supplied from frequency converters, the constant stator flux operation is to be used. In this operation the converter provides a voltage direct phase-sequence with variable magnitude and variable frequency such as $U_1 / f_1 = const.$

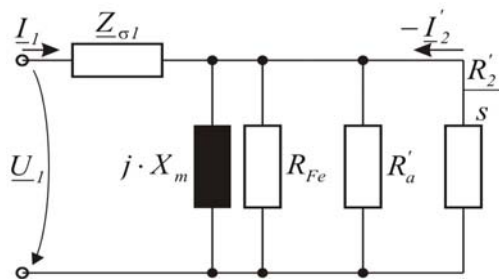


Figure 6. The simplified equivalent electrical diagram of the electromagnetic pump.

In this case the reference coordinate system is referred to the stator.

To obtain an estimate of the induced power into the melted metal the induced currents components and the magnetic flux-linkages components into the induced are to be computed.

The reference coordinate system is the stator and the inputs are the voltages and the currents through the stator winding.

3. IMPLEMENTATION OF BOCKER OBSERVER FOR DETERMINATION OF THE TRANSFERRED POWER TO THE MELTED METAL

The Bocker's observer provides an estimate of the magnetic flux linkages components, [3]. The voltages equations and the flux-linkages equations of the two-phased equivalent system represented in a coordinate system related to the stator are given by the following expressions, [4]:

$$\begin{aligned}
 u_{d1} &= R_1 \cdot i_{d1} + \frac{d\Psi_{d1}}{dt} & \Psi_{d1} &= L_1 \cdot i_{d1} + L_h \cdot i'_{d2} \\
 u_{q1} &= R_1 \cdot i_{q1} + \frac{d\Psi_{q1}}{dt} & \Psi_{q1} &= L_1 \cdot i_{q1} + L_h \cdot i'_{q2} \\
 0 &= R_2' \cdot i'_{d2} + \frac{d\Psi'_{d2}}{dt} + \frac{\pi}{\tau} \cdot v \cdot \Psi'_{q2} & \Psi'_{d2} &= L_2' \cdot i'_{d2} + L_h \cdot i_{d1} \\
 0 &= R_2' \cdot i'_{q2} + \frac{d\Psi'_{q2}}{dt} - \frac{\pi}{\tau} \cdot v \cdot \Psi'_{d2} & \Psi'_{q2} &= L_2' \cdot i'_{q2} + L_h \cdot i_{q1}
 \end{aligned} \tag{6 - 9} \tag{10 - 13}$$

From the (10 - 13) set of equations the currents are expressed. Afterwards the results are introduced into the relations (6 - 9). The following set of equations is then obtained:

$$\begin{aligned}
 \frac{d\Psi_{d1}}{dt} &= -R_1 \cdot \frac{1}{\sigma \cdot L_1} \cdot \Psi_{d1} + R_1 \cdot \frac{1-\sigma}{\sigma \cdot L_h} \cdot \Psi'_{d2} + u_{d1} \\
 \frac{d\Psi_{q1}}{dt} &= -R_1 \cdot \frac{1}{\sigma \cdot L_1} \cdot \Psi_{q1} + R_1 \cdot \frac{1-\sigma}{\sigma \cdot L_h} \cdot \Psi'_{q2} + u_{q1} \\
 \frac{d\Psi'_{d2}}{dt} &= R_2' \cdot \frac{1-\sigma}{\sigma \cdot L_h} \cdot \Psi_{d1} - R_2' \cdot \frac{1}{\sigma \cdot L_2'} \cdot \Psi'_{d2} - \frac{\pi}{\tau} \cdot v \cdot \Psi'_{q2} \\
 \frac{d\Psi'_{q2}}{dt} &= R_2' \cdot \frac{1-\sigma}{\sigma \cdot L_h} \cdot \Psi_{q1} - R_2' \cdot \frac{1}{\sigma \cdot L_2'} \cdot \Psi'_{q2} + \frac{\pi}{\tau} \cdot v \cdot \Psi'_{d2}
 \end{aligned} \tag{14 - 17}$$

Subsequently the given set of equations is rewritten in the matrix form as follows:

$$\begin{cases} \frac{d\hat{X}}{dt} = A \cdot \hat{X} + B \cdot U \\ \hat{Y} = C \cdot \hat{X} \end{cases} \tag{18 - 19}$$

where:

$$A = \begin{bmatrix} -\frac{R_1}{\sigma \cdot L_1} & 0 & \frac{R_1 \cdot L_h}{\sigma \cdot L_1 \cdot L_2'} & 0 \\ 0 & -\frac{R_1}{\sigma \cdot L_1} & 0 & \frac{R_1 \cdot M}{\sigma \cdot L_1 \cdot L_2'} \\ \frac{R_1 \cdot L_h}{\sigma \cdot L_1 \cdot L_2'} & 0 & -\frac{R_2'}{\sigma \cdot L_2'} & -\frac{\pi}{\tau} \cdot v \\ 0 & \frac{R_1 \cdot L_h}{\sigma \cdot L_1 \cdot L_2'} & +\frac{\pi}{\tau} \cdot v & -\frac{R_2'}{\sigma \cdot L_2'} \end{bmatrix}, \quad B = \begin{bmatrix} 1 & 0 \\ 0 & 1 \\ 0 & 0 \\ 0 & 0 \end{bmatrix},$$

$$C = \begin{bmatrix} \frac{1}{\sigma \cdot L_1} & 0 & -\frac{1-\sigma}{\sigma \cdot L_h} & 0 \\ 0 & \frac{1}{\sigma \cdot L_1} & 0 & -\frac{1-\sigma}{\sigma \cdot L_h} \end{bmatrix} \text{ and the vectors: } \hat{X} = \begin{bmatrix} \Psi_{d1} \\ \Psi_{q1} \\ \Psi'_{d2} \\ \Psi'_{q2} \end{bmatrix}, \quad U = \begin{bmatrix} u_{d1} \\ u_{q1} \end{bmatrix}, \quad Y = \begin{bmatrix} i_{d1} \\ i_{q1} \end{bmatrix}.$$

This set of equations is also called the Bocker's observer.

The maximum of the induced reaction is achieved when the melted metal doesn't move, i.e. the induced speed is at zero with respect to the stator, $v = 0$. This approximation may also be used in normal operation of the pump because the speed of the melted metal is usually much smaller than the synchronous speed of the pump. For example, for a given unit the synchronous speed is $v_s = 19,8 \text{ m/s}$, while at rated (or nominal) operation the speed of the melted metal results $v_N = 0,8 \text{ m/s}$.

The system of differential equations (18 - 19) is to be transformed into a system of difference equations with the sampling period T_e and follows the following recursive equations:

$$\begin{bmatrix} \Psi_{d1}(k+1) \\ \Psi_{q1}(k+1) \\ \Psi'_{d2}(k+1) \\ \Psi'_{q2}(k+1) \end{bmatrix} = \begin{bmatrix} 1-T_e \cdot \frac{R_1}{\sigma \cdot L_1} & 0 & T_e \cdot \frac{R_1 \cdot L_h}{\sigma \cdot L_1 \cdot L_2} & 0 \\ 0 & 1-T_e \cdot \frac{R_1}{\sigma \cdot L_1} & 0 & T_e \cdot \frac{R_1 \cdot M}{\sigma \cdot L_1 \cdot L_2} \\ T_e \cdot \frac{R'_2 \cdot L_h}{\sigma \cdot L_1 \cdot L_2} & 0 & 1-T_e \cdot \frac{R'_2}{\sigma \cdot L_2} & 0 \\ 0 & T_e \cdot \frac{R'_2 \cdot L_h}{\sigma \cdot L_1 \cdot L_2} & 0 & 1-T_e \cdot \frac{R'_2}{\sigma \cdot L_2} \end{bmatrix} \cdot \begin{bmatrix} \Psi_{d1}(k) \\ \Psi_{q1}(k) \\ \Psi'_{d2}(k) \\ \Psi'_{q2}(k) \end{bmatrix} +$$

$$+ T_e \cdot \begin{bmatrix} 1 & 0 \\ 0 & 1 \\ 0 & 0 \\ 0 & 0 \end{bmatrix} \cdot \begin{bmatrix} u_{d1}(k) \\ u_{q1}(k) \end{bmatrix}$$

$$\begin{bmatrix} i_{d1}(k) \\ i_{q1}(k) \end{bmatrix} = \begin{bmatrix} \frac{1}{\sigma \cdot L_1} & 0 & -\frac{1-\sigma}{\sigma \cdot L_h} & 0 \\ 0 & \frac{1}{\sigma \cdot L_1} & 0 & -\frac{1-\sigma}{\sigma \cdot L_h} \end{bmatrix} \cdot \begin{bmatrix} \Psi_{1d}(k) \\ \Psi_{1q}(k) \\ \Psi'_{2d}(k) \\ \Psi'_{2q}(k) \end{bmatrix} \quad (21)$$

The structure of the flux reconstructor is represented in Figure 7.

By means of the flux reconstructor, and the system of equations (10 - 13) the induced currents components are determined.

The power transferred to the liquid metal may be determined from the balance of power as follows:

$$P_{2tot} = [i]^T \cdot [u] - [i]^T \cdot [R] \cdot [i], \text{ în care: } [i] = \begin{bmatrix} i_{d1} \\ i_{q1} \\ i'_{d2} \\ i'_{q2} \end{bmatrix}, [u] = \begin{bmatrix} u_{d1} \\ u_{q1} \\ u'_{d2} \\ u'_{q2} \end{bmatrix}, [R] = \begin{bmatrix} R_1 & 0 & 0 & 0 \\ 0 & R_1 & 0 & 0 \\ 0 & 0 & R'_2 & 0 \\ 0 & 0 & 0 & R'_2 \end{bmatrix} \quad (22)$$

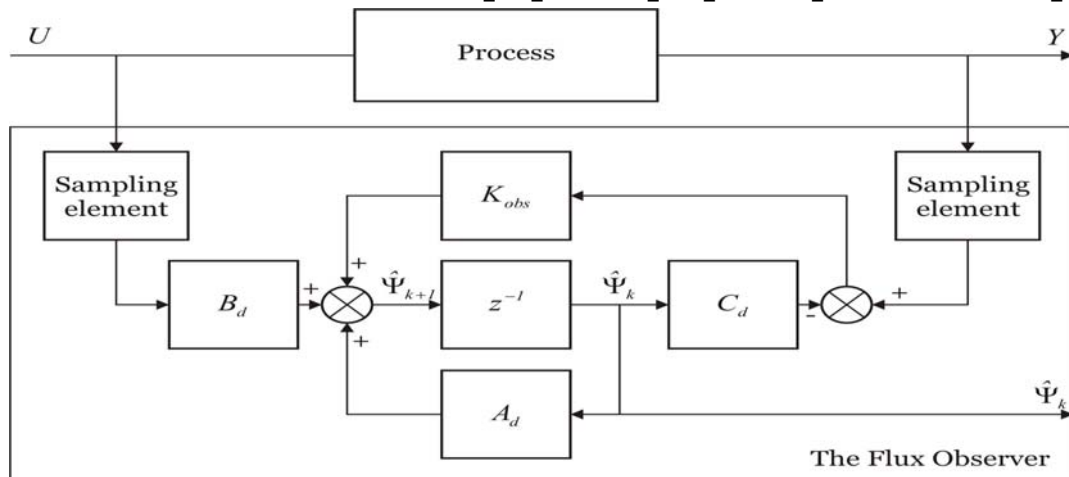


Figure 7. The flux observer.

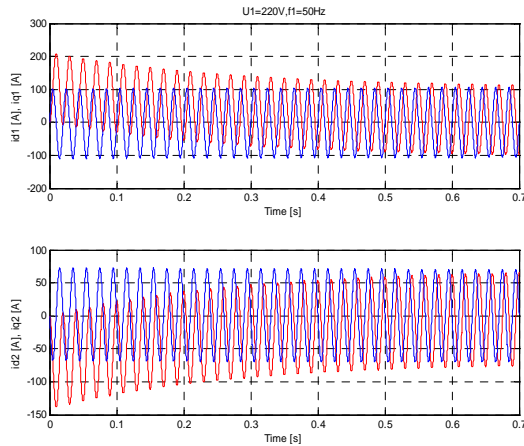


Figure 8. The currents components at start-up and in steady-state operation. Above: stator, below induced.

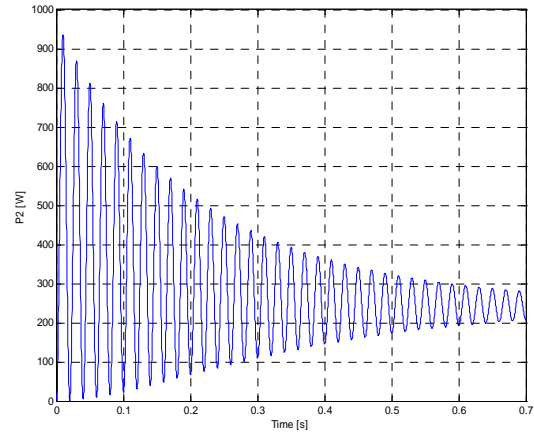


Figure 9. The transferred power to the induced at start-up and in steady-state operation- rated frequency.

The previous considerations have been implemented for a given induction electromagnetic pump designed with the procedure presented in [1]. The technical features of the pump are presented in Table 2.

Table 2. The technical features of the experimental induction electromagnetic pump.

No.	Denomination	Symbol	Units	Value
1	The rated supply voltage	U_{IN}	V	220
2	The rated frequency	f_{IN}	Hz	50
3	The rated flow rate	Q_{mN}	kg/s	22
4	No. of units	-	-	2
5.	Total power of a unit	P_t	W	9500
6.	The induced	-	-	cast-iron
7.	The pump's slope	s	°	10

The estimated values of the electric parameters of the pump are presented in Table 3. The computations have been performed according to the study [1]. To the practical implementation of the flux observer a software application has been conceived into the MatLab environment. The results are presented in Figures 8 and 9.

The currents components at start-up and in steady-state operation are presented in Figure 8.

Table 3. The estimated values of the electrical parameters of the experimental pump

No.	Denomination	Symbol	Units	Value
1	The phase resistance of the inductor	R_l	Ω	0.042361
2	The total inductance of the stator winding	L_l	H	0.0038067
3	The equivalent resistance of the melted metal referred to the number of stator turns	R'_2	Ω	5.9419e-006
4	The linkage inductance	L_m	H	0.0028573
5.	The inductancies coefficient	σ	-	0.75061

As seen from the computations, the induced reaction is rather weak in comparison with the classical induction machine. In Figure 9 the estimate of the induced transferred power is presented. At start-up, i.e. when the melted metal doesn't moves, the transferred power has a maximum while at normal operation the power decreases three times.

4. CONCLUSIONS

Within this paper an analysis of state observers implementation to estimate the transferred power to the melted metal into an electromagnetic pump is presented. This estimation is possible if a model of the system is available. The proposed method allows the magnetic flux components reconstruction. The computations performed into the MatLab environment are compatible to the experiments and design data of the pump under study. The further researches could enhance the usage of the observer to the melted metal flow rate estimation.

REFERENCES

- [1] Peşteanu, O. *Jgheab electromagnetic pentru transportul fontei topite*. Universitatea Transilvania din Braşov. Contract de cercetare nr. 126/1984
- [2] Fireşteanu, V. *Pomparea și antrenarea electromagnetică a metalelor topite*. Editura Tehnică, Bucureşti, 1986
- [3] Grellet, G., Clerc G. *Actionneurs électriques*, Edition Eyrolles, Paris, 2000.
- [4] Henneberger, G. *Electrical Machines 2*. Aachen University 2002.
- [5] Danila, A., A Direct- And Quadrature-Axis Approach To The Torque Estimation in an Eddy Currents Brake, In: International Symposium On Systems Theory, SINTES 13, Craiova – Romania, October 18-20 2007, pp 83 – 88.



ADAPTIVE GENETIC FUZZY SYSTEMS IN INDUSTRY: CURRENT FRAMEWORK AND NEW TRENDS

Tihomir LATINOVIC, Miroslav ROGIC, Milosav DJURDJEVIC

University of Banja Luka, Mechanical Faculty, BOSNIA & HERZEGOVINA

Abstract:

Adaptive genetic fuzzy systems are ability to solve different kinds of problems in various application domains. There is an increasing interest to mix fuzzy systems with learning and adaptation capabilities. Adaptive genetic fuzzy systems are very hybridizing the approximate reasoning method of fuzzy systems with the adaptive and evolutionary algorithms. Learning/optimization methods drawn from both fuzzy theory and genetic algorithms are used to find the optimal strategy. This paper provide an account of genetic fuzzy systems, with special attention to adaptive genetic fuzzy rule-based systems. After a brief introduction to models and applications of genetic fuzzy systems, critical evaluation is elaborated. The resulting expert system is an open system that uses frames, rules, fuzzy implication and connection matrices to produce a form of machine learning. Authors open questions for the future investigation of new trends in genetic fuzzy systems.

Keywords:

Fuzzy, Expert System, Genetic Algorithm

1. INTRODUCTION

Fuzzy systems successfully purposed to problems in classification [1.], modeling [2.] control [3.], in industry applications. The key for success was the ability of fuzzy systems to incorporate human expert knowledge.

One of the most approaches have been the hybridization attempts made in the framework of soft computing, were different techniques, such as neural and evolutionary, provide fuzzy systems with learning capabilities, as shown in Figure. 1. Neuro-fuzzy systems are one of the most successful and visible directions of that effort [4.,5.,6.]. A different approach to hybridization leads to genetic fuzzy systems (GFSs) [7.].

A GFS is basically a fuzzy system augmented by a learning process based on a genetic algorithm (GA). GAs are search algorithms, based on natural genetics, that provide robust search capabilities in complex spaces, and thereby offer a valid approach to problems requiring efficient and effective search processes [8.].

Genetic learning processes cover different levels of complexity according to the structural changes produced by the algorithm [9.], from the simplest case of parameter optimization to the highest level of complexity of learning the rule set of a rule based system. Parameter optimization has been the approach utilized to adapt a wide range of different fuzzy systems, as in genetic fuzzy clustering or genetic neuro-fuzzy systems.

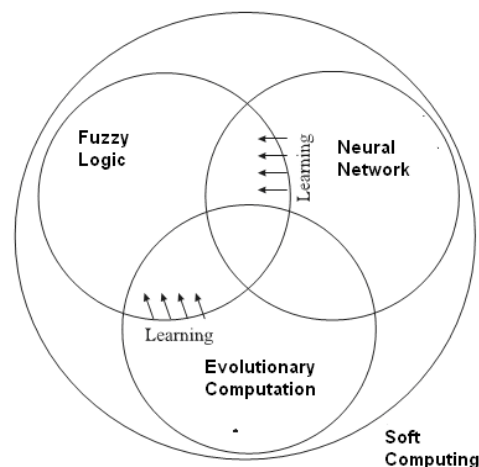


Figure 1 soft computing and learning in fuzzy system

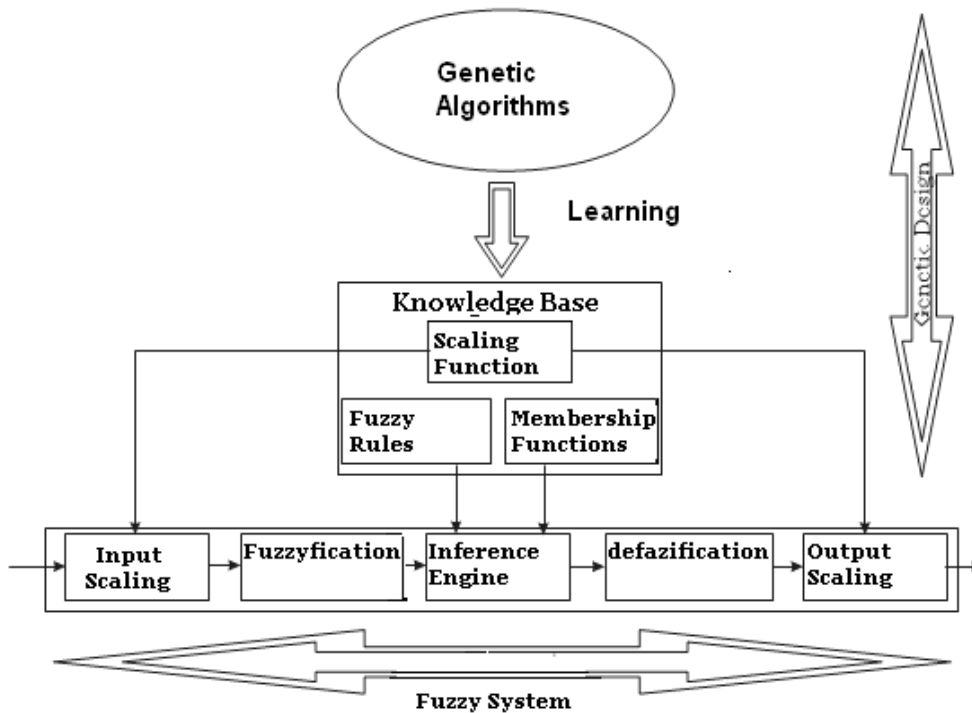


Figure. 2. Genetic design and fuzzy processing

Analysis of the literature shows that the most prominent types of GFRBSs are genetic fuzzy rule-based systems (GFRBSs) [10.], whose genetic process learns or tunes different components of a fuzzy rule-based system (FRBS). Figure. 2 shows this conception of a system where genetic design and fuzzy processing are the two fundamental constituents. Inside GFRBSs it is possible to distinguish between either parameter optimization or rule generation processes, that is, adaptation and learning.

2. GENETIC ALGORITHMS

GAs are general purpose search algorithms which use principles inspired by natural genetics to evolve solutions to problems [8.]. The basic idea is to maintain population of chromosomes (representing candidate solutions to the concrete problem being solved) that evolves over time through a process of competition and controlled variation.

A GA starts with a population of randomly generated chromosomes, and advances towards better chromosomes by applying genetic operators modeled on the genetic processes occurring in nature. The population undergoes evolution in a form of natural selection.

During successive iterations, called generations, chromosomes in the population are rated for their adaptation as solutions, and on the basis of these evaluations, a new population of chromosomes is formed using a selection mechanism and specific genetic operators such as crossover and mutation. An evaluation or fitness function must be devised for each problem to be solved.

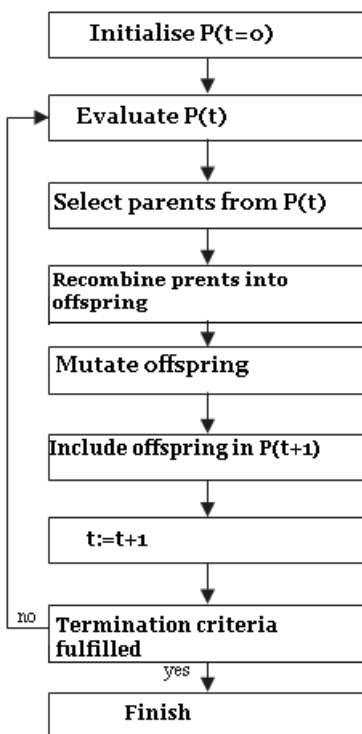


Figure. 3. Principal structure of a genetic algorithm

Given a particular chromosome, a possible solution, the fitness function returns a single numerical value, which is supposed to be proportional to the utility or adaptation of the solution represented by that chromosome.

Although there are many possible variants of the basic GA, the fundamental underlying mechanism consists of three operations: evaluation of individual fitness, formation of a gene pool (intermediate population) through selection mechanism, and recombination through crossover and mutation operators. Figure 3 illustrate this operation mode. The specific characteristics of the evaluation method are quite dependent on the application.

As previously stated, genetic learning processes cover different levels of complexity, from parameter optimization to learning the rule set of a rule based system. Genetic learning processes designed for parameter optimization usually fit to the description given in previous paragraphs, but when considering the task of learning rules in a rule based system, a wider range of possibilities is open.

3. GENETIC FUZZY RULE-BASED SYSTEM

The mean point is to employ an evolutionary learning process to automate the design of the knowledge base, which can be considered as an optimization or search problem.

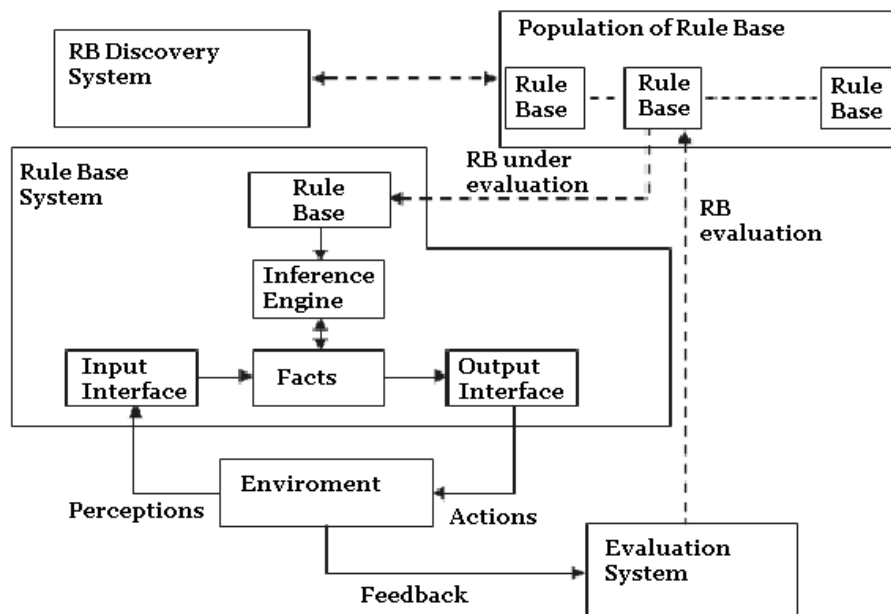


Figure. 4. Learning with the Pittsburgh approach

From the viewpoint of optimization, the task of finding an appropriate knowledge base (KB) for a particular problem, is equivalent to parameterize the fuzzy KB (rules and membership functions), and to find those parameter values that are optimal with respect to the design criteria. The KB parameters constitute the optimization space, which is transformed into a suitable genetic representation on which the search process operates.

The first step in designing a GFRBS is to decide which parts of the KB are subject to optimization by the GA. The KB of an FRBS does not constitute a homogeneous structure but is rather the union of qualitatively different components. KB of a descriptive Mamdani-type FRBS is comprised of two components:

- ✚ a data base (DB), containing the definitions of the scaling functions of the variables and the membership functions of the fuzzy sets associated with the linguistic labels, and
- ✚ a rule base (RB), constituted by the collection of fuzzy rules.

The decision on which part of the KB to adapt depends on two conflicting objectives: dimensionality and efficiency of the search.

A search space of a smaller dimension results in a faster and simpler learning process, but the obtainable solutions might be suboptimal. A larger, complete search space

that comprises the entire KB and has a finer dimensionality is therefore more likely to contain optimal solutions, but the search process itself might become prohibitively inefficient and slow.

First of all, it is important to distinguish between tuning (alternatively, adaptation) and learning problems:

- ✚ Tuning is concerned with optimization of an existing FRBS, whereas learning constitutes an automated design method for fuzzy rule sets that starts from scratch.
- ✚ Learning processes perform a more elaborated search in the space of possible RBs or whole KBs and do not depend on a predefined set of rules.

Summing up, the classical genetic learning procedures to evolve FRBSs are:

- ✚ Genetic tuning of the DB,
- ✚ Genetic learning of the RB,
- ✚ Genetic learning of the KB.

Although the review is by no means exhaustive, this section reviewed the most important approaches found in the literature.

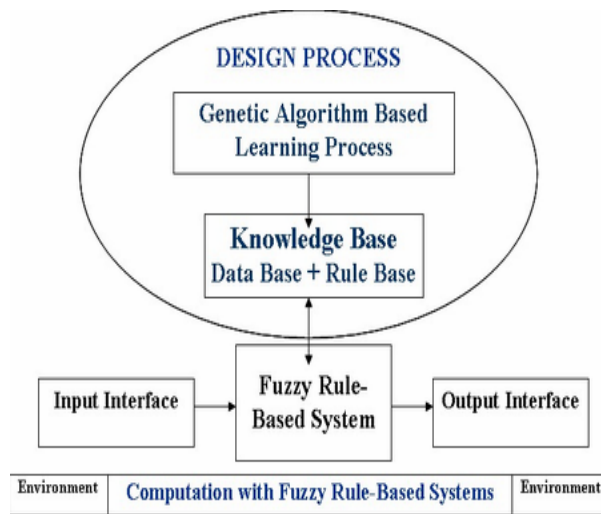


Figure 5. Genetic fuzzy systems

4. APPLICATIONS OF GENETIC FUZZY SYSTEMS

Authors provides a computational framework to address design, analysis and modeling problems in the context of uncertain and imprecise information. Its constituents fuzzy logic, neural networks, probabilistic computing and evolutionary algorithms are considered as complementary and synergistic partners rather than competing methodologies.

Neuro-fuzzy systems [5.] are by far the most prominent and visible representative of hybrid systems in terms of number of applications.

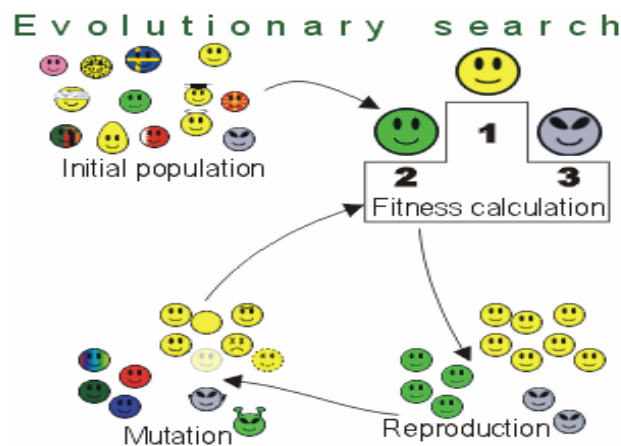


Figure 6. Evolutionary search

Compared to neuro- fuzzy systems, GFS applications until today remained less visible, in particular in an industrial setting.

In a second phase, the GA tunes the membership functions causing a local adaptation. Adaptation of membership functions for a controller with properly tuned scaling factors only results in a marginal improvement.

The role of the evolutionary algorithm is to adapt the number of rules and to fine tune the membership functions to improve the performance of fuzzy systems for estimation and control.

In [11.], Mizutani propose a hybrid neuro-genetic–fuzzy system for computerized colour prediction, a challenging problem in paint production.

Their architecture for colour paint manufacturing intelligence cannot be characterized as conventional GFSs in which the evolutionary algorithm optimizes the fuzzy knowledge base. Instead, colour expert knowledge is expressed by fuzzy rules.

Bonissone et al. apply evolutionary techniques to tune a fuzzy decision system [12.]. The fuzzy system automatically classifies the risk of an insurance application, which in turn determines the premium to be paid by the applicant.

In [14] Latinovic presents an approach to modeling genetic fuzzy real-time expert diagnostic system for PLC controlled manufacturing system in Tobacco Industry in Banjaluka. These approaches to modeling inspired by biological evolution are called evolutionary computation. It contains the design and engineering knowledge about the manufacturing system to be diagnosed.

The list of applications above indicates that GFSs can contribute to solve industrial and commercial problems. The major driving force behind this development is the need for low-cost solutions that utilize intelligent tools for information processing, design and optimization. GFSs can reduce the cost and time required to design, autonomously operate and maintain systems with a high degree of machine intelligence for control, prediction, modeling and decision making.

5. NEWTRENDS IN GENETIC FUZZY RULE-BASED SYSTEMS

In addition to the classical systems, here new directions to apply genetic (evolutionary) techniques to FRBSs are explored:

1. Genetic selection of fuzzy rule sets
2. Genetic feature selection
4. Learning knowledge bases via genetic derivation of data bases
5. Maintaining interpretability via multi-objective genetic processes
6. Genetic-based learning approaches considering different model structures
7. Genetic-based learning approaches with sophisticated genetic algorithms
8. Genetic-based machine learning approaches
9. Genetic fuzzy neural networks
10. Genetic fuzzy clustering algorithms

Until recently, there was no systematic procedure to design and develop fuzzy systems. A common approach was defining fuzzy systems based on expert knowledge and testing them to verify if the design is satisfactory. However, when expert knowledge is lacking or when considerable amount of data must be processed and analyzed, purely knowledge-based design approaches become limited.

Machine learning approaches have shown to be useful in these cases. For instance, neural networks can learn from data, but the linguistic representation of fuzzy rules and their transparency may be lost [13.].

GA-based approaches have been developed to learn:

- a) membership functions with fixed fuzzy rules ,
- b) fuzzy rules with fixed membership functions ,
- c) fuzzy rules and membership functions using (a) and (b) in alternate steps ,
- d) membership functions and RB simultaneously ,
- e) Rules and RB structure and parameters (granularity, rule antecedent aggregation operator, rule semantics, rule base aggregation operator, defuzzification, membership function shape and parameters) simultaneously.

6. CONCLUSIONS

The last decade has seen a large interest in technologies that have as their motivation some aspect of human function. Some of these, like artificial intelligence, can be seen to be rooted in the psychological domain. Others, like neural networks, genetic algorithms, and evolutionary programming, are inspired by reconsiderations of biological processes.

Common to all these so-called “intelligent technologies” is a need to represent knowledge in a manner that is both faithful to the human style of processing information as well as a form amenable to computer manipulation

This paper provided an account of the current status of GFSs after many years of considerable research and development effort. In addition to a brief overview of the field to address the classical models and applications, new trends have been identified. A critical evaluation of the contribution that GFSs bring to knowledge acquisition and fuzzy rule base design was conducted, and challenges for further developments in the field were outlined. From authors point of view we need to build hybrid intelligent systems that go beyond simple combinations.

Development of GFSs that offer acceptable trade-of between interpretability and accuracy is also a major requirement for efficient and transparent knowledge extraction. Discovery of more sophisticated and new evolutionary learning models of GFSs and its application to new areas and problems still remain as key questions for the future development trends of GFSs.

REFERENCES

- [1] Chi, H. Yan, T. Pham, Fuzzy Algorithms: With Applications to Image Processing and Pattern Recognition, World Scientific, Singapore, 1996.
- [2] W. Pedrycz (Ed.), Fuzzy Modelling: Paradigms and Practice, Kluwer Academic Press, Dordrecht, 1996.
- [3] D. Driankov, H. Hellendoorn, M. Reinfrank, An Introduction to Fuzzy Control, Springer, Berlin, 1993.
- [4] R. Fuller, Introduction to Neuro-Fuzzy Systems, Physica-Verlag, Wurzburg, 1999.
- [5] D. Nauck, F. Klawoon, R. Kruse, Foundations of Neuro-Fuzzy Systems, Wiley, New York, 1997.
- [6] P.P. Angelov, Evolving Rule-Based Models. A Tool for Design of Flexible Adaptive Systems, Physica-Verlag, Wurzburg, 2002.
- [7] D.E. Goldberg, Genetic Algorithms in Search, Optimization, and Machine Learning, Addison-Wesley, Reading, MA, 1989.
- [8] K. DeJong, Learning with genetic algorithms: an overview, Mach. Learning 3 (3) (1988) 121–138.
- [9] O. Cordo& n, F. Herrera, F. Ho+mann, L. Magdalena, Genetic Fuzzy Systems—Evolutionary Tuning and Learning of Fuzzy Knowledge Bases, World Scientific, Singapore, 2001.
- [10] E. Mizutani, H. Takagi, D.M. Auslander, J.-S.R. Jang, Evolving colour recipes, IEEE Trans. Systems Man Cybernet. (2000)
- [11] P.P. Bonissone, R. Subbu, K.S. Aggour, Evolutionary optimization of fuzzy decision systems for automated insurance underwriting, in Proc. of IEEE Int. Conf. on Fuzzy Systems FUZZ-IEEE’02, 2002
- [12] H. Takagi, I. Hayashi, NN-driven fuzzy reasoning, Int. J. Approx. Reasoning 5 (3) (1991)
- [13] Latinovic, T.; Jokanovic, S. & Rogic, M. (2008). A Genetic Fuzzy Real-Time Expert System in Tobacco Industry Banjaluka (2008)
- [14] D. Obradović, T. Latinović, K. Bošnjak, M. Šljivić: An Expert system with supports fuzzy rules: (Balcan Conference Solun Grece) 2002

energy of the turbine circuit. In this manner the energy transfer from the pump circuit to the turbine circuit is performed hydraulically.

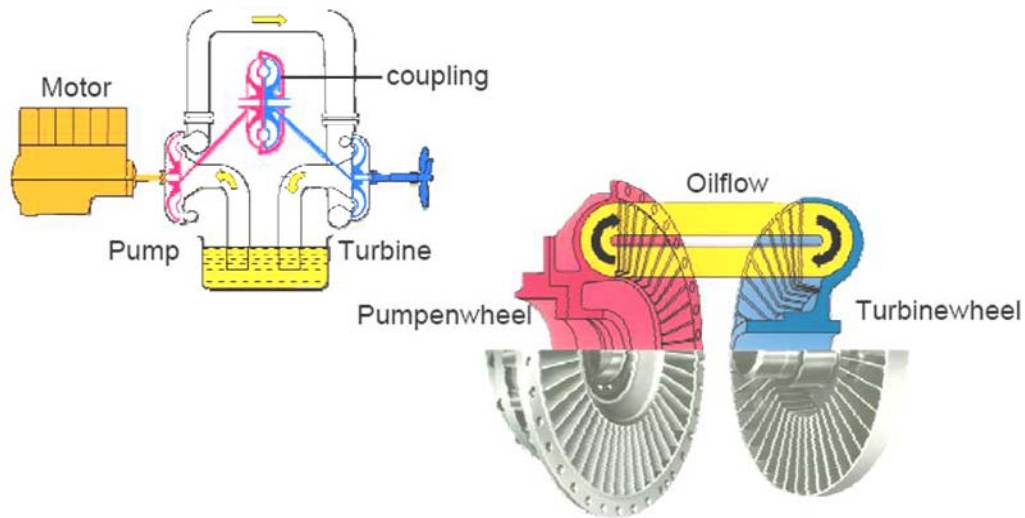


Fig. 2. The scheme of the principle of operation of the hydrodynamic coupler

2. THE ANALYSIS OF THE POSSIBILITY OF INSTALLING THE VOITH TURBOCOUPLER TVVS ON THE BELT CONVEYOR

The Voith couplers are specially designed to adjust to working with different working fluids:

- ✚ Oil-standard use,
- ✚ Water-especially in underground exploitation (TVV couplers),
- ✚ EP fluid (Environment Pollution-free Fluid) – biodegradable,
- ✚ Hi-fluid (High flash point fluid) - does not contain chlorinated hydrocarbon or phosphoric ester. The fluid density is smaller than water density.

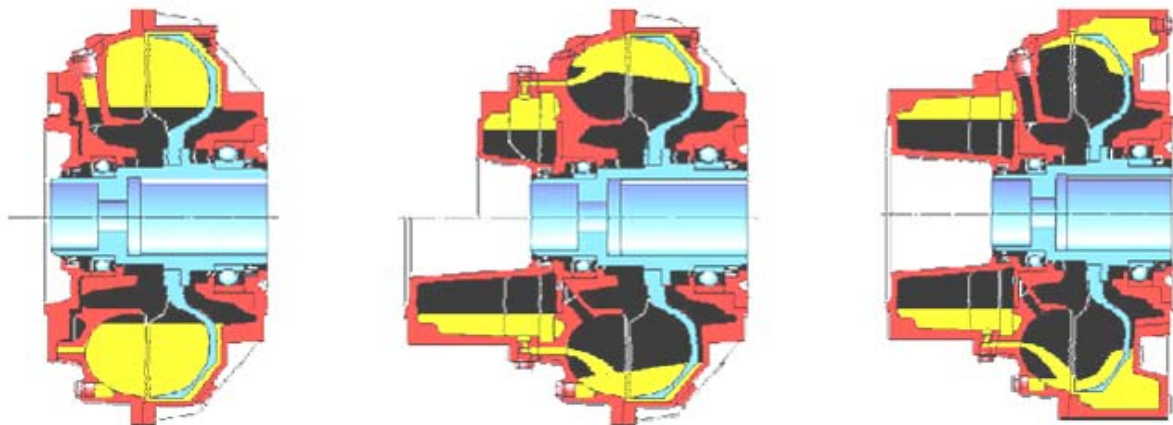


Fig. 3. The basic types of the couplers with the constant quantity of oil: T (on the left), TV/TVV (in the middle) and TVVS (on the right)

The consequences of irregular pouring of oil may be the following:

- ✚ When there is too much oil:
 - It takes more time to start the engine,
 - The engine cannot be started at all,
 - The engine cannot reach its nominal speed.
- ✚ When there is too little oil:
 - It takes more time to start the machine,
 - The machine cannot be started at all,
 - The machine operates with the increased slippage.

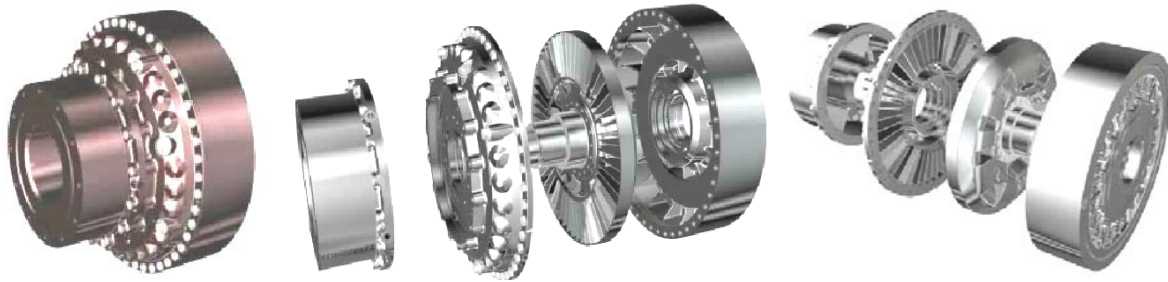


Fig. 4. The hydrodynamic coupler Voith 750 TVVS

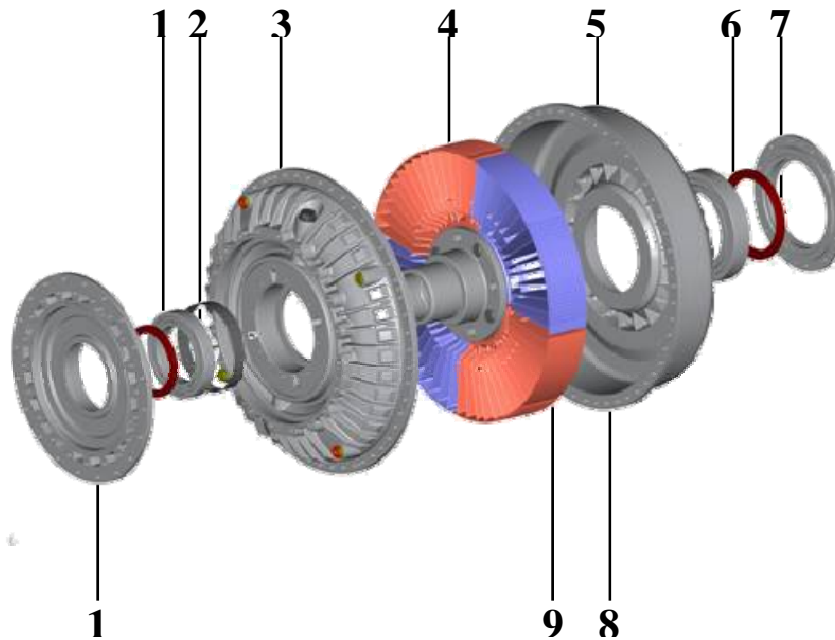


Fig. 5. The coupler parts: 1 - the radial sealing ring, 2 - the ball bearing, 3 - the outer working circuit, 4 - the inner working circuit, 5 - the coupler housing, 6 - the ball bearing, 7 - the radial sealing ring, 8 - the counterweight, 9 - the frictional covering, 10 - the lid

Table 1. The differences between the drive through the inner and the outer working circuit

	Drive through the outer working circuit	Drive through the inner working circuit
The weight of the coupler	Affects the reducer shaft.	Affects the engine shaft.
Inertia	Less inertia on the reducer side (fewer blows in the event of a sudden blockage).	Greater inertia on the reducer side.
Pouring of the fluids and the amount control	Easy - the coupler housing turns around even if the brake is closed.	The entire machine must be started in order to perform inspection.
Starting	Always acts the same at starting.	Emptying of the slowdown chamber depends on the characteristics of starting –the starting can be problematic during the blockage of the belt conveyor.
Cooling	Always the best possible.	Less-especially during the starting and blockage.
Starting characteristics	The Voith turbo couplers are optimal for starting the belt conveyors through the outer working circuit (the mixed profile in the inner working circuit).	
Slippage	Less.	Greater.
Brake installation	The construction with a shaft / additional brake flange necessary.	The lower price for the brake installed on the elastic coupler.

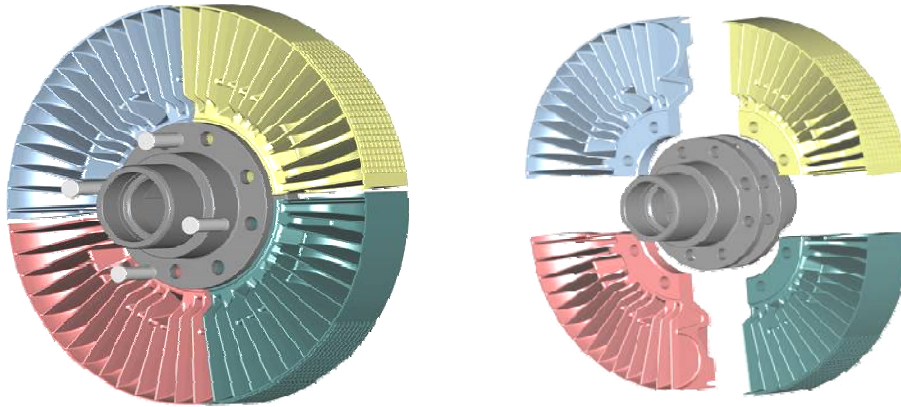


Fig. 6. The inner working circuit has freely movable separate segments

The special properties of TVVS coupler in comparison to the other types are:

- ✚ the lengthened slowdown chamber and the additional rim chamber,
- ✚ this type has thermal capacity increased by 15% which allows the coupler to be started more often,
- ✚ the heat removal is faster by 10% providing faster cooling and shortening the period between two consecutive starts.

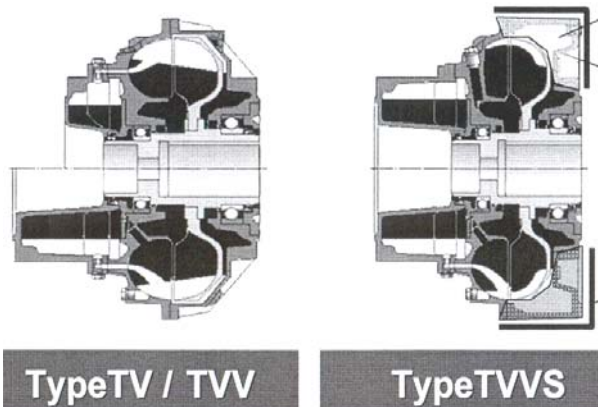


Fig. 7. The comparison of the different types of turbo couplers

3. CONCLUSION

Due to the characteristics of the hydrodynamic couplers, there exists the possibility of their application in belt conveyors in coal mines on condition of removing certain flaws which even this highly sophisticated equipment is not immune to. Generally speaking, the turbo couplers have many advantages and therefore should be included in exploitation as soon as possible.

REFERENCE

- [1] Krsmanović Lj., Gajić A.: *Turbomašine, hidrodinamički prenosnici snage*, Mašinski fakultet, Beograd, 1998.
- [2] Voith Turbo GmbH & Co. KG: katalogi, prilozi, aplikacioni programi, crteži, slike i ostalo.
- [3] Marković S., Erić D., Veličković D.: *Analysis of testing the hydrodynamic coupler on the belt conveyor used for open-pit mining in the coal mine*, 12th International scientific conference „Mechanical Engineering 2008“, Proceedings, Bratislava, Slovakia, 13÷14. November 2008.



WITH SPIDER8 ON RAILS

¹. Tiberiu Ștefan MĂNESCU, ². Ion SIMION, ². Nicușor Laurențiu ZAHARIA

¹. University “Eftimie Murgu”, Reșița, ROMÂNIA

². Romanian Railway Authority – AFER, București, ROMÂNIA

Abstract:

The carrying of heavy trains on large inclines can produce the breaking of the draw hook. The railway freight operator, want to carry long trains because of the economic reasons. This paper will present the steps of tests performing in purpose to measure the tensile forces from the locomotive draw hook equipped with strain gages. The purpose of the tests was increasing the tonnage of the trains on the inclines (the tonnage of the trains on the inclines is restricted by railway regulations).

Keywords:

Hottinger, Spider8, Catman, strain gauges

1. INTRODUCTION

Circulation on Romanian Railways is done under regulations in purpose to ensure optimal conditions of safety for passenger and freight trains.

From the point of view of passenger options there are alternatives at trains (cars, buses etc.), but regarding the freight transport there are some products which it will be always carry by the trains (cereals, oil, coal etc.).

If the freight trains run on plate ground, there aren't any problems if there is even one electrical locomotive of 5100 kW power. But, if the train run on inclines (which in Romania can have the value of 25‰) then a second locomotive it is necessary depending of the total length of train or his weight.

Romanian railways freight operators from Romania have electrical locomotives on four or six axles. If they use more than one locomotive at one train on the inclines the solve the problem of additional needed power, but another question appears: will the locomotive hook break it?

In purpose to measure the forces which appear in the drawing hook, one of the methods which can be used is applying strain gauges on the hook and measuring of the strains during the train's circulation.

2. MEASUREMENT POINTS, DEVICES AND TESTS

The measurements were performed with Hottinger Spider8 device connected to a laptop. The acquisition software used was Catman 4.5 also from Hottinger.

For simple loads (tensile/compression for example) it is necessary to glue strain gauges like those presented in figure 1.a.

Because any transducer is sensitive to different types of loads in the same time, the strain gauge glued on it, measure a strain witch represents the algebraic sum of the strains for each load type. The separation for each load type can be done if are glued more strain gauges.

In the tensile load, principal strain 1 is parallel with the longitudinal axe of the elastic element and principal strain 2 is perpendicular on principal strain 1.

The coupling hook it is an assembly of many articulated components. The thread axe where the strain gages were glued is load only with tensile forces. A full

Wheatstone bridge was used for measuring the tensile forces from the drawing hook of the locomotive (figure 1.b and figure 1.c.). The strain gauges were connected to Hottinger Spider8 measuring device.

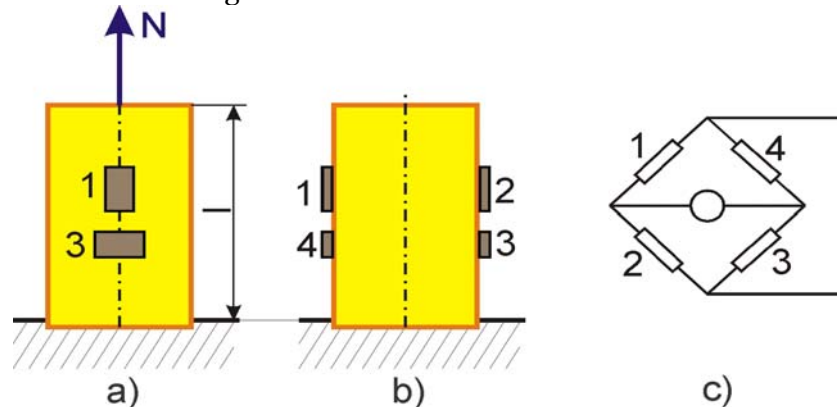


Figure 1 Tensile/compression loads transducer

In fig. 2 is shown the drawing hook of the locomotive which has strain gauges glued on it.



Figure 2 Drawing hook with strain gauges

The drawing hook was mounted the second locomotive and the first wagon of the train.

The measuring of tensile forces was performed in two variants of locomotive coupling: (EA+EC and EC+EC), where EA is electrical locomotive with six axles, 5100 kW power and EC is electrical locomotive with four axles, 3400 kW power.

The tests was done between railway stations Drobeta Turnu Severin – Șimian – Balota – Prunișor (Balota is the highest point of an incline with the maximum value of 29‰).

The performed tests were:

- ✚ Between railway stations Șimian and Balota the locomotives were coupled EA+EC, the train weight was 1218t;
- ✚ Between railway stations Drobeta Turnu Severin and Balota the locomotives were coupled EC+EC, the train weight was 1218t;
- ✚ Between railway stations Prunișor and Balota the locomotives were coupled EA+EC, the train weight was 2960t.

3. RESULTS

The maximum values of measured tensile forces are presented in table 1.

Table 1. The maximum values of measured tensile forces

Between	Force [kN]
Șimian – Balota	470,2
Dr. Tr. Severin – Balota	384,8
Prunișor – Balota	457,6

The graphic representation of the tensile forces it is shown in fig. 3÷5.

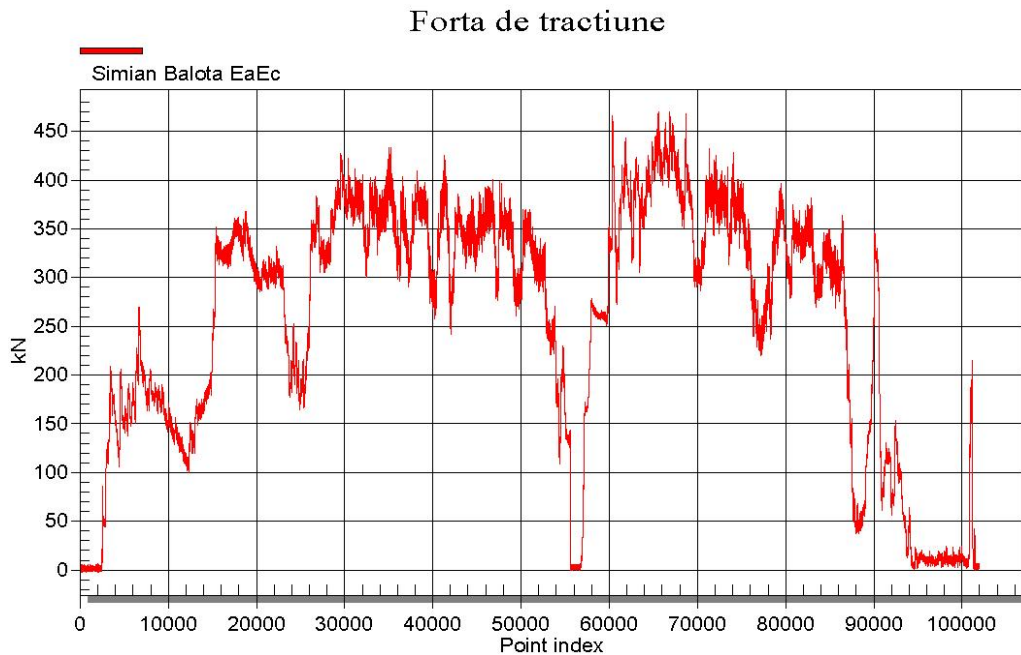


Figure 3 Locomotive coupled EA+EC

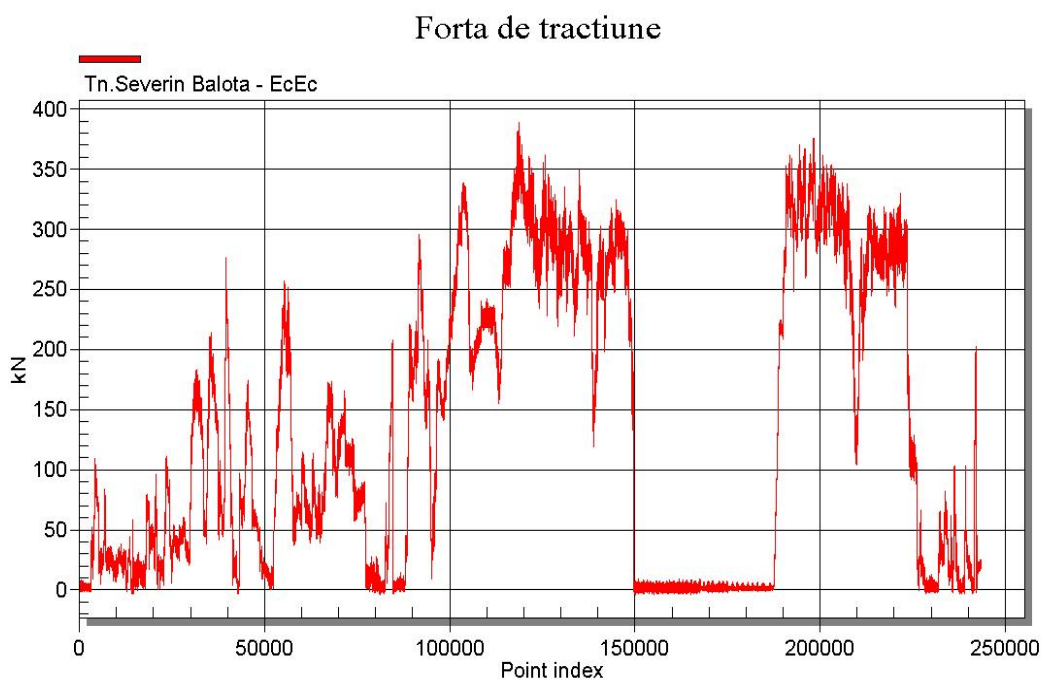


Figure 4 Locomotive coupled EC+EC

Forta de tractiune

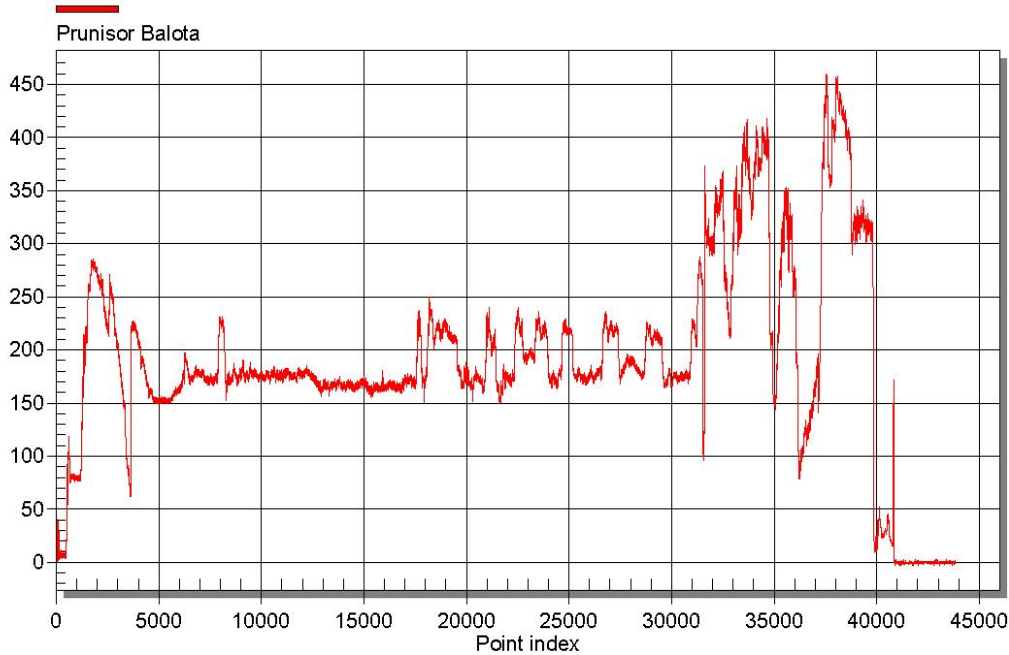


Figure 5 Locomotive coupled EA+EC

4. CONCLUSION

The results obtained after the finishing the tests can be used to adjust the weight of the train by increasing the weight of those but only if the technical condition of the locomotives is optimal especially from the point of view of weight balance on axle and good maintenance of the sanders.

In all cases which was study during those tests it was prove that when two locomotives are used is better that first to be an EC type locomotive.

REFERENCES

- [1] Hoffman, K. – *An Introduction to Measurement using Strain Gages*, HBM GmbH Darmstadt, 2005
- [2] Mănescu T.Ș., Copaci I., Olaru S., Creangă F. – *Tensometria electrică în cercetarea experimentală*, Ed. Mirton Timișoara, 2006
- [3] ***** – *Catman 4.5 User's Guide*, HBM GmbH, 2004
- [4] ***** – *Spider8 Operating Manual*, HBM GmbH, 2004
- [5] Mănescu T.Ș., Simion I., Zaharia N.L., Bîtea C.V., Bălan G. – *Measuring Of The Tensile Forces In The Draw Hook Of The Electrical Locomotives With Strain Gauges*, *The Annals of “Dunărea de Jos” University Of Galați* 2008.



EXAMINATION OF REFRIGERATOR ENGINES WITH THE METHOD OF VIBRATION DIAGNOSIS

Lajos TÓTH

University of Szeged, Faculty of Engineering, HUNGARY

Abstract

I have examined the bearings of three cooling-compressor engines with the intention to gather information on their status. Power of the engines 315 kW, rpm.: 2950/min. I have used a type SPM A2011 shock pulse analyzer for my examinations. With the help of this apparatus I have made shock pulse and effective vibrational force (horizontal, vertical, axial ways) measurements. I have made concluded from condition of the bearings, and the suggestion of the intervention.

Participating at: SECTION 5



ON THE ENERGETIC CHARACTERISTICS OF THE SHOCK INSULATORS OF RAILWAY VEHICLES

Ion COPACI

University „Aurel Vlaicu” Arad, ROMANIA

Abstract

The paper presents the results of experimental studies on the behaviour of bearing structures and shock insulators of railway vehicles during the shock caused by collisions.

The evolutions of energy parameters depending on the collision velocity are highlighted as well as the experimental values of certain kinematic and force parameters as response functions of the considered mechanical system to the action of excitations caused by the shocks that appear in use.

The paper contains notions related to the theory of shocks caused by collisions of railway vehicles as well as an experimental chapter which, together with the first part, highlight the importance of using shock insulators with a higher capacity for storing potential deformation energy, in order to reduce the maximum values of the response parameters of the considered mechanical system and also to protect the vehicles against the shocks that appear in use.

Keywords:

testing, collision, shock insulators, stored or dissipated potential deformation energy.

1. INTRODUCTION

Due to current tendencies to increase travel velocities and car masses by allowing increasingly larger axle loads, railway equipment shows a series of special problems regarding shock loads that appear during collisions. Collision of railway vehicles occurs during use, during car coupling operations, triage manoeuvres and during travel, as a consequence of sudden breaking or of a change in coupling systems [1].

The shock caused by railway vehicle collisions results in the transmission of forces and accelerations of considerable magnitudes, which determine:

- ✚ strains on the resistance structure of the cars (chassis, body) and bogies;
- ✚ strains of the internal equipment and facilities of passenger cars;
- ✚ strains of different devices, mechanisms, functional equipment of freight cars;
- ✚ accelerations transmitted to the transported freight, which can endanger their integrity and that of the anchoring or packaging systems;
- ✚ accelerations transmitted to passenger cars with considerable consequences on the comfort of the passengers.

In order to insulate and protect against longitudinal shocks, railway vehicles are equipped with shock insulators.

2. THE COLLISION PROCESS

The time evolution of the energetic parameters leads to the following observations on the collision process (figure 1) [3], [5], [6], [7]:

1. At the starting moment of the collision, $t = t_1 = 0$, the kinetic energy of the mechanical system composed of the vehicles, $E_c(t)$ is maximum.

2. On the interval $(0 - t_{12})$ the kinetic energy of the colliding car, $E_{c1}(t)$, decreases, and that of the collided car, $E_{c2}(t)$ increases. Their sum, $E_c(t)$, considerably decreases on the account of the transformation into stored potential energy by the bumpers W_e , cars $W_{ev} = W_{es} + W_{eb}$ and load W_{ei} .

3. At t_{12} , the kinetic energy of the cars is minimum:

$$E_c(t_{12}) = E_{c12} = \left[(m_1 + m_2) \cdot v_{12}^2 \right] / 2 \quad (1)$$

where:

m_1 – mass of the colliding car;

m_2 – mass of the collided car;

the stored potential energy being maximum:

$$E_p = W_e + W_{ev} + W_{ei} \quad (2)$$

4. On the interval ($t_{12} - t^*_{12}$) the process of transforming stored potential deformation energy into kinetic energy begins, together with the process of dissipating potential energy.

5. At the moment t^*_{12} the kinetic energy of the cars is equal to the kinetic energy of the cars at t_2 :

$$E_c(t^*_{12}) = E_c(t_2) - E^*_c = E^*_{c1} + E^*_{c2} \quad (3)$$

Furthermore, the sum between stored and dissipated potential energies (by the bumpers W_a , the cars W_{av} and the freight W_{ai}) is equal to the dissipated potential energy at t_2 :

$$(W_e(t^*_{12}) + W_{ev}(t^*_{12}) + W_{ei}(t^*_{12})) + (W_a(t^*_{12}) + W_{av}(t^*_{12}) + W_{ai}(t^*_{12})) = E_c - E_c(t^*_{12}) = E_c - E^*_c = W_a + W_{av} + W_{ai} \quad (4)$$

6. On the interval ($t^*_{12} - t_2$) the kinetic energy of the cars E^*_c remains constant, under the conditions of the compensation of the drop in stored potential deformation energy by dissipation of potential energy from the system.

7. At the moment t_2 the energy balance is:

$$E_c = (m_1 \cdot v_1^2) / 2 = E^*_c + (W_a + W_{av} + W_{ai}) \quad (5)$$

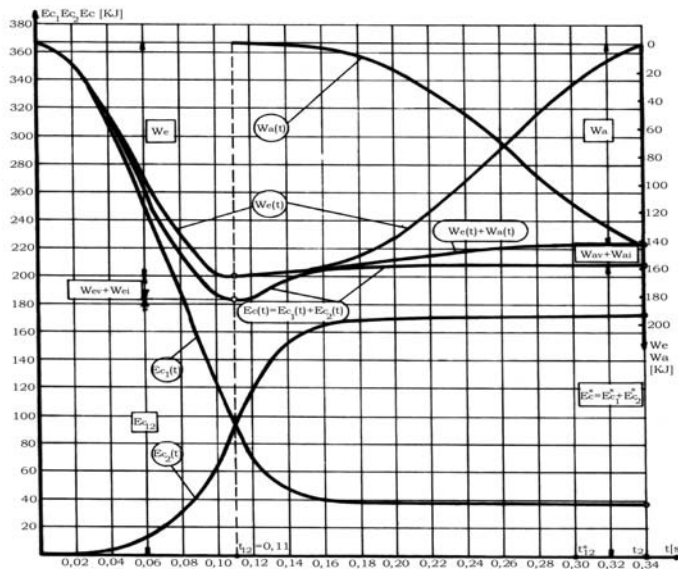


Figure 1

8. Using buffers with superior dynamic characteristics, which store an increased amount of potential deformation energy, has as a direct consequence the decrease of the effects caused by the shock due to collision.

The diagram in figure 1 was drawn experimentally for the motion and energetic parameters resulting from the collision process of two cars equipped with high capacity shock insulators, category C (UIC – 526-1), the colliding car having a mass $m_1=80$ t, and the collided car $m_2=80$ t, collision velocity $v_1=3,028$ m/s. The experimental determinations comprised of $a_2(t)$, the forces transmitted through the shock insulators $F(t)$, their contractions $D(t)$, their stored potential energy W_e as well as the dissipated energy W_a .

3. ENERGY FACTORS OF THE SHOCK CAUSED BY COLLISION

Against shocks that appear longitudinally during the use of the cars, the railway vehicles are equipped with shock absorbers (bumpers, central coupling dampeners) [8]. [9]. The use of bumpers or central coupling dampeners with high dynamic characteristics has the following consequences:

- ✚ the spectacular decrease of the maximum transmitted forces to the vehicles, with consequences on the protection of resistance structures by decreasing specific deformations and the stresses caused by the shock of collision;
- ✚ the lowering of the level of transmitted accelerations to the vehicles, down to a value that ensures a necessary protection of the freight, vehicle equipment and amenities, as well as an increased passenger comfort.

The following specific energy factors are defined, whose variation with the collision velocity $v = v_1 - v_2$ represents the energy characteristics of the shock caused by the vehicles' collision occurring on the time interval (0 - t_2):

1. The $2\beta = f(v)$ factor [2], which characterizes the shock of railway vehicles, represents the ratio between the potential deformation energy stored by the shock absorbers W_e and the potential energy stored by the system composed of the two vehicles E_p :

$$2\beta = W_e / E_p \quad (6)$$

2. The $2\lambda = f(v)$ factor is the ratio between the potential deformation energy stored by the bearing structures of the vehicles W_{es} and E_p :

$$2\lambda = W_{es} / E_p \quad (7)$$

If the vehicles are identical from this point of view, then $\lambda_1 = \lambda_2 = \lambda$.

3. The $2\delta = f(v)$ factor represents the ratio between the potential deformation energy stored by the elastic elements of the vehicles' suspensions W_{eB} and E_p :

$$2 \delta = W_{eB} / E_p \quad (8)$$

If the vehicles' suspensions are identical, it can be considered that $\delta_1 = \delta_2 = \delta$.

4. The $2 \chi = f(v)$ factor represents the ratio between the potential energy stored by the equipment and the freight of the vehicles W_{ei} and E_p :

$$2\chi = W_{ei} / E_p \quad (9)$$

If the vehicles are identical from this point of view, then $\chi_1 = \chi_2 = \chi$. It is obvious that:

$$2\beta + 2\lambda + 2\delta + 2\chi = 1 \quad (10)$$

It is extremely important to take into consideration the fact that the resistance structures, the elastic elements of the suspension, the equipment as well as the nature and quantity of the freight are established by criteria other than that of the response to the longitudinal shock caused by collisions. Thus, the only practical method of reducing the effects of the shock is to increase the potential deformation energy stored by the shock insulators. Hence, it becomes clear why the $2\beta = f(v)$ factor represents the specific energy factor that characterizes the shock phenomenon in railway vehicles. This specific energy characteristic directly influences the unwanted consequences of the shock.

4. EXPERIMENTAL STUDY

The 95 m³ liquid tank car on 4 axles with 22,5 t/axle, was put up to the collision testing, according to the testing conditions imposed by the UIC in report RP17 of the ORE B12 committee. The loaded car collision tests are presented, during which the tested car, with mass $m_2 = 90$ t, was loaded with water and equipped with category C buffers (according to UIC 526-1); the colliding car was a freight car with mass $m_1 = 80$ t loaded with sand equipped with category C shock insulators (according to UIC 526-1) [4].

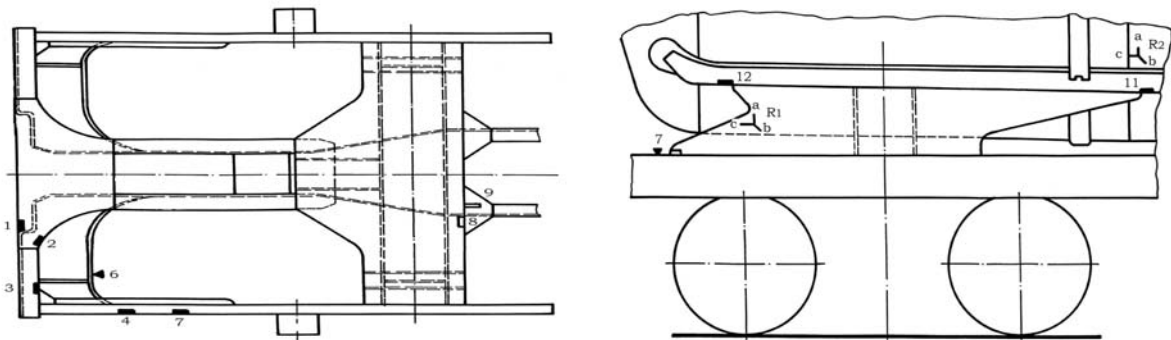


Figure 2

The placement of the transducers in order to experimentally determine the relative deformations is shown in figure 2, and the results of the measurements are presented in tables 1-3 (table 1 contains the results of the preliminary measurements, tables 2 and 3 show the results of the measurements for the series of 40 collisions).

Table 1.

Collision no.	V(km/h)	F ₁ (MN)	F ₂ (MN)	F(MN)	a (g)
1	8,9	0,48	0,57	1,05	3,04
2	11,2	0,70	0,79	1,49	4,19
3	13,5	0,92	1,05	1,97	5,33
4	15,0	0,98	1,14	2,12	6,09

Table 2.

Collision no.	V (km/h)	TER σ [N/mm ²]						
		1	2	8	11	4	6	9
10	15,0	243,1	-123,6	-173,0	-352,8	-164,8	214,8	-140,1
20	15,0	247,2	-119,5	-173,0	-342,0	-160,7	214,2	-144,2
30	15,0	239,0	-119,5	-181,3	-349,2	-160,7	226,6	-148,3
40	15,0	243,1	-119,5	-173,0	-352,8	-164,8	222,5	-140,1

Table 3.

Coll. no.	V (km/h)	TER σ [N/mm ²]			ROZETA R ₂ [N/mm ²]			
		3	7	12	σ_1	σ_2	σ_E	α (rad)
10	15,0	292,5	-243,1	214,2	-77,9	-162,1	140,4	1,61
20	15,0	271,9	-247,2	210,1	-77,9	-162,1	140,4	1,61
30	15,0	284,3	-243,1	214,4	-80,2	-162,8	140,1	1,60
40	15,0	271,9	-243,1	197,8	-76,6	-157,4	136,3	1,59

5. CONCLUSIONS

The study of the experimental results leads to the following conclusions:

- ✚ For a collision velocity of $v = 15$ km/h, the force transmitted to the shock insulators is in the range of (2,09 - 2,22) MN. The force $F = 3$ MN can be reached at velocities higher than the collision velocity of $v = 15$ km/h. Consequently, the repeated shock test (40 collision series) was conducted with the maximum collision velocity allowed by the RP17 ORE B12, meaning $v = 15$ km/h.
- ✚ The acceleration transmitted to the car at a collision velocity of $v = 15$ km/h is between (5,9 - 6,28) g, values that are inferior to those recorded in the case of using category A shock insulators.
- ✚ It is observed that the relative deformations and stresses, experimentally determined for the measurement points considered are below the flow limit $\sigma_c = 360$ N/mm², increased by 30% in accordance to the shock behaviour of the steels used in the construction of the railway car. Also, we consider that the use of shock insulators with a lower capacity for storing potential deformation energy would have led to the transmission of forces during the collision process that would have reached values of approximately 3MN, which would have led to the appearance of relative deformations in the most strained points which exceed the elasticity limit, thus creating the risk of occurrence of permanent deformations.
- ✚ The resistance structure of the chassis, the fixing elements for the tank on the chassis and the tank had an elastic behaviour. Residual deformations were not recorded at any measurement point. Investigations were conducted on the state of the car resistance structure, both visually and by using the penetrating liquid method, especially in the tank fixing region (transducers 11 and 12), as well as in the high strain areas (transducers 1 and 6) of the support beam. The collision testing prove that the technical solutions adopted correspond to the requirements imposed by vehicle use.

Using shock insulators with a high capacity for storing and dissipating potential deformation energy leads to the decrease of the unwanted effects of the shock caused by collision in the use of railway vehicles:

- ✚ permanent deformations of the elements of the resistance structures of railway vehicles;
- ✚ deterioration of amenities and functional equipment;
- ✚ ensuring the integrity of the transported freight and the fixing and packaging systems;
- ✚ eliminating the consequences that must be considered in appreciating passenger comfort.

REFERENCES

- [1] Copaci I., Trif E. ș.a. „Aplicarea metodei tensometrice pentru calcularea forței transmise și a lucrului mecanic înmagazinat de amortizoarele de șoc în timpul tamponării”. Revista Transporturilor și Telecomunicațiilor nr. 3 la al II-lea Simpozion Național de Tensometrie cu participare internațională, Cluj Napoca - 1980.
- [2] Copaci I. „Contribuții asupra comportării structurilor vagoanelor la solicitările provocate de șocul longitudinal produs la tamponare”. Teza de doctorat, Universitatea „Politehnica” Timișoara, 1996.
- [3] destinați echipării vehiculelor feroviare”. Simpozionul Internațional „UNIVERSITARIA ROPET 2003”, 16-18 octombrie, 2003, pag. 85-90.
- [4] Copaci I. „Cercetări asupra încercărilor de tamponare cu vagon gol și încărcat la vagonul cisternă pe 4 osii 95 mc pentru transport produse petroliere ușoare” - contract de cercetare I.C.P.V. Arad pentru "ASTRA" Vagoane Arad, 181/1993.
- [5] Sebe an I., Copaci I., „Teoria sistemelor elastice la vehiculele feroviare”, Editura Matrix Rom Bucure ti – 2008.
- [6] Tănăsioiu Aurelia, Copaci Ion, „Study on the Sock caused by Collision of Railway Vehicles”, International Journal of Mechanics, ISSN 1998-4448, pag. 67-76, www.naun.org/journals/mechanics.
- [7] Tănăsioiu Aurelia, Copaci Ion, „Study on the Behaviour of the Self-Unloading SSDT Train Upon the Shock Caused by Collisions”, WSEAS Conferences, Computer and Simulation in Modern Science, vol. II, ISSN 1790-5117, ISBN 978-960-474-032-1, www.wseas.org.
- [8] Aurelia Tanasoiu, Ion Copaci – Study on the evolution of kinematic parameters during the shock caused by railway vehicle collision, Simpozionul Internațional “INTERPARTNER” 22-27 sept. 2008, Alusta, Crimea.
- [9] Aurelia Tanasoiu, Ion Copaci – On the shock caused by railway vehicle collision, Al XVII-lea Seminar International de stiinte Tehnice, “INTERPARTNER” 22-27 sept. 2008, Alushta, Crimea, Ucraina.

ON THE STATIC AND DYNAMIC CHARACTERISTICS OF THE SHOCK INSULATORS EQUIPPING RAILWAY VEHICLES

Aurelia TĂNĂSOIU, Ion COPACI

Universitatea "Aurel Vlaicu" Arad, ROMANIA

Abstract

The paper presents theoretical notions regarding the shock due to collisions of railway vehicles as well as a study on the applied methodology used to experimentally determine the static and dynamic characteristics of the bumpers that equip railway vehicles. The experimental stand, the transducers, the measurement, recording and data processing apparatus are also presented.

The experimental force as a function of displacement (contraction) diagrams are presented for the shock insulators as well as the characteristics obtained during the static testing, both for normal temperature and extreme temperatures (+50°C and -40°C). Furthermore, the paper contains a study on the dynamic characteristics obtained for collision velocities between 6,15 km/h and 14,7 km/h with the appropriate conclusions regarding the category of classification of the elastic element that equips the studied bumpers (shock insulators) in order to categorize them in one of the A, B or C categories according to the international norms of the European railways, UIC 526-1.

Keywords:

shock insulators, static characteristics, dynamic characteristics

1. EXPERIMENTAL DETERMINATIONS

The testing for shock insulators [6], [8], [9], [10], [11] was conducted according to the prescription of the UIC 526-1 document. From the testing program presented in UIC 526 - 1 file the following tests were conducted:

1. Testing in order to determine the static characteristics;
2. Testing in order to determine the static characteristics at extreme temperatures -40°C and +50°C;
3. Testing in order to determine the dynamic characteristics.

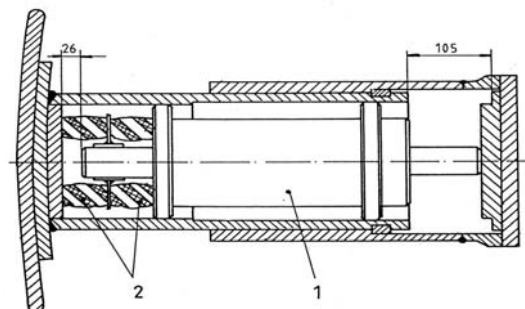


Fig.1 Shock insulator (1. Silicone dampener; 2. Rubber elastic elements)

1.1. Static characteristics

Test at +15°C. For the static test, a number of 2 shock insulators were studied (fig. 1) [4], [7]. The characteristic parameters of the category C shock insulators are imposed by the UIC 526-1 file and are the following:

- | | |
|---------------------------------|----------------|
| - Precompression force | 10 ÷ 50 KN; |
| - Force after 25mm compression | 30 ÷ 130 KN; |
| - Force after 60mm compression | 100 ÷ 400 KN; |
| - Force after 100mm compression | 400 ÷ 1000 KN; |

- stored energy (W_e) $\geq 12.500 \text{ J};$
- absorbed energy (W_a) $\geq 0,5 W_e.$

The experimentally determined characteristic diagrams of the shock insulators are shown in figures 2 and 3.

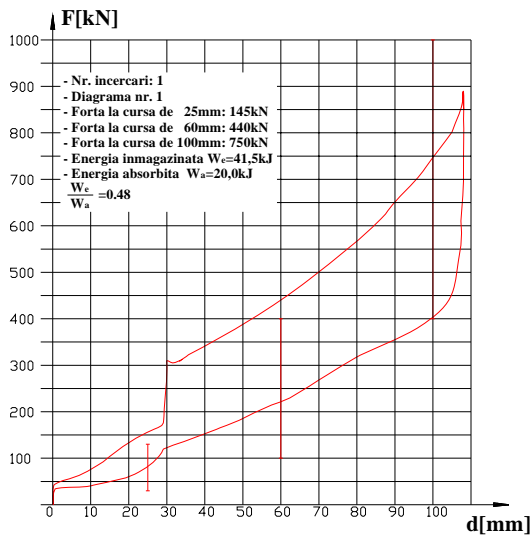


Fig. 2

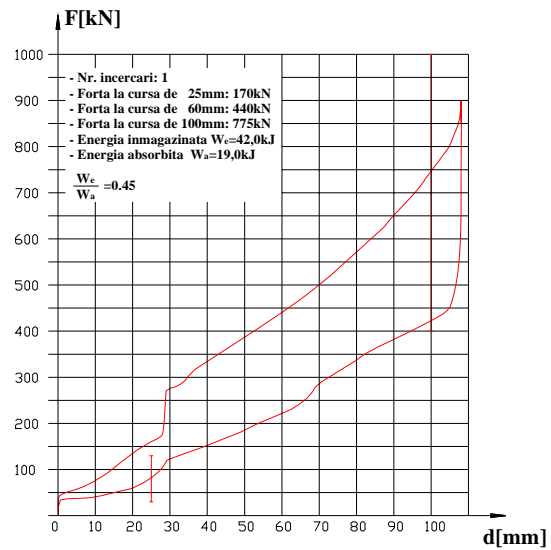


Fig. 3

From the analysis of the experimental results it is observed that for the two shock insulators tested, the force characteristics for the 25mm and 60mm compressions and the $\eta = \frac{W_a}{W_e}$ factor do not fall within the limits imposed by the UIC 526-1 file, while the other characteristics fit within the prescribed limits.

Test at +50°C. The test was conducted in a sealed climate controlled chamber where the shock insulators were introduced for a period of 8 hours. The heating was done with an air heater and the temperature control was done with a thermometer.. The results of the tests with the obtained parameter values are shown in figures 4 and 5.

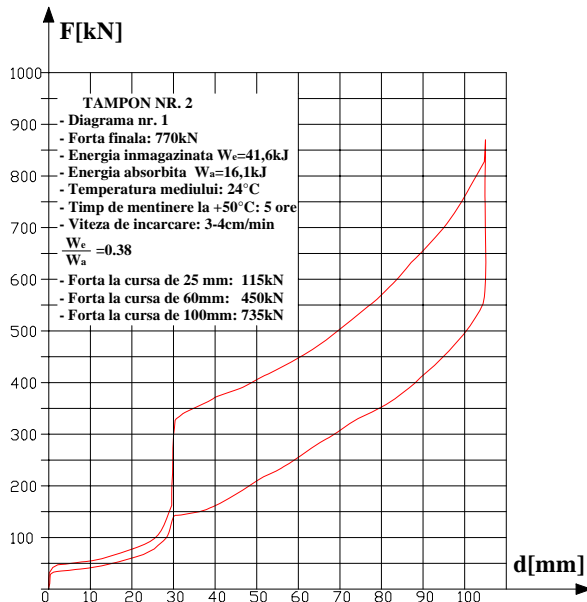


Fig. 4

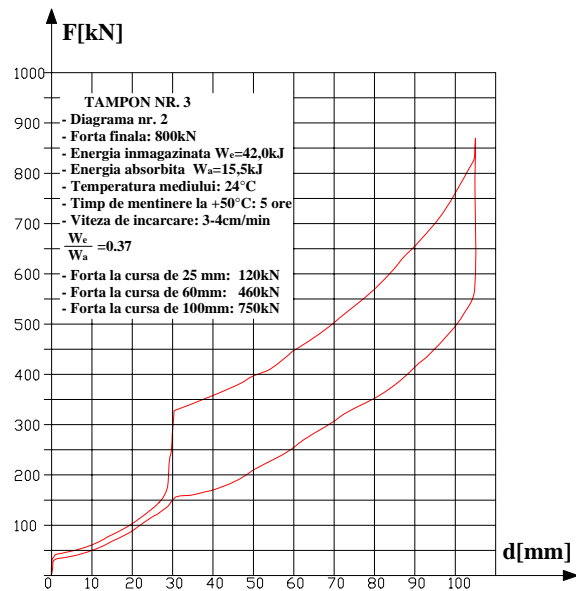


Fig. 5

Comparing the results from figures 2 and 4 for the first shock insulator, and from figures 3 and 5 for the second one, the following procentual differences are observed:

Shock insulator 1

- $\Delta F_{25} = 21 \%$

Shock insulator 2

- $\Delta F_{25} = 29,4 \%$

- $\Delta F_{60} = 2,2 \%$
- $\Delta F_{100} = 2 \%$
- $\Delta W_e = 0,2 \%$
- $\Delta W_a = 20 \%$
- $\Delta F_{60} = 4,5 \%$
- $\Delta F_{100} = 3,3 \%$
- $\Delta W_e = 0 \%$
- $\Delta W_a = 19,4 \%$

From the analysis of the above results it is observed that the shock insulators fit (with the exception of ΔF_{25} and the η factor) within the 20 % tolerance admissible by the UIC 526-1.

Test at -40°C. In order to conduct this test, shock insulator 2 was dismantled, the elastomer capsule together with the rubber elements were inserted into feutron where they were kept at -40°C for 16 hours. After the cooling time was done, the shock insulator was reconstructed and then the experimental determinations were carried out.

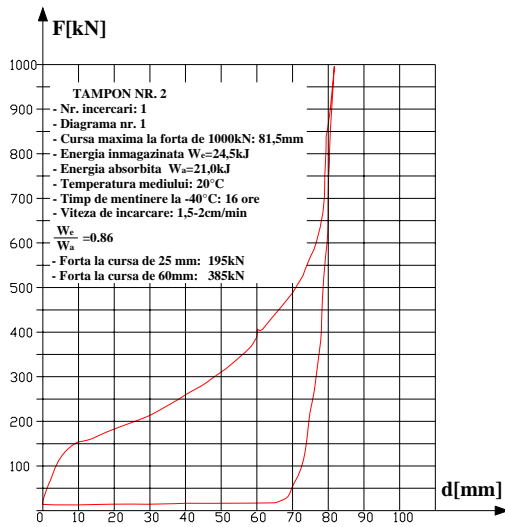


Fig. 6

The results of the tests together with the obtained parameter values are shown in fig. 6.

Comparing the results from figures 3 and 6, the following procentual differences are observed:

- $\Delta F_{25} = 34,4 \%$;
- $\Delta F_{60} = 22,5 \%$;
- $\Delta W_e = 41 \%$;
- $\Delta W_a = 5 \%$.

From the analysis of the results it is observed that during the -40°C testing the buffer no longer complies with the requirements of UIC 526-1. Furthermore, the buffer only underwent a compression of 81mm.

1.2. Collision testing in order to determine the dynamic characteristics of the shock insulators

Collision testing was conducted according to the prescriptions of UIC 526-1. The testing was done with two cars with masses of 80t (figure 7), the collided car being equipped with category C shock insulators [1], [5]. The colliding car was equipped with category A shock insulators with rubber elastic elements.

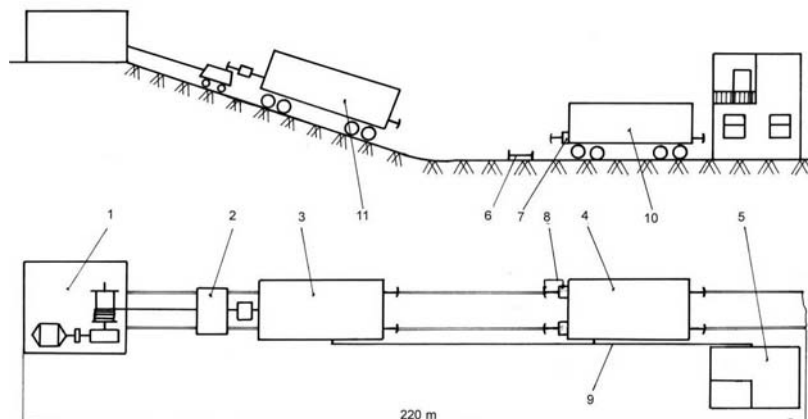


Fig. 7 Collision testing stand

(1.winch ; 2. Releasing cart ; 3. Colliding car ; 4. Collided car ; 5. Stand building ; 6. Velocity transducer ; 7. Force transducer ; 8. Displacement transducer ; 9. Connection cables ; 10. Acceleration transducers)

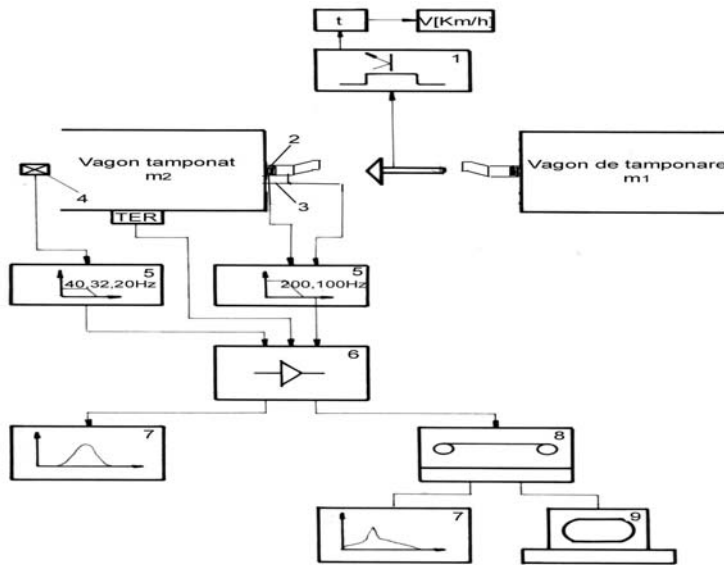


Fig. 8 Transducers, experimental data measurement, recording and analysis apparatus (1. Velocity transducer; 2. Force transducer; 3. Displacement transducer; 4. Acceleration transducer; TER. Resistive tensometric transducer; 5. Low-pass frequency filters; 6. Measurement amplifier; 7. Ultraviolet recorder; 8. Magnetic recorder; 9. Computer)

The transducers and the measurement apparatus used, as well as their placement are shown in fig. 8 [2].

The colliding car was launched at increasing velocities, up to 15 km/h towards the collided car. During the impact, the time evolutions of the following parameters were measured (table 1):

- force transmitted through the buffers F_1 and F_2 ;
- buffer compression D_1 and D_2 ;
- acceleration of the collided car „a”.

Table 1

No.	Velocity [km/h]	W_{e1} [kJ]	W_{e2} [kJ]	$W_{e\text{MEDIU}}$ [kJ]	F_1 [MN]	F_2 [MN]	F_{MEDIU} [MN]	a (0-20Hz) [g]
1.	6,15	7,5	9,0	8,25	0,381	0,297	0,340	1,41
2.	8,20	18,0	13,9	15,95	0,559	0,348	0,454	1,79
3.	10,14	30,5	22,1	26,30	0,725	0,478	0,601	2,27
4.	11,84	47,7	35,4	41,55	1,031	0,620	0,825	3,14
5.	13,84	57,3	38,2	47,75	1,297	0,930	1,113	4,48
6.	14,70	61,3	42,8	52,05	1,514	1,059	1,286	5,31

By eliminating time from the variations of force $F = f(t)$ and compression $D = f(t)$ the diagrams $F = f(D)$ were obtained. From these diagrams, the following parameters were determined: W_e - stored energy; W_a - absorbed energy and $\eta = \frac{W_a}{W_e}$ [3].

The $F = f(D)$ diagrams are shown in figures shown in figures 9 and 10.

$V = 10,14 \text{ km/h}$

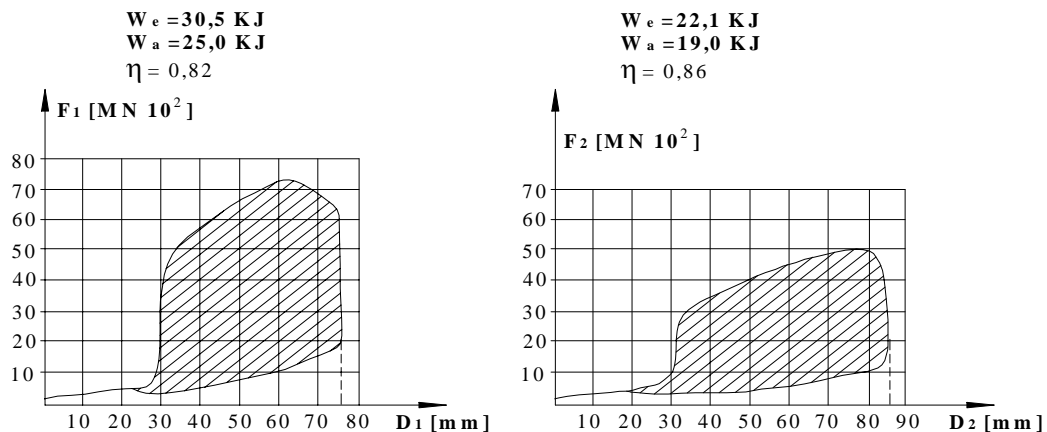


Fig. 9

V = 13,84 km/h

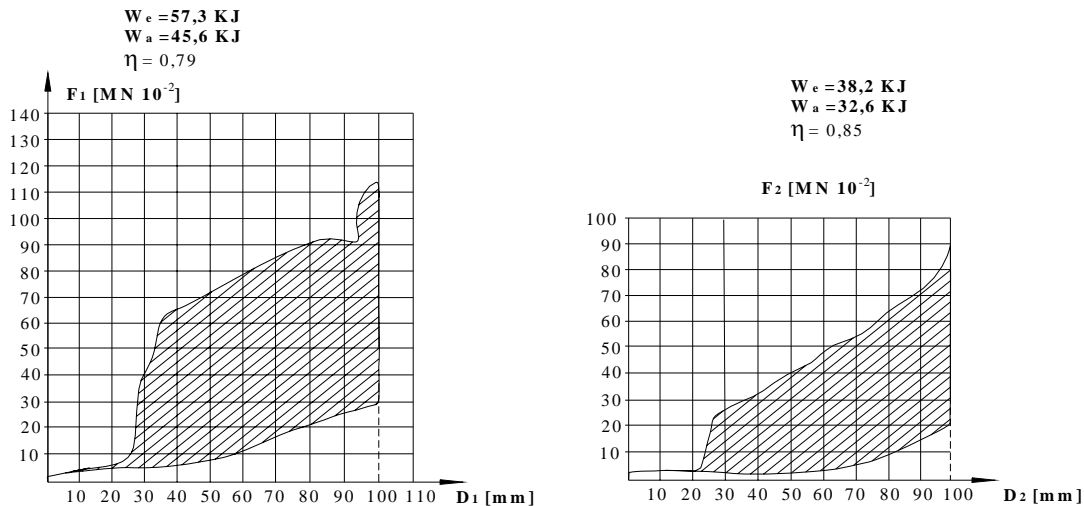
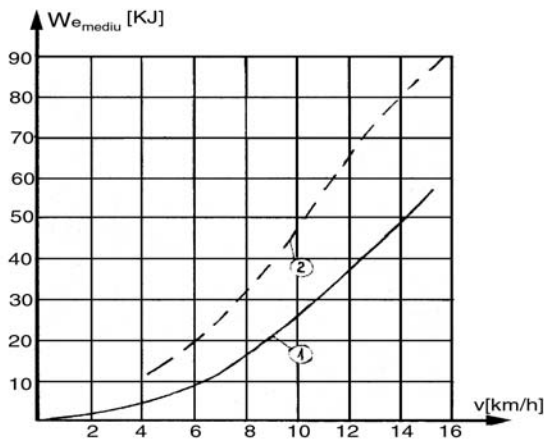


Fig. 10

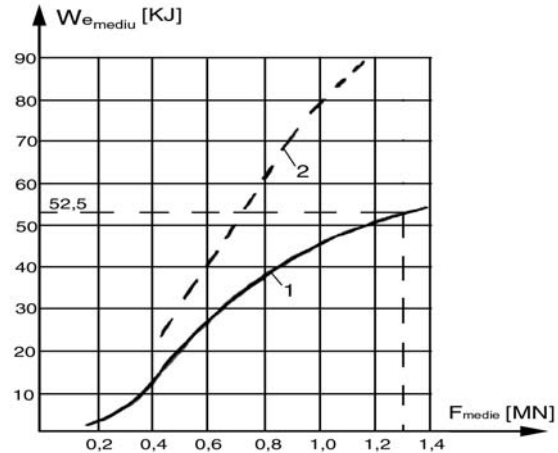
The variations of the average stored energy of the two shock insulators were represented as a function of the velocity of the collided car (figure 11), and of the average transmitted force through the two shock insulators (figure 12).

According to the diagram in figure 12, the average stored energy on the two studied shock insulators, $W_{e\text{MEDIU}}$, at the average force transmitted through the buffers of 1,3 MN is $W_{e\text{MEDIU}} = 52,5 \text{ kJ}$. According to the requirements of the UIC 526-1, for category C buffers it is necessary for a value in excess of 70 kJ to be reached.



1. Cat. C buffer with elastomers
2. Cat. C buffer ICPVA

Fig. 11



1. Cat. C buffer with elastomers
2. Cat. C buffer ICPVA

Fig. 12

2. CONCLUSIONS

After the analysis of the experimental results, the following conclusions can be drawn:

1. In regard to the static characteristics, the buffers do not correspond to the requirements of the UIC 526-1, the values of the absorption coefficient η corresponding to the force at 25 mm and 60 mm does not fit within the admissible limits.
2. For the extreme temperature tests, the studied buffers do not correspond to the UIC 526-1 norms. We point out that at -40°C the buffer only underwent a compression of 81 mm and it did not return to the initial displacement, by 31mm, which, in use, determines the altering of the clearance between car buffers.

3. In regard to the dynamic characteristics, the tested buffers do not correspond to the requirements imposed by the UIC 526-1 for category C buffers. The buffers fit within the limits imposed by category B buffers.

In conclusion, the tested buffers correspond to the norms of category B buffers in regards to the dynamic characteristics without fulfilling the requirements for the static characteristics at extreme temperatures..

REFERENCES

- [1] Copaci I., *Încercări experimentale pentru vehicule feroviare*, Editura Universității “Aurel Vlaicu” Arad, 1999;
- [2] Copaci Ion, Bocîi Liviu Sevastian, Sârb Mihai, *Determinarea experimentală a forței longitudinale la vehiculele feroviare echipate cu cuplă centrală*, The First International Railway Vehicles Symposium, 25-26 november 2005, Bucharest, ISBN 973-755-038-2, pag.109-112
- [3] Ion Copaci, Eleonora Trif, C-tin Nicolescu, *Aplicarea metodei tensometrice pentru calcularea forței transmise și a lucrului mecanic înmagazinat de amortizoarele de șoc în timpul tamponării*, Revista Transporturilor și Telecomunicațiilor nr.3 / 1980. Număr dedicat celui de al II-lea Simpozion Național de Tensometrie cu participare internațională. Cluj-Napoca 1980, pg. 33-39.
- [4] Copaci Ion, Olaru Stelian, ing. Tănăsioiu Aurelia *Fatigue - Resistance and Life Span of Railway Vehicle Bearing Structures Under Random Strains/Rezistența la oboseală și durata de viață la solicitări aleatoare ale structurilor portante ale vehiculelor feroviare*, The Knowledge Based Organization, Applied Mechanics, Military Technical Systems and Technologies Conference, pag. 218-225, “Nicolae Bălcescu” Land Forces academy, Sibiu, Noiembrie 2007.
- [5] Hoancă V., Copaci I., Otlăcan D., *Tampon pentru vagoanele de marfă de categoria C*, Sesiunea de Comunicări Științifice a Universității „Aurel Vlaicu”, Arad 1996.
- [6] Ioan Sebe an, Ion Copaci, *Teoria sistemelor elastice la vehiculele feroviare*, Editura Matrix Rom Bucure ti – 2008.
- [7] Tănăsioiu Aurelia – *Asupra rezistenței și fiabilității amortizorului ce echipează aparatul de tracțiune a vagoanelor de călători*, Sesiunea de comunicări științifice cu participare internațională „Cercetare științifică și educație în forțele aeriene”, pag. 410 – 417, AFASES – 2008 Brașov 16 – 17 mai.
- [8] Tănăsioiu Aurelia, Copaci Ion, *Study on the Sock caused by Collision of Railway Vehicles*, International Journal of Mechanics, ISSN 1998-4448, pag. 67-76, www.naun.org/journals/mechanics.
- [9] Tănăsioiu Aurelia, Copaci Ion, *Study on the Behaviour of the Self-Unloading SSDT Train Upon the Shock Caused by Collisions*, WSEAS Conferences, Computer and Simulation in Modern Science, vol. II, ISSN 1790-5117, ISBN 978-960-474-032-1, www.wseas.org.
- [10] Aurelia Tanasoiu, Ion Copaci – Study on the evolution of kinematic parameters during the shock caused by railway vehicle collision, Simpozionul Interna ional “INTERPARTNER”22-27 sept. 2008, Alusta, Crimea.
- [11] Aurelia Tanasoiu, Ion Copaci – On the shock caused by railway vehicle collision, Al XVII-lea Seminar Interna ional de tiin e Tehnice, “INTERPARTNER”22-27 sept. 2008, Alushta, Crimea, Ucraina.



THE INFLUENCE OF ELASTIC SYSTEMS ON THE TRAVEL SAFETY OF RAILWAY VEHICLES

TĂNĂSOIU Aurelia

Universitatea „Aurel Vlaicu” Arad, ROMANIA

Abstract

The paper presents experimental studies on the determination of the torsional rigidity of the bearing structures (carbody, bogies). The methods and the experimental technology of determining the torsional rigidity are revealed for the bearing structures of the chassis and bogies of the freight cars, as determining elements of travel safety.

Finally, a defining computational methodology is presented for establishing the derailment conditions (Nadal's formula) with the consequent conclusions.

Keywords:

torsional rigidity, force as a function of displacement variation, Y/Q ratio

1. INTRODUCTION

Travel safety is areas that belongs to the dynamics of railway vehicles and constitutes, together with bearing structure resistance and travel dynamics, preoccupations and lines of research that define the capacity of a vehicle to travel on the railway.

The possibility and chance of a vehicle to derail is in strict connection with the torsional capacity of the vehicle as a whole, wheel load, railway geometry and irregularities [3].

2. VERIFICATION OF WHEEL LOAD REPARTITION

The purpose of the test is determining the repartition and deviations of wheel loads. The trials were conducted in accordance with the recommendations of the testing program and the methodology of ERRI B55 Rp8, [8], [9], [10], [11].

The car was tested by positioning it successively with the two bogies on the stand with the tensometric transducers, rail type.

The car was tested for torsion by superimposing the effects of torsion on the basis of the car axle base and the bogie axle base. One of the points was put in a lifting-lowering motion, during which time at that point the displacement Δh and the sustainment force ΔF were measured. An analog process was used for the bogie frames.

With the values of the wheel loads determined during the torsion testing, hysteresis diagrams of the unloading were drawn. From these diagrams the decreases of the wheel loads ΔQ_{ij} were determined, which were compared to the admissible limits $\lim \Delta Q_i$, according to the norms of ERRI B55 Rp8.

With the measured values of ΔF and Δh , hysteresis diagrams were drawn. The values from the diagrams and the specific technical and constructive characteristics of the car were used in the computation of safety against derailment.

The torsion to which the car is exposed during testing simulates the crossing of the car over the irregularities of the rail [2], [3], [4], [5], [6], [7].

The torsion corresponding to the car (g^*), and the bogie (g^+) is computed using (1):

$$g^* = \frac{15}{2a^*} + 2, [\%]; \quad (1)$$

$$g^+ = 7 - \frac{5}{2a^+}, [\%] \quad (2)$$

where:

$2a^*$ is the car axle base;

$2a^+$ is the bogie axle base.

The values of the maximum admissible unloadings $\lim\Delta Q_j$ are computed for each axle, according to the following equations:

$$\lim\Delta q_j = \frac{\lim\left(\frac{Y}{Q}\right)_a - \frac{Y_{a0j}}{Q_{0j}}}{\lim\left(\frac{Y}{Q}\right)_a}, \quad \lim\Delta Q_j = \lim\Delta q \cdot Q_{0j} \quad (3)$$

where:

$\lim\Delta Q_j$ – the maximum admissible unloading of the wheel in order to ensure against derailment;

$\lim\Delta q_j$ – relative limit value of the unloading;

Q_{0j} – average wheel load at axle j ;

$\lim(Y/Q)_a = 1, 2$;

Y_{a0j} – transverse guidance effort at axle j on the exterior wheel of the curvature.

The condition that the car must satisfy in order to traverse the rail torsions without any risk of derailment is that the wheel unloadings observed during testing do not exceed the admissible limit values, computed with equation (2).

The unloadings ΔQ_j of the wheels are determined by measuring with the above mentioned installation. The measurement is done progressively, starting from the situation of the car resting on a straight railway, the carbody is torsioned, then the bogies, at the values g^* and g^+ computed with equations (1) imposed by ERRI B55 Rp8.

Finally, the following inequality is checked:

$$\Delta Q_{jk} < \lim\Delta Q_j. \quad (3)$$

In case the inequality is respected, the safety against derailment of the car is certified from the point of view of the torsional rigidity of the tested car.

3. DETERMINING THE TORSIONAL RIGIDITY

The torsional rigidity C_t^* of a carbody with own weight and the characteristics of the elastic elements of the suspension, are criteria of appreciating the travel safety of the car [1]. [12].

The torsional rigidity C_t^* is a characteristic of the carbody related to the axle base, expressed by a torsional moment ($\Delta F \times 2b_z^*$) applied to the carbody at an angular displacement $\left(\frac{\varphi}{2a^*}\right)$ resulting in:

$$C_t^* = \frac{2a^* \cdot \Delta F \cdot 2b_z^*}{\varphi} \left[\frac{\text{KN} \cdot \text{mm}^2}{\text{rad}} \right] \quad (4)$$

where:

$2b_z^*$ - distance between the suspension supports on the axle [mm];

$2a^*$ - car axle base [mm];

φ – angular displacement [rad];

ΔF – variation of the vertical force [KN].

The angular displacement φ [rad] can be expressed as:

$$\varphi = \frac{h}{2b_z^*} \quad (5)$$

And the expression of the torsional rigidity:

$$C_t^* = 2a^* \cdot (2b_z^*)^2 \cdot \frac{\Delta F}{h} \left[\frac{\text{KN} \cdot \text{mm}^2}{\text{rad}} \right] \quad (6)$$

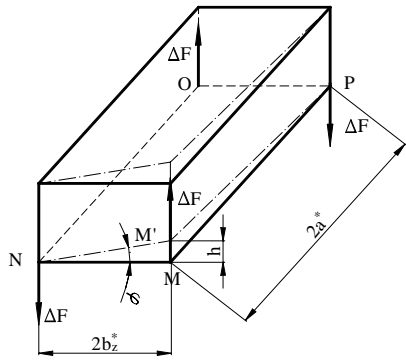


Figure 1. Geometrical characteristics of the car

It is sufficient for the $\frac{\Delta F}{h}$ ratio to be determined experimentally in order to determine the torsional rigidity C_t^* .

The experimental measurements in order to determine the $\frac{\Delta F}{h}$ or $\frac{\Delta F'}{h'}$ ratios can be conducted both for the carbody and the bogie frame. For the carbody, the measurements can be conducted both in the presence of the bogies or in their absence, and in the case of cars on two axles, both in the presence of the axles and in their absence.

Figure 2 shows the arrangements necessary in order to conduct the tests to experimentally determine the $\frac{\Delta F'}{h'}$ in the case of the vehicle without the bogies.

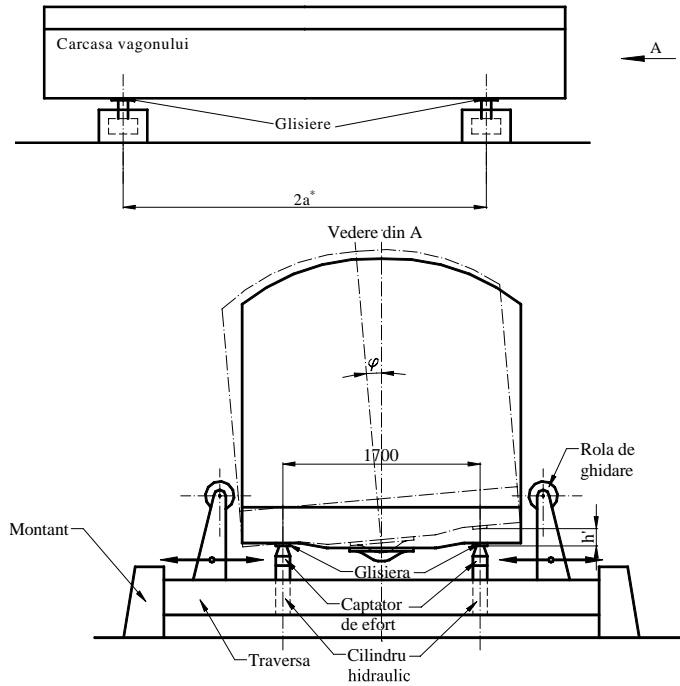
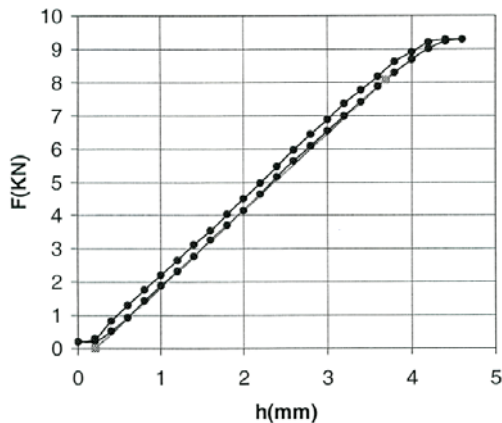


Figure 2. The necessary arrangements for the experimental determination of the $\frac{\Delta F'}{h'}$ ratio for the vehicle without the bogies.

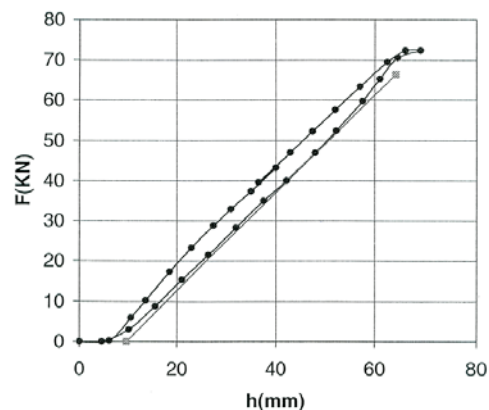
4. EXPERIMENTAL DETERMINATIONS OF THE WHEEL LOAD AND TORSIONAL RIGIDITY

Further on, experimental determinations of the wheel load and the torsional rigidity will be presented for the cistern car with 40m³ capacity [1], [2].



$$C_t^+ = 1,68138 \cdot 10^{10} \text{ KN} \cdot \text{mm}^2 / \text{rad}$$

Figure 3. Force-displacement diagram at the torsion of the bogie frame



$$C_t^* = 5,440012 \cdot 10^{10} \text{ KN} \cdot \text{mm}^2 / \text{rad}$$

Figure 4. Force-displacement diagram at the torsion of the chassis

Table 1

Tests	Imposed values by the testing program and procedures	Values obtained from the testing
Verifying wheel load repartitions, with Y25 Ls(s)d1 bogies and elastic gliders with equal 12 mm clearance	$\lim \Delta Q_{fz1} = 6,1149 \text{ KN}$	$Q_{11} = 29,9658 \text{ KN}$ $Q_{12} = 31,1832 \text{ KN}$ $\Delta Q_1 = 0,6087 \text{ KN}$ $\Delta Q_{\mu I} = 1,6376 \text{ KN}$ $\Delta Q_{fz1} = \Delta Q_1 + \Delta Q_{\mu I}$ $\Delta Q_{fz1} = 2,2462 \text{ KN}$
	$\lim \Delta Q_{fz2} = 5,9229 \text{ KN}$	$Q_{21} = 29,2961 \text{ KN}$ $Q_{22} = 29,9332 \text{ KN}$ $\Delta Q_2 = 0,3186 \text{ KN}$ $\Delta Q_{\mu I} = 1,6376 \text{ KN}$ $\Delta Q_{fz2} = 1,9562 \text{ KN}$
	$\lim \Delta Q_{fz3} = 5,9288 \text{ KN}$	$Q_{31} = 28,0350 \text{ KN}$ $Q_{32} = 31,2525 \text{ KN}$ $\Delta Q_3 = 1,6087 \text{ KN}$ $\Delta Q_{\mu II} = 1,2720 \text{ KN}$ $\Delta Q_{fz3} = 2,8807 \text{ KN}$
	$\lim \Delta Q_{fz4} = 5,6175 \text{ KN}$	$Q_{41} = 27,0843 \text{ KN}$ $Q_{42} = 29,0906 \text{ KN}$ $\Delta Q_3 = 1,0031 \text{ KN}$ $\Delta Q_{\mu II} = 1,2720 \text{ KN}$ $\Delta Q_{fz4} = 2,2751 \text{ KN}$

Table 2

Tests	Values imposed through the testing program	Values obtained from testing
Verifying the torsional rigidity, with Y 25 Ls(s)d1 bogies and elastic gliders with equal 12 mm clearance		$C_t^* = 1,68138 \cdot 10^{10} \text{ KN} \cdot \text{mm}^2 / \text{rad}$ $C_t^+ = 5,440012 \cdot 10^{10} \text{ KN} \cdot \text{mm}^2 / \text{rad}$
	$\lim (Y/Q)_a = 1,2$	$(Y/Q)_a = 0,926$
	$\lim \Delta Q_1 = 15,9084 \text{ KN}$	$\Delta Q_{11} = 4,950 \text{ KN}$ $\Delta Q_{12} = 4,320 \text{ KN}$
	$\lim \Delta Q_2 = 15,5465 \text{ KN}$	$\Delta Q_{21} = 6,880 \text{ KN}$ $\Delta Q_{22} = 5,540 \text{ KN}$
	$\lim \Delta Q_3 = 15,5575 \text{ KN}$	$\Delta Q_{31} = 7,120 \text{ KN}$ $\Delta Q_{32} = 4,160 \text{ KN}$
	$\lim \Delta Q_4 = 14,9709 \text{ KN}$	$\Delta Q_{41} = 6,280 \text{ KN}$ $\Delta Q_{42} = 4,010 \text{ KN}$

Car technical data

- weight $T = 24040 \text{ kg}$
- Average wheel load $Q_0 = 29,479 \text{ kN}$
- Load corresponding to the two stage primary suspension inflexion point (ERRI B 12 Rp 49) $F_{cz} = 26,2 \text{ kN}$
- Mounted axle weight (ERRI B 12 Rp 49) $Gr = 12,9 \text{ kN}$
- Car axle base $2a^* = 9360 \text{ mm}$
- Bogie axle base $2a^+ = 1800 \text{ mm}$
- Wheel base $2e = 1435 \text{ mm}$
- Distance between rolling circles $2b_A = 1500 \text{ mm}$
- Distance between suspension springs $2b_Z = 2000 \text{ mm}$
- Distance between gliders $2b_G = 1700 \text{ mm}$
- Rigidity – measured value $C_t^* = 5,440012 \cdot 10^{10} \text{ KN} \cdot \text{mm}^2 / \text{rad}$
- Bogie frame rigidity – measured value $C_t^+ = 1,68138 \cdot 10^{10} \text{ KN} \cdot \text{mm}^2 / \text{rad}$
- Primary suspension rigidity (ERRI B 12 Rp 49) $C_{z^+1(2)} = 1,004 \text{ KN} / \%$
- Glider springs rigidity (ERRI B 12 Rp 49) $c_G = 0,57 \text{ KN} / \%$

- Maximum relative deviation of wheel load $\Delta q_0 = 0,2$
- Wheel radius $r = 460$ mm
- Radius of the railway used in computation $R = 150$ m
- Gravitational acceleration $g = 9,81$ m/s²
- Derailment safety criterion $\lim(Y/Q)_a = 1,2$

Computation of the $(Y/Q)_a$ ratio is done according to ERRI B 12 Rp 49

- Torsioning at the car test $g^* = 15 / 2a^* + 2 = 3,603$ [%o]
- Torsioning at the bogie test $g^+ = 7-5 / 2a^+ = 4,222$ [%o]
- Exterior leading force $Y_a = 0,5319 \cdot Q_0 + 1,9062 = Y_a = 17,586$ [kN]
- Interior leading force $Y_i = -0,4923 \cdot Q_0 - 0,1512 = -14,664$ [kN]
- Transverse force in the axle box $H_y = -(Y_a + Y_i) = -2,922$ [kN]
- Absolute wheel load decrease due to the force
 $H_y \Delta Q_{H_y} = H_y \cdot r / 2b_A = -0,896$ [kN]
- Absolute maximum wheel load deviation $\Delta Q_{Fz0} = \Delta q_0 \cdot Q_0 = 5,896$ [kN]
- Absolute total diminution of the wheel load due to rail twisting on the basis of the bogie axle base

$$\frac{1}{C_{iA(2a^*)}} = \frac{10^3 \cdot (2b_A)^2}{C_i^+} + \frac{10^3 \cdot b_A^2 \cdot 4}{2a^+ \cdot b_z^{+2} \cdot c_{z1(2)}^+} \quad \Delta Q_t^+ = g^+ \cdot C_t^+ = 3,062 \text{ [kN]}$$

- Absolute total diminution of the wheel load due to rail twisting on the basis of the car axle base

$$\frac{1}{C_{iA(2a^*)}} = \frac{10^3 \cdot (2b_A)^2 \cdot 2}{C_i^*} + \frac{10^3 \cdot b_A^2 \cdot 2 \cdot 4}{2a^* \cdot b_z^{+2} \cdot 2 \cdot c_{z1(2)}^+} + \frac{10^3 \cdot b_A^2 \cdot 2 \cdot 4}{2a^* \cdot b_z^{+2} \cdot c_G} ; \Delta Q_t^* = g^* \cdot C_t^* = 2,419 \text{ [kN]}$$

$$(Y/Q)_a \text{ ratio} \left(\frac{Y}{Q} \right)_a = \frac{Y_a}{Q_0 - (\Delta Q_t + \max \Delta Q_{fz0} + \Delta Q_{H_y})} = 0,926$$

In order to perform the theoretical calculation regarding safety against derailment (Y/Q) , for the tested car, the following were considered:

- a. With the empty car the Ist suspension level (I) steps into action;
- b. In quasistatic conditions, it is acceptable in calculations, for the travel velocity, transverse acceleration and overheightening the use of the values: $v = 0$, $a = 0$, $u = 0$.

5. CONCLUSIONS

In conclusion, it can be considered that the value of the Y/Q ratio of 0,926 is situated under the UIC admissible limit of 1,2 and thus there is a certitude of the elimination of derailment.

Torsional rigidities C_t^* and C_t^+ of the car and bogie respectively, significantly influence travel safety since they can cause large values of the unloading ΔQ_t^* and ΔQ_t^+ when the bearing structures of the car and the bogie have large torsional rigidities and a low elasticity.

The existence of an adequate elasticity of the car and bogie structure thus leads to an improvement of the vehicle behaviour in regards to the derailment risk.

REFERENCES

- [1] Tănăsioiu Aurelia – *Asupra influenței rigidității echivalente a structurilor portante ale vehiculului feroviar în siguranța ghidării*, Simpozionul național de cale material rulant de cale ferată, ediția a III-a, 24 – 25 noiembrie 2006, pag. 37-42, Universitatea Politehnica din București
- [2] Tănăsioiu Aurelia – *Twisting stiffness influence of bearing structures of railway vehicles upon safety guidance*, Proceedings of the International Symposium, Research and Education in an Innovation Era, pag. 90 – 98, 16 – 18 noiembrie 2006, Universitatea „Aurel Vlaicu” din Arad

- [3] Tănăsioiu Aurelia - *On the Influence of Bearing Structure Elasticity of a Railway Vehicle on Guidance Safety/Asupra influenței elasticității structurilor portante ale unui vehicul feroviar în siguranța ghidării*, The Knowledge Based Organization, Applied Mechanics, Military Technical Systems and Technologies Conference, “Nicolae Bălcescu” Land Forces academy, pag. 226-230, Sibiu, Noiembrie 2007.
- [4] Tănăsioiu Aurelia, Copaci Ion, *Modelling of the Dynamic Interaction Vehicle-Railway Induced by High-Speed Trains*, ICEM 2007 Conferință Internațională de Electromecanică, A II-a Ediție, Petroșani, Mai 2007. Annals of the University of Petroșani, vol. 9 (XXXVI), ISSN 1454-9166, pag. 163-166, Universitas Publishing House, Petroșani, România, 2007.
- [5] Iliș Nicolae, Copaci Ion, Tănăsioiu Aurelia - *Factors Influencing the Railway Vehicle Guidance Safety*, - ICEM 2007 Conferință Internațională de Electromecanică, A II-a Ediție, Petroșani, Mai 2007. Annals of the University of Petroșani, vol. 9 (XXXVI), ISSN 1454-9166, nr. pag. 6, Universitaas Publishing House, Petroșani, România, 2007.
- [6] Nicolae Ilias, Ion Copaci, Aurelia Tanasoiu, Ioan Cioara, - *On the Influence of Bearing Structure Elasticity of a Railway Vehicle on Guidance Safety*, Congresul internațional “Metoda □i instrument în sisteme tehnologice”, Universitatea Tehnica Nationala, Institutul Politehnic Harkov, Ucraina, nr. 73/2007, ISSN 0370-808X, pg. 82-86.
- [7] Nicolae Iliă□, Aurelia Tănăsioiu, Ion Copaci, Aurelian Nicola – *Railway vehicle response to horizontal-transversal and vertical railway excitation*, Al XVI-lea Seminar Interna□ional de □tiin□e Tehnice, “INTERPARTNER”23-29 sept. 2007, Alushta, Crimea, Ucraina.
- [8] Aurelia Tănăsioiu, Ion Copaci, Nicolae Iliă□, Iosif Andras – *Railway vehicle response to diferent testing scenarios and procedures*, Al XVI-lea Seminar Interna□ional de □tiin□e Tehnice, “INTERPARTNER”23-29 sept. 2007, Alushta, Crimea, Ucraina.
- [9] Aurelia Tănăsioiu, Ion Copaci, Stelian Olaru, *Studii experimentale asupra capacită ii torsionale a vehiculelor feroviare*, International Symposium Research and Education in Innovation Era, 2nd Edition, University “Aurel Vlaicu” Arad, 20-21 noiembrie 2008.
- [10] Stelian Olaru, Aurelia Tănăsioiu, Ion Copaci, *Asupra ghidării la circula ia peste aparatele de cale*, International Symposium Research and Education in Innovation Era, 2nd Edition, University “Aurel Vlaicu” Arad, 20-21 noiembrie 2008.
- [11] ***** , ORE B55 RP8 *Conditions pour le franchissement des gauches de voie: valeurs recommandées des gauches et dévers de voie; calcul et mesure des valeurs caractéristiques déterminantes pour les wagons; contrôle des véhicules*, Utrecht, avril 1983
- [12] ***** , ERRI B12/DT 135 *Methodes de calcul d'application generale pour l'etude de nouveaux types des wagons ou de nouveaux bogies de wagons*, Utrecht octombrie 1995



ON THE DYNAMIC CHARACTERISTICS OF THE DAMPENER WITH ELASTIC RUBBER ELEMENTS USED ON A SUBURBAN TRANSPORT VEHICLE (EGYPT)

Mihai SÂRB, Ion COPACI, Aurelia TĂNĂSOIU

Universitatea "Aurel Vlaicu", Arad, ROMANIA

ABSTRACT

The paper presents a study on the determination of the elastic dynamic characteristics of the shock insulators that equip railway vehicles. The work underlines the fact that the most appropriate method for determining these characteristics is the colliding of vehicles in the conditions that mimic those that appear during their use.

The paper, by adopting original technical solutions, imposed the designing and production of force transducers and their attachment apparatus on railway vehicles in order to experimentally determine the diagrams for the static and dynamic characteristic of the dampener.



A CONSTRUCTIVE SOLUTION FOR A SOLAR COLLECTOR WITH ALUMINUM ABSORBER

Mirko DOBRNJAC, Tihomir LATINVIĆ

Banja Luka University, Faculty of Mechanical Engineering, BOSNIA & HERZEGOVINA

Abstract:

The paper presents a constructive solution of a solar collector made of a series of aluminum lamellas, placed in aluminum thermo-isolated box. The shape and the profile of lamella make the collector absorber original, and its design has a number of advantages compared to the usual technical solutions. A significant effort has been made to find the geometric profile of ribbed lamella, which would meet all the requirements, starting from design, production and assembly, to high thermal and electric power characteristics. The surface protection was made by way of special procedure of electrochemical protection, thus obtaining a high quality selective surface of absorber. The collector is intended for conversion of solar into thermal energy, and its vast application is possible in heating of sanitary or technological water in boilers, reservoirs, pools, etc.

Keywords:

Solar radiation, solar collector, absorber, aluminum lamella, heat conversion

1. INTRODUCTION

Solar energy, as an energy source is gaining in importance daily. There are several reasons for that, some of them are that solar energy is free and easily accessible to everyone, it is ecologically clean and does not pollute the environment. It is inexhaustible for both the present and future generations, and falls in the group of renewable energy sources. The reason why it has not been exploited sufficiently so far can certainly be found in its "dispersion", that is to say, its relatively low density compared to conventional sources, and in the fact that for its "capturing" and conversion relatively big solar surface should be installed which, already at the beginning, requires significant investment from an investor. This is why this investment is a privilege of well-off individuals and countries, which however, after a relatively short repayment period, provides free of charge and clean energy throughout its useful life. The ways of "capturing" solar energy are diverse. This paper focuses on an innovated technical solution of a solar collector designed for heat conversion, that is to say, primarily for hot water preparation. Photovoltage collectors that perform conversion of solar into electric energy also have a significant role as far as application is concerned, but they will not be discussed in this paper.

2. CONDITIONS AND POSSIBILITIES FOR USING SOLAR ENERGY

The power of the radiation of the Sun on the surface of the Earth is within the range of 1000 W/m^2 ^[2], which depends on a number of factors, latitude, position and the surroundings of the facility being radiated, cloudiness, etc. The time period during which solar energy can be efficiently and effectively used in our climatic area is from March through October and especially during the summer months when the abundance of the Sun is great and ranges from $1100\text{--}1500 \text{ kWh/m}^2/\text{year}$ (Figures 1. and 2.).

According to the PVGIS database, the average yearly global irradiation on horizontal plane in Europe is $1096 \text{ kWh/m}^2/\text{year}$. If we consider only built up areas, than the average is $1130 \text{ kWh/m}^2/\text{year}$. To better see the geographical distribution, the colors in the legend were modified to see the deviations from the value of $1000 \text{ kWh/m}^2/\text{year}$.

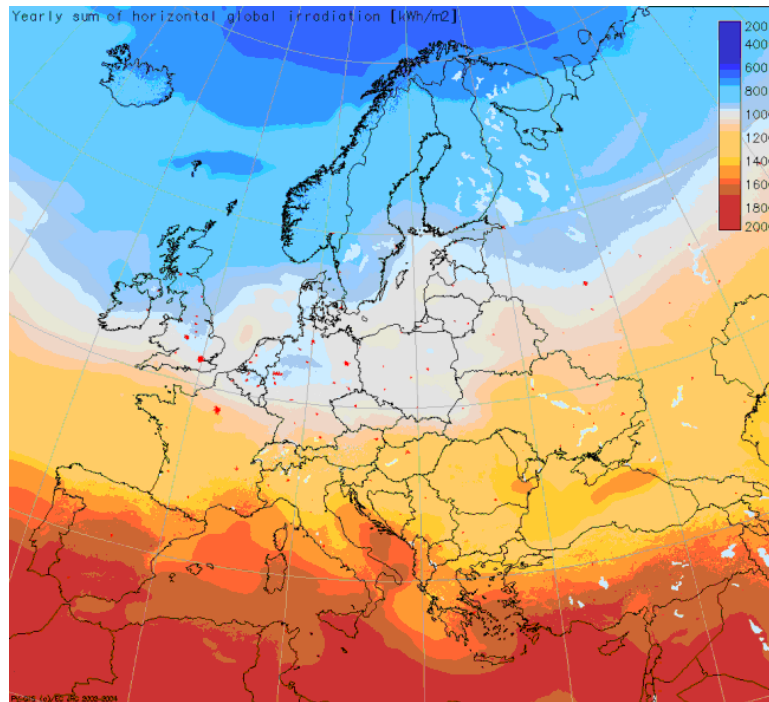


Figure 1. Yearly sum of global irradiation on horizontal surface [kWh/m²]

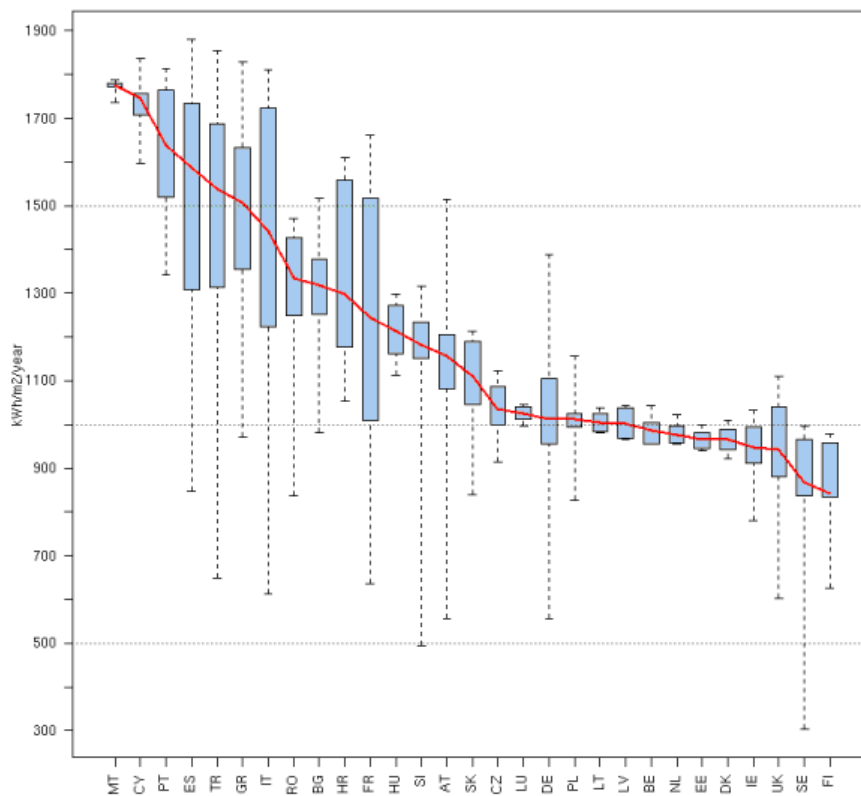


Figure 2. Global horizontal irradiation in EU25 countries [kWh/m²/year]

This time period coincides with naturally increased needs for water consumption due to bigger individual consumption, the summer season of bathing in outdoor pools, etc. That fact inevitably leads to the idea and the need for more intensive utilization of free and ecologically clean solar energy during that period, which can be efficiently solved by using solar collectors. The collectors have already found their place and application and are present in a number of different versions and technical solutions.

From the point of view of transformation technology, solar receivers, as devices that serve for capturing that is to say, receiving the energy of radiation of the Sun, can be divided into two basic groups, more precisely:

- ✦ collectors designed for thermal conversion, during which the energy of the Sun is directly converted to heat; their most frequent application is in heating systems and preparation of hot water for consumption;
- ✦ photovoltage panels designed for direct conversion of solar into electric energy which makes their use exceed the domain of thermal and technical systems and this is the reason for their much wider application in other fields too.

Of a number of collectors, i.e. systems, designed for thermal conversion, it is important to point out flat low-temperature receivers of solar energy, primarily because these systems are the cheapest and the simplest, and can easily find mass application, and thus produce significant economic and ecological effects.

There was a considerable number of producers of low-temperature solar panels of various types in the territory of former Yugoslavia; their production mostly stopped. However, the new producers with new solutions have been emerging. They are aware of the need and importance of using „free“ energy, especially having in mind that energy, being a strategically important resource is becoming more and more expensive every day. In addition

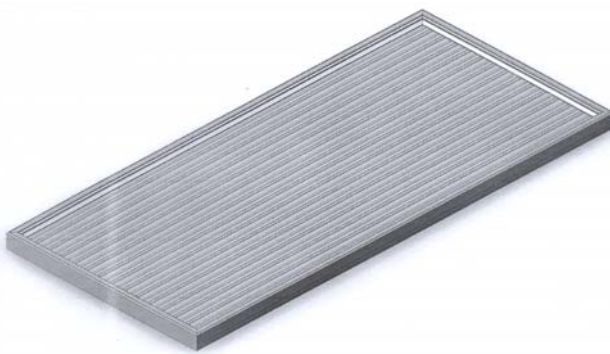


Figure 3. Solar collector

etc. This context was borne in mind while designing this technical solution of low-temperature flat solar collector (Figure 3). The aim was to achieve the biggest possible level of efficiency of heat conversion, decreasing the weight and the price, to accomplish longer duration of the device, as well as the simplest possible installation and operation.

to that, in recent years there has been a major change in overall attitude toward preserving the environment, and this has also been given a legal form in many countries and international organizations. The fact that classic energy sources, like coal and oil, are inevitably polluters, and that they incur additional expenses in terms of maintenance of the systems within permitted limitations of work, leaves more and more space for utilization of alternative, ecologically clean systems that use free energy of the Sun, the wind,

3. TECHNICAL AND GEOMETRIC CHARACTERISTICS OF THE ABSORBER

Having in mind that the absorber (Figures 4. and 5.) is the basic and the most important part of any solar receiver, it should be paid special attention during its constructive design. The efficiency of the entire device mostly depends on the absorber, but during the design process itself attention should be paid to technological possibility of making and installation of the elements, mass, price as well as to other factors.



Figure 4. The layout of the lamella of solar absorber

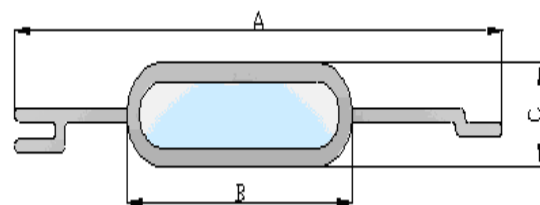


Figure 5. Lamella of absorber (cross-section)

In connection with that, aluminum was chosen as a material for making the absorber (i.e. aluminum alloy). It is significantly lighter than copper, material normally used for making this type of solar collectors. Weight is certainly something that should be taken into account, not only because of the price, but primarily because of the load on the roof structure, which can be significant, especially if a considerable number of collectors are placed on the roof, and having in that this type of load is frequently overlooked by civil engineers. Besides its being lighter, aluminum is also much cheaper material than copper and has good technical characteristics in the sense of heat conducting, the possibility of applying appropriate long-term surface protection, all of which provides the ground for expectation that this type of product can last longer.

The idea around the construction of the absorber itself was to assemble it of elements – lamellas, which are actually a substitute for usual classic collector pipes. The internal cross-section of the lamella through which the medium flows has a shape of a stretched circle; on the external cross-section two ribs from the left and the right side can be seen. The main task of the ribs is to directly conduct the collected energy of radiation from the surface which they cover to the medium.



Figure 6. Connected absorber lamellas (cross-section)

The edge of the rib is adjusted and shaped for fitting into and connecting with the adjacent rib (Figure 6.), so that after assembling all necessary ribs the final surface of the absorber is obtained, of a slightly wavy shape, but of quite satisfactory external appearance. In this way the laying of the cover upper sheet metal board has been avoided, which is in classic pipe collectors usually placed over the pipes and which serves as an absorber, but first of all as a mask - curtain. That role has been assumed here by lamellas. In this way, there is one less position in the assembly, and better conditions for transfer of heat to the medium are created by avoiding the contact resistances that inevitably appear with classic collectors on the place of contact of the upper board and the pipe. In this case the beams fall directly on the lamellas in which water flows.

Two aluminum collector pipes that have a role of a distributor, that is to say collector of the medium (most frequently water with addition of an anti-freeze agent), are connected from the upper and lower side of the lamella, thus ensuring circulation of the medium through the collector. However, if more than one passage through the same collector needs to be provided, then not all the lamellas are connected with a single collector pipe, but only a certain number of lamellas, whereby the medium is returned back through the collector by the subsequent same number of lamellas thus making more passages through the collector. This can be done thanks to the fact that the number of lamellas installed in one collector is not limited, nor is their length which is obtained by cutting lamellas to the desired length from the finished profile. This ensures the projected speed of circulation through the collector, and an influence is made on the ratio of heat transmission from the wall to the fluid, as well as on the overall circulation resistance, output temperature of the fluid, etc. Also, the frame of the collector box does not limit forming of the size of the collector, because the frame itself is formed according to the requirements of the collector dimensions from custom-made Al profiles. Therefore, during designing of a concrete solar system (e.g. water heating for the needs of hotels, multistorey buildings, pools, etc.), it is easy to form a collector of certain dimensions adjusted to that specific requirement.

The surface protection of the absorber itself has a key role in absorption of the radiation of the Sun; having said that, it is necessary to achieve the goal of the biggest possible absorption and the smallest possible emission and reflection of radiated energy on the surface of the absorber. A selective coating was applied by way of an electrochemical process; it was kept during a certain time period in the solution of exactly determined concentration in order to obtain a coating of necessary chemical composition and thickness. Besides good absorption characteristics, this coating also shows good persistence during the exploitation conditions, unlike classic coatings that most frequently peel and decay with time. The

selection of the process itself of applying and achieving the best selective coating has been done in accordance with the diagram in Figure 7 [3], which shows dependence of emissivity on thickness of oxide coatings formed in solutions of different acids.

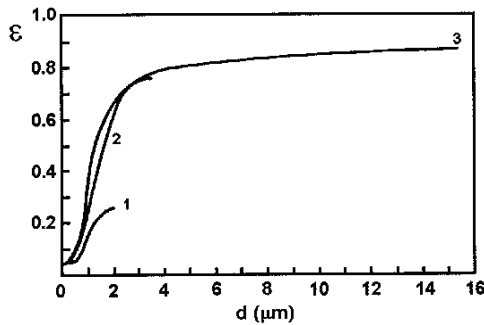


Figure 7. Emissivity depending on thickness of oxide coating made in solution of 1. phosphorous, 2. chrome and 3. sulphur acid

Protection of the box-frame of the absorber has also been done by way of electrochemical protection with parameters that underline more permanent resistance to atmospheric influences.

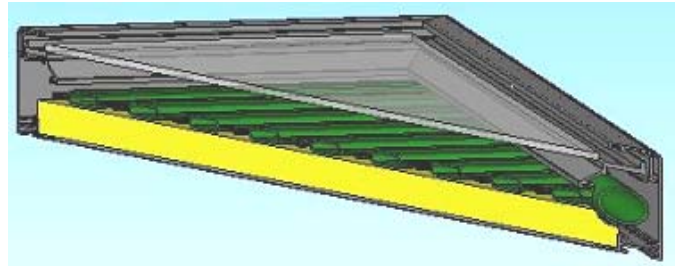


Figure 8. Cross-section of solar collector

Thermal isolation and protection of the absorber (Figure 8) against external influences has been done in the aluminum box which is isolated with polyurethane foam from the bottom side, and from the upper side with one glass board. Dimensions of the box, as well as of the thermal isolation and the glass board are reduced to minimum, having in mind that the operation of this absorber is preferred during the summer time as well as the transitional period when maximum energy effects are obtained.

4. INSTALLATION AND USE OF THE COLLECTOR

The collector has been designed for assembling in classic solar installations for preparing hot water in individual or joint containers for several consumers, for supplementary heating of the facilities, as a support to classic heating system, for supplementary heating of water in outdoor or indoor swimming pools, etc.

The hot water container should also be equipped with the pipe heater through which exchange of heat from the fluid-carrier of the heat to the consumer hot water is carried out. Besides standard components, the pump, the expansion receptacles and the pipe installations, there should be also automation installed in the system that will perform regulation of processes, that is to say, start and end of circulation, in order to prevent the loss of already accumulated heat in the container and increase the efficiency of the entire system. If there are more collectors installed in the system, their connecting can be done in a series, in parallel or in a combined manner, depending on the requirement of the project itself. The support structure is being adapted and delivered depending on the characteristics of the place of installation (gable roof, flat surface, etc.).

Figure 9. [1] presents a diagram for rough selection of size, i.e. number of solar collectors and hot water containers.

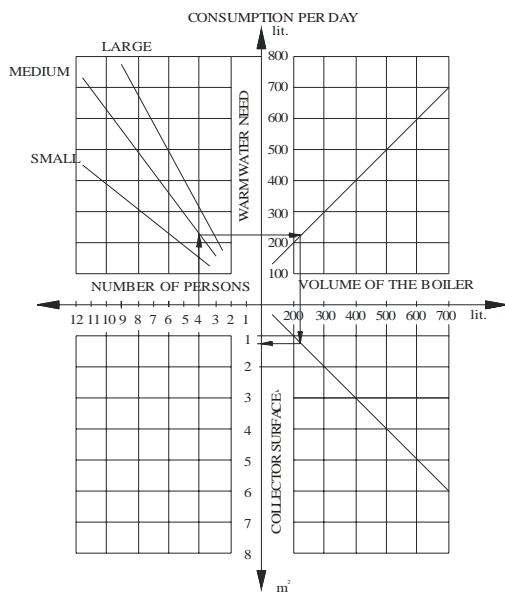


Figure 9. Determining the size of the boiler and the collector depending on the size of the household

5. CONCLUSION

The paper presents an original technical solution of a solar energy receiver, designed for heat conversion, which can be effectively used for preparation of hot water in boilers, containers, pools, etc. A solar receiver of high technological and energy performances is obtained through significantly adjusted geometric shape of the

absorber, quality surface protection and simple assembly of pre-fabricated elements. This is more than enough as a reason for the beginning of serious application this ecologically clean system in our area of, which ensures capturing and the use of abundant and free of charge heat of the Sun. In this way significant savings in the consumption of expensive conventional fuels will be achieved, especially having in mind that those fuels are polluters of the environment that is already to a large degree jeopardized and the protection of which will have to be intensively implemented in all countries in the world, on the basis of both current and future International treaties. Bearing in mind that these standards are to a large degree already in effect in EU countries, their application in our country is also expected, as well as the significant support to these projects by the Government. This solution also helps achieve considerable financial effects and savings compared to the utilization of conventional energy resources.

REFERENCES

- [1] Lambic M.: Prirucnik za solarno grejanje, Naucna knjiga, Beograd, 1992.
- [2] Osmanagić Muzafer: Niskotemperaturna konverzija sunceve energije, RU "Djuro Djaković" Sarajevo, 1987.
- [3] Pavlovic T., Cabric B.: Fizika i tehnika solarne energetike, Gradjevinska knjiga, Beograd, 1999.
- [4] Šúri M., Huld T.A., Dunlop E.D. Ossenbrink H.A., 2007. Potential of solar electricity generation in the European Union member states and candidate countries. Solar Energy, 81, 1295–1305, <http://re.jrc.ec.europa.eu/pvgis/>.



THE INFLUENCE OF LOW TEMPERATURES ON THE MECHANICAL CHARACTERISTICS OF THE 34MoCrNi15X-RS STEEL UNDERGOING SHOCK-BENDING, DEPENDING ON THE SAMPLING POSITION

WEBER Francisc

University "Politehnica" Timisoara, Faculty of Engineering Hunedoara, ROMANIA

Abstract

The paper introduces the tests of shock bending undergone over the 34MoCrNi15X-RS steel, carried out on Mesnager test bars (the groove depth $h = 2\text{mm}$), under low temperatures. The test bars were longitudinal, respectively cross-sectional samples of semi-finished sections of ingot middle. We first described the cooling room we used, then gave the experimental results obtained and analyzed the influence of the main alloy elements on the values of resilience.

Keywords

shock bending, low temperatures, cooling room.

1. GENERAL NOTIONS

The principle of the shock-bending test consists in breaking at a single blow, with a pendulum hammer, under determined conditions, of a test bar having a groove at its middle, **U** or **V** shaped, freely placed on two supports.

The shock-bending test is dealt with in **SR EN 10045-1:1993**, where general considerations are being given with respect to the conditions for low temperature tests. Although this European norm replaces **STAS 6833 -79**, which sets the conditions for shock-bending under low temperatures, the **standard** products are still being processes according to the national standards.

In order to carry out shock-bending tests under low temperatures we need the following elements: test bars of a well-determined shape and size; a cooling-room for cooling the test bars down and a pendulum-hammer provided with a scale, (Charpy hammer). The special character of this test consists in the fact that the test bars are being cooled down in a cooling room, which is out of the work area of the pendulum-hammer. Generally it is necessary to, sub-cool the test bars in the cooling room and to reduce the handling time to 5 seconds at most.

2. THE ROOM FOR COOLING TEST BARS

We used for the tests a cooling room built by the author, which uses as cooling agent solid carbon dioxide and as cooling medium acetone or ethylic alcohol. We thus have a liquid cooling agent.

This cooling room [3], cylinder-shaped, is shown schematically in fig.1.

Between the inner pot (1) made of stainless steel and the exterior one (2) there is a thermal insulation(5) made of mineral cotton. At the top, the two pots are connected by a textolite flange (3) provided with a mounting (9) made of asbestos plate. Between the posts, at the bottom, there is an oak grate (6) to support the inner pot.

In order to level the temperature of the cooling agent, the room has a stirring device (4), mounted on the cover of the room through the leading hub (13) and worked upon by means of a textolite piece (14).

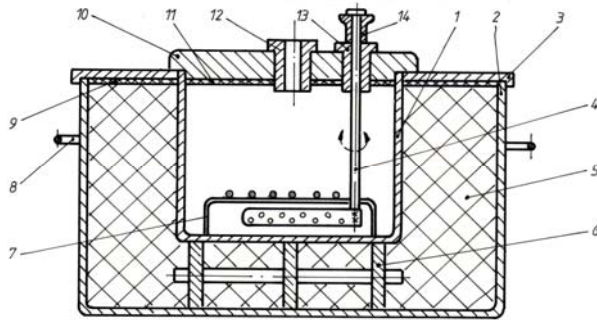


Fig.1. Cooling room with liquid cooling agent

On the bottom of the pot there is a stainless steel wire grate (7) on which the test bars to be cooled are placed.

The cooling room has a cover (10) made of textolite, muffled with asbestos (11), and meant to close the workroom at the top. The cover is provided with a leading hub (12) through which the thermometer or the thermo-couple can be introduced, in order to measure the temperature of the cooling agent.

3. THE TEST BARS USED IN THE TEST

The **34MoCrNi15X-RS** steel is used for welded joining. Unlike with other steel grades, the determination of the mechanical characteristics is carried out on test bars that are samples of rolled sections that have undergone thermal treatments.

The experiments have been carried out on Mesnager-type test bars (the groove depth $h = 2$ mm) that are longitudinal, respectively cross-sectional samples of semi-finished sections of ingot middle. The low temperature used for shock-bending tests was -30°C (243K).

4. THE RESULTS OF THE EXPERIMENTS AND CONCLUSIONS

As a result of the shock-bending tests at room and low temperature (-30°C) for the **34MoCrNi15X-RS** steel, we obtained medium values for every three steel charge and they were given in table 1.

Table 1. The Chemical Structure and the Values of Resilience KCU2 for the 34MoCrNi15X-RS Steel

Charge No.	C %	Mn %	S %	P %	Cr %	Ni %	Mo %	+20°C(293K)		-30°C(243K)	
								L	T	L	T
								[J/cm ²]		[J/cm ²]	
1	0,31	0,47	0,015	0,018	1,56	1,44	0,16	96,33	53,66	65,33	43
2	0,32	0,52	0,012	0,020	1,40	1,45	0,16	171	62	123,66	40
3	0,33	0,43	0,008	0,018	1,46	1,64	0,19	166	62,66	145	45,33
4	0,32	0,44	0,010	0,018	1,55	1,45	0,21	172	90,66	148,33	66
5	0,31	0,50	0,012	0,017	1,60	1,42	0,17	166	78,33	119	54,66
6	0,33	0,44	0,022	0,024	1,46	1,42	0,22	139	68,66	85	45
7	0,38	0,57	0,010	0,016	1,54	1,45	0,22	134,6	91,33	89	61,33
8	0,32	0,55	0,016	0,018	1,55	1,51	0,18	182,6	62	141,33	56,33
9	0,34	0,57	0,015	0,018	1,46	1,49	0,17	138,6	68	93,66	46,33
10	0,33	0,47	0,020	0,020	1,58	1,44	0,17	162,3	72	118,66	58
11	0,34	0,51	0,014	0,025	1,74	1,42	0,25	148	56	91,66	35
12	0,35	0,59	0,011	0,014	1,48	1,57	0,20	186,6	118,6	137,33	82,33
13	0,35	0,44	0,013	0,018	1,51	1,54	0,17	147,6	68,33	105,33	42,66
14	0,36	0,45	0,020	0,019	1,48	1,51	0,23	155,6	66,33	107,33	44
15	0,35	0,44	0,016	0,018	1,48	1,46	0,21	131,3	60,33	108,33	46,33

The variation of resilience at low temperature according to the main elements of the chemical composition is as follows: the influence of Nickel contents - fig.2.a.; the influence of Chrome contents - fig.2.b and the influence of Carbon contents - fig. 2.c.

By analyzing the graphs in the given figures we notice that the values of resilience we obtained for test bars that are cross-sectional samples are smaller than for the longitudinal ones; yet, a certain equal distance is preserved between the variation curves, which show that different contents in **Ni**, **Cr** and **C** have no influence upon these differences.

Fig.2.a shows an increase in the value of resilience alongside with the increase in the contents of **Ni**. For the longitudinally sampled test bars the value KCU2/-30 is higher than the minimum one required for room temperature tests ($\text{KCU2} = 62,5 \text{ J/mm}^2$). Even for the cross-sectionally sampled test bars taken from charges having contents in **Ni** higher than

1,6%, KCU_{2/-30} is higher than KCU₂. These results prove that nickel is the alloy element that ensures steel a high tenacity even at low temperatures.

The chrome contents required by this steel grade are 1,40... 1,70%. Fig.2.b shows a decrease of resilience KCU_{2/-30} when the contents in chrome increase.

Fig.2.c. proves that resilience KCU_{2/-30} has a maximum value for both longitudinally and cross-sectionally sampled test bars, when the contents in carbon are 0,34%, which corresponds to the mean of the interval 0,30%...0,38% carbon, requested by this steel grade.

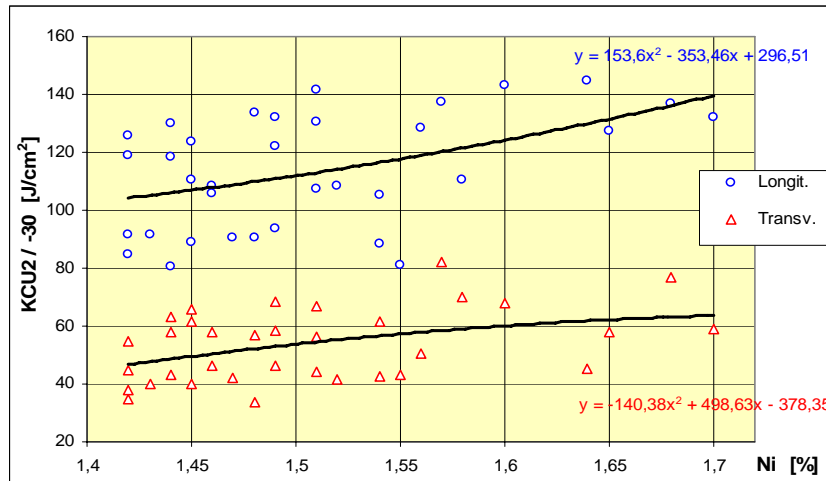


Fig.2.a. The variation of resilience KCU_{2/-30} according to the contents in Ni

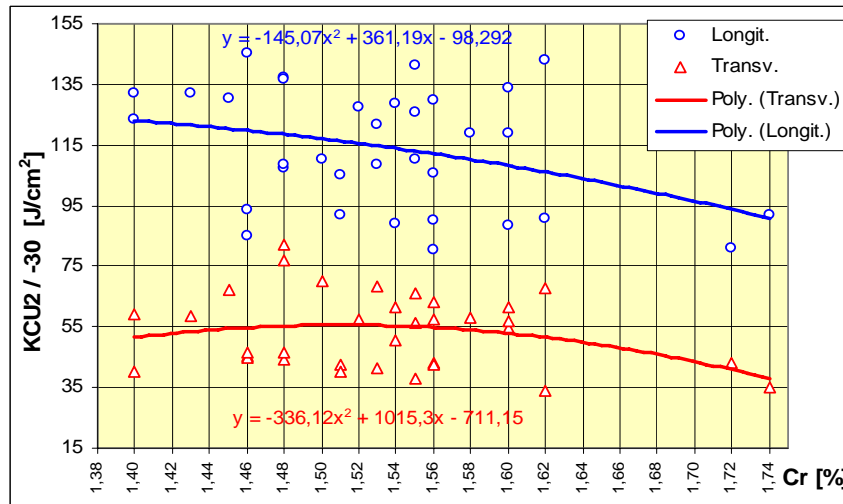


Fig.2.b. The variation of resilience KCU_{2/-30} according to the contents in Cr

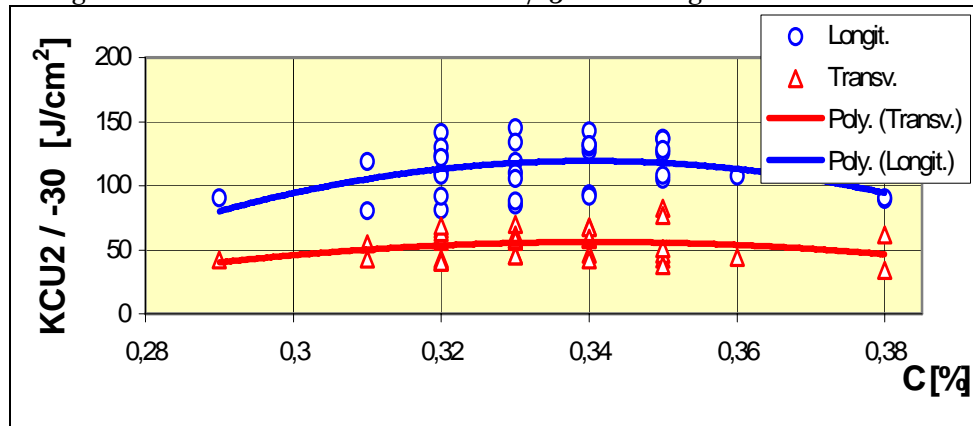


Fig.2.c. The variation of resilience KCU_{2/-30} according to the contents in C

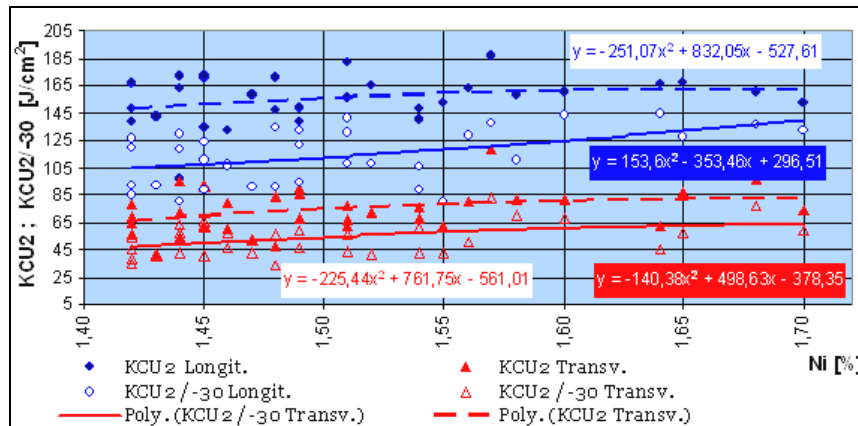


Fig.3 The variation of resilience $KCU_2 / KCU_2/-30$ according to the contents in Ni

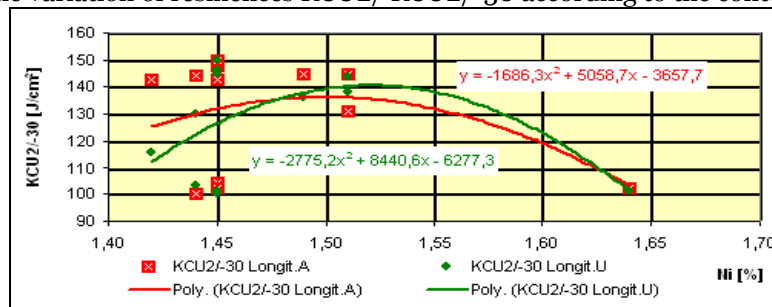


Fig.4. The variation of resilience $KCU_2/-30$ for longitudinal test bars sampled from ingot butt, respectively ingot crop, according to the contents in Ni

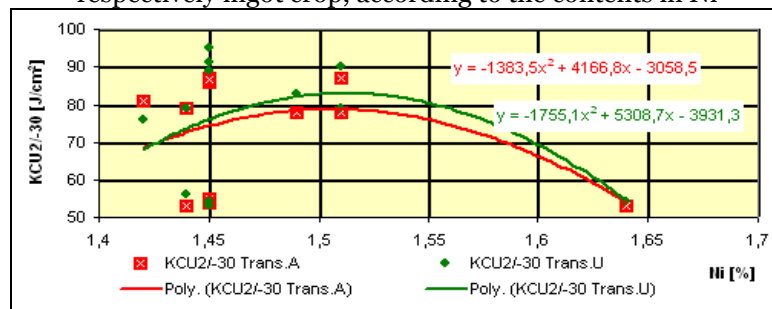


Fig.5. The variation of resilience $KCU_2/-30$ for cross-sectional test bars sampled from ingot butt, respectively ingot crop, according to the contents in Ni

Fig.3 gives the comparative variation diagrams for resilience at room temperature (KCU_2) respectively at low temperature ($KCU_2/-30$), for test longitudinal and cross-sectional bars, according to the contents in nickel.

The maximum values of resilience correspond to the contents of 1,7% Ni, which represents the top limit of the domain requested by this chemical structure and steel grade.

For the **34MoCrNi15X-RS** steel we performed tests at -30°C on test bars coming from ingot butt (**A**), respectively ingot crop (**U**).

The variation of resilience for low test temperatures depending on the contents in nickel and the place of sampling is given as follows: for the longitudinal test bars sampled from ingot butt, respectively crop - fig.4 and from the cross-sectional test bars sampled from ingot butt, respectively crop - fig.5.

REFERENCES

- [1] Atanasiu, C., s.a. Încercarea materialelor, vol. I, Editura Tehnică, București 1982
- [2] Tapalaga, I., s.a. Criogenia în construcția de mașini, Editura Dacia, Cluj-Napoca, 1988.
- [3] Weber, F. Contribuții la studiul comportării oțelurilor la temperaturi scăzute, Teza de doctorat, Timișoara, 1988.
- [4] Weber, F. Studiul influenței temperaturii scăzute și a locului de prelevare a epruvetei asupra caracteristicilor mecanice, la încovoierea prin șoc, a oțelului 34MoCrNi16X, Analele Facultății de Inginerie Hunedoara, Tomul I, Fascicola 3, pag 49-54, Hunedoara 1999



THE TORSION MECHANICAL CHARACTERISTICS UNDER LOW TEMPERATURE OF 34MoCrNi16X STEEL

WEBER Francisc

University "Politehnica" Timisoara, Faculty of Engineering Hunedoara, ROMANIA

Abstract

The paper introduces the torsion tests under low temperature for steel grade 34MoCrNi16X, carried out on round test bars, respectively on thin-walled tubular test bars, thus achieving a homogenous bi-axial strain. We described the shape and dimensions of the test bars, the test machine, the cooling room we used and we gave the experimental results we obtained.

Keywords

low temperatures, cooling room, torsion tests.

1. GENERAL NOTIONS

The torsion test is not subject of international norms, although it constitutes a way of examining metal behavior under the force of tangent strains. The results of the test allow considerations on the tenacity of metals [3] by the determination of their torsion resistance and deformability.

The low temperature tests are carried out, methodologically, as in the case of tests at room temperature, the particular characteristic consisting in the fact that the mechanical trial has to be done in the moment the entire mass of the test bar has a certain low temperature, within a certain limit tolerance for the testing temperature [1]; [3].

In the cross-sections of the test bar on which torsion momenta are applied, there appear tangent strains, and the sections twist around their axis at an angle φ which, up to a certain limit is proportional to the distance l between the planes of the charging couples [1]; [2]; [3]. The maximum angular deformation, called specific slide is calculated by means of relation:

$$\gamma_{\max} = \frac{r \cdot \varphi}{l} = \frac{d \cdot \varphi}{2 \cdot l} \quad (1)$$

The maximum tangent strain, called torsion resistance is calculated by means of relations:

$$\tau_r = \frac{12M_t}{\pi d^3}, \quad \text{for the circular-section test bars;} \quad (2)$$

$$\tau_r = \frac{12M_t}{\pi(D^3 - d^3)}, \quad \text{for the ring-section test bars.} \quad (3)$$

2. EXPERIMENTAL TEST STAND

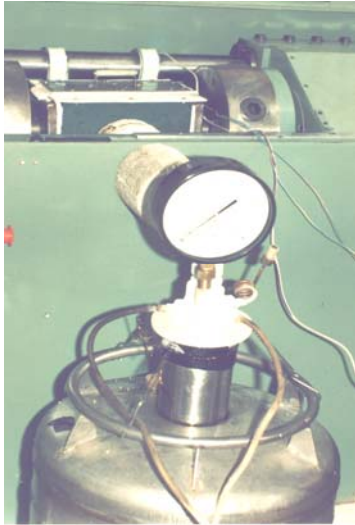
For the torsion tests under low temperatures, we used test stand made up of:

- the torsion test machine;
- the cooling room;
- Dewar vessel for keeping the solid nitrogen;
- device for the automatic regulation of low temperature.

The torsion tests for the circular, respectively ring-section test bars have been carried out on a machine model MODELL TAD III, available in the laboratory of Material Resistance of the Engineering Faculty of Hunedoara. This machine, described in [4]; [5] and [7] has the following characteristics:

- ✚ the loading rate, expressed in rotations/min has four work values (6, 12, 30, respectively 60 rot/min.), button selected;

- ✚ the mechanism for measuring the torsion momentum has four work domains (15, 30, 75 and respectively 150 Kf·m), to be obtained by attaching standard weights to its pendulum;
- ✚ the torsion test can be carried out clockwise or anticlockwise.



Picture 1. The cooling room mounted on the torsion test machine

For the torsion test under low temperatures we attached a cooling room [4]; [5]; [7] using nitrogen vapors as cooling agent to the test machine.

In order to store the liquid nitrogen we used a 40 l Dewar vessel. In the case of using nitrogen vapors as cooling agent we used a charge resistance immersed in the liquid nitrogen and warmed up so that the vapors at the upper part of the Dewar vessel be exhausted through a transfer pipe connected to the cooling room.

The device of automatic temperature regulation [4]; [6] controls the charge resistance and ensures a flow of nitrogen vapors, at a pre-selected temperature and over the period covering the entire torsion test.

Picture 1 shows the cooling room mounted on the torsion test machine as well as the Dewar vessel with its pressurizing system.

3. THE TEST BARS USED IN THE EXPERIMENT

The aim of the experiment consists in the determination of the torsion characteristic curve of the material, showing the dependency of the tangent strain τ on the specific slide γ . This curve is obtained by processing the diagram drawn by the recording system of the test machine, which represents the dependency between the torsion momentum (M_T) and the torsion angle (φ).

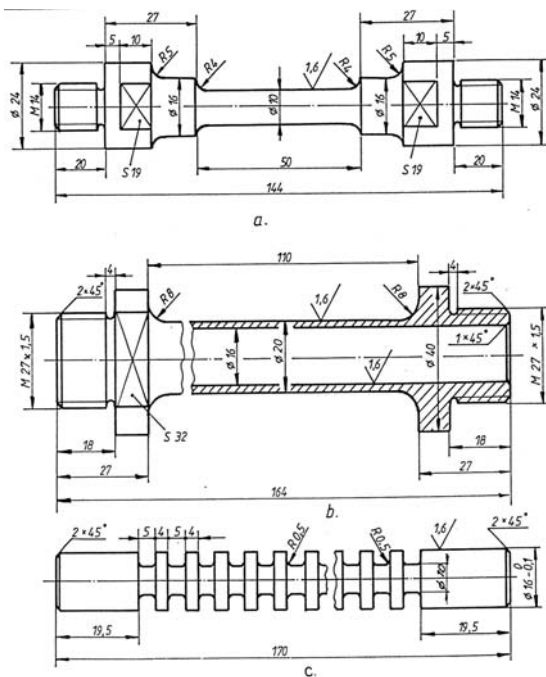


Fig.1. The shape and dimensions of the test bars used for torsion tests at low temperatures

the circular-section test bar (fig.1.a.) have the calibrated area 50 mm long and the diameter of 10mm ($L/d = 10$), and the joining radius between this zone and the ends is 4 mm.

The tubular test bars with thin walls have the shape and dimensions given in fig.1.b. Thus, the calibrated area is 110 mm long, the exterior diameter of 20 mm and the inner diameter of 16 mm, and the wall is 2 mm thick ($L/d = 5,5$; $D/s = 10$). The joining radius between this zone and the ends is 8 mm.

In order that the tubular test tube keep its stability along the torsion test we introduced in it an iron core, having the shape and dimensions given in fig.1.c. It has two cylindrical zones at the ends, while the central area is worked so as to allow the leading of the test tube long ring-shaped portions.

4. THE RESULTS AND CONCLUSIONS OF THE EXPERIMENT

The torsion tests have been done for the steel grade 34MoCrNi16X, which is a highly alloyed steel, worked by plastic deformation and used in machine parts (piston rods, shafts, large toothed wheels, etc.), after thermal treatment. The chemical structure, the mechanic characteristics, the thermal treatment applied, etc. observe STAS 791-88.

Out of the characteristic curves, fig.2 gives the ones obtained for circular-section test-bars for test temperatures of +20°C, -40°C and -80°C and fig.3 those resulting from torsion tests on ring-shaped test bars at test temperatures of +20°C and -40°C. For each level of the test temperature we used two test tubes, the charging rate being 6 rot/min.

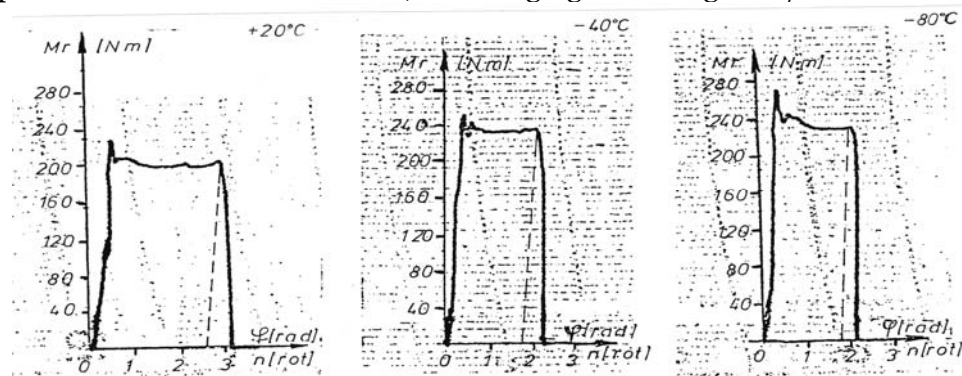


Fig.2. The torsion characteristic curves for the cylindrical test rods made of 34MoCrNi16X

The torsion resistance has been calculated by means of relations (2), respectively (3) and the specific glide by formula (1).

The magnitudes measured and calculated are given in table 1 (for the cylindrical test bars) and in table 2 (for the thin-walled, tubular test bars).

Table 1. The mechanic torsion characteristics of 34MoCrNi16X steel determined on cylindrical test bars

No.	Test temperature [°C]	(M _r) _{max}		n [rot]	φ _{max} [rad]	τ _r [N/mm ²]	γ _{max} [rad]
		[kgf.m]*	[N.m]				
1	+20	22,51	220,823	2,53	15,88	843,909	1,588
2		21,78	213,661	2,41	15,13	816,538	1,513
Media		22,14	217,193	2,47	15,51	830,223	1,551
1	-20	22,82	223,864	2,24	14,06	855,531	1,406
2		22,61	221,804	2,18	13,69	847,658	1,369
Media		22,71	222,834	2,21	13,87	851,594	1,387
1	-40	24,75	242,797	1,73	10,86	927,886	1,086
2		23,94	234,851	1,68	10,55	897,519	1,055
Media		24,34	238,824	1,70	10,70	912,703	1,070
1	-60	25,32	248,389	1,65	10,36	949,257	1,036
2		24,95	244,759	1,59	9,98	935,384	0,998
Media		25,13	246,574	1,62	10,17	942,321	1,017
1	-80	27,22	267,028	1,62	10,17	1020,489	1,017
2		28,12	275,857	1,58	9,92	1054,230	0,992
Media		27,67	271,442	1,60	10,05	1037,359	1,005

* The scales of the test machine are standardized in kgf.m

Table 2. The mechanic torsion characteristics of 34MoCrNi16X steel determined on tubular test bars

No.	Test temperature [°C]	(M _r) _{max}		n [rot]	φ _{max} [rad]	τ _r [N/mm ²]	γ _{max} [rad]
		[kgf.m]*	[N.m]				
1	+20	53,25	522,382	1,98	12,43	511,934	1,11
2		54,12	530,917	1,90	11,93	520,298	1,07
Media		53,68	526,649	1,94	12,18	516,116	1,09
1	-40	68,25	669,532	1,62	10,17	656,141	0,91
2		67,52	662,371	1,71	10,73	649,123	0,96
Media		67,88	665,951	1,66	10,45	652,631	0,94

* The scales of the test machine are standardized in kgf.m

The characteristic curves of the cylindrical test bars differ from those obtained for steel grade 10Ni35R, [4] inasmuch as after the maximum value for the torsion momentum has

been reached, at the end of the linear variation zone, it decreases and then stays approximately constant up to the breakpoint (see fig.2).

The explanation consists in the fact that, as steel possesses a relatively high resistance to torsion, in the zone in which it passes from the elastic behavior to the elasto-plastic, respectively plastic one, there arises a heating which is only partially compensated by the low temperature.

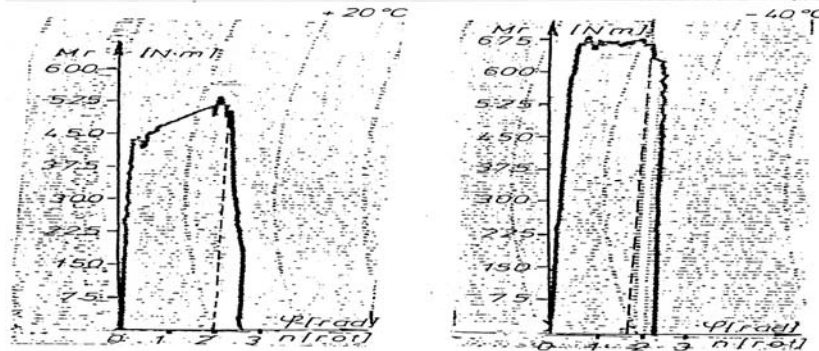


Fig.3 The torsion characteristic curves for tubular test bars made of 34MoCrNi16X

Fig.4 gives the variation curves of characteristics τ_r and γ_{max} with respect to the test temperature for the circular-section test bars.

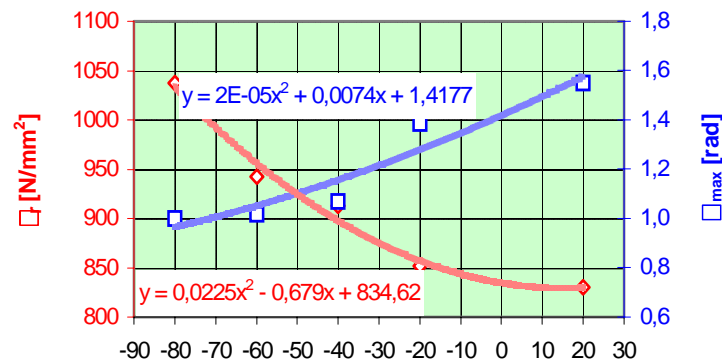


Fig. 4.The variation of the mechanical torsion characteristics with respect to the test temperature

We noticed an increase of the resistance to torsion, respectively a diminishing of the specific glide as the test temperature decreased. At -80°C the resistance to torsion is approximately 25% higher than the one obtained for +20°C.

For the ring-cross section test bars, the resistance to torsion at -40°C is 26% higher than at +20°C.

REFERENCES

- [1] Atanasiu, C., ș.a. Încercarea materialelor, vol. I, Editura Tehnică, București, 1982; Diter, G.E. Metalurgie mecanică, Editura Tehnică, București, 1970.
- [2] Tăpălagă, I., ș.a. Criogenia în construcția de mașini, Editura Dacia, Cluj-Napoca, 1988.
- [3] Weber, F. Contribuții la studiul comportării oțelurilor la temperaturi scăzute, Teza de doctorat, Timișoara, 1988
- [4] Weber, F. Încercarea la răsucire a oțelului 10Ni; 35R pe epruvete tubulare, Buletinul științific "Acta Universitatis Cibiniensis" vol. XXXIV, pag.309-316, Sibiu, 1999.
- [5] Weber, F., Hodor, I. Instalație experimentală, cu azot lichid, pentru reglarea temperaturilor scăzute - Analele Universității "Eftimie Murgu" Reșița, Fascicola II, pag 415-420, Reșița, 1996.
- [6] Weber, F. The Behavior of OL 37 - 2k Steel Wires under Torsion at Low Temperatures, Buletinul științific al Universității "POLITEHNICA" Timișoara, Seria Mecanică, Tom 44(58), Fascicola 2, pag 49-56, Timișoara, 1999.

DYNAMICS OF WORKING PROCESS OF FLAT SIEVES

Radu ILEA

Banat Agricultural University of Timisoara, ROMANIA

Abstract:

The operation of separation of seeds is realized due to the vibration of sieve. The operation of separation is analyzed with the help of the particle model which executes vibration motions on a plane with friction. There are analyzed displacement regimes of particle by forward sliding and back sliding without detachment. Because of velocity discontinuity which appears as consequence of friction between particle and plan or of dropping on plan in the case of detachment, vibro-impact motion regimes appear. That is why, for the study of motion, there are applied the specific methods, concerning the vibro-impact regimes.

Keywords:

Motion, flat sieves, dynamic model, sliding regimes

1. INTRODUCTION

Generally, the phenomenon of vibro-transfer is essentially influenced by the material behavior, characterized by composition, humidity, adherence, nature etc. In the first approximation, the experiences shown that the material can be schematized by a simple material particle which moves with friction on the vibrating surface (Figure 1).

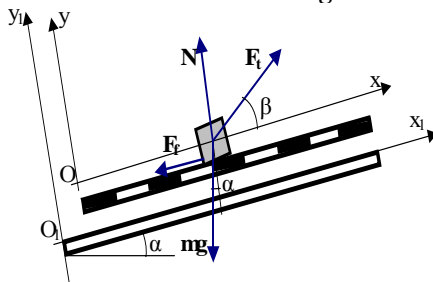


Figure 1. Dynamic model

The particle of mass m is supposed to be placed on the vibrating plan, inclined to the angle α , in relation to the horizontal surface. It is supposed that the vibrating plan executes a vibration translation motion on a direction which makes the angle β with the inclined plan and it has the amplitude r . Thus, a current point of the plan executes a vibration displacement, given by the law $r \sin \psi$, on a direction which makes the angle β with the inclined plan, where $\psi = \omega t$. So, in relation to the fixed frame $O_1x_1y_1$, the coordinates of the point O , the origin of the mobile frame Oxy , bound to the inclined plan, (figure 3.1), at a certain moment are

$$x_0 = r \cos \beta \sin \psi \quad \text{and} \quad y_0 = r \sin \beta \sin \psi . \quad (1)$$

The differential equation of relative motion of particle of mass m has the form

$$m \bar{a}_r = \bar{F}_f + \bar{N} + m \bar{g} + \bar{F}_t . \quad (2)$$

Because the transport force of inertia is $\bar{F}_t = -m \bar{a}_t$, where a_t is the acceleration of transport of particle, identical to the acceleration of the point O , the components of the transport force of inertia are

$$\begin{aligned} F_{tx} &= -m \ddot{x}_0 = m r \omega^2 \cos \beta \sin \psi , \\ F_{ty} &= -m \ddot{y}_0 = m r \omega^2 \sin \beta \sin \psi . \end{aligned} \quad (3)$$

As consequence, the differential equation of relative motion (2) has the following projections on the axes of the frame Oxy :

$$\begin{aligned} m \ddot{x} &= -\mu N \text{sign} \dot{x} + m r \omega^2 \cos \beta \sin \psi - m g \sin \alpha , \\ m \ddot{y} &= N + m r \omega^2 \sin \beta \sin \psi - m g \cos \alpha . \end{aligned} \quad (4)$$

Taking into account that there are considered only the motions of particle, in contact to the plan, it must be put $y=0$, so that from the second equation (4), it results

$$N = m (g \cos \alpha - r \omega^2 \sin \beta \sin \psi) . \quad (5)$$

2. CHARACTERISTICS OF MOTION OF SLIDING

As a principle, the particle which is situated in the rest position, at a certain moment becomes to slide on the plan, forward or back.

For the beginning it is supposed that the particle executes a forward sliding motion in relation to the sieve. On the particle act the force of weight mg , the normal reaction N , and the force of friction $F = \mu N$; the motion of transport being a translation, the Coriolis force of inertia is null.

If the expression (5) of the normal reaction N is introduced in the first differential equation in (4), it arrives at the following relation:

$$\ddot{x} = -\frac{g \sin(\alpha + \phi)}{\cos \phi} + \frac{r\omega^2 \cos(\beta - \phi)}{\cos \phi} \sin \psi, \quad (\psi = \omega t). \quad (6)$$

This relation represents the fundamental equation for the study of the forward motions of sliding on the vibrating sieve.

The beginning moment of the forward sliding is denoted by $t = t_1$ and so, $\psi_1 = \omega t_1$. It can mention that this moment corresponds to the condition that the acceleration \ddot{x} to be null.

If the acceleration (6) is made equal to zero, it is obtained the following equation, in the initial moment of the forward motion of sliding:

$$\sin \psi_1 = \frac{g}{r\omega^2} \cdot \frac{\sin(\alpha + \phi)}{\cos(\beta - \phi)}. \quad (7)$$

Taking into account the relation (7), the fundamental equation (6) can be also written

$$\ddot{x} = r\omega^2 \frac{\cos(\beta - \phi)}{\cos \phi} (\sin \psi - \sin \psi_1). \quad (8)$$

The forward motion of sliding is characterized by $t > t_1$ and so, $\psi > \psi_1$.

Considering the function $\dot{x} = \dot{x}(t)$, if $\ddot{x} > 0$, the function \dot{x} is increasing. Thus, from the moment $t = t_1$ when the velocity is nullifying, i.e. $\dot{x}(t_1) = 0$ and $\ddot{x} > 0$, it results $\dot{x} > 0$. So, the forward motion of sliding takes place. Thus, from the relation (8), written for the moment given by ψ_1 it must be satisfied the inequality

$$\sin \psi > \sin \psi_1. \quad (9)$$

From the relation (7), written for ψ_1 it can be supposed that $\psi_1 \in (0; \frac{\pi}{2})$ which, in accordance to the inequality (9), leads to the condition $\psi \in (\psi_1; \pi - \psi_1)$.

By integrating the differential equation of sliding motion which begins for $t = t_1$ it is found

$$\dot{x} = -r\omega \frac{\cos(\beta - \phi)}{\cos \phi} [\cos \psi - \cos \psi_1 + \sin \psi_1 \cdot (\psi - \psi_1)]. \quad (10)$$

The forward regime of sliding stops at the moment $t = t'_1$, respectively the angle $\psi = \psi'_1$ which corresponds to the nullifying of the relative velocity, $\dot{x} = 0$. So, by nullifying the expression of \dot{x} , it is deduced the equation

$$\sin \psi_1 = \frac{\cos \psi'_1 - \cos \psi_1}{\psi_1 - \psi'_1}. \quad (11)$$

This equation permits the calculus of the moment $t = t'_1$, corresponding to the cessation of sliding.

The distance, covered in the case of the forward sliding is given by the integral

$$s_{1,2} = \int_{t_1}^{t'_1} \dot{x} dt \quad (12)$$

Taking into account the relation (10), after the effecting of calculus, the integral (12¹) becomes

$$s_1 = -\frac{r \cos(\beta - \phi)}{\cos \phi} \left[\frac{(\psi'_1 - \psi_1)^2}{2} \sin \psi_1 + \sin \psi'_1 - \sin \psi_1 - (\psi'_1 - \psi_1) \cos \psi_1 \right]. \quad (13)$$

If in the relation (13) it is replaced $\sin \psi_1$ given by the equation (11), then for the displacements with forward sliding, it can be written the relation

$$s_1 = \frac{r \cos(\beta - \phi)}{\cos \phi} \cdot \Phi(\psi_1), \quad (14)$$

In an analogous way it is treated the case corresponding to the back motion of sliding. By back sliding it means the relative motion with friction of the material particle on the vibrating sieve, in the negative direction of the Ox axis, i.e. in opposite direction to the transporting one.

Taking into account that the force of friction is orientated in the positive direction of the Ox axis and projecting the differential equation of the relative motion, it is obtained

$$m\ddot{x} = \mu N - mg \sin \alpha + mr\omega^2 \cos \beta \sin \psi \quad (15)$$

or, if it is taken into account the equation (2), it results

$$\ddot{x} = -\frac{g \sin(\alpha - \phi)}{\cos \phi} + r\omega^2 \frac{\cos(\beta + \phi)}{\cos \phi} \sin \psi. \quad (16)$$

This relation represents the fundamental equation for the study of the back motions of sliding on the vibrating sieve.

The back sliding begins at the moment $t=t_2$ and $\psi_2 = \omega t_2$, when $\ddot{x} = 0$.

From the expression (16) of the acceleration, made equal to zero, it is obtained the equation

$$\sin \psi_2 = \frac{g}{r\omega^2} \cdot \frac{\sin(\alpha - \phi)}{\cos(\beta + \phi)}. \quad (17)$$

Taking into account the relation (17), the fundamental equation (16) can be also written as follows:

$$\ddot{x} = r\omega^2 \frac{\cos(\beta + \phi)}{\cos \phi} (\sin \psi - \sin \psi_2). \quad (18)$$

Because the back motion of sliding begins at the moment $t=t_2$ and it corresponds to the interval $t > t_2$, respectively $\psi > \psi_2$, in the same way as in the previous case, it is considered the function $\dot{x} = \dot{x}(t)$ which, for $\ddot{x} < 0$, is a decreasing one. Thus, beginning with the moment $t=t_2$ for which $\dot{x}(t_2) = 0$, the velocity \dot{x} is negative ($\dot{x} < 0$), so that a back motion of sliding takes place.

In accordance to the relation (18) and from the condition $\ddot{x} < 0$, it results

$$\sin \psi < \sin \psi_2. \quad (19)$$

Supposing ψ_2 given by the relation (17) in the first quadrant, i.e. $\psi_2 \in (0; \frac{\pi}{2})$, it results that the angle ψ must be in the interval $\psi \in (\pi - \psi_2; 2\pi)$.

By the integration of the differential equation (18), it is obtained the expression of the velocity:

$$\dot{x} = -r\omega \frac{\cos(\beta + \phi)}{\cos \phi} [\cos \psi - \cos \psi_2 + \sin \psi_2 \cdot (\psi - \psi_2)]. \quad (20)$$

The end of duration of the back sliding is obtained by nullifying the expression of the velocity \dot{x} , given by the relation (20). The final moment, denoted by $t = t'_2$, respectively the angle $\psi = \psi'_2$, is obtained by solving the transcendental equation

$$\sin \psi_2 = \frac{\cos \psi'_2 - \cos \psi_2}{\psi_2 - \psi'_2}. \quad (21)$$

The distance, covered in the case of the back sliding, is given by the integral

$$s_2 = \int_{t_2}^{t'_2} \dot{x} dt \quad (22)$$

Taking into account the relation (20), after effecting the calculus, becomes

$$s_2 = -\frac{r \cos(\beta + \phi)}{\cos \phi} \left[\frac{(\psi'_2 - \psi_2)^2}{2} \sin \psi_2 + \sin \psi'_2 - \sin \psi_2 - (\psi'_2 - \psi_2) \cos \psi_2 \right]. \quad (23)$$

If in the relation (23), it is replaced $\sin \psi_2$ given by the equation (21), then for the displacements with back sliding, it can be written the relation

$$s_2 = \frac{r \cos(\beta + \phi)}{\cos \phi} \cdot \Phi(\psi_2), \quad (24)$$

If during the time $T = \frac{2\pi}{\omega}$, the material particle moves by forward and back sliding, the advance in the positive direction of the axis O_1x_1 has the value

$$S = s_1 - s_2 ; \quad (25)$$

and the average velocity of particle is

$$v_m = (s_1 - s_2) \frac{1}{T} = (s_1 - s_2) \frac{\omega}{2\pi} . \quad (26)$$

The graphical representations of the absolute velocity v , transport velocity v_t and displacement s_t with sliding along the vibrating sieve, on which there are superposed the slips s_1 and s_2 , are shown in Figure 2, for a cycle of vibration.

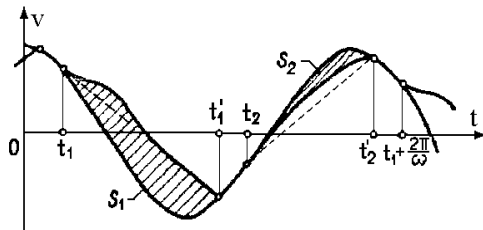


Figure 2. Absolute velocity, transport velocity and displacement

3. CONCLUSIONS

All obtained results correspond to the case of sliding motion, without detachment, i.e. for $N > 0$. In accordance to the relation (5), it results

$$\sin \psi < \frac{g}{r\omega^2} \cdot \frac{\cos \alpha}{\sin \beta} . \quad (27)$$

The analysis of possible motion regimes can be more easily made with the help of the kinematical index:

$$K = \frac{r\omega^2}{g} . \quad (28)$$

Thus, a condition for do not exist detachment, in accordance to the relation (5), is that the equation $N=0$ do not have solution, that leads to the inequality

$$K < \frac{\cos \alpha}{\sin \beta} . \quad (29)$$

Now, it is supposed the condition (27) as satisfied, so that all regimes of motion are with sliding, only. The characteristic indexes of forward and back motions of sliding are denoted by the parameters

$$K_{1,2} = \frac{\sin(\alpha \mp \phi)}{\cos(\beta \pm \phi)} . \quad (30)$$

As consequence, the relation (7), with the notations (29), becomes

$$\sin \psi_{1,2} = \frac{K_{1,2}}{K} . \quad (31)$$

For the beginning, it is considered $K_1 < K_2$. Then, there are the following possible situations:

- $K_1 < K < K_2$ for which the angle ψ_2 can not exist, situation that corresponds to a sliding motion, forward only (AI_t);
- $K < K_1 < K_2$ when no one of the angles of motion initiation is possible, that corresponds to the situation of rest (R);
- $K_1 < K_2 < K$, situation when both types of sliding are possible ($\psi_1 < \psi_2$), and the regime of motion is with forward and back sliding ($AI_t + AI_p$).

For the situation when $K_1 > K_2$ the possible cases are as follows:

- $K_2 < K < K_1$ for which the moment ψ_1 does not exist, which shows that the only possible regime of motion is with back sliding (AI_p);
- $K < K_2 < K_1$, where initial moments for motions with sliding do not exist, i.e. there is the rest, only (R);
- $K_2 < K_1 < K$ where there are possible solutions for both initial moments ($\psi_1 < \psi_2$) and so, the regime of motion is with forward and back sliding ($AI_t + AI_p$).

Finally, in accordance to the relations (31), it can be written

$$K_1 - K_2 = - \frac{\sin 2\phi \cos(\alpha + \beta)}{\cos(\beta + \phi) \cos(\beta - \phi)} . \quad (32)$$

The conditions $K_1 < K_2$ are realized if $\cos(\alpha + \beta) > 0$, that leads to $\beta < (\pi/2) - \alpha$. The other situation, $K_1 > K_2$ can appear if $\cos(\alpha + \beta) < 0$, i.e. only for $\beta > (\pi/2) - \alpha$.

REFERENCES

- BRINDEU, L., Vibrații și vibropercuții. Bazele mecanicii, vibrațiilor și vibropercuțiilor. Ed. „Politehnica”, Timișoara, 2001.
- BRINDEU, L., Vibrații și vibropercuții. Metode și dezvoltări analitice, Ed. „Politehnica”, Timișoara, 2005.

- [3] BRÎNDEU, L., ILEA, R., BIRÓ, I., HEGEDŰS, A., HERIȘANU, N., Studiul vibropresării prin alunecare, A X-a Conf. de Vibrații Mecanice, Vol.I, Timișoara, 2002, pp.125-130.
- [4] ILEA, R., Dinamica sitelor utilizate în construcția mașinilor agricole, Teza de doctorat, Universitatea „Politehnica”, Timișoara, 2001.
- [5] SILAȘ GH., BRÎNDEU L., “Sisteme vibropercutante”, Ed. Tehnică, București, 1986

THE ATTEMPT TO TRACTION OF THE INSULATION OF THE CABLE LAY-UPS FROM CARS

Teodor VASIU, Adina BUDIUL-BERGHIAN

University Politehnica Timisoara, Faculty of Engineering Hunedoara, ROMANIA

Abstract

The correct operation of the cars is the result of correctness output of the execution and the fitting ensembles, building blocks and the marks components. After make, each among these are submissive of a specific testing which have the fate to confers them a certainty of good operation in exploitation.

The cable lay-ups, as components of the electric plant, are submissive of attempts which visa the workstations and the insulation. In this work are analyzed the insulations of a cable lay-ups. The results, obtained abaft their attempts to traction, are processed with specialized software Weibull+ + 7, who permits the determination of reliability parameters of the cable lay-ups and therewith we can do appreciations about material quality used to the manufacture of the coatings and the correctness they were made.

1. INTRODUCTION

The electric equipment of the cars has the role assured the electric energy for the input of electric apparatus as much stationary, quotients and to the movement of the cars.

Component of electric equipment is: the feeder plant, the consumers and the central office with the specific annexes. This rearward contains the contact with spanner, isolators, switches, safeties etc. and the cable lay-ups which do the connection between elements of the electric equipment.

The conductors, as and components ale the cable lay-ups, can be down stress and of high stress. They are made from multiform cupriferous wire, of section and different insulation (figure 1). The conductors who have approximate same direction are made grouped with special par tape and are fixed with staples and metallic or plastic clamping jaws. They are put in places safe from leakages of oils, fuels, water and how much beyond the which part emanates excessive heat (across 100°C).

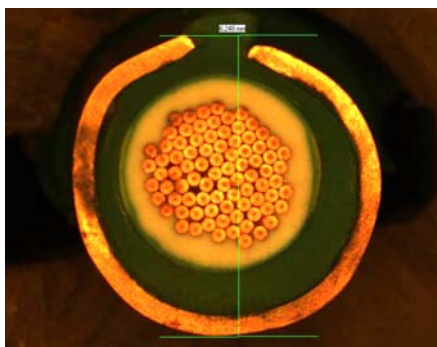


Figure 1. Section through the electric conductor



Figure 2. Section through the terminal

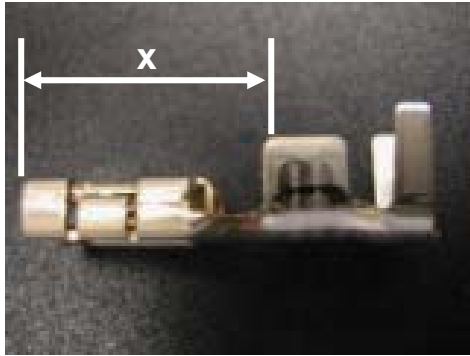


Figure 3. Clamping jaw

The conductor terminals (figure 2) used for the fixation to the elements of electric equipment are made in the shape of mules, clamping jaws (figure 3), clamping ring, clutches from brass latten or bronze. All the terminals are protecting with fittings of rubbers or plastics, of diverse forms.

2. Procedures of quality

The quality auditing activity of the cable lay-ups is done in special workspaces for ultimate check, utilizing the documents, the middles and the specific proper methods.

The documents of quality are constituted from: procedures and cautions of specific quality of the place of labor, standards of quality, plugs of measurements and specific registrations.

Used-up middles to the check quality can be: standards, equipments of testing, gauges and check (the tape measure, the ruler, caliper, micrometer and dynamometer) and specific characters (section the thread, color the thread, the bandage type, plan of dusk, numerical codes components).

The quality auditing methods can be: visual checkout, compare to the standards, measure, monitoring and functional testing.

Testing to traction the insulation of the cable lay-ups

In this paper is analyzed the comportment to traction of the insulation cable lay-up with following nominal sizes:

<i>Strip Length (mm):</i>	<i>6.00</i>
<i>Conductor crimp height (mm):</i>	<i>2.80</i>
<i>Conductor crimp width (mm):</i>	<i>4.20</i>
<i>Insulation crimp height (mm):</i>	<i>6.35</i>
<i>Insulation crimp width (mm):</i>	<i>6.36</i>

A number of 10 of identical cable lay-ups were stretched by a special machine up to rupture the insulations. Is registered the values of the forces (table1) which results the deterioration of the insulations.

Table 1. Experimental results

Nº	Insulation crimp height [mm]	Tensile result [N]
1	6.350	27.41
2	6.340	29.18
3	6.370	27.77
4	6.370	22.61
5	6.350	17.00
6	6.360	19.58
7	6.350	27.14
8	6.370	25.64
9	6.370	20.94
10	6.370	24.41

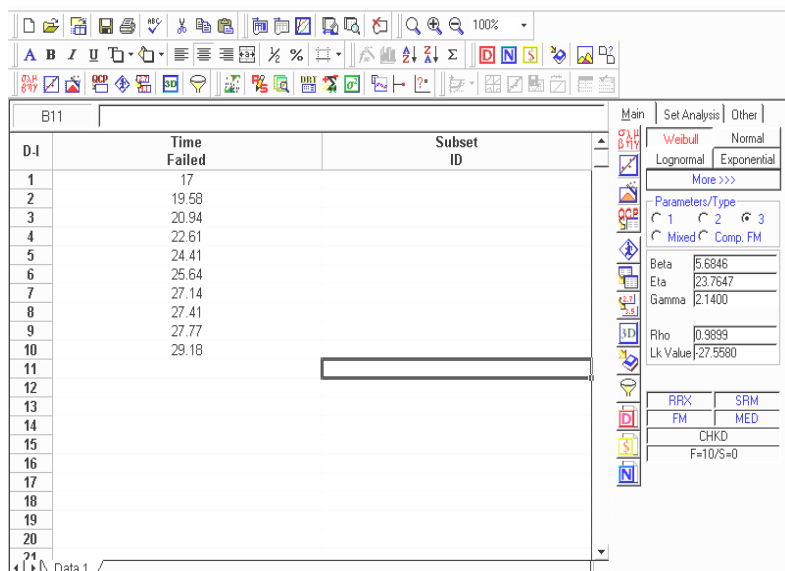


Figure 4 Introducing of experimental data

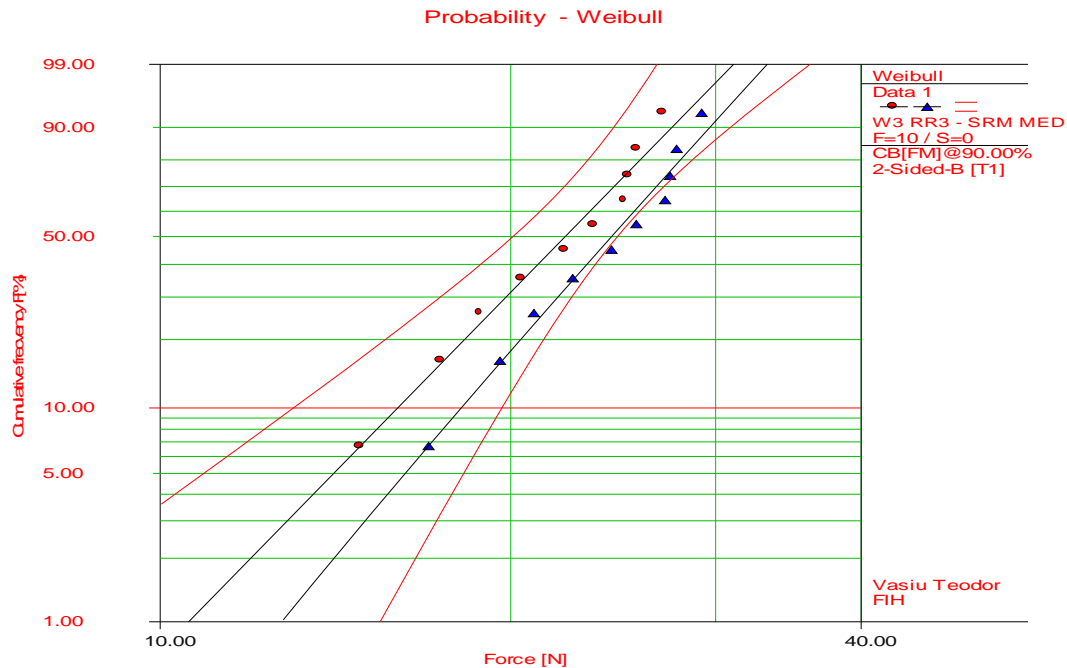
The insulations of the cable lay-ups are subdued also of a thermal stress which consists to heating of the samples to 120°C and maintain their 120 of hours, thereto is done just a visual check of integrity of the insulations.

The processing of experimental date

The values of the forces of destruction are entered in the program Weibull++7 of the Reliasoft corporation, just as is seen in the figure 4.

Launching in execution of the program show that the repartition rule values, of forces which destroy the insulations, is Weibull with three parameters: $\beta = 5.6846$, $\eta = 23.7647$ și $\gamma = 2.14$; which fact is can also see from the Allan-Plait diagram (figure 5).

ReliaSoft's Weibull++ 6.0 - www.Weibull.com

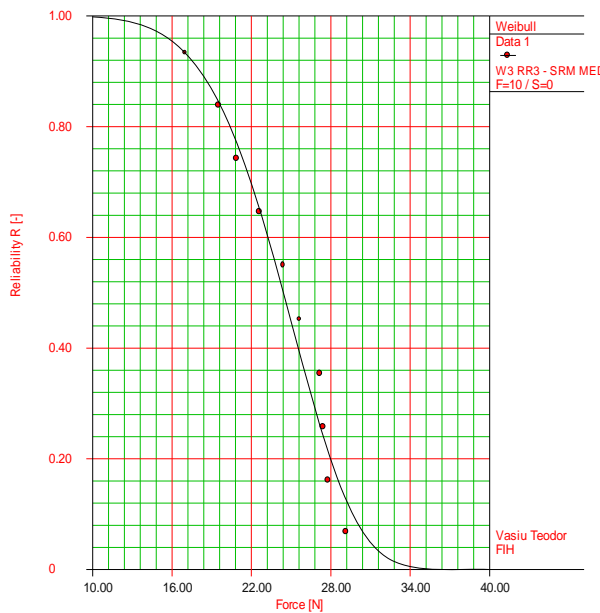


$\beta=5.6846, \eta=23.7647, \gamma=2.1400, \rho=0.9899$

Figure 5 Allan-Plait diagrams

Knowing the rule of repartition it can be traced the reliability of the insulations of the cable lay-ups depending on force tensile (figure 6), the variation accordingly the failure rate (figure 7) and the Likelihood function surface (figure 8).

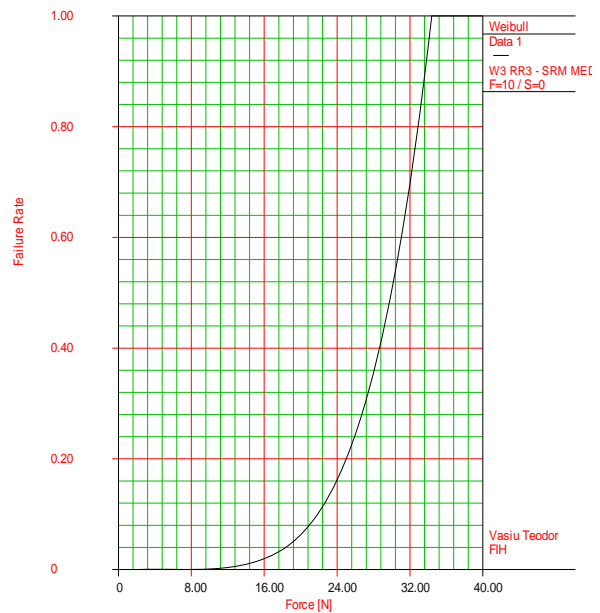
ReliaSoft's Weibull++ 6.0 - www.Weibull.com



$\beta=5.6846, \eta=23.7647, \gamma=2.1400, \rho=0.9899$

Figure 6 Reliability depending on tensile force

ReliaSoft's Weibull++ 6.0 - www.Weibull.com



$\beta=5.6846, \eta=23.7647, \gamma=2.1400, \rho=0.9899$

Figure 7 Failure rate depending of tensile force

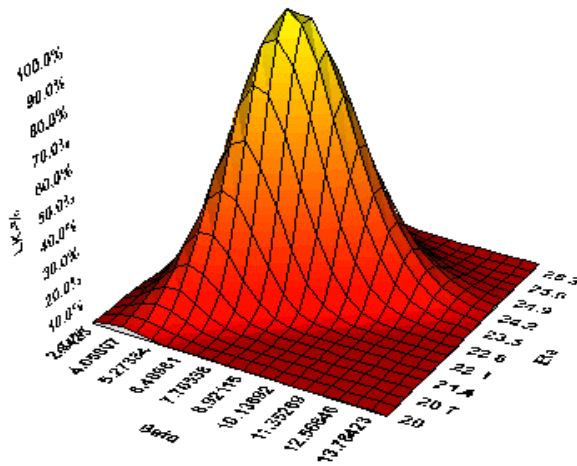


Figura 8 Likelihood function surface
improvement the material from which is executed insulations. Last solution, which presupposes the enlargement of reliability is proves always the viability in time.

3. CONCLUSIONS

The value parameter β show that insulations are in last period of life (the material from which they are made is olden), in which the ruptures can appear anytime to stretch forces bigger of 2N ($\gamma = 2.14$). Between 2 and 8N is estimates that appear just fissures which must be analyzes carefully of the electricians auto. Across 8N (the failure rate grows suddenly opening with this value) can appear detachments of insulations, fact that can produce short-circuits whose consequences are hard to advance.

In other words, is recommended either the carefully leverage the cable lay-ups, either

REFERENCES

- [1] Baron, T., ș.a., *Calitate și fiabilitate - manual practic*, vol. 1 și 2, Editura Tehnică, București, 1988.
- [2] Mihoc Gh., Muja A., Diatcu E., *Bazele matematice ale teoriei fiabilității*, Editura Dacia, Cluj-Napoca, 1976.
- [3] Vasiu T., *Fiabilitatea sistemelor electromecanice*, Editura Bibliofor, Deva, 2000.
- [4] ***, ReliaSoft Weibull++7 software.

SOLUTIONS FOR BREED THE AVAILABILITY OF THE PARALLEL GANG SHEARS ASSIGNED FOR CUTTING THE METALLURGICAL PRODUCTS

BUDIUL BERGHIAN Adina, VASIU Teodor

„Politehnica” University of Timisoara, Engineering Faculty of Hunedoara, Revolutiei str., no.4, ROMANIA

Abstract:

In this paper proposed some solutions for the decrease of the unschedule stops of the 8000Kn shear with parallel gang assigned for cutting the metallurgical products. Analysis of data collected through observation of operation/failure of the shear allow construction of the so-called Pareto diagram, which is an analysis and assessment method that at the same time allow identification of several failures on which should be droved with priority. Based on the study which has been performed is proposed solutions meant to increase the availability of the 8000 kN shear, existent in exploitation.

1. INTRODUCTION

Analyse yes obtained from the observation operation/breakdown of the scissors permits the construction of the Pareto diagram which is a method of analysis and of permissive evaluation therewith the identification of the categories of which bugs must resolve without delate.

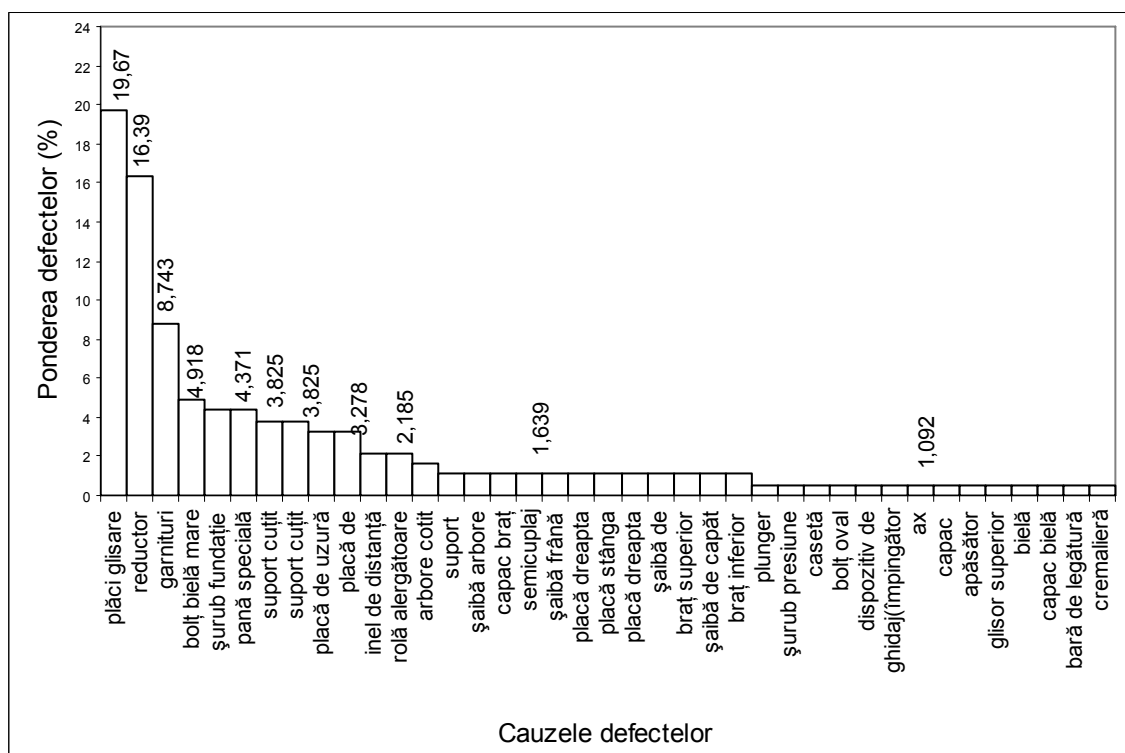


Figure 1. Pareto Diagram for scissors of 8000kN.from the framework of the line of rool S.F.1

From the figure 1. consisted as through his decrease the dismissal of the bonus fourteen guys of out of order, the number accidental stops are reduced with approximate 80% [2].

According to the results obtained by *Pareto diagram*, elements with the highest percentage of failure weight observation (19,67%) are the *sliding plates* which are mounted on the shear body, at the contact area of the upper slide.

2. SOLUTIONS FOR BREED THE AVAILABILITY

Sliding plates are performed currently from CuZn37. As per gives obtained from exploitation and through the determination reaction from the translational couple is can caused the speed of effeteness volumetrically scilicet $v=0,42380\text{mm}^3/\text{s}$.

A proposal for the decrease of the speed of coupled respectively is the execution sliding plates from steel OL60 and these veneering with an alloy a cast-iron appointed sormait for witch by-pathes characteristic date in the table 1.

Table 1. Characteristic date of the alloy a cast-iron appointed sormait

sormait	Addition agents [%]								
	C	Si	Mn	P	S	Ni	Cr	Cu	Mo
	3,46	3,28	1,35	0,066	0,070	2,0	21,65	-	-

The sormait due to of a big content of silicon (3,28%), assure a higher resistance to abrasive effeteness and the mechanical sock. In this choice the cemented carbide he considered the chemical composition satisfies following condition:

- ✚ the contents of carbon and the chromium, of which it depends the amount of primary carbides the eutectic, assure a optimal combination between resistor to effeteness and the tenacity of the layer applied;
- ✚ the content silicon, manganese, molybdenum, nickel and cooper am thus choosed that the plated its layer don't contains the pearlite in the structure.

Experimental tests to determine the wear speed for the coupling sormait-OT50-3 have been accomplished on an existent installation at the Specialized Laboratory of the faculty of Engineering in Hunedoara, the results being shown in figure 2.



Figure 2. Installation for attempms

The attempms they did so that coupled cylinder-disk is like with the bearing load from couple Sliding plates - upper slide.

Following of tests has been determined a volume wear speed of $4,71 \cdot 10^{-3} \text{mm}^3/\text{s}$, which is much lower that the one obtained through exploitation.

Also, according to the same Pareto diagram, at the 4th position is placed the pin of the upper bar with a weight observation of failures of 4,918%. This pin is manufactured of OLC 35 and the diameter of 370mm. In that coupling, pin – big connecting rod, appears the

phenomenon of semi-wet friction. This leads to high values of friction coefficient, intense wear.

Another proposals meant to reduce the non-programmed entity shutting downs are manufacturing the pin of 28TiMnCr12 and its cementation (face hardening). This type of steel [3], after the thermic specific treatment has a top-side constitute from martensite of return with erect content of carbon, verry hard and a resistant core but tenacios ghift with a ferrito structure. The manganese from the content of the steel raises resistance traction, limit of flow the steel, and the chromium confers the great effeteness resistance and good qualities of chip removal.

Forwards, has been performed the analysis of pin resistance by the method of finite element using a specialized software (Algor) in the two alternatives of materials: *OLC35 and 28TiMnCr12*.

3. ANALYSE THE RESISTOR OF THE BOLT THROUGH METHOD OF FINITE ELEMENTS

Analyse the mechanical systems through the method of finite elements, represents solution mathematics of the engineering problems, what it has to base division the studios bodies in discreet elements (finite) formally of a cubbies or tetrahedrons. Analyse through the method of finite elements permits the determination of the stress distribution, specifically strains, to the movements, analyse vibrations, etc, for requirement of connection and load yes. Analyse the mechanical systems through the method of finite elements can be done with matrical calculation complex utilizing software packages such as: Algor, Ansys, Cosmos, etc. Afterwards, is presented the analyse of the pin resistance with help of the program Algor4.

Analyse of the pin resistance with software specialized presupposed run next stages:
- the transfer of the pin model from Inventor in Algor (stp. format) and the settlement type of the analyse (static analyse), the figure 3.

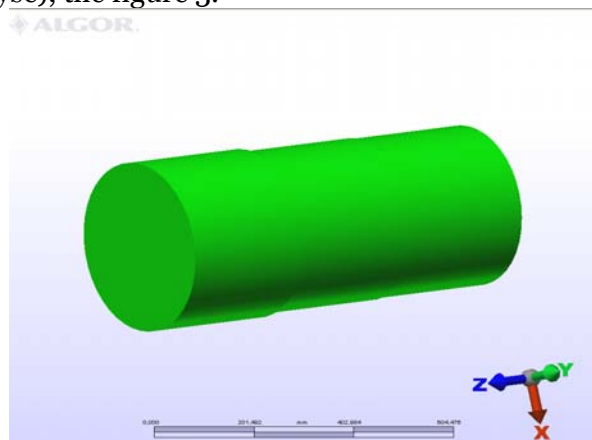


Figure 3. Transfer of the pin model

- the settlement parameters digitization and the digitization (mesh area) the model (figure 4.)

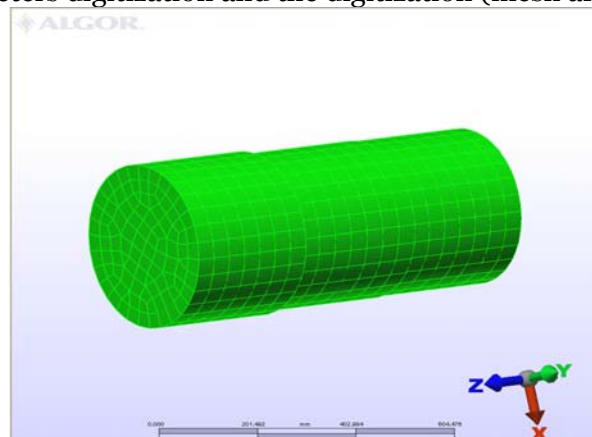


Figure 4. Digitization the model

- the settlement of the compulsions motional in the linkers, respectively shall kept the motion of rotation around axis Z as per the figure 5;

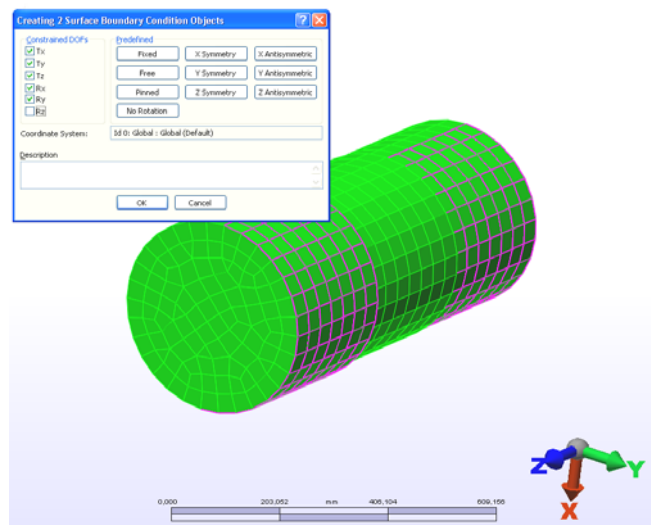


Figure 5. Settlement of the compulsions motional

- the settlement of the load: reaction from couple big bolt has the maxim value $7,384 \cdot 10^6 \text{N}$. With this value, can cause the bearing load between elements (71,27Mpa), as per figure 6;

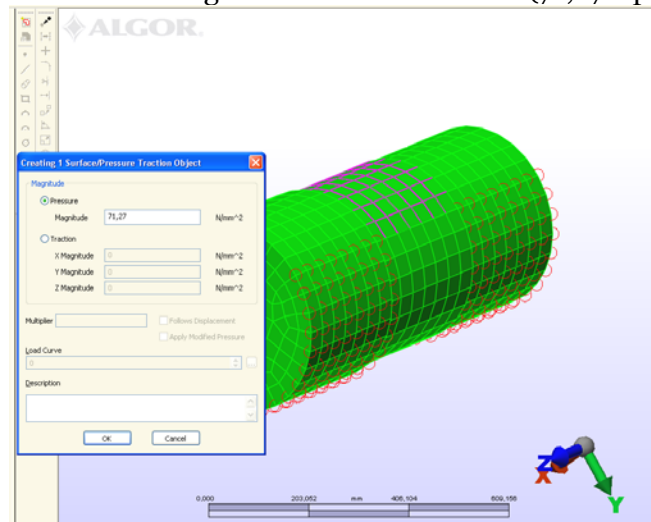


Figure 6. Settlement of the load

- analyse own said the bolt executed from OLC35, the state tensional von Mises (figure 7), the specific deformation (figure 8) and the nodal movements (figure 9);

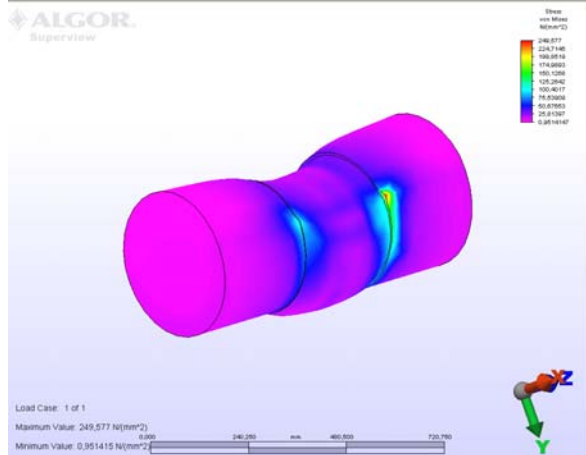


Figure 7. The state tensional

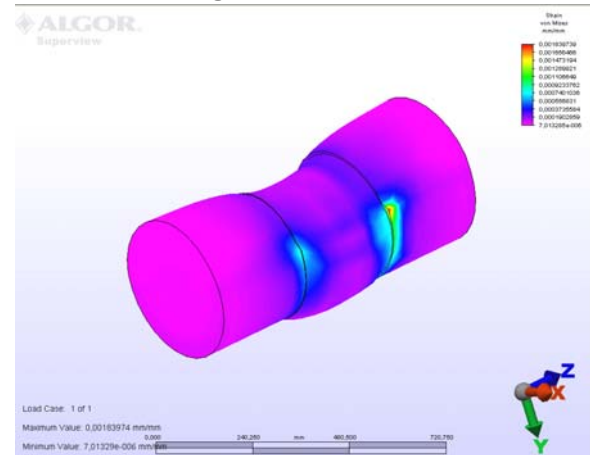


Figure 8. The specific deformation

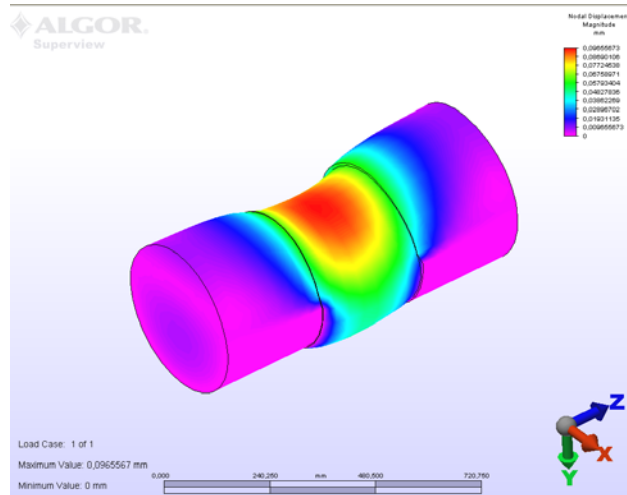


Figure 9. The nodal movements

Afterwards, is presented the analyse of the bolt executed from 28TiMnCr12, the state tensional von Mises (figure 10), the specific deformation (figure 11) and the nodal movements (figure 12):

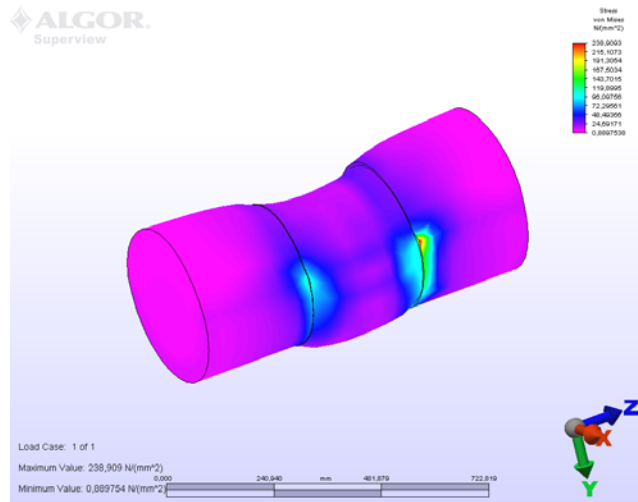


Figure 10. The state tensional

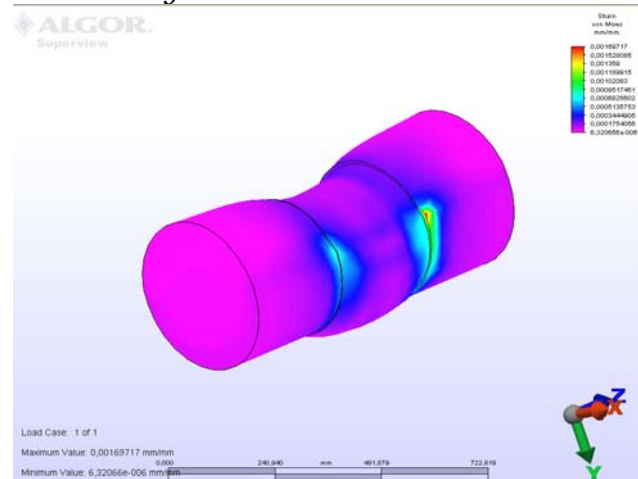


Figure 11. The specific deformation

From analysis presented on the two types of materials has been ascertained that in the situation of the cementation alloyed steel, 28TiMnCr12, both specific deformations and node movements are smaller for the same burden.

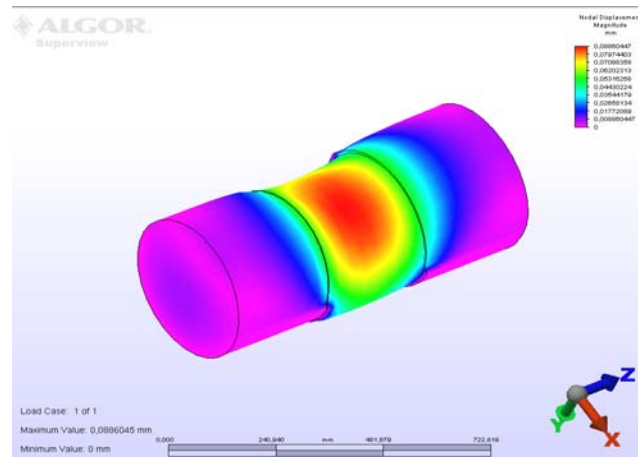


Figure 12. The nodal movements

Other proposals meant to reduce the non-programmed entity shutting downs are manufacturing the pin of OL37 and its plating with polytetrafluor-ethylene. The polytetrafluor-ethylene abbreviated PTFE [5], [6], can replaced material metallic antifrictions in certain conditions presenting the plasticity, good thermic resistance and reduced friction coefficient. Is proof to the low and higher temperatures and presented the chemical resistance to the most corrosive agents. It present notably non-adhesiveness.

The features the mechanics for polytetrafluoroethyls are presented in the table 2.

Table 2. The features the mechanics for PTFE

Mechanical property	Method of test ISO(ASTM)	Stone	Valori
Attempts to traction:			
- Limit of flow/resistance to rupture through traction	527	MPa	15,2/28
- The breaking elongation through traction	527	%	300
- The module of longitudinal elasticity	527	MPa	625
- The module of transversal elasticity	(D790)	MPa	562
Hardness Shore	2039-1	Sh.D	57
Densitate	-	g/cm ³	2,17
To temperature	-	°C	-200...250

The dynamic friction coefficient, without lubrication is contained between 0,04... 0,1.

3. CONCLUSIONS

Consequently, the proposed solutions: plating of sliding plates with Sormait, manufacturing of the pin of OL37 steel and its plating by polytetrafluor-ethylene and manufacturing the pin of cementation alloyed steel using a specific thermal and chemical treatment are accomplishable and relative easy from technological point of view and with the best practical results.

The suggested solutions, if they shall be selected, can reduce the times of maintenance preventively.

BIBLIOGRAPHY

- [1] Budiul Berghian, A- *Contribuții privind îmbunătățirea fiabilității mecanismelor tip foarfecă pentru debitat produse metalurgice*, teză de doctorat, 2007;
- [2] Budiul Berghian, A.,- *Stadiul actual privind mecanismelor de debitat produse metalurgice*, Referat, doctorat nr. 1;
- [3] Cheșa, I., ș.a., - *Alegerea și utilizarea oțelurilor*, Editura Tehnică, București, 1984;
- [4] ***- *Algor User guide*
- [5] *** - *Typical property data Teflon*, www.ptfeparts.com
- [6] *** - *Typical properties of PTFE*- www. Boedeker.com



INTERACTIVE AND COLLABORATIVE LEARNING IN MECHANICAL ENGINEERING USING INTERNET

ALIC Carmen, MIKLOS Cristina, MIKLOS I.Zsolt

University "Politehnica" Timisoara, Faculty of Engineering Hunedoara, ROMANIA

Abstract:

In the process of preparing tomorrow's engineers and scientists, the universities are facing the challenge of gradually teaching students a reality of modern mechanical engineering, namely the mechanisms that occur from the interaction between different parts of complex technical systems. The use of Internet in the classroom offers the opportunity of efficiently adopting methodologies and advanced learning systems that can help the students to expand their views and explore new frontiers. This paper describes our experience concerning the possibility of using dedicated software (via Internet), for an interactive and collaborative learning in mechanical engineering.

Keywords:

mechanical engineering, educational dedicated software resources.

1. INTRODUCTION

Globalization and advances in information technology have prompted a change in the credentials of the engineers today. Industry needs engineers who can work in a distributed, multifunctional, cross-cultural and multidisciplinary avenue. For responded to this change, in the process of preparing tomorrow's engineers and scientists, the universities are facing the challenge of gradually teaching students a reality of modern engineering, namely the mechanisms that occur from the interaction between different parts of complex technical systems.

The formal lecture, the oldest teaching methods, has been widely use in higher education for centuries. But lecturing alone cannot ensure that students become active learners. Generally, using lectures in combination with other kinds of instruction, such as discussion and cooperative learning, can increase their effectiveness.

The activities used to reach students with different learning styles are very important, while people have different preferences for processing new information. One recent "*hot topic*" in higher education has been the different ways in which students learn: some students prefer to learn by listening, others like visual representations, and still others learn by doing. Incorporating of various resources into lectures and seminar applications improves the chance of understanding of concepts by students with different learning styles. Possibilities include demonstrations, role plays, discussions, simulations, problem-solving, real-world applications, or multi-media.

2. USING OF THE DEDICATED EDUCATIONAL SOFTWARE IN MECHANICAL ENGINEERING EDUCATION

In mechanical engineering education, the concepts developed in the mechanics of materials course, essential in preparation for design courses in the engineering technology disciplines, provide the designer with the tools needed to choose an appropriate material and to establish the necessary sizes for the machine or structure. For the student, the key to success in the course is to develop technical problem-solving skills by working a number of problems taken from a wide variety of mechanical and structural situations.

This paper exposed our experience on the use of the educational software, exemplified with the software called MDSolids, [2], a computer program dedicated to aid students in the study of Mechanics of Deformable Solid. MDSolids was conceived as a tool to help students solve and understand homework problems typically used in the mechanics of materials course and consists of a number of modules, Figure 1a, each focusing on a type of problem typically studied. The software features educational routines for beams, flexure, torsion members, columns, axial structures, statically indeterminate structures, trusses, section properties, Mohr's circle analysis and stress and strain transformations.

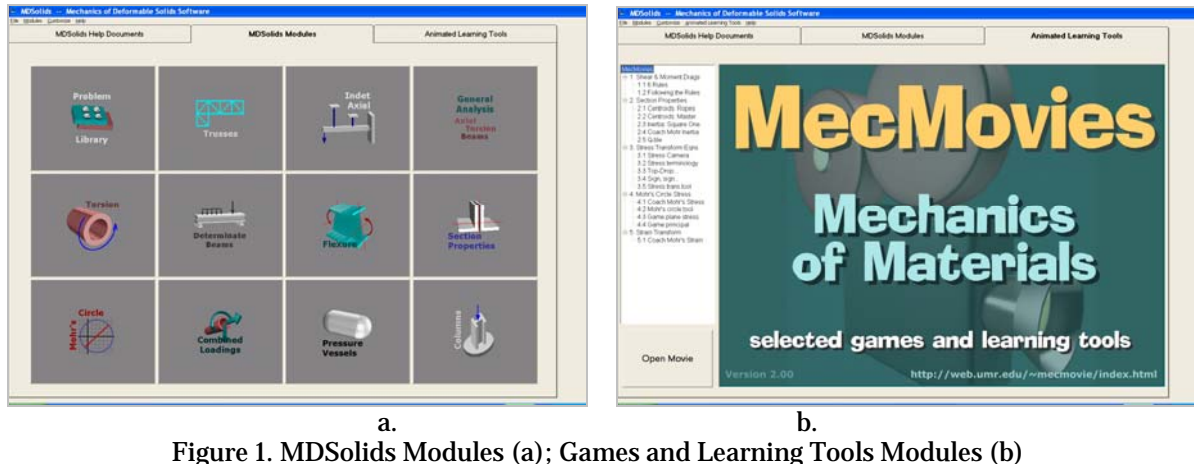


Figure 1. MDSolids Modules (a); Games and Learning Tools Modules (b)

Also, MDSolids contains modules of Animated Games and Learning Tools, Figure 1b, for topics such as: Shear force and bending moment diagrams, Section properties (centroids, moment of inertia, Q), Stress transformation equations and Mohr's circle stress and strain transformations.

Concerning the MDSolids style, this educational software varies from a slideshow presentation of lecture notes to a MathCAD- or TKSolver-type of equation worksheet to a full structural analysis software package. The analysis routines are grouped in modules devoted to particular problem types. These modules focus on specific mechanics of materials concepts and problem-solving methods. MDSolids is powerful enough so that many different combinations of structure configuration and loading can be solved within each module, and it is coordinated so that results from one module can be used in related modules. The modules are constructed so that data for a particular problem can be entered directly and intuitively from a textbook (see Figure 3). MDSolids does not require the user to know a particular sign convention or to enter the data in a particular set of units. Where necessary, the software presents these options in either a pictorial or descriptive fashion.

MDSolids' solutions give the final number and, also, show a picture of how the structure deforms and how the stresses are distributed.

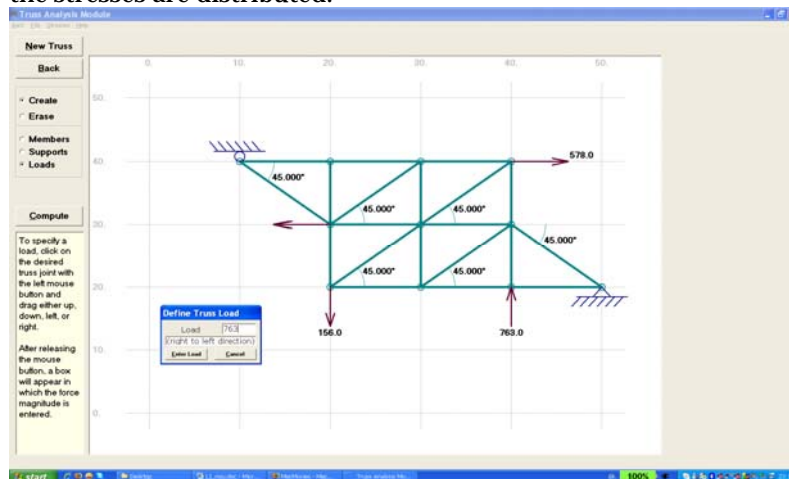


Figure 3. Sample of particular values entering

So, for the student, MDSolids can be helpful in several ways:

- ✚ The MDSolids solution can confirm the results obtained by hand calculations. If the hand calculations are incorrect, the complete solution provided by MDSolids can be used to track down errors in the hand calculations.
- ✚ The solution of typical mechanics of materials problems can be somewhat lengthy. With the MDSolids solution as a reference to keep the hand calculations on track, more problems can be attempted and solved. This problem-solving practice is essential to firmly understand the concepts.
- ✚ MDSolids can build confidence in the problem-solving method needed for the various types of problems included in the modules. The software can also help the student to develop a "feel" or intuition for what the correct answer should be. Confidence in the method plus engineering intuition about the outcome will conquer most of the difficulties commonly encountered in the mechanics of materials course. (Figure 4 and Figure 5).

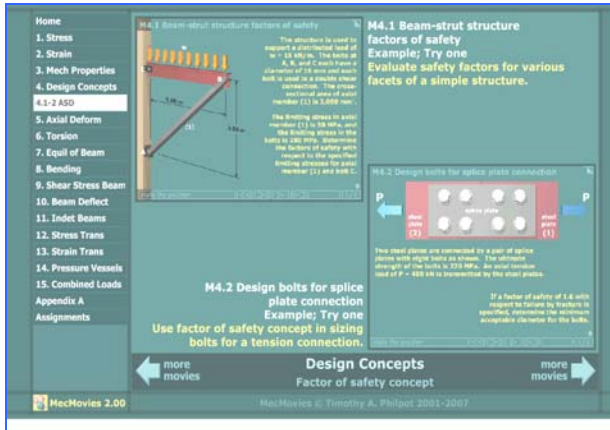


Figure 4. The Safety factor Concept in MecMovies Module

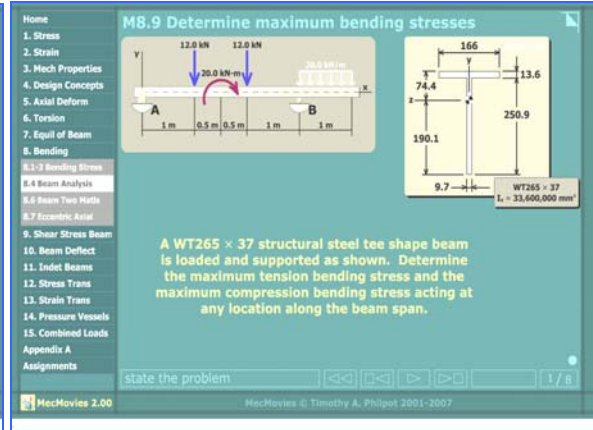


Figure 5. Beam analysis in the Design Concepts Module of MecMovies

MDSolids provides brief text commentary describing the solution, Figure 6. These explanations can help students develop the problem solving skills needed to succeed in the mechanics of materials course. The mechanics of materials course can be a much more satisfying educational experience if students get some extra help from a program such as MDSolids so that they can get themselves on the right track from the start.

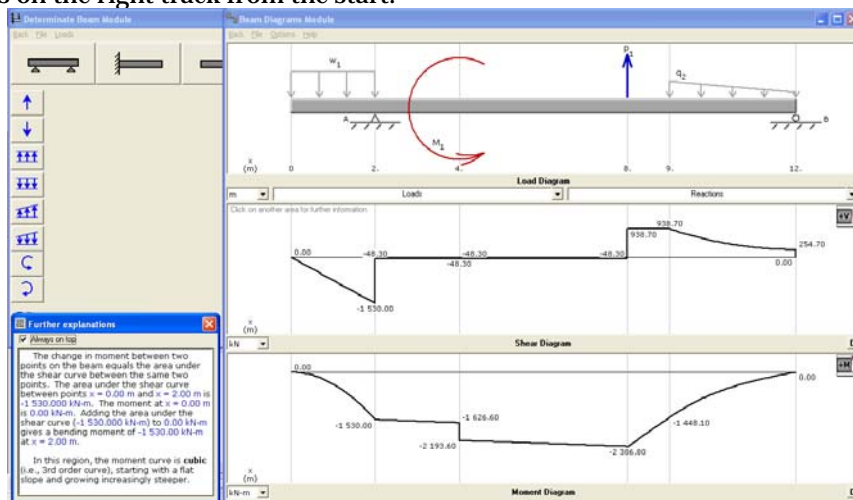


Figure 6. Comments on the solution in the describing box

MDSolids has a Help folder to provide additional information about using the software and the software “navigator”. The Help folder also contain a number of files with worked examples that describe the procedures used to solve the problems. The MDSolids Navigator is intended to help the software in the context of Mechanics of Materials studies. At opening of a book that corresponds to class textbook, will find a list of problems that can be solved and explained by MDSolids. By click on a problem number, the MDSolids Navigator will briefly describe the steps that are required to make MDSolids solve the problem.

3. DISCUSSIONS, APPROACHES AND INTERPRETATIONS

To develop the student understands of the mechanics of materials topics, homework assignments are the primary device used. The typical assignment can be somewhat lengthy; therefore, only selected problems can be assigned. Professors may expect that their students will work enough extra problems so that the fundamentals are firmly grasped, but students sometimes struggle just to keep up with the homework and exam schedule. To supplement the student’s educational development, the self-study potential offered by software would seem to be the ideal means of filling the gap between the material presented in lectures and the understanding and skills expected in homework and exams.

Educational Benefits to use dedicated software, with on-line accessibility:

- ✚ This can help students study mechanics of materials and develop the necessary problem solving, skills in several ways that are not inherent in lectures or customary assignments.
- ✚ Obtain correct Solutions and Intermediate Results: when learning a new concept, it’s very helpful

to use the correct solution as a benchmark. Knowing that the problem has been solved correctly gives the student confidence in their problem-solving skills and thereby provides a foundation for more challenging problems. Every textbook provides answers to selected problems for this reason. Software can provide the student with the correct solution for a particular problem, but in addition to the final answer, software can provide intermediate solutions that can be used to confirm the calculations along the way. These intermediate results can be helpful in tracking down faults in the problem-solving approach.

- ✚ What-If Analyses: Observing a cause-and-effect relationship can be quite helpful to students. For example, a student can develop a sense of the column buckling phenomenon without calculating a single number by assuming various end support conditions and then observing the effects on the buckled shape. This can help students to develop engineering intuition that will help them know what the correct solution should be before they calculate a single number.
- ✚ Availability: In the evening hours, during weekends or when working at home (which may be distant from the classroom), students don't have access to professors, graduate assistants, or others who can help them understand the course material. Having a versatile software tool at hand to supplement the textbook and lecture notes can be a big asset.
- ✚ Repetition: Some people must see or perform more repetitions involving a concept before they begin to fully understand it. Time limits the number of examples that can be presented in lectures and textbooks can present only a few examples. With software, students can drill themselves, trying various numeric combinations for a particular problem type until they feel confident in their understanding of the concepts.
- ✚ Visualization: Software can depict deformations or show stress distributions produced in the problem being considered. Visualization of the material's behavior in response to the loads acting on it can help the student to understand the relevant theory and to develop engineering intuition.

4. CONCLUSIONS

According to the exposed ideas, for a modern education in mechanical engineering field, there is a need to change the traditional lecture based of a passive learning methodology to an active technology using interactive and collaborative learning and the facilities offered by the information technology.

A very good and already experienced example can be the using of MDSolids software (by Timothy A. Philpot at Murray State University, [2]). That offers students numerical, descriptive, and visual results and details that illustrate and explain many types of problems in introductory mechanics of solids courses.

Compared with traditional instruction techniques, the using of educational software supports a learner's development of basic concepts and problem-solving skills through self-study.

REFERENCES

- [1] http://cee.mines.edu/On-line_Resources.htm , On-line Resources in Education
- [2] <http://www.mdsolids.com/> MDSolids Educational Software
- [3] <http://www.merlot.org/merlot/index.htm> , Merlot, Multimedia Educational Resource for Learning and Online Teaching
- [4] <http://www.needs.org>, MDSolids, Premier Award for Excellence in Engineering Education Courseware.
- [5] Alic, C., Miklos, C. – Fundamente de mecanica. Teorie si aplicatii. ISBN 978-973-52-0478-5, Ed. Mirton Timisoara, 2008.
- [6] Staab, G., Harper, B.-Use of Computers in Mechanics Education at Ohio State University, Int. J. Engng Ed. Vol. 16, No. 5, pp. 394, 2000 0949-149X/91, Great Britain.
- [7] Jennifer Kadowec, J., Von Lockette, P., Constans, E., Sukumaran, B., Cleary, D. - Hands-on Learning Tools for Engineering Mechanics, American Society for Engineering Education, Annual Conference & Exposition 2002.



INTEGRATION OF INTERACTIVE MULTIMEDIA LEARNING SOFTWARE INTO MECHANICAL ENGINEERING COURSE'S

ALIC Carmen, MIKLOS I.Zsolt, MIKLOS Cristina

University "Politehnica" Timisoara, Faculty of Engineering Hunedoara, ROMANIA

Abstract:

The integration of Information Technology in the applied educational activities of mechanical engineering, offers an excellent opportunity of improving the level of understanding achieved by the students. This paper describes the progress and results of our project, in testing the use of specific pedagogical resources in the teaching process of basic engineering disciplines, such as Fundamentals of Mechanical Engineering, Mechanics of Materials and Mechanical Vibration, in the inter disciplinary laboratory-classroom.

Keywords:

interactive desktop applications, virtual laboratory modules and experiments, computer based simulations, Java Applets

1. INTRODUCTION. CURRENT MECHANICAL ENGINEERING EDUCATIONAL SOFTWARE

The complexity of many of current mechanical systems has been growing exponentially. Unfortunately, it can be said that, generally, the Romanian higher education system has not kept pace with these needs. Existing undergraduate and graduate science and engineering programs need to incorporate more material on engineering educational software. An approach to using computers to enhance engineering mechanics education at our faculty involved the use of computer interactive desktop applications, virtual laboratory modules and experiments, computer based simulations, Java Applets, etc. This approach was motivated by the fact that the concepts taught in introductory engineering mechanics courses are often difficult for students to visualize and fully grasp. According to [6], an effective multimedia program should clarify abstract topics that are difficult to understand using traditional teaching media and focus on teaching concepts rather than entertaining students with shallow special effects. Software is currently being developed for Mechanics fundamentals, Dynamics and vibration and Strength of materials which focuses on illustrating theory, presenting relevant examples, and supplying quizzes for users to work. Many students first encountering mechanics have problems identifying what is wanted, how to decompose the problem into simpler segments, and what information they need to solve the problem. For such students, the authors believe that a directed learning procedure similar to that presented as examples in this paper is an appropriate procedure.

2. THE CASE STUDY

As a teacher team that has expertise in engineering of mechanical systems field, we have proposed two year ago a project for an interdisciplinary virtual laboratory-classroom equipped with computers network and educational software. This laboratory is currently operational in our faculty and is dedicated our students, future mechanical engineers, who can use here innovative and advanced educational software solutions. In this interdisciplinary laboratory, over the winter semester of the current academic year, we have developed a test program regarding the use of specific pedagogical resources in the teaching process of basic engineering disciplines, such as Fundamentals of Mechanical Engineering,

Mechanics of Materials and Mechanical Vibration. This test program is continued during the summer semester in aim to investigate how educational soft wares can aid our students to involved their design and structural analysis competences.

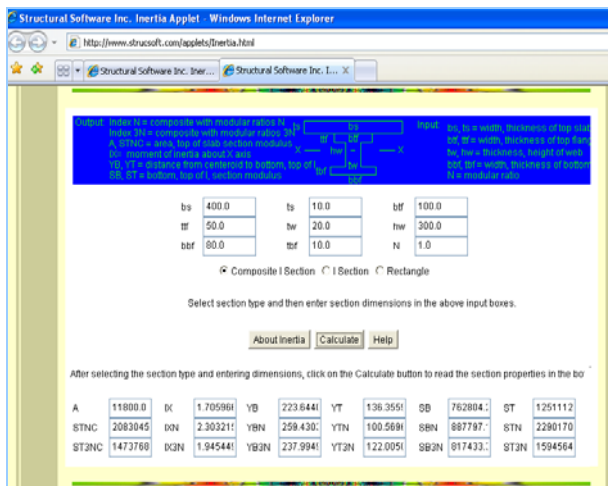
During the preparation period of this test program, our team devotes considerable resources to identifying the latest developments of dedicated and, if it is possible, free accessible software's, in order to update and review the packages installed on the network. In Figure 1a-1f and Figure 2a-2d, we are exemplified some of teaching resources used in our virtual laboratory-classroom.

In the domain of mechanical engineering, most of the current existing educational software can be grouped, generally, in the following categories: tutorials, worksheets, and basic analysis packages.

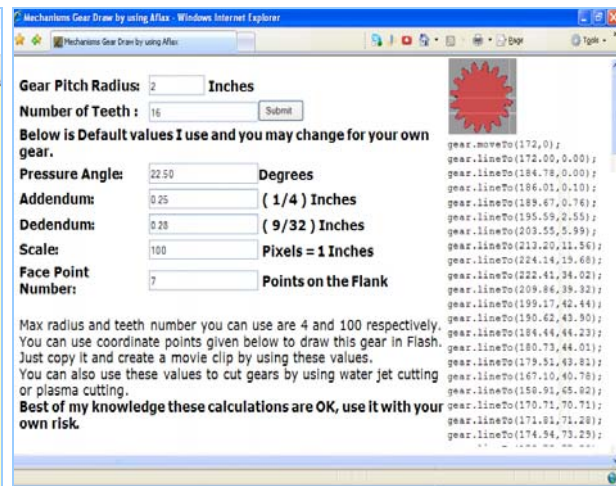
- Tutorials direct the student through a series of prepared screens, each focused on a specific concept or skill. In this manner, tutorials are like lectures delivered in a different format. Tutorials such as the Multimedia Engineering series feature impressive presentation complete with animation, video clips, and audio files. [2]. Despite excellent presentation, however, tutorial products are limited in applicability. The student must follow the sequence of the tutorial presentation in the same way that they would follow along in a lecture. Also, the student must master the concept presented by the tutorial and then apply that concept to the particular problems that they are asked to solve in their homework assignments.

- Worksheets for equation-solving software such as Mathcad, MATLAB, etc, have also been developed to supplement the mechanics engineering courses [3]. One drawback of worksheets is that the student must be somewhat familiar with the host software package in order to use the worksheet. This disadvantage can also be viewed as an advantage since worksheets encourage the student to develop some command of the equation-solving software, and familiarity with the equation-solving software is a skill that is useful in later engineering courses. However, to the student whose immediate goal is learning the mechanics of materials concepts, the added burden of gaining proficiency with the equation-solving software can be daunting.

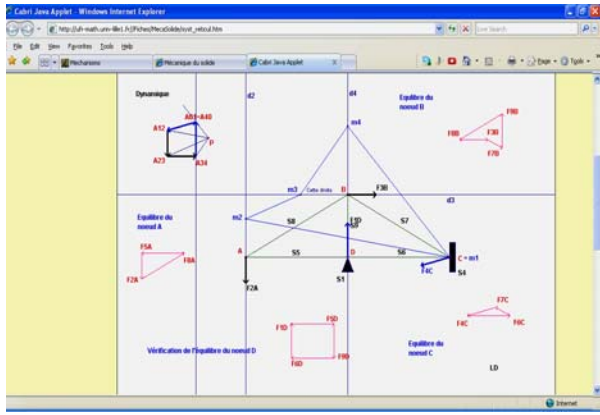
- Basic analysis packages have been included in several widely available mechanics of materials textbooks such as [4], [5]. These programs are useful as tools for assisting students in fundamental skills such as plotting shear and bending moment diagrams or performing Mohr's circle calculations. Basic analysis programs may require students to define nodes and elements and to assign section properties and material constants to the elements.



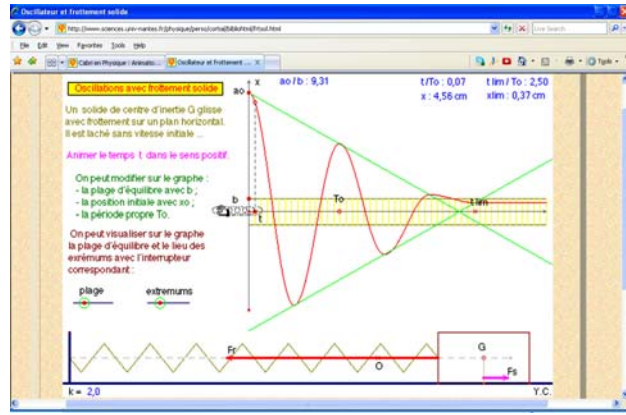
a. Inertia.class Applet
(source Structural Software, Inc.,
<http://www.strucsoft.com>)



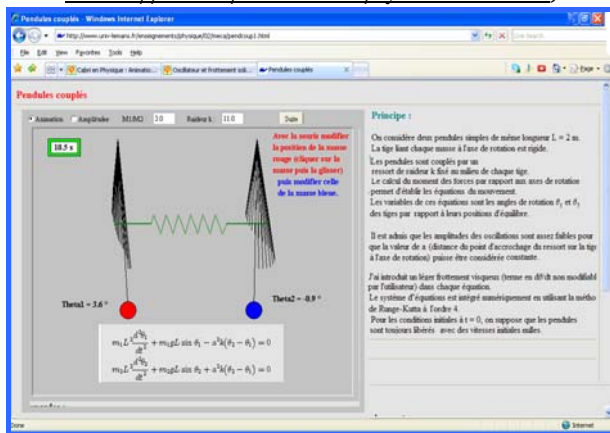
b. Mechanism Applet
Index, Linkage Mechanisms, Gears,
Pneumatic Systems (source of the applet
http://www.mekanizmalar.com/gear_draw.cgi)



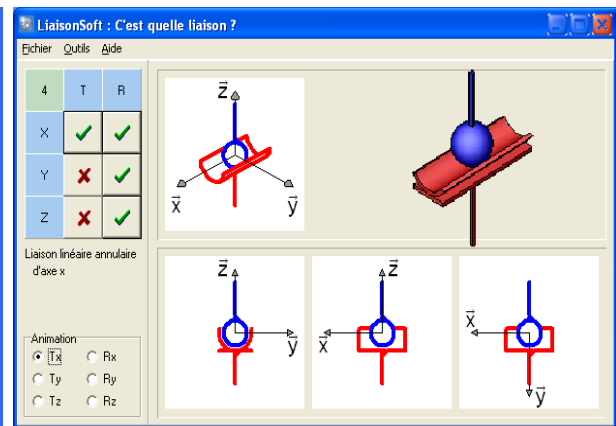
c. Cabri Java Applet
Equilibre de systèmes réticulés
(source Laboratoire virtuel- Université de Lille, France,
http://ufr-math.univ-lille.fr//Fiches/MecaSolide/syst_reticul.htm)



d. Cabri Java Applet
Oscillateur. Ressort avec frottement
(source Laboratoire-Université Nantes,France,
<http://www.sciences.univ-nantes.fr>)

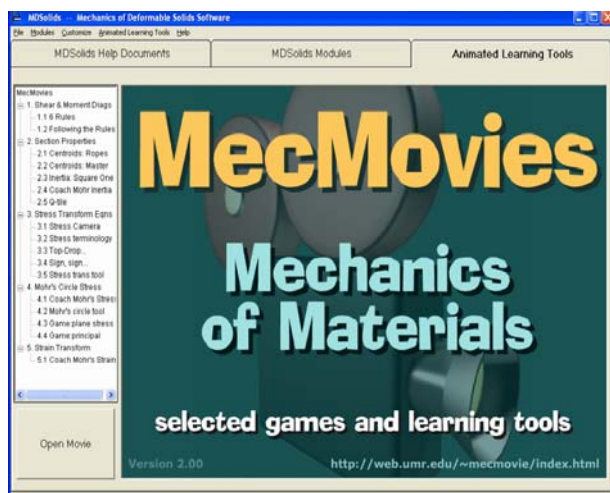


e. Cabri Java Applet
(source Laboratoire-Université Nantes,France,
<http://www.sciences.univ-nantes.fr>)

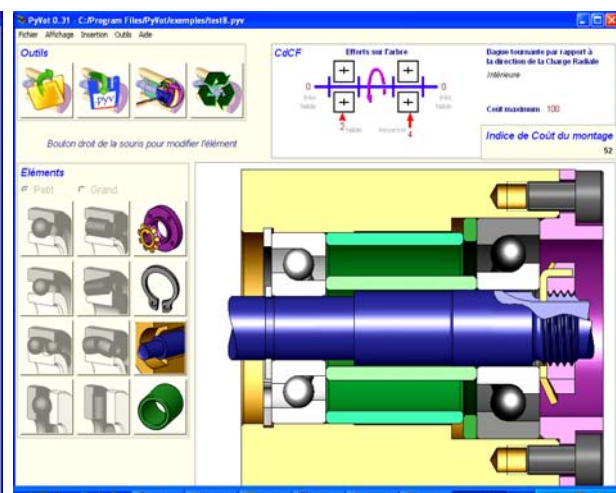


f. Educational software MecaTools
(source Laboratoire-Université Nantes,France,
<http://www.mecatools.new.fr>)

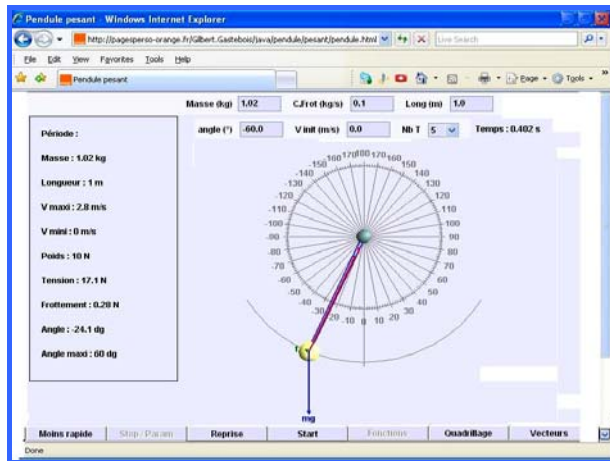
Figure 1. Teaching resources used in the virtual laboratory-classroom
Java Applets and Educational software



a. Educational software Mdsolids
Animated Learning Tools Module
(source <http://www.mdsolids.com>)

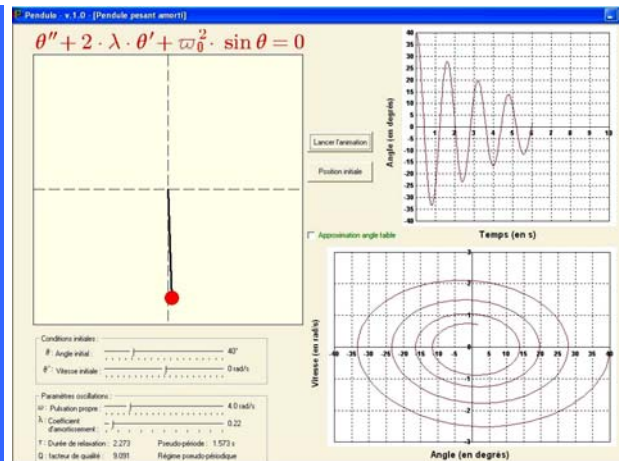


b. Educational software PyVot
Bearing assembly Analyzer
(source <http://pyvot.fr>)



c. Educational software

Simulations in physical sciences
(source <http://pagesperso-orange.fr/~java/accueil.htm>)



d. Educational software Pendulo
Engineering sciences

(source <http://www.sciences-edu.net/>)

Figure 2. Educational dedicated software used in the virtual laboratory.

Input for these programs has typically been very text-based, often requiring a user's manual to ensure that the proper data and sign conventions are used and to help in interpreting the program output.

The novice engineer may feel overwhelmed by the attention to detail needed to set up an analysis model and may have difficulty visualizing and interpreting the resulting tables of numerical output.

3. ANALISES, DISCUSIONS, APPROACHES, INTERPRETATIONS

The final goals of our work initiative in the virtual laboratory-classroom are listed below. These objectives are more detailed described in the laboratory project proposition.

1. Use hands-on and visualization tools to aid students in problem formulation and enhance learning opportunities.
2. Integrate software simulation experiences into lectures.
3. Ensure that the equipment that is developed has an impact on core courses in Statics and Solid Mechanics as well as advanced courses in the Mechanical engineering programs.
4. Improve the critical thinking and problem solving skills of students by engaging them in the learning process, allowing individual experimentation and providing for interchangeability of the tools.
5. Ensure material is taught in variety of ways to benefit students with various learning styles.

During the implementation period of the project, we consistently that, generally, a fairly consistent part of the educational softwares are developed from the professor's point of view, emphasizing lecture topics or permitting the student to perform more advanced calculations.

But, to be successful, educational software should be developed from the student's point of view. Rather than forcing the student to solve a problem posed by the software, the software should solve the problem of interest to the student.

To do this, educational software must be:

- ✚ versatile in the types of problems that can be solved;
- ✚ strongly visual to illustrate the behavior of materials or of mechanical systems;
- ✚ informative in explaining how and why the calculations are performed;
- ✚ intuitive and easy-to-use so that the student is presented with just the right amount of information and analytical power.

4. CONCLUSIONS

Today, engineering education can be considered realizing the potential of multimedia as learning and teaching tool.

The use of computer multimedia offers several tools that are useful in general engineering education and, particularly, in mechanical engineering education. Classical engineering graphics topics using a combination of animation, audio description, and interactive exercises can help the students

The most important benefit provided by multimedia can be considered the possibility of interaction. Many studies indicating that interacting with information can be a positive effect on learning since people remember/internalize more information if they interact with it (e.g. hears, see, and do).

Multimedia provides an excellent means of generating interaction through interfaces that require the user to make choices and perform actions.

Results of surveys indicate that the use of multimedia educational software in the virtual laboratory-classroom was extremely well received by the students and helped with the understanding of the training material in mechanical engineering field in mechanical engineering domain.

REFERENCES

- [1] Lieu, D.K. - *Using Interactive Multimedia Computer Tutorials for Engineering Graphics Education*, University of California, Journal for Geometry and Graphics, Volume 3 (1999), No. 1, 85-91
- [2] Malalasekera, A., Walsh, S. J. *Comparison of Approaches to a Multimedia Presentation*, Conference ICL2007, September 26 -28, 2007, Villach, Austria
- [3] Wilson, H., Louis H. Turcotte, H.,L., Halpern, D. - *Advanced Mathematics and Mechanics Applications Using Matlab*, ISBN 1-58488-262-X, 2002.
- [4] Philpot, T., A. - *Bridging the Gap between Mechanics of Materials Lectures and Homework with MDSolids*, The Technology Interface/Spring 1998, Murray State University.
- [5] Craig, R.R. *MechSolid in Mechanics of Materials*, John Wiley & Sons, 1996. New York, N.Y.
- [6] Owen, E. F. Helps, C. R. G. *Planning effective multimedia programs for technical education*, Proc. 1996 Frontiers in Education Conf., IEEE (1996) pp. 1047-1050.
- [7] Alic, C., Miklos, Z., Miklos, C. *Computer Aided Design Methods for an Optimal Quality of Conception and Exploitation of the Pre-Stressed Bolted Joints*, ISBN: 978-80-553-0069-6, Management of Manufacturing Systems MMS-2008, The 3rd Conference With International Participation, Prešov, Slovakia.
- [8] Alic, C., Barboni, D. *Upon the implementation of the Multidisciplinary Laboratory equipped with Educational Software*, Symposium “Didactic Methods Between Traditional And Modern” Lugoj, Colegiul Național ”Coriolan Brediceanu” , 2009.
- [9] Alic, C., Miklos, C., Miklos, Z. *Kinematic and Dynamic Analysis for EP3 asymmetric pantograph mechanism used in railway electric traction with SAM 5.0 Programs* ISBN 86-85211-92-1, *The 5th International Symposium about Shaping, Industrial and Product Design*, "KOD 2008". p.181-186, Novi Sad, Serbia.



EVALUATION OF THE SMOKE DEGREE AND CO₂ EMISSION IN CORRELATION WITH THE DISTANCE COVERED BY ROAD VEHICLES

PADURE Gelu, NEGREA Virgiliu Dan

„Politehnica”University of Timisoara, ROMANIA

Abstract

The paper presents the evaluation of the smoke degree in correlation with distance covered by a road vehicle, based on experimental measurements and theoretical modellations through mathematical functions. The evolution of CO₂ emission is evaluated using a specific software (DEKRA)

Key words:

smoke degree, CO₂ emission, DEKRA

1. GENERAL

The particles emitted by diesel engines consist mainly of soot, generated during the combustion (carbon graphite) and hydrocarbons adsorbed or condensed. Particles are defined in the law of the material (except water) that is collected on a Teflon filter to shift gas emitted by motor burned, previously diluted with filtered air, dilution with clean air is provided to meet the filter temperature be less than 52 ° C to avoid volatilization of hydrocarbons and water condensation.

Measurement of particle is based on previous definition and involves a complicated procedure, which involves diluting the exhaust gas (or part of them), the precise measurement of the ratio of dilution, weighing filters before and after sampling in a controlled atmosphere, knowing the exact diluted gas flow passing through the filter during sampling.

Since particle measurement is an operation with many phases, expensive and lengthy, there were many attempts to correlate measurements with gravimetric particle measurements of smoke index, using ordinary fummeter (Bosch, Hartridge) or other instruments not placed on the market. Most studies on this subject have obtained correlations between the numbers of smoke and soot concentration measured in undiluted exhaust emissions. Therefore, it will applicativitatea existing correlations in smoke-soot mass emission estimates for particulate matter and will investigate the relationships between particles, soot and smoke, and in correlation with the distance traveled by vehicles.

2. MEASURED VALUES

Measurements were made on a car brand Volkswagen Sharan - 1.9 TDI with measuring devices owned by two measuring stations, measuring smoke according with TÜV - Germany rules, in connection with Annexes XIa and IXa StVZO (a), respectively the tests in relation with Annex VIIIa and IXa StVZO (b).

For the two types of tests, the following values were selected:

- at relanti speed: according to (a) – $n_o = 700 \dots 950$ rpm
according to (b) – $n_o = 770 \dots 940$ rpm
- at rated speed: according to (a) – $n_n = 4700 \dots 5200$ rpm
according to (b) – $n_n = 4800 \dots 5200$ rpm
- for absorption coefficient KM: according to (a) – $K_M = 0.43 \text{ m}^{-1}$
according to (b) – $K_M = 1.85 \text{ m}^{-1}$
- number of kilometers covered: 20.000 km

Table 1 and figure 1 presents data for the smoke, estimated by the coefficient of absorption K_M , depending on the number of km traveled.

Table 1

Crt. no.	Absorbtion coefficient Hartridge $K_M [m^{-1}]$	Traveled distance [km]
1.	0,43	20.000
2.	0,9	30.000
3.	1,25	40.000
4.	1,51	50.000
5.	1,751	60.000
6.	2,0	70.000

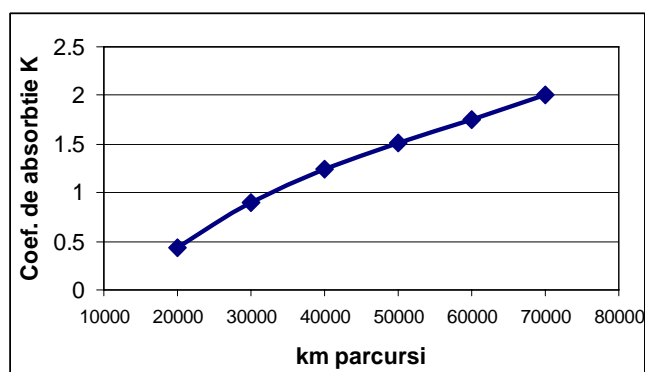


Figure 1. The absorbtion coefficient evolution vs. traveled distance

Table 2 give the data obtained through the exploitation of the DEKRA Soft Programme - Germany - 2007, for the route fuel consumption C_c [l/100km], specific CO_2 emissions - E_{CO_2} [g / km], that the total mass of CO_2 exhausted - M_{CO_2} [kg], depending on the number of km traveled by car.

Table 2

Crt. no.	Route fuel consumption C_c [l/100km]	Nr. of km traveled [km]	Specific emission of CO_2 E_{CO_2} [g/km]	Absolute emission of CO_2 M_{CO_2} [kg]
1.	6,8	20.000	180,2	3604,8
2.	6,9	30.000	182,9	5485,5
3.	7,0	40.000	185,5	7420,0
4.	7,1	50.000	188,1	9407,5
5.	7,2	60.000	190,8	11448,0
6.	7,3	70.000	193,9	13541,5

3. MATHEMATICAL MODELS

In all technical fields and not only, for studying of a certain process for establishing of a mathematical model, as a form of expression of the synthetic target and deployment process, that can later be used in different theoretical approaches. It follows that establishing the mathematical model based on experimental data is one of the main aims pursued by carrying out tests which should not be so to be repeated.

Obtaining non-linear models is more difficult due to the lack of a general theory that the uniform linear, therefore, most often resulting study nonlinear processes in particular cases. There are some treatment unit and the non-linear models, but still only valid for certain special cases, such as the polynomial models.

Thus, the size of the result y and x variable factorial model has polynomial general form:

$$y = \sum_{i=0}^m a_i x^i \quad (1)$$

For example, for a two-degree polynomial expression (1) becomes:

$$y = a_2 x^2 + a_1 x + a_0 \quad (2)$$

Relations were presented in full polynomial structure, so with all the expression characteristics terms. If using an unfully polynomial structure, missing at least one term, for example, in absence of the free term model (2) becomes:

$$y = a_2 x^2 + a_1 x \quad (3)$$

Using a cubic polynomial expression, relation (1) takes the form:

$$y = a_3 x^3 + a_2 x^2 + a_1 x + a_0 \quad (4)$$

Obviously, if considered a linear model, then the relationship (1) became:

$$y = a_1 x + a_0 \quad (5)$$

Starting from data presented in Table 1, considering the evolutionary curve of the

absorption coefficient Hartridge K_M according to the distance D traveled by the vehicle as a parable of second degree and applying relation (2), the following relationship which considers the evolution of K_M is obtained:

$$K_M = -0,023 \cdot D^2 + 0,521 \cdot D - 0,52 \quad (6)$$

The coefficients a_0 , a_1 și a_2 of the relationship (20) were obtained by applying the experimental results. Thus were obtained the following values:

$$a_0 = -0,52 ; a_1 = 0,521 ; a_2 = -0,023$$

There was not found major deviations from the experimental curve (Figure 1), the calculation curve is well overlapped above the theoretical, obtained by mathematical modeling - fig. 2.

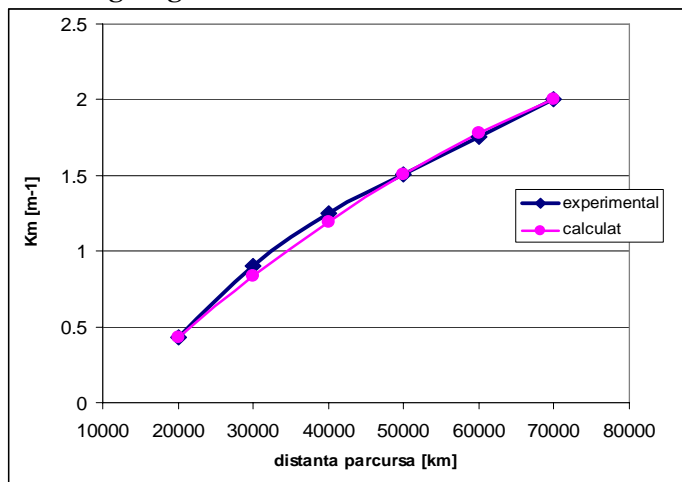


Figure 2. Comparison between absorption coefficient – experimental and calculated

For the intermediate points, i.e. those who have not served for establishing the constants a_0 , a_1 , a_2 , there was obtained deviations between 1.52 ... 4.32%, which are acceptable from a technical standpoint.

Accepting the mass particle content (GFC) evolution as a parable of a second degree, with the coefficients a_0 , a_1 , a_2 determinated as reasoning presented above ($a_0 = -0,016$; $a_1 = 0,062$; $a_2 = -0,002$), the following function is obtained:

$$GFG = -0,002 \cdot D^2 + 0,062 \cdot D - 0,016 \quad (7)$$

In Figure 3 presents graphically dependence $GFG = f(D)$. Deviations between theoretical and experimental points are below 2%, which corresponds to the aim pursued.

Table 3

Crt. no.	No. of km traveled D [km]	Absorption coefficient K_M [m^{-1}]	Mass particle content GFG [g/m^3]	Hartridge smoke degree HSU [%]
1.	20.000	0,43	0,10	1,0
2.	30.000	0,90	0,16	1,4
3.	40.000	1,25	0,20	1,9
4.	50.000	1,51	0,24	2,3
5.	60.000	1,75	0,28	2,5
6.	70.000	2,00	0,32	2,7

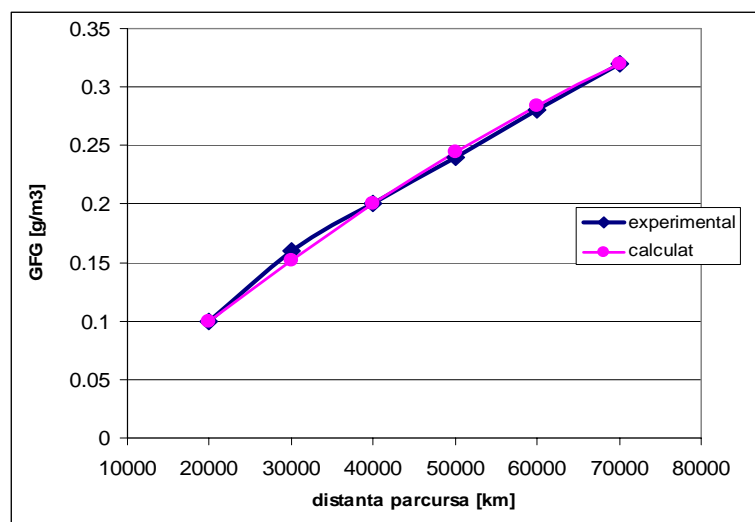


Figure 3. Comparison between mass particle content (experimental and calculated) vs. traveled distance

Modeling the evolution of CO₂ emission and route fuel consumption in relation to distance traveled for the analyzed car was realized also by functions. Experimental data for calibration are presented in Table 4.

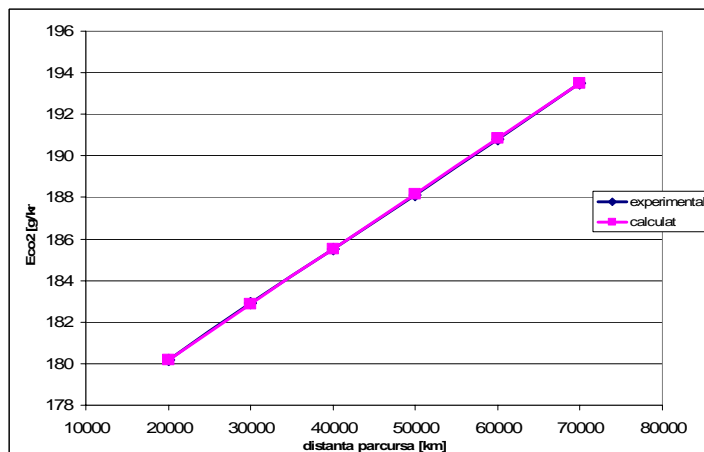
Table 4

Nr. crt.	Route fuel consumption C _c [l/100km]	Nr. of km traveled D [km]	Specific emission of CO ₂ E _{CO₂} [g/km]
1.	6,8	20.000	180,2
2.	6,9	30.000	182,9
3.	7,0	40.000	185,5
4.	7,1	50.000	188,1
5.	7,2	60.000	190,8
6.	7,3	70.000	193,9

Specific emission of CO₂ - estimated through DEKRA 2007 software, the function which describes the evolution is linear type:

$$E_{CO_2} = 2,66 \cdot D + 174,88 \quad (8)$$

It finds a good correlation of experimental data with those obtained by mathematical modeling with functions, deviations were recorded are virtually negligible.


 Figure 4. CO₂ emissions in correlation with traveled distance

Using the DEKRA - Germany 2007 software, it could be determined the evolution of route specific fuel consumption, the specific and absolute emission of CO₂ according with the distance traveled by an automotive car, with an concrete example of calculation.

4. CONCLUSIONS

Based on own measurements, there were established the evolution the level of smoke degree and particles emissions in relation to the distances covered. Experimental researches are performed on the smoke opacity measured in relation with the distance traveled by the car equipped with a diesel engine. There are presented graphically and tabular variation for K_M absorption coefficient based on the distance traveled. These allows establishing how the distance traveled values influence this factor.

REFERENCES

- [1] Negrea, V.D., Sandu, V., *Combaterea poluării mediului în transporturile rutiere*, Ed. Tehnică, București, 2000.
- [2] Negrea V.D., ș.a., *Transporturile și dezvoltarea lor durabilă*, SMAT 2008, Craiova, octombrie 2008.
- [3] Pădure, G., *Studii și cercetări privind evaluarea noxelor produse de către motoarele cu ardere internă*, teză de doctorat, Timișoara, 2000.
- [4] *** *Leitfaden zu Kraftstoffverbrauch und CO₂ Emissionen – Ausgabe 2007 - VDA*



AN EXPERIMENTAL ANALYSIS ABOUT THE FRACTURE OF THE WHEELSET-AXLES OF THE 5100 KW ELECTRIC LOCOMOTIVE

¹. Eugen GHITA, ².Lucia VILCEANU, ¹. Ramon BALOGH, ¹.Monica DOBRA

¹. "POLITEHNICA" University of Timisoara, Mechanical Engineering Faculty, ROMANIA
². "POLITEHNICA" University of Timisoara, Faculty of Engineering Hunedoara, ROMANIA

ABSTRACT:

The paper is focused on some experimental analysis performed in the Testing Materials Laboratory belonging to I.C.M. Resita regarding the appearance of cracks in the wheelset-axles of the 5100 kW electric locomotives. Chemical, traction, bending dynamic and torsion tests are performed for different wheelset-axles, different rolling distances and different working conditions which for the "stick-slip" phenomenon occurred.

Keywords:

locomotive, wheelset-axles, mechanical test, crack, stick-slip.

1. INTRODUCTION

The proper against skating device of the C.F.R. 5100 kW electric locomotives is not very efficient when a high level difference has to be raised. As an example, when a heavy train is trailed on an important level difference (as it is the Brasov – Predeal railway route), some important oscillations of the wheelset-axles appeared. The main reason is that for difficult traction conditions, the adherence limit is exceeded. The driving torque on the wheels is divided into non-equal parts, so the "stick-slip" phenomenon of the wheelset-axles is present, which mean an alternate torsion and slip state. Because of the elastic assembling of the wheels on the axles, the whole ensemble will oscillate with a proper frequency.

When the phenomenon takes place in the framework of the micro-sliding domain [1],[2] which means in the framework of a perfect adherence, the oscillation are of a high amplitude. The possible consequences is the appearance of a high state of stress in the wheelset-axles. But the final and the most dangerous consequence is represented by the fracture of the wheelset-axles ensemble [3]. This is the reason why the analysis of the wheel set-axles became obviously necessary [4]. It means both a mechanical,chemical analysis and an experimental non-destructive analysis, in order to detect possible crack initiating locations in the volume of the wheelset-axles.

2. LABORATORY EXPERIMENTAL ANALYSIS

During the time and according to railway administration regulations, the experimental analysis often avoids the appearance of the wheelset-axles fractures. The main studied wheelset-axles types are presented in table 1:

Tabel 1.

Nr.	Locomotive type	Number of wheelset on the locomotive	Rolling distance [km]
1	060-EA-006	2	306.000
2	060-EA-040	2	481.000
3	060-EA-012	2	476.000
4	060-EA-024	6	391.000

Especially for the wheelset-axles number 3 and 4, some detailed chemical, mechanical and metallographic researches were performed, but the conclusion were drawn for all four investigated cases.

1.1. Chemical analysis

The chemical analysis of the wheelset-axle materials conduce to the partition of the chemical elements presented in table 2:

Table 2.

Wheelset nr.	C[%]	Mn[%]	Si[%]	Cr[%]	Ni[%]	Mo[%]	P[%]	S[%]	Cu[%]
3	0,32	0,47	0,24	1,49	1,59	0,40	0,011	0,010	0,08
4	0,33	0,52	0,27	1,49	1,62	0,26	0,011	0,010	0,08

When compare the above mentioned concentrations with the imposed chemical element concentration of the wheelset-axles belonging to 7350 HP electric locomotive, it is observed that the values are placed into the accepted range by the wheelset-axles producers.

The content of 0.40% Mo on the wheelset-axles number 3, in comparison with 0.30% Mo prescribed content, will not present a non-favourable factor.

1.2. Traction test

The standardized traction specimen are in accordance with now-days regulations (it presents a 16 mm diameter on the calibrate circular parts). Tests were performed on an universal (traction-compression) testing machine.

The results are presented in the framework of table 3:

Table 3.

Wheel set-axles number	Number of specimen	Yield point [MPa]	Ultimate strength [MPa]	Proportional necking [%]
1	1	730	900	17,50
2	1	700	880	18,75

1.3. Dynamic bending test

The dynamic bending test specimens were manufactured both longitudinally and cross-section directionally. It means that a double number of specimens were tested, and results are presented in table 4:

Table 4.

Wheelset-axles number	Number of the specimen	Longitudinal toughness [MPa m]	Transversal toughness [MPa m]
3	1	775	425
3	2	750	337,5
3	3	800	462,5
3	4	675	462,5
3	Average	750	422
4	1	1000	500
4	2	775	450
4	3	1050	512,5
4	4	875	525
4	Average	925	497

1.4. Torsion test

The torsion loading represents the main loading which produces the stick-slip phenomenon. The obtained results, presented in table 5, are in accordance with the official prescriptions and regulations of the Railway Romanian Authority (A.F.E.R.):

Table 5.

Torsion torque [Nm]	Diameter of the specimen [mm]	Yield point [MPa]	Shearing ultimate strength [MPa]
940	20	598,7	783,4
980	20	624,2	770,7
960	20	611,4	777
920	20	586	764,3
920	20	586	764,3
910	20	579,6	757,9

3. CONCLUSIONS

- ✚ The aspect of the cross-section fracture zone represents the main juridical factor when a wheelset-axles accident takes place. The shiny zone parts (figure 1) represent the fatigue area inside where the cracks grow in time.

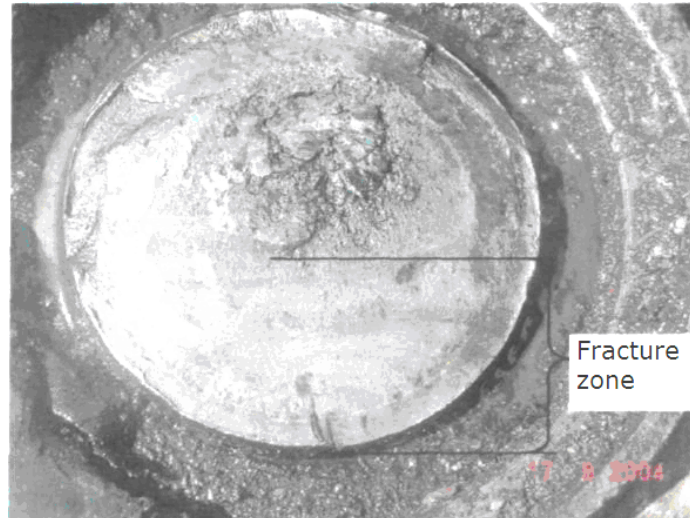


Figure 1. The aspect of the fracture zone in the body of the wheelset



Figure 2. The aspect of the fracture zone in the extremity of the wheelset (lubrication boxes)

- ✚ For the wheelset-axles nr.1, the aspect of the crack propagation is represented as two single independent cracks growing on the free wheel.
- ✚ For the wheelset-axles nr.2, the crack is developed in a continuous circular direction.
- ✚ For the wheelset-axles nr.3, the orientation of the crack is similar, but through the cross-section of the free wheel.
- ✚ For the wheelset-axles nr.4, the crack is located under the gear wheel. These are the most dangerous types of cracks. It may be detected only by an ultrasound control. The ultrasonic crack detection is usually performed by using an a lightweight, compact and handy-portable flaw detector designed for use on large workpieces and in high-resolution measurements. The complementary equipment consist in a mobile push-cart on the rail and three touching heads (a normal one and two bending touching heads).The equipment (figure 3) is able to detect fatigue cracks in the rail head, horizontal cracks in the rail head and in the transient area between the rail head and the rail core as well cracks which are initiated from the holes.

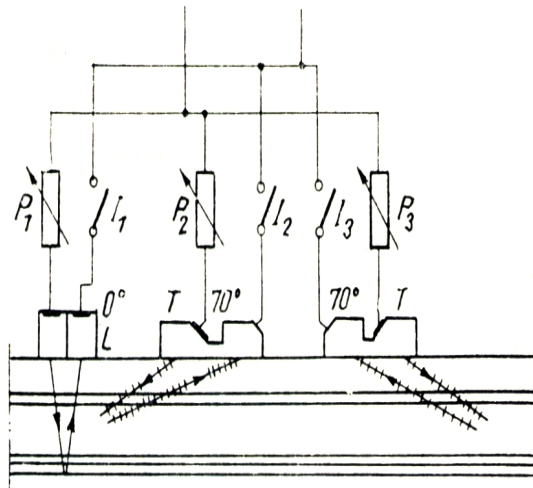


Figure 3. The mobile ultrasonic detection push-cart with three touching heads

The rail profile generates disturbed responses which have to be separated from the faults responses. Anyway, the experimental procedure is able to conduce to: the detection of the location of the cracks, the crack critical length and orientation. It may be calculated: the stress intensity coefficient at the top of the crack, the propagation rate, the estimated life-time of the wheelset for different locations and lengths of the detected cracks.

REFERENCES:

- [1] E. Ghita, “Strength on wheel-rail contact”, Ed. Mirton, Timisoara, 1998.
- [2] E. Ghita, Gh. Turos, “Dynamics of railway vehicles”, Ed. Politehnica, Timisoara, 2006.
- [3] M. Trusculescu, “Materialotehnica”, vol I, “Structural metallurgy”, Ed. Politehnica, Timisoara, 2003.
- [4] T. Mitelea, “Metalografia imbunatatirilor sudate”, Ed. de Vest, 2006.



ASPECTS REGARDING THE LIFE-TIME OF WIRES BELONGING TO A STEEL WIRE ROPE

Lucia VILCEANU¹, Eugen GHITA², Vasile PUTAN¹

¹“Politehnica” University of Timisoara, Faculty of Engineering Hunedoara, ROMANIA

²“Politehnica” University of Timisoara, Faculty Mechanical Engineering, ROMANIA

Abstract

The paper presents an analysis regarding the influence of working typical factors about the shallow destruction phenomena between wires in contact. It was studied the influence of contact pressure and the relative displacement between wires concerning the life-time of wire ropes. There is presented as a conclusion that the life-time of wires is decreasing at the increasing of the average pressure between the wire rope and the wrapping up roll. The destruction phenomenon of wires is increasing when increasing the frequency of the alternant bending process of wire rope around the roll.

Keywords:

wire rope, shallow destruction, life-time, contact pressure, fretting corrosion.

1. INTRODUCTION

The fretting corrosion belongs to the range of phenomena going to fracture of steel machine parts under different variable forces. The fretting corrosion conduce to decreasing of fatigue limit to (1,5...3) times. The above mentioned phenomena takes place between contact surfaces in a relative motion, when friction forces are acting on small contact areas due to roughness of joining surfaces. In the same time, heat is locally emitted producing punctual welding processes. A transfer of metallic powder between contact surfaces is produced. Because of chemical reactions with the oxygen included in atmosphere, the metallic powder is turning into oxides and nitrides. The degree of wear has high values in case of dry fretting, and small values in case of lubrication [3]. For wire ropes the influence factors about the fretting corrosion are as follows: the contact pressure, the amplitude and the frequency of relative displacement, the state of stress in the common contact area.

The interpretation of the fretting corrosion phenomena is based on the observation that high values of the contact stresses are located in the contact area. These stresses in correlation with relative displacements of contact surfaces are producing fractures of small particles. Taking into account the influence of the emitted heat, because of friction, the oxides are produced going to a wearing effect and facilitating the appearance of the fatigue cracks.

For the steel wire ropes subjected to a tensile test, the fretting corrosion is produced between the component wires as well between the external wires and the wrapping up roll. The favorable effect of lubrication about the life-time of wire ropes is unanimously accepted.

2. THE FACTORS OF INFLUENCE CONCERNING THE DESTRUCTION PROCESSES INTO THE CONTACT AREAS

2.1. Contact pressure

The contact compression, together with other loadings, conduces to a three-axis state of stress. The final result may be the appearance of the critical state, going to fracture, in layers

as far as a half of the breadth of the contact ellipse [1]. Hertz's formula is usually used in order to calculate the maximum contact pressure between the wire rope and the wrapping up roll.

The relation is valid only for elastic deformations:

$$p_0 = -\frac{3 \cdot P_0}{2\pi \cdot a \cdot b} \quad [\text{N/mm}^2], \quad (2.1)$$

where: P_0 [N] - pressing on force between bodies in contact;

a, b [mm]- half-axis of the contact ellipse:

$$a = 1,4 \cdot \nu \cdot \sqrt[3]{\frac{P_0}{E \cdot \sum \rho}}, \quad b = 1,4 \cdot \nu \cdot \sqrt[3]{\frac{P_0}{E \cdot \sum \rho}} \quad (2.2)$$

$\nu = 0,33$ - Poisson's ratio;

$E = 2,1 \cdot 10^5 \text{ N/mm}^2$ - Young's modulus;

$\sum \rho$ - the amount of curvatures of contact surfaces.

The average pressure between wire rope and wrapping up roll is expressed as:

$$p_m = \frac{2 \cdot T}{D \cdot d} \quad [\text{N/mm}^2], \quad (2.3)$$

where: T [N] - traction force;

D [mm] - diameter of roll;

d [mm] - diameter of wire rope.

The formula may be used for multi-layer wire ropes. The maximum contact pressure between wires may be written as $p_{0\max} = 2\sigma_r$, where σ_r [N/mm²] represent the strength at fracture of wire. When exceeding this value, the momentary destruction is not produced, but a decreasing of the life-time always appears.

2.2. The friction between wires

The estimation of friction coefficient at high pressures on the surfaces of wires is very necessary especially for the manufacturing process of wires. The influence of the diameter of wire about the friction coefficient may be neglected. It may be considered that the well known dependence between friction coefficient and perpendicular force remain still valid. As a lubricant very often used for wire ropes, the oil ensure suitable values for the friction coefficient.

2.3. The relative displacement of wires

The amplitude of relative displacement between the contact surfaces of wires is due to different values of stretching stresses in wires as well to different deformations of adjacent wires because of the bending process at different diameters [4]. The relative displacement of wires is caused by the diameters of layers, the length of the volute line for a single step having the following formula:

$$L = 2 \cdot \pi \frac{r}{\cos^2 \alpha} \quad (2.4)$$

where: r [mm] - the radius of the layer;

α - the wrapping up angle of wires in a layer.

There is very difficult to take into account all the above mentioned influence factors for the destruction phenomena of wires. The difficulty is caused by the relative dependence between factors. So, the principle of superposition regarding the effects of the influence factors may not be used. It is of a great practical importance to establish perceptually the decrease of the fatigue limit of wires when the wires are separately leaded in comparison with the same parameter for the wire as a component part of the wire rope.

3. THE EXPERIMENTAL ANALYSIS OF THE INFLUENCE OF PRESSURE AND RELATIVE DISPLACEMENT ABOUT LIFE-TIME OF A WIRE ROPE

There are considered the following stresses:

- traction produced by the force T , going to the stress in wire rope

$$\sigma_t = \frac{T}{A} \quad (2.5)$$

- primary bending because of the wrapping up around the roll with a diameter **D**, going to the stress in wire rope

$$\sigma_i = \pm E \frac{\delta}{D} \quad (2.6)$$

δ [mm] - diameter of wire;

$E = 2,1 \cdot 10^5 \text{ N/mm}^2$.

The fatigue tests conduce to fractures of wires especially in the contact area between the wire rope and the drain of roll. So, this contact zone will be analyzed. For fatigue and life-time tests, loading cycle is characterized by the following parameters:

$$\sigma_{\max} = \sigma_t; \quad \sigma_{\min} = \sigma_t - \sigma_i; \quad \sigma_{\text{med}} = \sigma_t - \sigma_i / 2 \quad \text{and} \quad \sigma_{\text{am}} = \sigma_i / 2$$

For the particular case $\sigma_t = \sigma_i$ a pulsate bending cycle is obtained. Moreover, a pulsate compression cycle will be added having the maximum pressure p_o in the volute zone and o in the stretching zone of the wire rope. So, the life-time N_s of wire, which was loaded under a pulsate cycle with $\sigma_{\max} = \sigma_t$, may be compared with the life-time N_c of a wire, which was loaded under a similar cycle and an added pulsate pressure ($o \dots p_o$). Because only the fatigue limit for a symmetrical cycle may be estimated for wires, the Soderberg's diagram is used. The diagram is approximated as a part of an ellipse having the half-axis σ_{-1} and σ_c . Instead of σ_c may be used the strength at fracture σ_r .

So, the following formula will be obtained:

$$\sigma_{-1Nc} = \frac{\sigma_o \cdot \sigma_r}{\sqrt{4 \cdot \sigma_r^2 - \sigma_o^2}} \quad [\text{N/mm}^2], \quad (2.7)$$

The fatigue tests have been performed [2] in the Laboratory of Strength of Materials from the Mechanical Engineering Faculty of Timisoara. A loading machine Schenk has been used for fatigue tests in the framework of life-times in the proximity of the value $N = 10^6$ cycles. The method of loading steps has been preferred in order to estimate the fatigue limit. The principle of the method consists in modifying the level of loading function of the level of stress obtained for the previous test. If the previous specimen has been fractured, the following specimen will be loaded at a smaller level of stress. For the opposite case, it will be used a higher level of stress. The test will continue until the whole range of specimen will be loaded. Results are presented in Table 1.

The advantage of the method consists in grouping the results around an average value. The drawback consists in the impossibility to perform simultaneously different specimens. So, the result of the previous test is necessary.

Table 1

σ [N/mm ²]	fractured wires •	N=10 ⁶ cycles			
		$i = \sigma_i - \sigma_o$	n	i.n	i ² .n
350	•	50	1	50	2500
340	o •	40	2	80	3200
330	• • • o •	30	5	150	4500
320	o • • o o o •	20	7	140	2800
310	o o ••	10	4	40	400
300	o	0	1	0	0
		$\Sigma =$	20	460	13400

The fatigue limit of wire may be calculated by using the following formula:

$$\sigma_{-1Ns} = \sigma_1 + \frac{\Sigma(i \cdot n)}{\Sigma n} = 300 + \frac{460}{20} = 323 \quad [\text{N/mm}^2], \quad (2.8)$$

where: σ_1 - is the reference level of stress, arbitrarily estimated for the smallest value of loading during the test.

The fatigue tests of wire ropes have been performed on a special loading machine designed by the lamented prof.dr.eng. Lazar Boleantu [2]. An usual wire rope **17 - 6x37 -160 S-Z**, STAS 1513-80, with the diameter of a single wire $\delta = 0,8 \text{ mm}$ and the area of the cross-section $A = 112 \text{ mm}^2$, has been tested.

There is emphasized in Figures 1 and 2 the life-time of wire rope for three different loading steps characterized by the stress $\sigma_t = T / A$ and by the diameter of roll. For every step, three specimens have been tested. The dispersion of results for a single loading step is located into the area of a rectangle. The hachure indicates the loading step for a fatigue pulsate cycle. It may be observed a relative small difference between the averages values of life-time for the two loading frequencies as well a favorable effect of low loading frequency about the life-time of wire rope.

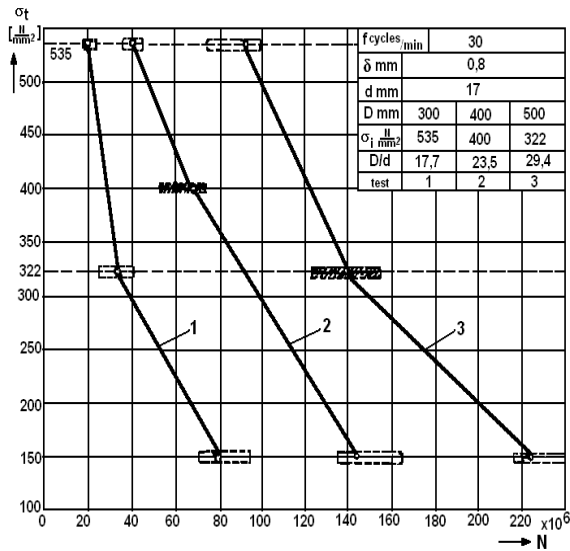


Fig. 1

Tests performed at frequencies of 30 cycles/min

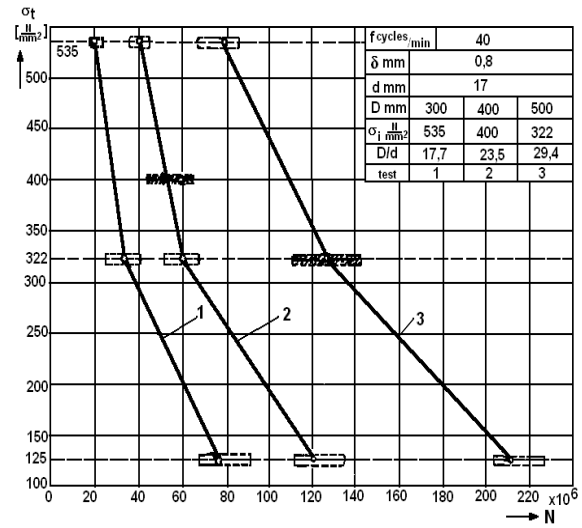


Fig. 2

Tests performed at frequencies of 40 cycles /min

The decreasing coefficient, regarding the fatigue limit of a wire belonging to a wire rope in comparison with the strength of a single wire for life-time $N = 10^6$ cycles, has been

$$c_\sigma = \frac{\sigma_{-1N_s}}{\sigma_{-1N_c}} \quad (2.9)$$

Results are presented in Table 2.

Test	1	2	3
D [mm]	300	400	500
$\sigma_o = \sigma_t = \sigma_i = E\delta/D$ [N/rnm ²]	535	400	322
σ_r [N/mm ²]	1600		
$\sigma_{-1N_c} = \frac{\sigma_o \cdot \sigma_r}{\sqrt{4 \cdot \sigma_r^2 - \sigma_o^2}}$ [N/rnm ²]	266	208	163
σ_{-1N_s} [N/mm ²]	323		
$c_\sigma = \frac{\sigma_{-1N_s}}{\sigma_{-1N_c}}$	1,23	1,55	1,98
N_s [cycles]	10^6		
N_{cmediu}	(19968) 19748	(68058) 51684	(138764) 124096
$C_N = N_s / N_c$	50	14,75	7,24
p_m [N/mm ²]	22,4	13,2	8,55
p_o [N/mm ²]	7850	6420	5540
$\Delta\varepsilon = \frac{2\delta^2}{D(D+2\delta)}$	$1,39 \cdot 10^{-5}$	$0,8 \cdot 10^{-5}$	$0,5 \cdot 10^{-5}$

There are presented in Fig. 3 the variations of c_σ and C_N for the pulsate testing cycle $\sigma_o = \sigma_t = \sigma_i$, corresponding to the average pressure p_m . It may be observed that if c_σ is increasing, C_N is decreasing. In the same time, the increasing of p_m has a non-favorable influence about the life-time of wire rope. There is presented in Fig. 4 the variation of C_N function of the average pressure p_m between wire rope and wrapping up roll. The parameter $\Delta\epsilon$ is representing the relative displacement between the layer of wires in contact with the roll and the internal layer located in the near vicinity, divided by the unit of length. There is ascertained a high value of the increasing slope of C_N when increasing the average pressure p_m , for high values of $\Delta\epsilon$.

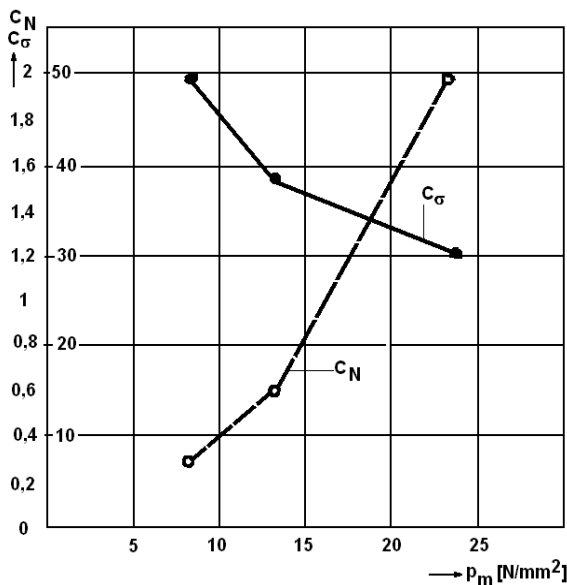


Fig.3. The variations of c_σ and C_N for the pulsate testing cycle

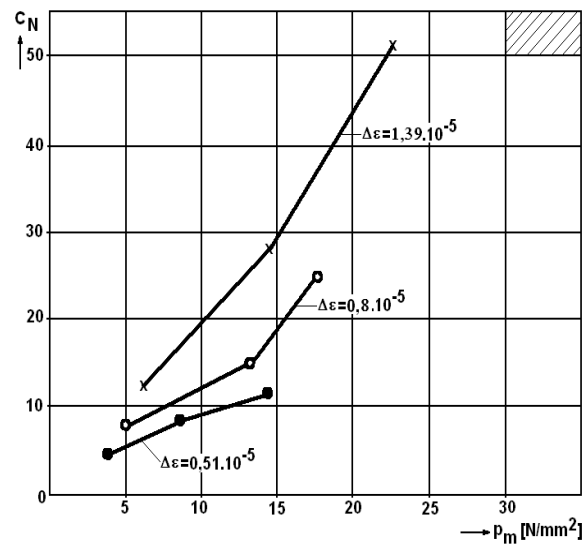


Fig.4. The variation of C_N function of the average pressure p_m

4. CONCLUSIONS

- ✚ The life-time of wires belonging to a wire rope is decreasing at increasing of the average pressure between the wrapping up roll and the wire rope. The dependence is valid for bending pulsate loading cycles (Fig. 3), as well for an uneven loading cycle (Fig. 4).
- ✚ At constant pressure, the life-time of wire rope is decreasing at increasing of $\Delta\epsilon$, the relative displacement between the layer of wires in contact with the roll and the internal layer located in the near vicinity (Fig.4). As increase because of the bending loading of wires due to wrapping up and bending of wire rope around the roll.
- ✚ Tests performed at frequencies of 30 respectively 40 cycles /minute prove that the destruction process increase when the frequency increase too, going to decreasing the life-time of wire rope. The reason consists in increasing the level of friction force between wire rope and roll because of increasing the angular acceleration. In the same time because of increasing the friction force, there is also increasing the local maximum pressure but is decreasing the elliptical contact surface. Both consequences have a non-favorable influence about the life-time of wires due to increasing the amplitude of contact pressure.
- ✚ A strongly increasing of the value of coefficient C_N , in case of bending loading cycles, is observed after a comparative analysis between a pulsate cycle (Fig.3) and an uneven cycle (Fig.4). A favorable effect about the life-time of wire ropes is obtained by superposing a compression or a traction stress over a contact compression stress.
- ✚ After analyzing the dispersion fields of the number of cycles (the rectangles in Fig.1 and 2) it may be observed the increasing of dispersion when increasing the number of cycles until the appearance of fracture. The explanation consists in the timely cumulative effect of wear. That is because the contact pressure and the bending-traction effects have an

insufficiently importance. The wear is strongly dependent on the friction coefficient between wire rope and wrapping up roll, as well between wires of the same wire rope. So, in order to decrease the level of wear it is necessary to decrease the friction coefficient by using a suitable lubrication. In the same time it is necessary to decrease the starting and the breaking accelerations which have an important influence about the relative sliding between the wire rope and the wrapping up roll.

REFERENCES

- [1] Babeu, T. – *The Basic Theory for Resistance of Materials*, Mirton Publishing House, Timisoara, 1998.
- [2] Boleantu, L. – *Studies regarding the resistance of tensile steel ropes and steel wires*, Scientifical Engineer Degree's Thesis, lito IPT, 1968.
- [3] Tudor, A. – *The real contact of friction surfaces*, Romanian Academy Publishing House, Bucharest, 1990.
- [4] Vîlceanu, L. – Resistance and working life at steel wire ropes in contact, in Mirton Publishing House, Timisoara, 2003.



CONSIDERATIONS REGARDING THE TESTING OF ELECTRICAL APPARATUS WITH THE TYPE OF PROTECTION “INCREASED SAFETY”

Martin FRIEDMANN, Lucian MOLDOVAN

¹INCD-INSEMEX Petroșani, ROMANIA

Abstract:

Increased safety “e” represent a type of protection applied to electrical apparatus in which additional measures are applied so as to give increased security against the possibility of excessive temperatures and of the occurrence of arcs and sparks in normal service or under specified abnormal conditions.

Keywords:

Type of protection, increased safety, type tests

1. GENERALITIES

Evaluation and testing of equipments that compose an explosion-proof system, in purpose of certification, is very important considering the existing explosion risk which has to be minimized to ensure peoples health and security, as well as to prevent goods damage and, not in the last instance, to protect the environment.

The type of protection increased safety “e” applies to electrical apparatus with a rated value of supply voltage not exceeding 11 kV r.m.s. a.c. or d.c. Additional measures are applied to ensure that the apparatus does not produce arcs, sparks, or excessive temperatures in normal operation or under specified abnormal conditions.

The principle for the type of protection increased safety is represented by carefully choose of the materials used for construction of such kind of apparatus, assurance of certain clearances and creepage distances in such manner that the probability of a failure to occur and to result an electric arc or spark to be reduced at an acceptable level; as well as to ensure an adequate degree of protection for the apparatus enclosure.

For the certification of electrical apparatus with type of protection increased safety, this should be submitted to type tests and routine tests.

In the type tests category are included the tests to determine the maximum surface temperature (to include the apparatus in a certain temperature class), tests for resistance to impact, dielectric strength test, tests for degree of protection (IP) and, if necessary, tests for thermal endurance to heat and cold, resistance to light, resistance to chemical agents and other tests which are specific for different types of apparatus.

The tests for thermal endurance to heat and cold, determination of surface temperature for luminaries and electric motors; and determination of time t_E for electrical rotating machines now can be done at INCD-INSEMEX. The apparatus needed to run these tests was in part acquired with funds from National Authority for Scientific Research in the Nucleu Program.

2.1. Tests for thermal endurance to heat and cold

The thermal endurance to heat shall be determined by submitting the enclosures or parts of enclosures in non-metallic materials, on which the integrity of the type of protection depends, to continuous storage for four weeks at (90 ± 5) % relative humidity at a temperature of (20 ± 2) K above the maximum service temperature, but at least 80 °C.

In case of a maximum service temperature above 75 °C, the period of four weeks specified above shall be replaced by a period of two weeks at (95 ± 2) °C and (90 ± 5) % relative humidity followed by a period of two weeks in an air oven at a temperature of (20 ± 2) K higher than the maximum service temperature.

The thermal endurance to cold shall be determined by submitting the enclosures and parts of enclosures of non-metallic materials, on which the type of protection depends, to storage for 24 h in an ambient temperature corresponding to the minimum service temperature reduced by at least 5 K but at most 10 K.



Figure 1. Control and monitoring panel for climatic chamber Vötsch, type VC 7060

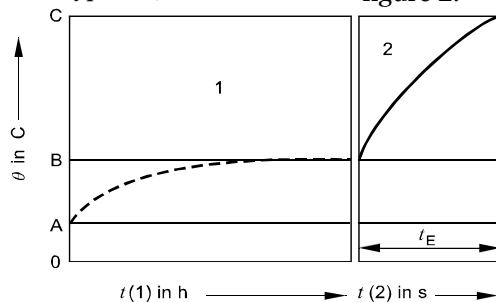
The test rig designed for these tests consists in a climatic chamber Vötsch type VC 7060, having a capacity of 0,6 m³, and the temperature can be adjusted in the range -70 ÷ +180 °C. The result of test is considered positive if the exposed apparatus shows no deteriorations that affect the type of protection.

2.2. Test of rotating electrical machines.

Determination of time t_E

Time t_E represents the time taken for an a.c. rotor or stator winding, when carrying the initial starting current I_A , to be heated up to the limiting temperature from the temperature reached in rated service at the maximum ambient temperature.

The diagram illustrating determination of time t_E is given in figure 2.



Key

- A Highest permissible ambient temperature
- B Temperature in rated service
- C Limiting temperature
- t Time
- θ Temperature
- 1 Temperature rise in rated service
- 2 Temperature rise during stalled rotor test

Figure 2 – Diagram illustrating the determination of time t_E

The temperature rise in stalled motors shall be determined experimentally as follows:

- ✚ With the stalled motor initially at ambient temperature, rated voltage and rated frequency shall be applied.
- ✚ The stator current measured 5 s after switching on shall be considered to be the starting current I_A .
- ✚ The temperature rise in the rotor cage (bars and rings) shall be measured by thermocouples and measuring instruments having a small time constant compared with the rate of temperature rise, or by temperature detectors or other means. The highest of the temperatures obtained during these measurements is the one to be considered.
- ✚ The average temperature rise of the stator, determined from resistance measurements, is taken as the temperature rise of the winding.
- ✚ When the stalled motor test is made at a voltage less than rated voltage, the measured values shall be increased proportionally to the ratio of those voltages, directly for the starting current and according to the square of the temperature rise. Saturation effects, if any, shall be taken into account.

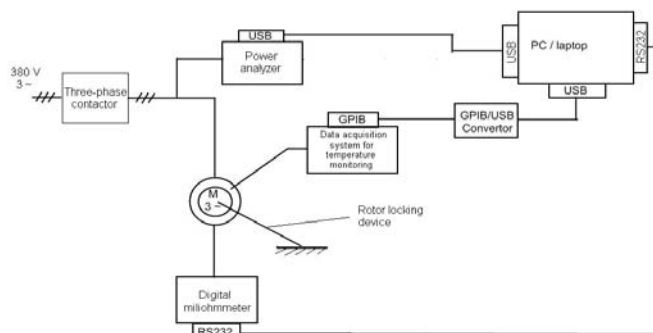


Figure 3. Block diagram of the test rig used to determine time t_E

The block diagram for the test rig used to determine time t_E is given in figure 3. To fulfil the test rig the following apparatus was acquired: power analyzer Fluke 435, milliohmmeter Crompton DO5001, data acquisition system Agilent 34970A with thermocouples, laptop Dell Latitude D830.

The role of Fluke 435 power analyzer is to measure and record the important parameters (voltage, current, frequency, power factor, etc.) during the test.

The Crompton DO5001 milliohmmeter measure and record the

values for the stator winding resistance in cold state and after the test..

The data acquisition system Agilent 34970A with thermocouples is used to measure and monitor temperature during test.

2.3. Determination of maximum surface temperature for electrical rotating machines

In order to determine the maximum surface temperature the following apparatus is used: power analyzer Fluke 435, milliohmmeter Cropico DO5001, data acquisition system Agilent 34970A with thermocouples, tachometer Lutron L1236L, laptop Dell Latitude D830.

To determine the maximum surface temperature the following steps should be covered:

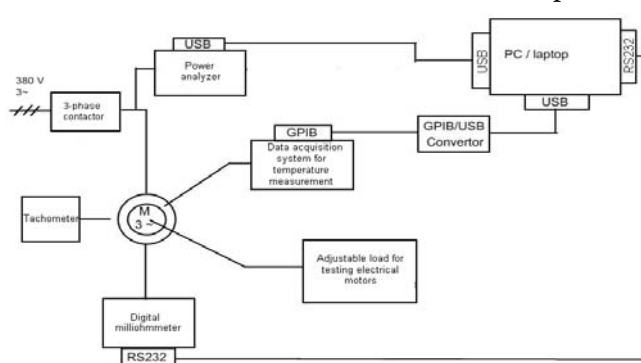


Figure 4. Test rig to determine maximum surface temperature for electrical rotating machines

- ✚ build-up experimental mounting according block diagram from figure 4, and connect the electric motor to adjustable load test rig;
- ✚ the stator winding resistance is measured and recorded, in „cold” state, with the help of Cropico DO 5001 microohmmeter;
- ✚ the thermocouples connected to Agilent 34970A data acquisition system are placed in points considered to be the hottest points during motor running;
- ✚ the adjustable load test rig is powered-on and the electric motor is driven on low speed;

- ✚ the electric motor is powered-on through a 3-phase contactor;
- ✚ the load is adjusted until the motor speed reaches nominal speed (rotation speed is measured with the help of Lutron 1236L tachometer);
- ✚ in this configuration, the system will function until the maximum temperature in normal functioning is reached, according SR EN 60079-0 and SR EN 60079-7 (temperature rising is lower than 2 K/ hour);
- ✚ after reaching the maximum surface temperature, the motor is powered-off and the adjustable load rig is driven so as to give a quick stop of the motor.
- ✚ the stator winding resistance is measured and recorded, with the help of Cropico DO 5001 microohmmeter;

Table 1: Delay time after power-off required to determine temperature in rated service

Rated power, (kW)/(kVA)	Delay time after power-off, (s)
$P \leq 50$	30
$50 < P \leq 200$	90
$200 < P \leq 5000$	120

The rotor temperature is measured with thermocouples placed on the rotor through some holes effected in the drive-part shield. Delay time after power-off to determine overtemperature in rated service is presented in table 1.

Temperature and winding resistance recording is made for at least 2 minutes after motor power-off, in reason to set-up the cooling curve for rotor and stator winding.

Data referring to electrical parameters during test (voltage, current, frequency, power factor, etc.) are viewed and recorded through the power analyzer, and transferred to a PC after the test.

The maximum temperature reached in stator winding at rated service is determined with the following formula:

$$\theta_2 = \Delta\theta + \theta_a$$

$$\Delta\theta = \frac{R_2 - R_1}{R_1} \times (k + \theta_1) + \theta_1 - \theta_a$$

where

- R_1 – winding resistance value in cold state, in Ω ;
- R_2 – winding resistance value in warm state, in Ω ;
- θ_1 – winding temperature value in cold state, in $^{\circ}\text{C}$;
- θ_2 – winding temperature value after heating test, in $^{\circ}\text{C}$;
- θ_a – temperature value for the cooling environment (ambient);
- k – reciprocal temperature coefficient for resistance at 0°C for conductive material; $k = 235$ – for copper; $k = 225$ for aluminium;
- T_{amb} – maximum ambient temperature (generally 40°C);

The maximum surface temperature is determined as the temperature measured in the hottest point of the motor, with the following formula:

$$T_{max} = T_{amb} + \Delta\theta$$

in this case $\Delta\theta$ represents the highest rise of temperature (measured in points where the thermocouples were placed).

2.4. Determination of maximum surface temperature for luminaries designed for main supply

In order to determine the maximum surface temperature for luminaries the following apparatus is used: ac power source Kikusui type PCR 1000M, data acquisition system Agilent 34970A with thermocouples, laptop Dell Latitude D830.

To determine the maximum surface temperature of luminaries designed for main supply the following steps should be covered:

- build-up experimental mounting according block diagram from figure 5;
- the thermocouples connected to Agilent 34970A data acquisition system are placed in points considered to be the hottest points during functioning.
- for tubular fluorescent lamps with main supply a diode will be connected in series with the lamp, and the luminaire supplied with a voltage equal to 110% of rated voltage;

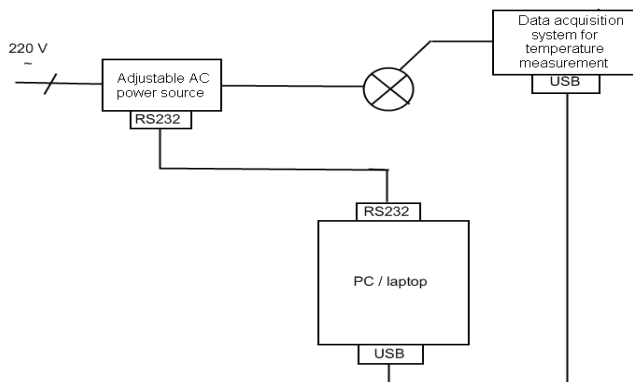


Figure 5. Test rig to determine maximum surface temperature for luminaires designed for main supply

- in this configuration, the all system will function until the maximum temperature in normal functioning is reached (temperature rising is lower than 2 K/ hour). The temperature is monitored by data acquisition system Agilent 34970A with thermocouples;
- when thermal equilibrium is reached the ac power source output of powered-off, and the data corresponding to electrical parameters during test are saved on PC;
- after approximately 1 minute from power-off the ac power source output the temperature recording is stopped and the data is saved on computer;
- the maximum surface temperature is determined with the following formula:

$$t_{\max} = t_{\text{inc}} + (t_{\text{amb max}} - t_{\text{amb inc}})$$

where

t_{inc} – temperature recorded during test (°C) in the hottest spot;

$t_{\text{amb max}}$ – maximum ambient temperature to which the equipment is designed to work;

$t_{\text{amb inc}}$ – ambient temperature during test;

- In the end of the test, the temperature should not exceed the temperature specified for the specific temperature class (80 °C for T6, 95°C for T5, 130°C for T4, 195°C for T3). The temperature at the rim of the lamp cap and at the soldering point of the lamp cap shall not exceed the limiting temperature.

3. CONCLUSIONS

The purpose of the paper is to underline the new test that can be done at INCD INSEMEX Petrosani for electrical apparatus with increased safety „e” type of protection. These tests are: thermal endurance to heat and cold, determination of surface temperature for luminaries and electric motors; and determination of time t_E for electrical rotating machines. The apparatus needed to run these tests was in part acquired with funds from National Authority for Scientific Research in the Nucleu Program.

REFERENCES

- [1] M. Friedmann, L. Moldovan, M. Magyari, A. Martinescu, *Implementation of new evaluation and testing methods for electrical apparatus with type of protection increased safety in order to correlate with European legislation and conformation with HG 753/2004, Phase IV Report, 2008, INCD-INSEMEX Petrosani*
- [2] SR EN 60079-0:2007, *Electrical apparatus for explosive gas atmospheres. Part 0: General requirements*
- [3] SR EN 60079-7:2004, *Electrical apparatus for explosive gas atmospheres. Part 7: Increased safety “e”*
- [4] S. Burian, J. Ionescu, M. Darie, L. Moldovan, et al., *Technical apparatus for potentially explosive atmospheres. Group II, 2nd edition revised, Europrint Oradea publishing house, 2006, ISBN 973-7735-32-3*



THEORETICAL AND EXPERIMENTAL ASPECTS REGARDING THE SEALED EFFICIENCY OF DIESEL ENGINES COMBUSTION CHAMBERS

Adriana TOKAR, Daniel OSTOIA, Arina NEGOIȚESCU

University Politehnica of Timisoara, Bv. Mihai Viteazu, no.1, ROMANIA

Abstract

In this paper are presented theoretical and experimental aspects accomplished on a diesel engine concerning piston rings dimensioning and verification, hydrodynamic lubrication between piston rings and cylinder and also aspects concerning the elastic pressure. The sealed efficiency of combustion chambers is emphasized through energetic losses and pollution degree for wearing piston rings.

Key words:

piston rings, diesel engine, hydrodynamic lubrication, sealed efficiency, elastic pressure

1. INTRODUCTION

Along with technical developments, the piston ring, cylinder and piston geometry and construction, together with the corresponding technologies and materials they are made of, were continuously improved. Modern engines are less polluting, operate with higher pressures and temperatures and are more durable. The only fact that has not been changed is the basic function of the piston rings. They provide an adequate compression and reduce the thermal stress of the piston contributing to the exhaustion of a major part of the heat absorbed by it. The piston rings also restrain gases to infiltrate into the crankcase and control the assembly lubrication realizing with cylinder a III group friction connect that provides at the same time the piston assembly direction in its alternative motion.

The selection of piston rings is very important, those being the principal elements of study as they are the ones that together with the piston are executing the translation motion. This is an obligatory condition for hydrodynamic lubrication into the assembly and provides in this way the wear reduction of both elements.

The gases infiltrated behind the lubrication piston ring flow through the exhausted holes of the accumulated oil. Therefore is no longer provided a superior elastic medium pressure in comparison with the one of the compression piston rings. The consumption decreases when the p_E pressure increases as a result of the oil film thickness reduction.

It is estimated that an acceptable consumption can be obtained for a value of film thickness between the piston rings and cylinder less than $2\mu\text{m}$. An important influence is exerted by the oval form of the piston coating and by the clearance of the piston into the cylinder.

2. THEORETICAL STUDIES ON THE DIMENSIONING AND FUNCTIONAL REQUIREMENTS OF THE PISTON RINGS UP IN THE PISTON RING-CYLINDER

2.1. CRITERIA OF FOR CONTROL AND DIMENSIONING PISTON RINGS

The operating requirements of piston rings of any type impose the existence of a adequate maintained in time and at high temperature elasticity, a determined repartition of pressure on the cylinder mirror, its processing in an adequate geometrical form which must provide a sealed position on the operated surface. Besides these basic requirements, a high fiability is necessary. For providing these requirements, the shape of piston rings is a cut ring. The cutting (joint) gives the piston rings elasticity in operation.

At present, for piston rings dimensioning the following objectives must be accomplished:

- ✚ The adoption of the medium elastic pressure p_E and pressures distribution;
- ✚ The determination of the piston ring basic dimensions, a and h ;
- ✚ The determination of the piston ring shape in free-state and joint s_o , so that to provide the adopted distribution of pressure;
- ✚ The verification of tensile stress generated at the piston ring fit and the size of the operating joint;
- ✚ The determination of joints from piston ring way;
- ✚ The determination of piston rings number.

The study of thermal and lubrication phenomena is very important for the wears and frictions reduction into the piston ring-cylinder connection.

2.2. CRITERIA CONCERNING THE DIMENSIONING AND VERIFICATION OF THE PISTON RINGS

The operating requirements of piston rings of any type impose the existence of a adequate maintained in time and at high temperature elasticity, a determined repartition of pressure on the cylinder mirror, its processing in an adequate geometrical form which must provide a sealed position on the operated surface. Besides these basic requirements, a high fiability is necessary. For providing these requirements, the shape of piston rings is a cut ring. The cutting (joint) gives the piston rings elasticity in operation.

At present, for piston rings dimensioning the following objectives must be accomplished:

- ✚ The adoption of the medium elastic pressure p_E and pressures distribution;
- ✚ The determination of the piston ring basic dimensions, a and h ;
- ✚ The determination of the piston ring shape in free-state and joint s_o , so that to provide the adopted distribution of pressure;
- ✚ The verification of tensile stress generated at the piston ring fit and the size of the operating joint;
- ✚ The determination of joints from piston ring way;
- ✚ The determination of piston rings number.

The study of thermal and lubrication phenomena is very important for the wears and frictions reduction into the piston ring-cylinder connection.

2.3. Theoretical studies concerning the parabolic shape of piston rings

At present the theoretical and experimental researches on the piston ring-cylinder connection show important progresses on the following directions:

- a. The determination of some designing criteria accepted for piston rings and cylinders of internal combustion engines;
- b. The elaboration of theoretical models for the lubricated regime;
- c. The determination of the influence factors on the wear in the connection and improvement of its elements fiability;
- d. The execution of test banks and methodologies for measuring the oil film thickness, friction force, wears and thermal regime in the connection.

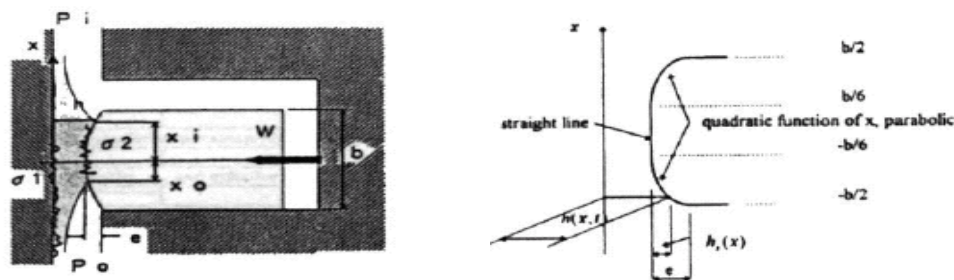


Figure1 The parabolic shape of the piston ring surface

As a general observation, all theoretical studies present the analytical modelling of the piston ring shape as a parabolic one (Fig.1).

2.4. CONSIDERATIONS ON THE HYDRODYNAMIC LUBRICATION IN PISTON RING - CYLINDER CONNECTION

As it is known [5], the following conditions are necessary for accomplishing the hydrodynamic regime:

1. The presence of lubricate in the connection;
2. The motion presence on connection surfaces;
3. The presence of a keyway.

If it is taken into account the presence of roughness, it will also appear a fourth condition which shows that for restricting their influence on hydrodynamic flow is necessary that the ratio: $2h_L / (R_{a1} + R_{a2}) > 5$

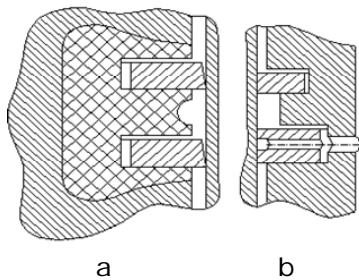


Figure 2 Space buffered of oil accumulation between the piston rings [5]

Where h_L is the lubricate film thickness, and $(R_{a1} + R_{a2}) / 2$ is medium value of elements roughness in the connection.

The latest considerations [5] show that for piston ring-cylinder connection the values bigger than 3 can be acceptable.

A possibility of the consumption reduction C_{us} is the execution of a buffer space of the oil accumulation.

The localization of this space under the first compression piston ring leads to the decrease of the rate of rise of pressure in that area. So, this piston ring is stable on the inferior side and the sealing will be improved. This solution is recommended for small distances between the two piston rings especially when their canals are executed in a piston insertion (Fig.2a).

The buffer space can be executed above the lubricated piston ring by reducing the piston packing leather diameter with no more than 1mm (Fig.2b). So it will be provide a “liquid piston ring” which restrains the oil infiltration to the combustion chamber. It will be obtained a special efficiency that is a sum of many solutions including the forming of piston rings sets to increase the sealing.

2.5. ELEMENTS REFERING TO THE WORKING PISTONS RINGS BEHAVIOUR CALCULUS

In reality, modifications from the theoretical free shape appear and therefore the distribution is no longer constant because fixing through heating does not remove completely the material tensions.

The pressure distribution is modified in operation because of two causes:

- ✚ The piston rings and cylinder are wearing, changing their contact conditions;
- ✚ The piston ring is inserted on the cylinder not only by its elastic force but also by the infiltrate gases behind it.

In this case, the pressure is $p = p_E(1 + \gamma)$, where $\gamma = p_s / p_E$. These cases are evaluated through relative wear u_T / a of the piston ring external side and the pressure p_τ / p between the piston ring and cylinder after a period of time τ . By noting with \bar{p}_τ the medium pressure after τ , it will be obtained the adjusted pressure:

$$\bar{p}_\tau = p + (\bar{p}_\tau - p_\tau) \quad (1)$$

The construction conditions need for a certain distribution an analytical expression of the piston ring pressure which is due to its own elasticity $p_{E\psi}$ determined by ψ angle (Fig.3).

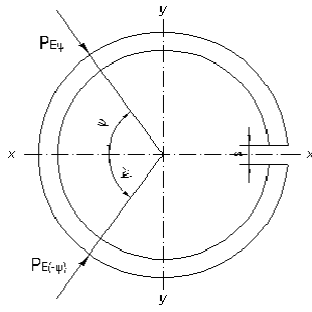


Figure 3 Diagram for the pressure developed by the piston ring

Because $p_{Eψ}$ is a periodic function with $2π$ period (the angle $ψ$ variation is between $−π$ și $π$), its development is used in Fourier series, so:

$$p_{Eψ} = p_0 + p_1 \cdot \cos ψ + p_2 \tag{2}$$

$$p_{Eψ} = p_0 + p_1 \cos ψ + \dots + p_n \cos nψ + q_1 \sin ψ + \dots + q_n \sin nψ \tag{3}$$

where $p_0, p_1 \div p_n, q_1 \div q_n$ are constant.

Related to x-x axis which passes through the middle of the joint, the piston ring load is symmetrical. Therefore $p_{Eψ}$ is an even function - $p_{Eψ} = p_{E(-ψ)}$ so the condition $q_1 = q_2 = \dots = q_n = 0$ is satisfied.

Under the peripheric pressure action the piston ring is in equilibrium which means that the pressures resultants on the two axis are null. The loading symmetry nullifies the resultant on the y-y axis.

$$- p_{Eψ} \cos(\pi/2 - ψ) = p_{E(-ψ)} \cos[-(\pi/2 - ψ)] \tag{4}$$

The equilibrium condition on the x-x axis is:

$$\int_0^\pi p_{Eψ} \cos ψ dψ = 0 \tag{5}$$

Because: $\int_0^\pi \cos ψ dψ = 0$; $\int_0^\pi \cos^2 ψ dψ = \frac{\pi}{2}$; $\int_0^\pi \cos ψ \cos nψ dψ = 0$;

This condition is accomplished if the second term is null meaning $p_1 = 0$.

The $p_{Eψ}$ pressure is expressed depending on the medium elastic pressure:

$$p_E = \frac{1}{2\pi} \int_0^{2\pi} p_{Eψ} dψ = \frac{1}{2\pi} \left(p_0 \int_0^{2\pi} dψ + p_2 \int_0^{2\pi} \cos 2ψ dψ + \dots + p_n \int_0^{2\pi} \cos nψ dψ \right) \tag{6}$$

Because: $\int_0^\pi \cos^2 ψ dψ = 0$, $p_E = p_0$, is obtained, and the expression of the piston ring

developed pressure results as:

$$p_{Eψ} = p_E \left(1 + \sum_{n=2}^\infty v_n \cos nψ \right) \tag{7}$$

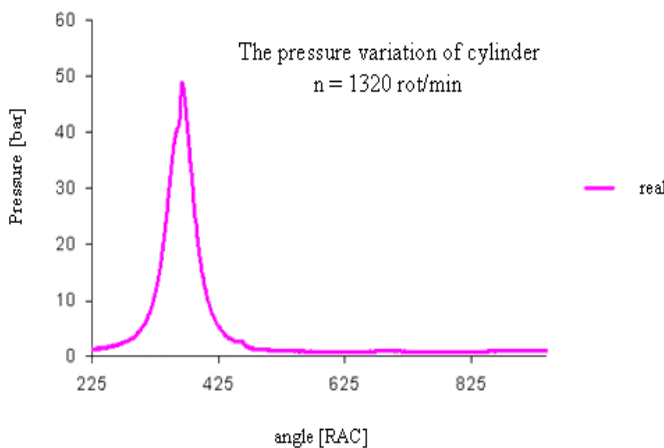


Figure 4 Pressure variations into the cylinder for engine with new piston rings

where $v_n = \frac{p_n}{p_E}$

The parenthesis from the relation (7) is the correction coefficient of the medium pressure p_E for variable pressure piston rings.

In practice, a finite number of the sum terms from relation (7) are considered. Because this sum is rapid convergent, the number of terms taking into account up to $2n = 10 \dots 12$ are limited.

For the M511 diesel engine the cylinder pressure variation with new piston is presented in Fig.4.

3. EXPERIMENTAL DATA ON THE EVOLUTION IN TIME OF PISTON RINGS PERFORMANCES

Experimental research aims to study the behavior in service of the combustion chamber engine of the diesel engine M-511. There was studied the losses through non-sealing by using a device to vary the pressure in the combustion chamber.

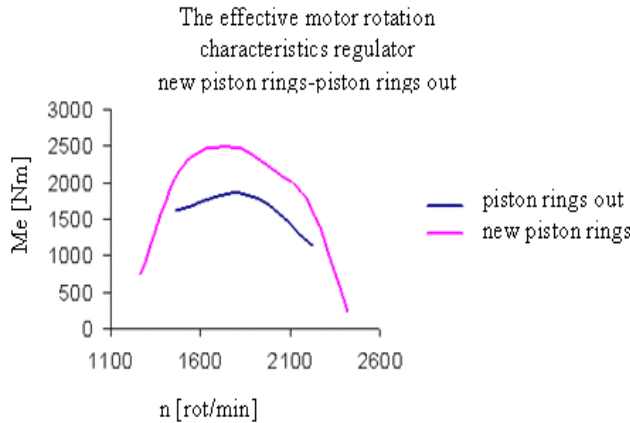


Figure 5 Variation of the effective rotation moment obtained for the new piston rings compared with wearing out ones

The efficiency of sealing the combustion chambers is revealed by energetic losses in the wearing out piston rings. In Fig.5 is presented the variation of the effective rotation moment obtained on the regulator speed characteristics of the engine equipped with new piston rings and wearing out piston rings.

In order to evaluate the evolution of wearing out both in the new and wear out piston rings case there were determined the energetic parameters for engine speed of 2200rpm obtaining on the engine regulator speed characteristics for partial load (Fig.6).

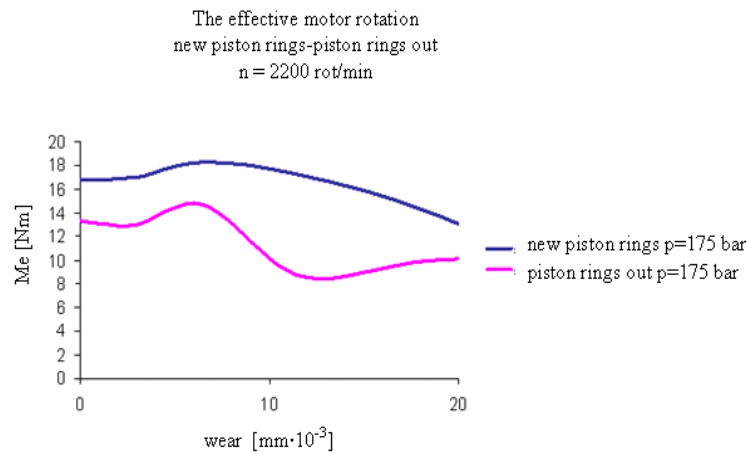


Figure 6 The effective rotation moment, new and wear out piston rings at constant engine speed

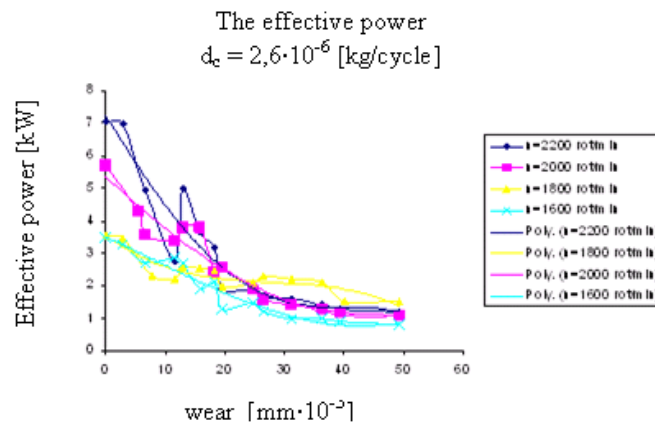


Figure 7 The effective power variation at the same engine speed and cyclical dose depending on wear out

4. CONCLUSIONS

The fuel mixture formation in the combustion chamber has a very important role on the combustion consequences and the on the energetic performances, but especially on pollution ones. Because of the losses of the combustion chamber, which are due mostly to the elements of the combustion chambers wear out, a reduction possibility of these effects would be that certain functional parameters to be modified so that the engine performances to be restored.

The effective power variation at the same engine speed and cyclical dose depending on wear is presented in Fig.7.

By knowing the losses evolution due to the wear out of the combustion chamber depending on the engine parameters (speed, power, fuel consumption, smoke degree), there can be made adjustments on the engine functional or constructive parameters in order to compensate these losses.

REFERENCES

- [1] Gaiginschi, R., Zătreanu, Gh., *Motoare cu ardere internă-Constructie și Calcul*, Editura “Gh.Asachi”, Iași 1995.
- [2] Jakobs,G. Influence of oil ring type and design on fuel and oil consumption, Internal Combustion Engine Research in Universities-C375/023, ImechE.
- [3] Negoțescu, A., Iorga, D., Mekki, C., Negrea, V.D., Ostoia, D., The Fuel Warning and vaporization in Diesel Engine-The VIII-th Conference, Societatea Inginerilor de Automobile din România, vol. I.C.E., ISBN 973-8212-00-4, Craiova-2000.
- [4] Ostoia Daniel, *Studii și cercetări privind controlul formării amestecului și al arderii asupra comportării în serviciu a camerelor de ardere în corelație cu regimul de noxe pentru motoarele diesel*, teză de doctorat, 2006.
- [5] Ostoia Daniel, Negoțescu Arina Speranța, *A study regarding the combustion chambers behaviour in correlation with emitted noxe sat diesel engines*-The 30th Annual Congress of the American Romanian Academy of Arts and Sciences (ARA), 5-10 July ,Chisinau-ISBN 9975-75-313-2.



EXPERIMENTAL DETERMINATION OF THE MECHANICAL STRESSES ON THE WARM ROLLING CYLINDERS

¹PINCA BRETOTEAN Camelia, ²TIRIAN Gelu Ovidiu

¹“Politehnica” University of Timisoara, Faculty of Engineering of Hunedoara,
Department of Engineering and Management, ROMANIA

²“Politehnica” University of Timisoara, Faculty of Engineering of Hunedoara,
Department of Electrical Engineering and Industrial Informatics, ROMANIA

Abstract:

The rolling mills cylinders are apply to thermo-mechanical stresses that are variable, complex, with extremely marked influences. Therefore, to intensify the rolling processes we need to observe the durability limits. To this purpose it is necessary to know the type of stress, the materials, and a detailed characterizes evaluation, to determine exploitation timing and to compare with previously established values. The paper presents experimental determinations of the mechanical stresses that take place during plastic deformation in rolling cylinders in exploitation. When being used, the laminating rolls are compared to the thermal tensions that cause thermal fatigue. This fatigue is the main cause for laminating rolls break.

Keywords:

experimental, mechanical, stresses, cylinders, fatigue, thermal

1. INTRODUCTION

The researches upon the stresses from the hot rolling mill cylinders represent an important scientific theoretical, experimental and economical issue. The calculus of the mechanical tensions which occur inside the laminating rolls are caused by the deformation process during the lamination, and they are the main elements for performing the sizing of the laminating rolls, as well as the main data for the calculus for the sizing of the rolling mill. We believe that the classical methods of rolls' sizing are not appropriate for most of the stages of the rolling process while producing rolls and laminated products.

This observation was remarked in [5] in which at page 489 say: „Although the solicitation of cylinders is a typical case of the variable solicitation, the usual calculus of dimensioning, is based merely on the static solicitation, without bareback is considered the fatigue”.

In the book [4] at page 95, the author show: “The resistance of the hot rolling cylinders”, with influence of different types tensional in at large, isn't studied” In the works written on this topic, rolling cylinders are calculated at static strains, which are wrongly considered to be constant in time. It is obvious that for the calculus of cylinders body, the determining of diameter based on the static bending moment does not correspond with the real exploitation strain, quite often thermal shocks lead to breakage of cylinders through shearing of caliber bead in the maximal sections. In the classical calculus of the cylinders, the decisive influence of thermal tension – with major effects in the rolling process – is not taken into consideration. Although rolling cylinder strain is a typical case of variable strain, the usual resistance calculus is based only on static strain, without considering the fatigue resistance in sizing the rolls. The replacement of cylinders takes place practically when the diameter is reduced below the minimum limit corresponding to normal wear, [2], [3].

We calculate mathematically the stresses in order to highlight them and to point out the fact that they do not influence the thermal fatigue of the laminating rolls very much, in order to compare them to those stresses caused by thermal influences.

2. CALCULATING THE MECHANICAL STRESSES

Nowadays specialized literature refers to the classical calculus methods used for the laminating rolls as, [2], [3], [5]:

- ✚ the pane of the rolls is calculated for a static bending;
- ✚ the journals of the rolls are calculated for twisting and bending;
- ✚ the journal blades are calculated for twisting tensions, meanwhile the blade is calculated for twisting and bending.

Forces acting on cylinders in rolling resistance classical calculation are presented in fig.1.

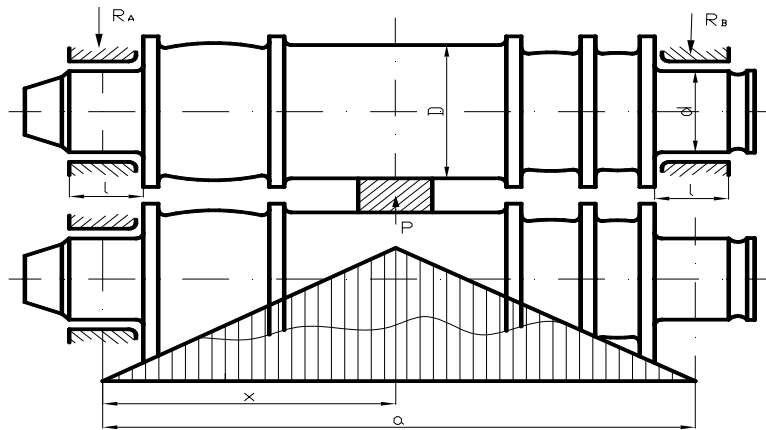


Figure 1. Representation of forces acting on cylinders rolling for the calculation of classical resistance

Nevertheless, we should note that the static stress we have considered for calculating the laminating rolls have not been too accurate as for time constant. The values of these „classic” tensions are determined in order to compare them to other tensions caused by temperature fields, [1].

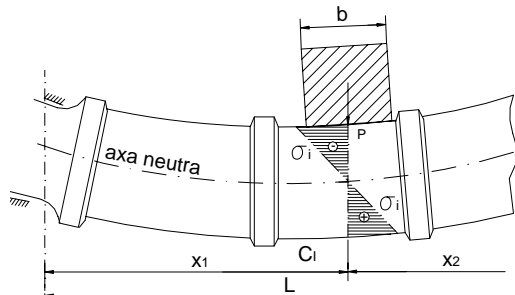


Figure 2. Roll stress caused by rotational bending stress

The bending and twisting stresses inside the pane rolls calibres of the laminating rolls are determined very accurately, avoiding any difficulty, according to current specialized literature, fig.2, [5].

According to fig. 2, bending stresses vary within the roll section, mainly in the compression deformation area, and have negative values. In the opposite side, there are only stretching stresses whose values are positive.

Bending stress are determined according to the relation (1).

$$\sigma_i = \frac{M_i}{I_z} \alpha_k = \frac{M_i r}{\pi R^4} \quad (1)$$

where: M_i – bending moment who stress the roll during the rolling process, considering that the rolling force is does not vary along length, [5].

$$M_i = P \left[\frac{x_1 x_2}{L} - \frac{b}{8} \right] \quad (2)$$

where: x_1, x_2 – the distance between the bearing and the axis of the rolled metal-plate; L – the distance between the axis of the bearings; R – the radius of the roll on the rolling gauge; b – the width of the rolling good corresponding shift of size; α_k – shape factor in case of tension concentration on the rolls already subject to calibration; P – the rolling force obtained after experiments (with an oscillograph); r – the distance from the neutral axis inside the radial section of the roll.

The pane of the rolls is subject to stress and twisting tensions caused by the rolling process. These tensions are determined according to relation (3).

$$\tau = \frac{\alpha_k M_t}{I_p} = \frac{M_t}{R^4} \alpha_k \quad (3)$$

where: M_t – twisting moment equal to rolling time, [5]; Δh – a reduced piece of the section, corresponding to the rolling design; r – the radius from the centre of the roll to the surface. The twisting moment is determining with relation (4):

$$M_t = 0,5F\sqrt{R\Delta h} \quad (4)$$

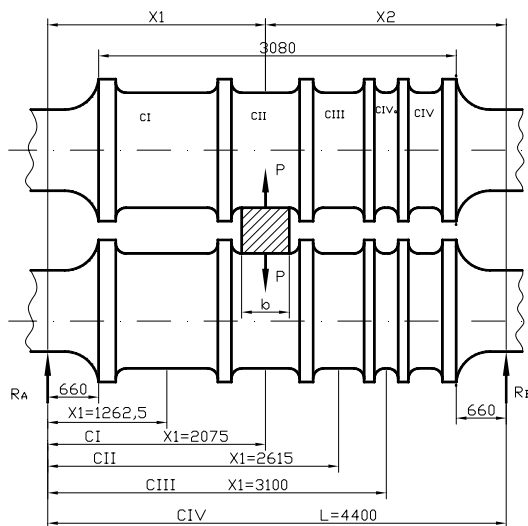


Figure 3. Calculus scheme for the lamination rolls

If we use the Exelud [2], [3], [4], [5] formula for contact pressure, the tension for the contact pressure is determined according to the relation (5); we use the results of the experiments for specific rolling parameters.

$$\sigma_{pc} = \frac{F_{max}}{B_m \sqrt{R\Delta h}} \quad (5)$$

where: F_{max} – the highest rolling force; B_{max} – the average width of the rolled goods – the deformation core; $\sqrt{R\Delta h}$ – the length of the contact arc; R – the radius of the rolling gauge; Δh – reducing the height of the rolled good during several use.

Fig. 3 describes the mathematical calculus method we have used for determining the twisting, bending, and contact pressure stress within the rolls of the rolling equipment. The rolling gauges are situated on their surface, according to their size, determined by the axis of the bearings. The rolling forces stress the gauges of the 9.2 tons ingot, according to the rolling scheme for each process during the rolling process. In order to determine the values of the forces, we have used the oscillograph to measure the parameters of the industrial rolling process – we have processed 10 ingots.

The experimental rolling mill is endowed with a plant for the determination of the lamination forces and of the variations of temperature fields in cylinders, which uses the electronic calculus technique, fig.4. The forces of lamination is measured in temporally experimentations of a help installation finded in the endowment rolling mill, in the aim verification of the stress from cylinders in order to subjected to excessive forces, which can produce ruptures or the damage of the rolling mill. In fig.5 presents the montage of tension-meter 1, which takes over half of rolling forces, transmits in bearing holder 3. The tension-meter is located under the axial bearing, lied on the head of the pressure screw 4, in a rigid metallic box, with the steel tie, at the superior cylinder's 5 equilibrate bend, fig.5, [4],[6].

Table 1. The results of the oscillograph analysis for industrial rolling

No. of stages	Gauge	Rolled good section [mm x mm]	Average rolling time [s]		$t_{mi} + t_{ri}$ [s]	Average rolling force F_m [kN]
			Time t_{mi}	Return time t_{ri}		
0	-	760/830 x 730/800	-	-	-	-
1	I	720 x 730/800	0,92	2,569	3,489	8527
2	I	640 x 735/800	0,889	4,505	5,394	11021
R	-	735/805 x 640	-	-	-	-
3	I	700 x 655	0,928	2,099	3,027	8555
4	I	610 x 680	1,174	3,030	4,204	10905
5	I	530 x 700	1,351	2,469	3,820	11010
6	I	450 x 720	1,161	6,110	7,271	10260
R	-	720 x 450	-	-	-	-
7	II	600 x 480	1,965	2,585	4,550	9582
8	II	500 x 505	1,614	4,812	6,426	9999
R	-	505 x 500	-	-	-	-
9	I	390 x 525	1,496	2,546	4,042	65543
10	I	330 x 545	1,526	5,540	7,066	7621
R	-	545 x 330	-	-	-	-
11	IV	430 x 355	2,297	2,257	4,554	8410
12	IV	350 x 375	4,349	6,114	10,463	8682
R	-	375 x 350	-	-	-	-
13	III	280 x 380	2,297	11,183	13,945	6927

The total value of the average rolling cycle of a 9.2 tons ingot 78,251 s = 1,304 minutes



Figure 4. The assembly of experimental rolling mill

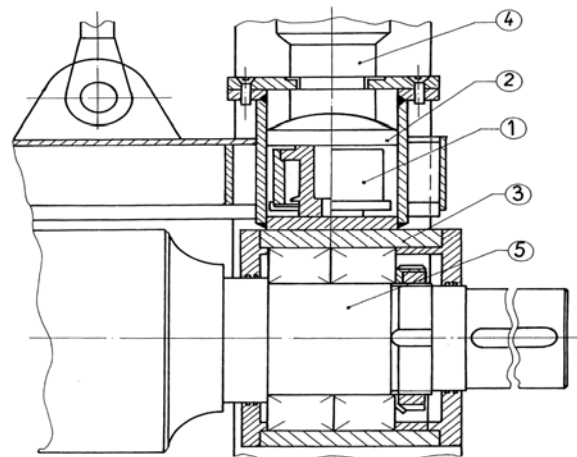


Figure 5. The tensiometer's montage with resistive transducers

The numerical calculus of stress caused by bending stress according with relation (1) is presented in table 2. The numerical calculus of stress caused by bending stress according with relation (3) is presented in table 3.

The process of stresses determination, when tensions are caused by the contact pressure, according to relation (5), corresponds to the result on the contact surface between the rolled good and the rolls. The numerical calculus has been performed according to new characteristic parameters, used for industrial rolling of 9.2 tons ingots – as in table 4.

Determination of stress caused by contact pressure by the relationship (5) corresponds to the effect of surface contact between laminate and cylinders. Calculations made after the parameters resulting from the characteristics of industrial rolling ingots of 9.2 tons are presented in table 5.

Table 2. Calculating the contact bending stresses on the roll surface

No. of stages	Gauge	Rolled good section [mm x mm]	Gauge radiu R [mm]	Coef α_k	Bending stresses [daN/mm ²]				
					σ_0 $\Delta r = 0$	σ_1 $\Delta r = 1,5$	σ_2 $\Delta r = 3$	σ_3 $\Delta r = 6$	σ_4 $\Delta r = 9$
0	-	760/830 x 730/800	-	-	-	-	-	-	-
1	I	720 x 730/800	620	1,39	5,09	5,08	5,07	5,04	5,02
2	I	640 x 735/800	620	1,39	6,91	6,57	6,55	6,52	6,49
R _s	-	735/805 x 640	-	-	-	-	-	-	-
3	I	700 x 655	620	1,39	5,21	5,19	5,18	5,16	5,13
4	I	610 x 680	620	1,39	6,63	6,61	6,59	6,56	6,53
5	I	530 x 700	620	1,39	6,66	6,64	6,63	6,60	6,56
6	I	450 x 720	620	1,39	6,18	6,17	6,15	6,12	6,09
R _s	-	720 x 450	-	-	-	-	-	-	-
7	II	600 x 480	592,5	1,39	8,55	8,53	8,51	8,47	8,42
8	II	500 x 505	592,5	1,39	8,55	8,53	9,51	8,47	8,42
R _s	-	505 x 500	-	-	-	-	-	-	-
9	I	390 x 525	620	1,39	4,26	4,05	4,04	4,02	4,00
10	I	330 x 545	620	1,39	4,49	4,48	4,47	4,45	4,42
R _s	-	545 x 330	-	-	-	-	-	-	-
11	IV	430 x 355	605	1,40	5,91	5,89	5,88	5,85	5,82
12	IV	350 x 375	605	1,40	6,02	6,07	6,05	6,02	5,99
R _s	-	375 x 350	-	-	-	-	-	-	-
13	III	280 x 380	600	1,40	5,80	5,78	5,77	5,74	5,71

 Tabelul 3. Calculation of winding tension for all crossings of a rolling cycle of Lingo 9.2 tonnes at depths r_i

No. of stages	Gauge	Rolled good section [mm x mm]	Gauge radiu R [mm]	Coef α_k	Tensions of twisting [daN/mm ²]				
					τ_0 $\Delta r = 0$	τ_1 $\Delta r = 1,5$	τ_2 $\Delta r = 3$	τ_3 $\Delta r = 6$	τ_4 $\Delta r = 9$
0	-	760/830 x 730/800	-	-	-	-	-	-	-
1	I	720 x 730/800	620	1,52	1,80	1,80	1,80	1,80	1,78
2	I	640 x 735/800	620	1,52	1,99	1,98	1,98	1,97	1,96
R _s	-	735/805 x 640	-	-	-	-	-	-	-
3	I	700 x 655	620	1,52	1,77	1,76	1,76	1,75	1,74
4	I	610 x 680	620	1,52	2,09	2,08	2,08	2,07	2,06
5	I	530 x 700	620	1,52	1,99	1,98	1,98	1,97	1,96
6	I	450 x 720	620	1,52	1,85	1,84	1,85	1,83	1,82
R _s	-	720 x 450	-	-	-	-	-	-	-
7	II	600 x 480	592,5	1,54	2,40	2,39	2,40	2,38	2,37
8	II	500 x 505	592,5	1,54	2,29	2,28	2,28	2,27	2,25
R _s	-	505 x 500	-	-	-	-	-	-	-
9	I	390 x 525	620	1,52	1,38	1,38	1,38	1,37	1,36
10	I	330 x 545	620	1,52	1,19	1,18	1,18	1,18	1,76
R _s	-	545 x 330	-	-	-	-	-	-	-
11	IV	430 x 355	605	1,51	1,92	1,91	1,91	1,90	1,89
12	IV	350 x 375	605	1,51	1,64	1,64	1,64	1,63	1,62
R _s	-	375 x 350	-	-	-	-	-	-	-
13	III	280 x 380	600	1,55	1,47	1,46	1,46	1,45	1,44

Table 4. Calculation of pressure stress on the contact surface of rolling cylinders in the area of hole deformation

No. of stages	Gauge	Rolled good section [mm x mm]	Gauge radius R [mm]	Reduction Δh [mm]	Average width B_m [mm]	Tension σ_{pc}	
						$\sqrt{R\Delta h}$	σ_{pc} [daN/mm ²]
0	-	760/830 x 730/800	-	-	-	-	-
1	I	720 x 730/800	620	40/110	765	261,1	4,26
2	I	640 x 735/800	620	80	767	222,7	6,46
R	-	735/805 x 640	-	-	-	-	-
3	I	700 x 655	620	35/105	640	255,1	5,23
4	I	610 x 680	620	90	655	236,2	7,04
5	I	530 x 700	620	80	682	222,7	7,24
6	I	450 x 720	620	80	707,5	222,7	6,51
R	-	720 x 450	-	-	-	-	-
7	II	600 x 480	592,5	120	467,5	266,6	7,68
8	II	500 x 505	592,5	100	497,5	243,4	8,25
R	-	505 x 500	-	-	-	-	-
9	I	390 x 525	620	115	514	267,0	4,76
10	I	330 x 545	620	60	536,5	192,8	7,36
R	-	545 x 330	-	-	-	-	-
11	IV	430 x 355	605	115	342,5	263,7	9,30
12	IV	350 x 375	605	80	362,5	220,0	10,88
R	-	375 x 350	-	-	-	-	-
13	III	280 x 380	600	95	365	238,7	7,94

3. RESULTS

According to the analysis of the twisting, bending, and contact pressure tensions we have already highlighted in Tables no. 2,3,4:

- ✚ the bending tensions (table 2) are the highest in case of the outside layer and go deep to 15-20 mm underneath the surface of the gauge; the highest values are $\sigma_I = 8,55$ daN/mm², and they grow smaller as they get closer to the core of the gauge. By the time they reach its axis, they are null.
- ✚ the twisting tensions (table 3) produced during the rolling (rolling time) have higher values. The highest value is $\tau_I = 2,29$ daN/mm² at the surface of the gauge. Thus, these tensions could be ignored. But still, we have to point out the general rule for determining the tensions inside the roll, where they get more and more small; and by the time they reach the axis they are null.
- ✚ other tensions caused by stress and contact pressure (table 4) influence only the surface of the gauges, in the area of the deformation core, and their highest value is $\sigma_{pc} = 10,88$ daN/mm².

Generally speaking, we could point out that mechanical tensions we have used for classical resistance calculus for the rolling process have insignificant values. These calculations are not valid in case of real industrial processes. If we consider the thermal tensions, we would be able to come up with a complete study about the genuine industrial process situations, because thermal influences are the main cause for thermal fatigue in case of lamination rolls. Those influences are also valid in case of favorable operation conditions when we use the lamination rolls.

REFERENCES

- [1] Pinca C., Tirian G.O. Socalici A.V –Researches upon the thermo- mechanic stresses to the hot rolling mill cylinders, 11th International Research/Expert Conference “Trends in the Development of Machinery and Associated Technology TMT 2007, Hammamet, Tunisia, 2007.
- [2] Toader St., Pinca C., Plesa D., The thermal fatigue of the hot rolling mill cylinders, Ed. Politehnica, Timisoara, 2004
- [3] Pinca C., - Researches and experiments regarding the thermal and the equivalent tensions from the hot rolling mills cylinders, in avoiding the growing thermal fatigue resistanc and the increase ofservice life, Grant No.58 GR/ 19.05.2006, Tema 3, Cod 45
- [4] Sicicov The thermal regime of the rolling cylinders” , Ed. Metalurgia, Moskva, 1974)pp. 95
- [5] Wusatowski Z., The bases lamination, Bucuresti, Ed. Tehnica, 1972
- [6] Pinca C., Tirian G.O., Vilceanu L- The effects of the thermal fatigue upon the hot rolling mill cylinders, Metalurgia Internațional, XIII (5), 2008, pp.25-33



THE USAGE OF TYPE SILUMINIU ALLOYS WITH MAGNESIUM FOR CASTING A VERY LARGE USED PIECES

BOBOESCU Remus, SPOREA Ion, BORDEAȘU Ilarie, TOKAR Adriana, BUJOR Victor

University Politehnica Timisoara, ROMANIA

Abstract:

ATSi₇Mg aluminum alloy is subjected to the processes of hardening and aging. The structural transformations are related mechanical properties of the alloy. The presence of the Mg₂Si phase is the main cause of increasing resistance of alloys Al-Si-Mg, but with the presence of stable phase Mg₂Si reduces refractivity of ternary alloys.

1. INTRODUCTION

Among the advantages of alloys siluminium ATSi₁₂; ATSi₁₀MnMg; ATSi₇Mg; ATSi₇MgTi is the used in humid atmosphere like maine atmosphere As the concentration of Si growth there is a decrease of the linear thermal expansion coefficient, but to obtain a raft structure raft in the cast [1] [2] [4] [5] [6] (the material is fragile and difficult to process).

For finishing the structure, increase the mechanical resistance and improve mechanical machining by cutting of type AAT siluminium (hipo and eutectic) is added to Na and Cl and salts containing F and Na, S, P, etc.. in the alloy. The hypereutectic alloys have much Si_I in the structure and is difficult to be modified with salts containing Na. A greater effect in modifying these alloys siluminiu hypereutectic is obtained with substances containing S or P [6] [7] [8] [9].

2. SYSTEM ALLOYS IN AL-SI + EA (ALLOING ELEMENTS)

System Al-Si alloys + Ea is one of most used in the casting aluminum alloy of great importance pieces because it possess superior mechanical and technological proprieties than other cast aluminum alloys (AAT).

The most typical alloy system Al-Si-Mg is widely used in casting of ATSi₇Mg (6-8% Si, 0.25-0.4% Mg, the rest). This alloy is used both in the hardening state (T4) and after partial aging (T5). Is is used for castings pieces with thin walls and complex shapes used in the condition of medium loaded forces (body pump, etc.). The advantages of alloy ATSi₇Mg are: good casting properties (high fluidity, minimum linear contractions) like as ATSi₁₂; the tendency of formation of small cracks hot high temperature; good mechanical strength and satisfactory plasticity; compared with ATSi₁₀MnMg not require autoclaves to pressure crystallization; is the possibility to used modifier containing Na as S, P, etc.[2]; Like disadvantages ATSi₇Mg shows: reduced machining by cutting; with increasing concentration of Mg decreases plasticity (mechanical R_m increases and the capability of machining); resistance to corrosion from HNO₃; reduced refractivity, which may increase with increasing concentration of Si, Mg or Cu.

The hardening basic phase of ternary alloys is Mg₂Si noted as β', the type chemical intermetallic component (determined by normal valence). Possess crystalline elementary cube network and does not form solid solutions α with its constituents, what is characteristic ionic combinations in contrast with benthonic phases type (ex: Mg₂Al₃).

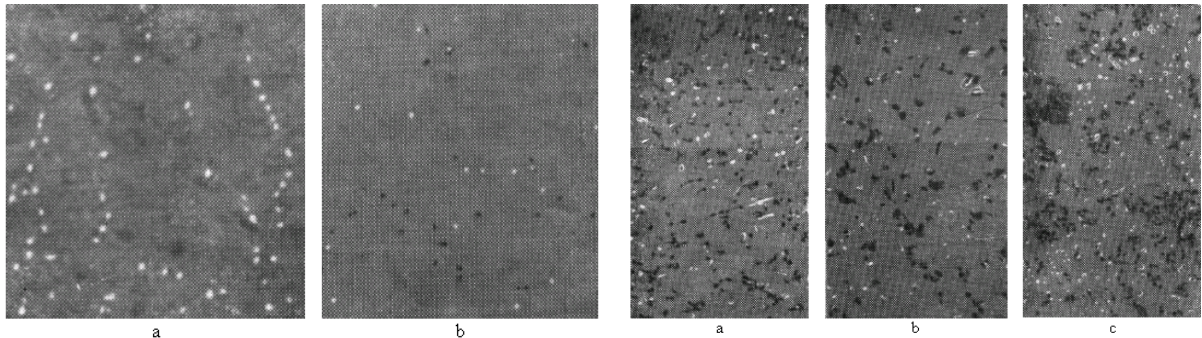


Fig. 1 Structure of alloy ATSi₇Mg (10000:1) aged a-135 °C/15 h and b- a-135 °C/15 h

Fig.2 Structure of alloy ATSi₇Mg(10000:1) aged a-165 °C in times:a15h b-25h, c-100h

Regarding the influence of Si and Mg on the effect of loss of mechanical resistance of alloys Al + Mg + Si at high temperatures [5], [6], [2], [8], it shows that the decomposition of α solid solution of Mg and Si in Al follow the next schedule:

1. Appear in the crystal network of solid solution the Guillet-P zone. There is a change to approaches atoms of Si and Mg and formation of metastable β' phase; (Mg_2Si) - the process is very intense at high temperatures and slow at ambient temperature. Reset of atoms position had place with the distortion is strong crystalline network and consequently there is as result strong growth mechanical resistance of siluminium type alloys at ambient temperature and reducing refractivity of temperature used in aging process (160-170°C and higher).
2. There are a formations of small grains mono-and two-dimensional phase metastable β' (Mg_2Si) which possess crystalline hexagonal network. It is believed that the training phase Mg_2Si is the main cause of increasing resistance of alloys Al-Si-Mg, but with the apparition of stable phase Mg_2Si the refractivity ternary alloys will be reduce. This clear happened at heated at 170-180°C retention time of 25h to return treatment.
3. Stable phase Mg_2Si is formed in alloys type siluminium in process to maintain at 185-220°C for several hours and at 300°C for 30 minutes to aging, with strong reduce resistance of alloy.

The alloy aging process at 180-225°C with reduced times of process can provide for ATSi₇Mg alloy high strength and low plasticity. Refractivity of these alloys can be strong increased by two ways:

- ✚ It strengthens the solid solution α by a complex process of alloying which assure the separation of the granular stable phases crystallized in form of branches
- ✚ make an bonding of Si free (elementary) in the stabile component ($Al_8Si_6Mg_3Fe$, Al_4Si_2Fe , Al_5SiFe etc.) An example of these components is phase Mg_2Si which is found in most siluminium alloys (ATSi₁₂, ATSi₇Mg, etc.)

Mg_2Si phase is formed through a series of transformations that strongly distorts the crystalline network of alloy and increases the mechanical resistance at ambient temperature (due to hardening and aging processes).

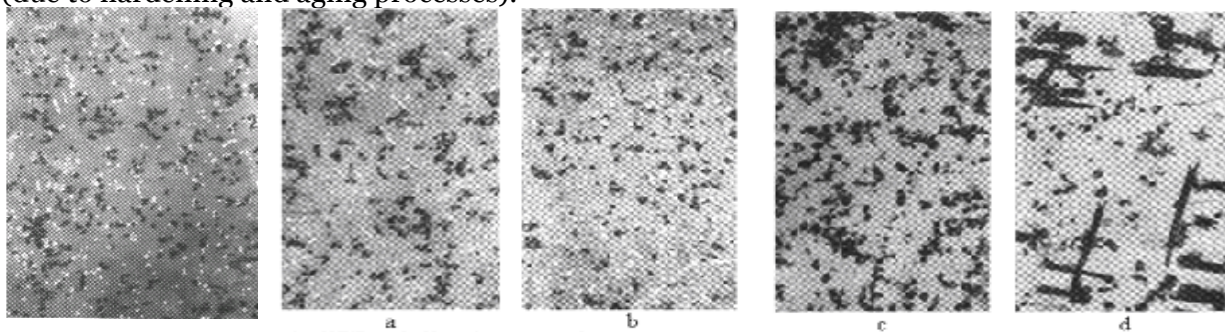


Fig. 3 Structure of alloy ATSi₇Mg (10000:1) aged a-175 °C/10 h

Fig. 4 Structure of alloy ATSi₇Mg(10000:1) aged:a-185 °C /15h , b-200 °C /10h, c-300 °C /10h, d-300 °C /100h.

3. INTERPRETATIONS

In work [8], [9] it shows that the ternary alloy system Al-Si-Mg, were first observed in aluminum matrix areas which characterize stages of ante-separation. There not was established neither by X-ray observations the differences in areas structure for aging alloys. Despite lack evidence of structural changes, increased of mechanical properties of ternary alloys is a fact. Only at a temperature of 150°C authors [9] in 1958 established that the separation distributed locally of Mg and Si take place.

It is believed (with network vacancies which are formed during the hardening process) atoms of alloying elements Ea begin to be collected in the chains without any order, after which the atoms slowly sits in an order determined the by network parameter (4.04 Å) and the chain gets the same format with the elementary cell of the matrix. At high temperatures the atoms of Ea formed construction areas least different of the matrix. It shows [9] that this phase β” move gradually in the phase β’ rebuilding the crystalline matrix is accompanied by a strong distortion which is the main cause of increasing the mechanical properties of alloys siluminium. But such a tensioned state of the crystalline network helps to reduce refractory of alloys. This is observed as a strong fact, in changing the structure of α solid solution alloy type ATSi₇Mg at 165 ° C in the ageing process where the decomposition of α solid solution takes place relatively quickly.

Figure 1 shows the solid solution alloy ATSi₇Mg in which ageing at 135 °C for 15 hours produce formation and deposition of fine dispersed elemental Si [5]. In addition to this Si there are deposits in the form round (white points) probably the Guillet areas or how to say „phase” β” .

We say that such products of the decomposing solid solution which is formed as chains in the alloys Al-Mg-Si is characteristic for the initial stage of aging. The structure of ATSi₇Mg aged at 150 °C for 15 h (Figure 1.b) confirms the words [16].

At higher temperatures the return process and the size of elementary high dispersed Si particles and a separation (white point) increase dramatically. (Figure 2). Structure of α solid solution after aging for 15 and 25 h (Figure 2 a, b) at 165 °C has many deposits of Si and formation of β” metastabile phase, and even the stable phase Mg₂Si (fig. 2 c)

From Figures 2 and 3 it is clear that with increasing aging temperature there is the decomposition of solid solution α is very intense and is formed by deposition metastabile phases that increase substantially with aging time. Very intense decomposition α solid solution had place at 175 °C with the maintenance of 10 h.

The figure 4 shows a large amount of fine and small and many particle high dispersed portions of Si_I (primary) that were formed after reset the network. Particles Mg₂Si (in the form of narrow white strips) are shown oriented.

Very suggestive is the alloy ATSi₇Mg old aged at 185 °C for 15 h (Figure 1 a). But I clearly see this in Figure 1 b α solid solution decomposition at the aging temperature of 200 °C, virtually ends after 10h. This produce reduced resistance of alloy ATSi₇Mg at temperature of 200 °C.

4. CONCLUSIONS

Technological processes of casting under pressure are widespread in the industry. The process ensures a quality cast alloy type siluminium such as good walls and lack risk of mechanical cracks at hot state and cold state. The proprieties of cast alloys type siluminium can be improved by thermal treatment named artificial aging. There are many ways to make these treatments. These have resulted in changing the structure of alloy, with the apparition Mg₂Si phase (composed intermetallic component). This has an effect to increase mechanical resistance.

REFERENCES

- [1] Sporea, I., Ghiță, M., Uroșu, D. – Ovlianii poperecinâh vânujdennâh kolebanii na kacestvo obrabotki rezaniem aluminievâh splavov. TT și TS – 98, Nr. 7-8, Penza, 1998, Rassia

- [2] Sporea, I., Dreucean, A., Paulescu, Gh. – Contribuții la studiul aşchiabilității prin strunjire a unor aliaje de tip silumin. Conf. a-III-a de PUPR, Timișoara, 1978.
- [3] Sporea, I., ș.a. – Studiul prelucrabilității prin aşchiere a aliajelor de tip silumin. BSTIPT, Tom 22 (36), Fasc. 1., 1977.
- [4] Sporea, I., ș.a. – Influența oscilațiilor asupra calității suprafețelor aşchiate BSCST, vol II, Hunedoara 2002.
- [5] Sporea, I., ș.a. – Studiul influenței vibrații sculei. BSTIPT, Tom 24 (38), Fasc. 1., 1997.
- [6] Sporea, I., ș.a. – Asupra eficacității modificării aliajelor de tip silumin. BSTIPT, Tom 22 (36), Fasc. 1., 1997.
- [7] Mandek, Fr., ș.a. – Considerații privind folosirea cochilelor din aliaje de Al fabricate prin turnare. Anal of the Univ. of Oradea, vol. III (XIII), 2004, Fascicle of MTE.
- [8] Mandek, Fr., Galea, I., Sporea, I. – Influența imperfecțiunii rețelelor cristaline asupra refractarității AA turnate în pistoane. A – IX-a ses. MAN AFT “Nicolae Bălcescu” Sibiu 2004.
- [9] Ion Sporea, Ilarie Bordeasu, Francisk Mandek –Aliaje de aluminiu refractare turnate în pistoane de motoare termice Editura Politehnica Timișoara 2008



STUDIES AND TESTS CONCERNING SMELTING CASTING ALLOY OF UNIVERSAL ALUMINIUM

Adriana TOKAR, Ion SPOREA, Arina NEGOITESCU

University Politehnica of Timisoara, ROMANIA

Abstract

The direct consequence use on a major scale a silumin alloy type at casting pieces which working at high temperatures, e.g. thermal engine pistons, is: finding, smelting an alloy that possess good mechanical and technological properties, with preservation of those properties for a long time. The most recommended are Al-Si alloys type, allied with addition agent (Ea) such as Cu, Mg, Mn, B, Ti, Cr, etc. Large used alloys are $ATSi_9Cu_2MgB$ and $ATSi_{10}MgMn$ but with the shortcoming technology and mechanical properties, has been necessary to find a “universal” cast alloy that has proven to be $ATSi_9Cu_3MgMnB$, which is studied in this paper and responded well to the demands of constructors and technologists requirements of the non-ferrous foundries.

Key words:

alloy, aluminium, thermal engine, pistons, casting

1. INTRODUCTION

In automotive industry is good to have a cast aluminium alloy (AAT) which correspond to the requirements of foundries technology, to have high mechanical strength both at ambient temperature and at high temperatures (resistance duration), dimensional stability over time, regardless of operating conditions, etc.

For developing (creating) a new alloy (made of AAT), with high technological and mechanical proprieties called UNIVERSAL DESTINATION Alloy, the basis for it had in mind the following considerations [1]....[4]:

1. Si content should be around 8-10%, to ensure high casting properties, which allow casting of PT by any method (in FAF, in shell, with lost models (fusible), centrifugal, under low or high pressure, etc.) without appear casting cracks.
2. Solid solution α must have a high quality of supersaturate in Ea, to allow during the aging process to obtain a high density of ultra-dispersed particles (micro-heterogeneous) inside s.s. α grains. This allows achieving high flow limits and mechanical resistance.
3. Alloy components -Ea- and inclusion, in the alloy crystallization should not form particles occur on the separation of the s.s. α . [5]...., [7].

Following research [1], [2] developed a new alloy cast in AAT, which possesses a chemical composition (8-11%Si; 3-4%Cu; 0,13-0,35%Mg; 0,1-0,3%Mn; 0,01-0,1B; 0,4%Fe, rest aluminium) and notes $ATSi_{9,5}Cu_3MgMnB$. Alloy has received a fast use at casting the various PT. In figure 1 (2.78) is shown typical PT, cast of this alloy, pieces that once was made by plastic deformation with very high costs.

To note that the proportion of Mg and Cu content in this alloy is other compared to $ATSi_9Cu_2MgB$. That alloy has characteristics of resistance much higher, both at ambient temperature and at higher temperatures. The complex configuration of PT and walls thickness, and the operation of the PT must be considered on load composition of the alloy development. As before, the highest is Si content (but $Si < 12\%$), the greater is eutectic quantity, this means that has highest properties of casting and PT hermetically. However,

with increasing Si content of alloy increases the tendency towards abortion gas, therefore PT is formed in a high porosity. For casting the complexity PT (complex configuration), with wall thickness 3-4mm is sufficient for the load to be 9% Si.

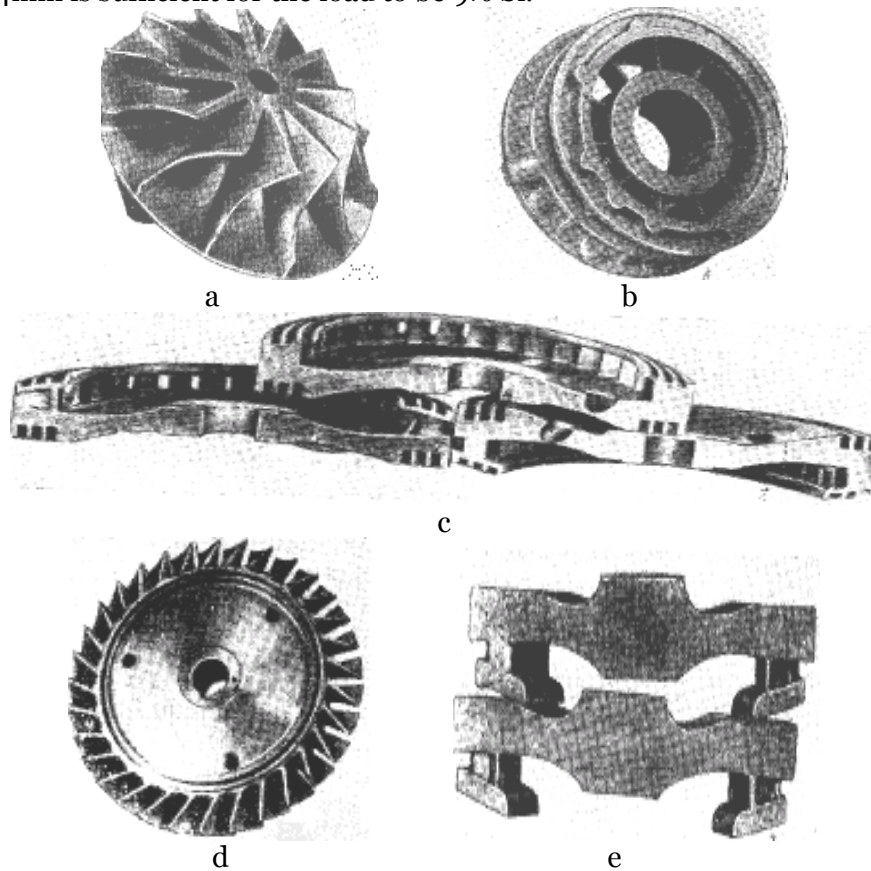


Fig.1 Pieces of great complexity cast of polynar alloy $ATSi_{10}Cu_3MgMnB$:
a- centrifugal; b- precision; c- section of the turbine body; d- Precision; e- Shell (microstructure)

With increasing content of Cu, refractory alloy increases, but plasticity (A) decreases at ambient temperature. If the PT in this alloy is intended to work long time at high temperatures the content that should be at upper limit, and if working at ambient temperature, then at lower limit.

The increasing of Mg content leads to increase refractory alloy, but decreases plasticity at ambient temperature. To increase plasticity, in PT, the content of Mg should be kept at the lower limit, same for Fe content. In this situation the content of Mn should be 0.8% and the content of Fe = 0.2-0.3%.

If PT is accomplished by stamping of semi liquid state, then permitted Fe inclusion even 0.4%. This has a great technical and economic meaning, because in the use of Al load (waste) technical with high content of Fe.

Ti and B are introduced in the alloy as modifier.

2. $ATSi_9Cu_5MgMnB$ ALLOY STRUCTURE

The alloy $ATSi_9Cu_3MgMnB$ as you can see possesses a complex chemical composition. Depending on the chemical composition fluctuation, Fe content in the PT and the rate of crystallization, phases of the alloy composition may change strongly. Alloy structure in a cast (especially in parts of the massive and high content of Cu) may have the following phases: α , Si, Mg_2Si , $CuAl_2$, $AlSiMnFe$ (figure 2, (2.79)). In case of very slow crystallization (at $T \approx ct$, in equilibrium) can form $W(Al_xMg_5Si_4Cu_4)$ phase which is seen in figure 3 (2.80).

Taking into account that in the $ATSi_9Cu_3MgBTi$ alloy can be eutectic with different melting temperatures (because of the complexity phase component, which depends on the rate of crystallization) and also considering the differential thermal analysis (figure 4 (2.81)) for PT is recommended two regimes of hardening:

- ☛ heating at 500°C/4h + 515°C/10h followed by cooling in water temperature 20-30°C;
- ☛ heating at 490°C/4h + 500°C/4h + 515°C/6h and cooling in water temperature 20-30°C.

The first hardening regime is recommended to PT in the shell or PT with thin walls cast in FAT (when the cooling rate of casting is great - $v_{cr} \gg 0$). The second hardening regime is recommended for large size PT with thermal node (joints massifs).

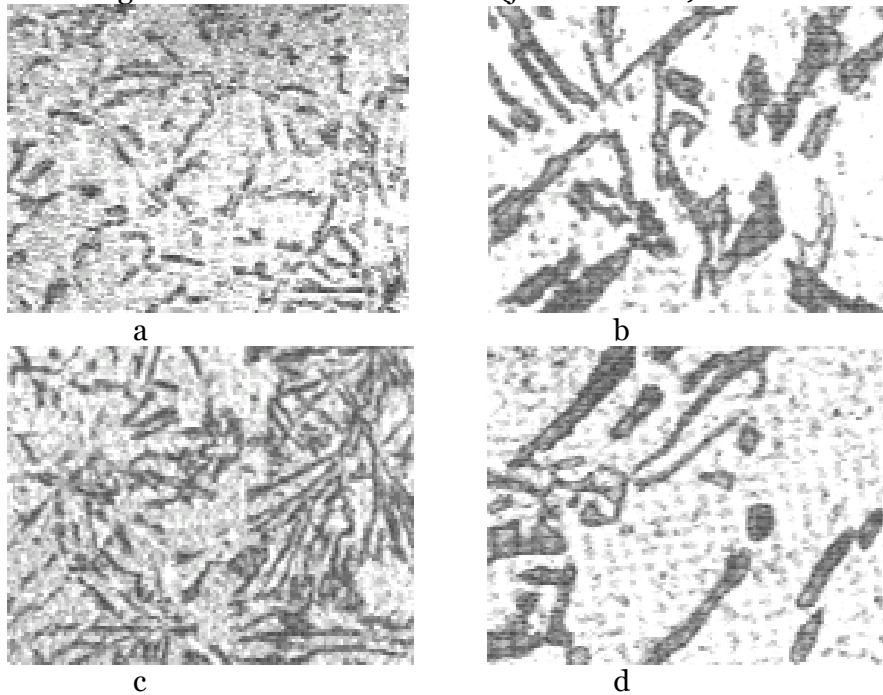


Fig.2 ATSi₉Cu₃MgMnB alloy structure: a- cast (100:1); b- cast (500:1); over TT; c- 100:1; d- 500:1



Fig.3 Type of crystallization phase W(Al_xMg₅Cu₄Si₄) la

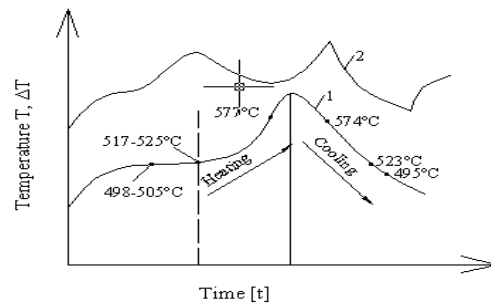


Fig.4 Direct thermal analysis curves (1) and differential (2) of the ATSi₉Cu₃MgBTi

Mechanical properties of ATSi₉Cu₃MgMnB hardening after the first regime and the aging after the regime 165°C/22h or 175°C/7h, with air cooling are shown in figure 5 (2.82). At 20°C has HB=120daN/mm² and decrease with test temperature increase.

4. CONCLUSIONS

The physical properties of the alloy ATSi₉Cu₃MgMnB practically are the same as those of the alloy ATSi₉Cu₂MgB, and the casting of the alloy as ATSi₁₀MgMn. The cutting process is better [5], than the two mentioned alloys. The welding is good.

To confirm the correctness of the choice of aging regime is shown in figure 6 (2.83) s.s.α alloy structure ATSi₉Cu₃MgMnB in hardening state and cast in forms of mixture formation.

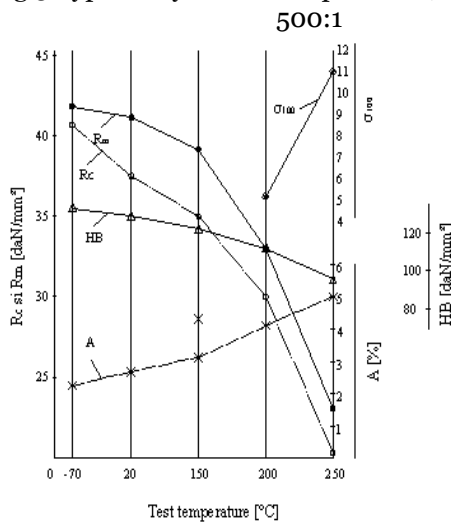


Fig.5 ATSi₉Cu₃MgMnB proprieties determined on sample of Φ12mm cast in shell

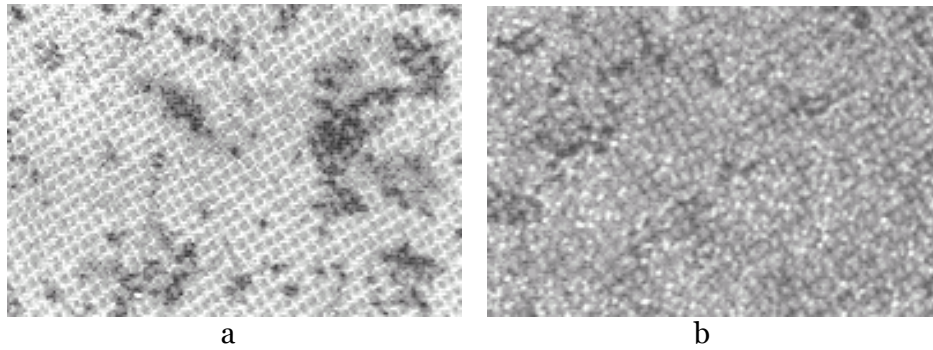


Fig. 6 ATSi₉Cu₃MgMnB structure alloy in hardening state after casting in: a- FAT and b- shell (10000:1)

Note that the cooling was the first stage of aging, this mean that, they have managed to form ZGP and agglomerations of Si ultra-dispersed particles what were separately from s.s.α. In comparing these pictures, you can see that ZGP density in solid solution alloy ATSi₉Cu₃MgMnB, cast in FT, is much reduced, comparative to s.s.α of the alloy cast in shell. This can be explained by the fact that: supersaturate degree of s.s.α in the last sample, in all probability, is higher, and the degree of distortion R_{cr} of s.s.α also higher, which accelerates the process of form ZGP, and ultra-dispersed particle of elementary Si.

REFERENCES

- [1] Sporea Ion, Bordeasă Ilare, Mandek Francisc, *Aliaje de aluminiu refractare turnate în pistoane de motoare termice*, Ed. Politehnica, Timișoara, ISBN 2008
- [2] Tokar Adriana, Sporea, Ion, ș.a *Influence of heat treatment on the alpha coeficient, the piston-cylinder clearance with Dacia engines*, Scientific Conference-13th-edition with international participation, Engineering series, no.2, ISSN 1844-4856, Tîrgu Jiu, 2008.
- [3] Tokar Adriana, Sporea Ion, Olariu Mircea ș.a, *Considerations regarding the refractoriness of aluminium alloys intended for casting into heat engine pistons*, The 14th International Conference, The Knowledge-Based Organization, ISSN 1843-6722 Sibiu, 2008.
- [4] Tokar Adriana, Bujor Victor, Sporea, Ion, *Refractoriness of alloz from the polznar szstem Al-Cu-Mg-Si-Mn-Ti etc used on piston casting for heat engines*, International Congress Automotive Safetz and Environment SMAT, Tom II, E19(97), ISBN 978-606-510-253-8, Craiova, 2008
- [5] Sporea Ion, Ghiță Mihai, Uroșu D., *O vlianii poperecinâh vânuya kolebanii na kacestro obrâb. rezaniem aluminiemvâh splarov.*, TT i TS-98, Nr,7-8, Penza, 1998, Rassia.
- [6] Sporea Ion, ș.a., *Studiul prelucrării prin aşchiere a aliajelor de tip siluminii*, BST al IPT, Tom. 22(36), Fasc.1, Timișoara 1977.
- [7] Sporea Ion, Dreuceanu Aurel, Paulescu Gheorghe, *Contribuții la studiul aşchiabilității prin strunjire a unor aliaje de tip silumin*, Conferința a-III-a PUPR, Timișoara, 1978



MEASURING THE PRESSION FIELD IN AN INVERTED AIR FILTER

¹Sorin RAȚIU, ¹Corneliu BIRTOK-BĂNEASĂ, ²Liviu MIHON

¹Politehnica University Timișoara, Faculty of Engineering Hunedoara, ROMANIA

²Politehnica University Timișoara, Faculty of Mechanical Engineering Timișoara, ROMANIA

Abstract:

This article presents a concept regarding the design of an efficient air filter for internal combustion engines, and more precisely: the super-absorbing air filter. The collection effect is being described by measuring the pressure fields with a digital manometer under air flow action.

Keywords:

air filter, internal combustion engine, pressure fields

1. INTRODUCTION

The correct filtration of the air that circulates inside the cylinders of the internal combustion engine is essential for preserving the good functioning of the engine over time. The obstruction of the admission of various impurities from the atmospheric air significantly lowers the wearing out of the moving parts of the engine.

Unfortunately, in addition to its air filtration function, the air filter displays a significant gas-dynamic resistance of the absorbed air. If the air filter is not periodically cleaned and the car circulates frequently in a dusty area, both the absorption pressure p_a and the filling coefficient η_V are dramatically decreased.

There are currently on the market several constructive variants of air filters, which differ according to the filtering principle:

- ✚ filters with filtering cell,
- ✚ inertia filters,
- ✚ combined filters.

These air filters have the following *disadvantages*:

- the presence of the filtering element inside the box induces an enhanced gas-dynamic resistance of the absorbed air (generating the phenomenon of insufficient absorption);
- storage of impurities inside the filter affects the self - cleaning feature of the filtering element;
- the filtering element can not be visualized and it has to be dismantled for the impurity level to be checked;
- incapacity of the air filter to significantly increase the speed of the absorbed air;
- incapacity of the air filter to cool the absorbed air;
- impossibility of the air filter to create a slight effect of overfeeding during the functioning of the engine.

2. THE INVERTED SUPER ABSORBING FILTER

The inverted super absorbing filter consists of a cylindrical filtering element, bordered at its anterior part by an internal diffuser fused to a joint cylinder. At its posterior part, the cylindrical filtering element is embedded concentric-axially (2/3 of its length) in a mono-block complex, which consists of an external diffuser for air collection, followed by a direction-invertor (figure 1).



Figure 1. The inverted super absorbing filter

For an optimum air collection and absorption yield, the inverted super absorbing filter is set along the geometrical axis of the car.

Due to its geometry, the external diffuser (figure 2) with direction-invertor (figure 3) ensures a very good collection, causing the inversion of the absorbed air flux by 180°, which is thus directed through the filtering element towards the internal diffuser (towards the exit of the filter).

The external diffuser with direction-invertor covers the filtering element (for 2/3 of its length) up to a very precise distance from the exterior of the element, which ensures the collection and inversion of the air flux. Cooling radiators are located on the outside of the direction-invertor.

the element, which ensures the collection and inversion of the air flux. Cooling radiators are located on the outside of the direction-invertor.

2.1. The external diffuser for air collection with direction-invertor

The cooling radiators consist of external wings, which cover 80% of the external surface of the direction-invertor. They maintain a low temperature of the direction-invertor and generate, consequently, a thermal equilibrium between the surface of the wall and the absorbed air. As a result, the temperature of the air is significantly decreased before it enters the air filter.



Figure 2. The external diffuser for air collection



Figure 3. The direction-invertor

2.2. The filtering element

The filtering element (figure 4) has a cylindrical shape. It consists of a micron size cardboard, which forms the lateral surface of the filtering element (in a radial section, the micron size cardboard has a W shape).



Figure 4. The filtering element



Figure 5. The internal diffuser and joint cylinder

The cardboard ensures a micron size filtration and is covered on the outside with a millimetric sieve, which allows a rough millimeter size filtration of the air. The micron size cardboard and the millimetric sieve are fixed at the two open ends by silicone rings, for an optimum sealing and concentric – symmetrical alignment with both the internal diffuser of the anterior part and the mono-block complex of the posterior part.

2.3. The internal diffuser for air acceleration

The internal diffuser for air acceleration has a taper shape and ensures the connection between the contact surface and the joint cylinder (figure 5). Due to its constructive geometry, the internal diffuser has the capacity of increasing the speed of the absorbed air. Taper-shaped cooling radiators are located on the outside of the internal diffuser. Because of their taper shape, they redirect the air flux towards the external diffuser, which allows a concentrated flow of the air and a minimum gas-dynamic resistance. They maintain a low temperature of the diffuser and generate, consequently, a thermal equilibrium between the surface of the wall and the absorbed air. As a result, the temperature of the air is significantly decreased before it leaves the inverted filter.

The purpose of the joint cylinder is to link the air filter to the admission gallery of the engine.

The internal diffuser for air acceleration, the filtering element and the mono-block complex (the external diffuser for air collection with direction-invertor) have varying dimensions according to the swept volume of the engine, so that the bigger the swept volume, the larger the dimensions of the diffuser and vice-versa.

The inverted super absorbing filter improves the filling coefficient and is useful for engines that employ air filters set in the opposite direction of the flow of the absorbed air (filters set up at the rear of the Bugatti, Ferrari, Lamborghini engines).

2.4. Conclusion regarding the inverted super absorbing filter

The inverted super absorbing filter has the following *advantages*:

- being in direct contact with the air, the filtering element ensures a minimal gas- dynamic resistance of the absorbed air, increasing therefore the level of absorption and collection of the air, and consequently boosting the air filling coefficient of the engine cylinders;
- possibility of self-cleaning of the filtering element;
- the level of impurities on the filter can be readily evaluated: the filtering element can be easily visualized without previously dismantling the filter;
- the speed of the absorbed air both at the entrance and the exit of the filter is considerably increased;
- significant capacity of the air filter to cool the absorbed air;
- the air filter creates a slight effect of overfeeding during the functioning of the engine, which is proportional with the speed of the car;
- this air filter fulfils new tasks, in addition to its classical function of air filtration: increases the degree of absorption and collection, the speed of the absorbed air, cools down the absorbed air and inverts the air flux by 180°

3. DESCRIPTION OF THE EXPERIMENTAL SETUP

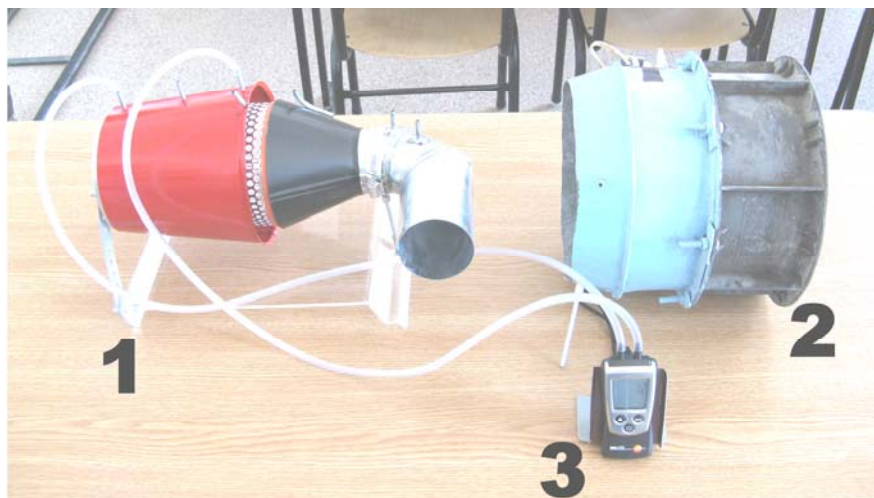


Figure 6. General view of the experimental setup:
1- inverted super-absorbing filter; 2- constant flow ventilator;
3- digital manometer

3.1. The inverted super-absorbing filter

The inverted super-absorbing filter consists of a cylindrical filtering element (C), bordered internally by a diffuser (D) fused to a joint cylinder (E). The cylindrical filtering element is embedded concentric-axially (90 % of its length) in an external air collector (A), bordered at its posterior part by an internal cone (B) (Figure 7).



Figure 7. Inverted super-absorbing filter. Constituting elements

For an optimum air collection and absorption yield, the inverted super aspirant filter is set longitudinally with respect to the geometrical axis of the car.

3.2. The external axial collector with the internal cone

Due to its geometry, the axial external collector A with the internal cone B (Figure 7, 8 and 9) ensures a very good air collection. It causes the inversion of the absorbed air flux by 180°, which is therefore directed through the filtering element towards the internal diffuser (towards the exit of the filter).



Figure 8. The external axial collector with the internal cone (longitudinal view)

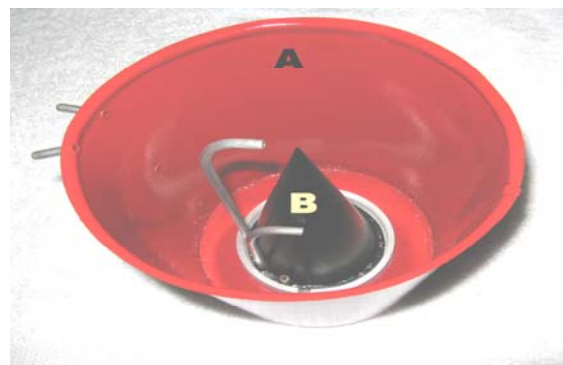


Figure 9. The external axial collector with the internal cone (radial view)

The axial external collector with internal cone covers the filtering element (for 90 % of its length) up to a very precise distance from the exterior of the element, which allows an optimal collection and inversion of the air flux. There are 4 pressure plugs on the outside of the axial external collector and 3 pressure plugs around the internal cone.

3.3. The cylindrical filtering element

The filtering element is cylindrically shaped (Figure 10). It consists of a piece of cardboard with micron-size pores, which forms the lateral surface of the filtering element (in a radial section, the cardboard piece has a W shape).



Figure 10. The filtering element

The cardboard ensures a micron-size filtration and is covered on the outside with a sieve with millimetre-size pores, which allows a rough millimeter-size filtration of the air. The cardboard and the sieve are fixed at their open ends by silicone rings, for an optimum sealing and concentric – symmetrical alignment with both the internal diffuser at the anterior part and the mono-block complex at the posterior part.

3.4. The internal diffuser for air speed acceleration.

The internal diffuser for air acceleration D (figure 11) has a taper shape and ensures the connection between the filtering element C and the joint cylinder E (Fig. 7). Due to its geometry, the internal diffuser has the property of increasing the speed of the expelled air. Its taper shape directs the air flux towards the external axial collector, which allows a concentrated air flow and a minimum gas-dynamic resistance.



Figure 11. The internal diffuser

4. MEASURING METHODOLOGY

The static pressure is measured in the external axial collector via the pressure plugs 1, 2, 3, 4, inside the filtering element (at 1/2 its length) via plug 5, at the entrance of the internal diffuser via plug 6 and inside the joint cylinder via plug 7 (figure 12). All these pressure plugs were designed perpendicular to the air flow.

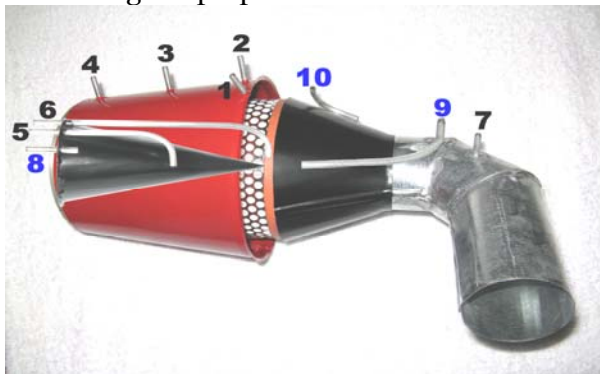


Figure 12. Pressure plugs



Figure 13. The digital manometer TESTO 510



Figure14. Filter with the internal cone



Figure15. Filter without the internal cone

The dynamic pressure is measured at the basis of the internal cone via plug 8, at the exit of the internal diffuser via plug 9 and at the external surface of the internal diffuser via plug 10 (figure 12). These pressure plugs were designed axial to the air flow.

The measurements were performed with the digital manometer TESTO 510 (0-100hPa) described in Figure 13. Pressure measurements relative to the atmospheric pressure were carried out at each pressure plug, at various distances

5. ANALYSIS OF RESULTS AND CONCLUSIONS

A significantly higher collection yield is observed in the presence of the internal cone (figure 14, Tabel 1) compared to when the internal cone is missing (Figure 15 and Tabel 2). The following graphs show the effect of the presence or absence of the cone on the pressure fields recorded at various distances from the ventilator: 0, 20, 40 cm.

Table 1. Static Pressure values (with internal cone)

distance	Plug 1	Plug 2	Plug 3	Plug 4	Plug 5	Plug 6	Plug 7
0	44	28	33	50	26	14	8
5	38	25	30	42	22	11	7
10	33	23	28	36	20	11	10
15	31	23	28	34	21	13	10
20	32	26	30	37	22	13	13
30	32	26	33	39	27	20	14
40	32	27	34	40	28	20	16
50	29	24	29	32	23	17	14

Table 2. Static Pressure values (without internal cone)

distance	Plug 1	Plug 2	Plug 3	Plug 4	Plug 5	Plug 6	Plug 7
0	39	26	35	50	20	8	3.5
5	30	19	25	36	15	4.5	2
10	20	15	20	29	13.5	3	1
15	16	13	19	21	13	3	1
20	17	14	19	22	11.5	2	1
30	15	13	18	22	12	2	2
40	15	13	19	22	12	3	2

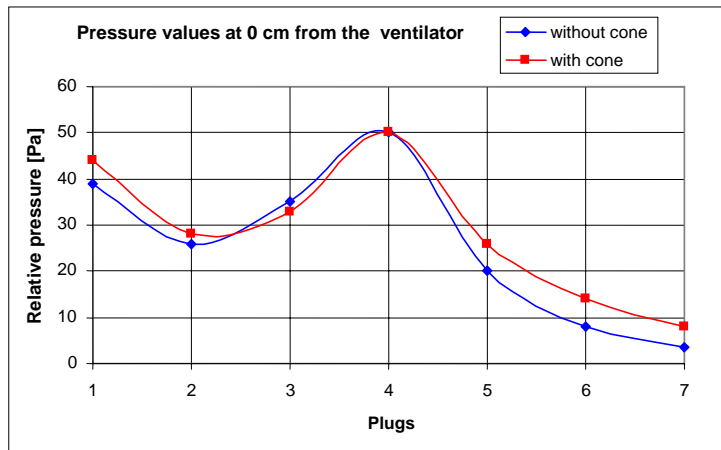


Figure 16. Comparative pressure values in the filter at 0 cm form the ventilator

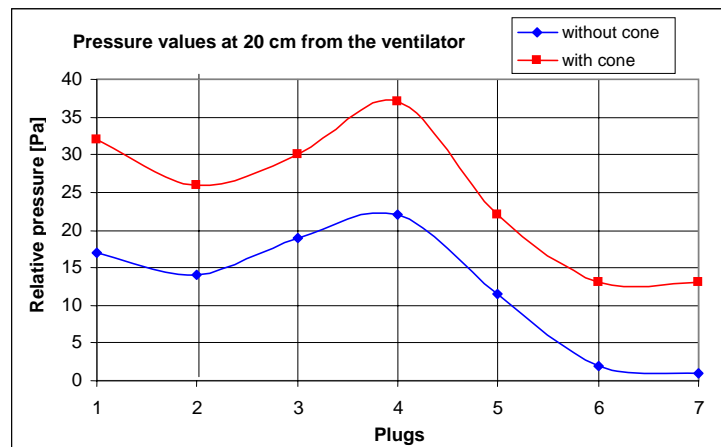


Figure 17. Comparative pressure values in the filter at 20 cm form the ventilator

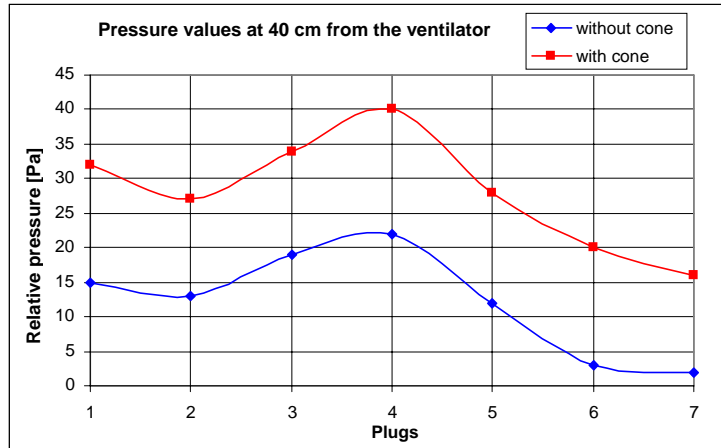


Figure 18. Comparative pressure values in the filter at 40 cm form the ventilator

The following graphs display the relative pressure fields measured at each plug vs the distance between the filter and the ventilator:

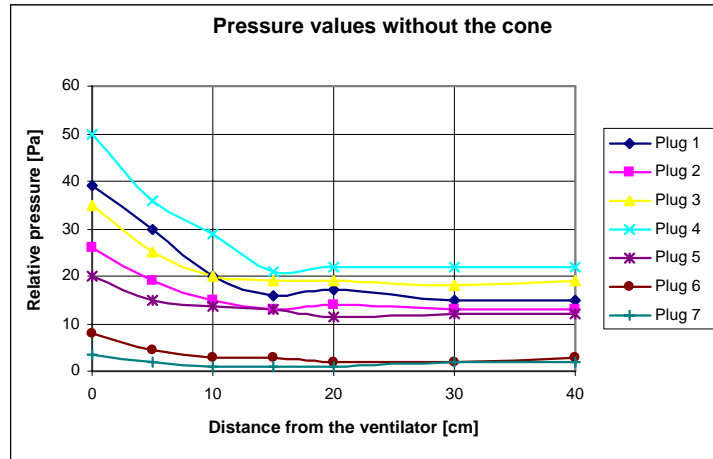


Figure 19. Relative pressure in the filter in the absence of the cone

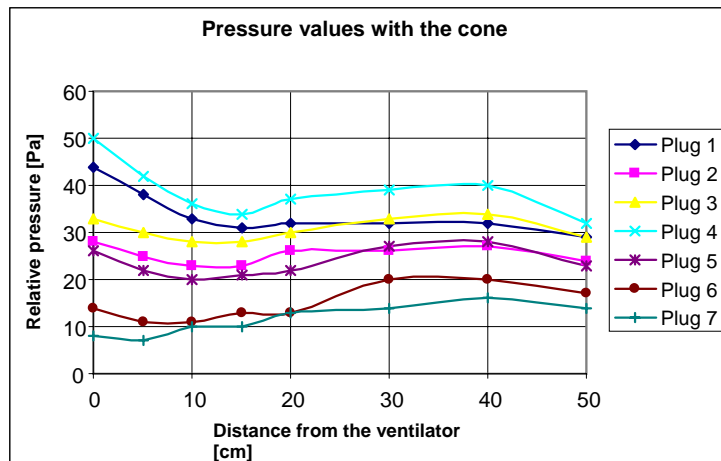


Figure 20. Relative pressure in the filter in the presence of the cone

The inverted super-absorbing filter improves the filling coefficient and is useful for engines that employ air filters set in the opposite direction of the flow of the absorbed air (filters set up at the rear of the Bugatti, Ferrari, Lamborghini engines).

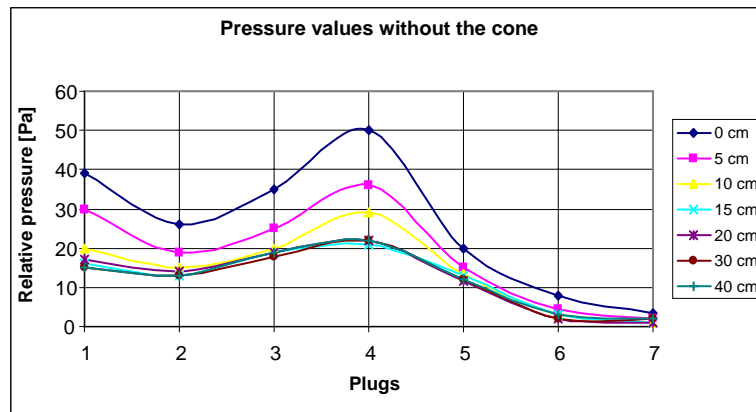


Figure 21. Comparative pressure values in the filter at various distances form the ventilator in the absence of the cone

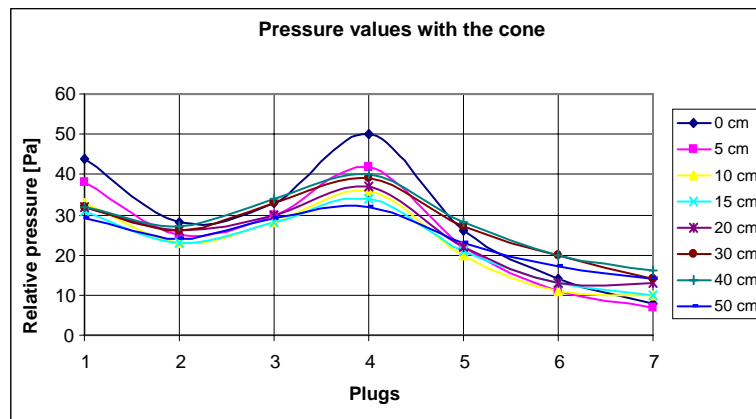


Figure 22. Comparative pressure values in the filter at various distances form the ventilator in the presence of the cone

6. CONCLUSIONS REGARDING THE INVERTED SUPER-ABSORBING FILTER

The inverted super aspirant filter has the following advantages:

- being in direct contact with the air, the filtering element ensures a minimal gas-dynamic resistance of the absorbed air, increasing therefore the level of absorption and collection of the air;
- possibility of self-cleaning of the filtering element;
- the level of impurities on the filter can be readily evaluated: the filtering element can be easily visualized without having to dismantle the filter;
- the speed of the absorbed air both at the entrance and the exit of the filter is considerably increased;
- the air filter creates a slight effect of overfeeding during the functioning of the engine, which is proportional with the speed of the car;
- this air filter fulfils new tasks, in addition to its classical function of air filtration: increases the degree of absorption and collection, the speed of the absorbed air, cools down the absorbed air and inverts the air flux by 180°.

BIBLIOGRAPHY:

- [1] www.corneliugroup.ro;
- [2] McComb, W.D. – Turbulența fluidelor, Editura Tehnică, București, 1997;
- [3] Abăitancei, D., ș.a. – Motoare pentru automobile și tractoare, Editura Tehnică, București, 1980;
- [4] Rațiu, S., Mihon, L. – Motoare cu ardere internă pentru autovehicule rutiere, Procese și Caracteristici, Editura Mirton, Timișoara, 2008;
- [5] Ionescu, D.Gh., ș.a. – Mecanica fluidelor și mașini hidraulice, E.D.P. București, 1980.



LABORATORY MEASUREMENTS OF LIGHT-DUTY VEHICLE POLLUTION AND FUEL CONSUMPTION

¹MIHON Liviu, ¹OSTOIA Daniel, ²ALIC Carmen Inge, ²RAȚIU Sorin

¹ Politehnica University of Timisoara – Faculty of Mechanical Engineering Timisoara

² Politehnica University of Timisoara – Faculty of Engineering Hunedoara, ROMANIA

Abstract:

The present paper present a method used in simple applications in order to determine the fuel consumption of a light-duty vehicle starting from the exhaust gases quantity and depending the testing cycle type. Are covered the EU, US and Japanese cycles and are presented the mesurements done on a twin-roll dynamometer.

Keywords:

fuel consumption, dynotest, driving cycles, carbon balance method

1. INTRODUCTION

Many countries have regulations on the measurement of exhaust gas emissions of passenger cars and light trucks. Pollution regulations define measurement conditions and the limit values for emissions of the following pollutants: carbon monoxide (CO), unburnt hydrocarbons (HC), nitrogen oxides (NOX), and particulate matter for diesel engines (compression-ignition engines). "Fuel consumption" regulations define the measurement conditions for both consumption and carbon dioxide (CO₂) emissions for passenger cars.

These measurements are taken on chassis dynamometers that can simulate different regulatory driving cycles: urban and extra-urban cycles in most countries and also motorway cycles, especially in the United States. Trucks, earth-moving vehicles and farm vehicles do not have to comply with any regulations on pollution or fuel consumption once fully assembled. Only their engines are subjected to laboratory pollution measurements with upper limits on the following emissions: CO, HC, NOX, particulate matter and exhaust fumes. As these engine measurements do not include tyre rolling resistance, we will not investigate them any further in this document. However, just as for passenger cars, progress in truck engine, vehicle and tyre design is helping lower pollution levels.

2. TEST PRINCIPLES

The vehicle is set up on a chassis dynamometer which simulates the resistance to forward movement experienced when driving on roads. During the test, the exhaust gases are collected then analyzed to determine:

- ✚ for pollution measurements: the mass of carbon monoxide (CO), hydrocarbons (HC), nitrogen oxides (NOX) and, for diesel engines, particulate matter. The results are given in g/km.
- ✚ for fuel consumption measurements: the mass of carbon monoxide (CO), total hydrocarbons (THC) and carbon dioxide (CO₂) in g/km. Fuel consumption is then calculated using the "carbon balance method".

3. POLLUTION AND FUEL CONSUMPTION MEASUREMENTS

- ✚ Speed (tolerance of ± 2 km/h with respect to the theoretical speed)
- ✚ Time (tolerance of ± 1 s)

- # Braking effort
- # Temperature in the test chamber (between 20 and 30 °C)
- # Air humidity
- # Engine tuning: as per manufacturer’s specifications
- # No heating, lighting or air-conditioning
- # Fuel: reference fuel as defined by the Directive
- # Vehicle: run in for at least 3,000 km and kept at between 20 and 30 °C for at least 6 hours before the test.

Pollution measurements

- # Size: the widest size specified as original equipment by the automobile manufacturer. If more than 3 sizes are certified, it is choosed the second widest. The model is not indicated in the test report.
- # Run in at the same time as the vehicle or with between 50 and 90 % of original tread depth.
- # Tyre pressure specified by the manufacturer, as used for the preliminary road test to adjust the dynamometer. Important: May be raised by up to 50 % if the measurements are recorded on a twin-roll dynamometer.

Measured parameters:

- # Mass of CO, HC, NO_x, and, for diesel engines, particulate matter.

Fuel consumption measurements

- # One of the tyres specified as original equipment by the automobile manufacturer. Tyre pressure as recommended for the load and speed, adjusted if necessary to test bed operation.

Measured parameters:

- # Mass of CO, THC, CO₂.

Calculated parameters:

- # Fuel consumption in l/100 km.

4. DYNAMOMETER ADJUSTMENT

The dynamometer must be able to reproduce all the forces to which a running vehicle is subjected:

- # rolling resistance forces,
- # inertial forces,
- # internal frictional forces,
- # aerodynamic forces.

The dynamometer is calibrated either using data obtained from a road coastdown test or from calibration tables stipulated in the Directive.

Dynamometers

There are two types of dynamometer: single-roll and twin-roll.

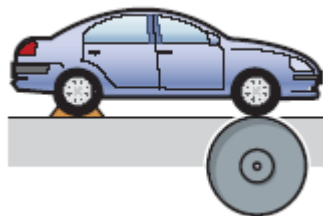


Figure 1. Car on a single - roll dynamometer

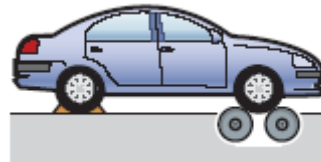


Figure 2. Car on a twin - roll dynamometer

Note: Tyre deformation is greater on a single-roll dynamometer than on a road, and still greater on a twin-roll dynamometer. Dynamometer-generated rolling resistance is greater than road-generated rolling resistance. At a normal tyre pressure, the deformation inflicted by a twin-roll dynamometer could even damage the tyre. European Directives therefore allow the tyre to be inflated up to an extra 50 % for twin-roll dynamometer tests.

5. DETERMINING FUEL CONSUMPTION BY THE CARBON BALANCE METHOD

The **carbon balance method** may be used to calculate fuel consumption from the quantity of carbon found in the exhaust gases collected.

Even with the complex chemical transformations taking place in an internal combustion engine, the relationship between fuel consumption and carbon emissions can be stated relatively simply:

- ✚ The main four fuels currently used are made almost exclusively of saturated hydrocarbons (alkanes). Saturated hydrocarbons are composed of carbon (C) and hydrogen (H) only, in known proportions.
- ✚ When combustion takes place, all the carbon from the fuel is emitted in the exhaust gases, combined with oxygen from the air in the form of carbon dioxide (CO₂), carbon monoxide (CO) or as unburnt hydrocarbons (HC, also referred to as VOC – Volatile Organic Compounds).

The calculation formulae are given in the following relations:

Fuel consumption calculation (according to Directive 1999/100/EC):

Petrol Vehicles :

$$C = \frac{0,1154}{\rho} \cdot [(0,866 \cdot THC) + (0,429 \cdot CO) + (0,273 \cdot CO_2)] \quad (1)$$

Diesel Vehicles :

$$C = \frac{0,1155}{\rho} \cdot [(0,866 \cdot THC) + (0,429 \cdot CO) + (0,273 \cdot CO_2)] \quad (2)$$

Liquefied petroleum gas (LPG) vehicles :

$$C_{norm} = \frac{0,1212}{0,538} \cdot [(0,825 \cdot THC) + (0,429 \cdot CO) + (0,273 \cdot CO_2)] \quad (3)$$

Natural gas vehicles (NGV) :

$$C_{norm} = \frac{0,1136}{0,654} \cdot [(0,749 \cdot THC) + (0,429 \cdot CO) + (0,273 \cdot CO_2)] \quad (4)$$

where:

C - fuel consumption in litres per 100 km (for petrol, LPG or diesel) or in cubic metres per 100 km for NGV

THC - total hydrocarbon emissions measured, in g/km

CO - carbon monoxide emissions measured, in g/km

CO₂ - carbon dioxide emissions measured, in g/km

ρ - test fuel density measured at 15 °C. A reference fuel density is used for LPG and natural gas.

6. CARBON AND CO₂ EMISSIONS PER LITRE OF FUEL CONSUMED

Even if the exact amount of CO₂ produced by one litre of fuel depends on various factors such as temperature, ambient pressure and fuel quality, the following may be considered typical values:

- ✚ 1 litre of petrol used produces 2.35 kg of CO₂, i.e. 0.64 kg of carbon;
- ✚ 1 litre of diesel used produces 2.66 kg of CO₂, i.e. 0.72 kg of carbon.

E.U. DRIVING CYCLE

The European regulatory driving cycle is the same for both fuel consumption and pollution measurements. Automobile manufacturers thus take both sets of measurements during a single test. The cycle simulates 4.052 km of urban driving (part ONE) and 6.955 km of extra-urban driving (part TWO – driving on expressways and bypasses).

Specifications:

Maximum speed: 120 km/h

Average speed for part one: 18.7 km/h

Average speed for part two: 62.6 km/h

Total simulated distance: 11.007 km

Total duration: 19 min 40 s

Regulatory driving cycle as defined by European Directive 98/69/EC

applicable to passenger cars and light-duty trucks (weighing ≤ 3.5 t)

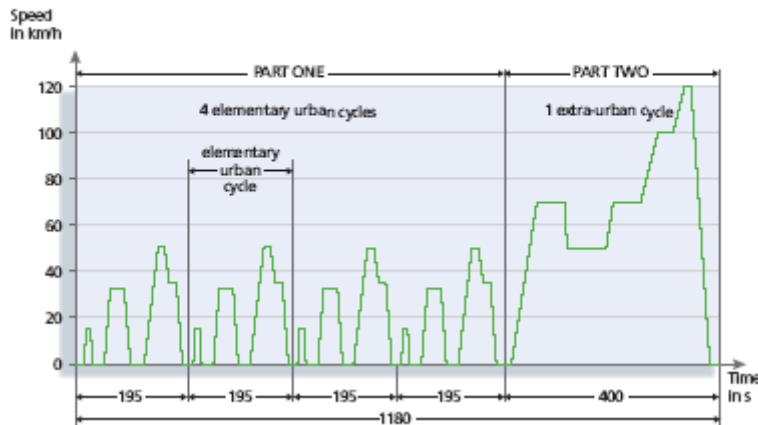


Figure 3. EU driving cycle

- ✚ Part ONE comprises four "elementary urban cycles", each made up of 15 successive phases (idling, acceleration, steady speed, deceleration, idling, etc.).

The urban cycle was drawn up in 1958 after following a Renault Dauphine car in Paris. It therefore represents a very slow urban cycle.

- ✚ Part TWO comprises one extra-urban cycle made up of 13 phases.
- ✚ Exhaust gases are collected continuously throughout the cycle.

U.S. DRIVING CYCLES

Driving cycle FTP 75

(urban driving)

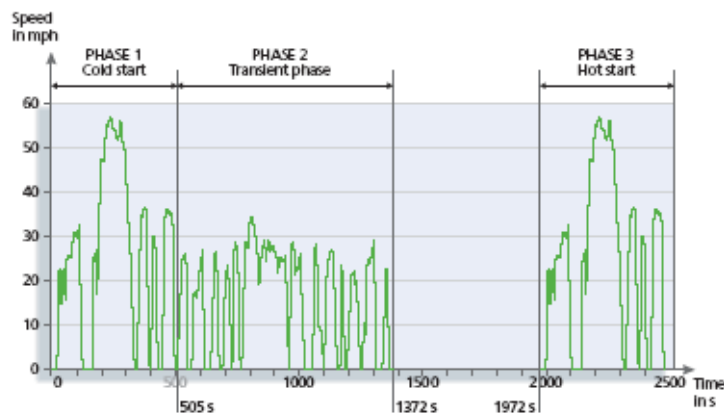


Figure 4. US driving cycle

Specifications:

- Average speed: 21.2 mph (34.1 km/h)
- Maximum speed: 56.7 mph (91.2 km/h)
- Total rolling time: 31 min 17 s (1,877 s)
- Stopping time: 10 minutes
- Distance travelled: 11.04 miles (17.8 km)
- Weighting factors:
 - PHASE 1 = 0.43
 - PHASE 2 = 1
 - PHASE 3 = 0.57

There are three American regulatory driving cycles used in the certification of passenger cars and light-duty trucks with respect to pollutant emissions:

- ✚ **FTP 75**: cycle simulating urban driving from a cold start followed by a hot-start urban cycle;
- ✚ **SFTP-US06**: "aggressive" motorway driving;

✚ **SFTP SC03:** urban driving with air-conditioning on (not shown here).

Fuel consumption measurements are based on the **FTP 75** cycle and the normal motorway driving cycle **HWFET**.

Driving cycle SFTP US06
("aggressive" motorway driving)

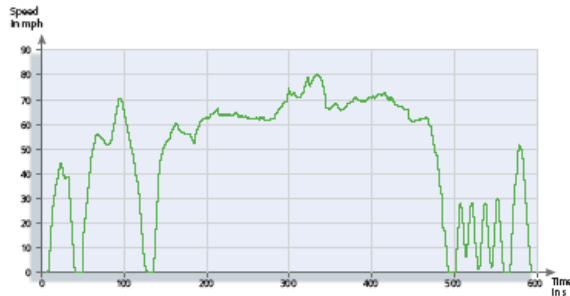


Figure 5. US driving cycle – aggressive motorway driving

Specifications:

Average speed: 48.4 mph (77.9 km/h)
Maximum speed: 80.3 mph (129.2 km/h)
Total rolling time: 9 min 56 s (596 s)
Distance travelled: 8.01 miles (12.9 km)

Driving cycle HWFET
(normal motorway driving)

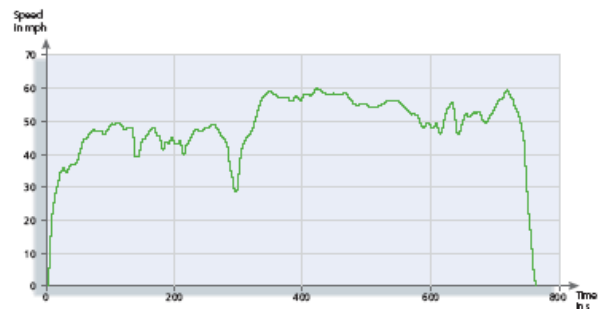


Figure 6. US driving cycle – normal motorway driving

Specifications:

Average speed: 48.3 mph (77.7 km/h)
Maximum speed: 60 mph (96 km/h)
Total rolling time: 12 min 45 s (765 s)
Distance travelled: 10.26 miles (16.5 km)

JAPANESE DRIVING CYCLES

There are currently two Japanese regulatory driving cycles:

- ✚ One hot-start cycle known as 10-15 mode for measuring the pollution and fuel consumption of passenger cars and light trucks.
- ✚ One cold-start cycle known as 11 mode applied in addition to 10-15 mode for measuring the pollution of petrol-driven passenger cars and lightduty trucks. 10-15 mode simulates urban driving (three "10-mode" elementary cycles) followed by peri-urban driving (one "15-mode" elementary cycle). It is a hot-start cycle, with the measurements only beginning after 15 minutes of rolling at 60 km/h, a measurement during idling then a further 5 minutes' rolling at 60 km/h and finally a "15-mode" elementary cycle, which means a total warm-up time of more than 20 minutes. Measurement results are given in g/km.

11 mode simulates another urban trip, this time from a cold start. Measurement results are given in g/test.

10-15 mode
(hot-start urban driving cycle)

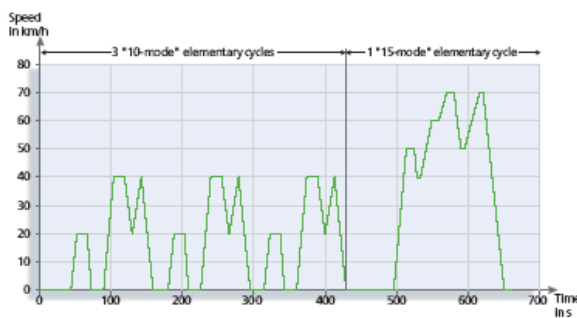


Figure 7. 10-15 mode Japanese cycle
Specifications:

Average speed: 22.7 km/h
Maximum speed: 70 km/h
Total rolling time: 11 min (660 s)
Distance travelled: 4.16 km

11 mode
(cold-start urban driving cycle)

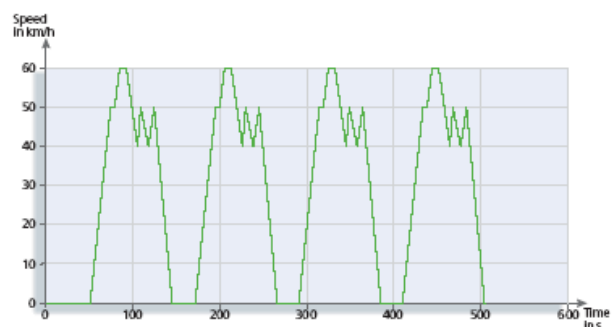


Figure 8. 11 mode Japanese cycle
Specifications:

Average speed: 29.1 km/h
Maximum speed: 60 km/h
Total rolling time: 8 min 25 s (505 s)
Distance travelled: 4.084 km

7. PRACTICAL APPLICATION

On the MAHA LPS 3000 dynamometer is loaded the correspondent driving cycle (figure 9) and when all the measurement devices are set and the exhaust gas analyser are ready, the measurement is started and datas are saved in tables and displayed as graphics (figure10).

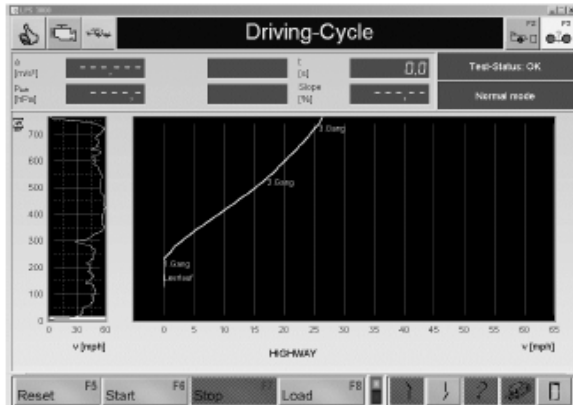


Figure 9. Loading the corresponding driving cycle for light-duty vehicle

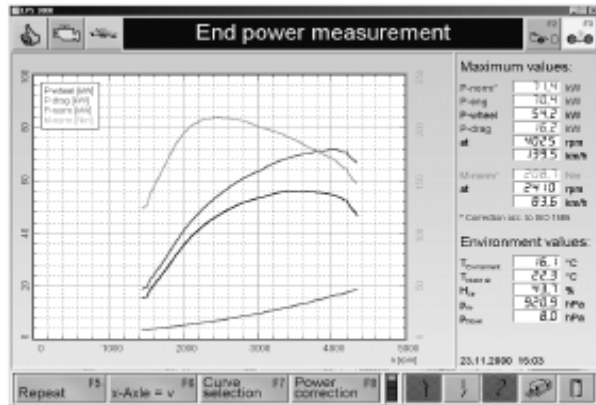


Figure 10. Graphics for analyzing the performances of the vehicle's engine

Applying the formulas 1 – 4, depending the engine's type, we have the values for fuel consumption, values that could be compared with official datas from car manufacturer, or could be used for analyzing the working of the engine.

REFERENCES

- [1] Bosch, Automotive Handbook, 5th Edition, SAE Publisher, 2005
- [2] MAHA, Chassis Dynamometer LPS 3000 for Passenger Cars – Standard Operating Instructions and User's Manual, 2006
- [3] Rațiu, S., Mihon, L. – Internal Combustion Engines for Road Motor Vehicles, Processes and Characteristics, Mirton Publishing House, Timisoara, 2008;

MODALITIES OF REDUCING THE LEAKAGE FLOW IN MECHANICAL SEALING

Veronica ARGESANU, Mihaela JULA, Ioan LAZA

Politehnica University Timisoara, ROMANIA

Abstract

The paper presents the connection between the contact pressure on the sliding ring, the size of the interstice and the pressure of the sealed fluid determined experimentally as well as the modalities of reducing the flow discharge.

Keywords

Leakage, unsealing, flow discharge

1. GENERAL CONSIDERATIONS

In the case of the mechanical seals, the sealing is obtained by a small interstice between two rings with front contact surfaces, which are in relative motion (figure 1).

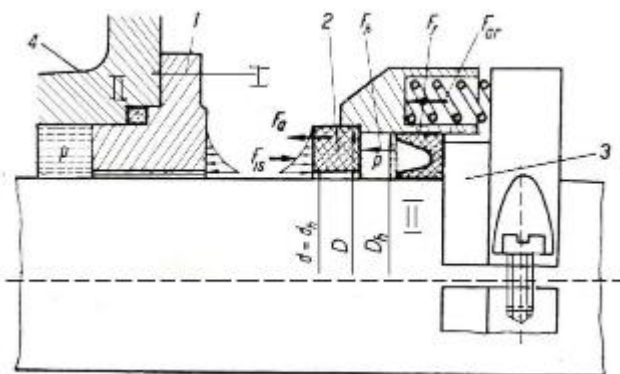


Figure 1

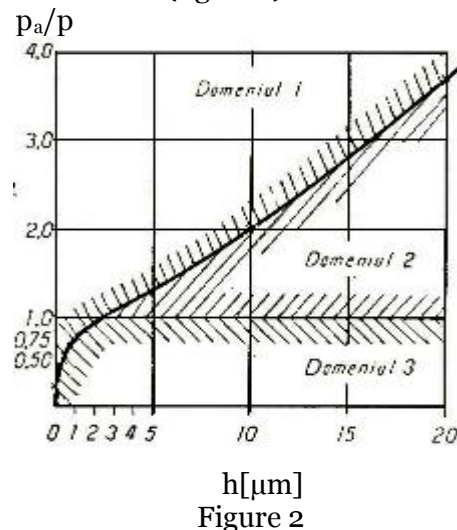


Figure 2

Experimentally it has been observed that there is a connection between the contact pressure on the sliding ring p_a , size of the interstice h and the pressure of the sealed fluid p (figure 2).

In the field noted 1 there is no pressure forming in the interstice $p_{is} \approx 0$ and $p_a = p_{ar} + k_p$. The interstice contains fluid that is leaking through the contact surface irregularities. There is a limit lubrication discharging rapidly to a dry friction that can lead to rapid wear.

Fluid losses marked Q are given with the help of the empirical equation:

$$Q = \pi d (p - p_e \pm p_z) 60 S h^2 / p_a^2 \quad (1)$$

where:

- d - Entrance diameter of the fluid in the interstice
- p - The pressure of the sealed fluid
- p_e - external pressure
- p_z - pressure due to centrifugal force
- S - Interstice specific coefficient
- h - Interstice size
- p_a - axial contact pressing

It can be noted that the fluid loss through leakages is largely influenced by the size of the interstice and by the contact pressure.

Seals in this area are characterized by a stable operation, low pressure in the interstice and loss of fluid through minimal leakage.

In the field noted 2 there is a pressure p_{is} in the interstice that can grow to the amount of fluid pressure p . The interstice is a friction joint with a low coefficient of friction. Loss of fluid can be calculated quite precisely with the equation noted 1.

In the field noted 3, the seal has the most favorable conditions for friction in the interstice, but at the same time also the greatest loss through leakage.

In the interstice it is established a laminar leakage; the losses by leakage of fluid can be calculated by the relationship:

$$Q = \pi(p - p_e \pm p_z) d_m^3 h^3 / 12 \eta b \quad (2)$$

where: d_m - average diameter of the ring
 η - dynamic viscosity of the fluid

2. LOSS OF FLUID THROUGH UNSEALING

2.1 Parameters that determine the loss of fluid

Mechanical sealing behavior is influenced by:

- ✚ relationship between the acting surface of the fluid and the frontal contact surface $k = A_h/A$;
- ✚ relative speed of sliding between the contact surfaces and the sealed fluid pressure
- ✚ the couple of materials of the two sliding rings in contact;
- ✚ the sealed medium, its lubrication and cooling properties, its chemical behavior, the content of impurities;
- ✚ the shape of the interstitial of the surfaces in contact, influenced by the nature of mechanical and thermal strains that appear during operation;
- ✚ roughness of the surfaces in contact their deviation from the geometrical shape;
- ✚ friction, vibrations, pressure shocks, continuous working or with stops, the ability of heat dissipation, lubrication direction in relation with the direction of the centrifugal forces;
- ✚ Temperature of the sealed medium and contact surfaces and their evolution in time.

2.2 Ways of reducing the flow discharge

The ratio of surfaces $k = A_h/A$ may range from positive, over unitary or sub unitary, or even negative.

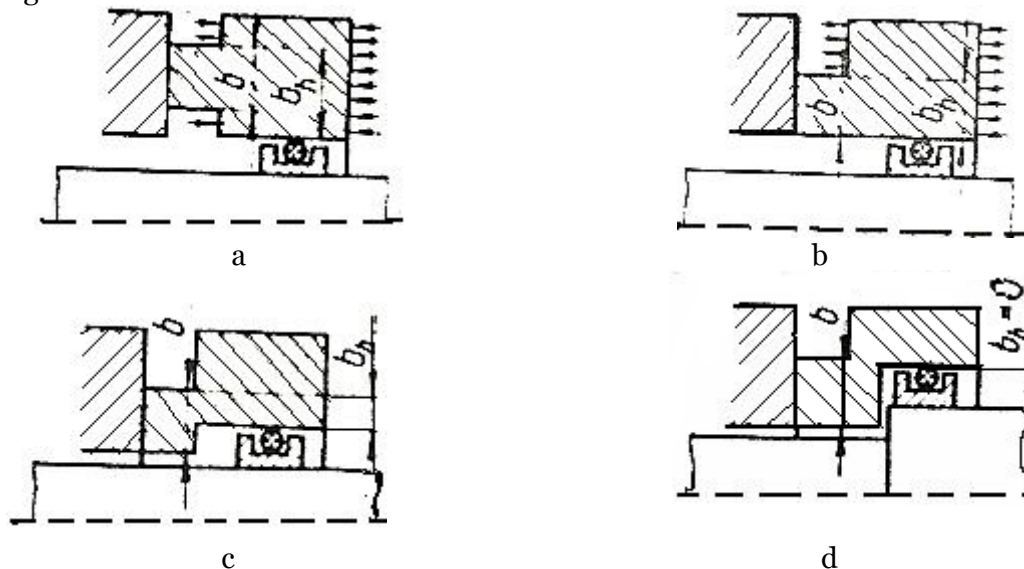


Figure 3

- a) $k > 1$ loaded sealing or unbalanced
- b) $k = 1$ balanced sealing or unloaded
- c) $k < 1$ balanced sealing or unloaded
- d) $k = 0$

The “loaded” seals situate in fields of operation 1 and 2 with minimum loss through the interstice.

In the unloaded constructions the pressing on contact surfaces is made by the spring force.

Experimental research [2] showed that pressure in the interstice is dependent on the ratio k and viscosity (figure 4). For joint studies with low viscosity (propane or butane), the seal must be designed with a value $k = 0.7$ in order not to lose contact between sealing surfaces r_e , while for water a value $k=0.58 \div 0.6$ is enough. For high viscosity mediums (oils) $k = 0.3 \div 0.4$. Normally, mechanical sealing show radial plane surfaces, with the great manufacturing advantage of simplicity.

$p/p_1, A$

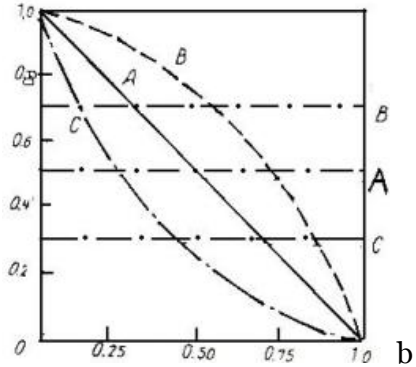


Figure 4

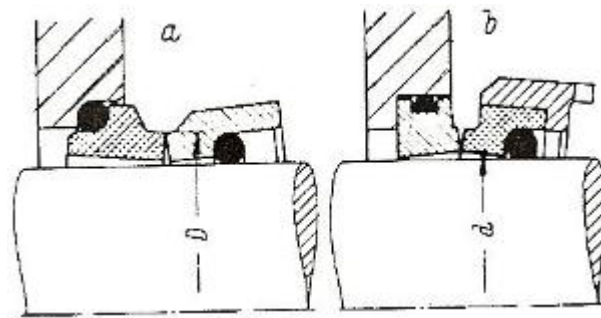


Figure 5

The configuration of the area may suffer modifications due to heat or wear, applied torsion moment, radial or axial forces; the rings deform and the interstice becomes convex, concave or tilted with peripheral contact, internal or external (figure 5). If the operating conditions remain constant, by choosing a suitable couple of materials in contact, wear can gradually restore the parallelism to the ring surfaces, if time and contact pressure is convenient. Besides geometry, the roughness of the rings surfaces in contact has a considerable influence on losses. If the roughness rises losses do to unsealing rise also.

As in the friction-wear process appear strong heating in the area of contact thus leading to deformations of the interface, results that in heavy operating conditions in particular (pressures, high speeds) in order to reduce the flow out of sealing constructive measures are necessary to diminish wear.

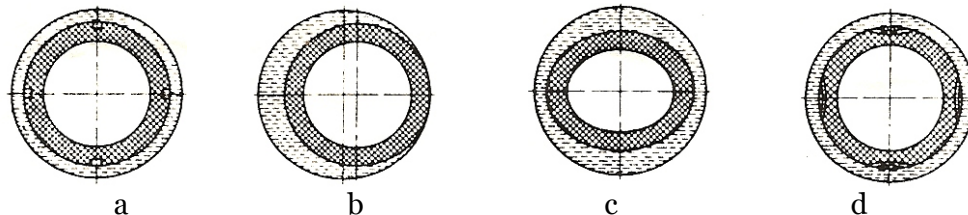


Figure 6

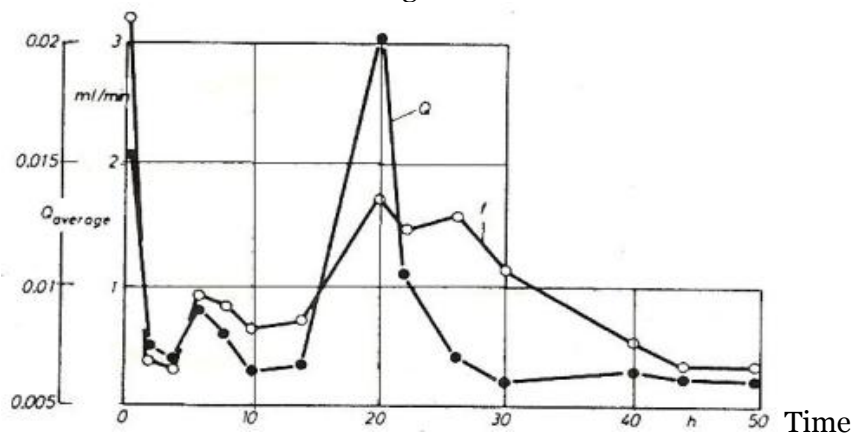


Figure 7

Figure 6 presents the construction of sealing surfaces in contact with frontal circular channels eccentric friction surfaces, elliptical rings, circular ring channels, with effect on the hydrodynamic lubricating film between sliding surfaces.

Figure 7 presents the interdependence between the flow loss Q and the coefficient of friction for a high pressure seal with frontal sealing surfaces with radial channel.

3. CONCLUSIONS

The geometry of a mechanical sealing interstice, its roughness, can be changed depending on working conditions. In turn they influence the force pressing the two rings, the pressure of the interstice, losses through leakage of the fluid and even the friction conditions.

Leak flow rate may thus rise even when constant operating conditions are present. In mechanical sealing the condition that the lubricant has no pressure in the interstice (see fig.2 in area X) is very important to ensure the stability of operation and minimum losses due to fluid leakage.

BIBLIOGRAPHY

- [1] Cristea, V.; - Etansari, E.T. Bucuresti 1973;
- [2] Greiner, H.; - Rotating seals for high pressure product eng., February 1986, S 140/43;
- [3] Mayer, E.; - Axiale Glaitringdichtungen VD I – Verlag GmH Dusseldorf 1974



THERMO ELASTIC INSTABILITY WITHIN A CLASS IV FRICTON JOINT

Veronica ARGESANU, Mihaela JULA, Ioan LAZA

Politehnica University Timisoara, ROMANIA

Abstract

With a class IV couple of friction joint there are conditions when the disturbances of the pressures on the interface increase, decrease or remain unchanged. When the two materials of the joint are identical a relative stability is formed regarding this phenomenon, while a good heat-conducting material coupled with a heat insulator, depending on certain characteristics of sliding speed, creates instability. Equation of this paper specifies the threshold for instability.

Keywords:

Thermo elastic instability; Solutions; Temperature wave

1. INTRODUCTION

With a class IV friction joint (annular joint), which is the primary sealing of a frontal sealing, may appear situations in which pressure disturbances within the interface decrease, increase, or remain constant. These in turn are influenced by the properties of the materials in contact, coefficient of friction and relative sliding velocity.

The increase of the pressure disturbances in the interface leads to an increase in contact pressure and the local temperature. Adjacent to the zones with low pressure the surfaces can detach leading to important losses by leakage.

Materials of the same type making the joint tend to a relative stability when speaking of this phenomenon, while a joint composed of a good heat conductor material and a insulator will always show characteristics of relative sliding speed, from which instability appears.

The sliding contact at relatively high speeds is associated with a macroscopic instability, so that on a flat and uniform contact area will appear disturbances of local pressure.

This leads to negative effects upon the contact area from the point of view of heating and wear.

The simplified configuration of the primary sealing (class IV friction joint) is presented in Fig. 1. For such geometry, if the pressure is uniform in the interface, the temperature slowly rises until it hits a nominal value determined by the operating parameters.

If instead the uniform distribution of the pressure is disturbed even sparsely (which can be expressed as a Fourier series or waves along the contact surface) the disturbance may diminish, may remain unchanged or may rise. Thus, the stability of the pressure distribution can be investigated according to the behavior of waves of initial disturbance.

The problem is assumed to be ideal linear, with a linear heat transfer, thermal expansion and elastic displacement so that:

- ✚ the solution found is for the pressure wave produced at the surface of the semi-infinite ring extremity when there is a temperature wave of constant amplitude moving with constant speed;
- ✚ there is a relationship between the pressure wave and the heat produced by friction, generated at the limiting value, where it is assumed that another plate slides over and takes over the pressure distribution.

As an additional restriction of harmful waves it is assumed that there is no disruption at the extremities of the distance corresponding to the circumference of the tube (fig 1).

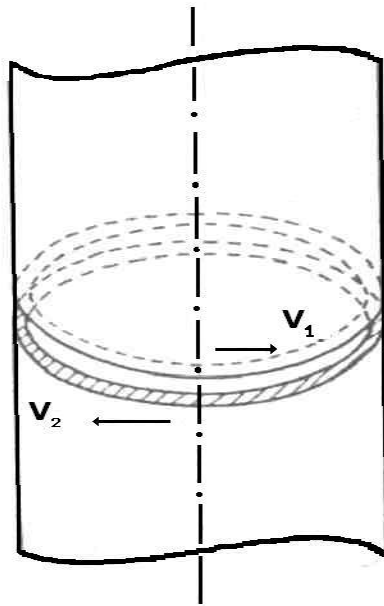


Figure 1

This implies that the harmonic components of the disturbance, complete one or more numbers of cycles over the specified length.

The combination of properties of materials in contact and operating conditions which satisfy the entire set of conditions will be considered to define the circumstances of a specified wavelength disturbance, without diminution or amplification.

2. SOLUTIONS FOR A TEMPERATURE WAVE WITH CONSTANT MOVEMENT

If referred to one of the plates marked with 1, the edge temperature perturbation can be expressed:

$$T = T_0 * \sin \omega(x-vt) \quad (1)$$

where:

- T_0 is the constant for temperature
- $\omega = 2n\pi/L$ the measure of wave number
- x – is measured along the contact surface
- v - Instantaneous transverse velocity of the wave along the contact surface

Heat transfer equation:

$$\frac{\delta^2 T}{\delta x^2} + \frac{\delta^2 T}{\delta y^2} - (\delta T / \delta t) / k = 0 \quad (2)$$

$$-\infty \leq x \leq \infty$$

$$0 \leq y \leq \infty$$

with $T=0$ when $y \rightarrow \infty$; y is measured perpendicular to the contact surface

Solution for body number 1:

$$T_1 = T_0 e^{-b_1 y} \sin(\omega x - \omega v_1 t + a_1 y) \quad (3)$$

where:

$$b_1 = \{ \omega^2 / 2 + \omega / 2 [\omega^2 + (v_1 / k_1)^2]^{1/2} \}^{1/2} \quad (4)$$

$$a_1 = \{ -(\omega^2 / 2) + \omega / 2 [\omega^2 + (v_1 / k_1)^2]^{1/2} \}^{1/2} \quad (5)$$

where:

- k – material diffusion capability
- K - material conductivity
- p - pressure
- c_p – specific heat

The heat flow (q_1) is given by the equation:

$$q = -K(\delta T / \delta y)_{y=0} = -KT [a_1 \cos(\omega x - \omega v_1 t) - b_1 \sin(\omega x - \omega v_1 t)] \quad (6)$$

Surface temperature will be:

$$T = T_0 \sin \omega t \quad (7)$$

and

$$q_1 = K_1 T_0 (b_1 \sin \omega x - a_1 \cos \omega x) \quad (8)$$

For the second body (which moves in the opposite direction relatively to the temperature wave with the speed v_2):

$$T_2 = T_0 e^{-b_2 y} \sin(\omega x - \omega v_2 t - a_2 t) \quad (9)$$

Where a_2 and b_2 correspond to the (4) and (5) equations with the correct changes for indices. Thus:

$$q_2 = -K_2 (\delta T_2 / \delta y_2)_{y_2 \rightarrow 0} = K_2 T_0 [a_2 \cos(\omega x - \omega v_2 t) - b_2 \sin(\omega x + \omega v_2 t)] \quad (10)$$

If the wave is stationary and plate is moving relative to it:

$$q_2 = K_2 T_0 (b_2 \sin \omega x + a_2 \cos \omega x) \quad (11)$$

and

$$q = q_1 + q_2 = T_0 [(K_1 b_1 + K_2 b_2) \sin \omega x + (K_2 a_2 - K_1 a_1) \cos \omega x] \quad (12)$$

3. STATE OF THERMO ELASTIC STRESS IN A PLATE SUBJECTED TO A WAVE OF TEMPERATURE THAT MOVES UNIFORMLY

The thermo elastic equation of a plate depending on the potential of displacement Ψ is:

$$\delta^2 \Psi / \delta x^2 + \delta^2 \Psi / \delta y^2 = (1 + \nu_0) \alpha T_0 e^{-by} \sin(\omega x + ay - \omega vt) \quad (13)$$

where: α - coefficient of thermal expansion
 ν_0 - Poisson's coefficient

The speed v of the surface on the direction of y is zero ($v_{y \rightarrow 0}$) and $\Psi \rightarrow 0$ when $y \rightarrow \infty$, $\delta \Psi / \delta y \equiv v$, resulting in:

$$\Psi_1 = (Ae^{-\omega y})(C \cos \omega x + D \sin \omega x) + (k_1/v\omega)(1 + \nu_1) \alpha_1 T_0 e^{-b_1 y} \cos(\omega x + a_1 y) \quad (14)$$

Coefficients C and D are evaluated to meet the condition on the limit. Results that the surface pressure p_1' will be:

$$p_1' = E_1 \alpha_1 T_0 k_1 [-(\omega - b_1) \cos \omega x + a_1 \sin \omega x] / v_1 \quad (15)$$

A similar equation can be written for the body numbered 2. At the moment of contact between the two bodies each surface will suffer a displacement equal and contrary till the equalization of tensions:

$$p_1'' = E\omega\delta/2 \quad \text{with } \delta = \delta_0 \sin \omega x \leftarrow \text{thermal layer thickness}$$

As a result:

$$p = -E_1\omega\delta/2 = p_1' + p'' \quad (16)$$

$$p = E_1\omega\delta/2 = p_2' + p'' \quad (17)$$

Given the fact that p must be identical for the two bodies (according to the law of balance) δ can be eliminated

$$p = E_1 E_2 T_0 \{ [\alpha_2 k_2 (\omega - b_2) / v_2 - \alpha_1 k_1 (\omega - b_1) / v_1] \cos \omega x + [\alpha_2 k_2 a_2 / v_2 + \alpha_1 k_1 a_1 / v_1] \sin \omega x \} / (E_1 + E_2) \quad (18)$$

According to the principles of equilibrium, the heat generated by friction must be equal to the heat from the interface if:

$$mp(v_1 + v_2) = q \quad (19)$$

$$(K_1 b_1 + K_2 b_2) \sin \omega x + (K_2 b_2 - K_1 b_1) \cos \omega x = (v_1 + v_2) \mu E_1 E_2 \{ [\alpha_2 k_2 (\omega - b_2) / v_2 - \alpha_1 k_1 (\omega - b_1) / v_1] \cos \omega x + [\alpha_2 k_2 a_2 / v_2 + \alpha_1 k_1 a_1 / v_1] \sin \omega x \} / (E_1 + E_2) \quad (20)$$

To satisfy the equation (20):

$$K_1 b_1 + K_2 b_2 = (v_1 + v_2) \mu E_1 E_2 [\alpha_2 k_2 a_2 / v_2 + \alpha_1 k_1 a_1 / v_1] / (E_1 + E_2) \quad (21)$$

$$K_2 b_2 - K_1 b_1 = (v_1 + v_2) \mu E_1 E_2 [\alpha_2 k_2 a_2 (\omega - b_2) / v_2 - \alpha_1 k_1 a_1 (\omega - b_1) / v_1] / (E_1 + E_2) \quad (22)$$

So for bodies of the same material: $v_1 = v_2 = v/2$, and equation (21) reduces to:

$$\mu E \alpha k a / b K = 1 = \mu E \alpha k \{ [1 + [1 + (v/k\omega)^2]^{1/2}] / [1 + [1 + (v/k\omega)^2]^{1/2}] \}^{1/2} / K \quad (23)$$

and for two bodies of which, one is good conduit for heat and other heat isolated:

$$k_1 \rightarrow 0, K \rightarrow 0, v_2 \rightarrow 0, \text{ and } v_1 \rightarrow v. \text{ If } v > 1, a_1 \rightarrow \omega(v_1/2k_1\omega)^{1/2}$$

$$a_2 \rightarrow v_2/2k_2; b_1 \rightarrow \omega(v_1/2k_1\omega)^{1/2}; b_2 \rightarrow \omega[1 + (c_2/k_2 \omega)^2/8]$$

and equation (21) reduces to:

$$v_1 = v = 2K_2 \omega (E_1 + E_2) / \mu E_1 E_2 \alpha_2 \quad (24)$$

4. CONCLUSIONS

The equations from above serve to provide the terms depending on which the pressure disturbance in a frontal sealing interface increases. In this case load concentrations occur in small portions of the contact surfaces, resulting in damage or separation of the rings.

For materials of the same type, instability occurs only at a high coefficient of friction. Initial size of the uniform load has little influence on the general temperature which may alter the properties of the materials. Role of slip velocity is also small.

In case the material has different properties from the point of view of transfer of heat produced by friction will be taken from the heat-conducting body and the limit between stability and instability depends on the relative sliding velocity.

BIBLIOGRAPHY

- [1] Dow, T.A; Burton, R.A. “Initiation of thermo elastic instabilities of sliding contact in the absence of wear”, *Wear*, 19 (1972)
- [2] Dow, T.A; Burton, R.A. “The role of wear in the initiation of thermo elastic instabilities in sliding contact”, *J. Lubric. Technol*; 95(1973); ASME Paper No 72- Lub. -45
- [3] Mayer, E. “Mechanical Seals”, Newness Butterworths London-Boston, 1973

STUDY REGARDING MASS REPARTITION TO ROAD VEHICLE WITH MULTIPLE DESTINATIONS

Ioan LAZA, Daniel OSTOIA, Lucian MOLDOVAN

University "Politehnica" of Timisoara, ROMANIA

ABSTRACT

This paper presents a study regarding to distribution of mass road vehicles for multiple destination: for freight transport and people transport. Category of this road vehicle is N1 with the maximum mass allowance 3500 kg. Main producers of this categories of road vehicle achieve common platforms, subsequently has transformed to the final type destination. The distribution of mass road vehicles on the axes is different because the mass center of freight is different after transformation.

Some aspects of this new situation which appear to modification of freight are presented in the case of vehicle from category N1.

1. INTRODUCTION

The study realized in this paper is the road freight vehicle type "lightly truck" (figure 1) with next principal parameters:

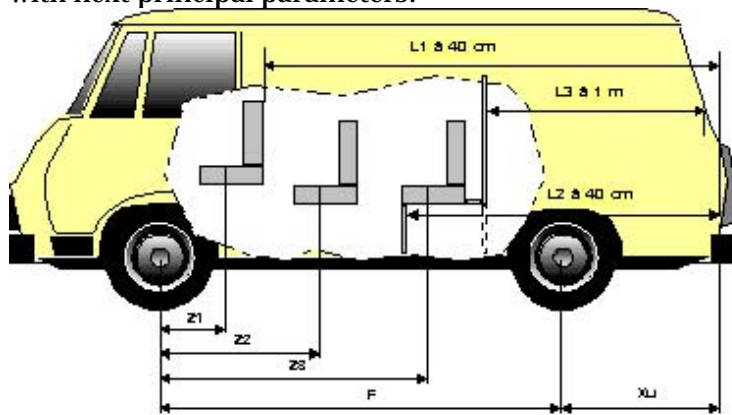


Figure 1 Parameters of road vehicle

L1-measured in meter: The length of space charge before transformation (this data can be measured or can be take from producers of road vehicle);

L2-measured in meter: The length of space charge measured to +40 centimeter height regard to floor vehicle;

L3- measured in meter: The length of space charge measured to +1 meter height regard to floor vehicle;

F-measured in meter (wheel base)

Xu-rear overhang

Z1-measured in meter: distance from mass center of front seats and rear axle

Z2- measured in meter: distance from mass center second line of seats and rear axes

Z3- measured in meter: distance from mass center third line of seats and rear axle

Yc- measured in meter: distance from mass center of load and rear axle

FZ(1,2 and 3)- measured in meter: distance from mass center of seats and rear axes

PTAC-measured in kilo: admissible maximum mass (for category N1 is 3500kg)

PV- measured in kilo: own vehicle mass (without driver, a fuel tank is 90% full)

PV1- measured in kilo: own vehicle mass to front axes E1

PV2- measured in kilo: own vehicle mass to front axes E2

POM- measured in kilo: own vehicle mass in driving conditions (European Directive CE 98/14

$POM = PV + 75 * 0,1M$ (M-mass of 100 % fuel from fuel tank)

CM- measured in kilo: mass of load

CMAR- measured in kilo: load distribution on the rear axes

CMAV- measured in kilo: load distribution on the front axes

E1- measured in kilo: maximum load to front axes

E2- measured in kilo: maximum load to rear axes

C.U.- measured in kilo: real load (=PTAC)

N-number of the seats including driver seat

2. THE STUDY

2.1. Condition imposed

- For vehicle with admissible maximum mass (for category N1 is 3500kg), and the seat number is $N \leq 7$ and the body structure is tip BB VAN, after classification from European Directive 98/14/CE (for vehicle with multiple destination, people transport with luggage or freight transport in the same compartment) it is necessary to verify the ratio of luggage mass and people mass following relation:

$$PTAC - (POM + (N1) \times 68) > (N1) \times 68$$

- For other cases if the people mass including the driver is less with 60% from real load C.U. then:

$$75 \times N = \dots < (PTAC - PV) \times 0,6$$

- For the cases if the vehicle is with two line of seats, PTAC must be more 2400 kg

2.2 Dimensional Checking and design description

- L3 must be more or equal then 1meter
- If the vehicle has just one line of seats L2 must be more or equal then $0,5 \times L1 + 0,3$
- If the vehicle has two line of seats L2 must be more or equal then $0,4 \times L1$
- If Yc value is negative it is necessary a certification from producer to accept this value and it must be included into condition the maximum load on front axes
- It is forbidden to separated the first line of seats with the second line of seats
- The space for passengers must be separated from the space of freight with rigid closure with a resistance of 800KN/m^3
- If the vehicle has more than two line of seats is necessary to assembled the stuck window

3. MASS DISTRIBUTION ON AXES

3.1. Driver and passengers

1. first line of seats

Driver mass and passengers: $P1 = 75 \text{ kg} \times \text{passengers number}$

$P1 = \dots \text{kg}$

$Z1 = \dots \text{m}$

$F - Z1 = \dots \text{m}$

$P1AV = (P1 \times (F - Z1)) / F = \dots \text{kg}$

$P1AR = (P1 \times Z1) / F = \dots \text{kg}$

2. second line of seats

mass passengers: $P2 = 75 \text{ kg} \times \text{passengers number}$

$P2 = \dots \text{kg}$

$Z2 = \dots \text{m}$

$F - Z2 = \dots \text{m}$

$P2AV = (P2 \times (F - Z2)) / F = \dots \text{kg}$

$P2AR = (P2 \times Z2) / F = \dots \text{kg}$

3. third line of seats (optional)

mass passengers: $P3 = 75 \text{ kg} \times \text{passengers number}$

$P3 = \dots \text{kg}$

$Z3 = \dots \text{m}$

$F - Z3 = \dots \text{m}$

$P3AV = (P3 \times (F - Z3)) / F = \dots \text{kg}$

$P3AR = \dots \text{kg}$

$P3AR = (P3 \times Z3) / F = \dots \text{kg}$

3.2. Load mass

$CM = PTAC - (PV + P1 + P2 + P3)$

$CM = \dots \text{kg}$

$CMAV = (CM \times Yc) / F = \dots \text{kg}$

$CMAR = (CM \times (F - Yc)) / F = \dots \text{kg}$

3.3. Calculation with passengers

	Total	Front	Rear
Vehicle mass	PV=	PV1	PV2
Driver and passengers AV (first line of seats)	P1=	P1AV=	P1AR=
Passengers on second line of seats	P2=	P2AV=	P2AR=
Passengers on third line of seats	P3=	P3AV=	P3AR=
Load	CM1=	CM1AV=	CM1AR=
Maximum load	PTC1=	E1=	E2=
Maximum authorized load	PTAC=		

3.4. Calculation without passengers

Vehicle mass	PV=	PV1	PV2
Driver (1)	P1= 75kg	P1AV=	P1AR=
Load	CM2=	CM2AV=	CM2AR=
Maximum load	PTC1=	E1=	E2=
Maximum authorized load	PTAC=		

Calculation condition:

1. CMAR= maximum load on axes: E2-PV2-P1AR

Calculation: $CM = (CMAR \times F) / (F - Y_c)$

$CM = PTAC - PV - 75 \text{ kg}$

E1 must be more of minimum mass authorized

$CM_{AV} > \text{minimum mass authorized} - PV1 - P1AV$

If the condition is not achieved:

$CM_{AV} = \text{minimum mass authorized} - PV1 - P1AV$

$CM = (CM_{AV} \times F) / Y_c$

4. ANALISES, APROCHES

For the example of repartition of mass it was made a calculation for a vehicle CITROEN JUMPER L3H2 with extra four seats.

PTAC=3500 kg (maximum authorized mass)

E1 max=1850 kg

E2 max=2000 kg

F=4,078 m

L1,L2,L3=3.68,2.79,2.655 m

Xu=0.959 m

Z1=0.95 m

Z2=1.755 m

Z3=0 -

$Y_c = (L2/2) - X_u = 0.436 \text{ m}$

PVconst=2050 kg

E1 const=1290 kg

E2 const=760

Cab mass=145 kg

E1 cabine=38 kg

E2 cabine=107 kg

1	Categoria	AUTOUTILITARA N1				
2	Caroseria	BB furgon				
3	Marca	CITROEN				
4	Tipul Varianta	Y/CBMFC/JUMPER				
5	Numărul de omologare Anul fabricației	BF15231811U37E4 / 2007				
6	Numărul de identificare	VF7YCBMFC11137366				
7	Masele (Kg)	Proprie	2050	Totală max. autorizată	3500	
		Sarcină utilă max. autoriz.	1450	Sarcina pe cirligul de remorcare	100	
		Maximă autorizată pe axe	Față	1850	Mijloc	
			Spate	2000	Pe rola de șenilă	
Remorcabilă cu disp. de frinare	2500	Remorcabilă fără disp. de frinare	750			

Figure 2 - Example before transformation

$PV_{transf} = PV_{const} + \text{cabine} = 2195 \text{ kg}$

$E1_{transf} = E1_{const} + E1_{cabine} = 1328 \text{ kg}$

$E2_{transf} = E2_{const} + E2_{cabine} = 867 \text{ kg}$

Tank fuel mass=70 litres

$POM = PV_{transf} + 75 -$

$(0,1 \times 70 \times 0,9) = 2263.7 \text{ kg with petrol}$

N=5 passengers number

Condition

1. $PTAC \leq 3500\text{kg}$ and maximum of number passengers is 7
 $PTAC - (POM + (N-1) * 68) > (N-1) * 68$
 The results : $964,3\text{kg} > 272\text{kg}$

Repartition of load

Driver and passengers

*P1=75kg*3 passengers
 (including the driver)

$$* P1AV = [P1 * (F - Z1)] / F$$

$$* P1AR = [P1 * Z1] / F$$

*P2= 75 * 3 passagers

$$* P2 AV = [P2 * (F - Z2)] / F$$

$$* P2 AR = [P2 * Z2] / F$$

P3= 75 0 passengers

$$* P3 AV = [P3 * (F - Z2)] / F$$

$$* P3 AR = [P2 * Z2] / F$$

The results:

P1= 150
 P1AV= 115,06
 P1AR= 34,94
 P2= 225
 P2AV= 128,17
 P2AR= 96,83
 P3= 0
 P3AV= 0
 P3AR= 0

The results:

CM= 930
 CMAV= 99,4
 CMAR= 830,6

Calculation with passenger

- * $PTC1 = P_{vtransf} + P1 + P2 + P3 + CM$
- * $E1 = E1_{transf} + P1AV + P2AV + P3AV + CM1AV$
- * $E2 = E2_{transf} + P1AR + P2AR + P3AR + CM1AR$

Driver and load

		* $CM = PTAC - (PV + P1 + P2 + P3)$
PTC1 max. laod	3500	* $CMAV = [CM * Yc] / F$
PTAC	3500	* $CMAR = [CM * (F - Yc)] / F$
E1=	1670,63	
E1max	1850	
E2=	1829,37	
E2max	2080	

5. CONCLUSIONS

The results obtained can lead to the following conclusion:

- ✚ it is necessary to make a repartition of mass to vehicle with multiple destinations for safety driving condition;
- ✚ the method can be used for the increased the degree of safety for the vehicle with multiple destination from N1 category;
- ✚ some aspects can be used to vehicle with special destination (ambulance, etc.)

REFERENCES

- [1.] Stoicescu Aurel, Proiectarea performantelor de consum si de tractiune ale automobilelor, Editura Tehnica Bucuresti 2007
- [2.] Stoicescu Aurel, s.a., Dinamica autovehiculelor pe roti, Editura Didactica si Pedagogica Bucuresti 1981
- [3.] ***-www.citroen-jumper.com



METALLOGRAFIC ASPECTS OF THE ELEMENTS MAKING UP A STEAM BOILER

Amalia Ana DASCĂL

“Politehnica” University of Timisoara, Faculty of Engineering of Hunedoara,
Department of Engineering and Management, ROMANIA

Abstract:

OLT 35K steel is part of the non-allied steel category, used for the achievement of tubes that work at high temperature. Specimen has been taken from this tube type, placed in a steam boiler, from which strip drive test-bars were manufactured. Afterwards, they were tried on driving, at ambient and high temperature, close to the ones used in operation, so as to determine the mechanical features of the material, after a certain period of use. Conclusions made, concerning the influence of temperature on how the OLT 35K steel deals with high temperature, can be taken from the results and, in this way, you can estimate the remaining life-length of both that material and implicitly that of the source equipment.

Keywords:

high temperature, thermal resistant steel, mechanical testing, life-length, mechanical feature

1. GENERAL APPRECIATION

In the context of the present economy, the technological process must be done with high efficiency of transformation. Nowadays, this efficiency can be grown only by high pressure and temperature of the technological process, this being the reason for which the development of a steel scale is required, and especially the ones with low allied degree, as they are less expensive.

In the same time, decisions on the material are essential in all fields of industrial practice, because any technical activity has to finally result in a resistance structure or a functional device. And, each new technological process brings about the development of a new material as the achievement of structures and/or device is being conditioned by their existence and usage.

Choosing the right steel, in point of the required features, the acquisition price and the manufacture price, as well as in reserve, has always been a priority in the eyes of designers and industry manufacturers.

Work Temperature is an element considered more and more interesting because, in a special way, you can assert that the new technological development depends, in many sectors, on the manner you deal with *how materials behave at high temperature*.

The reliability and quality of the elements which work at high temperature and pressure is part of the reliability of electrical and thermic energy production units. The working of these units at best parameters is very important because if not the social and economic implications can be huge.

Choosing and using the right steel, in point of the required mechanical features, for a special field of usage, cannot be made without knowing the real behavior of the material, which relies on theoretical and **experimental research**.

The mechanical features of metals, obtained by testing made with bars, liable to different requirements that are close to the conditions of operation of the elements strength, allow the quality check of their material, fixing the maximum limits of requirements, being essential elements that stand at the discretion of that technologist's designer.

2. TEST-BARS USED IN TESTING

Test-bars, generally having the shape and size of those found in testing at ambient temperature, are used in mechanical experiment at high temperature. Because test-bars are heated in different precincts, it is necessary that the shape and size of the holding extremity is built in such a way to allow their assembly in the holding jaws of the testing machineries. There are situations when, between the extremities of the test-bars and the ones of the holding jaws, some prolonged rods made from metals resistant at high temperature, have to be assembled.

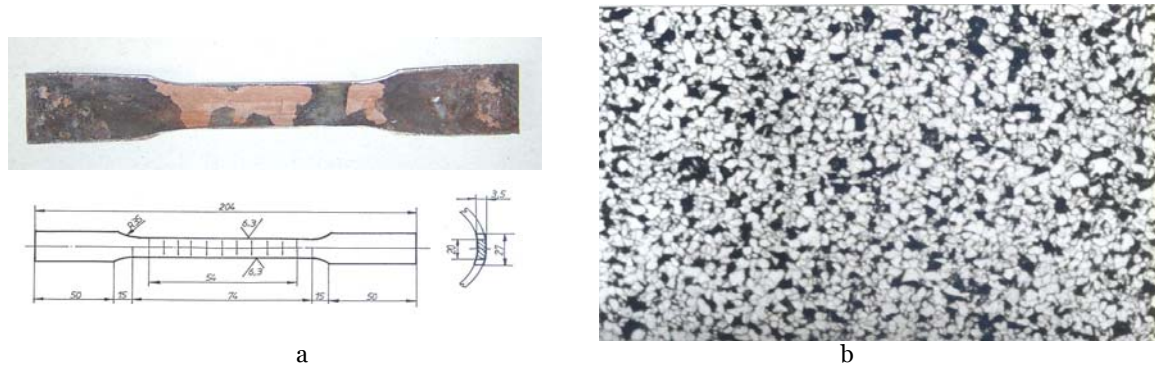


Figure.1. The shape and size of test-bars used in testing: a) test-bar drawn from focus; b) the metallographical structure resulted from the chemical analysis

Ring-shaped transversal samples have been drawn for metallographical analysis, looking at emphasizing the morphology of transformation stages from the material, and establishing the seed size, likely oxidation or decarburization phenomena and other structure faults.

For the OLT 35K tube material, drawn from the focus and shown in fig.1.b, and after the optical microscope study, it seemed that it offered a ferrite-perlite structure, with a 7-8 outline of real seed, proceeding from SR ISO 643-93, and the tube walls had not have a decarburized structure.

After the metallographical analysis, it is found that the tested material is part of the adherent standard, but stating that small size of molybdenum can be detected. Analysing this fact, in accordance with [2], we can state that, in small amounts, molybdenum is fighting against the reversible return brittleness. Dissolved in ferrite and forming carbides, molybdenum improves the resistance features and to a certain extent, the plasticity features of annealed or normalized steel, just like the case at study. Molybdenum also improves the usage resistance and stops the sliding process, by forming carbides, ascertaining a sensitive growth in the steel resistance at high temperature.

Therefore, molybdenum is the ally element that provides the mechanical resistance of steel used at high temperature.

3. TESTING

OLT 35K steel – STAS 8184-80 is part of the non-allied steel category, used for manufacturing tubes that work at high temperature. Steel is elaborated in electrical ovens, Martin ovens, in converters with oxygen spraying or other equivalent methods.

The chemical make-up of the used material (drawn from focus), for the experimental testing, is shown in table 1. The mechanical features guaranteed on the delivered products as tubular, established on longitudinal drawn test-tubes, under ambient testing atmosphere, are given in table 2.

Table 1. The chemical make-up of the OLT 35K steel, drawn from focus

Material	C [%]	Mn [%]	Si [%]	S [%]	P [%]	Cr [%]	Ni [%]	Cu [%]	Mo [%]
Focus – OLT 35K	0,15	0,76	0,34	0,011	-	0,19	0,20	0,17	0,01
STAS 8184-80	Max. 0,17	Min. 0,45	0,15... 0,35	Max. 0,045	Max. 0,040	Max. 0,30	Max. 0,30	Max. 0,30	-

Table 2. The guaranteed mechanical features for OLT 35K steel

Steel type	Breaking resistance R_m [N/mm ²]	The conventional running limit $R_{p0,2}$, [N/mm ²], min.	After breaking percentage elongation A, [%], min	The narrowing value of the section Z, [%], min.	Impact value KCU 300/2 min.
OLT 35K	350...450	230	26	60	60

Table 3. The driving mechanical features of the OLT 35K steel

Testing temperature [°C]	Breaking force F_{max} [N]	Breaking resistance R_m [N/mm ²]	After breaking percentage elongation A[%]	The narrowing value of the section Z [%]
20°C	34435	491,92	90,00	37,85
100°C	33800	482,85	85,00	44,07
200°C	27350	390,71	72,22	55,00
300°C	34900	498,57	71,29	33,60
400°C	34200	502,85	64,81	29,57
500°C	39380	562,57	78,70	33,14

In the field of high temperature, driving testing has been made on a universal machinery by adjusting a genuine conception of heating precincts, [1].

Figure 2. a÷f shows the F-Δl curves, obtained for a share of the tested tubes, and the values of the resulted mechanical features are synthesized in table 3.

The testing made for establishing the mechanical driving features have taken place between +20°C...+500°C. The values shown in chart 3 represent the average of the mechanical features obtained in sets of 3 bars, tested at each level of temperature. Variation diagrams of the driving mechanical features were outlined by using these values, depending on the testing temperature. Therefore, in fig.3, it is shown the R_m feature variation, and in fig.4 that of A and Z feature.

Fig.5 shows a share of OLT 35K bars, drawn from the focus and tested at temperatures of: +20°C, +100°C, +200°C, +300°C, +400°C and +500°C.

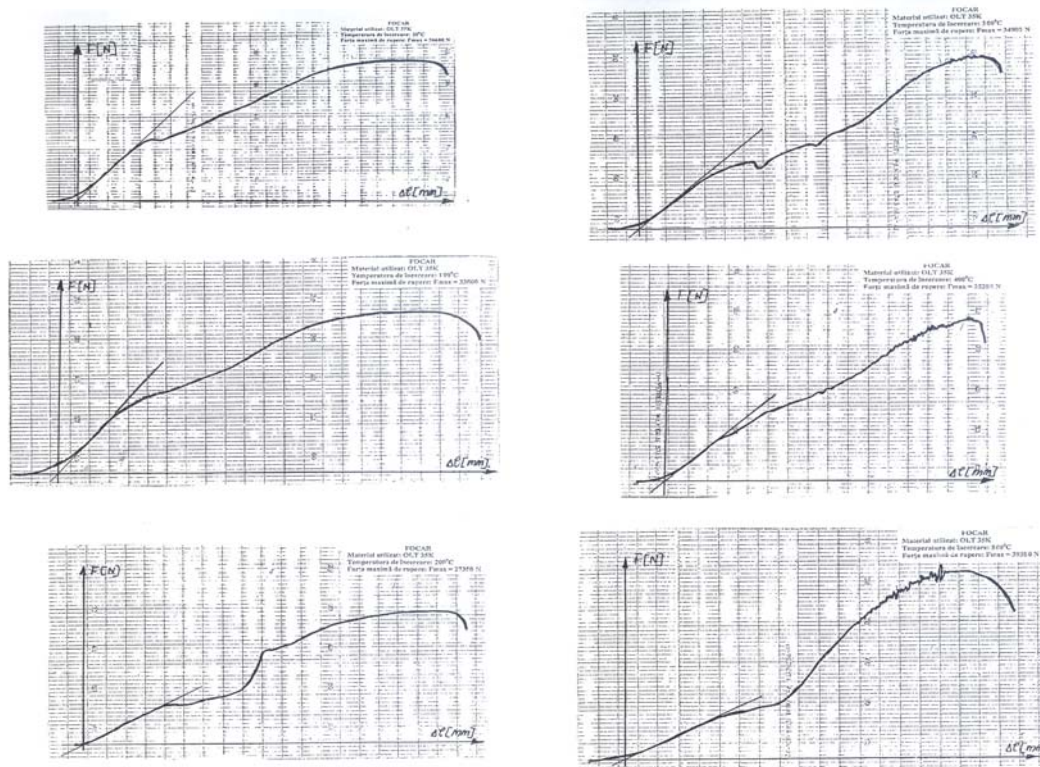


Fig.2. a÷f. F-Δl diagrams, at different temperature, obtained for OLT 35K, focus

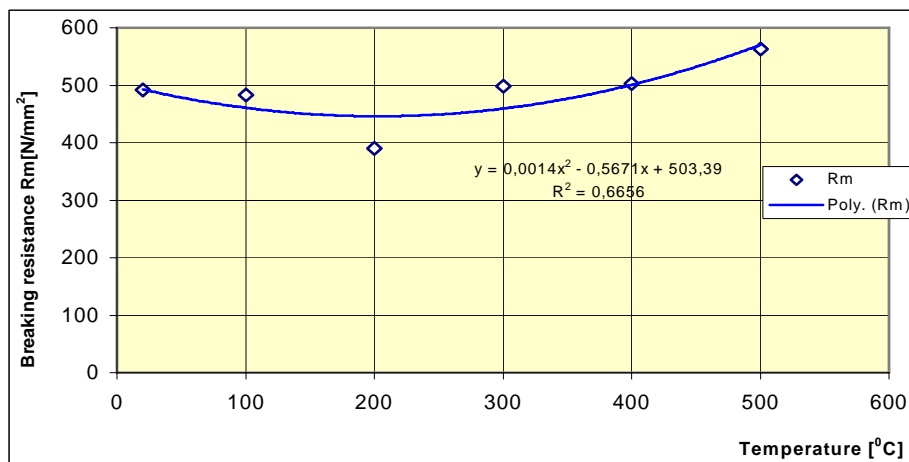


Fig. 3. Variation of characteristics R_m for steel OLT 35K, by temperature

Looking at the dates, you can find out that while the temperature gets high, the breaking resistance R_m and the after breaking percentage elongation gets lower, the first one reaching the temperature of 200°C and the second, 300°C. This could be explained by the fact that steel has lost some of its initial plasticity and resistance features, and still the breaking resistance experimentally established did not decline below the standard required values, for ambient temperature, by working in the focus of a steam boiler.

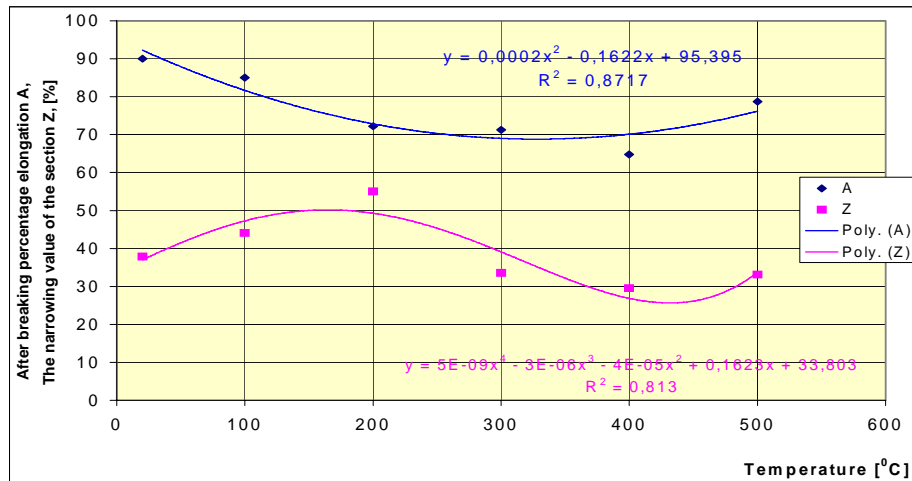


Fig.4. Variation after breaking percentage elongation A and The narrowing value of the section Z, for steel OLT 35K, by temperature

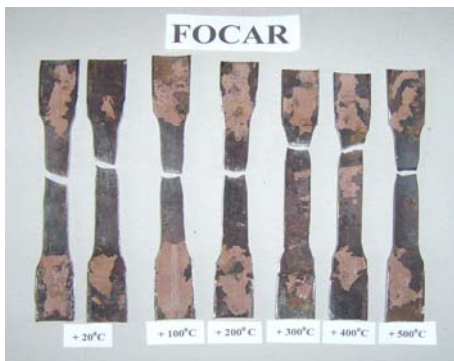


Fig.5. Share of bars, drawn from focus and tested at different temperature

The after breaking percentage elongation is valued between 90%, at temperature of 20°C (maximum) and 64,81%, at temperature of 400°C.

The narrowing value of the section is maximum valued at 55%, for the temperature of 200°C and minimum at 29,57%, for the temperature of 400°C.

Analysing the appearance of the broken test-bars surface, you can say that temperature influences the critical tangen tension value from the sliding layouts and especially the diffusion process of carbon, so that at a temperature between 250...300°C, the diffusion speed of carbon atoms is great, which makes the dislocation movement possible (in accordance with Ludes lines), that are taking place in the material.

4. CONCLUSIONS

Following the metalographical analysis and the testing, it can be concluded that materials still offer great mechanical resistance features, as in the structure of the analysed steel there is a sufficient quantity of perlite and ferrite and fine granulation, which gives an important reason for continuing their exploitation.

A primordial objective to all thermal-electrical power stations is to extend the functional length of the elements that work at high pressure and temperature. This extent of the functional length cannot be done in any way, without knowing the real behavior of the material, but only by both strict use of the safety conditions and maintaining the best functioning parameters.

Avoiding the appearance of damage requires a good knowledge of mechanical, physical, chemical, metalographical and any type of features, in as many conditions as possible, close to the ones in exploitation, which means knowing the real behavior of the material, knowledge that is based on theoretical research and experimental testing.

REFERENCES:

- [1] Lăpușan, A., *Contributions brought to the study of steel behavior at high temperature*. Doctoral thesis, Timișoara, 2004.
- [2] Cheșa, I. etc., *Choosing and using steel*. The Technical Publishing, Bucharest, 1984.
- [3] Dieter, G.F., *The mechanical metallurgy*. The Technical Publishing, Bucharest, 1970.
- [4] Mocanu, D.R. etc., *Testing materials, vol. I. Destructive testing of metals*. The Technical Publishing, Bucharest, 1982.
- [5] Nădășan, Șt. etc., *The handbook of the technician, from the metal testing laboratory*, The Didactics and Pedagogic Publishing, Bucharest, 1969.
- [6] Nădășan, Șt. etc., *Metal analysis and testing*. The Technical Publishing, Bucharest, 1965.
- [7] *** *Technical indications for the projection, execution, assembly, repair, installation, exploitation and check of the steam and hot water boilers*. C1-85, I.S.C.I.R Collection, Bucharest, 1986.



REGISTRATION AND PROCESSING OF FUNCTIONAL PARAMETERS VALUES FOR INTERNAL COMBUSTION ENGINES

Sorin RAȚIU, Ștefan MAKSAY, Ana JOSAN

University Politehnica of Timișoara, Engineering Faculty of Hunedoara, ROMANIA

Abstract:

The article represents a study regarding the creation of a correlation between the functional parameters of the internal combustion engines, both diesel and petrol ones, with the help of the MATLAB mathematic software. The values of these parameters were registered with the help of the mega macs 55 equipment, in real time, the motor vehicles running in urban traffic.

Keywords:

internal combustion engine, correlations, mathematic software, intelligent diagnosis, OBD

1. INTRODUCTION

The best results in tracking down defects immediately after their appearance can be reached if the motor car systems performance is permanently supervised, which involves the development of certain on board diagnosis techniques and equipment. Their evolution has been and is closely linked to the evolution of motor car construction. Thus, the appearance of microprocessor-operated systems has enabled a considerable increase in the number of objectives monitored and the number of registered and analyzed parameters.

The OBD (On Board Diagnostic) system monitors the engine performances and evacuation emissions, including the self-test sensors during vehicle running, to make sure it works. The board computer can identify a problem before it is tracked down by the vehicle driver, warning him/her about the failure by displaying a bright light. Most bright witnesses will display "Check Engine," "Service Engine Soon" or an engine symbol.

As soon as the OBD detects a problem, a failure code (error) is registered in the motor vehicle computer. When the vehicle is placed on an OBD I/M checking tester, this code will help the technician track down and repair the defect.

OBD-II is a new standard introduced in the second half of the '90, insuring the engine and chassis, equipment accessories and car installation control almost entirely. OBD II is an extensive set of standards used by SAE, and adopted by EPA and CARB (California Air Resource Board).

Certain motor vehicle models equipped with OBD-II are not 100% compatible. There are three basic OBD-II protocols used, each with minor variations of the communication model between the board computer and scanning outrigger.

Based on the OBD-II protocols, and connecting a mega macs 55 tester, the main functional parameters were registered for two types of engines. These values were transferred to the MATLAB mathematic software, with whose help different correlations were created.

2. ENGINE TESTING

The study was conducted on two different engines, petrol and diesel, and the data were obtained with the help of the mega macs 55 equipment from Gutmann company.

The diagnosis of the engine management was made in urban traffic, the equipment being connected through the OBD coupling to the engine command central unit. The data prevailed are displayed in the form of the data shown in the pictures below.

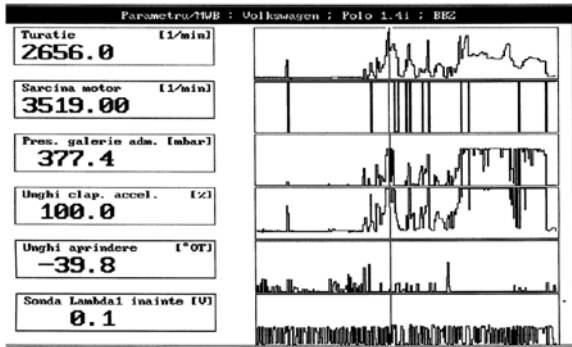


Figure 1. VW Polo, 1.4i engine

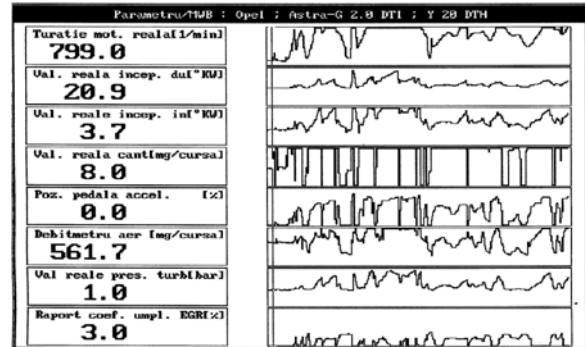


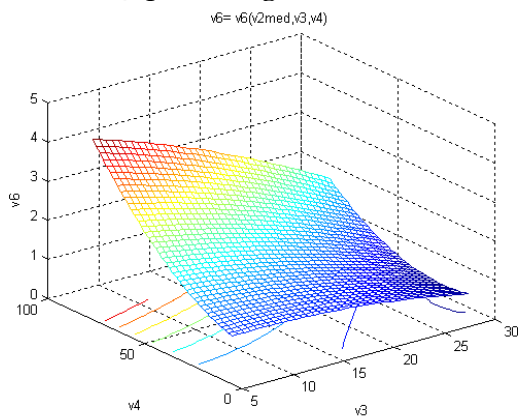
Figure 2. Opel Astra 2.0 DTI engine

As it can be observed, the system allows the registration of the engine functional parameters in graphic form, and by moving the cursor along the abscissa, in the left side of the display one can see the actual values of these parameters at a certain point in time.

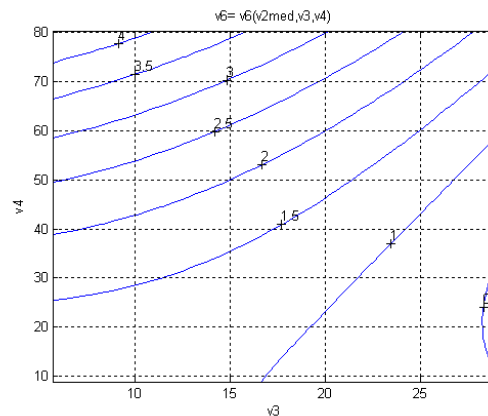
3. PROCESSING OF EXPERIMENTAL DATA

Following the measurements made in traffic, in a 15 minute interval, the data were introduced in a specialized processing program, thus a series of correlations being made, from which conclusions can be drawn referring to engine running in different revolutions and charges specific to urban traffic.

The study was conducted on the diesel engine fitted on the Opel Astra model and on the VW Polo 1.4i petrol engine.

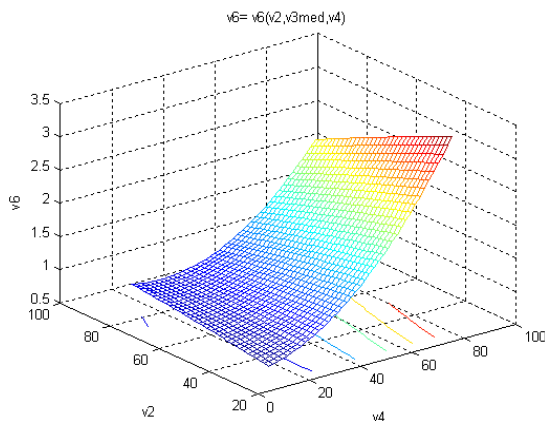


a.

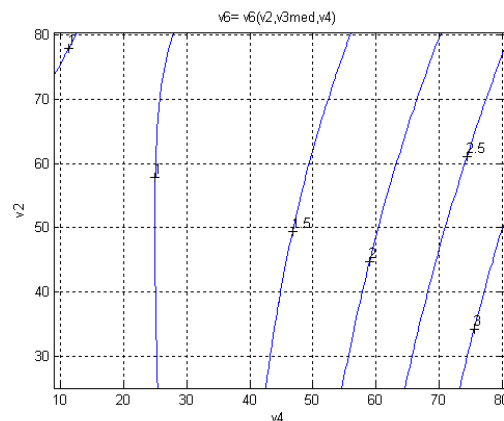


b.

Figure 3. Real value of the oversupply pressure (v6) function of the real quantity injected (v3) and the acceleration lever position (v4) for the Opel Astra engine



a.



b.

Figure 4. Real value of the oversupply pressure (v6) function of the real advance in the injection (v2) and the acceleration lever position (v4) for the Opel Astra engine

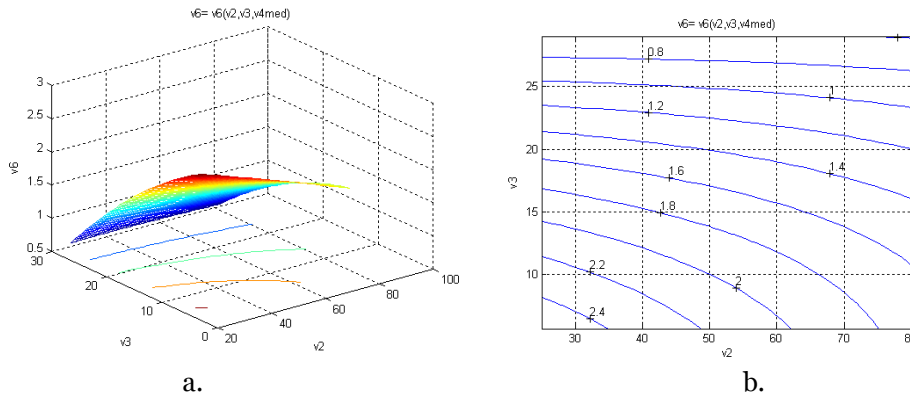


Figure 5. Real value of the oversupply pressure (v_6) function of the real advance in the injection (v_2) and the real quantity injected (v_3) for the Opel Astra engine

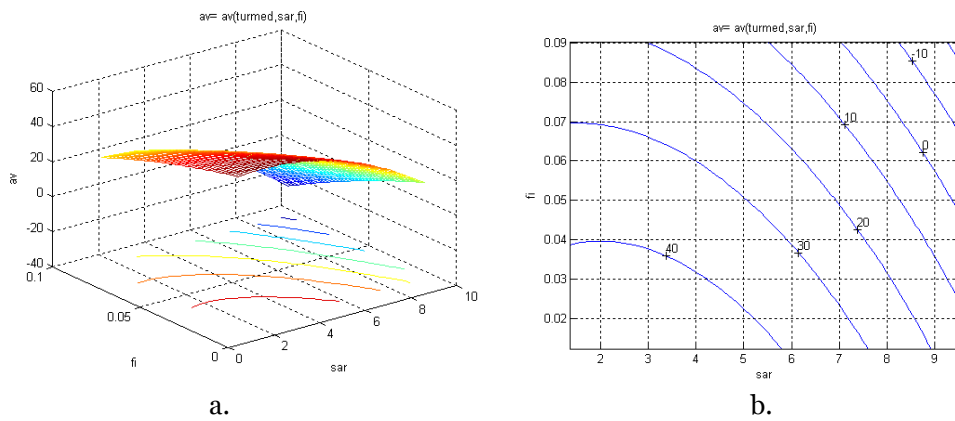


Figure 6. Value of the advance function of load and the acceleration choke opening angle for the VW Polo 1.4i engine

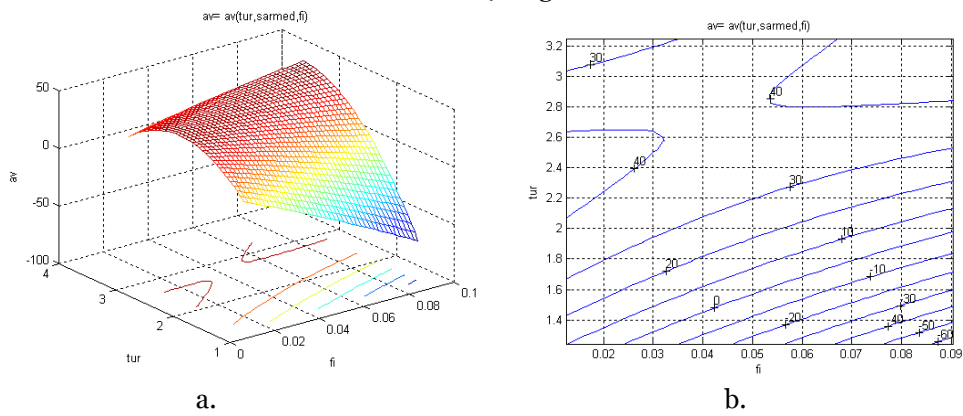


Figure 7. Value of the advance function of revolution and the acceleration choke opening angle for the VW Polo 1.4i engine

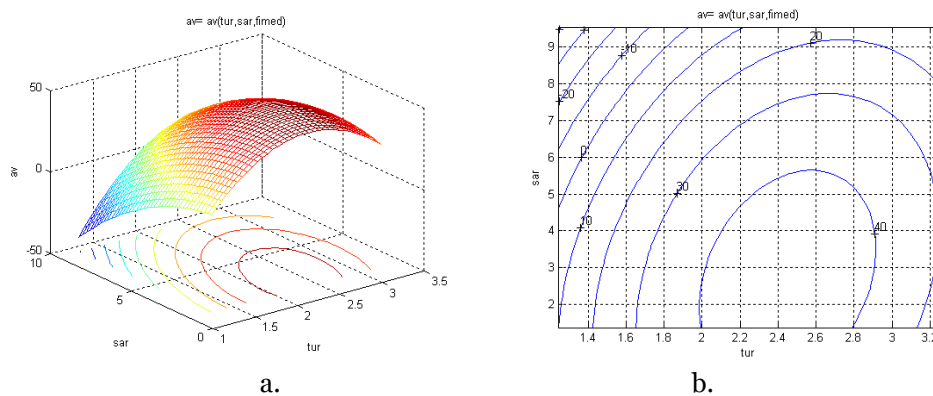


Figure 8. Value of the advance function of revolution and load for the VW Polo 1.4i engine

4. ANALYSIS OF RESULTS AND CONCLUSIONS

The registration system of the engine functional parameters allows only the sequence visualization of the prevailed data, based on which conclusions can be drawn regarding the functioning of different components.

Once these data are introduced in a specialized processing program, they can offer global information regarding the correlations which the command electronic unit makes during engine running between the different components that interact with one another.

BIBLIOGRAPHY:

- [1.] Mega Macs 55 – User Guide;
- [2.] Rațiu, S., Mihon, L. – Internal Combustion Engines for Road Motor Vehicles, Processes and Characteristics, Mirton Publishing House, Timisoara, 2008;
- [3.] MATLAB software – User Guide.



STUDY ON THE VARIATION OF CONVENTIONAL FLOW LIMIT DEPENDING ON THE MAIN ALLOY ELEMENTS FOR THERMORESISTANT STEEL

Amalia Ana DASCĂL

“Politehnica” University of Timisoara, Faculty of Engineering of Hunedoara,
Department of Engineering and Management, ROMANIA

Abstract:

The paper presents the results of the research made under laboratory experimental testing, on OLT45K steel, intended to the manufacturing of tubes, used at high temperature in the make-up of thermal-energetic installation. Mechanical driving testing has been made at the temperature of 450°C, on shares of test-bars drawn out of a number of 50 charges, with a view to achieving the optimization of the chemical composition of this steel type. The optimization, under experimental dates, suggests alternatives of combinations among the main elements of the chemical composition, so as the steel can be elaborated with superior mechanical features at high temperature. The obtained results have a large feasibility area, and can be also endorsed for other steel types and mechanical features for which the optimization is viewed, therefore being very useful to technologists, in the process of achieving a certain type of steel.

Keywords:

high temperature, thermal resistant steel, mechanical testing, life-length, mechanical feature.

1. GENERAL APPRECIATION

Generally, any research elaboration implies some stages: gathering the dates, their modeling and the decisional working out. The informational pattern-making follows 3 steps: manual, mechanical and automatic.

Its results have to be presented in a shape which makes them utilizable by the beneficiary, no matter the pattern-making method.

A new and important problem, raised in the study of multidimensional reparations, concerns the bound among the analysed variables and through them, among the phenomena they represent, known as **correlation**. It includes two fundamental problems: the first consists in describing the medium variation law of a variable depending on another (or other) variable(s), known as the **problem of regression** and settled under the regression function, and the irrespective of the linked variable measures.

Estimating and sizing the thermal-electric power station pipes is extremely detailed and expensive, regarding the use of the finite element programmes, as it is very hard to specify all the testing which the pipe system is to be requested, during the estimated life length. Extreme situations and possible exploitation accidents are also hard to estimate.

This is the reason of choosing as a subject of the paper the making of multiple correlations, II figure, which offers information on the influence of two of the chemical composition elements on the technical running limit at the temperature guaranteed by the metal manufacturer. From the graphical representation and knowledge of the outline values, we can establish the desired value of the mechanical feature, for any content of an element found in the chemical composition. We can also establish the best variation fields of these elements, varying with the desired values of the studies parameter.

2. EXPERIMENTAL DATES

The numerical studies had as starting point the driving experimental testing at heat, made on shares of test-bars drawn out of a number of 50 charges of OLT 45K steel, endorsed into an electrical oven equipped with a spring, whose chemical composition is presented in [1] paper.

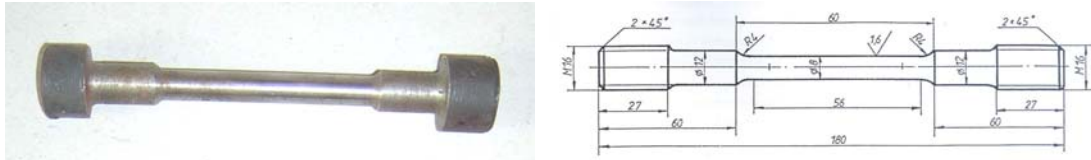


Fig.1 The shape and size of test-bars used in testing
Three test-bars have been tried for each charge, their shape and size being shown in fig.1.

3. ESTABLISHING THE NUMERICAL STUDIES

By using the experimental dates obtained after laboratory testing, it went forward to establishing some graph correlations, using MATLAB 5.0 programme. Files with experimental dates and those obtained by the rolling of the used programmes, can be found in [1] paper. The numerical results, obtained by rolling the programme are sizable, for which they are not presented in the paper. Then, the graphs obtained by mathematical pattern-making of the results.

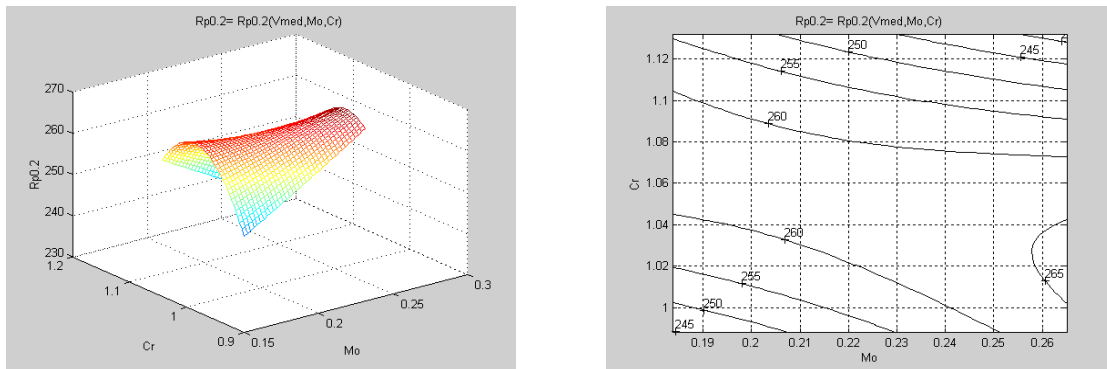


Fig.2 The variation of the technical running limit $R_{p0.2/450}$, containing manganese and silicon, taking into consideration the medium percentage of carbon

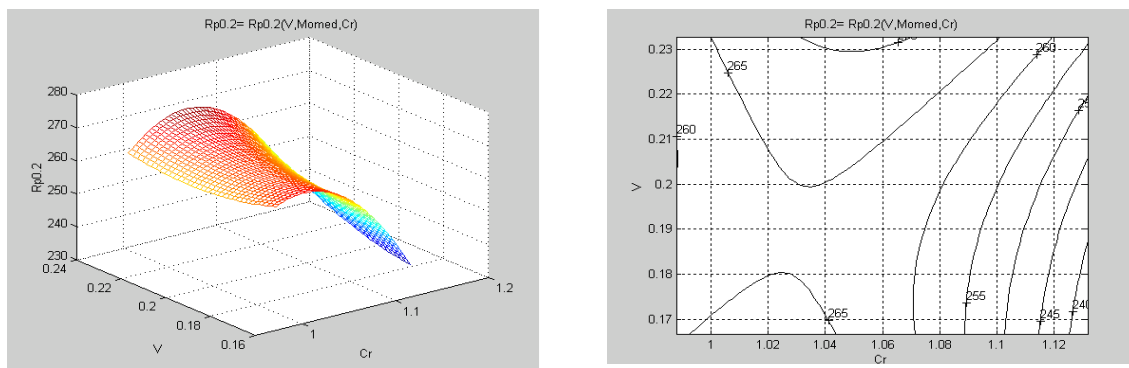


Fig.3 The variation of the technical running limit $R_{p0.2/450}$, containing carbon and silicon, taking into consideration the medium percentage of manganese

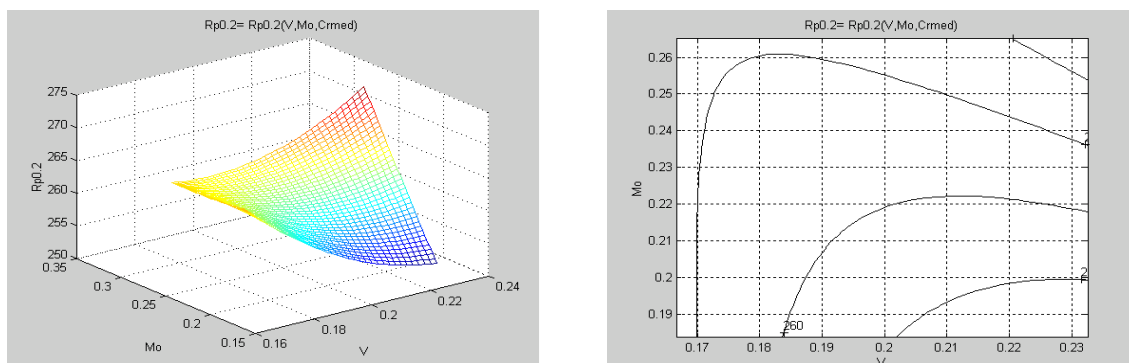


Fig.4 The variation of the technical running limit $R_{p0.2/450}$, containing manganese and carbon, taking into consideration the medium percentage of silicon

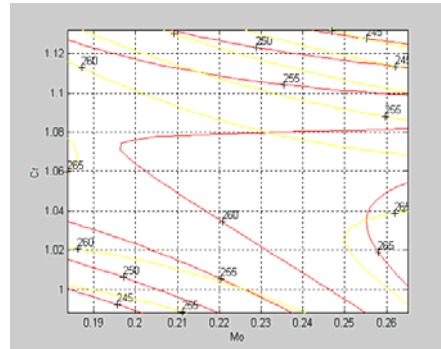
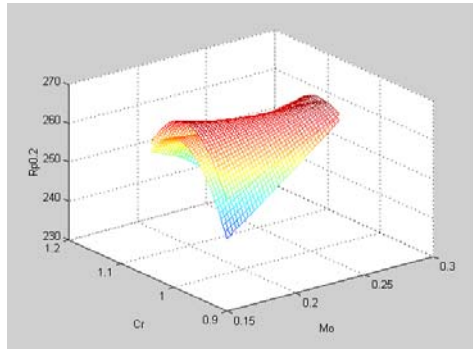


Fig.5 The delimitation of the best field for the technical running limit $R_{p0.2/450}$, depending on the manganese and silicon content, taking into consideration the medium percentage of carbon

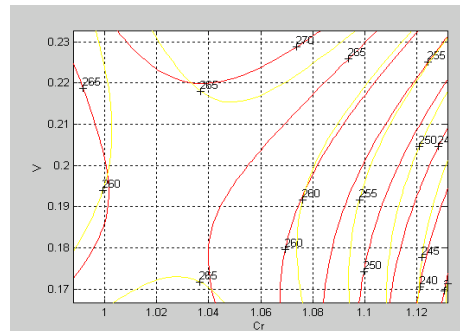
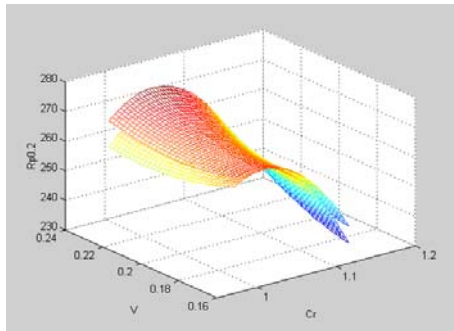


Fig.6 The delimitation of the best field for the technical running limit $R_{p0.2/450}$, depending on the carbon and silicon content, taking into consideration the medium percentage of manganese

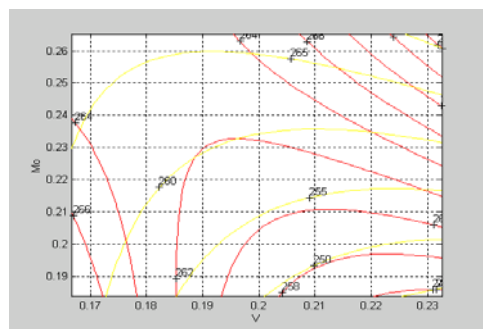
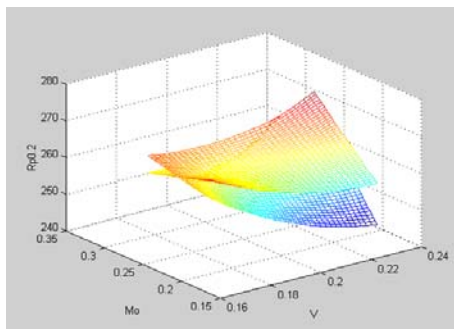


Fig.7 The delimitation of the best field for the technical running limit $R_{p0.2/450}$, depending on the carbon and manganese content, taking into consideration the medium percentage of silicon

Because of the huge size of dates found in such a processing of experimental dates, we stopped, focusing on the mechanical feature $R_{p0.2/450}$, which must be guaranteed by the metal manufacturer, for the analysed steel.

The most important feature of this steel category at high temperature is the conventional running limit at heat. This is the reason why the study has been made for establishing combinations of the best chemical composition and through the working process, for the steel to have superior mechanical features. Therefore, the obtained results follow the way of the conventional running limit for combinations of three main elements of the chemical composition. Through the multidimensional numerical pattern-making of the experimental dates, it was tried the finding of a modeling of the dependent variable, considering the independent variables x, y, z as:

$$u = C_1 \cdot x^2 + C_2 \cdot y^2 + C_3 \cdot z^2 + C_4 \cdot x \cdot y + C_5 \cdot y \cdot z + C_6 \cdot z \cdot x + C_7 \cdot x + C_8 \cdot y + C_9 \cdot z + C_{10} \quad [1]$$

The variation limits of the variable are:

$$[\%C] = 0,16...0,23; [\%Mn] = 0,51...0,83; [\%Si] = 0,16...0,35; R_{p0.2/450} = 169...255.$$

The medium values and the medium square deviation of the variables are:

$$[\%C]: 0,18563...0,01886; [\%Mn]: 0,66375...0,09545; [\%Si]: 0,235...0,047697; [R_{p0.2/450}]: 08,95...17,193$$

The correlation coefficient is valued: $r_f = 0,65599451703118,$

and the deviation from the regression area is: $s_f = 12,97668845383391$

The maximum established on the 50 charges sample is given by:

$$\begin{aligned}
 R_{p_{0,2}} = & 19828,0654 \cdot [\%C]^2 - 268,3624 \cdot [\%Mn]^2 + 571,8135 \cdot [\%Si]^2 + \\
 & -2984,07 \cdot [\%C] \cdot [\%Mn] + 148,8591 \cdot [\%Mn] \cdot [\%Si] + 1182,9936 \cdot [\%Si] \cdot [\%C] + \\
 & -5668,4577 \cdot [\%C] + 962,9562 \cdot [\%Mn] - 672,8277 \cdot [\%Si] + 472,3753
 \end{aligned} \quad [2]$$

These 4 dimensional surfaces allow a *saddle point* of coordinates:

$$[\%C] = 0,19417; [\%Mn] = 0,79343; [\%Si] = 0,2842; R_{p_{0,2}/450} = 208,473.$$

The existence of the saddle point is very important as it assures a stability of the feature close to this point, being it preferable or avoidable. In this case, it is preferable. The behavior of these hyper surfaces close to the saddle point can only be studied as tabular, which means ascribing values on concentric spheres of the studied point to the independent variable. Because of the fact that this surface cannot be represented in 4 dimensional spaces, it has been chosen the successive replacement of each independent variable, with its medium value, and obtaining the following equations:

$$\begin{aligned}
 R_{p_{0,2}} C_{med} = & -268,3624 \cdot [\%Mn]^2 + 571,8135 \cdot [\%Si]^2 + 148,8591 \cdot [\%Mn] \cdot [\%Si] + \\
 & + 409,0382 \cdot [\%Mn] + 453,2345 \cdot [\%Si] + 103,3764
 \end{aligned} \quad [3]$$

$$\begin{aligned}
 R_{p_{0,2}} Mn_{med} = & 571,8135 \cdot [\%Si]^2 + 19828,0654 \cdot [\%C]^2 + 1182,9936 \cdot [\%Si] \cdot [\%C] - \\
 & -574,0225 \cdot [\%Si] - 7649,1341 \cdot [\%C] + 993,3067
 \end{aligned} \quad [4]$$

$$\begin{aligned}
 R_{p_{0,2}} Si_{med} = & 19828,0654 \cdot [\%C]^2 - 268,3624 \cdot [\%Mn]^2 - 2984,07 \cdot [\%C] \cdot [\%Mn] - \\
 & -5390,4542 \cdot [\%C] + 997,938 \cdot [\%Mn] + 345,8392
 \end{aligned} \quad [5]$$

These surfaces which belong to the 3 dimensional spaces can be represented and therefore interpreted by technologists. The surfaces are shown in fig.2, fig.3, fig.4, fig.5, fig.6 and fig.7. For a more exact analysis, the corresponding level curves have been shown next to these. The knowledge of the level curves allow the establishing of the two independent variable values, so as $R_{p_{0,2}/450}$ can be obtained, within the limits required or imposed by the beneficiary.

By looking at the graphs shown in fig.2, and considering %C an average, you can estimate that maximum values of $R_{p_{0,2}/450}$ feature can be obtained for 0,50% Mn and 0,14% Si, values which are close to the inferior limit of the composition imposed by standard. From fig.3, considering % Mn an average, you can say that maximum values of $R_{p_{0,2}/450}$ (230 N/mm²) features can be obtained for C concentrations within the 0,12 – 0,14% limits and Si within the 0,15 – 0,18% limits, subfields which are close to the inferior limit of the composition imposed by standard. From the graphs shown in fig.4, and considering % Si an average, you can estimate that while the C and Mn grow, the $R_{p_{0,2}/450}$ conventional running limit grows as well. The diagrams in fig.5, fig.6 and fig.7 show the limits of the maximum field, where the metallurgic engineer can choose the element percent of the chemical composition, in order to obtain steel having the desired features of the manufacturer. Knowledge of the level curves for these maximum fields allows the correlation of the two independent variable (the contents of the chemical element) so that $R_{p_{0,2}/T}$ can be obtained within the limits asked by the beneficiary.

CONCLUSIONS

These results allow the establishing of the best C, Mn, Si contents from the chemical composition of 12VMoCr10, so that, by the end of the elaboration, steel can possess certain imposed mechanical features.

The analysis has been done for 3 elements of the chemical composition, being able to enlarge it for both other elements, depending on the desired chemical composition and other types of steel.

Taking into consideration that the way in which one charge is done has a deep importance on the mechanical features of the steel, knowledge of these correlations is really significant for the engineer, because he is the one to estimate the values of the imposed parameter, depending on the chemical composition which allows him the adjustment of the chemical composition during the elaboration, in order to obtain the features desired by the beneficiary.

REFERENCES:

- [1] Lăpușan, A. – *Contributions brought to the study of steel behavior at high temperature*, Doctoral thesis, Timișoara, 2004.
- [2] Todorean, I. – *The mathematical study of experimental dates*. The Academy Publishing, Bucharest, 1976.
- [3] Maksay, Șt. – *Special Mathematics*, The Polytechnic Publishing, Timișoara, 2001.
- [4] Taloi, F. – *The optimization of metallurgic process*. The Didactics and Pedagogic Publishing, Bucharest, 1982.



APPLICATION OF THE SQUIRREL CAGE ASYNCHRONOUS MACHINE WORKING AS SINGLE PHASE GENERATOR IN MICROHYDRO POWER PLANTS

Sorin Ioan DEACONU, Marcel TOPOR, Gabriel Nicolae POPA, Diana BISTRIAN

“Politehnica” University of Timisoara, Faculty of Engineering of Hunedoara,
Department of Electrical Engineering and Industrial Informatics, ROMANIA

Abstract:

Today the hydroenergy potential of Romania is used only in proportion of 60 %. There are in work several project concerning the arrangement of several water flows (Jiu, Strei, Bistrita, Mures). This will increase the overall percent up to 70 % in 2020.

However it remains an important percent of usable potential which can be integrated by technology upgrade or building of new power plants.

The asynchronous generator is a more efficient solution for small installed power and especially where the electric consumers are single phase and the electrical grid is isolated from the main grid.

Keywords:

asynchronous machine, single phase generator, mathematical model

1. INTRODUCTION

Power is the vital input for economic development for any developing country. Technologies being at its zenith, many methods for the generation of power have been developed. Owing to the perpetual increase in energy needs it is difficult to meet the growing demand by exploiting energy from the limited conventional sources such as coal, oil, gas, etc. In consequence a greater emphasis is now being given to the harnessing of energy from non conventional energy sources such as wind, micro and mini hydro and solar [1].

As a result of increasing environmental concern, more and more electricity is generated from renewable energy. The main advantage of electricity generation from renewable sources is the absence of harmful emission and the infinite availability of the prime mover that is converted to electricity [2].

With continuing energy crises, utilities in poor country's are finding it increasingly difficult to establish rural area electrification. The cost of supplying electrical power through grid to such areas is becoming excessively high to the large investments in transmission lines losses. For these reasons the stand-alone decentralized power generating stations using non-conventional energy sources like wind, micro and mini hydro are being considered for electrifying rural and remote areas [1].

Taking into account its simplicity of use and its modest cost compared to a synchronous machine, the asynchronous machine is as susceptible to function in generating in power stations of production of the electric energy. In this case, the slip is negative and the rotor turns in the direction of the spinning field pattern at a slightly higher speed. The generator provides the active power to the utility, but the reactive power necessary to its supply is provided by the utility. An isolated operation of the induction generator is possible. The convert of renewable energy is mainly equipped by both asynchronous generators and capacitors of self- excitation [3].

In many papers is investigated the ability of some dynamic self- asynchronous generator models to predict the output voltage depending of the variation of turbine speed (figure 1).

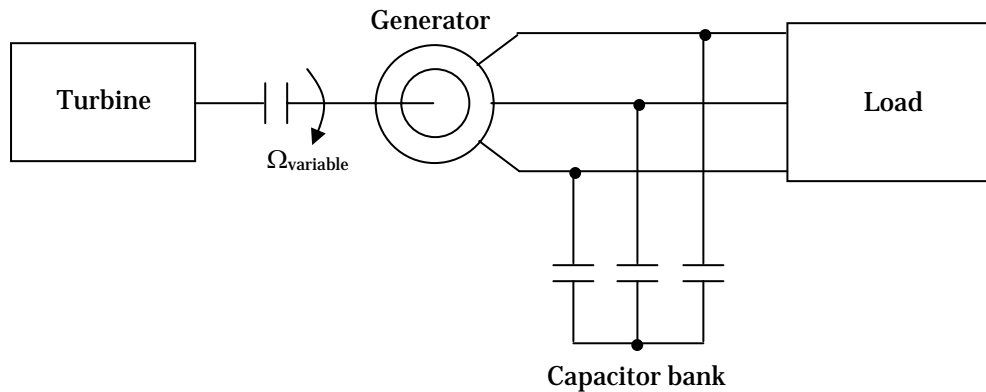


Figure 1 Self-excited asynchronous generator

Low-power generators (say up to 10 kW) invariably feed a single-phase supply system. Since it has been found that a normal single-phase asynchronous motor cannot be effectively used as self-excited generator, a specially designed two-winding single-phase has been proposed in [4]. Since this requires modified manufacturing procedures, and hence is expensive, the alternative of using off the shelf three-phase load asynchronous motor as a self-excited asynchronous generator to feed single-phase load appears attractive. This requires a suitable balancing system to achieve balanced winding currents and to obtain maximum output with minimum losses [5].

Large numbers of exploitable small hydro sites exist in several countries with capacities ranging from 5 to 50 kW, mostly needing to feed single-phase loads. The use of three-phase asynchronous motors as self-excited asynchronous generator to feed such loads makes practical sense. The present paper provides theoretical support to such promising technologies.

2. STATEMENT OF THE PROBLEM

When the rotor speed of asynchronous machine is greater than the synchronous speed of air gap revolving field, then the same asynchronous machine can be act as asynchronous generator.

As a generator asynchronous machine has severe limitation. Because it lacks a separate DC field current, an asynchronous generator needs AC excitation current. The self excitation phenomenon using external capacitors is well known. If an appropriate capacitor is connected across the terminals of an externally driver asynchronous machine as shown in figure 1, an emf is induced in the machine winding to the excitation provided by the capacitor [1],[6].

Induced voltage and current will continue to rise until the VAR supplied by the capacitors is balanced by the VAR demanded by the machine, a condition that is essentially divided by on saturation of the magnetic circuit.

Let us consider that the machine has an initial residual flux (or same means are provided to inject an initial current into the stator windings), and the rotor is propelled by some external mechanical power source, such as on fuel engine, hydraulic turbine, etc. If external capacitors of adequate values are connected to the stator windings, self excitation occurs. The magnitude of the generated voltage will depend among other things on the capacitance value, the load current, and the load power factor. Considering steady state operation it is possible to observe three regions clearly differentiated: a) a stable zone corresponding to operation in the saturated region of the magnetic core; b) an unstable zone, corresponding to operation on the linear region of the magnetic core; and c) a region of no-generation. In the first case the linear curve of the excitation capacitors intersect the core magnetizing curve at a well defined point. In the second case, the intersection is not well defined, far it occurs at an infinite number of points. In the third case, the only intersection occurs at the origin as is shown in figure 2 [6].

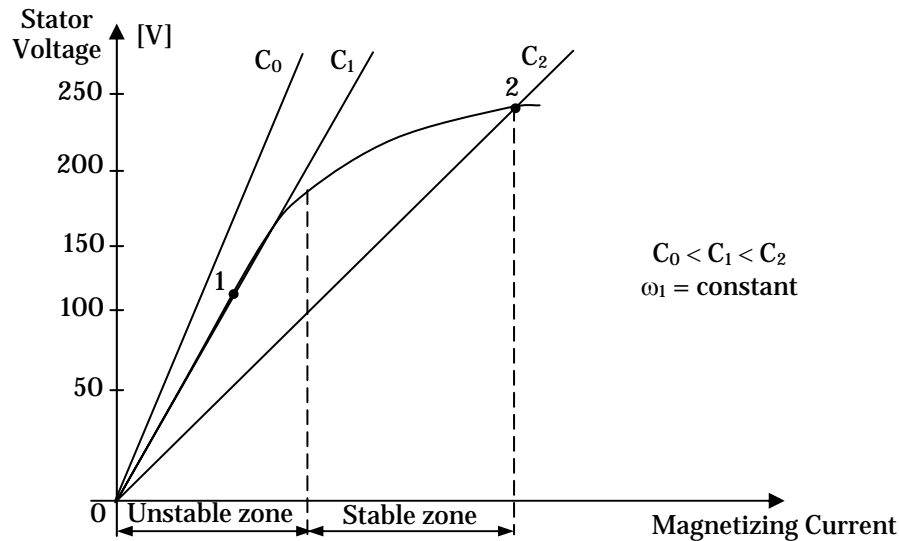


Figure 2 Magnetizing characteristic of a self-excited asynchronous generator

Let us assume that the machine is actually operating at point 1 in figure 2. If a capacitor of value C_2 is connected, the new generated voltage will be determined by the machine characteristic curve, and will evolve from point 1 to point 2 with a definite time constant. Conversely, if the capacitor is reduced from a value C_1 at point 1 to a value C_0 , smaller than C_1 , the magnetizing current will not be compensated by an identical but leading current component. In this case, the machine will first try to save the situation by dropping some of its magnetizing current in order to reach another stable operating point along its magnetizing curve. This results in a lower air gap voltage and a consequently lower flux; the slip will increase and finally the machine will stop generating (intersection at origin in figure 2). Fortunately, the time constants involved in either situation (voltage increase or decrease) are lower than the generation period, this fact allows corrective commutation actions to be taken to keep the average leading current around its required value [6].

3. EXCITATION REQUIREMENTS OF SELF-EXCITED ASYNCHRONOUS GENERATOR (SEAG)

The minimum capacitance (C_m) for the excitation of asynchronous generator is obtained from no load test. On no load, the capacitor current (I_c) must be equal to the magnetizing current (I_m), under stable operating:

$$I_m = I_c \quad (1)$$

$$\frac{U}{X_m} = \frac{U}{X_c} \quad (2)$$

$$X_c = X_m \quad (3)$$

where

$$X_c = \frac{1}{2\pi f \cdot C} \quad (4)$$

From no-load test we calculated the magnetizing reactance X_m by applying the rated voltage of the machine and find out the magnetizing current (I_m). The value of minimum capacitance C for self-excitation is

$$C_m = \frac{1}{2\pi f} \cdot \frac{I_{m\text{phase}}}{U_{\text{phase}}} \quad (5)$$

The most serious problem with an asynchronous generator is that its voltage varies widely with changes in load, especially reactive load. In order to maintain constant voltage, reactive current must be controlled from no load to full load. Hence special technologies

must be employed to increase the effective capacitance during starting and decrease it during normal operation. [1].

In self-excited mode, output frequency and voltage are affected by speed, the load and terminal capacitor. Changing any of above parameter will change the frequency and magnetizing reactance of asynchronous generators [1].

The schematic diagram of a three phase delta connected self –excited asynchronous generator feeding a three phase unbalanced load is shown in figure 3. The delta connection is deliberately here since a star connected three phase asynchronous motors has be reconnected in delta to feed single phase loads.

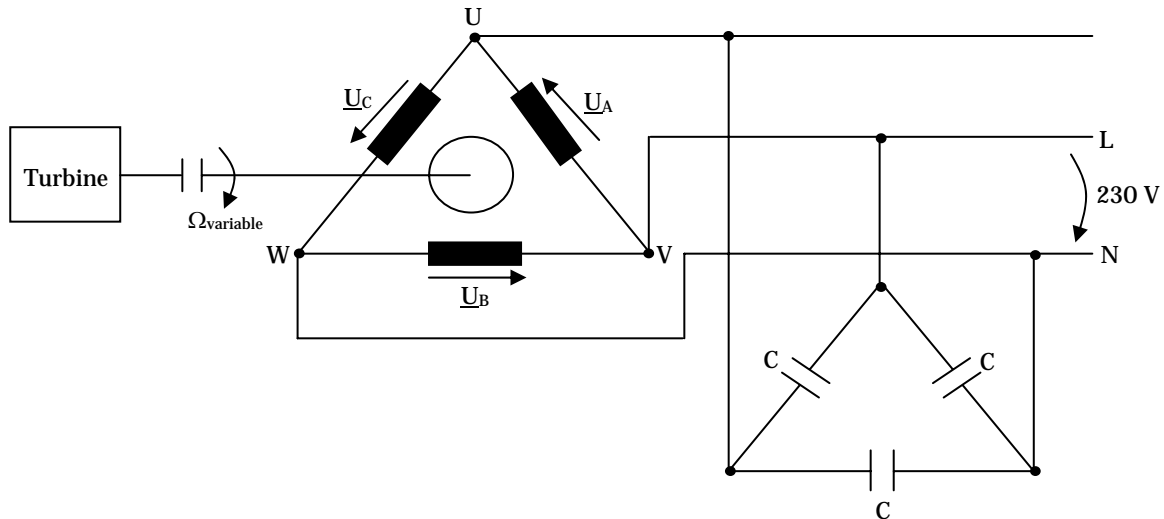


Figure 3 Schematic diagram of self-excited asynchronous generator

4. SIMULATION RESULTS OF THE SEAG

In order to evaluate the operating principles of the self excited asynchronous generators we consider two situations: three phase operation in grid connection mode and single phase connection mode.

4.1. Three phase grid connected operation of the SEAG

The equivalent model of the SEAG operating in three phase mode is presented in fig. 4.

The equivalent per phase impedance seen by the terminals [7] represented in equation (6) is :

$$\underline{Z} = R_1 + jX_1 + \frac{1}{\frac{1}{jX_m} + \frac{1}{R_m} + \frac{1}{R_2/s + jX_2}} \quad (6)$$

where R_1 , X_1 is stator resistance and reactance, R_2 , X_2 is rotor resistance and reactance R_m , X_m magnetizing equivalent resistance and reactance, s is slip , F is frequency , $v = n_s/n_r$.

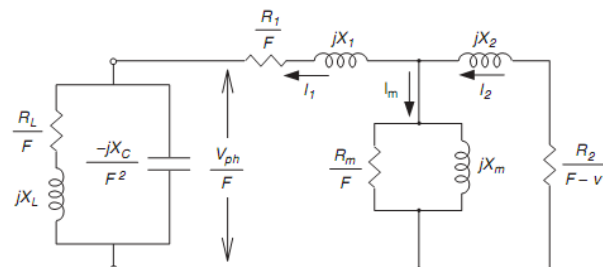


Figure 4 Equivalent circuit diagram of self-excited asynchronous generator

In order to simulate the operation of the SEAG it is necessary to use the d-q model of the SEAG. The d-q model of the induction generator in flux linkage state variables is given in equation (7):

$$\begin{cases} p\lambda_{qs} = V_{qs} - (R_s / L_{1s})(\lambda_{qs} - \lambda_{mqsat}) \\ p\lambda_{ds} = V_{ds} - (R_s / L_{1s})(\lambda_{ds} - \lambda_{mdsat}) \\ p\lambda_{qr} = \omega_r V_{qr} - (R_r / L_{1r})(\lambda_{qr} - \lambda_{mqsat}) \\ p\lambda_{dr} = \omega_r V_{qs} - (R_r / L_{1r})(\lambda_{dr} - \lambda_{mdsat}) \end{cases} \quad (7)$$

where V_{ds}, V_{qs} represents d, q axis voltages $\lambda_{qs}, \lambda_{ds}$ d, q axis flux linkages, $\lambda_{mqsat}, \lambda_{mdsat}$ d-q saturated magnetizing flux, R_s, R_r stator and rotor resistance, L_{1s}, L_{1r} stator and rotor inductance, ω_r rotor speed.

The d-q model of the load side that consists of the excitation capacitors C_s in parallel with an inductive load is given by equation (8):

$$\begin{cases} pQ_{qs} = -I_{qs} - I_{qL} \\ pQ_{ds} = -I_{ds} - I_{dL} \\ pI_{qL} = (V_{qs} - R_L I_{qL}) / L \\ pI_{dL} = (V_{ds} - R_L I_{dL}) / L \end{cases} \quad (8)$$

where I_{qs}, I_{ds} is d, q axis current, Q_{qs}, Q_{ds} charge across excitation capacitor, R_L, L load resistance and inductance, Q_s represents the charge across the excitation capacitor. The mechanical equation that describes the prime mover is:

$$\frac{d\omega_r}{dt} = \frac{P}{2J} (T_L + T_e) \quad (9)$$

$$T_e = (3/2)(P/2)(\lambda_{ds} I_{qs} - \lambda_{qs} I_{ds}) \quad (10)$$

where T_e is the asynchronous generator electromechanical torque, T_L is the mechanical load torque, p is the induction generator number of poles, J is the total inertia of the generator and the prime mover machine.

The parameters of test machine are given table 1. The simulation model of the SEAG is build in PSIM software (figure 5). The setup consists in two asynchronous identical machines from which one acts as prime mover. The prime mover machine is a electric drive running a constant speed above the synchronous speed of the SEAG generator.

Table 1. SEAG data

Parameter name	Symbol	Value
Stator resistance	Rs	0.294
Stator inductance	Ls	0.00139
Rotor resistance	Rr	0.156
Rotor inductance	Lr	0.00074
Magnetising inductance	Lm	0.041
Moment of inertia	J	0.0131
Friction factor	F	0.002985
Pole pairs	p	2

The main steady state characteristics of SEAGs are to be obtained at constant (given) speed though a prime mover, such as a constant speed small hydroturbines, does not have constant speed if unregulated.

The self excitation transients of the of the three phase generator operating in grid conection mode with three phase output are presented in fig. 6 and 7.

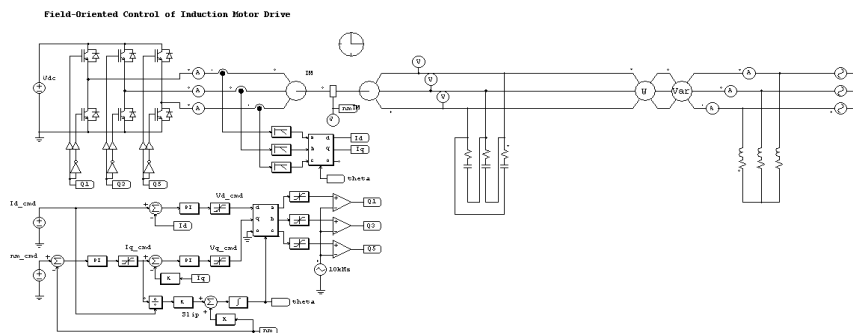
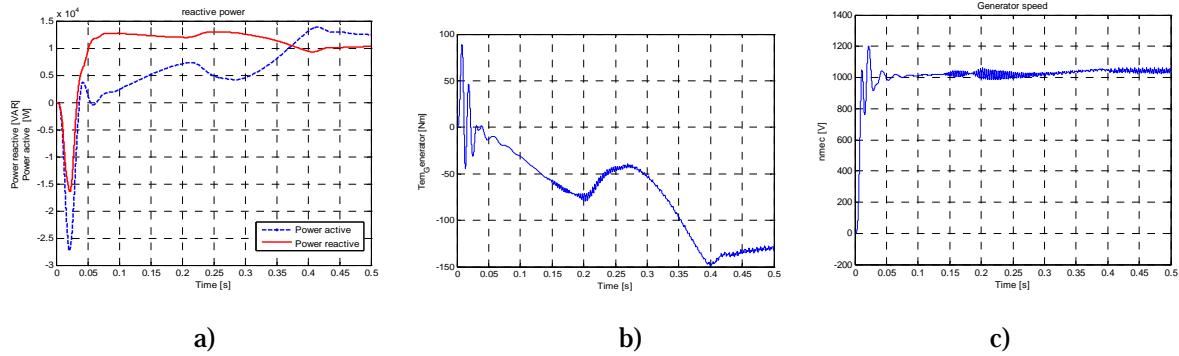
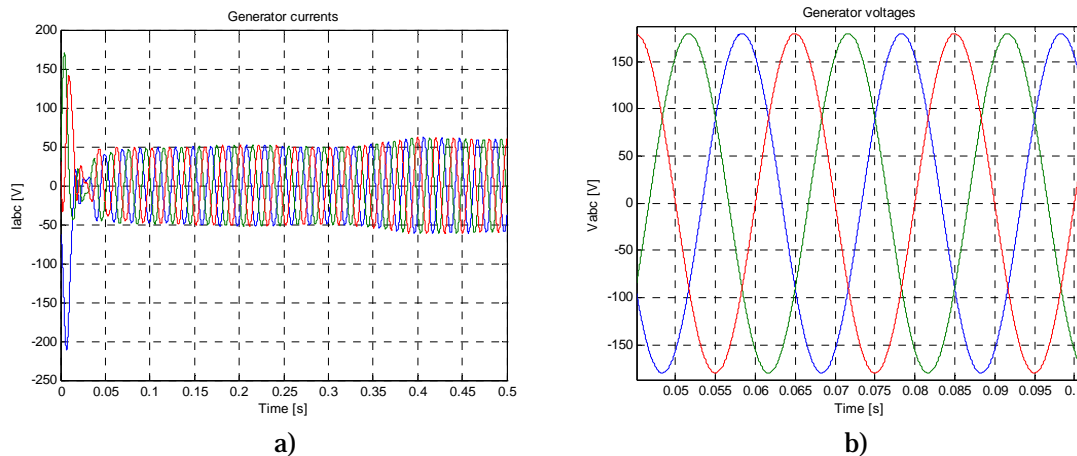


Figure 5 PSIM model of the three phase SEAG



a) Figure 6 Simulation results when SEAG is connected to a 3 phase grid
 a) active and reactive power; b) electromagnetic torque; c) speed

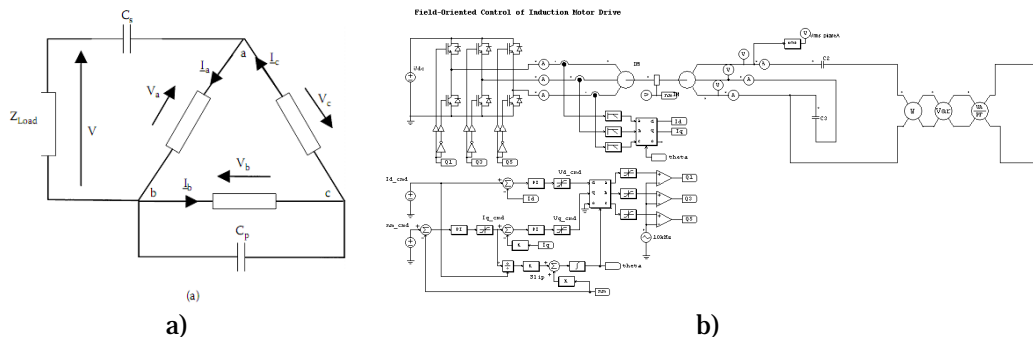


a) Figure 7 Simulation results of generator currents and voltages

The reactive and active energy of SEAG during the startup function working as stand alone generator in three phase grid is presented in fig. 6a. As it can be noticed the required reactive energy varies during generator wakeup and reaches a minimum when the generator is running in steady state mode. The active power in the three phase grid also changes sign during generator wakeup injected/absorbed. The electromagnetic torque of the generator presents no pulsations.

4.2. Simulation of three-Phase SEAG with Single-Phase Output

When the SEAG is operating with a single phase load, the machine operates under unbalanced conditions thus it is imposed a different connection of the SEAG excitation capacitors. We consider here Steinmetz capacitor excitation connection [8] presented in figure 8 a.



a) Figure 8 SEAG Steinmetz excitation connection and PSIM simulation test model

For the simulation of the SEAG in this operation mode we have implemented the generator model into the PSIM software figure 8 b. The single phase electromagnetic torque of the SEAG is presented in fig. 9.

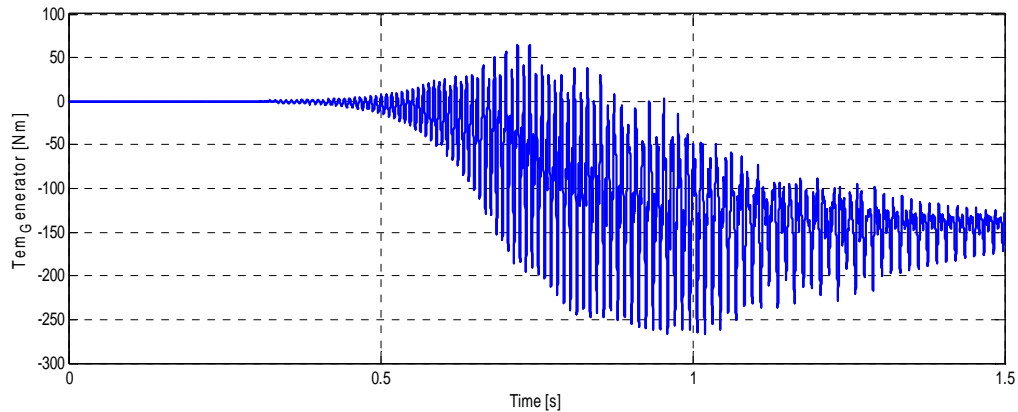


Figure 9 Electromagnetic torque of the SEAG operating in single phase grid connection

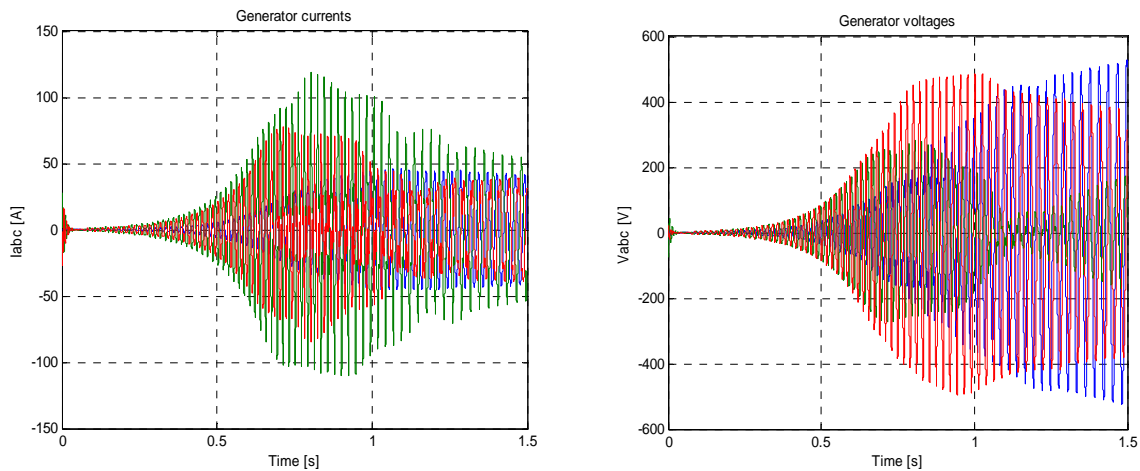


Figure 10 Generator currents and voltages when the SEAG is connected to one phase grid

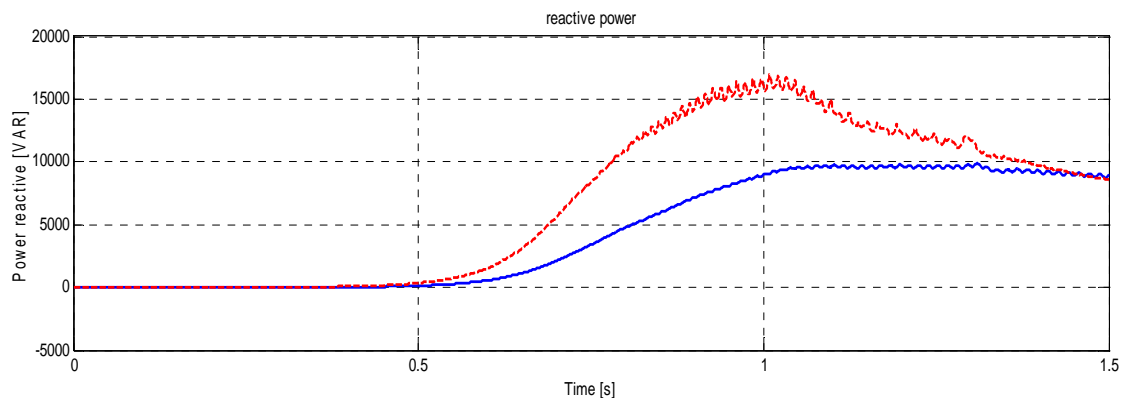


Figure 11 Active power and reactive power of the SEAG

Figure 10 and 11 shows transients of the SEAG during startup of the generator.

5. CONCLUSION AND FUTURE WORK

In the present paper we consider the operation of the single phase SEAG during self excitation process for two situation three phase grid operation and single phase grid operation. The necessary reactive power is evaluate in both cases. As it can be observed the torque pulsations are not negligible and the current pulsations are present. In order to operate the SEAG in single phase grid connection a special attention should be accorded to symmetrisation scheme and capacitor selection.

REFERENCES

- [1] Chandra, T.S., Bishnu, P.M., Voltage Regulators for Self Excited Induction Generator, IEEE Transactions on Energy Conversion, Vol.20, no. 4, April 2004, pp 460÷463.
- [2] Slothweg, J.G., Polinder, H., King, W.L., Dynamic Modeling of a Wind Turbine with Doubly Fed Induction Generator, Proceedings of IEEE Power Engineering Society Summer Meeting, vol. 1, pp.644-649, 2001.
- [3] Elhafyani, M.L., Zouggar, S., Benkaddour, M., Zidani, Y., Permanent and Dynamic Behaviors of Self-excited Induction Generator Society, volume 7, no. 1, January 2006. pp. 49÷53.
- [4] Nigel, S., Motors as generators for microhydro power plant, ITDG publishing 2003, ISBN 1-85339-286-3.
- [5] Singh, B., Kasal, G., Chandra, A., Kamal, A.H., Battery Based Voltage and Frequency Controller for Parallel Operated Isolated Asynchronous Generators, IEEE International Symposium on Industrial Electronics, ISIE 2007, Proceedings, pp. 883÷888.
- [6] Suarez, E., Bartolotto, G., Voltage-Frequency Control of a self-excited Induction Generator, IEEE Transaction on Energy Conversion, vol.14, no 3, September, 1999, pp. 394÷401.
- [7] Farret Felix A., Simões M. Godoy, Integration of Alternative Sources of Energy Wiley-IEEE Press 2006 ISBN 0471712329.
- [8] Boldea Ion, Variable Speed Generators (Electric Power Engineering Series) CRC Press 2005 ISBN: 0849357152.



YIELD FACTORS OF A PHOTOVOLTAIC PLANT

¹Cristian P. CHIONCEL, ²Dieter KOHAKE, ³Ladislau AUGUSTINOV,
⁴Petru CHIONCEL, ⁵Gelu Ovidiu TIRIAN

^{1,3,4}“Eftimie Murgu” University, Resita, ROMANIA

² FH Gelsenkirchen, GERMANY,

⁵ “Politehnica” University of Timisoara, Faculty of Engineering Hunedoara, ROMANIA

Abstract:

The paper gives the definition of the main yield factors that characterizes the performances of a photovoltaic plant. This are analyzed for a grid connected photovoltaic plant at the University in Resita, in use since spring 2008, were the main climatic and technique parameters of the photovoltaic plant are monitorised and heaped in an data base for further analysis.

Keywords:

yield factors, photovoltaic plant, photovoltaic system

1. INTRODUCTION

Accurate and consistent evaluations of photovoltaic (PV) system performance are critical for the continuing development of the PV industry. These performance parameters allow the detection of operational problems; facilitate the comparison of systems that differ with respect to design, technology or geographic locations.

2. SPECIFIC YIELD FOR SOLAR PHOTOVOLTAIC PLANTS

Parameters describing energy quantities for the PV system and its components have been established by the International Energy Agency (IEA) Photovoltaic power System Program and are described in the IEC standard [1]. The generally definition of yield factors of power plants, expressed in simplified terms, describes how many times energy generated during plant operation covers the energy used for constructing the plant. An exact definition would be: 'The yield factor is the ratio of net energy production during plant life and the cumulative energy used for construction, operation and operating supply items'. This concept is only meaningful in the context of using regenerative energy sources, as photovoltaic plants, insular ore grid connected.

Three of the IEC standard 61724 performance parameters [2] may be used to define the overall system performance with respect to the energy production, solar resource and overall effect of system losses. These parameters are the performance ratio, final PV system yield and reference yield.

The final PV system yield Y_f is the net energy output E_{PV} divided by the nameplate d.c power $P_{maxG,STC}$ (STC – Standard Test Condition 1000 W/m², 25°C) of the installed PV array. It represents the number of hours that the PV array would need to operate at its rated power to provide the same energy. The units are hours or kWh/kW:

$$PR = \frac{AC - \text{GridinjectedEnergy}}{PV\text{SystemEnergyInSTC}} \quad (1)$$

The Y_f normalizes the energy produced with respect to the system size, being a convenient way to compare the energy produced by PV systems of differing size.

The specific plant losses are described through L_c - capture losses, losses that are caused by obfuscation, temperature grown, mismatching, limitation through dust, losses generated by energy conduction in the photovoltaic modules and L_s – system losses, caused by inverter, conduction and loses of passive circuit elements.

The reference yield Y_r is the total in-plane irradiance H divided by the PV's reference irradiance G . It represents the under ideal conditions obtainable energy. If G equals 1 kW/m², then Y_r is the number of peak sun hours or the solar radiation in units of kWh/m². The Y_r

defines the solar radiation resource for the PV system. It is a function of the location, orientation of the PV array, and month-to month and year-to-year whether variability:

$$Y_A = \frac{E_{PV}}{P_{\max G,STC}} \quad (2)$$

To compare on different locations mounted grid connected PV systems, the performance ratio is a decisive value [2]. The performance ratio is the Yf divided by the Yr. By normalizing with respect to irradiance, it quantifies the overall effect of losses on the rated output due to: inverter inefficiency, wiring, mismatch and other losses when converting from d.c. to a.c power, PV module temperature, incomplete use of irradiance by reflection from the module front surface, soiling or snow, system down-time and component failures.

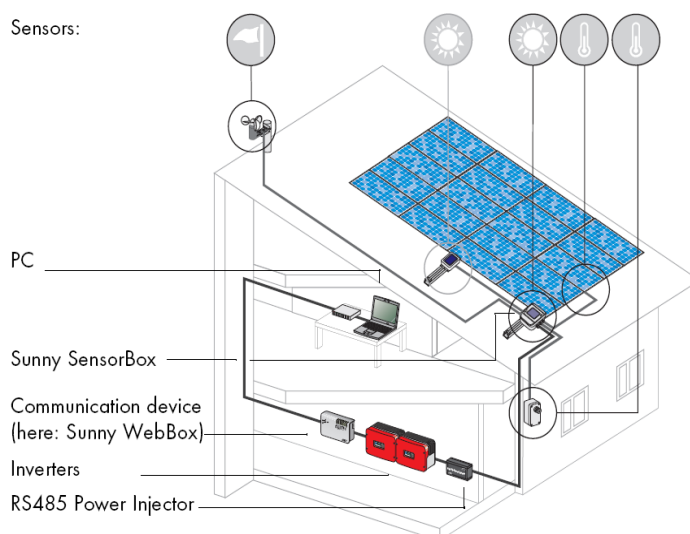
$$Y_f = \frac{E_{PV,AC}}{P_{\max G,STC}} \quad (3)$$

Performance ratio PR values are typically reported on a monthly or yearly basis. Values calculated for smaller intervals, such as weekly or daily, may be useful for identifying occurrences of component failures. Because of losses due the PV module temperature, PR values are greater in the winter than in the summer and normally fall within the range 0.6 to 0.8. If the PV module soiling is seasonal, it may also impact differences in PR from summer to winter. Decreasing yearly values may indicate a permanent loss in performance. Considering the increasing degree of effectiveness, the performance ratio PR factor can reach ideal annual values between 0.8 and 0.84.

The PR being a dimensionless quantity that indicates the overall effect of losses [5] on the rated output, does not represent the amount of produced energy, because a system with low PR in a high solar resource location might produce more energy than a system with a high PR in a low solar resource location. However, for any given system, location and time if a change in component or design increase the performance ratio PR, the final yield Yf increase accordingly. PR values are useful for determinations if the system is operating as expected. Large decrease in PR indicates events that significantly impact performance, such as inverters not operating or circuit-breaker trips. If the PR decrease moderate or small, it indicates that a less severe problem exists. The performance ratio PR can identify the existence of a problem, but not the cause. To identify the cause of the existing problem, a research at the site is needed.

3. GRID CONNECTED PHOTOVOLTAIC PLANT AT THE UNIVERSITY ‘EFTIMIE MURGU’ RESITA

The grid connected photovoltaic system [3] mounted at the ‘summer theater’ of the University ‘Eftimie Murgu’ Resita, since middle of may 2008, is putted together from four high performance standard solar modules of type Multisol 150, manufactured by Scheuten Solar – Germany [6], with a total capacity of 600W/h. The system is completed with a Sunny Boy 1100 inverter and a completely online monitoring system of the PV, made from a Sunny Webbox and the Sunny Sensorbox. This monitoring system [4], build up like in figure 1, allows a detailed supervision of the PV plant, produced energy, measuring and saving values of solar radiation, ambient and module temperature, wind speed and direction.



The measured values and the current energy yield are visualized and archived in the Internet, through the sunny web portal [7], figure 2.

Figure 1 Complete scheme, photovoltaic and monitoring system

4. SPECIFIC YIELD FOR THE SOLAR PHOTOVOLTAIC GRID CONNECTED SYSTEM AT THE EFTIMIE MURGU UNIVERSITY

This paragraph allows us an overview of the specific yield factor Y_A for the grid connected photovoltaic system, for a time period of almost one year, from middle of May 2008 until the end of March 2009. Figure 3 represents the energy production and the specific yield factor for this period. A more detailed, daily, overview of the yield factor in the analyzed period is given in table 1.

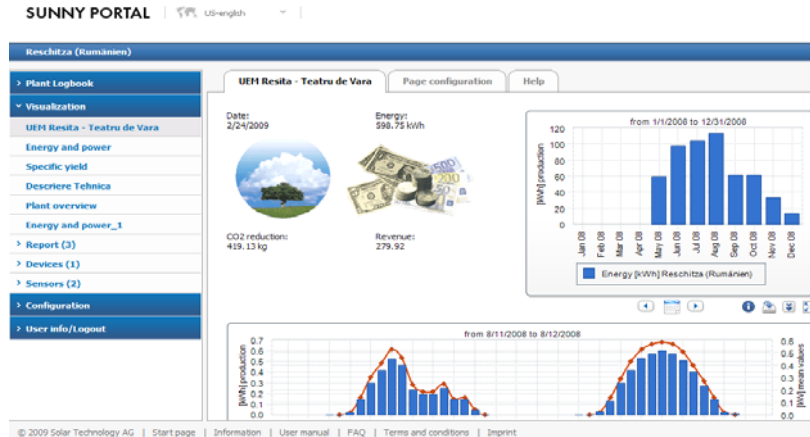


Figure 2 Sunny web portal on-line monitoring

Energy production and Specific Yield

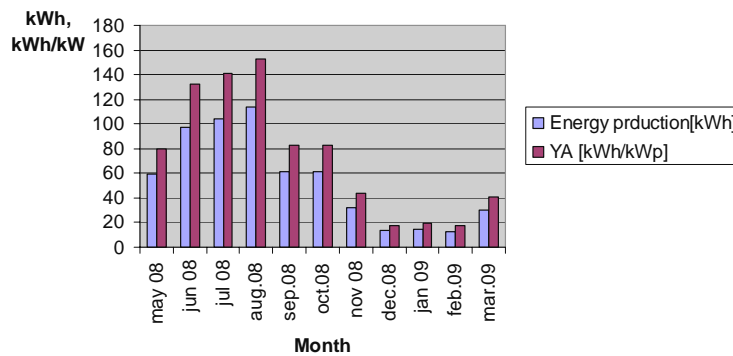


Figure 3. Energy production and array yield
Table 1 Daily Specific Yield Factor

	Specific Yield Factor - YA [kWh/kWp]										
	may 2008	jun. 2008	jul. 2008	aug. 2008	sept. 2008	oct. 2008	nov. 2008	dec. 2008	jan. 2009	febr. 2009	mart. 2009
1	0,00	4,72	5,78	6,49	5,65	4,64	1,57	2,30	0,12	2,32	0,00
2	0,00	5,15	5,99	5,80	4,54	1,59	1,61	1,84	0,00	1,69	0,03
3	0,00	6,11	5,76	5,69	5,39	3,80	2,68	0,27	0,22	0,85	1,31
4	0,00	5,22	4,96	5,61	5,18	2,43	2,28	0,51	0,24	1,15	3,62
5	0,00	3,65	3,92	5,81	5,24	0,12	1,12	1,68	0,24	0,97	1,05
6	0,00	2,12	6,08	6,28	5,68	2,51	1,70	0,16	0,77	3,26	4,73
7	0,00	1,78	5,80	5,78	4,82	2,89	2,35	0,12	2,16	2,66	0,30
8	0,00	2,16	4,51	5,76	2,97	2,54	1,24	0,38	0,01	1,89	0,39
9	0,00	2,45	4,95	2,46	5,73	2,09	1,66	0,49	0,64	0,09	3,11
10	0,00	1,96	3,22	4,81	5,28	2,88	2,95	1,74	1,11	1,93	1,61
11	0,00	5,34	5,99	4,73	3,82	3,89	2,69	0,85	0,38	0,32	2,53
12	0,00	4,46	5,81	6,08	3,86	4,27	2,53	0,19	1,07	0,00	0,97
13	0,00	3,88	5,65	5,86	0,82	3,59	2,36	0,54	0,76	0,00	0,72
14	0,00	2,96	4,61	5,28	1,07	2,09	1,28	1,73	0,65	0,00	3,95
15	1,58	2,32	1,15	5,85	0,15	3,50	2,30	1,24	0,22	0,00	6,35
16	5,59	5,27	3,53	4,95	0,69	3,59	2,36	0,88	0,08	0,00	0,50
17	4,68	5,70	5,11	5,28	0,57	0,12	0,20	0,89	1,70	0,00	0,80
18	5,39	3,41	4,97	6,14	0,35	4,23	1,27	0,05	2,57	0,00	0,24
19	4,70	3,41	5,93	6,23	1,07	3,64	0,39	0,12	2,03	0,00	3,11
20	5,24	5,36	6,12	5,97	0,55	3,89	2,24	0,08	2,32	0,00	4,77
21	3,72	5,89	5,08	5,57	0,69	3,62	0,09	0,11	0,45	0,00	1,85
22	0,76	6,00	0,51	4,45	1,64	3,61	0,38	0,49	0,80	0,00	5,15
23	4,85	1,89	1,23	4,26	3,14	3,43	0,14	0,15	0,46	0,00	0,00
24	6,62	5,58	2,19	1,89	2,51	0,18	0,95	1,70	0,22	0,00	0,00
25	4,74	5,84	1,11	4,53	0,64	0,30	0,16	0,01	0,31	0,00	0,00
26	5,05	5,70	2,70	6,18	0,80	0,64	0,04	0,08	0,20	0,00	0,00
27	5,85	5,20	6,09	3,89	0,58	3,39	0,77	0,04	0,95	0,00	0,00
28	5,73	1,76	5,11	3,59	1,73	3,20	1,88	0,05	0,08	0,00	0,00
29	6,08	5,95	5,70	1,26	2,66	1,76	1,18	0,00	0,09	0,00	0,00
30	5,59	6,03	6,14	3,97	4,89	1,15	2,57	0,01	0,18	0,00	0,00
31	5,32	0,00	6,14	5,23	0,00	3,15	0,00	0,01	0,55	0,00	0,00

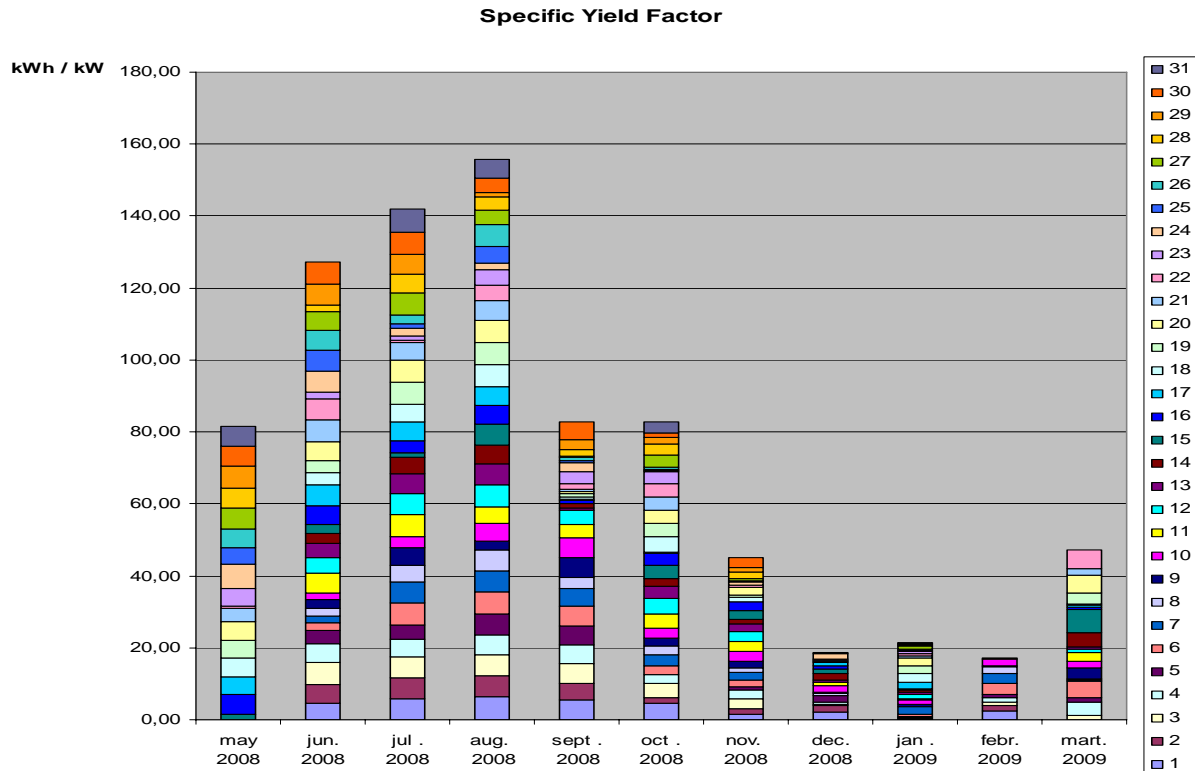


Figure 4 Daily yield factor, May 2008 – March 2009

5. CONCLUSIONS

Analyzing the specific yield factor, the photovoltaic plant owner can have a permanent look of the time, in hours expressed, that the system works in STC and obtains indicate or a higher energy production. As shown, during summer the yield factor has a much higher density in June, July and August and the lowest in December, January and February.

REFERENCES

- [1] IEC, `Photovoltaic System Performance Monitoring – Guidelines for measurement, Data Exchange and Analysis, IEC Standard 61724`, Geneva, Switzerland, 1998
- [2] Energy yield factors for the generation of electrical energy, www.sealnet.org
- [3] Cristian P. Chioncel, Petru Chioncel, Berinde Florin, Gilbert-Rainer Gillich *Monitoring system for photovoltaic power plant*, Analele Universității “Eftimie Murgu” Reșița, Fascicola de Inginerie, ISSN 1453-7394, 2006
- [4] Cristian P. Chioncel, Dieter Kohake, Petru Chioncel, Nicoleta Gillich *Solar photovoltaic monitoring system implemented on the location Resita*, Analele Universității “Eftimie Murgu” Reșița, Fascicola de Inginerie, ISSN 1453 – 7394, 2008
- [5] www.iea-pvps-task2.org Performance of Photovoltaic-Anlagen: Resultate einer internationalen Zusammenarbeit im IEA-PVPS Task 2
- [6] www.scheutensolar.com
- [7] www.sunnyportal.com



PERFORMANCE RATIO OF A PHOTOVOLTAIC PLANT

¹Cristian P. CHIONCEL, ¹Ladislau AUGUSTINOV, ¹Petru CHIONCEL,
¹Nicoleta GILLICH, ²Gelu Ovidiu TIRIAN

¹“Eftimie Murgu” University, Resita, ROMANIA

² UPT – Faculty of Engineering, Hunedoara, ROMANIA

Abstract

Based on the grid connected photovoltaic plant at the University ‘Eftimie Murgu’ in Resita, injecting energy in the public grid since spring 2008, we define and analyze the performance ratio and the final yield factor. With these two factors given, we are able to assure a critic overview of the plant performance.

1. INTRODUCTION

To be able to choose the right photovoltaic equipment, starting from modules through inverters, for grid connected plants, at least one year of consistent evaluations of system performance are needed. One of those performance parameters that allow the detection of operational problems and facilitate the comparison of systems is given by the final yield factor and the performance ratio.

2. YIELD FACTOR AND PERFORMANCE RATIO FOR GRID CONNECTED SOLAR PHOTOVOLTAIC PLANTS

The International Energy Agency (IEA) for Photovoltaic Power System Program has define, based on existing experience, a number of performance parameter for photovoltaic plants, that are now concentrated in the IEC standard [1], concept that are only meaningful in the context of using regenerative energy sources, as photovoltaic plants, insular ore grid connected. The main parameters are performance ratio and the final PV system.

The performance ratio PR is defined as the energy output E_{PV} that is injected in the grid, AC part, divided by the nameplate d.c power $P_{maxG,STC}$, obtained in Standard Test Condition (STC - 1000 W/m², 25°C) of the installed PV array. It represents the number of hours that the PV array operates at its rated power.

$$PR = \frac{AC - GridinjectedEnergy}{PVSystemEnergyInSTC} \quad (1)$$

Performance ratio PR values are typically reported on a monthly or yearly basis. Another yield value is the final Yield factor. As the performance ratio, it expresses plant performance on the AC site. It is definite as the monthly grid injected energy divided to the nameplate power of the photovoltaic generator in standard test conditions. The result offers an overview referring to monthly pro one kWp plant power, in the grid injected energy, ore the so called monthly specific energy production.

$$Y_f = \frac{E_{PV,AC}}{P_{maxG,STC}} \quad (3)$$

PR values calculated can be also calculated for smaller intervals, such as weekly or daily. This is may be useful for identifying occurrences of component failures. Depending on geographical location and season the PR values fall normally within the range 0.2 to 0.8. If PR decreases yearly, this may indicate a permanent loss in performance. Ideal annual values for the performance ratio PR factor are between 0.8 and 0.84.

PR does not indicate the amount of produced energy, because a system with low PR in a high solar resource location might produce more energy than a system with a high PR in a low solar resource location. But however, for any given system, location and time an increase of the performance ratio PR supposes accordingly an increase of the final yield Y_f too.

If PR registers a deep decrease, that indicates events with significant performance impact, like inverters that are not operating proper. When the PR decrease moderate, this indicates that the plant has less severe problems. So, based on the performance ratio PR analyzes, it can be clearly identified if the systems work like plant ore problems exist, but not the cause.

3. GRID CONNECTED PHOTOVOLTAIC PLANT AT THE UNIVERSITY ‘EFTIMIE MURGU’ RESITA

The grid connected photovoltaic system [3] mounted at the University ‘Eftimie Murgu’ Resita, has in his structure, following components: four high performance standard solar modules of type Multisol 150, manufactured by Scheuten Solar – Germany [6], with a total capacity of 740W/h; a Sunny Boy 1100 inverter and a completely online monitoring system [7] of the PV system: Sunny Webbox and Sunny Sensorbox (solar radiation, ambient and module temperature, wind speed and direction).



Figure 1. The solar photovoltaic modules and equipment at the “E.Murgu” University Resita

4. PERFORMANCE RATIO AND FINAL YIELD FACTOR FOR THE GRID CONNECTED PV SYSTEM AT THE “EFTIMIE MURGU” UNIVERSITY

In this paragraph we will obtain an overview of the final yield factor Y_f for the grid connected photovoltaic system, from May 2008 until the March 2009. Figure 2 represents the monthly performance ratio; figure 3 the final yield factor for this period. A comparison between those two plant performances indicators are given in figure 4.

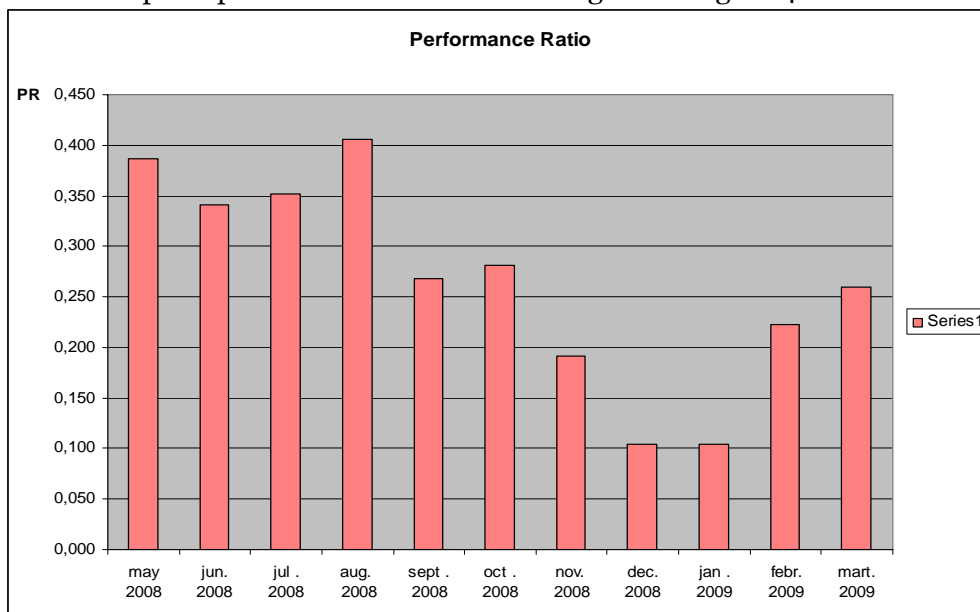


Figure 2. Monthly grid connected PV system performance ratio, May 2008 – March 2009

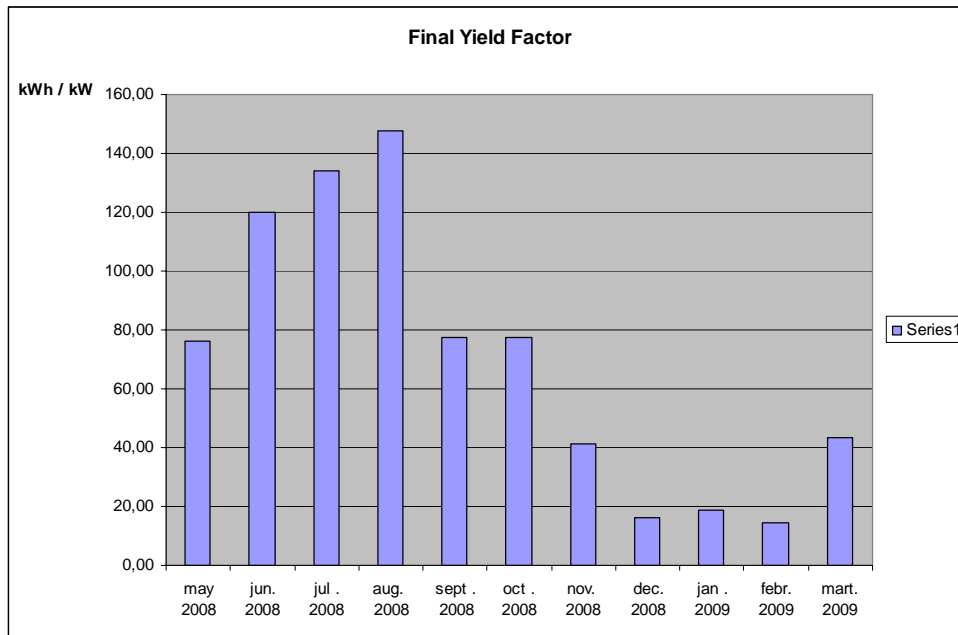


Figure 3. Final yield factor, May 2008 – March 2009

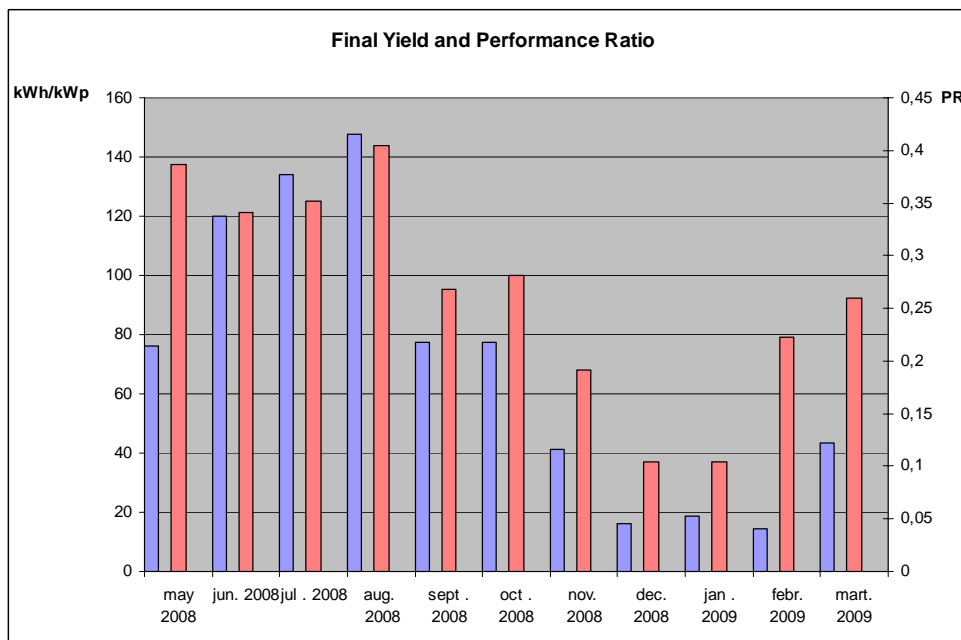


Figure 4. Comparison between Final Yield and Performance Ratio, May 2008 – March 2009

5. CONCLUSIONS

Based on the analyze of the final yield factor and the performance ratio of an photovoltaic grid connected plant, we can always have a overview of the plants performance and check in the right if we register system losses.

REFERENCES

- [1.] IEC, `Photovoltaic System Performance Monitoring – Guidelines for measurement, Data Exchange and Analysis, IEC Standard 61724`, Geneva, Switzerland, 1998
- [2.] Energy yield factors for the generation of electrical energy, www.sealnet.org
- [3.] Cristian P. Chioncel, Petru Chioncel, Berinde Florin, Gilbert-Rainer Gillich *Monitoring system for photovoltaic power plant*, Analele Universității “Eftimie Murgu” Reșița,

- Fascicola de Inginerie, ISSN 1453-7394, 2006
- [4.] Cristian P. Chioncel, Dieter Kohake, Petru Chioncel, Nicoleta Gillich *Solar photovoltaic monitoring system implemented on the location Resita*, Analele Universității “Eftimie Murgu” Reșița, Fascicola de Inginerie, ISSN 1453 – 7394, 2008
- [5.] www.iea-pvps-task2.org *Performance of Photovoltaic-Anlagen: Resultate einer internationalen Zusammenarbeit im IEA-PVPS Task 2*
- [6.] www.scheutensolar.com
- [7.] www.sunnyportal.com



PREDICTION OF THE SIGNALS USING THE NEURONAL NETWORKS

¹ Gelu Ovidiu TIRIAN, ¹Stela RUSU-ANGHEL, ²Camelia PINCA-BRETOTEAN

¹ "Politehnica" University of Timisoara, Faculty of Engineering of Hunedoara,
Department of Electrical Engineering and Industrial Informatics, ROMANIA

² "Politehnica" University of Timisoara, Faculty of Engineering of Hunedoara,
Department of Engineering and Management, ROMANIA

Abstract:

This paper work refers to the prediction problems which are used with the help of the neuronal networks. The network is made of a neuron whose function is linear and who has the past few 5 input values of the useful signal $x(t)$ – this signal must be predicted.

The training algorithm is Widrow-Hoff. This algorithm decreases the number of square errors between the output of the network and the required value, and it eventually establishes the "weight" factor.

Keywords:

Prediction, algorithm, neuronal networks, signal

1. INTRODUCTION

This identification [2], [3] is based on some neuronal methods and it has been lately used a research method due to mathematical research about the approximation properties of the neuronal networks - MLP (Multilayer Perceptron) and RBF (Radial-Basis Function) type [1]. The development of this new domain has been spectacular due to a remarkable contribution of some Automatics scientists. They have used the MLP networks for the non-linear identification and they have decided to use the RBF-type patterns. Thus, we have to point out the fact that the most important automatic application of those techniques, who are specific for the neuronal networks, is the use of the MLP features with sinoid nodes inside the hidden layer(s). On the other hand, those companies who produce technical-scientific software have begun developing specific facilities for the neuronal networks, so that the first version of the Neuronal Network Toolbox (NNT) should be enclosed in the MATLAB 4.2 environment – it had a major impact on the interest of the automatics specialists. NNT, from the earliest to the most recent version, has been designed to cover a range of applications of the neuronal networks, the designers had no intention to develop the Simulink blocks simultaneously [4]. These blocks are used for designing dynamic patterns.

2. NEURONAL NETWORKS. TRAINING NEURONAL NETWORKS

The neuronal networks can be made of simple processing elements, such as perceptrons or neurons (Figure no. 1), and they make up one-layer networks, or of multiple elements and they make up multi-layer networks [1]. All these network-types enclose some elements that are distributed within the connection „weights" amongst different layers that make up each network [6]. The properties of the neuronal networks are: contain memory, shape acknowledgment, control and identification of the non-linear processes, etc. These properties are obtained through learning, such as in the case of the physiological systems. Specific training algorithms could be used in order to determine the values of those weights/percentages who represent the solution to the problems we solve by using the neuronal networks. The training algorithms could be divided in two separate categories: supervised instruction methods and non-supervised instruction methods. In the case of those methods belonging to the first category, the instruction is called supervised because we know both the input and the output sizes. The system is shaped up with the help of a neuronal network and the weight amongst the layers have random values. By comparing the input sizes that we already know and those of the output of the network (after we have used the input data set), we get an error signal. This signal helps us establish

and adjust the weights amongst the layers of the network, in order to diminish a performance criterion [8].

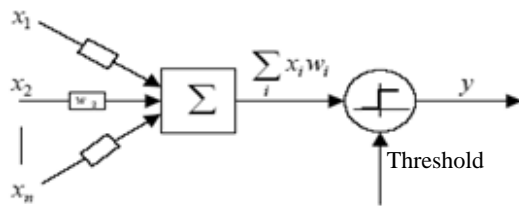


Figure no. 1 Classic perceptron model

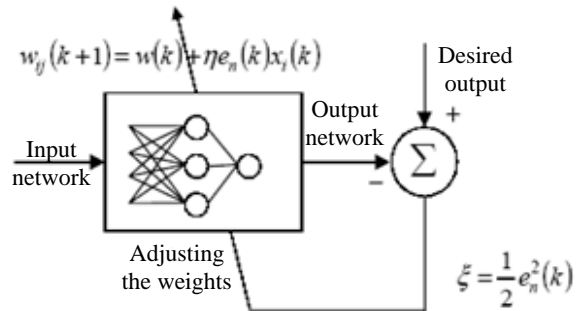


Figure no. 2 Supervised instruction mechanism for neuronal networks

The non-supervised learning methods do not use already-known input sizes during the training stage of the neuronal network, by using only the input sizes for adjusting the weights. Thus, we can establish some input categories who correspond to some inputs from the data set, or „winner take all” outputs – in this case, the output neuron who has the highest activity wins and turns active, meanwhile the others do not work. This method is called self-organisation and we could use it successfully in matters of shape acknowledgement.

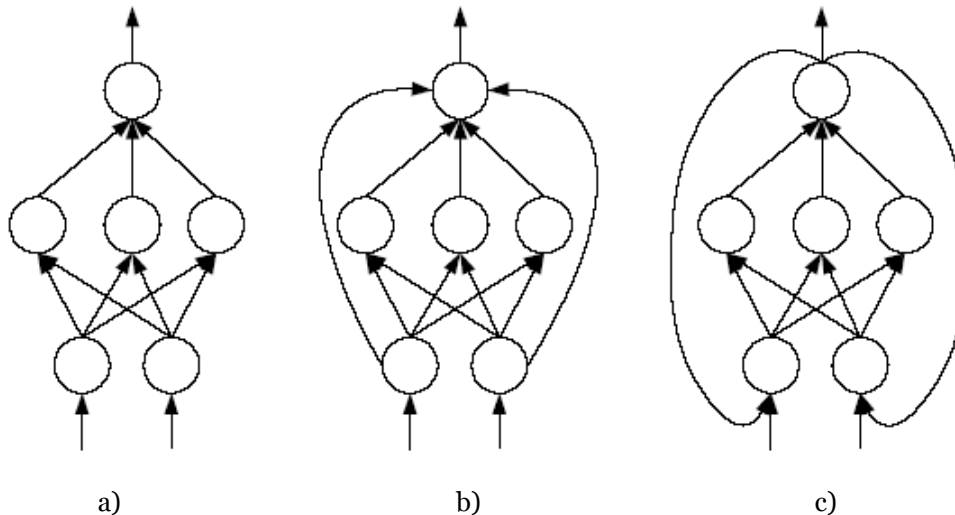


Figure no. 3 „Feed forward” neuronal networks topologies a), b) and „feedback” neuronal networks topology c)

According to this topology, the artificial neuronal networks could be classified in two categories - „feedback” and „feed forward”. In the case of a „feed forward” network the neuronal output is sent to other neurons who do not receive any information from the input neurons from the surface layers - Figure 3 a) and b).

3. NEURONAL NETWORKS USED FOR SIGNAL PREDICTION

The design of the linear prediction neuron is described in Figure no. 4. The network is made of a linear active neuron and the input receives the last five values of the useful signal $x(t)$ - this signal must be predicted [4], [7].

We write the matrix P , $p = [x(t) \ x(t-1) \ x(t-2) \ x(t-3) \ x(t-4)]$, and the five delay values of the $x(t)$ signal, who are going to be represented at the input of the neuronal network. The matrix and the values are going to represent the data we need for the supervised training, by using the Widrow-Hoff algorithm. This algorithm decreases the sum of the square errors between the output and the required value, and establishes the weight vector who is able to solve the problem.

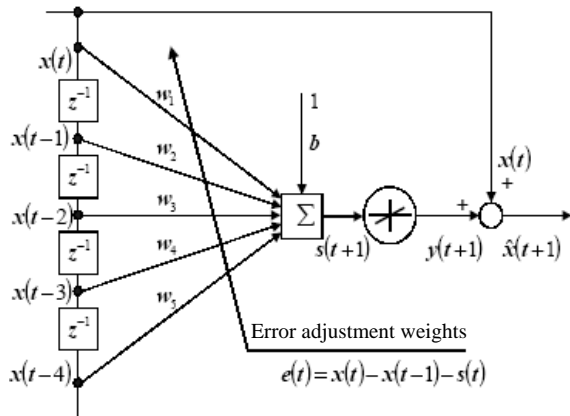


Figure no. 4 Linear prediction neuron

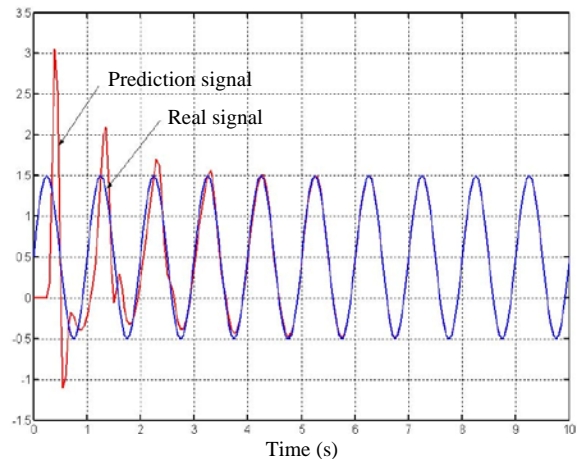


Figure no. 5 The proposed sinusoidal signal (blue) and the network predicted signal (red)

We consider a sinusoid signal $x(t) = 0.5 + \sin(2 \cdot \pi \cdot t)$ - in Figure no. 5 it is coloured in blue. The learning ratio of the training algorithm is $\eta = 0.1$, considering that it is constant during the training process. The network turns active and the training algorithm is used for a period of 200 steps. We could see that after about 100 repetitions the network is able to predict the signal we propose – Figure no. 5, where the red signal represents the output of the neuronal network during the training process. Figure no. 6 describes the prediction error - the difference between the real and the predicted signal. This signal tends to reach 0 after a certain time.

Figure no. 7 describes the values of the simple perception weights during the training process. The identification time of the process lasts according to the value we choose for the learning ratio. If we want a faster identification then, the value must be increased, but the values we have estimated during the first stages reach important values. We could also use another training method that should vary the learning ratio throughout the process, for improving the methods.

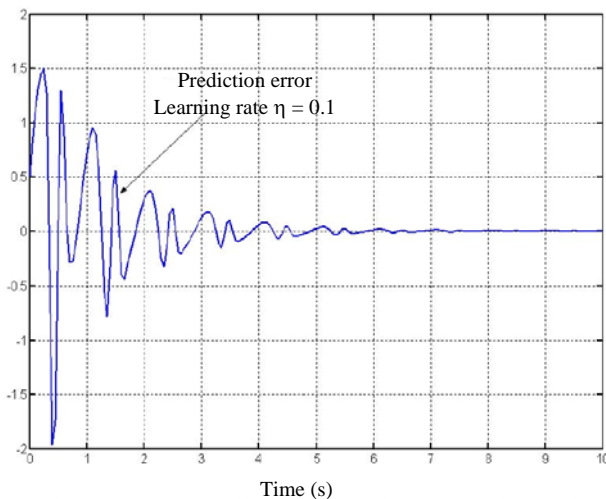


Figure no. 6 Prediction error between the real and predicted signal

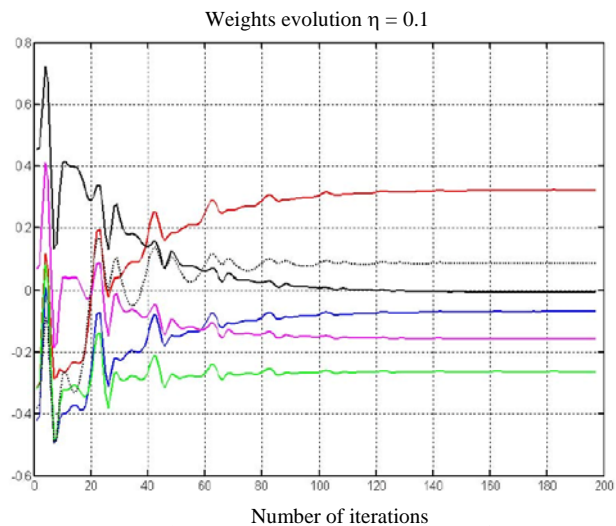


Figure no. 7 The evolution of the weights during the training process

4. CONCLUSIONS

All the neuronal networks could be made of simple processing elements, such as perceptions or neurons, so they should make up some single-layer networks, or made of several elements and they should make up some multi-layer networks. The „information” within all these networks is distributed within the connection weights amongst the different layers that make the network. Studies have proven that the prediction of the neuronal networks signals is extremely effective.

This paper work has described the linear neuron used for predictions, the training process, and the results we had obtained. The network is made of one neuron, according to the linear active process, which has the last five input values we have to predict.

REFERENCES

- [1] Dumitrescu, D., Costin, H. „Rețele neuronale teorie și aplicații” Editura Teora, 1996.
- [2] Ljung, L. “System Identification” Theory for the User Prentice Hall, Inc., Englewood Cliffs, New Jersey 07632.
- [3] Ljung, L., Soderstrom T. “Theory and Practice of Recursive Identification”, MIT Press, 1983.
- [4] Muktani, M, Marie, M. ”Engineering Application of Matlab 5.3”, Springer, 2000.
- [5] Narendra, K. S., Parthasaraty, K. “Identification and Control of Dynamical Systems Using Neural Networks”, IEEE Transactions on Neural Networks, vol. 1 nr. 1 1990, pag. 4-27.
- [6] Tirian G.O. „High speed neuronal estimator for the command of the induction machine” International multidisciplinary scientific symposium ”UNIVERSITARIA SIMPRO 2006” October, 13-14, pg.62...65, 2006.
- [7] G.O.Tirian „Abordari moderne in estimarea si identificarea sistemelor”, Referat doctorat, Timisoara, 2005.
- [8] Widrow, B., Lehr, M. A. “30 Years of Adaptive Neural Networks: Perceptron, Madaline and Backpropagation”, Proceedings of IEEE, vol. 78 nr. 9 1990, pag. 1415-1439



ERROR HANDLING AND MESSAGES WITH APPLICATION SERVER ABAP

¹CRISTEA Ana Daniela, ²BERDIE Adela Diana

¹ NWCON Technology Consulting GmbH, GERMANY

²University of Timisoara , Faculty of Engineering Hunedoara, ROMANIA

ABSTRACT

Application Server ABAP is an integrated part of the application platform within SAP NetWeaver. In this paper we will present the tools and concepts we can use to develop solid ABAP based applications, that deal with the error and problem situations occurring in our programs. We catch exceptions and describe it for the end user. We use client-side validation and server-side validation to inform the user about the program status and exceptions occur. ABAP offers us full support to do that through exception classes, message classes, assistance classes, a special Hook method in Web Dynpro ABAP, a special control structure for catching exceptions and more.

1. INTRODUCTION

SAP NetWeaver is an infrastructure software that supports the integration and development of heterogeneous system landscapes as they are typically found in companies today [1].

Application platform of the SAP NetWeaver integration platform has two stacks: ABAP stack and Java stack or Application Server ABAP and Application Server Java with two programming interfaces ABAP and respective Java.

Application Server ABAP (AS ABAP) offers us through ABAP language many possibilities to handle the exceptions that occurs in our applications, offers us tools to develop robust programmes. A good user interface catch exceptions and describes for the user the errors that occurs.

One of the key quality criteria for software is the robustness of a program. It should be able to deal with the situation and should not crash [2].

In ABAP we have classical exception handling and class based exception handling. The SAP documentation [3] recommends us to use class based exception handling where every exception class derives directly or indirectly from the CX_ROOT super-class.

To structure possible exceptions we have three abstract exception classes that derive from CX_ROOT super-class. Fig. 1 shows the exception classes relationship [4].

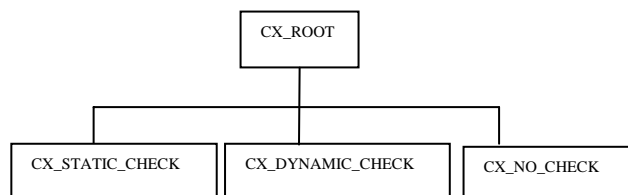


Fig. 1 The tree of exception classes in ABAP

We can handle an exception in an ABAP programme with TRY - ENDTRY control structure. Fig. 2 shows an example of catching and handling exceptions.

The messages that we can use in ABAP language are "A" termination message, "E" error message, "I" information message, "S" status message, "W" warning message , "X" exit message and define how the ABAP runtime should process the message [5].

When an exception is raised using RAISE EXCEPTION, the runtime environment searches for a handler. Once a handler is found, the control flow processes the code of the handler before continuing. If no handler can be found, the program ends with a runtime error.

We can use catch CX_ROOT to catch all errors that occurs.

```

Report      YTRY_ENDTRY      Active
19  FIELD-SYMBOLS <fs_ytb_student> LIKE LINE OF it_ytb_student.
20  DATA: oref TYPE REF TO zcx_exception_otr,
21         text TYPE string.
22
23  START-OF-SELECTION.
24  text = pr_matr.
25  TRY.
26      SELECT mandant matricol nume datan ex_promovate
27      FROM ytb_student
28      INTO TABLE it_ytb_student
29      WHERE matricol = pr_matr.
30  LOOP AT it_ytb_student ASSIGNING <fs_ytb_student>.
31      WRITE:/ <fs_ytb_student>-mandant,
32             <fs_ytb_student>-matricol,
33             <fs_ytb_student>-nume,
34             <fs_ytb_student>-datan,
35             <fs_ytb_student>-ex_promovate.
36  ENLOOP.
37  IF sy-subrc <> 0.
38      RAISE EXCEPTION TYPE zcx_exception_otr
39  EXPORTING
40      textid = zcx_exception_otr=>zcx_exception_otr1
41      parameter1 = text.
42  ENDIF.
43  CATCH zcx_exception_otr INTO oref.
44  MESSAGE oref TYPE 'I'.
45  ENDTRY.
    
```

```

TRY.
  [try_block]
[CATCH cx_class1 cx_class2 ...
  [catch_block]]
  ...
[CLEANUP [INTO oref].
  [cleanup_block]]
ENDTRY.
    
```

Fig. 2 TRY-ENDTRY structure example

2. THE STUDY

2.1 WORKING WITH EXCEPTION CLASSES AND TEXTS FOR XCEPTIONS

Each exception has assigned a text that describes the exception and can be for example Online Text Repository (OTR) text or text from a message class.

OTR is a central place for texts that offers us tools for its processing and administration. The texts that are stored here can contain maximum 255 characters [6].

We can create our own exception classes as global classes with Class Builder or as local classes in our programs. Some of the advantages of using class-based exception handling are [7]:

- ✚ Object-oriented concept of inheritance
- ✚ Exception classes have integration with ABAP message concept
- ✚ Exception class can hold many different types of exceptions

```

Function module  YFM_WITH_EXCEPTION_CLASS      Active
Attributes      Import      Export      Changing      Tables      Exceptions      Source code
4  ** IMPORTING
5  ** REFERENCE (IN_IDPROD) TYPE YTIPD-IDPROD
6  ** EXPORTING
7  ** REFERENCE (EXP_YTIPD) TYPE YTAB_YTIPD
8  ** RAISING
9  ** YCX_EXCEPTION_CLASS_OTRTEXT
10 **
11 data oref type ref to ycx_exception_class_otrtxt.
12 try.
13 select *
14 from ytipd
15 into table exp_ytipd
16 where idprod = in_idprod.
17 if sy-subrc <> 0.
18 raise exception type ycx_exception_class_otrtxt
19 exporting
20 textid = ycx_exception_class_otrtxt=>ycx_exception_txt
21 id = in_idprod.
22 endif.
23 catch ycx_exception_class_otrtxt into oref.
24 message oref type 'E' display like 'I'.
25 endtry.
26 endfunction.
    
```

Fig. 3 Exception class and Function Module

Fig. 4 shows the new defined exception id and attribute for this exception class. In the Text tab we can find the exception id YCX_ECEPTION_TXT that we have used in our Function Module.

Class Interface: YCX_EXCEPTION_CLASS_OTRTEXT (Implemented / Active)

Exception ID	Text
CX_ROOT	An exception occurred
YCX_EXCEPTION_CLASS_OTRTEXT	Action not supported!
YCX_EXCEPTION_TXT	The id &id& don't exist!

Attribute	Level	Visi...	Re...	Typing	Associated Type
<CX_ROOT>	Consta...	Publ...	<input type="checkbox"/>	Type	S0TR_CONC
CX_ROOT	Consta...	Publ...	<input type="checkbox"/>	Type	S0TR_CONC
TEXTID	Instanc...	Publ...	<input checked="" type="checkbox"/>	Type	S0TR_CONC
PREVIOUS	Instanc...	Publ...	<input checked="" type="checkbox"/>	Type Re...	CX_ROOT
KERNEL_ERRID	Instanc...	Publ...	<input checked="" type="checkbox"/>	Type	S380ERRID
YCX_EXCEPTION_TXT	Consta...	Publ...	<input type="checkbox"/>	Type	S0TR_CONC
YCX_EXCEPTION_CLASS...	Consta...	Publ...	<input type="checkbox"/>	Type	S0TR_CONC
ID	Instanc...	Publ...	<input type="checkbox"/>	Type	YTIPD-IDPROD

Fig. 4 The structure of YCX_EXCEPTION_CLASS_OTRTEXT

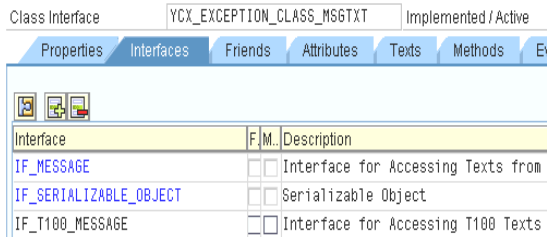


Fig. 5 Exception class with message class

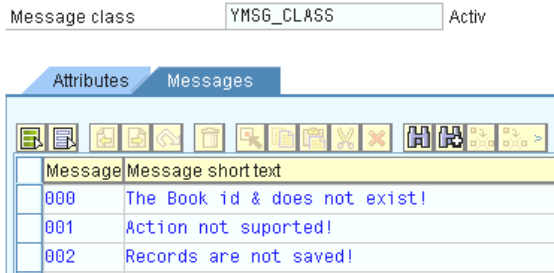


Fig. 6 Message Class YMSG_CLASS

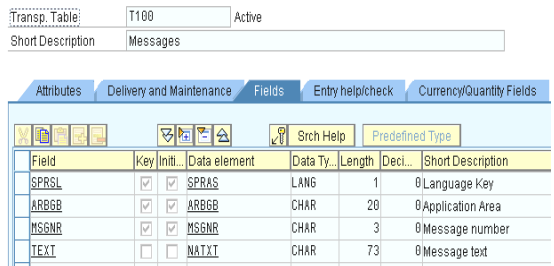


Fig. 7 The structure of T100 database table

Each exception id can be mapped to a message id from our message class. In Fig. 8 is shown a mapping example. As can be seen when we use text from a message class we have a restriction to maximum four placeholders. We can assign maximum four attributes from the exception class.

Fig. 9 illustrates the way we can use our exception class into an ABAP class that selects data from a database table through the help of SQL statements.

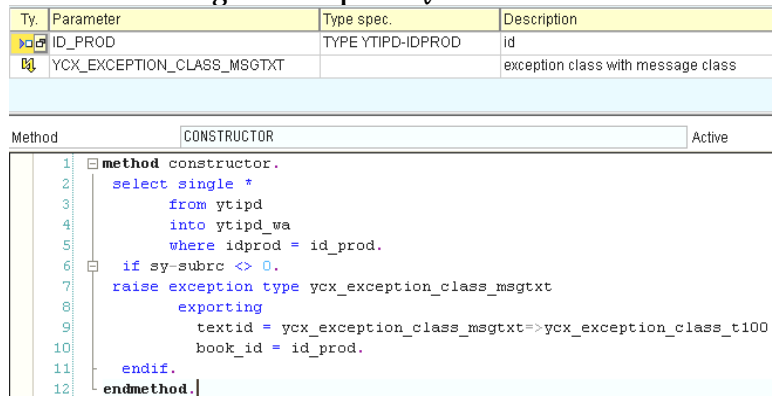


Fig. 9 ABAP class and exception class

B. Exception class with text from a message class

We create an exception class YCX_EXCEPTION_CLASS_MSGTXT with text from a message class. In this case exception class implements the interface IF_T100_MESSAGE and we can use exception texts from database Table T00.

Fig. 5 shows the defined exception class.

Before we can use this class we have to create a Message Class and assign it to our exception class. In Fig. 6 we presented the Message Class YMSG_CLASS, created with Message Maintenance SE91.

Messages are stored in the database Table T100 that has columns as: message number, short text, language key. Fig. 7 shows the structure of this table.

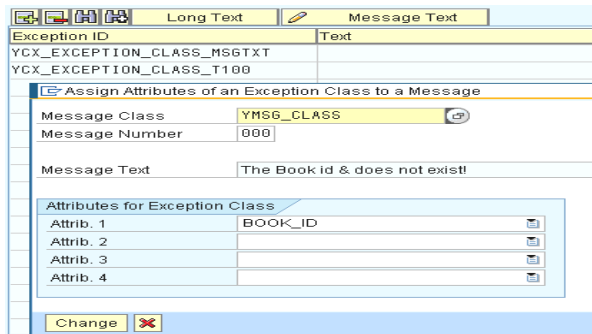


Fig. 8 Exception id mapped to message class and message number

2.2. MESSAGES, EXCEPTIONS AND WEB DYNPRO ABAP

Web Dynpro ABAP is the SAP Framework that uses Model View Controller MVC paradigm in order to build reusable multi-component web business applications.

Through a What You See Is What You Get view editor we can simply drag and drop the UI Elements that we need and we have fully support to work with messages [8].

The presentation of messages in the client is controlled by Web Dynpro Framework and Hook method wddobeforeaction() can us help to react to user inputs [9].

A. Exception class and Web Dynpro ABAP

Web Dynpro ABAP offers us support to work with exception classes through methods of the Message Manager.

In Fig. 10 we present the way we can use in a Web Dynpro application, the class defined hereinbefore. What is more important is the fact that we can catch the proper exception and show it in browser in a MessageArea UI Element.

```

4      data lr_node type ref to if_wd_context_node.
5      data ls_data type if_view_books=>element_search.
6      data: lv_idprod type ytipd-idprod.
7      lr_node = wd_context->get_child_node( 'SEARCH' ).
8      lr_node->get_attribute( exporting name = 'IDPROD'
9                             importing value = lv_idprod ).
10     data oref type ref to ycx_exception_class_msgtxt.
11     try.
12         create object model exporting id_prod = lv_idprod.
13         l_value_wa = model->ytipd_wa.
14     catch ycx_exception_class_msgtxt into oref.
15         data: l_current_controller type ref to if_wd_controller,
16               l_message_manager type ref to if_wd_message_manager.
17         l_current_controller ?= wd_this->wd_get_api( ).
18         l_message_manager = l_current_controller->get_message_manager( ).
19         * report message
20         l_message_manager->report_exception(
21             message_object = oref ).
22     entry.
    
```

Fig. 10 Catch and show of the exception message

All the messages that are shown with Web Dynpro ABAP are displayed as default at the begin of the screen. In our case we want to change this position and in this purpose we use a MessageArea UI Element. In fig. 11 we show the proper User Interface.

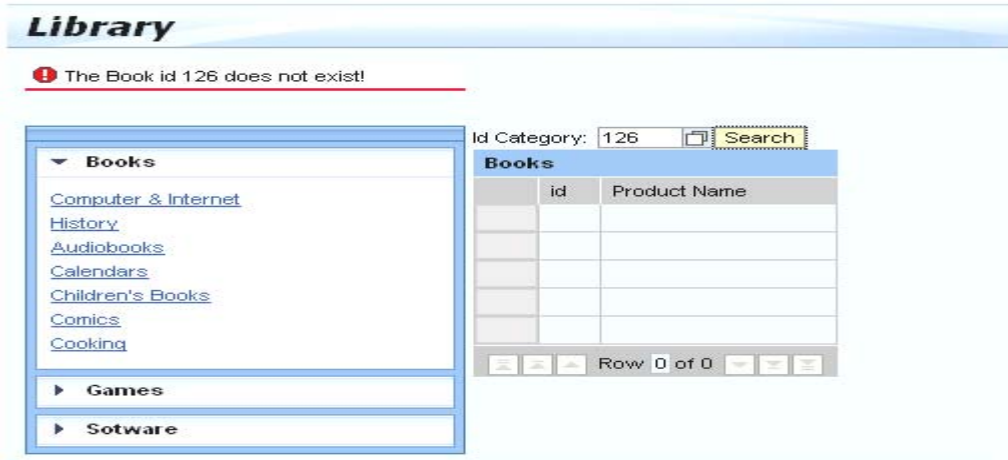


Fig. 11 The User Interface with Web Dynpro ABAP

B. Assistance class and Web Dynpro ABAP

An assistance class is a regular ABAP class that inherits the CL_WD_COMPONENT_ASSISTANCE. Every Web Dynpro component has assigned just an assistance class that we can use as Model or to work with text symbols.

The class CL_WD_COMPONENT_ASSISTANCE provides central functions by which a Web Dynpro component can access text symbols of the assistance class [10]. As advantages of using assistance class we can specify [11]:

- ✚ Method calls of the assistance class have more performance as calls of methods of a Web Dynpro controller.
- ✚ Manage dynamic texts

In Fig. 12 we present the text symbols that we have defined for a created assistance class YCL_ASSISTANCE_CLASS_MSG.

Sym	Text	dLen	mL...
000	The registration data are successful saved!	44	60
001	All Fields have to be filled!	28	30
002	Email adress it is wrongh. Pleas restore!	41	60

Fig. 12 Text symbols of assistance class

Ty.	Parameter	Type spec.	Description
Y	FIRST_NAME	TYPE YREGISTRATION-FIRSTNAME	First Name
Y	LAST_NAME	TYPE YREGISTRATION-LASTNAME	Last Name
Y	EMAIL	TYPE YREGISTRATION-EMAIL	Email
Y	MESSAGE	TYPE YREGISTRATION-MESSAGE	Message
EX	YCX_EXCEPTION_CLASS_MSGTXT		exception class with message class

```

Method: INSERT_VALUES Active
1 method insert_values.
2 data: provider_wa like line of search_wa.
3 call function 'YFM_SEARCH' importing value = linet.
4 try.
5     provider_wa-id = linet + 1.
6     provider_wa-firstname = first_name.
7     provider_wa-lastname = last_name.
8     provider_wa-email = email.
9     provider_wa-message = message.
10    insert provider_wa into table search_wa.
11    insert registration from table search_wa.
12    if sy-subrc <> 0.
13        raise exception type ycx_exception_class_msgtxt
14        exporting
15            textid = ycx_exception_class_msgtxt->ycx_no_saved.
16    endif.
17 endtry.
18 endmethod.
    
```

Fig. 13 Method of our assistance class

```

View: VIEW_BOOKS Active
Method List: ONACTIONSAVEDATA
13 importing value = lv_firstname ).
14 lr_node->get_attribute( exporting name = 'LASTNAME'
15 importing value = lv_lastname ).
16 lr_node->get_attribute( exporting name = 'EMAIL'
17 importing value = lv_email ).
18 lr_node->get_attribute( exporting name = 'MESSAGE'
19 importing value = lv_message ).
20 try.
21 model->insert_values( first_name = lv_firstname
22 last_name = lv_lastname
23 email = lv_email
24 message = lv_message ).
25 catch ycx_exception_class_msgtxt into orref.
26 data: l_current_controller type ref to if_wd_controller.
27 l_message_manager type ref to if_wd_message_manager.
28 l_current_controller => wd_this->wd_get_api().
29 l_message_manager = l_current_controller->get_message_manager().
30 report message
31 l_message_manager->report_exception(
32 message_object = orref ).
33 endtry.
Scope: METHOD onactionsavedata ABAP Ln 1 Col 1
    
```

Fig. 14 Web Dynpro and assistance class

We have to specify that for client-side validation we can use even messages that are defined directly in the message class but is not recommended to involve the message texts directly in coding. In Fig. 16 we present the corresponding User Interface in Web Dynpro ABAP.

In our assistance class we define a new method INSERT_VALUES with which we can insert in the database table the informations that the user enter in the registration form. Fig. 13 shows the method coding.

To show a message to the user when he doesn't enter a proper value or to inform him that the data are successful saved (client-side validation) we use text symbols defined in our assistance class. When an exception occurs we use the exception class. Fig. 14 illustrates the way we can use the assistance class as model in our Web Dynpro application and the way we can catch the exceptions.

Through the attribute WD_ASSIST and the method WD_COMPONENT_ASSISTANCE ~GET_TEXT() we can access text symbols of the assistance class from our component controller, Fig. 15.

```

View: VIEW_BOOKS Active
Method List: ONACTIONSAVEDATA
34 data text type string.
35 text = wd_assist->if_wd_component_assistance-get_text( key =
36 '000' ).
37 if lv_firstname is not initial and lv_lastname is not initial and
38 lv_email is not initial and lv_message is not initial.
39     l_current_controller ?= wd_this->wd_get_api().
40     call method l_current_controller->get_message_manager
41     receiving
42     message_manager = l_message_manager.
43     call method l_message_manager->report_success
44     exporting
45     message_text = text
    
```

Fig. 15 Access of text symbols from assistance class

Library

The registration data are successful saved!

First Name: *	<input type="text" value="MARINESCU"/>
Last Name: *	<input type="text" value="ANDREI"/>
Email: *	<input type="text" value="MARINESCU.ANDREI@WEB.DE"/>
Message: *	<div style="border: 1px solid #ccc; padding: 2px;"> I NEED A GOOD PHP BOOK! I NEED A ADVICE. THANKS! </div>

Books

Games

Software

Registration

[Registration Form](#)

Fig. 16 User Interface with Web Dynpro ABAP

3. CONCLUSIONS

In this paper we have presented some of the concepts to develop robust software by ABAP programming language. When we develop an application we have to plan a good exception and messages handling to describe in detail the error situation, to check the data input from the user and to show the program status. We have seen the advantages of using the new class based exception concept of the ABAP language and some of the tools that Web Dynpro ABAP gives us in order to simplify the message and error handling.

REFERENCES

- [1] L. Heilig, S. Karch, O. Brottcher, C. Mutzig, J. Weber, R. Pfenning, SAP NetWeaver: The official Guide, Galileo Press 2008
- [2] Horst Keller, Sascha Kruger, ABAP Objects, Galileo press 2007
- [3] http://help.sap.com/saphelp_nw04s/helpdata/en/a0/ff934258a5c76ae10000000a155106/frameset.htm
- [4] Horst Keller, The official ABAP reference, Galileo Press, 2005
- [5] http://help.sap.com/saphelp_nw04s/helpdata/en/5f/8b2e16880111d194cb0000e8353423/frameset.htm
- [6] http://help.sap.com/saphelp_nw04/helpdata/en/4a/fff13a62d1ad6de10000000a11405a/frameset.htm
- [7] Rich Heilman, Thomas Jung, Next Generation ABAP Development, Galileo Press 2007
- [8] The 14th international conference, The knowledge based organization, November 2008, Cristea Ana Daniela, Adela Diana Berdie, Osaci Mihaela, User Interfaces with Web Dynpro ABAP and Web Dynpro Java, “Nicolae Balcescu” land Forces Academy publishing Haus Sibiu, 2008.
- [9] Ulli Hoffmann, Web Dynpro for ABAP, Galileo Press 2007
- [10] http://help.sap.com/saphelp_nw04s/helpdata/en/21/ad884118aa1709e10000000a155106/frameset.htm
- [11] Karl-Heinz Kühnhauser, Discover ABAP, Galileo Press, 2008



CONTRIBUTIONS TO THE IMPLEMENTATION OF THE TELEMETRIC PROGRAMMABLE AUTOMATS BY RTU TYPE FOR AUTOMATION, MONITORING AND CONTROL INSTALLATIONS

OPREA Constantin, BARZ Cristian, SEREGHI Alexandru

North University, Baia Mare, ROMANIA

Abstract:

The equipment RTU (Remote Terminal Unit) monopolize much more the sphere of industrial applications who necessities the control and monitoring from distance of the processes, stored under histories form of land events, take some measures in case of damage or to alert the personal. So, with help of SCADA interface (Supervisory Control And Data Acquisition) all the process can be monitoring and controlling with the computer help. In the paper an application created with the help of the RTU Tbox equipment is presented, application used for the monitoring of a solar installation for the processing of hot water. The application is located in a mountain area, the solar system being made up of collectors with a surface of 2x16 mp, two 500 liter reservoirs and two heat switches.. It also presents an application for monitoring and control of a production line, made from 16 hydraulic presses, with the help of software SCADA Ethernet Tview. Because the major products realized by beneficiary (hub from auto) get to the export where the customs want a strict monitoring the times of vulcanization, of the temperatures and pressures uses, it is necessary to search the best solutions who permit a production control from computer and who can accomplish some conditions impose.

Obs.: The final results will be presented through online link, with authors' access only.

Key words:

technological lines automation, Remote Terminal Unit, control and monitoring

1. INTRODUCTION

RTU equipment is a device installed at distance from the centre of control, who acquires the data from the process. They are coded in an easy format to be transmitted to the control centre. Also, the RTU equipment can take the commands from the control centre, dispose of modules of inputs and outputs for the interaction with the process and of course by multiple module communications. A typical RTU dispose of communication interfaces (serials, interfaces Ethernet (LAN), GSM or GPRS, Radio, PSTN etc), by a processor, interfaces with digital or analogue inputs/outputs.

The systems of monitoring and control from the distance dispose of SCADA (*Supervisory Control and Data Acquisition*) type interfaces for visualizing in real time the applications from the field. The SCADA type software is already very well known due to the success obtained in applications such as those of power, water, oil products distribution, leading completely automatic lines in real time etc...

A SCADA system will control and monitor a local process or one from far away through communication channels and RTU-s from the field.

2. THE RTU CONCEPT – PRESENT AND FUTURE

With the help of inputs/outputs, a RTU will read/command the equipments from the field; it will connect to the devices with serial communications through the communication ports, all the processed information and events being stocked as historical (datalogging) in the memory assigned for this purpose. Once stocked, the information can be accessed

through different ways: through SCADA type software, through emails, through *SMS* messages, through a structure of files transferred by *FTP* (File Transfer Protocol) or through *Internet Explorer* browsers (Fig.1).

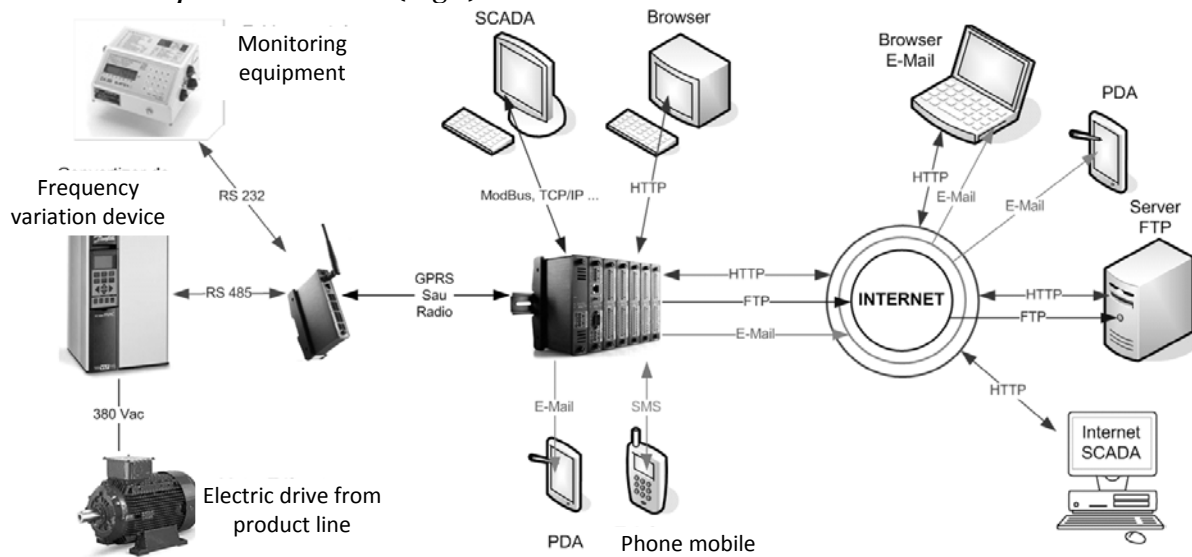


Fig. 1. The principle scheme

The data transfer from RTU to SCADA equipments is done through standard communication protocols; among the most popular transfer protocols for industrial applications, I mention the *Modbus* protocol (*Modbus ASCII*, *Modbus RTU*, *Modbus TCP/IP*). The SCADA software can be connected locally to the RTU through the *Modbus RTU* protocol or through the *Modbus TCP/IP* if the software is of *Internet SCADA* type. RTU equipment will generally communicate with a serial device (gas, water, power meter, frequency variation device etc.), with the help of *Modbus ASCII* protocol.

Presently, there is a tendency of the great producers of PLC (*Programmable Logic Controller*) equipments to develop and attach to PLCs the characteristics of actual RTU equipments: memory for *datalogging* (events journal) or multiplication of communication ports, but as long as there will be processes situated on field and far away from the control centre, RTU equipment is the answer.

RTU-s of the future will be equipped with faster and faster processors and multi-processors, with communication modules allowing higher and higher speeds for data transfer and a higher and higher capacity of stocking the historical from the process. The wired communication lines between different RTU equipments will remain of actuality, but the transfer protocols and the speeds will increase considerably. Wireless communications between RTU equipments will be used when the distances between them increase, or when the communication is done through SCADA type interfaces.

3. THE HARDWARE AND SOFTWARE ARCHITECTURE OF RTU [3]

The hardware architecture of RTU equipments has the following variants:

- ✚ **Modular** – each module having previously established and dedicated functions (ex.: the power source module, the processor module, input/output communication modules). The modular series has the advantage of being able to develop the application in time by simply adding new input/output modules, it disposes of processors faster than 32 bits and it is set up in the DIN automatic case on runner.
- ✚ **The “All in One” concept**, meaning everything in one carcass, contains the processor, the communication modules and a fix number of digital and analogue inputs/outputs in the same carcass.

The systems type SCADA permit the monitoring and control of the equipments from the field with help of computer; to a simple command from *mouse* or *keyboard* its possible to give commands to process, all these can be monitored online on the screen of the operator.

The softwares type SCADA dedicated to the monitoring and control of the RTU equipment has in general the next facilities:

- ✦ they are *Data Collecting Centres*: they gather all the information and history from the RTU storing them in databases;
- ✦ they are *Supervisors*: by connecting to the RTU (local or wireless) and listing the parameters in real time;
- ✦ they are *WebServers*: allowing users to access the list of history, alarms etc., by means of the classical network (LAN) and of a *Internet Explorer browser*.

The field data can be collected:

- ✦ *locally*, through a *Ethernet* connection or a serial connection using the RS232, RS485 communication ports. The data transfer is done in this case by means of standardized communication protocols (TCP/IP, Modbus TCP/IP, Modbus ASCII, Modbus RTU, etc.);
- ✦ *wireless* by means of GSM/GPRS modems, Radio, PSTN etc. for real time monitoring or through FTP, E-mail services for acquiring history.

Generally speaking in order to insure continuity in acquiring data from the field, one uses a redundant configuration of communication, namely if the local communication fails the SCADA software will switch the application to another local or wireless communication line so that no data within the process is lost.

At the same time with the data acquisition these will be stored in a database which will allow the future visualization of the entire history of the process in graphics, alarm lists or chronologies, being able to be exported in different formats (SQL, MySQL, Oracle, Access etc.).

The SCADA software administrator has access to a control panel which will allow the configuration of all communication, acquisition, authentication parameters. (Fig. 2).

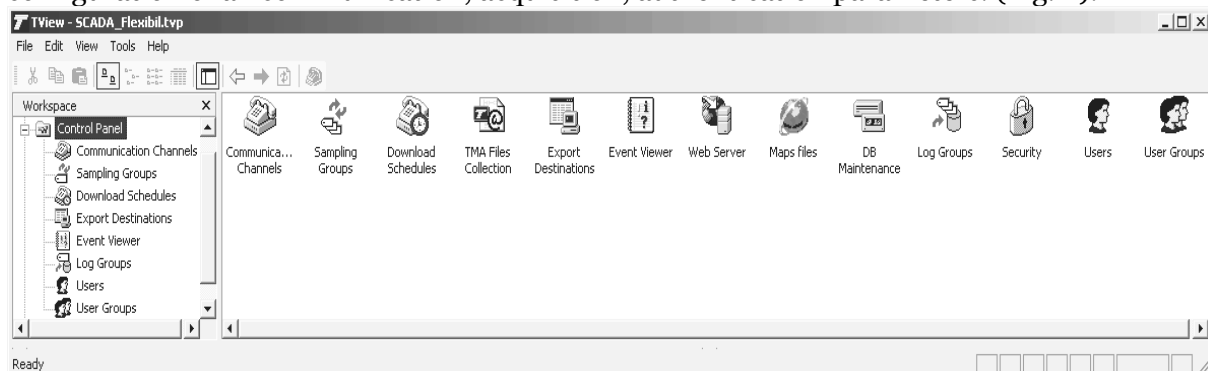


Fig. 2. The control panel

In general, the control panel has a series of interfaces like this:

- ✦ *the configuration of communication*: through LAN (Local Area Network), or through a modem (serial, GSM/GPRS etc.); one can configure redundancy groups for those cases when one of the communication lines fails, the next available line taking over the process data (Fig. 3);

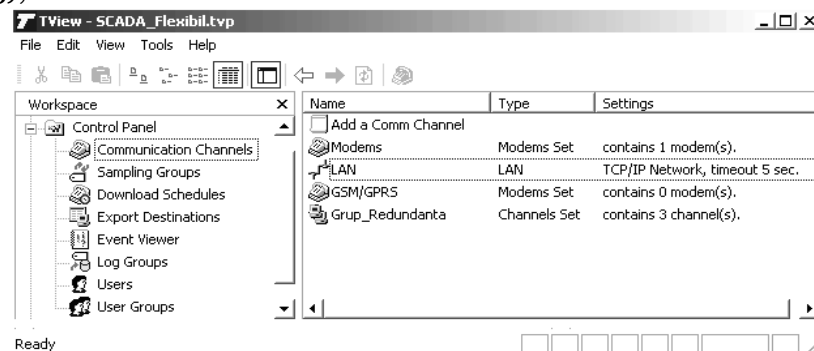


Fig. 3. Communication configuration interface

- ✦ *access level and user configuration*, having the possibility to add/delete with every user which has access to the SCADA interface (Fig. 4). The authentication is done with

username and password, the level of access being: without access rights, reading rights, reading and editing rights, these being established by the SCADA administrator

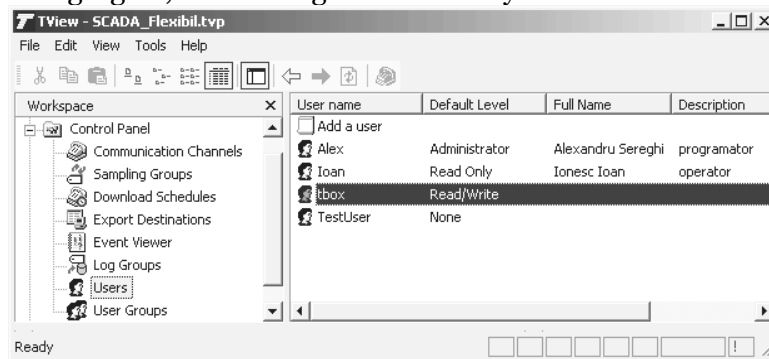


Fig. 4. Access level and user configuration interface

- ✚ visualization of events which happen during SCADA usage. One can thus monitor the location from where users will access the monitoring and control interfaces, the warnings or error which can occur during the usage of the program, thus filling in the list of the SCADA interfaces advantages.

The software architecture of RTU equipments

The software met in the development of RTU applications is grouped in that of:

- ✚ **Programming** of the automation (programming the internal PLC);
- ✚ **Monitoring and control** of the conducted process (SCADA type software).

Programming Software of RTU equipments

New interfaces for programming RTU equipments dispose of more and more advanced programming tools and more intuitive windows for creating and administrating a programme.

The following steps intervene in the programming of RTU equipments:

- ✚ **The configuration of the RTU's properties:** it allows the selection, the adding and the modification of the application's main parameters, starting from communication parameters (the Modbus address, TCP/IP, communication drivers with equipments on field or other SCADA type software) up to things related to the security of communication ports or of the application itself;
- ✚ **The adding of input/output modules:** RTU equipments disposing of a high diversity of modules, from the classic ones with digital inputs/outputs, analogues on 14 bits or modules with temperature inputs (for PT100, PT1000 drills, etc), up to GSM/GPRS, PSTN, optical communication modules etc. Other RTU equipments or, through standard protocols, other equipments such as temperature controllers, measuring equipments (debits, levels, movements...), frequency variation devices etc, generally any equipment disposing of a communication port, can be added to the existing configuration of RTU equipments, due to the many ways of communication;
- ✚ **The realisation of Tags:** a *Tag* is the location of the RTU equipments' registers memory in which the value of a parameter (digital – a single memory bit, or analogue – 8, 16 or 32 memory bits) will be found. Each Tag will represent a direct or indirect link with the inputs or outputs from the process, in the programme which will be developed in the future (in *Ladder*, *Basic*, *Statement List*, *Function Block* etc.);
- ✚ **The realisation of the programme:** *Ladder* language, the most often used language in programming RTU equipments, represents the structure of the programme under the form of a ladder; *Basic* language presents the advantage of developing complex programme lines, but the most important fact is that the code lines are executed by the processor more rapidly compared to other programming languages, thus resulting a shorter scanning cycle;
- ✚ **The realisation of alarms:** is one of the elements which makes the difference between a RTU and classic PLCs. The interfaces with alarm lists allow the choosing of any event from the process we desire to start an alarm. The alarms will automatically be saved in a historic, enabling us to use them in the programme or send them towards the service personnel by SMS, Email, FTP etc.

- ✚ *The realisation of Datalogging:* is another distinct element specific to RTU equipments, being responsible for stocking the main parameters to be monitored, forming the historic of the process. The digital measures’ passing from an estate to another can be stocked, but also the variations in time of the analogue measures.

The monitoring and control Software of RTU equipments

SCADA type interfaces allow the visualizing and control of field processes with the help of the computer; commands can be given towards the process by a simple mouse or key touch, all these being visualized in real time on the screen in front of the operator.

SCADA type software dedicated to monitoring and controlling from the distance of RTU equipments generally dispose of the following main facilities:

- ✚ They are *Data Collecting Centres:* they get all the information and historical from RTU equipments and stock them into data bases;
- ✚ They are *Supervisors:* through the connection to RTU (local or wireless) and display of parameters in real time;
- ✚ They are *WebServer:* allowing the access of users to the lists of historic, of alarms etc, through the classic network (LAN) and an *Internet Explorer* type *browser*.

The field data can be collected:

- ✚ *Locally,* through an *Ethernet* or serial connection using RS232, RS485 communication ports. The data transfer is done in this case through standard communication protocols (TCP/IP, Modbus TCP/IP, Modbus ASCII, Modbus RTU, etc.);
- ✚ *Wirelessly,* through GSM/GPRS, Radio, PSTN etc. modems for monitoring in real time or through FTP, Email services for historic acquisitions.
- ✚ Together with the data acquisition, it will be socked in a data base which will later allow the visualizing of the entire historic of the process in graphics, alarm lists or chronologies, being ready for export in different formats (SQL, MySQL, Oracle, Access etc.).

4. CONCLUSIONS

In conclusion we will present an application created by means of the RTU *TBox* equipment and namely monitoring a solar hot water production installation. The application is located in a mountain area, the solar system being made up of collectors with a total surface of 2x16 mp, two 500 liter reservoirs and two heat switches. The monitoring panel is equipped with a RTU *TBox* device specially designed for such applications, having 6 temperature inputs of the PT1000 type, 8 digital inputs, 2 analogue 4-20mA inputs, and 4 relay digital inputs. One of the main advantages of this type of equipment is the low energy consumption. Thus the monitoring panel was equipped with a 12Vdc battery, which in case of a power failure will continue to supply energy to the *TBox* equipment, thus the data acquisition being protected from any loss. The solar system supplier wanted a thermal energy threshold ensured with the implemented solution described above, so that it would be able to estimate the energy economy for the client achieved by introducing the solar panels. For this the following were required:

- ✚ heat and solar radiation monitoring by means of graphics according to time, with 10 minute acquisition rates and 10 day memory storage;
- ✚ water flow measuring;
- ✚ monitoring the recirculation pumps situation;
- ✚ sending through e-mail the database, process graphics, alarm lists every 24 hours;

The position of every sensor of the application is indicated in figure 5. The analogical radiation sensor with a 4-20mA output indicates the solar radiation in W/mp. The temperature sensors of the PT1000 type are linked to the system’s inputs and outputs on the closed system of the solar panels and to the reservoirs’ outputs. By means of relays one can monitor the situation of the recirculation pumps in the solar systems’ panels. The recirculation pumps are powered according to the temperature difference between the input and output of the solar panel. The measurement of the flow was done with the help of a debitmetru which sends impulses at every liter of water being used.

The program which will be executed in RTU *TBox* according to the requirements was developed during the first stage of the project. The program was edited with the *TWinSof*

programming software. TWinSof allows the manipulation of the project on the interface of Windows and Linux operation systems.

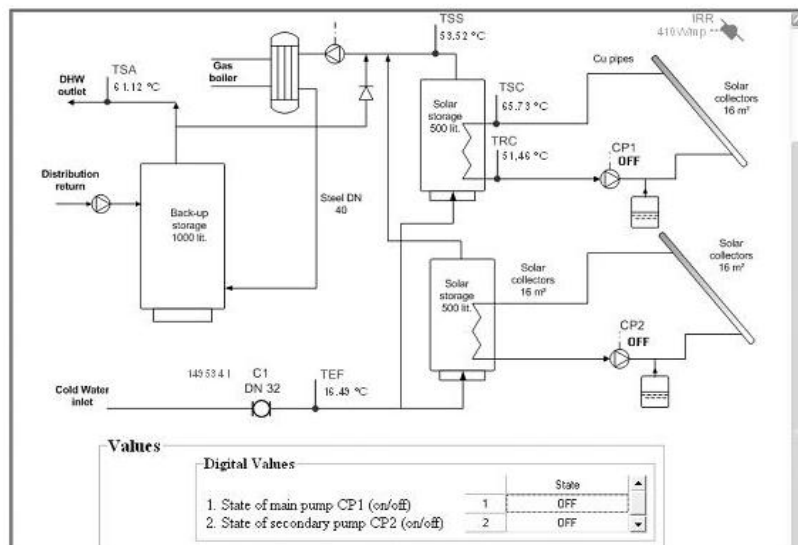


Fig. 5. Visualization interface

During the second stage of the project, once the RTU TBox was configured, the required graphics were configured, and a SCADA monitoring interface was created for field interventions and local visualization; this interface can be accessed by means of an Internet Explorer browser type. This interface was created in the WebFormEditor program, which is identical to TView in terms of the programming mode. The program graphics allows the creation of windows that are intuitive and in accordance with the field application, thus making it easy for the user to use the application. There are some *ActiveXs*, tables, and graphics available, with which one can develop user-friendly interfaces where the position of the sensors on the solar system plan is indicated. The temperatures, the flow, the situation of the pumps will dynamically indicate the values, according to the field values.

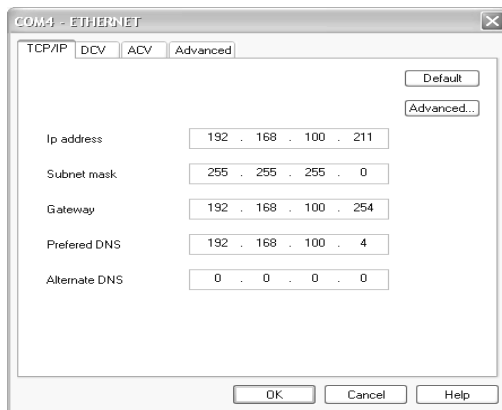


Fig. 6. Ethernet communication configuration

introduced the communication parameters (see Fig. 6).

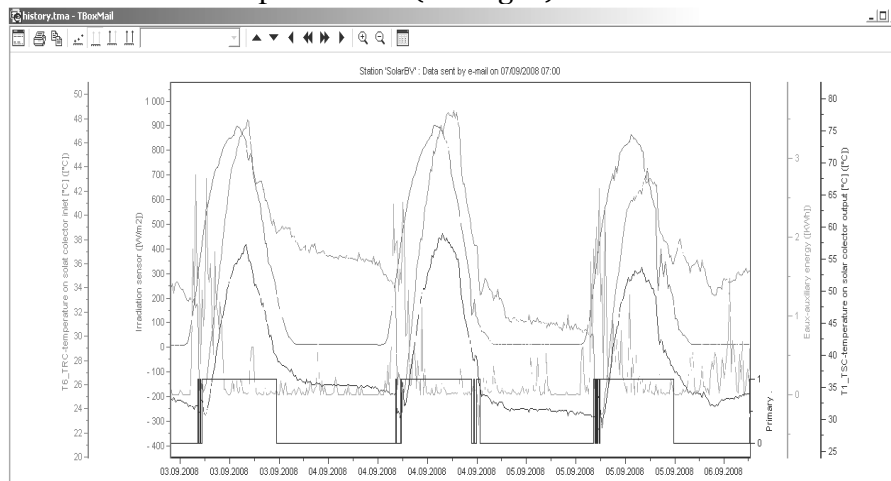


Fig. 7. Process graphic

The process graphics (Fig. 7) sent via e-mail contain all the monitoring data. Upon opening the graphic one can select the desired parameters. The graphic can be exported under .csv format and can be integrated into Microsoft Excel applications. Whenever necessary one can set the parameters, shrink or enlarge the graphics, having the possibility to print or export them under different formats (.jpeg, .bmp, .wmf, .emf, .txt).

As a conclusion, we'll present an application realized with the help of RTU *TBox* equipment in the industry of rubber based products. The monitoring and control of the entire production line is made with the help of *SCADA Ethernet TView* programme.

- ✚ The production line which is to be automated is formed of 16 hydraulic presses. Because most of the products need a strict monitoring of the vulcanization time, of temperatures and of the pressures used, the best solution needed to be found for allowing a computer controlled production and for fulfilling the following conditions:
- ✚ To allow the adding/modifying/deleting, through a window, of new production receipts for each press and their registration in a data base;
- ✚ To allow two working regimes: *Manual* (the initial case without automation) and *Automat* (the case in which the RTU TBox equipment will take over the control of the press);
- ✚ To register and display as graphics the main parameters of the process indifferently of the chosen working regime;
- ✚ To indicate all the events of interest in the list of alarms;
- ✚ To allow the access to the visualizing/controlling of data through a computer linked to internet.

The hydraulic presses are controlled by a manipulator through a control panel. The superior and inferior moulds are warmed with the help of some resistances and of some controllers with a PID curl for adjusting temperature, which dispose of a RS485 communication port.

In the first stage of the project, the programme to be executed in RTU TBox was developed. The programme was edited with the help of TWinSof programming software. TWinSof allows the manipulation of the project under Windows and Linux operating systems. First, the development of a communication driver was needed for the controllers from the production hall with the purpose of reading temperatures and setting temperature thresholds according to each production receipt.

In the second part of the project, once the programming of RTU TBox was done, the SCADA interface of monitoring and control from the distance was realized with the help of *SCADA Ethernet TView* software. The graphics of the programme allows us to create more and more intuitive windows in concordance with the application from the field, so that it is much easier to use the application. We have at our disposal many ActiveXs, tables, graphics to develop friendlier interfaces, where the hydraulic presses are indicated to be placed in the production hall. The estate of the presses (*supplied/unsupplied* with tension, working regime selected *automatically/manually*, production cycle *finished/stopped/in work*) s indicated in real time through messages and bright indicators alongside each press.

Each press will receive a receipt guiding the production in the automated regime. These receipts are created and edited where the most important parameters are the vulcanization time, pressures and prescribed reference temperatures. All receipts are saved in the table with *EntranceData* of the data base. In time, the receipts table will contain more and more registering, and in order to ease the finding of receipts and their reediting we developed a small filter with different searching criteria.

Returning to the process and to its monitoring in real time, windows can be created for each press, in which each parameter from the process can be visualized, indifferently of the working regime (automatic or manual).

The pressure and temperatures will indicate values in a dynamic way, corresponding to the values from the field. When the press works in automatic regime, the green arrow from the group of times will indicate the phase of the process in which the manipulator is found; in the table with production cycles, the stage of production can be followed with the exact number of successful/unsuccessful charges.

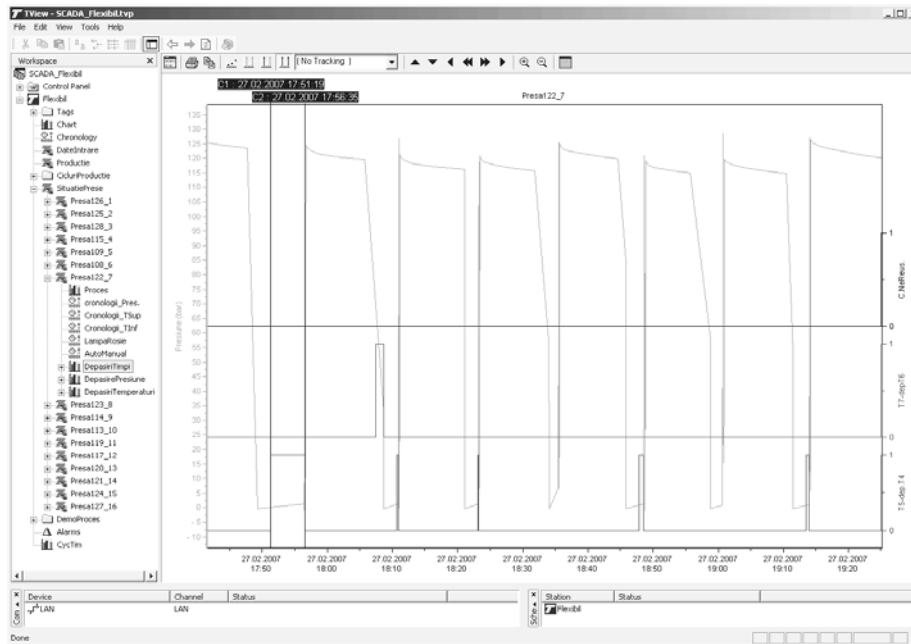


Fig. 8. Trial pressure

One of the greatest advantages of SCADA interfaces is the possibility of superposing the monitored parameters on graphics. In Figure 8 we can visualize pressure, superior temperatures, estate of the process (automatic/manual) and the situation of the bright indicator (Red Lamp) which indicates the end of vulcanization time and requires the intervention of the manipulator. Whenever we need, the parameter scales can be set, graphics can be increased or decreased, also having the possibility of printing and exporting them under different formats (.jpeg, .bmp, .wmf, .emf, .txt, .csv).

REFERENCES

- [1] Bolton, W., *Programmable Logic Controllers*, Fourth Edition Elsevier Newnes, Burlington, 2006
- [2] Oprea, C., Al., Sereghi, Cr., Barz, Ol., Chiver, *Contributions to DOMOTIC house automation for an optimum confort and safe ambiance*, A IV-a Conferință Internațională de Inginerie electrică și energetică EPE 2006, Buletinul Institutului Politehnic din Iași, Tom LII (LVI), Fasc. 5A, pg. 135 – 140, ISSN 1223-8139, Iași, 2006
- [3] Techno Trade, *TBoxMS – Remote Terminal Unit*, version 1.11, e-Book, 2007.
- [4] Techno Trade, *TView – Advanced Supervisory Software for Telemetry Applications*, version 2.51, e-Book, 2007.
- [5] x x x - MELSS AUTOMATION CASE STUDY ,Jan 2009 – www.melssautomation.com
- [6] x x x - www.scada.ro
- [7] x x x - www.cse-semaphore.com
- [8] x x x - www.automatizari-scada.ro
- [9] x x x - www.wizcon.com

WORKING WITH ABAP PERSISTENT DATA

CRISTEA Ana Daniela*, BERDIE Adela Diana**, OSACI Mihaela**

* NWCON Technology Consulting GmbH, GERMANY

**University of Timisoara , Faculty of Engineering – Hunedoara, ROMANIA

ABSTRACT

SAP NetWeaver is the SAP integration platform that provides integration layers “People Integration”, “Information integration”, “Process Integration” and where the application platform is based on Application Server Java and Application Server ABAP so called ABAP stack and Java stack. Both application servers work with a different database schemas that cannot be locate in the same database. Relational database tables are most used to store persistent data with Application Server ABAP and have two database interfaces open SQL and Native SQL. In this paper we make a presentation of the ways we can access an ABAP database schema through classical ABAP tools as Function Modules and until to object-oriented access via Object Services.

1. INTRODUCTION

SAP NetWeaver is the SAP technology platform that SAP use to distribut its technology as a proprietary product, an entire group of so-called usage types (Application Server, Business Inteligence, SAP NetWeaver Portal ...) [1].

The usage type SAP NetWeaver Application Server (AS) plays a central role in SAP NetWeaver and is subdivided in two usage types Application Server ABAP and Application Server Java with two programming interfaces ABAP and Java and two separated database schemas.

In Fig. 1 [2] we present the Application Server ABAP which we use to develop ABAP applications.

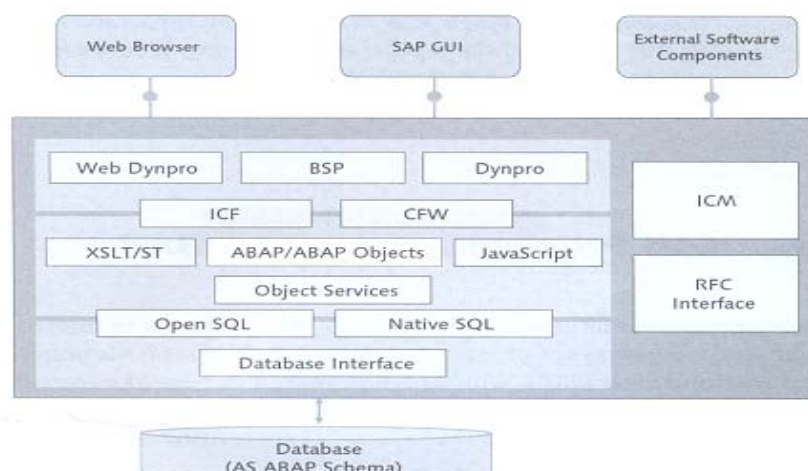


Fig. 1 Application Server ABAP [2]

As we can see the most of the AS ABAP can be divided in three layers: presentatin layer (Web Dynpro ABAP, Dynpro, BSP), application layer (ABAP/ABAP Objects, XLT/ST, JavaScript) and persistence layer with two interfaces Open SQL and Native SQL.

In this paper we present the way we can access the Database through Open SQL statements and Object Services. For this purpose we decouple the presentation logic from the application logic through Function Modules, usual ABAP classes and persistent classes.

ABAP supports both procedural (Function Modules, subroutines) and POO programming styles (Object Services, classes) and can be used easily to implement GUI-oriented (Dynpros) or browser-based (BSP, Web Dynpro) User Interfaces [3].

Function modules are procedures that are defined in function groups (special ABAP programs with type F) and can be called from any ABAP program. To create Function Modules and Function Groups we used Function Builder from ABAP Workbench. [4]

With help of Persistence Classes all SQL statements are hidden from developer and provides instead set and get methods to access the database.

We present follow some of the advantages of using a new abstraction layer through Object Services: [5]

- ✚ Flexibility via Abstraction - we can simply substitute the coding in the business objects class with methods from Web Services instead of the persistent objects;
- ✚ Functionality via Abstraction - It allows for a more complex mapping than a one-to-one relationship with the database;
- ✚ Simplicity via Abstraction

With help of persistent objects we can use fast and easy the ZIP compression technology available in ABAP to compress and decompress the large data that we store in database as xstrings. For our application we have chosen to work with Web Dynpro ABAP framework because that offers us many advantages as for example What You See Is What You Get view editor with drag and drop support for UI elements so that we can use better concentrate of the business process.

2. THE STUDY

2.1 DATABASE EXAMPLE

To create a database table in the ABAP Dictionary we can use ABAP Dictionary Maintenance. To see all the tables and their relationship we can use table relationship Graphic. These tools are completely integrated in ABAP Workbench.

Normal application programs are not supposed to create any database table or to change their attribute and with open SQL statements we can only access database tables that we have created with the ABAP Dictionary tools [6]. To create a database table in our programs we can use native SQL, that offers us this possibility with the proper disadvantages.

To keep our application simple and easy to understand we have built a database that has six tables needed to manage the Products in a virtual Library, Fig. 2.

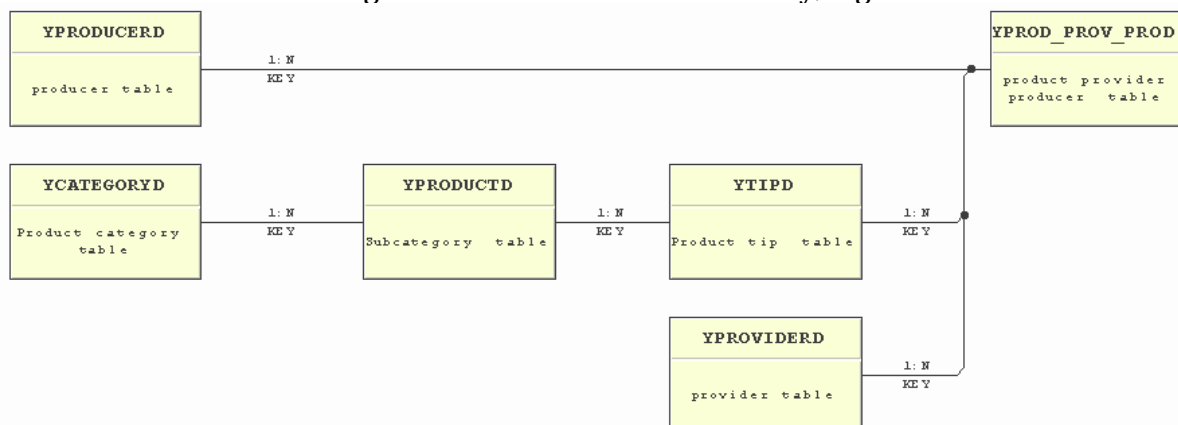


Fig. 2 The database used in our application

2.2. DATABASE ACCESS

Database tables are the most common data storage and we can access this ABAP database schema through Open SQL or Native SQL or we can build a new abstraction layer through Object Services.

2.2.1 Database access with Open SQL statements

SQL – Structured Query Language, is a largely standardized language for accessing relational database [7]. To access our database with open SQL statements we can use classical ABAP tools or ABAP Objects.

A. Classical ABAP tools and database access with Open SQL

Classical ABAP has no classes and object-oriented modularization just the procedural modularization with Function Modules and subroutines.

In our example we want to show in a Web Dynpro application all the Books and publisher information for a specific Author. For this purpose we build a Function Group where we integrate a Function Module YFM_SEARCH, Fig. 3.

Function modules can have the following interface parameters: Import parameters, Export parameters, Changing parameters and Tables parameters.

```

Function module YFM_SEARCH Active
Attributes Import Export Changing Tables Exceptions Source code
1 function yfm_search.
2
3   ***Local Interface:
4   *** IMPORTING
5   ***   REFERENCE(IN_IDPRODUCER) TYPE YSEARCH_VIEW-IDPRODUCER
6   *** EXPORTING
7   ***   REFERENCE(EXP_YTIPD) TYPE YTAB_VIEW
8   *** RAISING
9   ***   YCX_EXCEPTION_CLASS
10  ***
11  data oref type ref to ycx_exception_class.
12  try.
13    select *
14    from ysearch_view
15    into table exp_ytipd
16    where idproducer = in_idproducer.
17    if sy-subrc <> 0.
18      raise exception type ycx_exception_class
19      exporting
20        textid = ycx_exception_class=>ycx_exception_class_id
21        book_id = in_idproducer.
22    endif.
23  catch ycx_exception_class into oref.
  
```

Fig. 3 Function Module YFM_SEARCH

We used this Function Module in a Web Dynpro application to offer a search possibility for the user, Fig. 4.

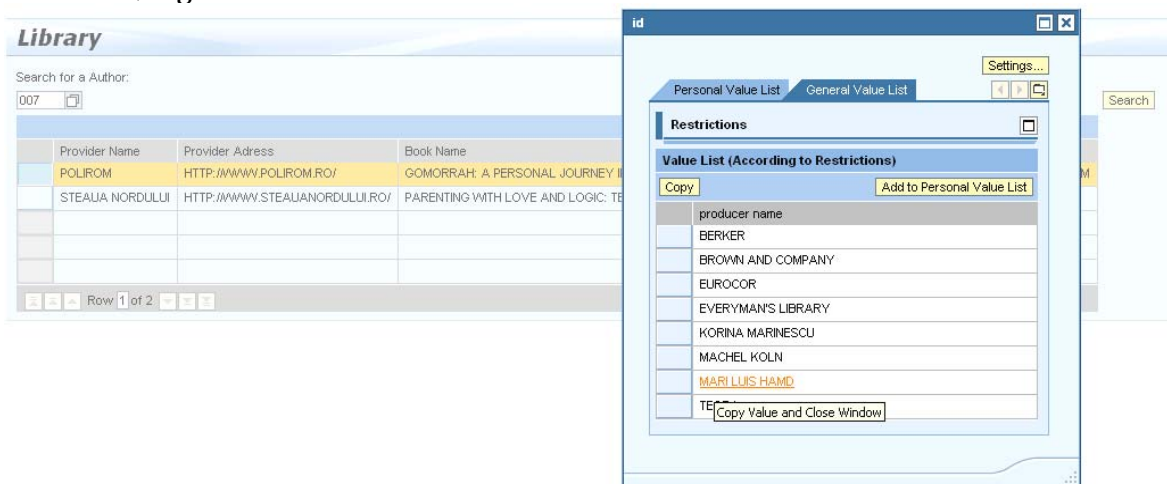


Fig. 4 The User Interface for YFM_SEARCH

Another example where we can use ABAP classical a Function Module is BAPI.

External access to the data and processes is possible by means of specific methods, so called BAPIs (Business Application Program Interfaces) that enable business functions in the SAP Systems to be integrated with business functions in non-SAP software, Fig. 5 [8].

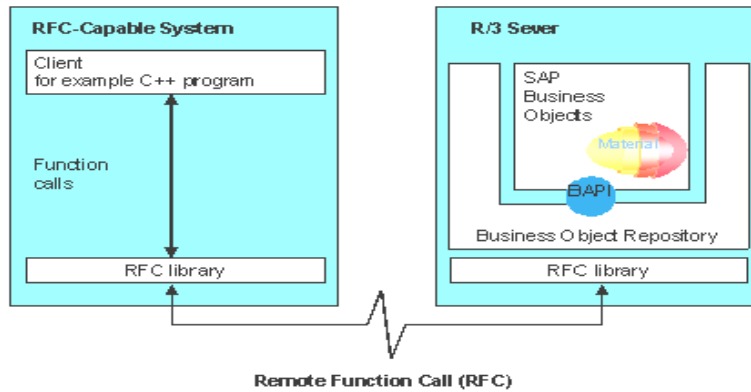


Fig. 5 Accessing a BAPI Function Module through RFC Calls [8]

We create a new Function Module named YBAPI_FUNCTIONMODULE, Fig. 6 with this module we can select all the Books that make part from a subcategory of Books category. After we save our Function Module we have to release him, to create an object YBAPI_OB with transaction SWO1 and to add a method (our Function Module YBAPI_FUNCTIONMODULE).

For example the code 001 represented Computer & Internet Books, code 002 represented History Books, Fig. 7.

Function module: YBAPI_FUNCTIONMODULE Active

Attributes Import Export Changing Tables Exceptions Source code

```

1 | function ybapi_functionmodule.
2 |
3 | *-- Local Interface:
4 | *-- IMPORTING
5 | *-- VALUE(IN_IDPROD) TYPE YBAPI_STRUCTURE-IDPROD
6 | *-- EXPORTING
7 | *-- VALUE(RESULT) TYPE BAPIRET2
8 | *-- TABLES
9 | *-- TABLEST STRUCTURE YBAPI_STRUCTURE
10 |
11 | select *
12 | from ytipd
13 | into table tablestt
14 | where idprod = in_idprod.
15 | if sy-subrc <> 0.
16 |   write in_idprod to msg_help.
17 | endif.
18 | endfunction.
                
```

Object type YBAPI_OB ✓ YBAPI_OB

- Interfaces
- Key fields
- Attributes
- Methods
 - YBAPI_OB.ExistenceCheck Check existence of object
 - YBAPI_OB.Display Display object
 - YBAPI_OB.YbapiModule function Module for BAPI
- Events

Fig. 6 Function Module YBAPI_MODEL_WD

IDPROD	IDCAT	PRODUCT_NAME
001	001	COMPUTERS & INTERNET
002	001	HISTORY
003	001	AUDIOBOOKS
004	001	CALENDARS
005	001	CHILDREN'S BOOKS
006	001	COMICS
007	001	COOKING

Fig. 7 Subcategory Books products from Library

Each function module underlying a BAPI and to use a BAPI method we need to know just some informations as for example the name of BAPI, the import parameters, the export parameters.

We import our BAPI in Web Dynpro ABAP as Model to build each view from our library web site, Fig. 8.

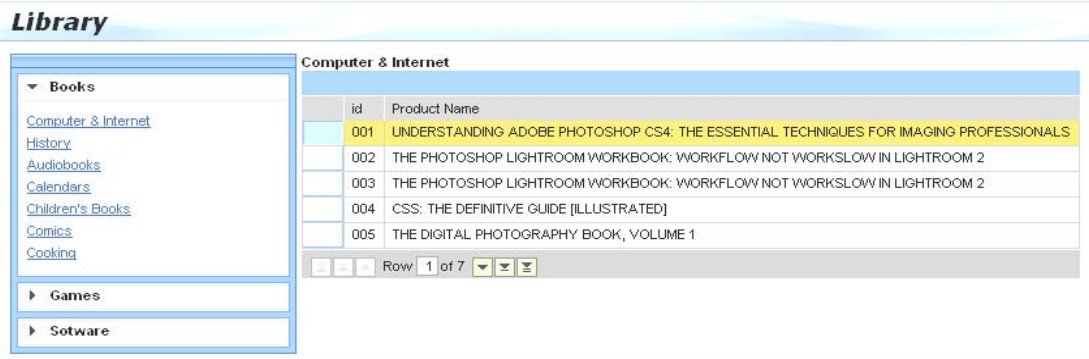


Fig. 8 The User Interface after service call creation

B. ABAP Objects and database acces with Open SQL

After a succinct presentation of the classical ABAP tools that we can use to access a database and that already existed before ABAP Objects, we use now ABAP Object concepts.

Object-oriented programming is based on the encapsulation of data and its associated functionality in classes [9]. In ABAP Workbench we can build global classes with help of Class Builder and local classes that are coded in our ABAP programs. The most important components of a class are methods and attributes. To show the use and structure of a class we create a global class YCL_ABAP_INSERT, and methods for the database insert. In Fig. 9 we presented the method INSERT_PROVIDER of the global class YCL_ABAP_INSERT.

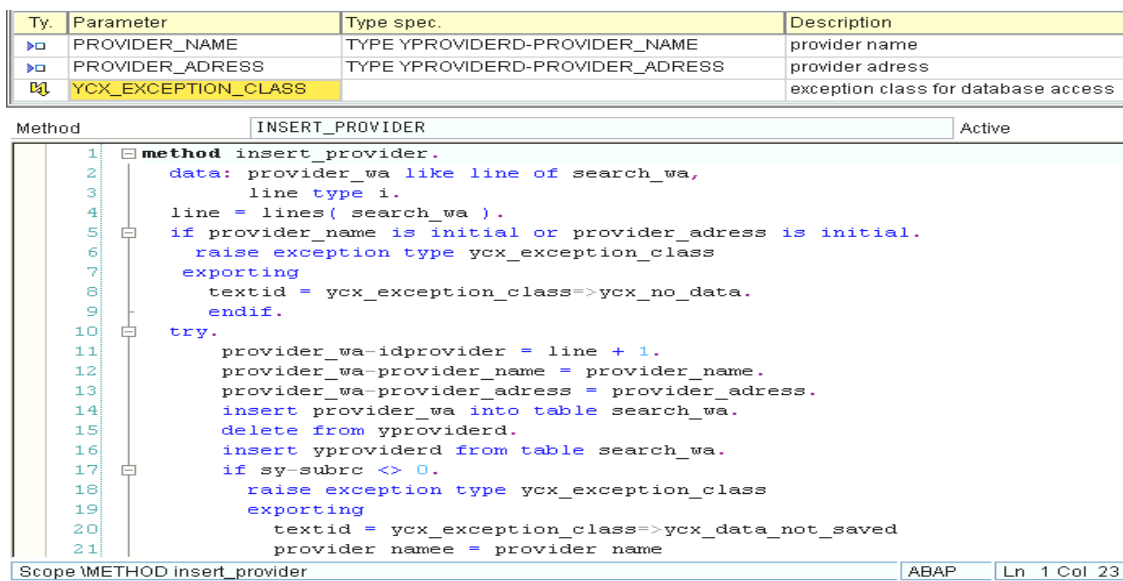


Fig. 9 ABAP Global Class, method INSERT_PROVIDER

The User Interface developed with Web Dynpro ABAP to show the use of the method INSERT_PROVIDER it is presented in Fig. 10.



Fig. 10 User Interface with Web Dynpro ABAP

2.2.2 Database access with Object Services

If we use in our applications ABAP Objects to develop object-oriented applications then we can store the data from objects in database through Persistent classes with help of Object Services.

Object Services offer us several services as:

- ✚ Persistence Service – that help us to manage persistent objects in the database
- ✚ Transaction Service – that help us to update persistent objects
- ✚ Query Service – that help us to search and load persistent objects

The components of the Persistence Service that are relevant to ABAP programmers are presented in Fig. 11 [10].

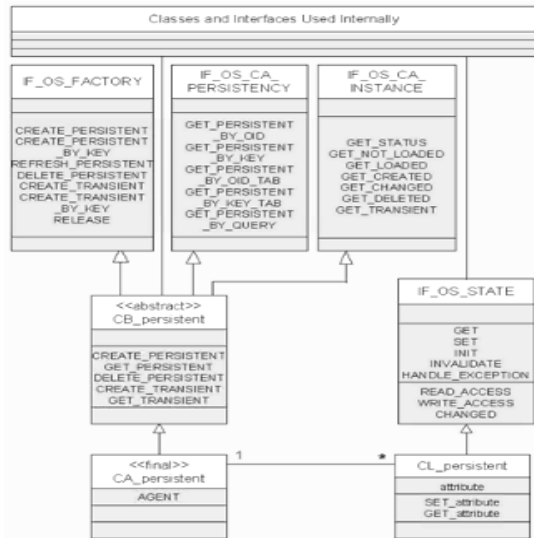


Fig. 11 The relevant components of the Persistence Service [10]

The Interface IF_OS_FACTORY through the method CREATE_PERSISTENT or CREATE_PERSISTENT_BY_KEY offers us the possibility to create a new persistent object.

The interface IF_OS_CA_PERSISTENCY through the method GET_PERSISTENT_BY_QUERY offer us the possibility to make a query for a database to import data from database tables that match conditions specify through proper parameters. Alongside GET_PERSISTENCE_BY_QUERY we can use the method GET_PERSISTENCE_BY_KEY_TAB to import persistent objects by specifying business key.

We create a persistent class YCL_PERSISTENT_ACCESS with help of Class Builder. As can be seen in Fig. 12 when we create a persistent class with the name YCL_<CLASS_NAME> or CL_<CLASS_NAME> the framework generate

for as two extra classes YCA_<CLASS_NAME> or CA_<CLASS_NAME> and YCB_<CLASS_NAME> or YCB_<CLASS_NAME>. After we define the persistent object the framework generate for us the SET and GET methods for the class attributes.

Fig. 12 ABAP persistent Class YCL_PERSISTENT_ACCESS

The attributes represented all the table fields and the generated get and set methods offer us the possibility to write and read individual fields in the database.

The main class it is YCL_PERSISTENT_ACCESS where we create our methods, the generated class YCA_PERSISTENT_ACCESS it is so called actor class that we use to manage our main class and the generated class YCB_PERSISTENT_ACCESS so called base class it is a abstract super class with the framework functionality.

We create a method SELECT_BOOKS, Fig. 13 that we can have all the Book records that we need to build a search possibility for a user.

Ty.	Parameter	Type spec.	Description
	IDPROD	TYPE YID	id
	VALUE(RETURNING_PAR)	TYPE OSREFTAB	OS: Table of References
	YCX_EXCEPTION_CLASS		exception class for database access


```

Method: SELECT_BOOKS Active
1 method select_books.
2   data: query_manager type ref to if_os_query_manager,
3         query          type ref to if_os_query,
4         agent          type ref to if_os_ca_persistency.
5   query_manager = cl_os_system=>get_query_manager( ).
6   agent = yca_persistent_access=>agent.
7   query = query_manager->create_query(
8         i_filter = `IDPROD = PAR1` ).
9
10  try.
11    returning_par = agent->get_persistent_by_query(
12      i_query = query
13      i_par1 = idprod ).
14    if lines( returning_par ) = 0.
15      raise exception type ycx_exception_class
16      exporting
17      textid = ycx_exception_class=>yxc_persistent_select
18      id = idprod.
19    endif.
20  catch cx_os_object_not_found.
21  catch cx_os_query_error.
22  endtry.
  
```

Fig. 13 Method SELECT_BOOKS - YCL_PERSISTENT_ACCESS

A persistent class is a Protected class. To consume our YCL_PERSISTENT_ACCESS persistent class in Web Dynpro we build a assistance class used as model. In Fig. 14 we presented the User Interface after we have build a proper Search Help for yproductd-idprod

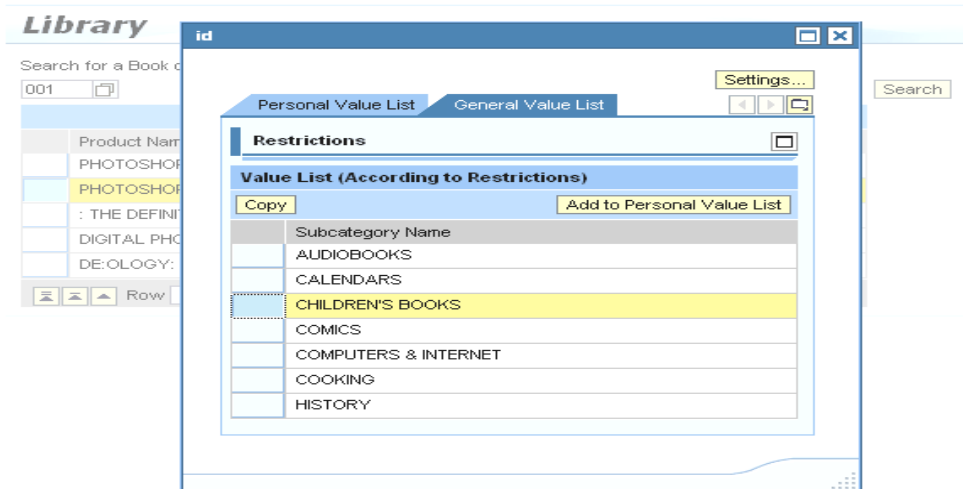


Fig. 14 User Interface with Web Dynpro ABAP

4. CONCLUSIONS

In this paper we have make a presention of some of posibilitys that we have to acces a ABAP Database schema. We have seen the classical ABAP tools through Function Modules and Function Groups but also the new ABAP Objects concepts. Function Modules are not just a yesterday technology are used today too for Remoute Function Calls (RFC), BAPI or from a ABAP class or Web Dynpro component to access a specific functionality. We have seen that Applicatios Server ABAP offer us many posibilitys to acces a database and samtimes we have to sacrifice pur object orientation for easier programming and we can combineate the old ABAP tools with the new ABAP object oriented concepts.

REFERENCES

- [1] Dan Woods, Jeffrey Word, *SAP NetWeaver for Dummies*, Wiley Publishing Inc. 2004
- [2] Horst Keller, Sascha Kruger, *ABAP Objects*, Galileo press 2007
- [3] Karl Kessler – Peter Tillert, Panayot Dobrikov, *Java Programing with the SAP Web Application Server*, Galileo Press 2005
- [4] http://help.sap.com/saphelp_nw04/helpdata/en/9f/db988735c111d1829f0000e829fbfe/frame set.htm
- [5] Rich Heilman, Thomas Jung, *Next Generation ABAP Development*, Galileo Press 2007
- [6] Horst Keller, *The Official ABAP Reference*, Galileo Pres 2005
- [7] Michael J. Hernandez, *Proiectarea bazelor de date*, Teora, 2003
- [8] http://help.sap.com/saphelp_nw04/helpdata/en/7e/5e11cf4a1611d1894c0000e829fbbd/frame set.htm
- [9] http://help.sap.com/saphelp_nw04/helpdata/en/c3/225b5654f411d194a60000e8353423/frame set.htm
- [10] http://help.sap.com/saphelp_nw04s/helpdata/en/ab/9d0a3ad259cd58e10000000a11402f/frame set.htm



CONSIDERATIONS ABOUT NEURO-FUZZY ADAPTIVE SYSTEMS

Gelu Ovidiu TIRIAN

“Politehnica” University of Timisoara, Faculty of Engineering of Hunedoara, Department of
Electrical Engineering and Industrial Informatics, ROMANIA

Abstract:

This paper work describes the shaping up of a system based on a input-output data set using ANFIS. First of all, we had to design the input-output data set to use during the training. The next step is to design a FIS structure that is going to be used in order to shape up a system who must be appropriate to the input-output data set. The FIS structure is going to be used in order to establish a primary set of functions needed during the training process.

Keywords:

neuro-fuzzy system, shaping up, structure , use

1. INTRODUCTION

The neuronal networks [1] could add high dynamic performance to the classical methods of adjustment, if they are used and designed properly [7]. This is possible if they adjust in real time, during the adjustment process [4]. Due to their ability of approximating the non-linear arbitrary functions, artificial neuronal networks are widely used in the domain of non-linear systems. Artificial intelligence could be also used successfully for parameter identification or for estimating different features of the process. The most important properties of the artificial neuronal networks (which are important for different applications during the automatic management) are: the ability of function approximation. Due to this ability of approximating arbitrary non-linear functions, artificial neuronal networks are highly important for the non-linear systems; information spreading; artificial neuronal networks have a parallel structure that allows the implementation of the systems' hardware; such an approach enables a highly margin degree in case of deficiencies than the classical alternatives; a parallel calculation higher degree; the ability of adaptation; the ability of generalization; neuronal networks could be used based on the data available previously - „off-line” learning or „on-line” learning (in real time): if the network is correctly used then, it has the ability of turning the data to a general outline, which is not possible in case of the data-set in use; shaping up the multi-variable systems; genuinely the neuronal systems have several inputs and outputs, and they are used in multi-variable systems; high degree of sturdiness in case of noise and incomplete inputs.

2. MULTI-LAYER NEURONAL NETWORKS. TRAINING METHODS.

Multi-layer neuronal systems are highly important for the domain of the artificial intelligence, because a lot of applications and classification and acknowledgement problems such as, the approximation of non-linear functions, the control and identification of the non-linear systems or the adaptation percolation - are solved out by using different types of networks. Multi-layer neuronal networks [5] eliminate a lot of limited features of the classical methods of the simple propagation or multi-layer perceptron – we refer to XOR. Generally speaking, such networks use feed forward propagation – meaning that in the case of those networks, there is no reaction amongst the neurons within the hidden layers or amongst those within the output and input layers, like those in Figure no. 1. Training methods for such network belong to the supervised methods, and they develop alongside the error back propagation algorithm - „back propagation” [7]. The main characteristic of these networks is the active function – it has both active continuous and/or derived non-linear functions, such as in Figure no. 2.

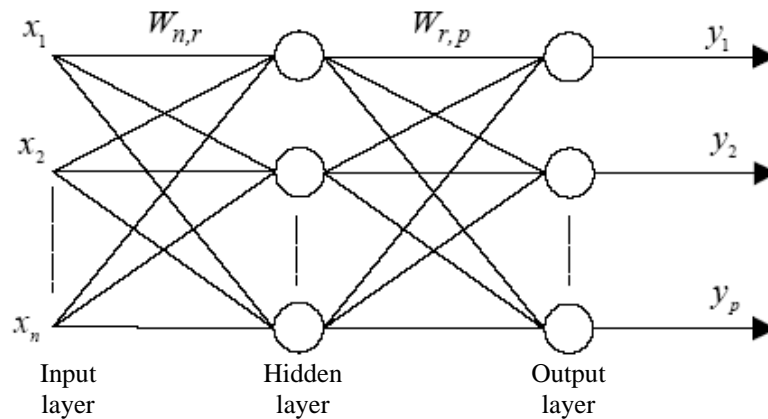


Figure no. 1 One hidden- layer neuronal network

The network in Figure no. 1 is made of one hidden layer who contains „n” neurons inside the input layer (n entries), „r” neurons inside the hidden layer, and „p” neurons inside the output layer [4]. The functions that make the neurons output layer active could be linear or sigmoid, meanwhile inside the hidden layer they must be sigmoid. In Figure no. 2 there are the most used functions that turn the multi-layer neuronal networks active, the sigmoid logarithmic function (left) and a hyperbole tangency function (right) are both coloured in blue, as well as their derivative functions - which are coloured in green.

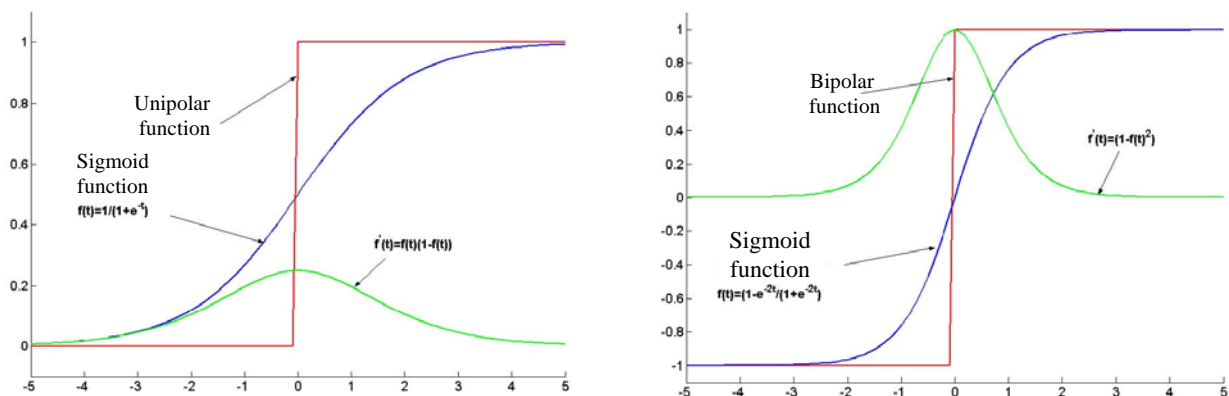


Figure no. 2 Functions that make multi-layer neuronal functions active

The error back propagation algorithm [7] uses three sets of data, one who turns the network active; other that is used for testing and validation of the weight we have come up with after the training stage; meanwhile the last one is the real data set. Choosing the data set for the training stage is highly important [29]. The data set must be representative for the matter under discussion, thus it should contain as much information as possible about the size-pairs of input values/output values we need. A correct data set will provide the network with the ability of generalization during the tests and the working process (real data sets), which reveal input values that have not been used during the training stage. Thus, the network shall come up with the right values at the output. We consider a training data set is made of „m” pairs who correspond to the most appropriate input and to the output vectors for the network:

$$(X^1, d^1), (X^2, d^2), \dots, (X^m, d^m) \quad (1)$$

In such conditions, when the input of the network uses the „k” data set, we could calculate the values for the output layer neurons, according to the moment when they turn active $s_j^k, j = 1 \dots p$; as well as for the active function f^i , when the output value is the following:

$$y_j^k = f^i(s_j^k), \quad j = 1 \dots p \quad (2)$$

We can define the square output error referring to the input vector X^k :

$$E_k = \frac{1}{2} \sum_{j=1}^p [d_j^k - y_j^k] = \frac{1}{2} \sum_{j=1}^p [d_j^k - f^i(s_j^k)] = \frac{1}{2} (e^k)^T e^k \quad (3)$$

Total error for all „m” data-sets is the sum of the E_k errors:

$$E = \sum_{k=1}^m E_k \quad (4)$$

3. NEURO-FUZZY ADAPTIVE SYSTEM (ANFIS)

In order to design a fuzzy model [2] we should make the following steps: outputs are associated to input member functions which are turned into laws in order to get a certain set of output features; the output feature changes into output member functions, and the latter turn into a single output value or a decision associated to the output. If we want to shape up such a system, based on an input-output data-set, we should use the ANFIS shaping [6].

During the first stage, we create the input-output data set which we are going to use during the training stage.

The next stage is to design a FIS structure which is going to be used in order to shape up a system which must acquire the input-output data pair.

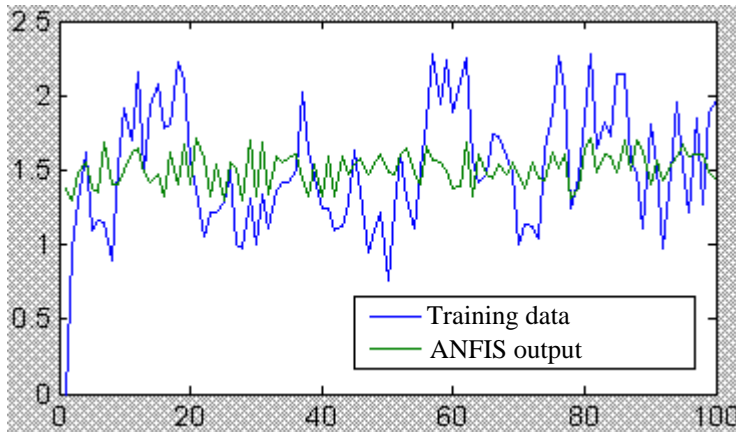


Figure no. 3 Process and network output

The FIS structure we have already created is going to be used in order to get a primary set of member functions used in training.

In order to check out the FIS system we have used, we should compare its output to the „y” input belonging to the training set. The output of the system we use and the „y” size we have obtained during experiments are described in Figure no. 3.

In order to identify [3] the ANFIS process, there is the possibility of using a graphical interface. Once we use this interface,

it is possible to upload the data set in order to turn the network active – these data is uploaded on the work space or on the disk. After we have uploaded the data, the output data are graphically described alongside some information about them (number of entries, number of entry pairs) - Figure no. 4.

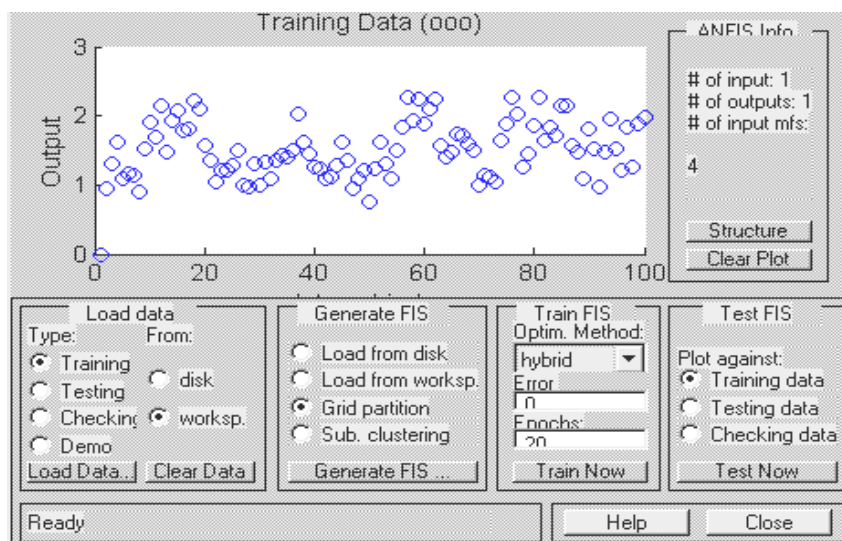


Figure no. 4 ANFIS graphic interface; training data

The next step is to define the FIS structure which is about to be used (Figure no. 5).

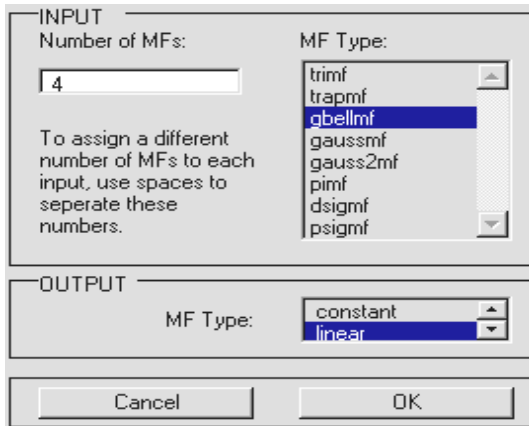


Figure no. 5 Choosing the FIS network parameters

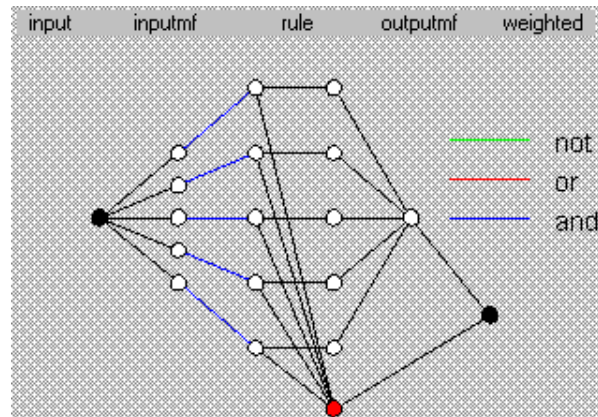


Figure no. 6 Network structure

The structure we have created could be graphically described. Therefore, the primary relations, the logical operations, and the implemented laws are ready to be performed - Figure no. 6.

After we have defined the parameters, we are able to perform the network training. The value of the error must be equal to 0; the best method of training is either ‘*hybrid*’ or ‘*back propagation*’ - the number of repeated stages to be performed. Figure no. 7 represents the evolution of the error during each stage of the training. If the training of the network is performed again then, it is going to work below the error value it had reached earlier. We see that once the number of periods increases, the error decreases, but not below to a certain value. That value is the limit. When it is reached, the number of repetitions does not cause a significant error decrease. If the number of repetitions increases, it reaches the “y” value of the output – Figure no. 8.

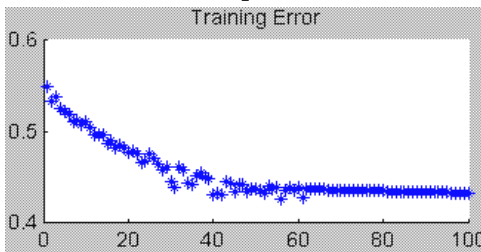


Figure no. 3.32 Evolution of ANFIS error

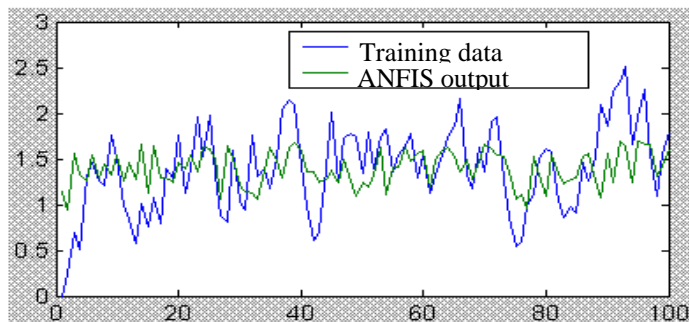


Figure no. 8 Evaluation of ANFIS after an increased number of repetitions

4. CONCLUSIONS

We have performed the shaping up of a system based on an input-output data set and we have used the ANFIS shaping-up method for that. We have created an input-output data set and we have created the FIS structure and the network training.

We have found out that once the number of periods increases, the error decreases, but it does not go below a certain margin. If it goes below that

margin, the number of repetitions is increased and it does not produce any significant decrease of the error. If the number of repetitions increases, we find out that it reaches the right “y” value.

REFERENCES

- [1] Dumitrescu, D., Costin, H. „Rețele neuronale teorie și aplicații” Editura Teora, 1996.
- [2] Hong, X., Harris, C.J., Wilson, P.A., „Neurofuzzy state identification using prefiltering”, IEE, 1999
- [3] Ljung, L. “System Identification” Theory for the User Prentice Hall, Inc., Englewood Cliffs, New Jersey
- [4] Narendra, K. S., Parthasaraty, K. “Identification and Control of Dynamical Systems Using Neural Networks”, IEEE Transactions on Neural Networks, vol. 1 nr. 1 1990, pag. 4-27.
- [5] Tirian G.O. „High speed neuronal estimator for the command of the induction machine” International multidisciplinary scientific symposium “UNIVERSITARIA SIMPRO 2006” pg.62...65, 2006.
- [6] G.O.Tirian „Abordari moderne in estimarea si identificarea sistemelor”, Referat doctorat, Timisoara, 2005.
- [7] Widrow, B., Lehr, M. A. “30 Years of Adaptive Neural Networks: Perceptron, Madaline and Backpropagation”, Proceedings of IEEE, vol. 78 nr. 9 1990, pag. 1415-1439



A STUDY ABOUT A RESISTIVE STEPPED TRANSDUCER USED FOR WATER LEVEL MEASUREMENT

Gabriel Nicolae POPA, Iosif POPA,
Sorin Ioan DEACONU, Corina Daniela CUNȚAN

”Politehnica” University of Timișoara
Engineering Faculty of Hunedoara, ROMANIA

Abstract:

In this work is analyzed a resistive stepped transducer used for water level measurement. For sending remote the information regarding the level, is used a level-frequency converter with an astable circuit with CD 4047. Experimentally it was determined the frequency modification from output depending on the water level in two situations: when the transducer’s steps above the water are wet and when these steps are dry. In both situations is found a non-linear frequency modification, depending on the level. Were calculated the transducer’s resistances in such way that the frequency will modify linearly with the level.

Keywords:

level, resistive transducers, level-frequency converters

1. INTRODUCTION

Electric measurement of the non-electric measures is applied on large scale in almost all domains. The advantages of the measuring electric methods against the non-electric methods are: high precision, high sensitivity, possibility for sending remote information, great adaptability, possibility and safety of recording, possibility to process the values obtained by measurement [1,2].

In practice, there are many conversion methods of the level of a liquid into an electric signal. When measuring the liquids level, there can be more measuring methods: with floating mechanism and electric transmission, impulse system for level’s remote measurement, capacitive measuring methods, methods based on radioactive radiations, methods based on pressure measurement, methods based on mass measurement, resistive methods [3,4,5,6]. Level’s measurement can be continuous or discontinuous [2].

2. RESISTIVE LEVEL TRANSDUCER WITH LEVEL-FREQUENCY CONVERTER

The resistive transducers are safe in operation and should achieve a conversion as good as possible of the level into another measure. An astable circuit alternates between two different output voltages. The output remains at each voltage level for a defined period of time. The astable circuit has two outputs, but no input [7].

The resistive level transducer with level-frequency converter is presented in fig.1.

The level-frequency conversion takes place in two steps: a level-resistance conversion achieved with the stepped level transducer itself (resistive transducer), followed by a resistance-frequency conversion made by a symmetric astable trigger circuit.

The integrated circuit CD 4047 is capable of operating in either the monostable or astable mode. It requires an external capacitor (between pins 1 and 3) and an external resistor (between pins 2 and 3) to determine the output pulse width in the monostable mode, and the output frequency in the astable mode. Astable operation is enabled by a high level or low level on the astable input. The output frequency, at 50% duty cycle, is determined by the timing components [7]. Features like astable circuit of CD 4047 [8]:

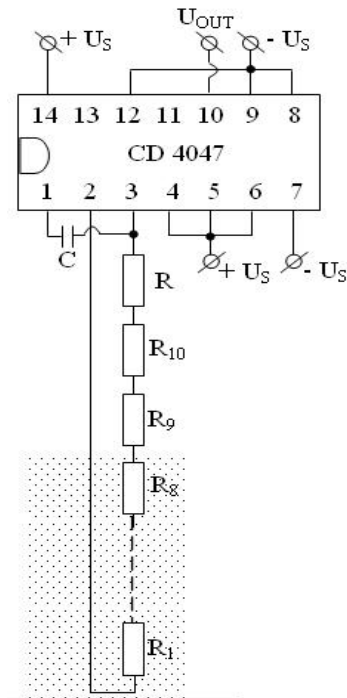


Figure 1. Resistive level transducer with level-frequency converter

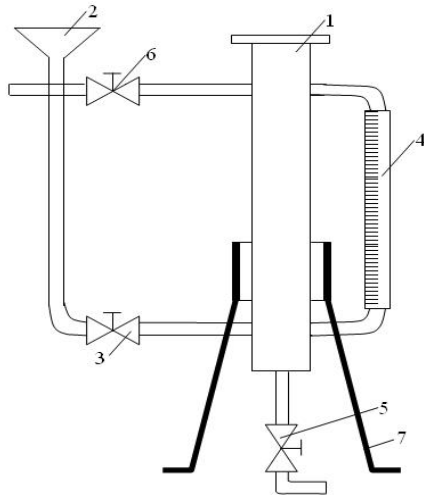


Figure 2. The tank used for checking the resistive transducer



Figure 3. The resistive transducer used in experiments

- wide supply voltage range: 3 ÷ 15 V;
- low power TTL compatibility;
- free-running or gatable operating modes;
- 50% duty cycle;
- good astable frequency stability:
 - typical=±2%+0.03%/°C at 100 kHz, U_s=10 V;
 - frequency=±0.5%+0.015%/°C at 10 kHz, U_s=10 V.

The astable trigger circuit has the integrated circuit CD 4047, the capacitance C and the transducer's resistors (R₁÷R₁₀). The resistive transducer is formed by putting in serial the resistances R₁÷R₁₀ (the steps of the transducer's resistances). By increasing the level, are short-circuited, in order, the resistances R₁, R₂, ..., R₁₀. The modification of the equivalent resistance from the transistors' bases leads to the frequency modification of the voltage U_{out}. For the symmetric astable circuit, the output signal's frequency is [8]:

$$f = \frac{1}{4.4 \cdot R \cdot C} \quad (1)$$

Its are chosen the transducer's resistances R₁= R₂...= R₁₀= 18 kΩ. It is notice in fig.1, that R_{CB}=R₂₃, the resistance between the pins 2 and 3 of CD 4047 (the resistance of transducer).

The transducer's resistances were introduced in plastic boxes with Φ 22 mm diameter and 30 mm length, and the boxes were filled with electrical insulating paste. The boxes where mounted on a stainless steel support. The transducer has the active length of 1 m, and the distance between two successive resistances is 10 cm. The resistances are serial, with tinned copper plates with the surface of 12.5 cm² and the distance against the metallic support of 1 cm (distance between plates). The resistive level transducer with level-frequency converter was practically tested into a tank of which principle diagram is presented in fig.3. In fig.2: 1 – tank, 2 – filler funnel, 3 – filler tap, 4 – tube scaled in level units, 5 – drain tap, 6 – vent valve, 7 – support. In fig. 3 is the resistive transducer used in experiments.

To determine the frequency's real values depending on resistivity, should be determined the resistivity of the water used in experiments. In order to determine the resistivity of the potable water, it was used the volt-ammeter measuring method of the resistance. This method was used in alternate current to avoid the water's electric polarization phenomena. It was used an experimental device formed by two plane-parallel plates of surface S₁=20.8 cm² and distance between them of l₁=1.8 cm in upstream (fig.4) and downstream (fig.5) montage.

The potable water resistances and resistivities for the upstream montage are determined with the relations:

$$R = \frac{U}{I} - R_{mA} \quad (2)$$

$$\rho = \left(\frac{U}{I} - R_{mA} \right) \cdot \frac{S_1}{l_1} \quad (3)$$

and for the downstream montage with:

$$R = \frac{U}{I \cdot R_v - U} R_v \quad (4)$$

$$\rho = \frac{U}{I \cdot R_v - U} R_v \cdot \frac{S_1}{l_1} \quad (5)$$

For the measuring instruments, $R_v=1000\Omega$ and $R_{mA}=275\Omega$. The measurement results and the calculation of resistances and resistivities are given in table 1. From table 1 it results the average value for the potable water resistivity used in experiments: $\rho_{avg}=52.35 \Omega \cdot m$.

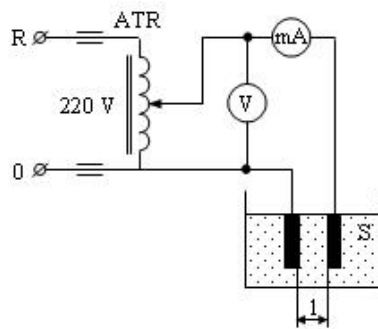


Figure 4. The volt-ammeter method – upstream montage

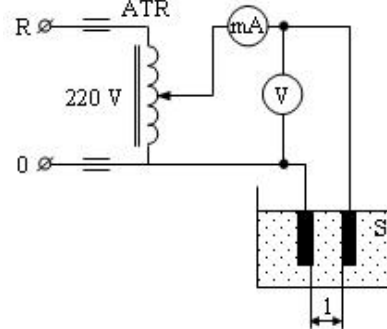


Figure 5. The volt-ammeter method – downstream montage

By measuring the resistances, the transducer has the following values for the resistance steps (fig.1,3): $R_1=17.66 \text{ k}\Omega$; $R_2=17.5 \text{ k}\Omega$; $R_3=17.3 \text{ k}\Omega$; $R_4=16.96 \text{ k}\Omega$; $R_5=17.12 \text{ k}\Omega$; $R_6=16.98 \text{ k}\Omega$; $R_7=17.26 \text{ k}\Omega$; $R_8=17.5 \text{ k}\Omega$; $R_9=17.08 \text{ k}\Omega$; $R_{10}=17.32 \text{ k}\Omega$ and $R_B=121.4 \text{ k}\Omega$ and $C=101 \text{ pF}$.

The measurements of the signal's frequencies from the circuit's output were made with the TRMS Protek 506 multimeter. To verify the operation of the transducer from fig.1, was measured the output frequency, by short-circuiting the resistance steps.

Table 1. Determination of water's resistivity

Electric Measures	Montage type						Average value
	upstream			downstream			
	1	2	3	1	2	3	
U [V]	0.52	0.88	1.75	0.26	0.63	0.75	-
I [mA]	0.78	1.15	2.4	0.8	1.825	2.34	-
R [Ω]	391	493	453	482	524	470	468.8
ρ [$\Omega \cdot m$]	45.2	56.8	52.5	55.6	60.6	54.2	54
Electric Measures	Montage type						Average value
	upstream			downstream			
	1	2	3	1	2	3	
U [V]	0.35	0.7	1.38	0.32	0.43	0.74	-
I [mA]	0.47	0.97	1.95	1.08	1.42	2.45	-
R [Ω]	469	445	435	421	434	433	439.5
ρ [$\Omega \cdot m$]	54.2	51.5	50	48.7	50	50	50.7

If the tank is empty ($h=0$), the transducer has all the resistances:

$$R_t = R_{1-10} = R_1 + R_2 + \dots + R_{10} \quad (6)$$

If the tank has $h=10\text{cm}$ of water, then the transducer's resistance is:

$$R_t = R_{2-10} = R_2 + R_3 + \dots + R_{10} \quad (7)$$

For $h=90 \text{ cm}$, the transducer's resistance is:

$$R_t = R_{10-10} = R_{10} \quad (8)$$

For $h=100 \text{ cm}$, the transducer's resistance is $R_t=0$.

For $U_s=10V$ it was made a comparative analysis in table 2, between the frequency's calculated values (f_c) and the measured ones (f_m). It was determined the relative error with:

$$\epsilon_r = \frac{f_c - f_m}{f_m} \cdot 100 \text{ [%]} \quad (9)$$

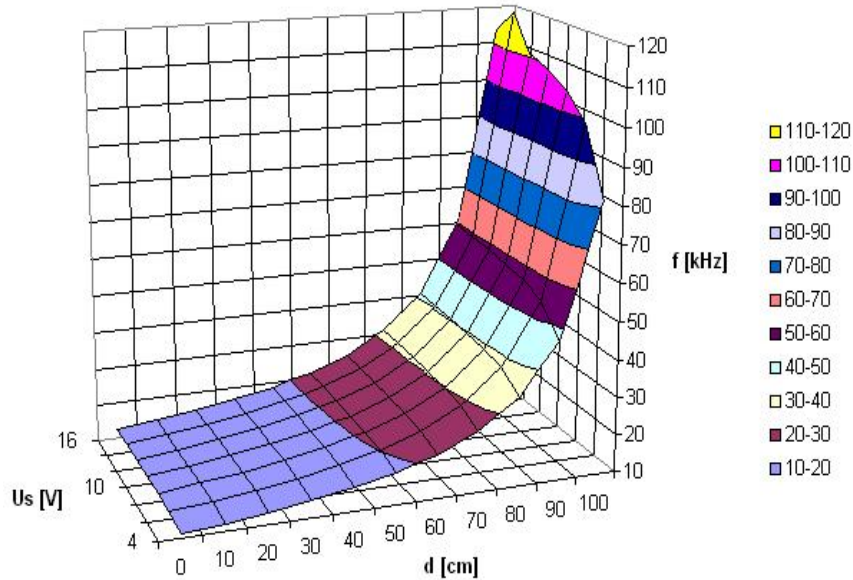


Figure 6. The output signal's measured frequency (f) depending on level (h) and supply voltage (U_s), when the resistance steps are short-circuited

From table 2, one can notice that, for the $h=0-100$ cm ϵ_r is acceptable, that validate the calculate frequency with (1).

In fig.7 and 8 were measured the circuit's output signal frequencies depending on h and U_s , in two situations:

- at a rapid water level modification, the superior resistance steps remain wet (fig.7);
- at a slow water level modification, the superior resistance steps having time to dry-up (fig.8).

The first situation is rarely met in practice than the second situation.

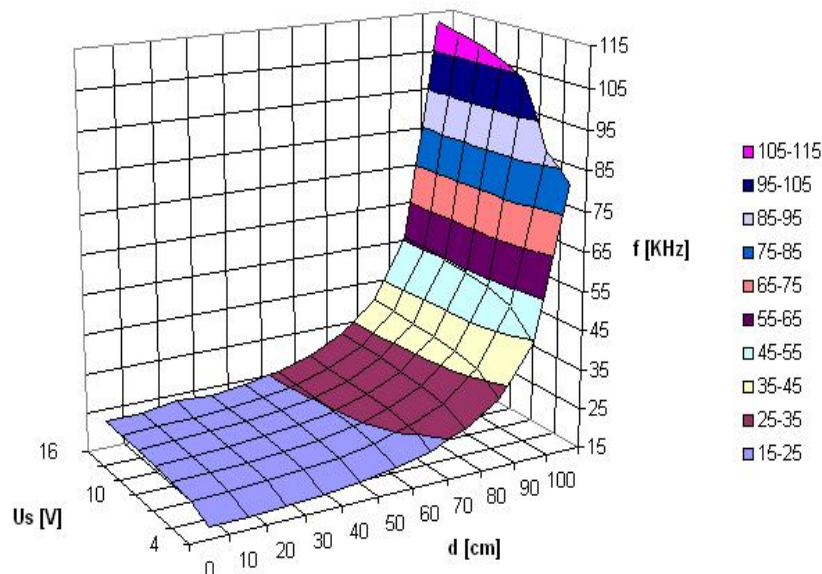


Figure 7. The output signal's measured frequency (f) depending on level (h) and supply voltage (U_s), when the transducer is introduced in water, the resistance steps above the water being wet

Table 2. The calculated and measured frequency depending on the level (by short-circuiting the steps) $U_s=10V$

h [cm]	0	10	20	30	40	50
f_c [kHz]	11.8	13.04	14.46	16.27	18.55	21.6
f_m [kHz]	12.39	13.44	14.73	16.32	18.34	21.04
ε_r [%]	-6.2	-4.66	-3.34	-1.99	-0.57	0.71
h [cm]	60	70	80	90	100	
f_c [kHz]	25.81	32.18	42.92	63.67	124.87	
f_m [kHz]	24.67	30.39	39.78	57.61	108.7	
ε_r [%]	2.01	3.41	5.01	7.08	9.73	

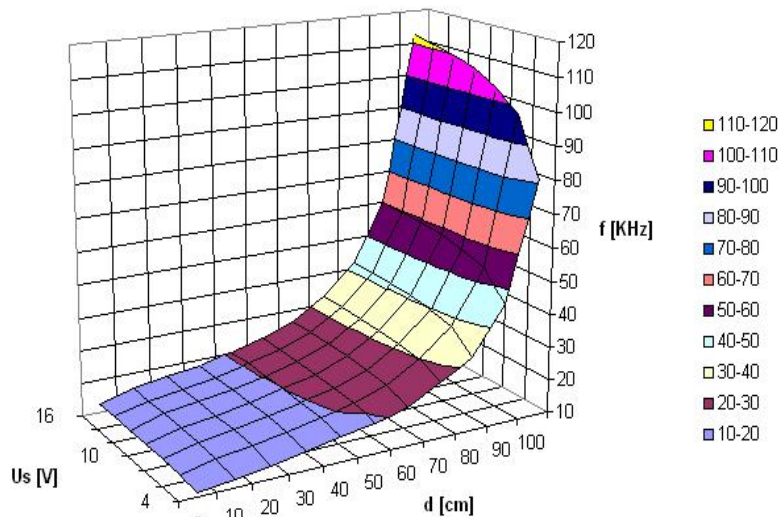


Figure 8. The output signal’s measured frequency (f) depending on height (h) and supply voltage (U_s), when the transducer is introduced in water, the resistance steps above the water being dry

For determining the signal’s frequency depending on the transducer’s resistance, it should be used the transducer’s electric model in real operation conditions (is taken into account the water resistance between the transducer’s plates). Further, the resistance steps above the water are assumed to be dry. The resistance between the plates, when the water is at their mid-height, is R_s :

$$R_s = \rho \cdot \frac{l}{S} \quad (10)$$

where ρ is the water resistivity, l is the distance between the transducer’s plates, and S is the common surface between the plates, when the water is at their mid-height. With the calculated data (ρ) and measured data (l , S) is obtained $R_s=1.68$ k Ω . For $h=0$ (fig.1), the transducer’s resistance is given by (fig.9):

$$R_{CB0} = \sum_{i=1}^{10} R_i \quad (11)$$

With the resistances’ measured values is obtained $R_t=R_{CB0}=294.08$ k Ω . For $h=10$ cm, in situation when the water is at the mid-height of the plate for the first step, the electric model of the transducer’s resistance is $R_t=R_{CB1}$ is presented in fig.10.

$$R_{CB1} = \sum_{i=2}^{10} R_i + \frac{R_1 \cdot R_s}{R_1 + R_s} \quad (12)$$

Is obtained $R_{CB1}=277.95$ k Ω . For $h=20$ cm, in situation when the water is at the mid-height of the plate for the first step, the electric model of the transducer’s resistance is $R_t=R_{CB2}$ is presented in fig.11. Step 1 is completely under water, the metallic plates being completely covered. Their equivalent resistance is $R_s/2$.

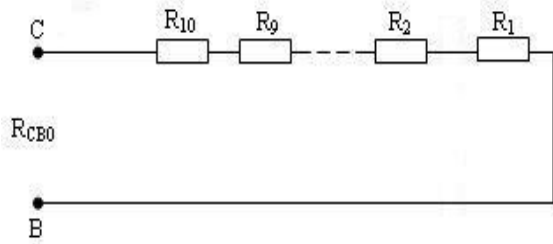


Figure 9. Electric model for h=0

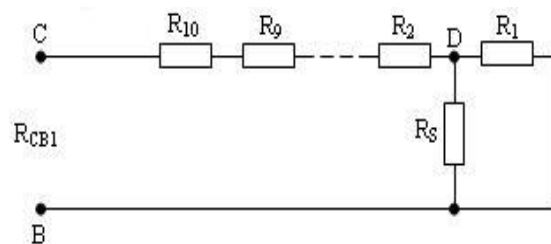


Figure 10. Electric model for h=10cm

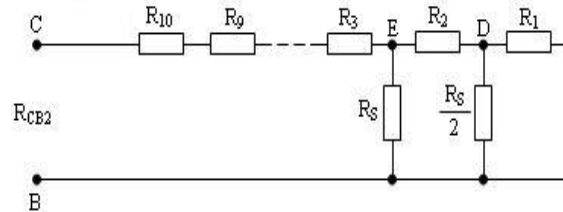


Figure 11. Electric model for h=20cm

$$R_{CB2} = \sum_{i=3}^{10} R_i + \frac{\left(\frac{R_1 \cdot R_s}{2 \cdot R_1 + R_s} + R_2 \right) \cdot R_s}{\frac{R_1 \cdot R_s}{2 \cdot R_1 + R_s} + R_2 + R_s} \quad (13)$$

Is obtained $R_{CB2}=260.45 \text{ k}\Omega$. Calculating little by little, are determined also the other values of the resistances for the other values of the water height (table 3). In table 3, f_m is the output signal's frequency when $U_s=10\text{V}$, and the resistance steps above the water are dry.

 Table 3. The measured and calculated frequency depending on R_{CBi}

h [cm]	0	10	20	30	40	50
R_{CBi} [k Ω]	190.7	99.69	69.1	52.87	42.82	35.98
f_c [kHz]	12.58	22.57	32.56	42.55	52.54	62.54
h [cm]	60	70	80	90	100	
R_{CBi} [k Ω]	31.02	27.26	24.32	21.95	20	
f_c [kHz]	72.53	82.52	92.51	102.5	112.5	

3. LINEARIZATION OF THE CHARACTERISTIC OF THE RESISTIVE LEVEL TRANSDUCER WITH LEVEL-FREQUENCY CONVERTER

The characteristics from fig.7 and 8 are non-linear. The issue is to determine the values of the transducer's resistances in such way that the frequency indication depending on level to be linear. Is imposed the modification of the output signal's frequency between 12.58 kHz and 112.5 kHz, with 9.992 kHz step. From (1) is calculated the resistance depending on frequency:

$$R = \frac{1}{4.4 \cdot f \cdot C} \quad (14)$$

This frequency interval is divided to the number of resistance steps of the transducer, and then, by (14) are determined the resistances R_{CBi} from the transducer's electric model (table 4). Further, is considered that when the water is at a certain level, the water covers half of the surface S common between the two plates, and the water's equivalent resistance is R_s . If the plates are completely covered, then the water's equivalent resistance is $R_s/2$. For $h=0$ (fig.9):

$$R_{CB0} = \sum_{i=1}^{10} R_i \quad (15)$$

From (15), it results $R_1=92.66 \text{ k}\Omega$. For $h=10 \text{ cm}$ (fig.10):

$$R_{CB1} = \sum_{i=2}^{10} R_i + \frac{R_1 \cdot R_s}{R_1 + R_s} \quad (16)$$

By making the difference between R_{CB1} (16) with R_{CB0} (15), is obtained:

$$R_{CB1} - R_{CB0} = R_1 - \frac{R_1 \cdot R_S}{R_1 + R_S} \tag{17}$$

From (27), $R_2=30.53 \text{ k}\Omega$.

Proceeding similarly by achieving the transducer’s electric model for each case in part, are obtained also the other resistance values which will determine a linear modification of the frequency depending on level.

Table 4. The resistances calculated and used in experiments for the circuit from fig.2 – linearized characteristic

Resistance	R_1	R_2	R_3	R_4	R_5
calculated [k Ω]	92.66	30.53	16.16	9.98	6.76
measured [k Ω]	93	30.6	16.18	9.95	6.7
Resistance	R_6	R_7	R_8	R_9	R_{10}
calculated [k Ω]	4.68	3.69	2.87	2.3	1.88
measured [k Ω]	4.65	3.7	2.87	2.3	1.89

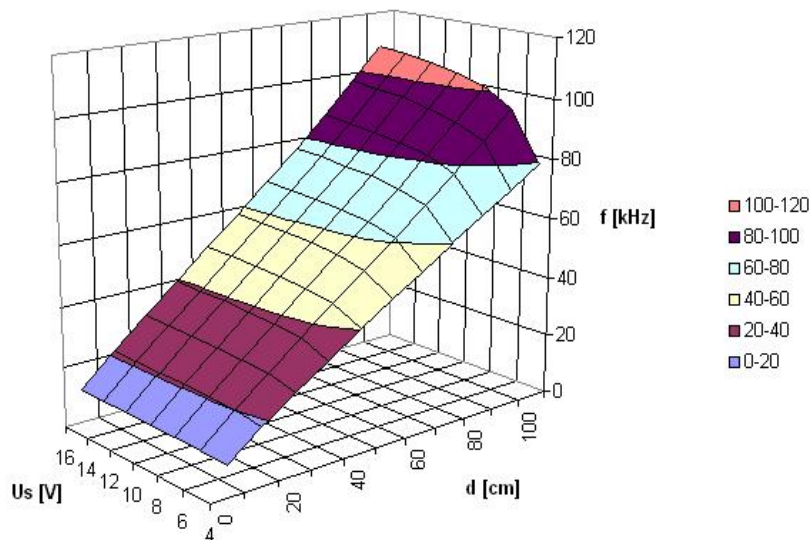


Figure 12. The measured frequency of the output signal (f) depending on level (h) and supply voltage (U_s) after linearization

4. CONCLUSION

It was analyzed a 10-step resistive transducer connected to an astable trigger circuit in such way to achieve the level-frequency conversion. The condition (wet or dry) of the resistances above the water influences the transducer’s operation. For equal values of the transducer’s resistance steps, the frequency depends non-linear on the water level. Were analytically determined the transducer’s resistance steps in such way that the frequency to depend linearly on the level. The transducer can be used in applications where the level does not fluctuate (does not modify up and down with high speed) in order that the insulating support of the resistances above the water to have time to dry-up. Can be also used other electronic circuits attached to this type of transducer, that should achieve the level-frequency conversion.

BIBLIOGRAPHY:

- [1] Grave, H.F. - Electrical Measurement of Non-electric Measures, Akademische Verlagsgesellschaft, Leipzig, Germany, 1965.

- [2] Ignea, A. - Electrical Measurement of Non-electric Measures, West Publishing House, Timișoara, Romania, 1995.
- [3] Wallace, W.D., Spielvogel, L.G. - Field Performance of Steam and Hot Water Electric Boilers, IEEE Transactions on Industry Applications, Vol.IA-10, No.6, november/december, 1974, pp.761-769.
- [4] Keeland, B.D., Dowd, J.F., Hardegree, W.S. - Use of Inexpensive Pressure Transducers for Water Level Measurement in Wells, Wetlands Ecology and Management, No.5, 1997, Kluwer Academic Publishers, Netherlands, pp.121-129.
- [5] Khan, S. and other - Capacitive Transducer Circuits for Liquid Level Measurement, International Journal of Computer Sciences and Engineering Systems, Vol.2, No.3, july, 2008, pp.195-197.
- [6] Cai, S., Lu, C., Wang, H. - Measurement Technology of the Physical Model Test in the Hydraulic Engineering, International Conference on Hydro-Science and Engineering, 1988.
- [7] Pfeiffer, W. - Impulse Technique, Darmstadt, Germany, 1976.
- [8] *** - CD4047BC, Low Power Monostable/Astable Multivibrator, Fairchild Semiconductor, U.S.A., 2002.



DISCSP-NETLOGO-EDUCATIONAL SOFTWARE MEANT FOR THE IMPLEMENTATION AND EVALUATION OF THE ASYNCHRONOUS SEARCH TECHNIQUES IN NETLOGO

MUSCALAGIU Ionel, MUSCALAGIU Diana, PETRAS Teodora, PĂNOIU Manuela

University „Politehnica” din Timisoara, Faculty of Engineering Hunedoara, ROMANIA

ABSTRACT:

The wide spreading of computer networks and of the Internet will result in the necessity of developing distributed software, which is supposed to work under these media, and to turn into account the advantages of a distributed and concurrent environment. The implementation of such techniques can be done in any programming language allowing a distributed programming, such as Java, by means of RMI. Nevertheless, for the study of such techniques, for the analysis of their completeness and for their evaluation, it is easier and more efficient to implement the techniques under certain distributed media, which offer various facilities, such as NetLogo.

In this article there is proposed a general implementation and evaluation model in NetLogo for the asynchronous techniques. This model, we believe, will allow the use of the NetLogo environment as a basic simulator for the study of asynchronous search techniques. This model can also be used for building educational software which can be used when studying the asynchronous search techniques with agents.

Keywords

Artificial intelligence, distributed programming, constraints, agents

1.INTRODUCTION

The adjustment of the software technologies to the distributed equipment represents an important challenge for the next years. The wide spreading of computer networks and of the Internet will result in the necessity of developing distributed software, which is supposed to work under these media, and to turn into account the advantages of a distributed and concurrent environment.

The constraint programming is a model of the software technologies, used to describe and solve large classes of problems as, for instance, searching problems, combinatorial problems, planning problems, etc. A large variety of problems in the A.I field and other domains specific to computer sciences could be regarded as a special case of constraint programming. Lately, the A.I community showed a greater interest towards the distributed problems that are solvable through modeling by constraints and agents. The idea of sharing various parts of the problem between agents that act independently and that collaborate between them using messages, in the prospective of gaining the solution, proved itself useful, as it conducted to obtaining a new modeling type called Distributed Constraint Satisfaction Problem(DCSP) [3,4].

There exist complete asynchronous searching techniques for solving the DCSP, such as the ABT (Asynchronous Backtracking) and DisDB (Distributed Dynamic Backtracking) [1,3,4]. There is also the AWCS (Asynchronous Weak-Commitment Search) [3,4] algorithm which records all the nogood values. The ABT algorithm has also been generalized by presenting a unifying framework, called ABT kernel [1]. From this kernel two major techniques ABT and DisDB can be obtained. The implementation of asynchronous search techniques based on distributed constraints can be done in any programming language allowing a distributed programming, such as Java, C, C++ or other. Nevertheless, for the study of such techniques, for their analysis and evaluation, it is easier and more efficient to

implement the techniques under certain distributed environment, which offer various facilities, such as NetLogo [8], [5,6,7].

NetLogo, is a programmable modelling environment, which can be used for simulating certain natural and social phenomena. It offers a collection of complex modelling systems, developed in time. The models could give instructions to hundreds or thousands of independent agents which could all operate in parallel. NetLogo is the next generation in a series of modeling languages with agents that began with StarLogo [8]. It is an environment written entirely in Java, therefore it can be installed and activated on most of the important platforms (Windows, Unix).

The aim of this article is to introduce an as general as possible model of implementation and evaluation for the asynchronous search techniques, in two possible cases: synchronous and asynchronous. This model can be used in the study of agents behavior in several situations, like the priority order of the agents, the synchronous and asynchronous case, leading, therefore, to identifying possible enhancements of the performances of asynchronous search techniques. This model can also be used in creating some educational software to be used in the study of asynchronous search techniques with agents by the students. For this purpose we have chosen the NetLogo environment, which is a programmable environment [8].

We will see the way one can simulate agents, how constraints can be implemented, how various measurement units for asynchronous techniques in the ABT and AWCS family can be implemented. Unfortunately, there is no distributed environment dedicated to modeling with distributed constraints, all the existent media are general ones, with more general targets. The implementation of agents and constraints implies a certain calculation effort, bigger or smaller, according to the performances of the given environment. The use of this support for educational software can ease the actual implementation of asynchronous techniques. This educational software can be approached by students on the site [7]

2. THE IMPLEMENTATION OF APPLICATIONS WITH AGENTS IN NETLOGO

2.1 The NetLOGO objects

The NetLogo world is made of agents. Each agent carries out a task, all the agents execute simultaneously and concurrently. The NetLogo language allows three types of agents: turtles, patches and the observer. The turtle type objects are agents that can move on in the NetLogo world, which is bidimensional and is divided in a grid of patches. Each patch is a square piece that represents the support on which turtle objects can move. The observer doesn't have a fixed location, it can be imagined as being situated above the world of turtles and patches objects. The observer can be regarded as a system agent that can initiate various operations for the other agents. NetLogo uses commands and reporters to tell the agents what to do (the commands and the reporters are NetLogo primitives). The commands are actions for the agents, but the reporters return certain values.

NetLogo allows the defining of different "types" of turtles, called breeds. Once a breed has been defined, we can establish a different behavior for it. Those objects are used for simulating various objects existent in DCSP problems. For example, the agents from the n queens problem can be defined using breed type objects (a construction of type breeds [queens]). That thing allows the fixing of a special behavior for each agent-queen. When breed type objects are defined, automatically there is created an agentset for each breed.

A very important problem is related to the way of execution of an agent's attached procedures, agent simulated using breed type objects. The DCSP applications require the simultaneous and asynchronous execution of the code attached to each agent. That thing is possible in NetLogo because the commands are executed asynchronously, each object of the "turtle" type or "patch" executes its list of commands as soon as possible. There are two ways of performing each agent's commands. The first one consists in "aligning" the commands executed by each turtle, through placing all the commands in the ask block. That way, the executed steps won't be synchronized. In exchange, using an ask command for each operation, a synchronization of all the operations performed by the agents will be obtained, each turtle will wait until the other turtle objects will finish their computations.

2.2. Modelling and implementing the process of the agents' execution

In this paragraph there is presented a solution of modelling and implementation for the existing agents' process of execution in the case of the asynchronous search techniques. That modelling, applying a technique for detecting the algorithms' termination, allows us to obtain two multi-agent systems that can be applied for implementing and evaluating the most outstanding asynchronous search techniques. That modelling can be used also for implementing most of the asynchronous search techniques, such as those from the AWCS family [3,4], ABT family [1], DisDB [1]. The modelling proposed in this paragraph allows the obtaining of implementations for asynchronous search techniques derived versions in which various situations that exist in reality are simulated: delays in supplying the messages, message management, etc. Implementation examples for those techniques can be found on the NetLogo site ([6] and in [5, 7]).

Any implementation for the asynchronous search techniques supposes the following two steps:

- ✚ programming the agents such as they run concurrently
- ✚ designing the user interface.

The modelling of the agents' execution process will be structured on two levels, corresponding to the two stages of implementation. The definition of the way in which asynchronous techniques will be programmed such that the agents to run concurrently and asynchronous will be the internal level of the model. The second level refers to the way of representing the NetLogo application, and is the exterior level. The first aspect will be treated and represented using turtle type objects. The second aspect (that is connected with the problem to be solved) refers to the way of interacting with the user, the user interface. Regarding that aspect, NetLogo offers patches type objects de tip and various graphical controls. Anyway, patches type objects will allow the simulation of the application's interface.

2.2.1. Agents' simulation and initialization

First of all, the agents are represented by the breed type objects (as we saw in the previous paragraph, those are of the turtles type). In there fig. 1 is presented the way the agents are defined together with the global data structures proprietary to the agents.

```

breeds [agents]
globals [variables that simulate the memory shared by all the agents]
agent-own [message-queue current-view nogoods messages-received_ok messages-received_nogood]
;message-queue contains the received messages.
;current-view is a list indexed on the agent's number, of the form [v0 v1 v2...], vi = -1 if we don't know the value o that agent.
;nogoods is the list of inconsistent positions [0 1 1 0 ... ] where 0 is a good position, and 1 is inconsistent.
;messages-received_ok and messages-received_nogood are variables that count the number of ok and nogood messages received by an agent.

```

Figure 1. Agents' definition in the case of the asynchronous search techniques

The initialization of the agents supposes building the agents and initialization of the necessary data structures for the agents' operation. For initialization there is proposed an initialization procedure for each agent, procedure presented in figure 2 (the procedure will be called setup). Typically the num-agents required for the running of the asynchronous search technique are built and the most important data structures are initialized.

```

to setup-agenții // the agents defined with the breeds [agenți] are used
; the num-agents agents are created and are initialized
create-custom-agenți num-agents [
  set messages-received_ok 0
  set current-view get-list num-agents -1
  set nogoods get-list num-agents 0
  set message-queue []
  ...
]
end

```

Figure 2. The initialization procedure for each agent-setup

2.2.2. Representation and manipulation of the messages

Any asynchronous search technique is based on the use by the agents of some messages for communicating various information needed for obtaining the solution. The manipulation of the messages supposes first of all message representation. This thing can be achieved in Netlogo by using some indexed lists. To represent complex messages that contain many information, Netlogo allows the use of lists of lists. The way of representation of the main messages encountered at the asynchronous search techniques is presented as follows:

- ✚ (list "ok" agent value agent_costs) – messages of the *ok* or *info* type;
- ✚ (list "nogood" agent current-view agent_costs) - messages of the *nogood* or *back* type;
- ✚ (list "add1" agent₁ agent₂ agent_costs)
- ✚ (list "remove1" agent₁ agent₂ agent_costs)

2.2.3. Definition and representation of the interface

As concerning the interface part, it can be used for the graphical representation of the DCSP problem's objects (queens or nodes) of the patch type. It is recommended to create an initialization procedure for the display surface where the agents' values will be displayed.

For the case of the graph coloring problem, the representation of nodes and links is done in the same way [5,6,7]. The two initialization procedures will be attached (using a setup procedure) to a start button of the application, as in the sequence in figure 3.

```
to setup
  ca
  setup-patches
  setup-nodes
  ask nodes [procedura_inicializare]
end
```

Figure 3. Setup procedure of the NetLogo application

3. IMPLEMENTATION AND EVALUATION METHODOLOGY FOR THE ASYNCHRONOUS TECHNIQUES

In this paragraph there is presented a methodology of implementation for the asynchronous search techniques in NetLogo, using the model presented in the previous paragraphs 2. That methodology supposes the identification of the application's objects, building the agents and of the working surface for the application. There are also built the communication channels between agents, routines for message handling and the main program of the application. The methodology contains more elements specific to NetLogo necessary for finalizing the implementation of the asynchronous search techniques. Any implementation based on the presented model, will require the following of the next steps.

P1. Defining the DCSP application's objects.

Starting from the type of problem that is implemented, it will be defined the objects of the DCSP application. In figure 4 is presented a solution of agents modelling and also for the working surface of the application. As in the modeling examples are proposed *breeds* [*queens*] (for modeling the agents associated to the queens from the problem of the n queens) or *breeds* [*vertices*] (for modeling the agents associated to each node from the problem of graph coloring).

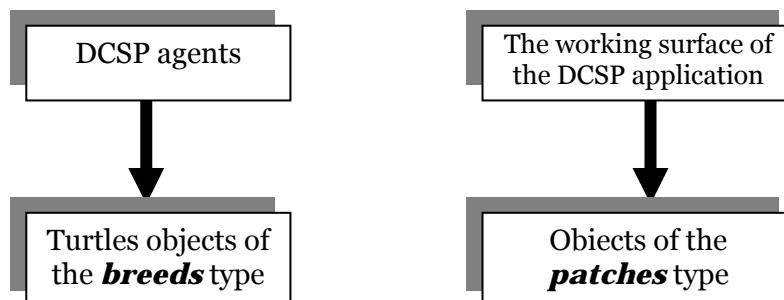


Figure 4. Identification of the objects of the DCSP application

In exchange, to model the surface of the application are used objects of the *patches* type. Depending on the significance of those agents, they are represented on the NetLogo surface. In figure 5 are presented two ways in NetLogo for representing the agents of the *queens* type, respectively *noduri*.

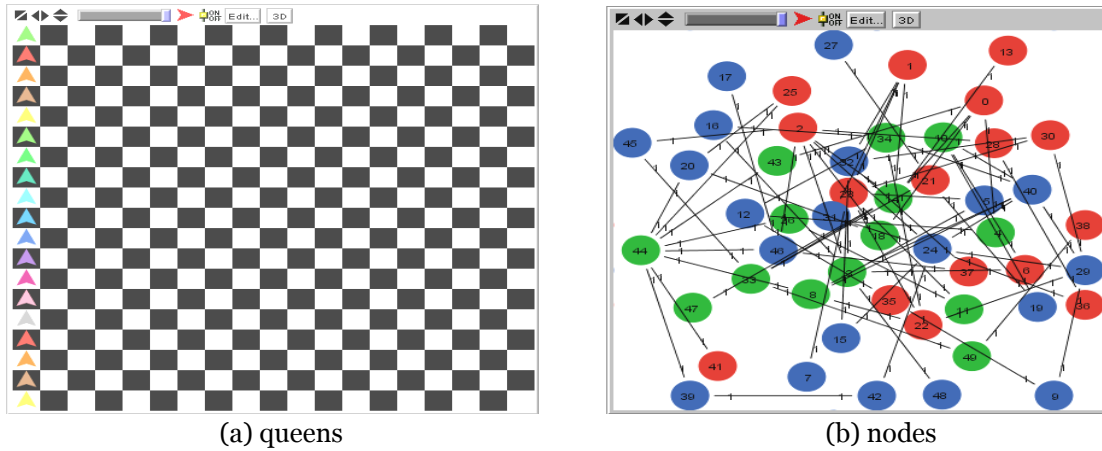


Figure 5. Examples of representation of the agents on the NetLogo surface

P2. Message handling. The FIFO type message channel.

Any agent keeps its working context at least as two proprietary structures: *current_view* and its *nogood* list. That context is used to take decisions, inclusively for building messages. For the proposed model, the data structures that store the working context of each agent can be simulated with lists. A representation solution is presented in figure 6 (a)

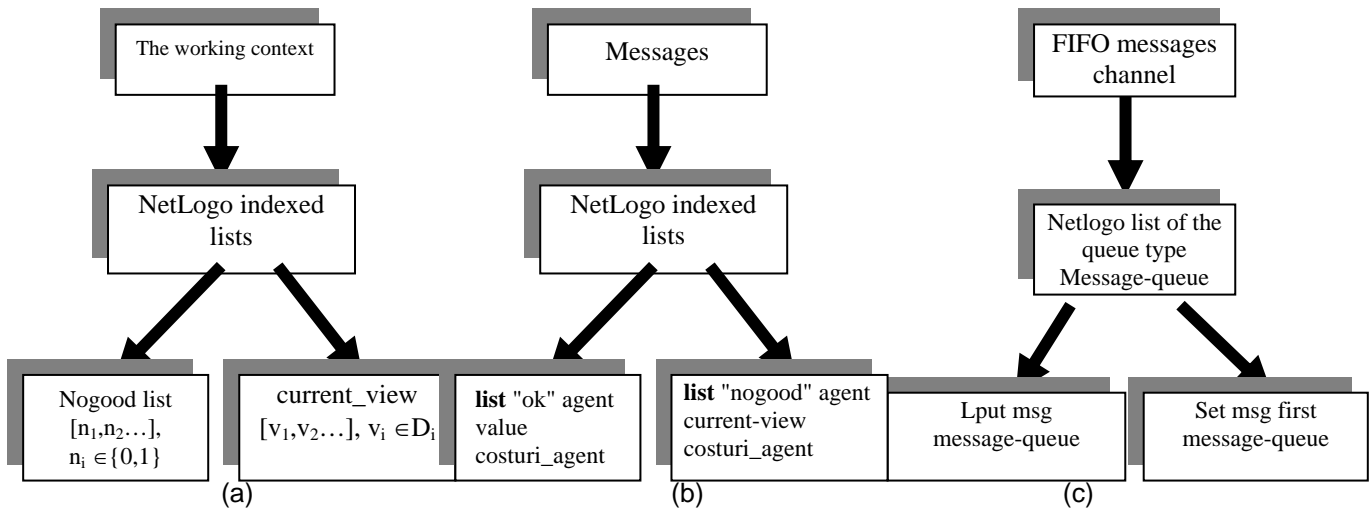


Figure 6. The necessary structures for message handling

```

to receive-message [msg]
  without-interruption [
    set message-queue lput msg message-queue]
end

to-report retrieve-message
  without-interruption [
    set msg first message-queue
    set message-queue butfirst message-queue]

to handle-message
  if (empty? message-queue) [stop]
  set msg retrieve-message
  if (first msg = "ok") [
    ok msg ]
  ...

```

Figure 7. Message handling

Message handling supposes first of all message representation. In figure 6.(b) is presented the way of representation of the main messages found at the asynchronous techniques. Simultaneous of message queues for each agent can be done using NetLogo lists, for which are defined routines of handling corresponding to FIFO principles (figure 6.(c)). These structures keep the messages received by each agent. Starting from NetLogo elements presented in figure 6, we can build three procedures for handling messages from the message queue, routines presented in figure 7. The first receive-message routine is used for receiving a new message, the second routine retrieve-message has as its purpose the extraction of a message from the waiting queue, being called in the message treatment routine. The last routine handle-message identifies the message type, calling the appropriate message handling routine.

P3. Application initialization and of each agent. “The main program” for application

The initialization of the application supposes the building of agents and of the working surface for them. When the agents are built the required initializations are also done. Usually, is initialized the working context of the agent (current-view), the message queues, the variables that count the effort carried out by the agent. In figure 8 are presented the two routines of application initialization and of agents initialization.

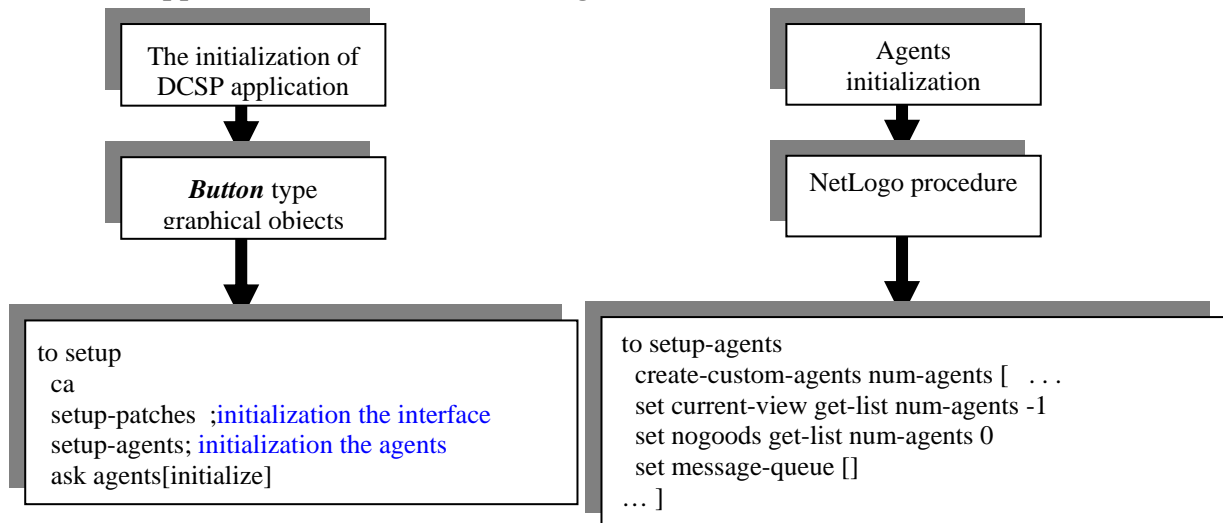


Figure 8. Initialization of the DisCSP application

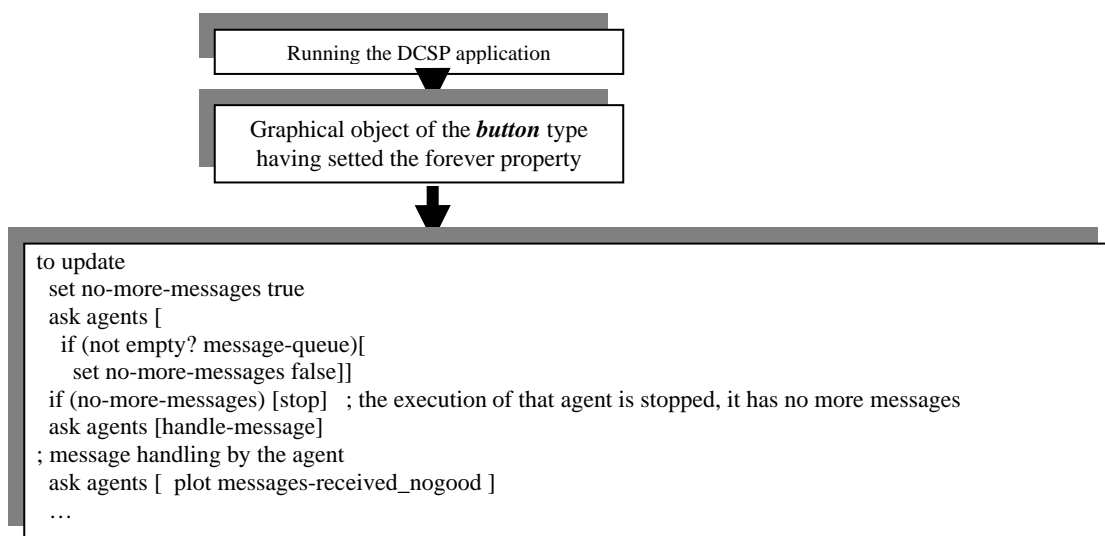


Figure 9. The procedure for running the DCSP application for the system SEIS

The working surface of the application should contain NetLogo objects through whom the parameters of each problem could be controlled: the number of agents, the density of the

constraints graph, the number of colors. These objects allow the definition and monitorization of each problem parameters.

For the application running is proposed the introduction of a graphical object of the button type and setting the *forever* property. That way, the attached code, in the form of a NetLogo procedure (that is applied on each agent) that will run continuously, until emptying the message queues and reaching the *Stop* command (which in NetLogo stops the execution of an agent). The solution presented in figure 9 is based on the utilization of the *ask* command. That NetLogo command executes a synchronization of each agent execution.

Another important observation is tied to attaching the graphical button to the *observer*. The use of this solution allows obtaining a solution of implementation with synchronization of the agents' execution. In that case, the *observer* will be the one that will initiate the stopping of the DisCSP application execution. In figure 9 the *update* procedure is attached and handled by the *observer*. These elements lead to the multi-agent system with synchronization of the agents execution (SEIS). If it's desired to obtain a system with asynchronous operation (SIEAS), will be used the second method of detection, which supposes another *update* routine. That new *update* routine will be attached to a graphical object of the *buton* type which is attached and handled by the turtle type agents.

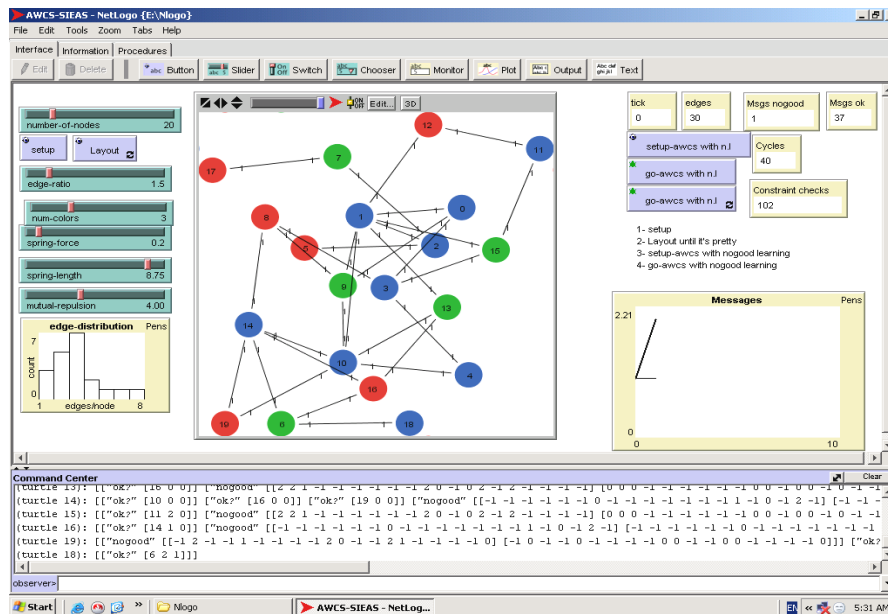


Figure 10. NetLogo implementation for AWCS technique- SEIAS

P4. Monitorization of the evaluation parameters

The model presented in this chapter allows storing the costs for obtaining the solution. That thing can be done using some variables attached to the agents. For counting the flow of messages it can be used a variable proprietary to each agent (*messages-received_nogood,etc*), variable that needs to be incremented in the moment of receiving a message. That variable is incremented in the routine of message manipulation *handle-message*. Also, for measuring the work effort carried out by the agents can be used two variables *nr_constraintc* and *c-ccks*. Those variables store the costs necessary for each agent. Thus, those costs should be measured.

Application of the methodology presented previously allows the implementation and evaluation of any asynchronous search technique. In figure 10 is captured an implementation for the AWCS technique that uses uses the multi-agent SIEAS system.

4. CONCLUSIONS

In this article was analysed the NetLogo environment with the purpose of building a general model of implementation and evaluation for the asynchronous techniques such as

they could use the NetLogo environment as a basic simulator in the study of asynchronous search techniques.

In this article was proposed a general model of implementation and evaluation for the asynchronous search techniques. The proposed model supposed the identification of NetLogo objects necessary for implementing the asynchronous search technique (agents, messages, message queues, agents ordering) and of the interface of interaction with the user. In this article was proposed solutions for simulating the objects of any DisCSP application. Also, were proposed solutions for counting the costs for obtaining a solution using different measuring units. That thing will allow the evaluation of performances for asynchronous search techniques and eventual improvements for them. Also, the model allows studying the behaviour of the agents for various techniques, studying the costs for each agent.

As a general conclusion, we think that the model we achieved can be used for the study and analysis of the asynchronous techniques, the model allowing their complete evaluation. Students can use the models on the site [7] to study, to understand the functioning of the asynchronous search techniques and, perhaps, to extend them. Starting from those models, they can develop other versions of the asynchronous search techniques.

BIBLIOGRAPHY

- [1] C. Bessiere, I. Brito, A. Maestre, P. Meseguer, Asynchronous Backtracking without Adding Links: A New Member in the ABT Family. *Artificial Intelligence*, 161:7-24, 2005
- [2] I. Muscalagiu, H. Jiang, H.E. Popa. “Implementation and evaluation model for the asynchronous techniques: from a synchronously distributed system to a asynchronous distributed system”, in *Proceedings of the 8th International Symposium on Symbolic and Numeric Algorithms for Scientific Computing (SYNASC 2006)*, Timisoara, Romania, *IEEE Computer Society Press*, 2006, pp. (209-216)
- [3] Yokoo M., E.H. Durfee, T. Ishida, K. Kuwabara (1998): *The distributed constraint satisfaction problem: formalization and algorithms*. *IEEE Transactions on Knowledge and Data Engineering* 10 (5)
- [4] Yokoo Makoto (2001): *Distributed Constraint Satisfaction- Foundation of Cooperation in Multi-agent Systems*. Springer
- [5] MAS Netlogo Models-a. <http://jmvidal.cse.sc.edu/netlogomas/>
- [6] MAS Netlogo Models-b. <http://ccl.northwestern.edu/netlogo/models/community>
- [7] MAS Netlogo Models-c. <http://discsp-netlogo.fih.upt.ro/>
- [8] Wilensky, U. *NetLogo itself: NetLogo*. <http://ccl.northwestern.edu/netlogo/>. Center for Connected Learning and Computer-Based Modeling, Northwestern University. Evanston, IL, 1999



EDUCATIONAL SOFTWARE FOR ANALYSIS OF PARALLEL ALGORITHMS USING PRAM MODEL

OPREAN Alexandru-Ștefan, DUȚĂ Tatiana-Elena, PĂNOIU Manuela

Department of Electrical Engineering and Industrial Informatics,
“Polytechnic” University of Timisoara, ROMANIA

Abstract

This paper presents visual interactive software which shows through simulation the parallel access memory for PRAM model. The software was implemented in Java. It was also performed a comparative study between a classic sequential algorithm and a parallel algorithm in terms of execution times.

Keywords:

Algorithm visualization, parallel access memory, Java, PRAM model

1. INTRODUCTION

The purpose of the theoretical models for parallel computation is to give frameworks by which we can describe and analyze algorithms. These ideal models are used to obtain performance bounds and complexity estimates. One of the models that have been used extensively is the parallel random access machine (PRAM) model [1]. A PRAM consists of a control unit, a global memory shared by p processors, each of which has a unique index as follows: P_1, P_2, \dots, P_p . In addition to the global memory via which the processors can communicate, each processor has its own private memory. Based on the different modes for read and write operations, the PRAM can be further divided into the following subclasses:

- ✚ EREW PRAM: Access to any memory cell is exclusive. This is the most restrictive PRAM model.
- ✚ ERCW PRAM: This allows concurrent writes to the same memory location by multiple processors, but read accesses remain exclusive.
- ✚ CREW PRAM: Concurrent read accesses are allowed, but write accesses are exclusive.
- ✚ CRCW PRAM: Both concurrent read and write accesses are allowed.

2. DESCRIPTION OF THE SOFTWARE

The target of this application is to help students in understanding the parallel and sequential algorithms. Another goal for this project is to show a comparative study between a classic sequential algorithm and a parallel algorithm in terms of execution times.

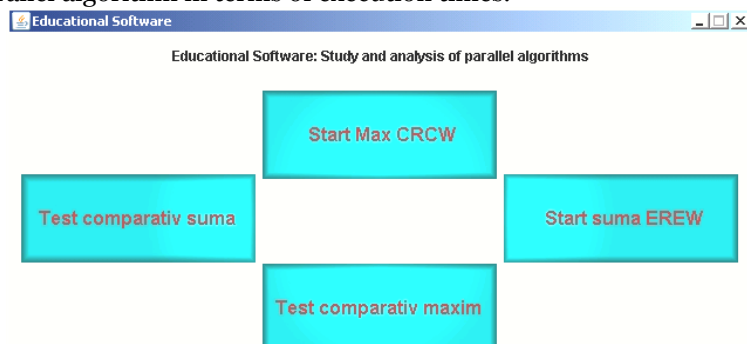


Figure 1. Main Menu

The application was implemented in Java as independent application. The application can easily convert in a Java applet. For simulation the It is made so that it possible for students and beginners to use the application. From the main menu that you can see in Figure 1 you can choose one of four options of the software:

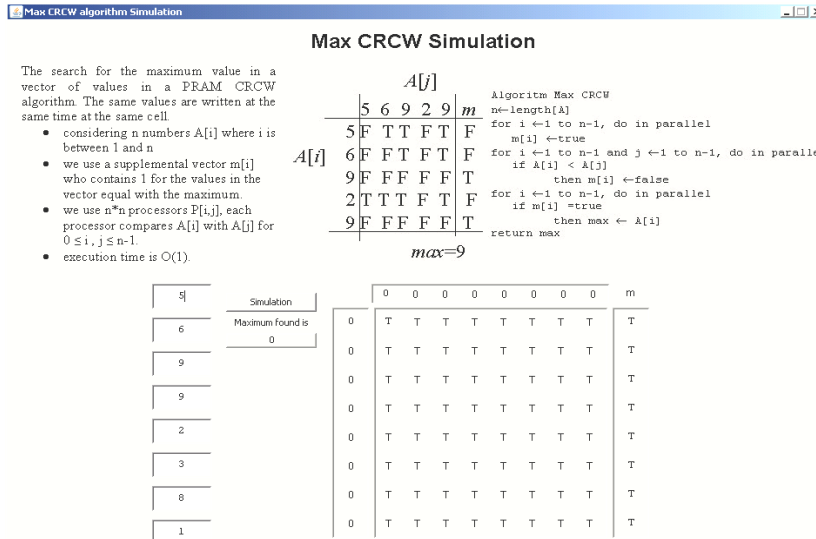
- ✚ Description of the PRAM CRCW maximum search algorithm
- ✚ Description of the PRAM EREW sum algorithm
- ✚ A comparative study between the PRAM CRCW maximum search algorithm and the classic sequential.
- ✚ A comparative study between the PRAM EREW sum algorithm and the classic sequential variant.

By selecting any of these options from the application interface a new window will open which will contain each part of the application.

Buttons are simulations realized with the help of images created with the 3D Button program.

2.1. Maximum search CRCW Simulation

This is the main frame for the Maximum Search algorithm simulation. This presents the steps taken by the Maximum Search CRCW algorithm.



The search for the maximum value in a vector of values in a PRAM CRCW algorithm. The same values are written at the same time at the same cell.

- considering n numbers $A[i]$ where i is between 1 and n
- we use a supplemental vector $m[i]$ who contains 1 for the values in the vector equal with the maximum.
- we use $n \cdot n$ processors $P[i,j]$, each processor compares $A[i]$ with $A[j]$ for $0 \leq i, j \leq n-1$.
- execution time is $O(1)$.

	$A[j]$					m
	5	6	9	2	9	F
$A[i]$	5	F	T	T	F	F
	6	F	F	T	F	F
	9	F	F	F	F	T
	2	T	T	T	F	F
	9	F	F	F	F	T

```

Algorithm Max CRCW
n←length[A]
for i ←1 to n-1, do in parallel
  m[i] ←true
  for j ←1 to n-1, do in parallel
    if A[i] < A[j]
      then m[i] ←false
  for i ←1 to n-1, do in parallel
    if m[i] =true
      then max ← A[i]
return max
    
```

$max=9$

The algorithm which searches for the maximum in a vector of values with the aid of the Maximum search CRCW (Concurrent Read Concurrent Write) algorithm is presented and simulated in our application.

The theory behind the algorithm is presented on the upper part. The simulation of the algorithm is made so that the user can input some 8 values for the vector. By pressing the Simulate button the process begins. First the top and left vectors are initialized with the values introduced by the user. Then

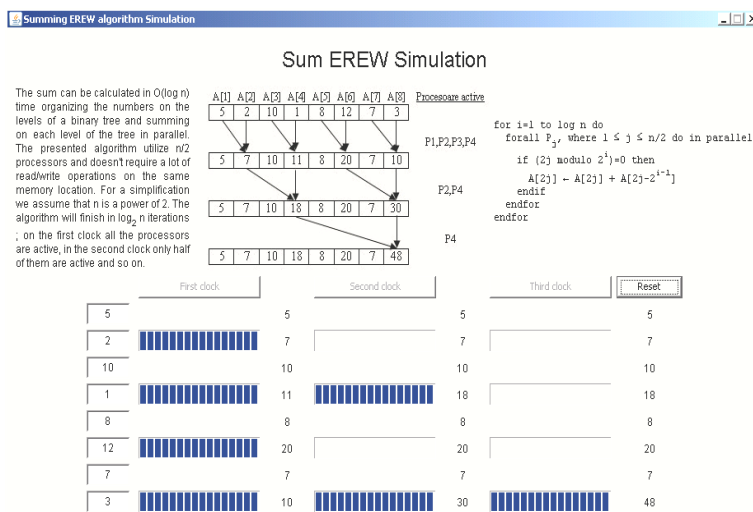
Figure 2. Maximum Search Simulation

the middle matrix is initialized with the start (F=False) value. The m vector is initialized also.

After the first phase the simulation of the algorithm is started. The middle matrix is obtained by the tests between $A[i]$ and $A[j]$. Meanwhile the m vector is obtained. After the m vector is found, the maximum value of the vector is found: where $m[i]$ is true, $v[i]$ is the maximum.

2.2. Summing algorithm EREW Simulation

This is the frame which presents the simulation for the summing EREW algorithm.



The sum can be calculated in $O(\log n)$ time organizing the numbers on the levels of a binary tree and summing on each level of the tree in parallel. The presented algorithm utilize $n/2$ processors and doesn't require a lot of read/write operations on the same memory location. For a simplification we assume that n is a power of 2. The algorithm will finish in $\log_2 n$ iterations ; on the first clock all the processors are active, in the second clock only half of them are active and so on.

$A[1]$	$A[2]$	$A[3]$	$A[4]$	$A[5]$	$A[6]$	$A[7]$	$A[8]$
5	2	10	1	8	12	7	3

```

for i=1 to log n do
  forall  $P_j$ , where  $1 \leq j \leq n/2$  do in parallel
    if  $(2j \text{ modulo } 2^i) = 0$  then
       $A[2j] \leftarrow A[2j] + A[2j-2^{i-1}]$ 
    endif
  endforall
endfor
    
```

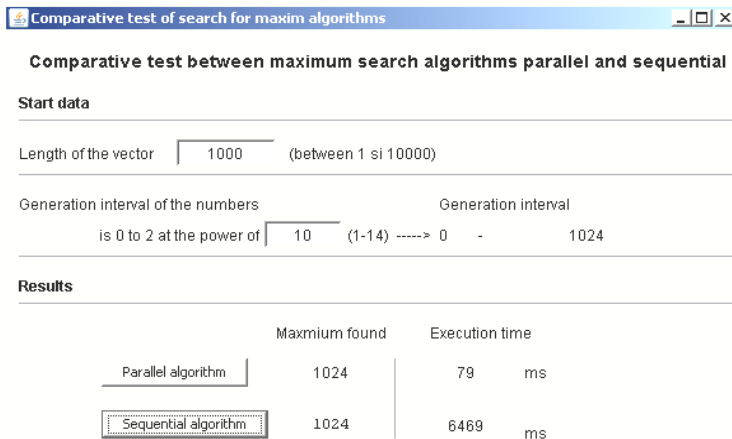
Processor active: $P1, P2, P3, P4$, $P2, P4$, $P4$

To simulate the summing algorithm in parallel the user must input some start values for the vector to be summed. To start the algorithm we first click the First Clock button. After the first clock of the simulation (the simulation is done by filling 4 progress bars showing that 4 processors are active) we can pass to the second clock of the simulation. In this clock, only half of the processors active in the previous clock are active (showed by only two progress bars). At the last clock only one processor is active. After this clock, the sum of all 8 values is in the last field on the down right part of the frame.

Figure 3. Summing algorithm Simulation

2.3. Comparative Study for the maximum search algorithms

In this frame we want to show the execution times for the classic sequential algorithm and the parallel CRCW algorithm. For this study we have made it possible for us to choose the length of the vector for the search and the maximum value of each value of the vector.



To run the comparative test of the two algorithms the user must insert the length of the vector and the generation interval for the values (this generation interval is found between 0 and 2 at the power of the value entered). In case the introduced data is wrong the application will show an error message. If we will not introduce a number in one of the input box, the application will show the next error message.

In case of a value lower of larger than the provided interval the application will show a attention message. In case the user didn't fill the start values and he wishes to execute the parallel or sequential algorithm the application will show another attention message.

Figure 3. Comparative Study for the maximum search algorithms

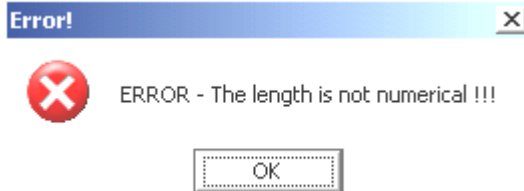


Figure 4. Error message

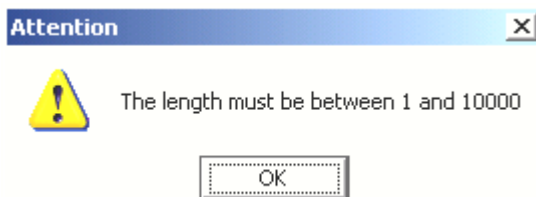


Figure 5. Attention message

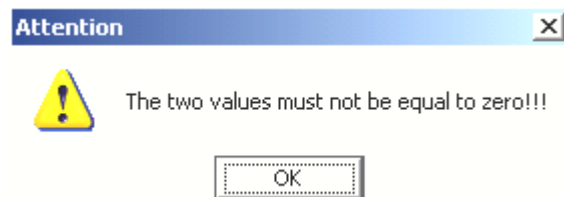


Figure 6. Attention message

2.4. Comparative study for the summing algorithms

This frame presents a comparative study for the execution times of the summing algorithms, the sequential and the parallel one.

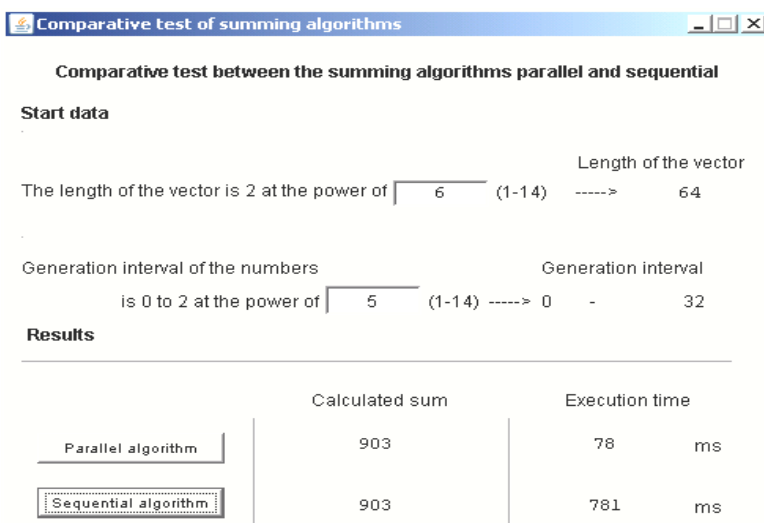


Figure 4. Comparative study for the summing algorithms

To start the comparative test between the two algorithms the user must fill in the initial data. If the values are not filled in, the application sends the user error or warning messages.

After the input parameters are filled in the two algorithms are executed and the application calculates and shows the execution times for the two algorithms. To verify if the two algorithms are working on the same set of numbers we can compare the two sums displayed. The results of some comparative tests are show in Table 1 for finding maxim algorithm and in Table 2 for

summing algorithm. The computer used for the test was an Intel Pentium Mobile, processor frequency 1,7 GHz, 1024 MB RAM, operating system Microsoft Windows Xp SP2.

Table 1 The run time for CRCW maximum search algorithm

Input data	Nr. crt of test	Parallel algorithm	Sequential algorithm
Vector length: 4096 (2^{12}) Values interval: 0 – 256 ($0 - 2^8$)	1.	1782 ms	44344 ms
	2.	1622 ms	44384 ms
	3.	1682 ms	44664 ms
	4.	1712 ms	47618 ms
	5.	1683 ms	48530 ms
Vector length: 4096 (2^{12}) Values interval: 0 – 256 ($0 - 2^8$)	1.	110 ms	721 ms
	2.	130 ms	771 ms
	3.	150 ms	721 ms
	4.	121 ms	741 ms
	5.	70 ms	731 ms

Table 2 The run time for EREW summing algorithm

Input data	Nr. crt	Parallel algorithm	Sequential algorithm
Vector length: 128 (2^7) Values interval: 0 – 256 ($0 - 2^8$)	1.	10 ms	731 ms
	2.	10 ms	771 ms
	3.	10 ms	751 ms
	4.	15 ms	721 ms
	5.	10 ms	761 ms
Vector length: 1024 (2^{10}) Values interval: 0 – 512 ($0 - 2^9$)	1.	30 ms	6740 ms
	2.	20 ms	6810 ms
	3.	10 ms	6829 ms
	4.	40 ms	6900 ms
	5.	31 ms	6659 ms

3. CONCLUSIONS

Analyzing the tests results it can be observe that form point of view of the execution time, the parallel algorithms are more efficient than the sequential algorithms, but the total cost of the parallel algorithm are higher in terms of processors numbers. Since a good sequential algorithm can sum the list of n elements and also find the maximum of the elements in $O(n)$, these algorithms is not cost optimal.

However, the PRAM model is a very useful model for study the parallel access to the memory, and the present application can do this an interactive manner, so that the students will better understand these concepts.

REFERENCES

- [1.] Hesham El-Rewini, Mostafa Abd-El-Barr, Advanced Computer Architecture and Parallel Processing, Wiley+Interscience, 2005
- [2.] Herlo D. - Metodologia educațională, Editura Universității „Aurel Vlaicu”, Arad, 2000
- [3.] Ioan Jurca – Programarea orientată pe obiecte. Limbajul Java, Editura de Vest, Timișoara, 2005
- [4.] Ștefan Tanasă, Cristian Olaru, Ștefan Andrei – Java de la 0 la expert, Editura Polirom, Iași, 2003
- [5.] Motogna, S. – Metode și tehnici de proiectare a algoritmilor, Editura Universității Babeș-Bolyai, Cluj Napoca, 1999



EDUCATIONAL SOFTWARE METHODS AND STRATEGIES FOR DESIGNING ALGORITHMS BACKTRACKING, GREEDY METHOD AND DYNAMIC PROGRAMMING

DUȚĂ Tatiana-Elena, OPREAN Alexandru, PĂNOIU Manuela

Department of Electrical Engineering and Industrial Informatics,
"Politechnica" University of Timisoara, ROMANIA

Abstract

This paper present visual interactive software which shows through simulation the main algorithms use in searching solutions in artificial intelligence. It was studies backtracking, greedy and dynamical programming algorithms. The software is multimedia educational software designed for acquisition and learning process and it can be seen as a modern method for teaching methodology. It was also perform a comparative study of these algorithms using some typical known problems.

Keywords:

Algorithm visualization, backtracking, dynamic programming, greedy algorithm

1. INTRODUCTION

The teaching art consists not only in the scientific strictness of exposing the subject matter to be studied, but also in including in this activity of all influence forms upon the student [1]. One of the main aspects of using computer for lessons is the development of the students creative thinking. An optimal mean in this case is the introduction in the computational training means of the interactivity elements. Educational software provides this important feature - it is interactive: it offers to the learner the opportunity to manipulate the model for achieving in a short time, a high volume of knowledge (more complex and stable).

This paper present not only one useful application to the study of solving algorithms with backtracking, greedy method and dynamic programming but also a comparative study of these algorithms in terms of executive time.

2. DESCRIPTION OF THE INFORMATICS SYSTEM

For informatics system design it was use a visual oriented object language, Borland C++ Builder. This environment is very useful because it generate a native code for Windows platform, which is the most used operating system.

Application interface is very simple. I have focused on the fact that all students and even beginners, in algorithms and programming tricks could use it. From the main menu, you can see in Figure 1, you can choose four paths of the project:

-  Presentation of Backtracking method
-  Presentation of Greedy method
-  Presentation of Dynamic Programming
-  A comparative study for these three algorithms earlier selected

By selecting any of these options from the application interface a new window will open which will contain the main menu for accessed algorithm.

The animation is realized using Xara 3D and starts the creation of the form.

Buttons are simulations realized with the help of images performed through program 3D Button. The effect of "push" the buttons is realized with Label type components, showing the explanatory text of the buttons.

Here are the main buttons for navigation. The name of each button will show the exact segment you want to make active. So, every time you click on *, from the book, you are accessing the "Theory" page where you'll find three more buttons. Each button is a links for another page, where you can find, depending on the button name, information about the accessed method.

The "POLITEHNICA" University of Timisoara
The Faculty of Engineering of Hunedoara
Domain: Industrial IT

Educational Software

METHODS AND STRATEGIES FOR THE DESIGN ALGORITHMS

BACKTRAKING, METHOD GREEDY AND DYNAMIC PROGRAMMING



Figure 1. Main Menu

constraint satisfaction problems. It is often the most convenient (if not the most efficient) technique for parsing, for the knapsack problem and other combinatorial optimization problems. It is also the basis of the so-called logic programming languages such as Prolog use for artificial intelligence. Backtracking can be applied only for problems which admit the concept of a "partial candidate solution" and a relatively quick test of whether it can possibly be completed to a valid solution. When it is applicable, backtracking is often much faster than brute force enumeration of all complete candidates, since it can eliminate a large number of candidates with a single test.

For backtracking algorithm simulation it was use the following well known problems: the N queen’s problem, the coloring maps problem, the horse jump on chessboard problem, and other problem that can be solve using backtracking. From these one, in this paper is present the map coloring problem.

The map coloring problem is a very well known problem and consists in finding the appropriate color to coloring a map so than two neighborhood regions on the map to have distinct colors. The graphical user interface for algorithm analyze in shown in fig. 3.



Figure 2. Main Menu Backtracking

By running a click on Applications, you'll find applications, made to exemplify through images and algorithm of this procedure. Also, through the window on the right corner of the interface, you can learn what each button contains, simply passing the mouse over it.

2.1. Backtracking algorithm simulation

Backtracking is a general algorithm for finding all (or some) solutions to some computational problem, that incrementally builds candidates to the solutions, and abandons each partial candidate c ("backtracks") as soon as it determines that c cannot possibly be completed to a valid solution, [3].

Backtracking is an important tool for solving

The simulation allows to visualize the algorithm step by step or to visualize entire algorithm. For the first case the user can push the “Step by step” button after each step. This means that appear a new color for the current region on the map, after pushing the above mentioned button. At the same time the stack variation is updated by increasing or decreasing the top of stack. During the simulation the user can see the stack variation and the map partially colored. The test map can be load from a file (a *.bmp file). In a frame is show also the algorithm implemented in C++. After a solution is found, this is displayed in a separate frame.

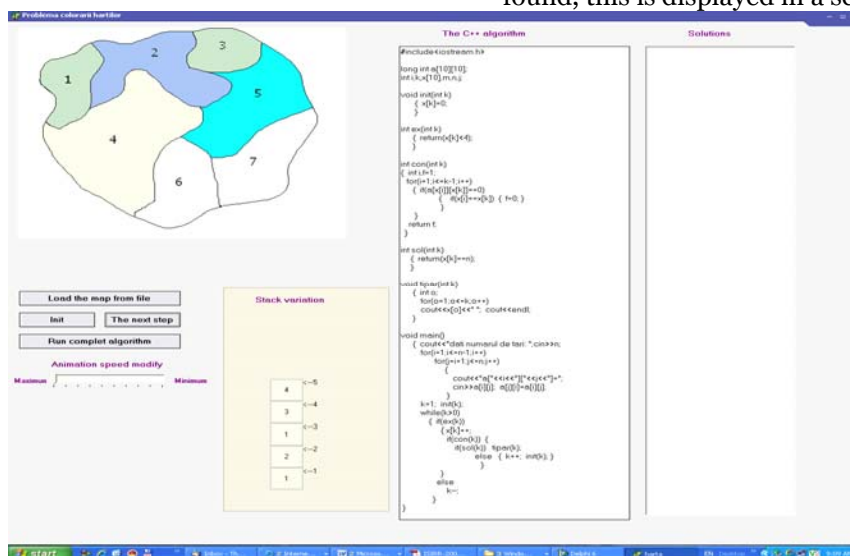


Fig. 3. The map coloring problem

2.2. Greedy algorithm simulation

A greedy algorithm is any algorithm that follows the problem solving meta-heuristic of making the locally optimal choice at each stage [4] with the hope of finding the global optimum. For example, applying the greedy strategy to the traveling salesman problem yields the following algorithm: "At each stage visit the unvisited city nearest to the current city". Greedy algorithms mostly (but not always) fail to find the globally optimal solution, because they usually do not operate exhaustively on all the data. Nevertheless, they are useful because they are quick to think up and often give good approximations to the optimum.

For Greedy algorithm simulation it was use the following well known problems: Dijkstra’s Algorithm, Connecting cities with minimum cost, Prim’s Algorithm, the Knapsack problem. These examples can be selected using a graphical user interface similar with the one presented in fig. 2.

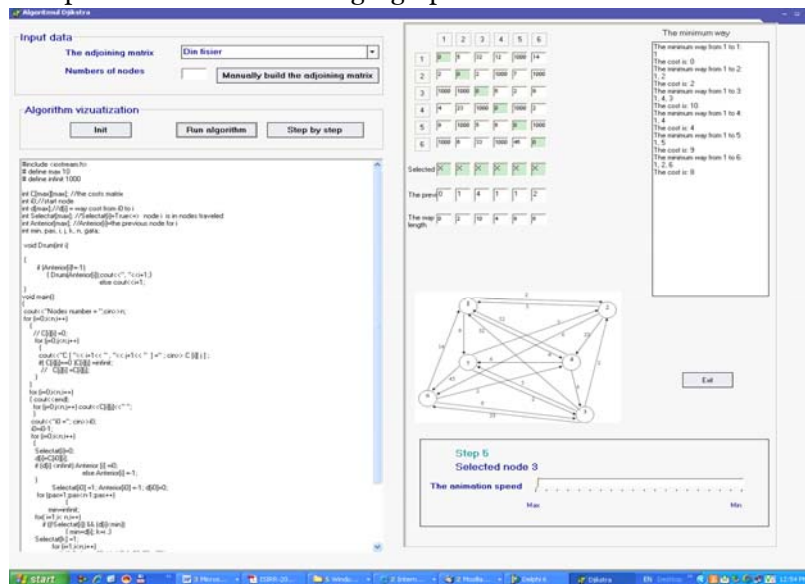


Fig. 4. The Dijkstra’s algorithm visualization

The Dijkstra’s algorithm visualization is exemplified in this paper. The graphical user interface is shown in fig. 4.

In this simulation, the user can build the adjoining matrix for the graph manually or be loading from a file. As the previous presented simulation, the user can run the entire algorithm using a desired animation speed or the algorithm can be run step by step. During the simulation, the user can see the costs matrix updating, a vector with selected nodes and the current length way in each moment. Finally, in a frame on the GUI, all the ways from all the nodes

to the selected start node are printed. The user can see also the algorithm implemented in C++ language.

2.3. Dynamical programming algorithm simulation

In computer science and also in mathematics, dynamic programming is a method of solving problems that exhibit the properties of overlapping subproblems and optimal substructure [5]. The method takes much less time than native methods. This method can be applied to many string algorithms including longest common subsequence, longest increasing subsequence, longest common substring. It can be also applied to many algorithmic problems on graphs can be solved efficiently for graphs of bounded treewidth or bounded clique-width by using dynamic programming on a tree decomposition of the graph. In this software was simulating the Roy – Floyd algorithm. This is a simple algorithm for determining dot-matrix graph roads. One execution of algorithm finds the shortest path between all pair vertices of the graph. In many practical situations the question is to determine a shortest way between two vertices of the graph. The graphical user interface is similar with the GUI for Dijkstra’s algorithm simulation and provides the same options. Another simulation was made for maze problem.

3. CONCLUSIONS. COMPARATIVE STUDY

Comparative study was possible after using backtracking algorithms, greedy and dynamic programming of some representatives problems. The conclusions are presented below.

3.1. Backtracking-Dynamic programming

Solving problems by dynamic programming is done in polynomial time, because each optimal "more general" is calculated from optimum "more private" searching in polynomial time, and the calculated optimum time is not recalculated later but switched to calculating the optimum "more general".

Therefore the method of dynamic programming may be considered as an alternative to the backtracking method. It is clear that the problems which may be solved through backtracking may be solved by dynamic programming as well. If the backtracking method is used you can obtain an algorithm that can reach (in the most unfavorable case) exponentially. Dynamical programming is more efficient that Backtracking.

If the dynamic programming method is used we can obtain a single optimal solution, unlike the backtracking method that generates all the optimal solutions.

3.2. Backtracking-Greedy

Although both methods offer solutions in the form of vector, the greedy method and backtracking method have the following differences:

- ✚ backtracking technique provides all the problem solutions, while greedy method is providing a single solution;
- ✚ greedy technique doesn't have a mechanism for going back (which is specific for backtracking method) that is why is impossible to achieve the global optimum.

Regarding the time running, Greedy algorithms are more efficient but it doesn't apply to whatever problem.

3.3. Greedy-dynamic programming

Both dynamic programming and greedy technique can be used when the solution to a problem is seen as the result of a sequence of decisions. The essential difference between greedy technique and dynamic programming is that the greedy method generates a single sequence of decisions, exploiting incompletely the optimality principle. In dynamic programming are generated more sub sequential decisions, taking in consideration the optimality principle, but considering only the best sub sequences, combining them in the final optimal solution. Although the total number of sequences of decisions is exponential, dynamic programming algorithms are often polynomial, the reduction of complexity due to the use optimality principle. Another important characteristic of dynamic programming is that it stores the optimum sub sequences, thus avoiding their recalculation.

Although the greedy algorithm does not guarantee obtaining the optimal solution, however it has the advantage that it is more efficient in terms of execution time and memory used than dynamic programming algorithm and the corresponding backtracking method.

Final conclusion is: when solving a problem by greedy method, execution time is polynomial (instant solution) for different input data. Solving through the backtracking method the execution time increases exponentially by the increase of input data's volume. For the dynamic programming method the execution in most cases is increasing polynomial with the input data. If recursively is used in solving a problem using dynamic programming, execution time increases exponentially with the input data.

REFERENCES

- [1.] E. Scalon, C. Tosunoglu, A. Jones, P. Butcher, S. Ross, J. Greenberg, Learning with computers : experiences of evaluation, Computer Education, Elsevier Science, 1998
- [2.] J. Trindade, C. Fiolhais, L. Almeida, Science Learning in Virtual Environments, British Journal of Educational Technology, 2002
- [3.] Donald E. Knuth (1968). The Art of Computer Programming. Addison-Wesley.
- [4.] Introduction to Algorithms (Cormen, Leiserson, and Rivest) 1990, Chapter 16 "Greedy Algorithms" p. 329.
- [5.] Bertsekas, D. P., 2000. Dynamic Programming and Optimal Control, Vols. 1 & 2, 2nd ed. Athena Scientific.
- [6.] Herlo D., Metodologia educațională, Editura Universității „Aurel Vlaicu”, Arad, 2000
- [7.] Mihai Oltean, Programare avansată în Delphi, Editura Albastră, Cluj-Napoca, 2000
- [8.] Pătruț B., Aplicații în Delphi, Editura Teora, București, 2001
- [9.] Sorin T., Inițiere în programarea vizuală, Editura L&S INFOMAT, București, 2002
- [10.] Vladimir-Ioan Crețu, Structuri de date și algoritmi, Editura Orizonturi Universitare, Timișoara 2000



EDUCATIONAL SOFTWARE FOR THE PRESENTATION OF HYPERBOLOID

IORDAN Anca, PĂNOIU Manuela

Technical University of Timisoara, Engineering Faculty of Hunedoara, ROMANIA

Abstract:

The informative society needs important changes in educational programs. The informational techniques needs a reconsideration of the learning process, of the programs, manuals structures, a reconsideration of the methods and organization forms of the didactic activities, taking into account the computer assisted instruction and self instruction. This paper presents a software package, which can be used as educational software.

Keywords:

Educational Software, Java, Hyperboloid, Distance Education.

1. INTRODUCTION

In the condition of informatics society whose principal source in the social-economic development is to produce and consumption the information, the complex and fast knowledge of the reality for rational, opportune, effective decisions is a desideratum which generate the necessity to form some superior level habituation in information manage for the whole population. The computers and their programs offer to the users powerful capabilities for the information manipulation: image and text visualize on the screen which can be manipulate later; memory storage of an important quantity of information, his accessing and selection of a part of them; possibility to realize a great volume of computation; possibility of equipment control and fast decisions; Computer Based Training [1]. This facilities offer to the microcomputers higher educational capabilities versus other technologies used in education and provide learning controlled based on many parameters: intellectual aptitude, level of knowledge, abilities, rhythm of work.

2. COMPUTER BASED TRAINING AS A DIDACTIC METHOD

The informatics society makes sensitive modification in education programs. In this scope, the school must prepare programmers, maintenance technicians, etc. In the same time it is necessary that the teacher make ready to use the computer in education process.

These informational techniques impose to reorganize the contents of the education process, of the programs, course books and manuals, to reconsider the methods and organization forms of didactic activities, which follow to be center on individualization of the teaching process [4].

The programmed teaching consist in information presentation in small units, logic structured, units that compose a program, the teaching program. The user will have possibility that after each sequence to have a knowledge about the measure of understanding the give information. The programmed teaching method organize the didactic action applying the cybernetic principles to the teaching-learning-evaluating activities level, considering like a complex and dynamic system, composed as an elements ensemble and inter-relations and develop his personal principles valid on the strategic level in any cybernetic organization form of teaching.

On the other hand, programmed teaching assume some principles which the teaching program must respect [6]:

- ✚ The small steps principle consists in progressive penetration, from simple to complex, in a subject content which logic divided in simple units series lead to minimal knowledge, which later will form an ensemble. This principle regards the subject division in contents/information units that give to user the chance to succeed in his teaching activities;
- ✚ The principle of personal rhythm of study regard mannerism observance and capitalization of each user of the program which will be able to make the sequences of knowledge learning or control, in a personal rhythm appropriate to his psycho-intellectual development, without time limits. The user can progress in the program only if he accomplished the respective sequence requirement;

- # The active participation principle, or active behavior, regard user effort trend into selection, understanding and applying the necessary information in elaboration of a correct answer. On each step the user is liable to an active participation to resolve the step job;
- # The principle of inverse connection, regard positive or negative inputs of user competence, refer to the success or breakdown in task performed;
- # The immediate and directly control of the task work precision with the possibility to progression to the next sequence, in case of success;
- # The repetition principle, based to the fact that the programs are based on return to the users initial knowledge.

The combined programming interposes the linear and branch sequence according to teaching necessities.

After linear and branch programming the computer aided generative teaching has appear, where the exercises are gradually present, with different difficulty steps and answers on the students questions.

The expert system consists of self-teaching training programs, tutorial strategies, and the usage of natural language, mixed initiative and some complex representation of knowledge usage [7].

The computer based programmed teaching realize learning process with a inputs flow – the command, an executive controlled system, an output flux – control and a control system functions which correct measure establish.

In such a system have tree stages of teacher perceive: teaching, evaluating and the feedback loop closing, the computer being present in all of tree stages.

3. HYPERBOLOID

A hyperboloid is a quadratic surface which may be one sheet or two sheets. The one sheet hyperboloid is a surface of revolution obtained by rotating a hyperbola about the perpendicular bisector to the line between the foci, while the two sheets hyperboloid is a surface of revolution obtained by rotating a hyperbola about the line joining the foci [2].

The one sheet hyperboloid is given in cartesian coordinates by [3]:

$$\frac{x^2}{a^2} + \frac{y^2}{a^2} - \frac{z^2}{c^2} = 1. \quad (1)$$

The parametric equations of an one sheet hyperboloid can be written as [5]:

$$\begin{aligned} x(u, v) &= a \cdot \sqrt{1 + u^2} \cdot \cos v; \\ y(u, v) &= a \cdot \sqrt{1 + u^2} \cdot \sin v; \\ z(u, v) &= c \cdot u. \end{aligned} \quad (2)$$

The two sheets hyperboloid is given in cartesian coordinates by [8]:

$$\frac{x^2}{a^2} - \frac{y^2}{a^2} - \frac{z^2}{c^2} = 1. \quad (3)$$

4. APPLICATION PRESENT

This paper presents a software package, which can be used as educational software to the course of analytical geometry for presentation of the hyperboloid. The application is implemented in Java, under Microsoft Windows operating system. The graphical user interface was structured in three parts:

- the theoretical presentation;
- the presentation of solved problems;
- the solution of representative types of problems.

From the application window it can selected by a main menu the following options:

- the determination of the first quadratic fundamental form of hyperboloid;
- the determination of the second quadratic fundamental form of hyperboloid;
- the graphic representation of hyperboloid;
- the plan tangent and the normal to the hyperboloid into a point.

In the figure 1 is represented hyperboloid of one sheet by using the following projections: ($\alpha=-145, \beta=-30, \gamma=90$), ($\alpha=145, \beta=-30, \gamma=60$), ($\alpha=45, \beta=0, \gamma=145$) and ($\alpha=-20, \beta=100, \gamma=150$).

In the figure 2 is represented hyperboloid of two sheets by using the following projections: ($\alpha=-145, \beta=-30, \gamma=90$), ($\alpha=45, \beta=150, \gamma=90$), ($\alpha=-60, \beta=60, \gamma=150$) and ($\alpha=120, \beta=-120, \gamma=45$).

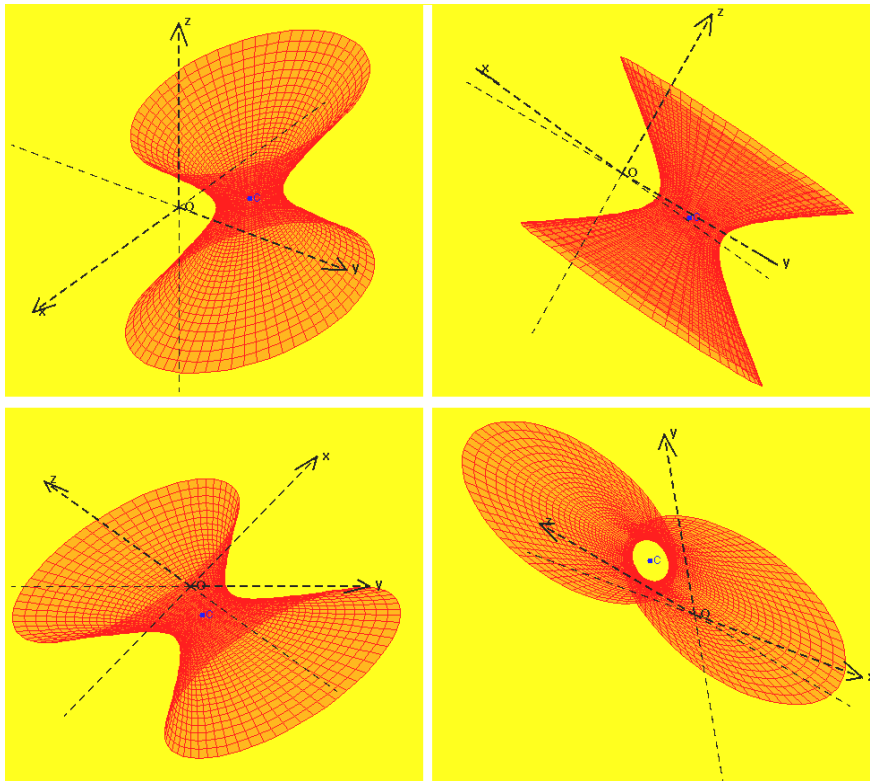


Figure 1. Hyperboloid of one sheet

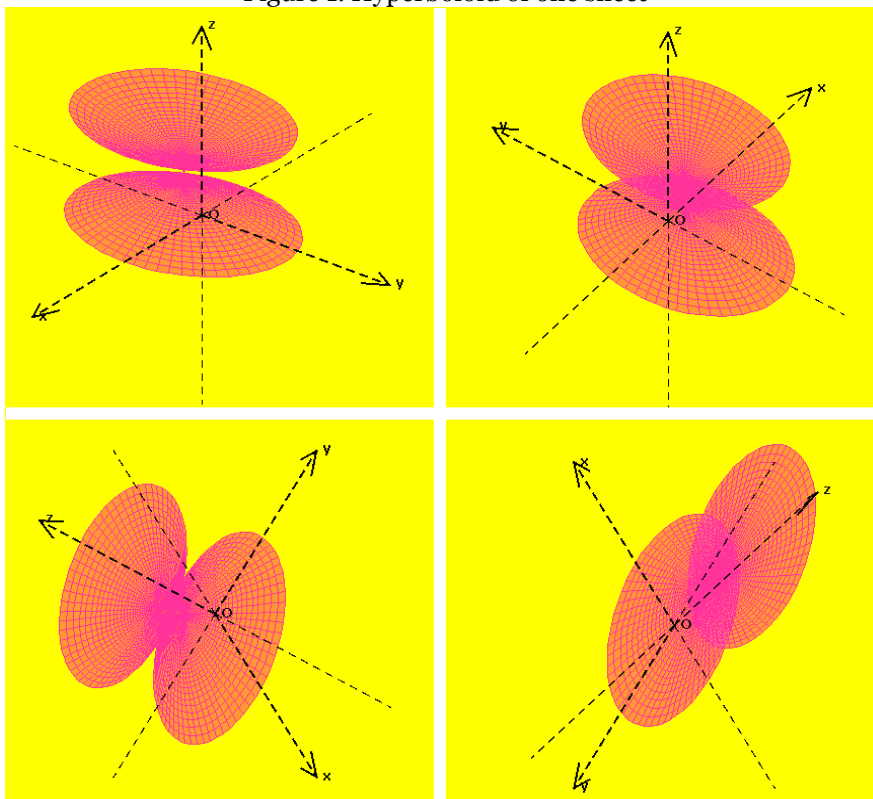


Figure 2. Hyperboloid of two sheets

The hyperboloid is draw by the following function:

```
public void desenare(Graphics2D g, int latime, int inaltime, Proiectie pr) {
    figura=new GeneralPath();
    Punct2D pct[[[=new Punct2D[61][61];
    pct=matrice(latime,inaltime,pr);
    int ij;
    for (i=0;i<60;i++)
```

```

for (j=0;j<60;j++) {
    GeneralPath fig=new GeneralPath();
    fig.moveTo((float)(pct[i][j].getX()),(float)(pct[i][j].getY()));
    fig.lineTo((float)(pct[i+1][j].getX()),(float)(pct[i+1][j].getY()));
    fig.lineTo((float)(pct[i+1][j+1].getX()),(float)(pct[i+1][j+1].getY()));
    fig.lineTo((float)(pct[i][j+1].getX()),(float)(pct[i][j+1].getY()));
    fig.closePath();
    if (culoare.equals(Color.black)) g.setColor(new Color(0,0,0,100));
    if (culoare.equals(new Color(155,65,30))) g.setColor(new Color(155,65,30,100));
    if (culoare.equals(Color.green)) g.setColor(new Color(0,255,0,80));
    if (culoare.equals(Color.blue)) g.setColor(new Color(0,0,250,100));
    if (culoare.equals(new Color(155,55,150)))
    g.setColor(new Color(155,55,150,120));
    if (culoare.equals(Color.red)) g.setColor(new Color(255,0,0,110));
    if (culoare.equals(new Color(250,70,150))) g.setColor(new Color(250,70,150,120));
    if (culoare.equals(Color.yellow)) g.setColor(new Color(255,0,0,70));
    g.fill(fig);
}
for (i=0;i<=60;i++) {
    figura.moveTo((float)(pct[i][0].getX()),(float)(pct[i][0].getY()));
    for (j=1;j<=60;j++) figura.lineTo((float)(pct[i][j].getX()),(float)(pct[i][j].getY()));
}
for (j=0;j<=60;j++) {
    figura.moveTo((float)(pct[0][j].getX()),(float)(pct[0][j].getY()));
    for (i=1;i<=60;i++) figura.lineTo((float)(pct[i][j].getX()),(float)(pct[i][j].getY()));
}
g.setColor(culoare);
g.setStroke(stil);
g.draw(figura);
}
    
```

In the figure 3 is represented the plan tangent and the normal to a hyperboloid of one sheet by using the following projections: ($\alpha=-145$, $\beta=-30$, $\gamma=90$), ($\alpha=-20$, $\beta=100$, $\gamma=150$), ($\alpha=-135$, $\beta=30$, $\gamma=120$) and ($\alpha=-135$, $\beta=20$, $\gamma=120$).

The plan tangent to a hyperboloid is draw by the following function:

```

public Plan3D plan_tangent(Punct3D P, double u, double v) {
    double A,B,C1,D;
    if (caz==1) {
        A=-b*c*Math.cosh(u)*Math.cosh(u)*Math.cos(Math.toRadians(v));
        B=-a*c*Math.cosh(u)*Math.cosh(u)*Math.sin(Math.toRadians(v));
        C1=a*b*Math.sinh(u)*Math.cosh(u);
    }
    else {
        if (u>=0) {
            A=-b*c*Math.sinh(u)*Math.sinh(u)*Math.cos(Math.toRadians(v));
            B=-a*c*Math.sinh(u)*Math.sinh(u)*Math.sin(Math.toRadians(v));
        }
        else {
            A=b*c*Math.sinh(u)*Math.sinh(u)*Math.cos(Math.toRadians(v));
            B=a*c*Math.sinh(u)*Math.sinh(u)*Math.sin(Math.toRadians(v));
        }
        C1=a*b*Math.sinh(u)*Math.cosh(u);
    }
    D=-A*P.getX()-B*P.getY()-C1*P.getZ();
    return new Plan3D(A,B,C1,D);
}
    
```

The normal to a hyperboloid is draw by the following function:

```

public Dreapta3D normala(Punct3D P, double u, double v) {
    double p,q,r;
    if (caz==1) {
        p=-b*c*Math.cosh(u)*Math.cosh(u)*Math.cos(Math.toRadians(v));
        q=-a*c*Math.cosh(u)*Math.cosh(u)*Math.sin(Math.toRadians(v));
        r=a*b*Math.sinh(u)*Math.cosh(u);
    }
    else {
        if (u>=0) {
            p=-b*c*Math.sinh(u)*Math.sinh(u)*Math.cos(Math.toRadians(v));
            q=-a*c*Math.sinh(u)*Math.sinh(u)*Math.sin(Math.toRadians(v));
        }
    }
}
    
```

```

}
else {
    p=b*c*Math.sinh(u)*Math.sinh(u)*Math.cos(Math.toRadians(v));
    q=a*c*Math.sinh(u)*Math.sinh(u)*Math.sin(Math.toRadians(v));
}
r=a*b*Math.sinh(u)*Math.cosh(u);
}
return new Dreapta3D(P,p,q,r);
}

```

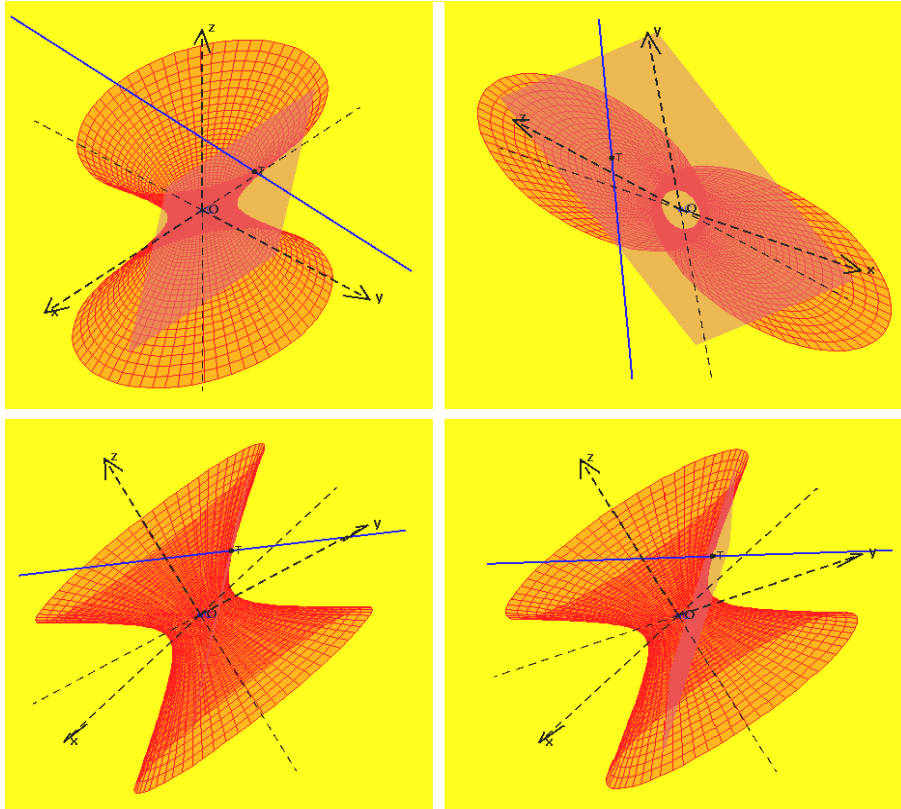


Figure 3. The plan tangent and the normal to a hyperboloid into a point

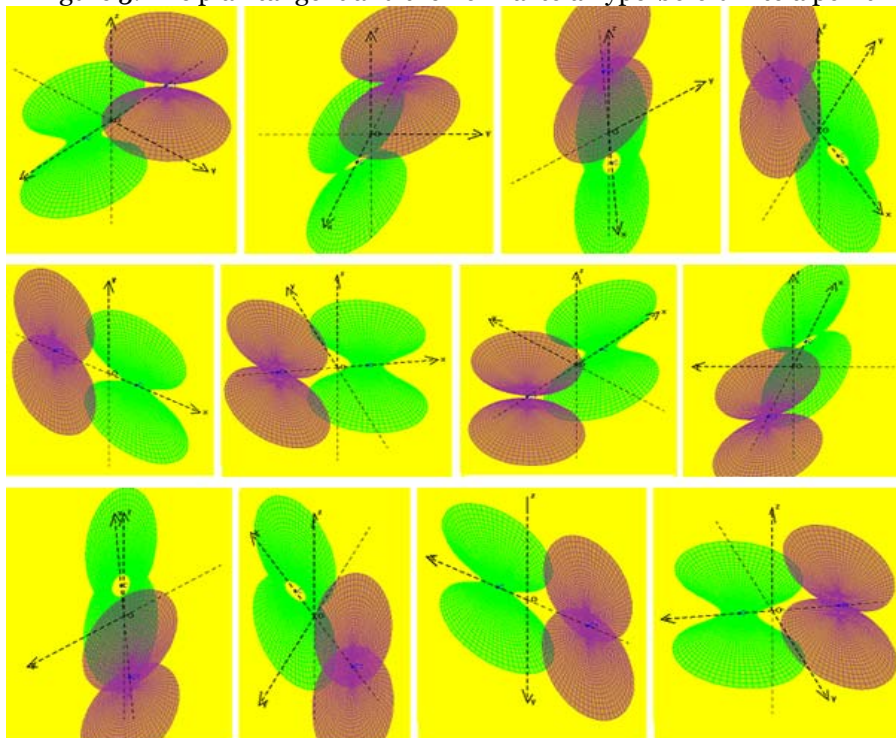


Figure 4. Animation achieved by rotation around the Oz axis

The interactive system allows the utilization of any orthogonal projection for representing the 3D geometric elements as bidimensional images in the projection plan. Specification of the desired projection is made by means of the three angles made by the three axis of the orthonormal benchmark from space with Ox axis from the projection plan.

After achievement of a 3D geometric construction there is the possibility to change the observation point by rotations around the Ox, Oy and Oz axis.

In the figure 4 is presented a sequence from the animation of a hyperboloid of one sheet and a hyperboloid of two sheets, animation achieved by rotation around the Oz axis. The presented sequence includes 12 bidimensional images obtained by using the following projections: $(\alpha=-145, \beta=-30, \gamma=90)$, $(\alpha=-115, \beta=0, \gamma=90)$, $(\alpha=-85, \beta=30, \gamma=90)$, $(\alpha=-55, \beta=60, \gamma=90)$, $(\alpha=-25, \beta=90, \gamma=90)$, $(\alpha=5, \beta=120, \gamma=90)$, $(\alpha=35, \beta=150, \gamma=90)$, $(\alpha=65, \beta=180, \gamma=90)$, $(\alpha=95, \beta=-150, \gamma=90)$, $(\alpha=125, \beta=-120, \gamma=90)$, $(\alpha=155, \beta=-90, \gamma=90)$ and $(\alpha=-175, \beta=-60, \gamma=90)$.

5. CONCLUSIONS

On this application, authors take into consideration the condition, which must accomplish a courseware, being made necessary steps. So, in elaboration and utilization of this application must take into consideration next criteria:

- ✚ To follow up the curriculum for a specific domain;
- ✚ To accomplish some teaching and learning strategy. In this kind of self-instruction and evaluation program it must find basic notions and representation and scanning notions. Animation and graphical modeling must represent the graphical construction way and also scanning of them;
- ✚ To exist the possibility to use parameterized variable, in conditions in which users have the possibility to input the variables value;
- ✚ To present a method in which the user can be informed about how can use graphical module, i.e. an interaction user-computer exist.

The presented application accomplishes these criteria, and for this we consider that is a good example of how educational software must be realized.

REFERENCES

- [1.] Adăscăliței A., *Instruire asistată de calculator. Didactica informatica*, Editura Polirom, 2007
- [2.] Andrica D., Țopan L., *Analytic Geometry*, Cluj University Press, 2004
- [3.] Brannan D.A., Esplen M. F., Gray J., *Geometry*, Cambridge: Cambridge University Press, 1999
- [4.] Glusac D., Radosav D., Karuovic D., Ivin D., *Pedagogical and Didactic-Methodical Aspects of E-learning*, 6th WSEAS International Conference on E-ACTIVITIES, Tenerife, Spania, 2007, pag. 67-75
- [5.] Henle M., *Modern Geometries: The Analytic Approach*, Upper Saddle River: Prentice-Hall, 1997
- [6.] Negret-Dobridor I., Panișoara I., *Știința învățării. De la teorie la practică*, Editura Polirom, 2005
- [7.] Nicola I., *Tratat de pedagogie școlară*, Editura Aramis, 2003
- [8.] Prasolov V.V., Tikhomirov V.M., *Geometry*, American Mathematical Society, 2001



DESIGN OF SEQUENCE DIAGRAMS FOR IMPLEMENTATION OF A DYNAMICAL SOFTWARE FOR DOING GEOMETRICAL CONSTRUCTIONS

IORDAN Anca, PĂNOIU Manuela

Technical University of Timisoara, Engineering Faculty of Hunedoara, ROMANIA

Abstract:

This paper presents a software package, which can be used as educational software. The informatics system, including modern methods and techniques, will lead the subject which is using it to gain experience in understanding and managing the knowledge from geometry field and will offer the comfortable and efficient access to the newest information and knowledge. The investigation can be oriented towards reaching of some precise purposes or can be an exploration.

Keywords:

UML, Sequence Diagram, Educational Software

1. INTRODUCTION

Unified Modeling Language (UML) is a standardized general-purpose modeling language in the field of software engineering [1]. UML includes a set of graphical notation techniques to create abstract models of specific systems.

The Unified Modeling Language (UML) is an open method used to specify, visualize, construct and document the artifacts of an object-oriented software-intensive system under development. UML offers a standard way to write a system's blueprints, including conceptual components such as: actors, business processes, system's components and activities, as well as concrete things such as: programming language statements, database schemas and reusable software components.

UML combines the best practice from data modeling concepts such as entity relationship diagrams, business modeling (work flow), object modeling and component modeling. It can be used with all processes, throughout the software development life cycle, and across different implementation technologies. UML has succeeded the concepts of the Booch method, the Object-modeling technique (OMT) and Object-oriented software engineering (OOSE) by fusing them into a single, common and widely usable modeling language. UML aims to be a standard modeling language which can model concurrent and distributed systems. UML is not an industry standard, but is taking shape under the auspices of the Object Management Group (OMG). OMG has initially called for information on object-oriented methodologies, that might create a rigorous software modeling language. Many industry leaders have responded in earnest to help create the standard.

UML models may be automatically transformed to other representations by means of QVT-like transformation languages, supported by the OMG. UML is extensible, offering the following mechanisms for customization: profiles and stereotype.

UML is not a development method by itself, however, it was designed to be compatible with the leading object-oriented software development methods of its time. Since UML has evolved, some of these methods have been recast to take advantage of the new notations (for example OMT), and new methods have been created based on UML. The best known is IBM Rational Unified Process (RUP). There are many other UML-based methods like Abstraction Method, Dynamic Systems Development Method, and others, designed to provide more specific solutions, or achieve different objectives.

It is very important to distinguish between the UML model and the set of diagrams of a system. A diagram is a partial graphical representation of a system's model. The model also contains a "semantic backbone" — documentation such as written use cases that drive the model elements and diagrams.

UML diagrams represent two different views of a system model [2]:

- Static view: Emphasizes the static structure of the system using objects, attributes, operations and relationships. The structural view includes class diagrams and composite structure diagrams.

- ✚ Dynamic view: Emphasizes the dynamic behavior of the system by showing collaborations among objects and changes to the internal states of objects. This view includes sequence diagrams, activity diagrams and state machine diagrams.

UML models can be exchanged among UML tools by using the XMI interchange format.

2. SEQUENCE DIAGRAMS

A sequence diagram in Unified Modeling Language (UML) is a kind of interaction diagram that shows how processes operate with one another and in what order [3]. It is a construct of a Message Sequence Chart. Sequence diagrams are sometimes called Event-trace diagrams, event scenarios, and timing diagrams.

A sequence diagram shows, as parallel vertical lines, different processes or objects that live simultaneously, and, as horizontal arrows, the messages exchanged between them, in the order in which they occur. This allows the specification of simple runtime scenarios in a graphical manner.

The UML 2.0 Sequence Diagram supports similar notation to the UML 1.x Sequence Diagram with added support for modeling variations to the standard flow of events.

If the lifeline is that of an object, it is underlined. Note that leaving the instance name blank can represent anonymous and unnamed instances.

In order to display interaction, messages are used. These are horizontal arrows with the message name written above them. Solid arrows with full heads are synchronous calls, solid arrows with stick heads are asynchronous calls and dashed arrows with stick heads are return messages. This definition is true as of UML 2, considerably different from UML 1.x.

Activation boxes, or method-call boxes, are opaque rectangles drawn on top of lifelines to represent that processes are being performed in response to the message (ExecutionSpecifications in UML). Objects calling methods on themselves use messages and add new activation boxes on top of any others to indicate a further level of processing.

When an object is destroyed, an X is drawn on top of the lifeline, and the dashed line ceases to be drawn below it (this is not the case in the first example though). It should be the result of a message, either from the object itself, or another.

A message sent from outside the diagram can be represented by a message originating from a filled-in circle ("found message" in UML) or from a border of sequence diagram ("gate" in UML).

UML 2 has introduced significant improvements to the capabilities of sequence diagrams [4]. Most of these improvements are based on the idea of *interaction fragments* which represent smaller pieces of an enclosing interaction. Multiple interaction fragments are combined to create a variety of *combined fragments*, which are then used to model interactions that include parallelism, conditional branches, optional interactions etc.

Some systems have simple dynamic behavior that can be expressed in terms of specific sequences of messages between a small, fixed number of objects or processes. In such cases sequence diagrams can completely specify the system's behavior. Often, behavior is more complex, e.g. when the set of communicating objects is large or highly variable, when there are many branch points (e.g. exceptions), when there are complex iterations, or synchronization issues such as resource contention [5]. In such cases, sequence diagrams cannot completely describe the system's behavior, but they can specify typical use cases for the system, small details in its behavior, and simplified overviews of its behavior.

3. PRESENTATION OF SEQUENCE DIAGRAMS UTILIZED TO IMPLEMENTATION OF A DYNAMICAL SOFTWARE FOR DOING GEOMETRICAL CONSTRUCTIONS

In the achievement of the interactive informatics system designed for studying geometry were aimed the following purposes:

- presenting of theoretical concepts and main results;
- interactive presentation of applications for each required subdomain;
- achievement of accurate drawings by replacing the pencil and ruler with the mouse.

By representing the diagrams related to the three steps: analysis, designing and implementation, the interactive informatics system will be described in a clear and concise manner. Utilization of the UML modelling language in the diagrams' achievement is featured by a rich syntactic and semantic rigour, and support for visual modeling.

The sequence diagram is used primarily to show the interactions between objects in the sequential order that those interactions occur. Much like the class diagram, developers typically think sequence diagrams were meant exclusively for them.

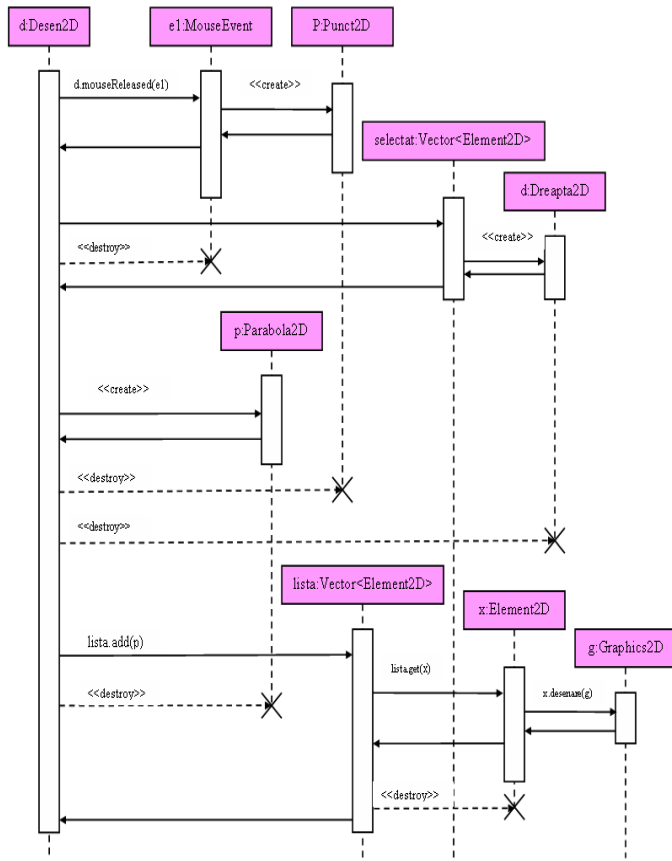


Figure 1. Sequence diagram for drawing a parabola

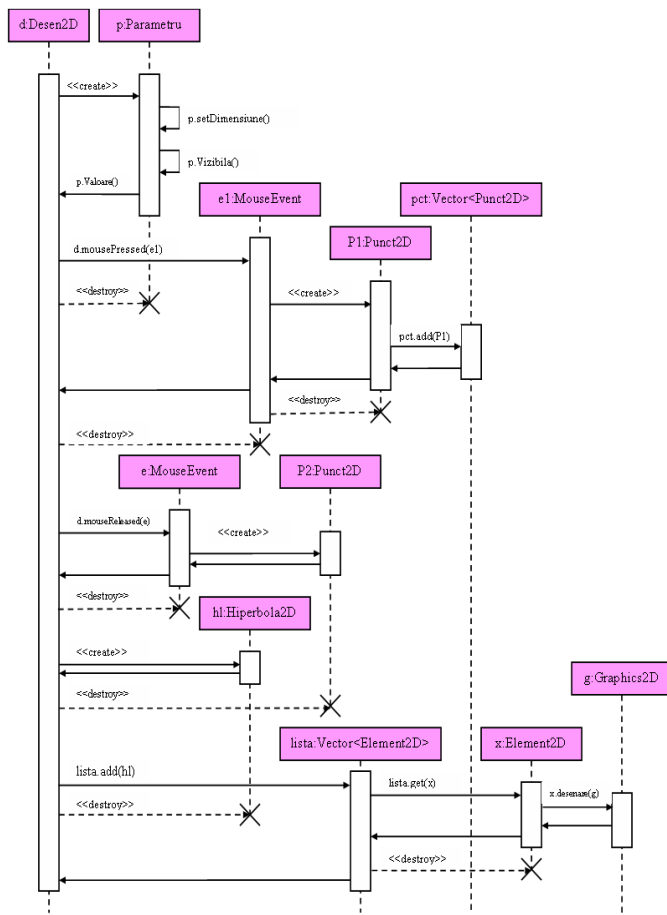


Figure 2. Sequence diagram for drawing a hyperbola

The diagram illustrates in figure 1 shows the interactions between objects, which have as purpose the drawing of a parabola. One can notice that there are interactions between nine objects, out of which the objects of *Vector<Element2D>*, *Desen2D* and *Graphics2D* type are already created, and the objects of *Element2D*, *Punct2D*, *Dreapta2D*, *MouseEvent* and *Parabola2D* type will instantiate during the interactions.

The diagram illustrates in figure 2 shows the interactions between objects, which have as purpose the drawing of a hyperbola. One can notice that there are interactions between eleven objects, out of which the objects of *Vector<Element2D>*, *Desen2D*, *Vector<Punct2D>* and *Graphics2D* type are already created, and the objects of *Element2D*, *Parametru*, *Punct2D*, *MouseEvent* and *Hiperbola2D* type will instantiate during the interactions.

The diagram illustrates in figure 3 shows the interactions between objects, which have as purpose the drawing the normal to a hyperbola. One can notice that there are interactions between nine objects, out of which the objects of *Vector<Element2D>*, *Desen2D* and *Graphics2D* type are already created, and the objects of *Element2D*, *Punct2D*, *Dreapta2D*, *MouseEvent* and *Hiperbola2D* type will instantiate during the interactions.

These objects are represented on *Ox* axis and, on *Oy* axis, are represented the messages ordered increasingly in time. At the beginning, the execution's control is undertaken by the object of *Desen2D* type which creates an instance of the *MouseEvent* class.

Now, the control is undertaken by this newly created instance that will allow to determining a point. Giving the control to the object of *Hiperbola2D* type, will verified if the created point belong to the hyperbola.

Giving back the control to the object of *Desen2D* type, further will be instantiated the object of *Dreapta2D* type, representing the normal to hyperbola, then will be destroyed the object of *Punct2D* type and the object of *Hiperbola2D* type.

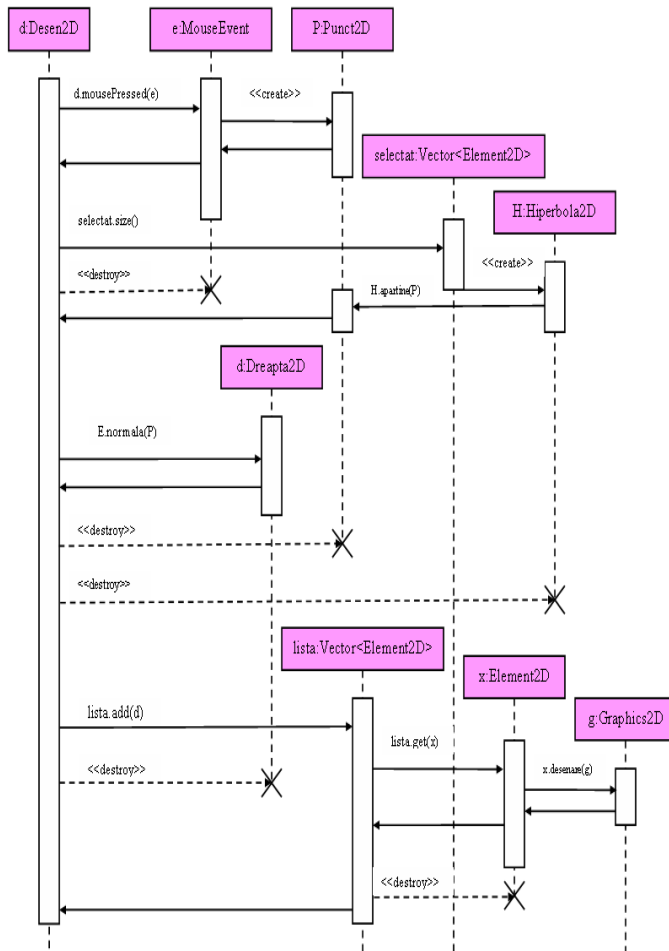


Figure 3. Sequence diagram for drawing a the normal to a hyperbola

Further, the execution's control is transmitted to the object of *Vector<Element2D>* type, in order to add the normal previously created in the list of 2D elements of the geometric construction, and then will be destroyed the instance of the *Dreapta2D* class. Finally, will be redrawn the geometric construction, which will include now also the normal to the previously created hyperbola by using the object of *Graphics2D* type.

4. CONCLUSIONS

The diagrams were achieved by an approach in a new manner, multidisciplinary, of the informatics application, including both the modern pedagogy methods, and the components specific to the discipline to be studied. Thus, was achieved the connection between the didactic actions and the purposes and objectives scientifically established, by elaborating of new methods and assimilating of new means, capable to increase the school efficiency, allowing the pupils and students to acquire the system required by knowledges and their application techniques in conditions as optimal possible.

REFERENCES

- [1.] Booch G., Rumbaugh J., Jacobson I., *The Unified Modeling Language User Guide*, Addison Wesley, 1999
- [2.] Fowler M., Scott K., *UML Distilled: A Brief Guide to the Standard Object Modeling Language*, Addison Wesley, Readings MA, USA, 2000
- [3.] Odell J., *Advanced Object Oriented Analysis & Design using UML*, Cambridge University Press, 1998
- [4.] Oestereich B., *Developing Software with UML*, Addison Wesley, 1999
- [5.] Rumbaugh J, Jacobson I., Booch G., *The Unified Modeling Language Reference Manual*, Addison Wesley, 1999



STUDY OF LOW-SIGNAL AMPLIFIERS WITH FIELD-EFFECT TRANSISTORS

Corina Maria DINIȘ, Corina Daniela CUNȚAN, Gabriel Nicolae POPA, Angela IAGĂR

Politehnica University Timișoara, Faculty of Engineering Hunedoara, ROMANIA

Abstract:

In this work are presented the types of amplifier stages with field-effect transistors, as well as the diagrams of the low-signal amplifiers achieved with TEC-J for the three connection types: common-source, common-grid and common-drain. Also, using the EWB-Multisim 8 program, it was simulated the operation of the amplifier with TEC-J in common-source connection, the amplifier with TEC-MOS in common-drain connection and the cascode amplifier with two TEC-J transistors .

Keywords:

TEC transistor, Voltage amplification, Current amplification, Amplifier, Simulation, Multisim 8

1. INTRODUCTION

The models which describe the operation at small signal variations have in view a description of the transistors' behavior in applications of amplifier stages' type. In these applications, the transistors are polarized in the characteristics' area where these are almost horizontal lines; against the collector, the transistors are equivalent with a controlled current generator and behave linearly. In the respective circuits' operation, the effect of the charges accumulated in junctions or other regions of the transistors is the one of some capacitors which produce phase differences and dampings with frequency.

The small signal variations are the voltage and current variations situated within an interval relatively restricted around some continuous components, interval where the device's behavior can be described by linear equations. The device's equivalent diagram is composed by linear components, of which values depend generally to the operation static point (the continuous components of voltages and currents through the device). The voltage and current variations are small, but the time-variation speeds are not neglectable, thereby the accumulations of electric charges in the device should be taken in consideration .

2. TEC-J and TEC-MOS BEHAVIOR AT SMALL SIGNAL VARIATIONS

The operation static point should be in the saturation region of the drain current (Fig. 1). In this operation regime, the equation of the TEC-J transistor is:

$$I_D = I_{DSS} \cdot \left(1 - \frac{V_{GS}}{V_P}\right)^2 \quad (1)$$

$$dI_D = 2 I_{DSS} \cdot \left(1 - \frac{V_{GS}}{V_P}\right) \cdot \left(-\frac{dV_{GS}}{V_P}\right) = 2 I_{DSS} \cdot \sqrt{\frac{I_D}{I_{DSS}}} \cdot \left(-\frac{dV_{GS}}{V_P}\right) \quad (2)$$

Using the same convention to note the variations and the components $v_{GS} = V_{GS} + v_{gs}$ and $i_D = I_D + i_d$, we have the correspondence:

$$dI_D \rightarrow i_d \text{ și } dV_{GS} \rightarrow v_{gs} \quad (3)$$

$$i_d = -2 \frac{\sqrt{I_D I_{DSS}}}{V_P} \cdot v_{gs} \quad (4)$$

The TEC-J transistor's slope is:

$$g_m = \frac{i_d}{v_{gs}} \Big|_{V_{DS}=\text{constant}} = -2 \frac{\sqrt{I_D I_{DSS}}}{V_P} \quad (5)$$

The higher the drain current, the higher the slope. The maximum slope of a TEC-J is obtained at $V_{GS} = 0$ and has the value:

$$(g_m)_{max} = |2 I_{DSS} / V_P| \quad (6)$$

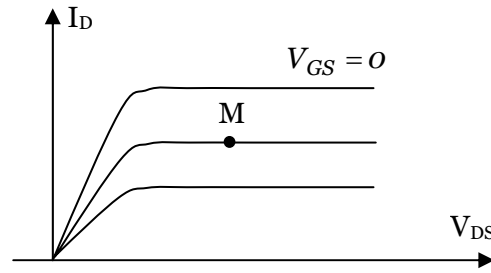


Fig. 1. TEC-J's operation point as amplifier

The small variations $v_{gs} > 0$ of the grid-source voltage produce the following effects:

- ✚ the drain current's increase due to the increase of the channel's conductance (the channels' area increases);
- ✚ the electric charge accumulated in the passing region of the grid-channel junction modifies in the source's region and, as result, is necessary a grid current to supply this modification

$$i'_g = C_{gs} \cdot \frac{dv_{gs}}{dt} \text{ where } C_{gs} \text{ is the barrier capacity of the grid-channel junction in the source's area;}$$

- ✚ the drain-source voltage modifies (following the modification of the drain current), which leads to the modification of the electric charge accumulated in the passing region of the grid-channel junction in the drain's region; a grid current is necessary to supply this charge modification

$$i''_g = C_{gd} \cdot \frac{dv_{gd}}{dt} \text{ where } C_{gd} \text{ is the barrier capacity of the grid-channel junction in the drain's area.}$$

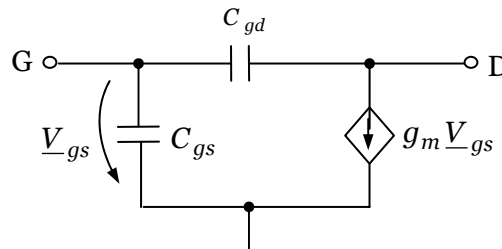


Fig. 2. TEC-J's equivalent diagram

TEC-MOS behavior is described by an equivalent diagram identical with the one from Fig. 2. Capacities C_{gs} and C_{gd} correspond to the TEC-MOS' sublayer grid capacities in the source's, respectively the drain's area. The TEC-MOS' equivalent slope is obtained starting from the transistor's equation in the drain current's saturation area.

$$I_D = k \cdot (V_{GS} - V_P)^2 \quad (7)$$

Is obtained the TEC-MOS transistor's slope:

$$g_m = 2 \sqrt{k I_D} \quad (8)$$

3. AMPLIFIER STAGES

The amplifier stage is the simplest constructive block of an amplifier. It contains one or maximum two transistors which operate in controlled current source regime. For TEC, this corresponds to the drain current's saturation area. Against the drain, the transistor behaves as a current generator controlled by the voltage V_{gs} . The three amplifier stages' types are based on the connections of the field-effect transistors:

- ✚ Common-source connection (Fig. 3);
- ✚ Common-grid connection (Fig. 4);
- ✚ Common-drain connection (Fig. 5).

The presented circuits include the resistances that ensure the transistors' polarization in the reminded regions. For the amplifier stages with TEC are presented, for exemplification, only the diagrams of the stages with TEC-J, but there are similar circuits also for TEC-MOS.

In order to simplify the diagrams, in some cases it was chosen the option of polarization from two sources. In this case, the components' number from the diagram is smaller and the equivalent diagrams for small signal variations are simpler.

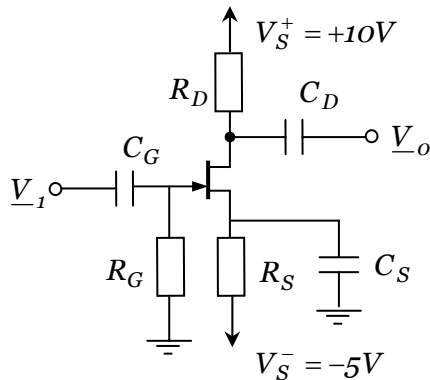


Fig. 3. Amplifier stage: Common-source

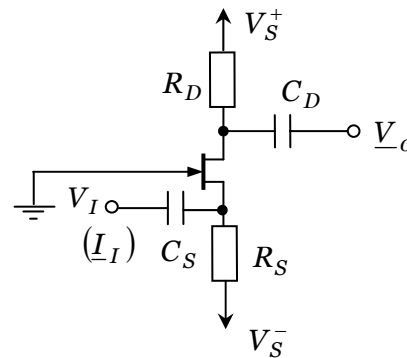


Fig. 4. Amplifier stage: Common-grid

Resistances R_G , R_S și R_D from the common-source amplifier stage (Fig. 3) ensures the TEC-J polarization in RAN. Capacitors C_G and C_D separate the input and output in d.c. from the TEC-J polarization and allow the coupling of the input and output signals, reason for which they are also called as coupling capacitors. The capacitor C_S , also called as decoupling capacitor, is short-circuiting to earth in a.c. the source TEC-J, where from the diagram's name. The resistance R_D has an important function also in a.c., as will be seen at amplification's calculation.

In the common-grid amplifier stage (Fig. 4), the TEC-J polarization in RAN is ensured by R_S and R_D and by the supply sources V_S^+ și V_S^- . The coupling capacitors C_S and C_D are separating in d.c. the amplifier stage from the rest of the circuit, and allow the input's and output's coupling to the circuit.

The common-grid amplifier stage: (Fig. 5), also called as repeater-on-source, is polarized from the supply sources through the resistances R_G and R_S . The input and output coupling is achieved with the coupling capacitors C_G and C_S .

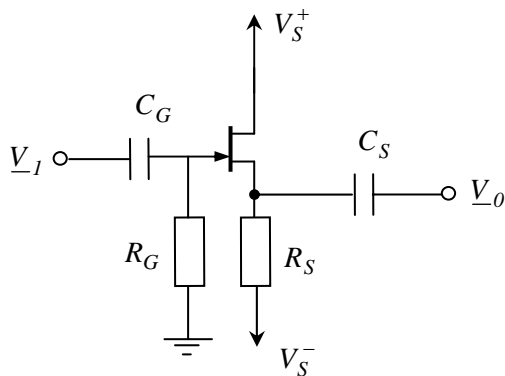


Fig. 5. Amplifier stage: Common-drain

In all diagrams, the coupling and decoupling capacitors (C_G , C_D , C_S) should have sufficiently high values, in order that their impedances at operating frequencies to be considered neglectable, respectively the voltage drops on the equivalent impedances don't matter. This condition is not only dependent by the capacitors' values and the signals' frequency, but also by the resistances from the circuit.

4. AMPLIFIERS WITH FIELD-EFFECT TRANSISTORS (TEC)

4.1. Amplifiers with field-effect transistor (TEC) in common-source connection

Study of an amplifier with TEC-J is very similar to the one of an amplifier with TEC-MOS, therefore here is presented only an amplifier with TEC-J. A typical diagram for such an amplifier is represented in fig. 7, and its model, in which for TEC-J are used the natural parameters, is given in fig. 8.

The role of the components e_g, R_G, C_i, C_e, R_S from fig. 7 and 8 is the following: e_g - signal source, which usually is of alternative signal; T - amplifying element; R_G - equivalent internal resistance of the signal source; R_{GR} and R_D - the TEC-J's polarization resistors; R_S - amplifier's charge (consumer); C_i, C_e - input capacitor which couples the signal mass at the amplifiers' input, respectively the output capacitor which couples the consumer's output to the charge.

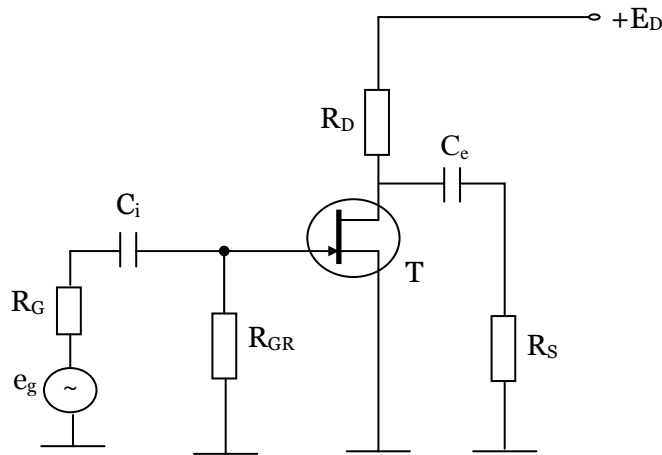


Fig. 7. Amplifier in common-source connection with TEC-J

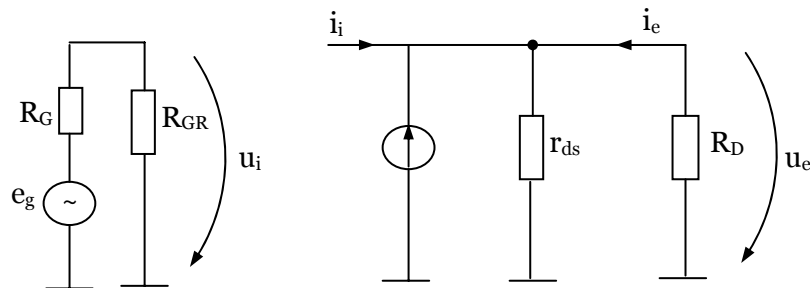


Fig. 8. Amplifier's low-signal equivalent circuit in common-source connection with TEC-J
Based on fig. 8, we have:

$$A_{us} = \frac{u_e}{u_i} = -\frac{g_m \cdot R_D}{1 + \frac{R_D}{r_{ds}}} \quad (9)$$

Because $r_{ds} \ll R_D$, the frequently used relation for the voltage amplification A_u is:

$$A_{us} = -g_m \cdot R_D \quad (10)$$

and the current amplification A_i is:

$$A_{is} = \frac{i_e}{i_i} \quad (11)$$

The current amplification is very high, but practically is less interesting because the TEC's control is made in voltage. However, a high A_i leads finally to an amplification in power A_p very high for a stage with TEC. For the input resistance R_i and output resistance R_e , having in view the obvious neglects, are obtained:

$$R_{is} = R_{GR} \quad (12)$$

$$R_{es} = r_{ds} \quad (13)$$

4.2. Amplifiers with field-effect transistor (TEC) in common-drain connection (repeater-on-source)

The amplifier in common-drain connection (fig. 9) is useful in applications with requirements in accordance with its properties, i.e.:

- ✚ Output signal in phase with the input one;
- ✚ Very high input resistance;
- ✚ Low input capacity;
- ✚ Low output resistance;
- ✚ Output signal undeformed by high amplitude at output;
- ✚ Voltage amplification slightly subunitary.

Current amplification A_i is very high:

$$A_{id} = \frac{i_e}{i_i} \uparrow \quad (14)$$

and the voltage amplification A_u is expressed by the relation (15) and has the value closed to 1.

$$A_{ud} = \frac{g_m \cdot R_D}{1 + g_m \cdot R_D} \quad (15)$$

$$R_d = r_{ds} \parallel R_{SU} \parallel R_S \quad (16)$$

The stage's own input resistance is given practically by the value of R_{GR} which should be chosen of an as high possible value, or, in some cases, equal with the value of the signal source's equivalent resistance R_G . The stage's own output resistance is low, having the value:

$$R_{ed} = \frac{1}{g_m + \frac{1}{r_{ds}}} \quad (16)$$

and the total one R_{et} :

$$R_{etd} \cong R_S \parallel R_{SU} \quad (17)$$

The stage's total input capacity is:

$$C_{idt} = C_{gd} + (1 - A_u) \cdot C_{gs} \cong C_{gd} \quad (18)$$

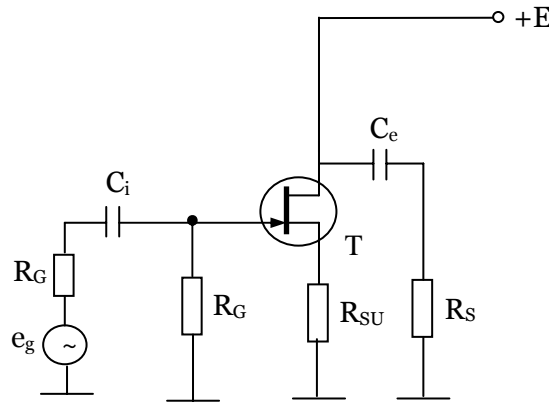


Fig. 9. Amplifier with TEC-J in common-drain connection

4.3. Amplifiers with field-effect transistor (TEC) in common-grid connection

The amplifier with TEC in common-grid connection (Fig. 10) is lesser used, and its main qualitative characteristics are the following:

- ⚡ High output impedance;
- ⚡ Low input impedance;
- ⚡ Unitary current amplification;
- ⚡ Low input → output transfer capacity;
- ⚡ The output signal is in phase with the input one.

Under mathematical aspect, the circuit's voltage amplification is:

$$A_{ug} = \frac{(1 + g_m \cdot r_{ds}) \cdot R_S}{R_S + r_{ds} + (1 + g_m \cdot r_{ds}) \cdot R_S} \cong g_m \cdot (R_S \parallel r_{ds}) \quad (19)$$

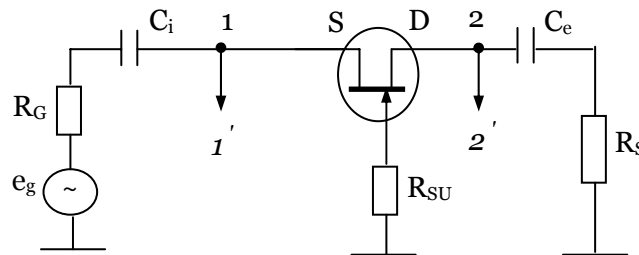


Fig. 10. Amplifier with TEC-J in common-grid connection

5. SIMULATION OF THE LOW-SIGNAL AMPLIFIERS’ OPERATION WITH TEC USING EWB-MULTISIM 8

The amplifier with TEC-J in common-source connection is a classic one (Fig. 11). Resistors R1 and R3 achieve the automatic polarization, R3 introducing also a negative reaction in d.c. Resistor R2 represents the drain charge of the transistor T, and Rs is the amplifier’s external charge.

Capacitors C1 and C2 achieve the galvanic separation of the amplifier from the signal source, respectively from the charge. The capacitor C3 decouples totally in a.c. the resistor R3 in order not to decrease the circuit’s voltage amplification.

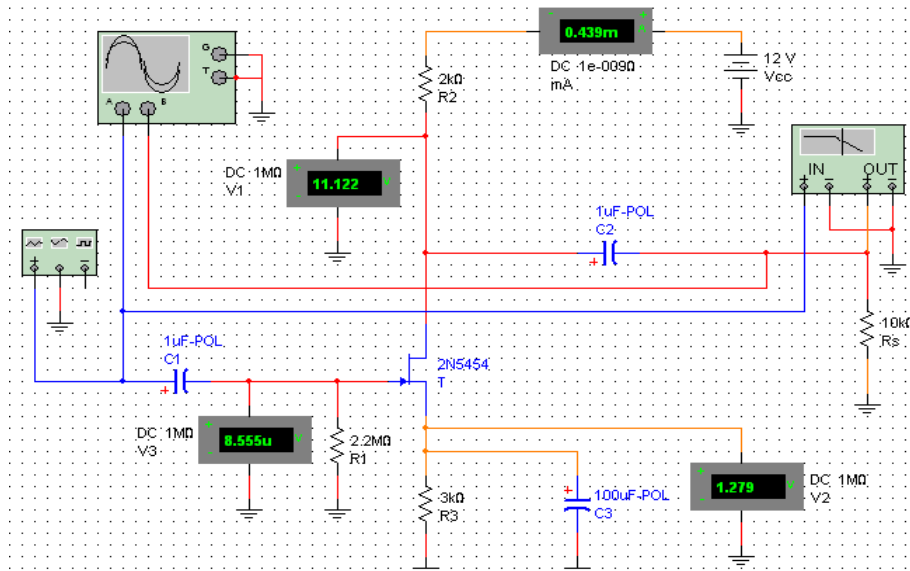


Fig. 11. The amplifier’s simulation diagram with TEC-J in common-source connection

It’s been achieved the simulation of this amplifier’s operation for the following values of the electronic components from diagram: $S_V = 1 \text{ mV}/10 \text{ kHz}$, $V_{cc} = 12 \text{ V}$, $T = 2N5454$, $R_1 = 2,2 \text{ M}\Omega$, $R_2 = 2 \text{ k}\Omega$, $R_3 = 3 \text{ k}\Omega$, $C_1 = C_2 = 1 \mu\text{F}$, $C_3 = 100 \mu\text{F}$, $R_s = 10 \text{ k}\Omega$. Were measured: the the circuit’s current consumption and the voltages in drain, the source and grid of the transistor T.

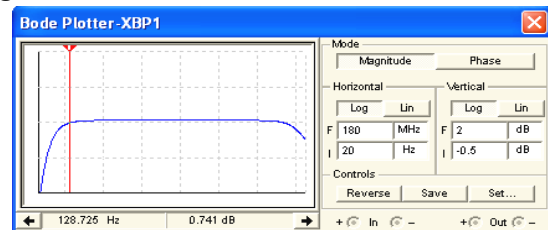
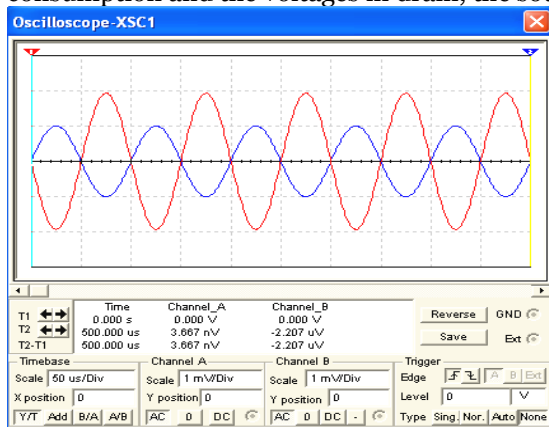


Fig. 13. Amplifier’s amplitude-frequency characteristic with TEC-J in common-source connection resulted further simulation

Fig. 12. Signals from the amplifier’s input and output with TEC-J in common-source connection resulted further simulation

Have been visualized on oscilloscope the signals from the amplifier’s input and output with TEC-J in common-source connection (fig. 12). The amplitude–frequency characteristic of this amplifier, resulted further simulation, is presented in fig. 13.

The amplifier with TEC-MOS transistor, repeater-on-source with bootstrap reaction, (Fig. 14), represents an apart amplifier type, used especially as adaption circuit for signal sources with extremely high internal resistance. The bootstrap connection applies by the capacitor C2, which, by the the positive reaction source-grid which introduces it, increases the amplifier’s input equivalent resistance (however very high in the presented case).

Resistors R1, R2 form the voltage divider from the grid of the transistor used for its polarization, and the resistor R3, of high value, has the role to ensure a high input resistance to the circuit. The resistor Rs contribute to establishing the drain current of transistor T, having in this case also the role of charge resistance.

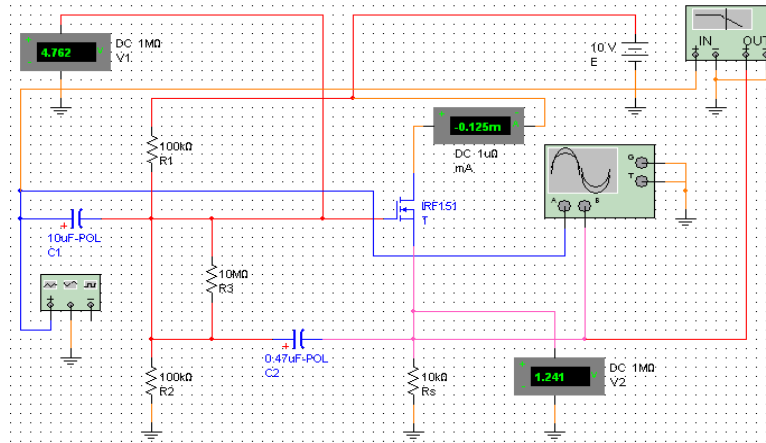


Fig. 14. Amplifier’s simulation diagram with TEC-MOS in common-drain connection (repeater-on-source)

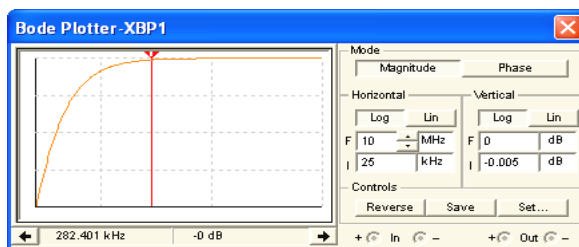


Fig. 15. The amplifier’s amplitude–frequency characteristic with TEC-MOS in common-drain connection resulted further simulation

It’s been achieved the simulation of this amplifier’s operation for the following values of the electronic components from diagram: $S_V = 100 \text{ mV} / 10 \text{ kHz}$, $E = 10 \text{ V}$, $T = \text{IRF151}$, $R_1 = 100 \text{ k}\Omega$, $R_2 = 100 \text{ k}\Omega$, $R_3 = 10 \text{ M}\Omega$, $C_1 = 10 \text{ }\mu\text{F}$, $C_2 = 0,47 \text{ }\mu\text{F}$, $R_s = 10 \text{ k}\Omega$.

Was measured the circuit’s current consumption, the grid voltage and the drain of transistor T. The amplitude–frequency characteristic of this amplifier, the resulted further simulation, is presented in fig. 15.

Following the simulation, were visualized on oscilloscope the signals from the amplifier’s input and output with TEC-MOS in common-drain connection (fig. 16).

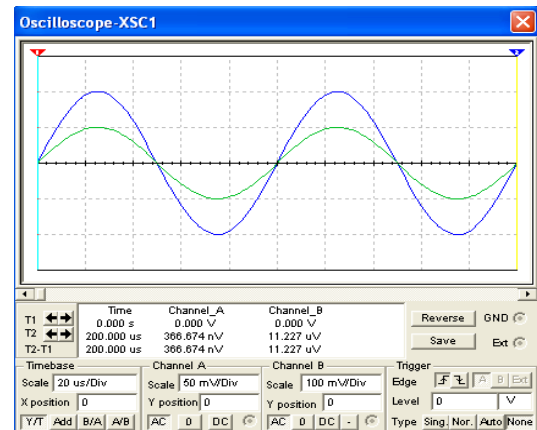


Fig. 16. Signals from the amplifier’s input and output with TEC-MOS in common-drain connection resulted further simulation

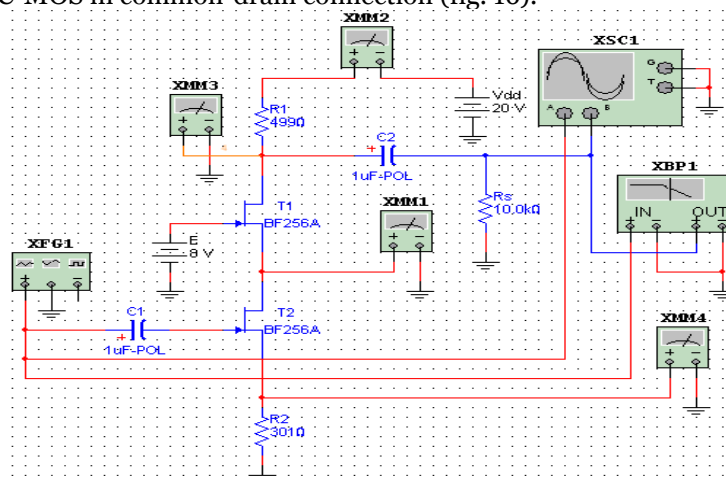


Fig. 17. Simulation diagram of the cascode amplifier with two TEC-J transistors

The cascode amplifier with two TEC-J transistors (Fig. 17) is used especially at high frequencies. Transistor T1 works in common-source connection and transistor T2 in common-grid connection, the coupling between the two transistors being direct. Thus, are ensured the equivalent input and output specific resistances and a high voltage amplification, comparable with the one of a classic amplifier

with two amplifier stages. Resistors R1 and R2 ensure the simultaneous polarization, convenient, of transistors T1, T2.

Capacitors C1, C2 achieve the galvanic separation between the amplifier and the SV signal source (XFG1 functions generator), respectively the charge Rs.

Was achieved the simulation of this amplifier's operation for the following values of the electronic components from diagram: SV = 1 mV/10 kHz, E = 8 V, Vdd = 20 V, T1 = BF256A, T2 = BF256A, R1 = 499 Ω , R2 = 301 Ω , C1 = C2 = 1 μ F, Rs = 10 k Ω .

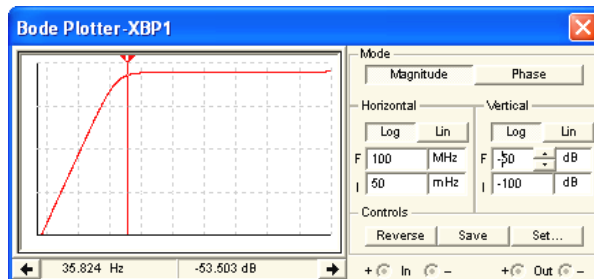


Fig. 18. The amplitude-frequency characteristic of the cascode amplifier with two TEC-J transistors

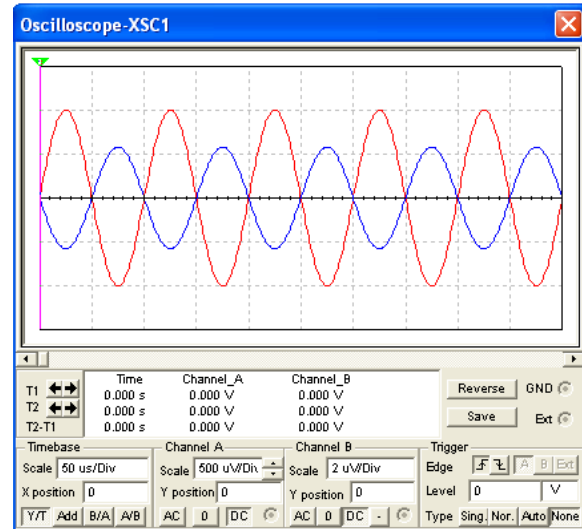


Fig. 19. Signals from the cascode amplifier's input and output with two TEC-J transistors

Was measured the circuit's consumption, the voltage in the source and drain of transistor T1, as well as the voltage in the source and drain of transistor T2. The amplitude–frequency characteristic of this amplifier, resulted further simulation, is presented in fig. 18.

In fig. 19 were visualized on oscilloscope the input and output signals of the cascode amplifier with two TEC-J transistors resulted further simulation.

6. CONCLUSIONS

Simulation of the low-signal amplifiers' operation with field-effect transistors has a very important role, being the intermediary step absolutely necessary between designing and achievement of the experimental model. Thus, the user can observe by simulation, without being necessary the practical achievement of the electronic circuit, the real behavior and can modify certain components in order to reach the desired result.

After the electronic diagram's achievement, by software can be performed an operational analysis, as well as the behavior in different duty regimes – d.c., impulses, transitory and stationary regimes, behavior with frequencies, etc – by means of the own measurement and diagnosis systems, as well as the software's specific facilities.

The main advantage offered by the EWB–Multisim 8 simulation program consists in high flexibility as regards the structure modification of the analyzed electronic circuits and their duty regimes, fact which allows an analysis and a diagnosis within a much more reduced time interval of the electronic circuits than the case when these would be physically achieved, allowing in addition a facile and large storage of information about the circuit's operation between different implementation options.

One can notice the time savings and the possibility of further data processing, especially the graphic dependencies for different measures, by means of the EWB–Multisim 8 program.

REFERENCES

- [1] Cătălin Daniel Căleanu, *Electronic devices and circuits, Experiments and Simulation*, „Politehnica” Publishing House, Timisoara, 2003
- [2] Thomas L. Floyd, *Electronic devices*, „Teora” Publishing House, Bucharest, 2003
- [3] E. Lakatoş, *Modeling of active semi-conductor devices*, Course notes, „MatrixRom” Publishing House, Bucharest, 2003
- [4] Ş. Lungu, O. Pop, *Modeling of electronic circuits*, “Science Book House” Publishing House, Cluj-Napoca, 2006
- [5] S. Paşca, N. Tomescu, I. Sztoljeanov, *Analogue and digital electronics*, „Albastra” Publishing House, Cluj-Napoca, 2004



SIMULATION OF SOME FAULTS IN THREE-PHASE ELECTRIC SYSTEMS USING THE PSCAD-EMTDC PROGRAM

Angela IAGĂR, Corina Maria DINIȘ, Gabriel Nicolae POPA, Ioan BACIU

Politehnica University Timișoara, Faculty of Engineering Hunedoara, ROMANIA

Abstract:

The main faults and abnormal regimes in the three-phase electric systems are short-circuit and phase interruptions, respectively overcurrents and system's stability loss.

Studying faults and abnormal operation regimes has a special practical importance, because these operation regimes produce malfunctions or even failures of the electric installation, if they are not removed on time.

In this work are analyzed few faults of three-phase electric systems by means of the PSCAD-EMTDC program.

Fault analysis with PSCAD can be used for protection relay coordination and for improving the system's performance and reliability.

Keywords:

Three-phase electric systems, Faults, Simulation, Reliability

1. INTRODUCTION

The most frequent faults in electric systems are short-circuiting. Short-circuits' appearance is caused by damaging the insulation or insulation space between phases, or between phase and ground, as result of the loads at rated voltage, or overvoltages that appear in electric installations [1,2].

Short-circuit can be: three-phase (or three-phase-to-earth), phase-to-phase (or phase-to-phase-to-earth) and single-phase (or phase-to-earth fault, produced in the grids with neutral directly grounded).

The three-phase short-circuit is also called as symmetrical fault, because the impedances on phases are equal. This short-circuits, by their consequences, represent the worst fault that might happen into an electric grid. From this reason, the three-phase short-circuit currents are taken as base when selecting the commutation electric devices and verifying them at thermal and electrodynamic stress, verifying the relay protection and automations etc [3-5].

The other short-circuits are called as asymmetrical faults. These are featured by the fact that the phenomena from each phase are produced differently. In these conditions, the phase impedances are unequal and the currents' three-phase system is asymmetrical. Determination of these currents is made by the symmetric components method.

In aerial electric grids, short-circuits are produced, in major cases, by external transitory causes: atmospheric discharges, indirect contact of some phases by foreign bodies etc. After a short time interval from disconnecting the faulty element, the causes might disappear and the insulation in the respective point resume to normal [6].

In these conditions, to prevent a long-term interruption of the consumers' power supply, are provided devices of high speed automatic reclosing (RAR), which connect after a preestablished time the disconnected supply circuits. Earth fault is not an immediate danger, because is not accompanied by big fault currents. However, earth fault of a phase determines the voltage increase of the healthy phases against ground. This increase leads to overstressing the insulation and the danger of its breakdown also in other point from the other phases. Thus, the fault is going to double-earth fault (bi-phase short-circuit to-earth) [7,8].

Beside short-circuits, in the electric systems appear also other faults, such as interruption of a phase. The study of this fault is necessary for designing the parallel lines' protections and to verify if the influence of the negative-sequence components (that appear at a phase interruption) upon generators is within the permissible limits. In case of long-term operation of a line in two phases, is also necessary to verify the influence on the telecommunication lines [4,6].

The main abnormal regimes in electric systems are overcurrents and system's stability loss.

Overcurrents are caused by a short-circuit external to the protected element, or by appearance of some overloads. Overcurrents don't need an immediate disconnection of the protected element, but neither can be admitted on an undetermined period, because they are causing overheating and, therefore, insulation's wear. Against overcurrents are provided delayed protections [4,6,8].

The system's stability loss can appear due to some short-circuits removed too late, or exceeding the permitted power transported through a line, which causes the dropping-out-of-step of the power plants operating in parallel [8].

Study of faults and abnormal operation regimes in three-phase electric grids has a special practical importance for protection relay coordination. The relay protection should ensure the installation's automatic disconnection when a fault or abnormal operation regime appears, dangerous for the installation. In case of faults and abnormal regimes which don't show an immediate danger, the relay protection is not controlling the installation's disconnection, but warns the appearance of the abnormal regime [9].

Automatic separation of the faulty installation from the rest of the electric system aims three objectives: to prevent the fault's increase, respectively extension of its effects by affecting other installations from the electric system and transforming the fault into a system emergency; to prevent the installation's damage where the fault appears, by rapid interruption of all possibilities to supply the fault; to reestablish a normal operation regime for the rest of the electric system, ensuring the consumer's supply continuity [10].

2. SIMULATION OF SOME FAULTS IN THREE-PHASE ELECTRIC SYSTEMS USING THE PSCAD-EMTDC PROGRAM

Calculation of some faults (short-circuits, phase interruptions, etc.) that appear during the three-phase systems' operation is a complicated procedure, needing to solve some equation systems with a great number of unknown quantities. To simplify the equations and the corresponding equivalent diagrams, can be used the symmetric components' method.

In case of a small circuit with linear elements, determination by normal analysis of the accurate solution is a problem easy to solve. Manual analysis of bigger circuits becomes, however, a very complex problem, being preferable the utilization of a simulation program.

Among the programs used in electric circuits' simulation can be enumerated: PSCAD-EMTDC, SPICE, OrCAD, Multisim.

PSCAD/EMTDC is a general-purpose time domain simulation program for multi-phase power systems and control networks. It is mainly dedicated to the study of transients in power systems. A full library of advanced components allows to precisely modeling interactions between electrical networks and loads in various configurations [11].

PSCAD is ideal for the analysis of electrical transients involving: asymmetrical faults, power line and cables, large non-linear industrial loads, protection relay coordination, arc furnace flicker, distributed power generator, rotating machines, embedded systems [11].

Further, are analyzed few faults of three-phase electric systems by means of the PSCAD-EMTDC program.

2.1 Short-circuit of a phase

Is admitted short-circuit of phase 1 into a circuit where the other two phases have equal impedances, and the voltage system is symmetric (Fig. 1). In simulation, short-circuit was modeled with a null impedance (phase 1 impedance).

Switch K_1 is closed, and after a second it opens. The electric diagram implemented in simulation is presented in Fig. 1. Simulation results are presented in Fig. 2-4.

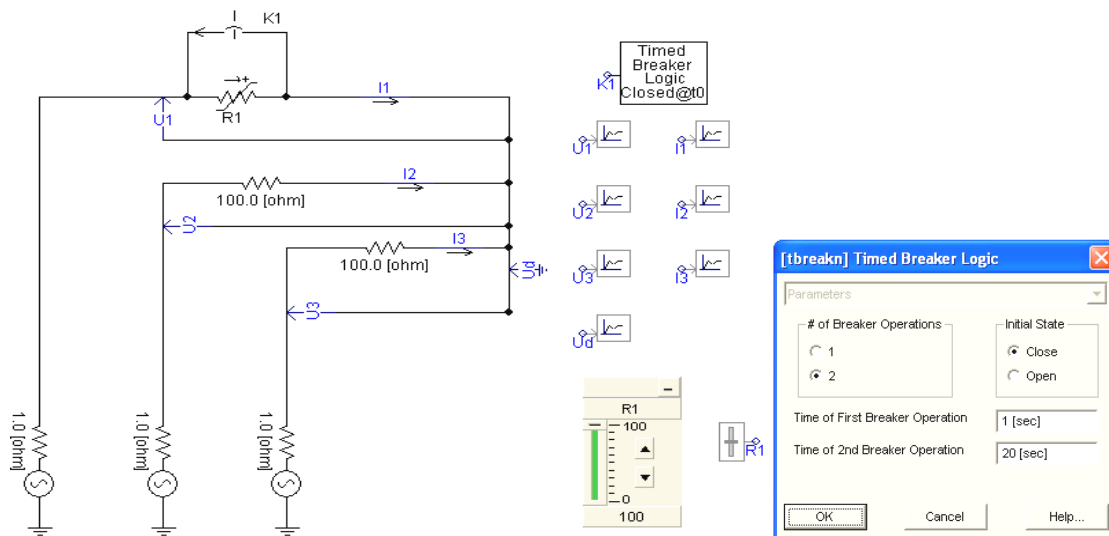


Figure 1. Electric diagram implemented in simulation. Switch K_1 configuration.

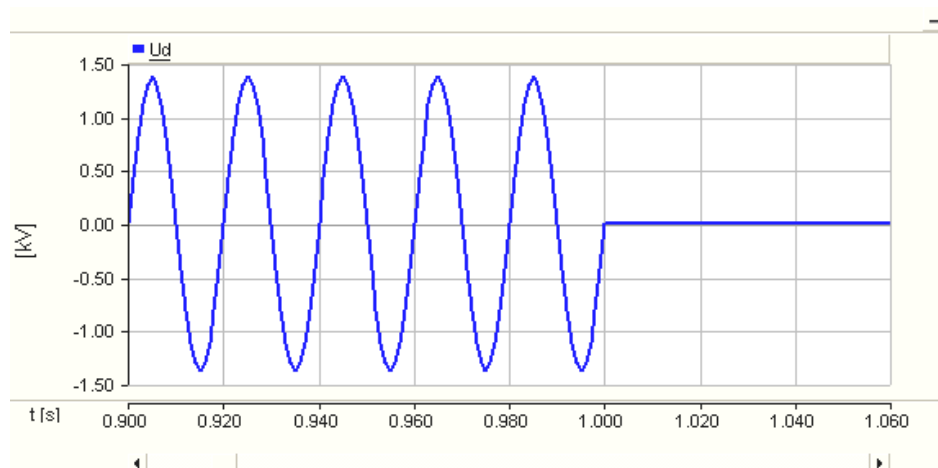


Figure 2. Simulation results. Neutral point displacement voltage.

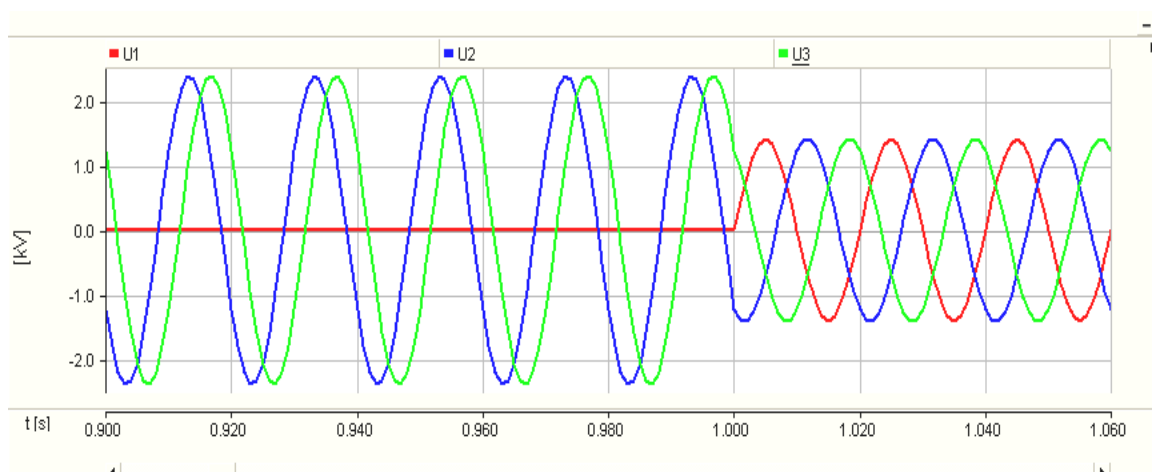


Figure 3. Simulation results. Voltages on receptor's phases.

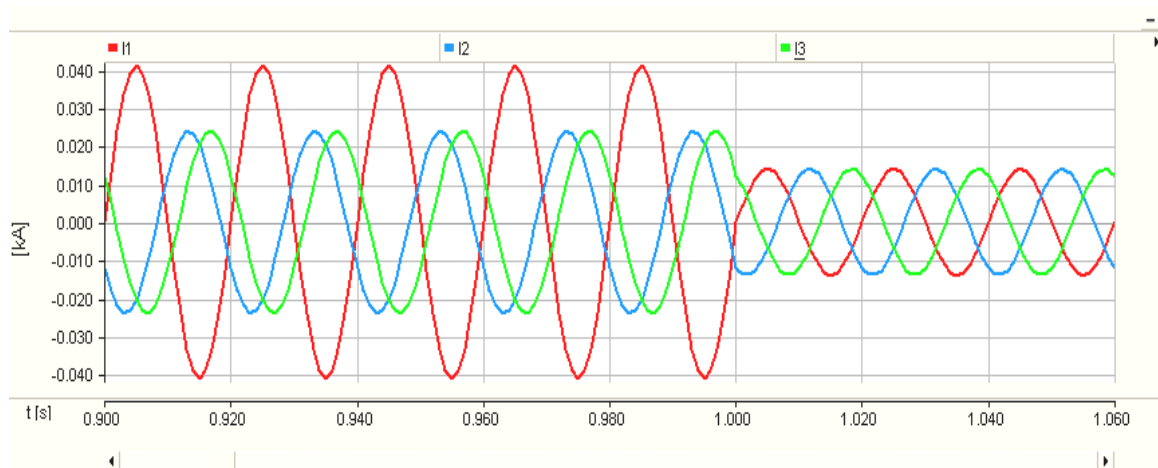


Figure 4. Simulation results. Currents absorbed from the grid.

It is found that voltages on phases 2 and 3 increase by $\sqrt{3}$ times during short-circuit of phase 1. As consequence, currents I_2 and I_3 increase (by $\sqrt{3}$ times) compared to rated currents. This currents are equal (as rms value) and dephased by $\pi/6$ radian. Short-circuit current I_1 increase very much (by 2,8 times) compared to rated current.

After 1 second, switch K_1 opens and the regime becomes symmetric (the receptor is balanced, and the supply voltage system is symmetric).

2.2 Interruption of a phase

Is admitted an interruption of phase 1 into a circuit where the three-phase receptor has the same impedances on phases, and the voltage system is symmetric. Interruptions on phases 1 were modeled with a static and infinite impedance.

Initially the switch K_1 is open and after a second switch K_1 closes. The electric diagram implemented in simulation is presented in Fig. 5. Simulation results are presented in Fig. 6 (voltages on receptor’s phases and currents absorbed from the grid).

It is found that the voltage on the interrupted phase increases (by 1,5 times), and the voltages on other phases decrease (by $\sqrt{3} / 2$ times) compared to rated voltages.

After 1 second the regime becomes symmetric because switch K_1 closes (the receptor is balanced, and the supply voltage system is symmetric).

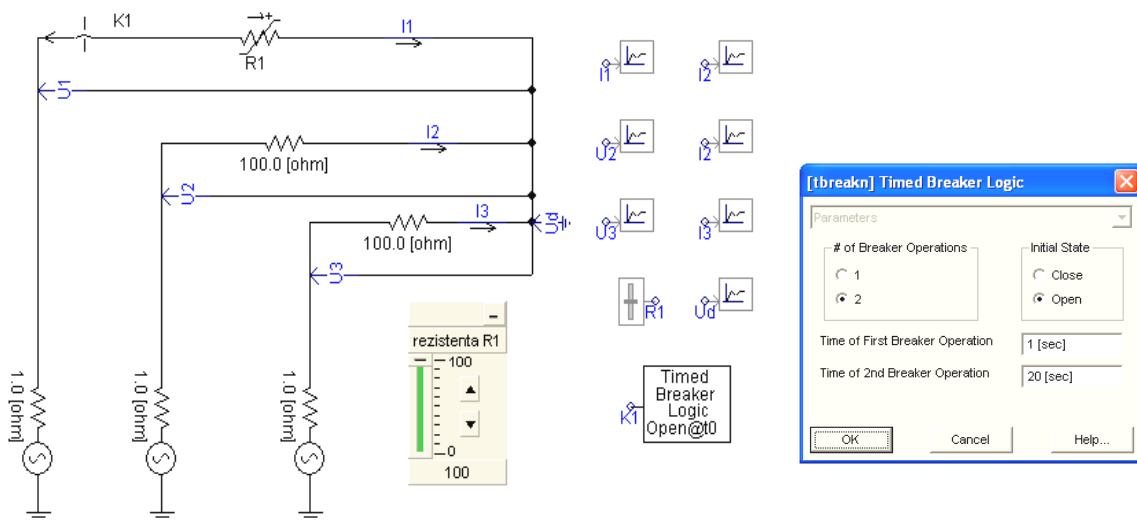


Figure 5. Electric diagram implemented in simulation. Switch K_1 configuration

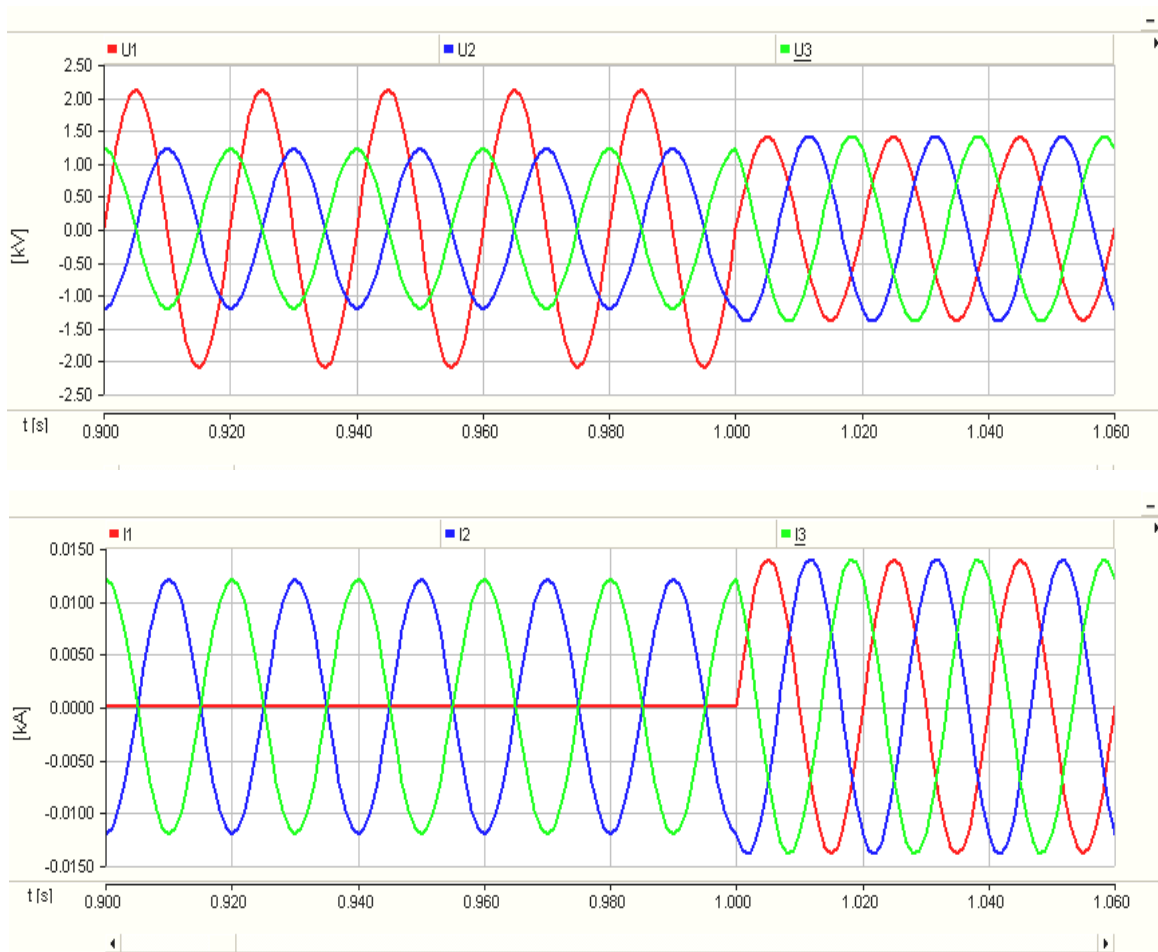


Figure 6. Voltages on receptor’s phases and currents absorbed from the grid.

2.3 Short-circuit on phase 1 and interrupting phases 2 and 3

Interruptions on phases 2 and 3 were modeled with static and infinite impedances, and short-circuit on phase 1 was modeled with a null impedance.

During the first two seconds switch K_1 is closed, and switches K_2 and K_3 are open. After 2 seconds, switch K_1 opens, and the other switches are closing. The electric diagram implemented in simulation is presented in Fig. 7, and simulation results are presented in Fig. 8, 9.

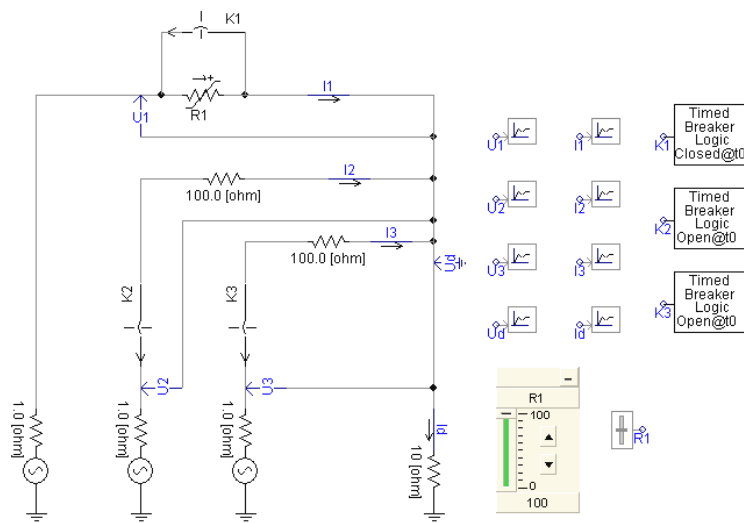


Figure 7. Electric diagram implemented in simulation.

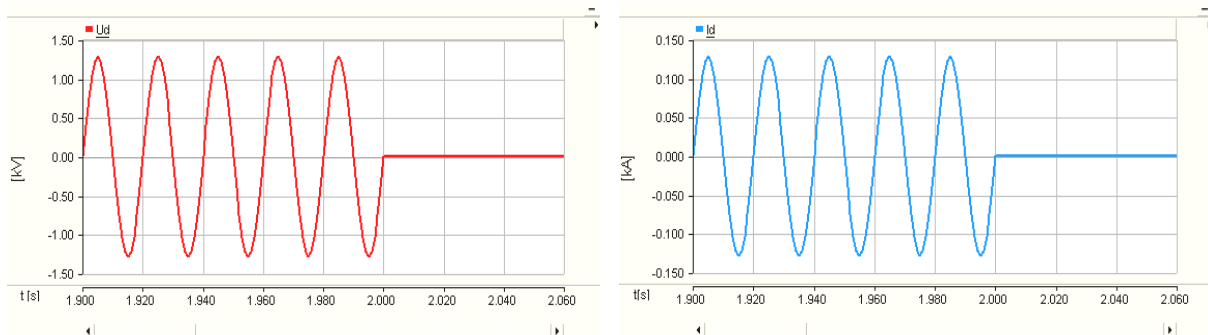


Figure 8. Neutral point displacement voltage and the neutral conductor current.

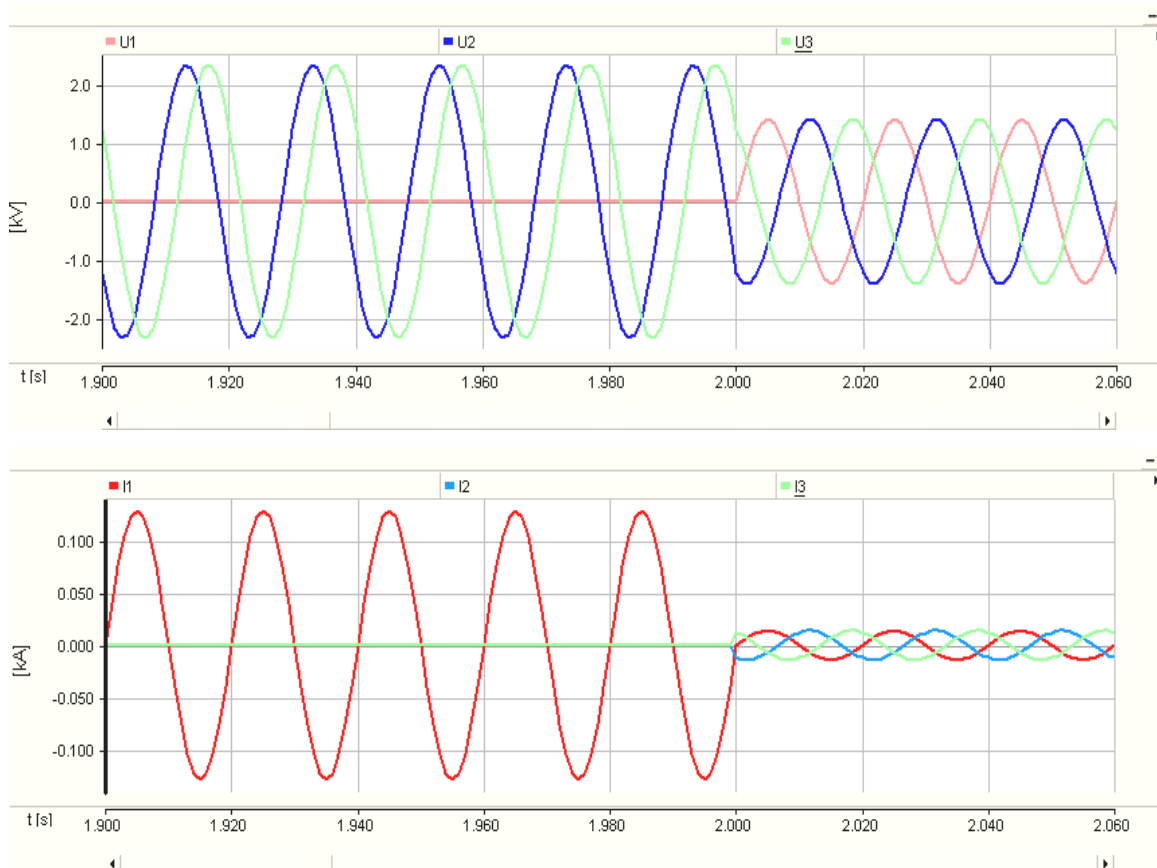


Figure 9. Voltages on receptor’s phases and currents absorbed from the grid.

During the fault, the voltages on phases 2 and 3 increase (by $\sqrt{3}$ times). Current I_1 is very high (increases by 21 times compared to rated current), and currents I_2 and I_3 are null. After two seconds, when switch K_1 closes, and switches K_2 and K_3 open, the regime becomes symmetric.

2.4 Short-circuit in two phases and interrupting one phase

It is considered short-circuit in phases 2 and 3 (without earth) and phase 1 interrupted. Short-circuits were modeled with null impedances, and interruption on phase 1 was modeled with a static and infinite impedance.

During the first two seconds, switches K_2 and K_3 are closed, and switch K_1 is open. After this period, switches K_2 and K_3 open, and switch K_1 closes. The electric diagram implemented in simulation is presented in Fig. 10, and simulation results are presented in Fig. 11-13.

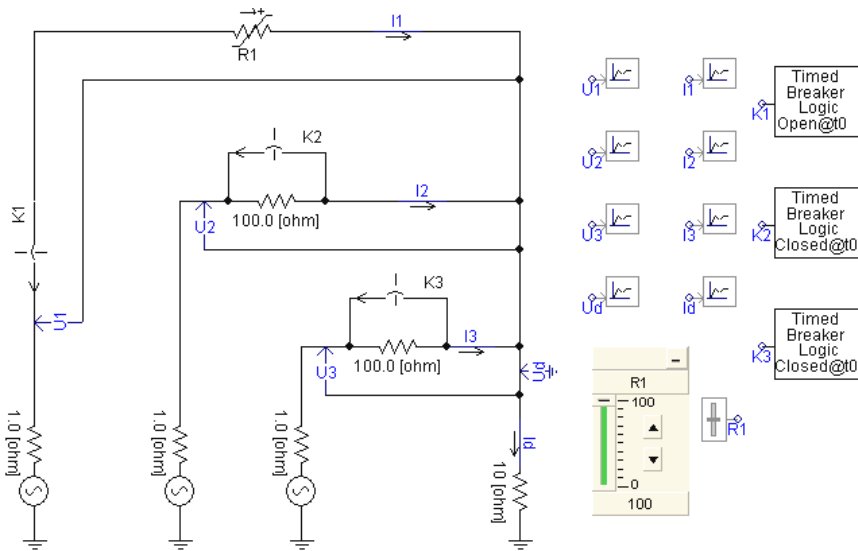


Figure 10. Electric diagram implemented in simulation.

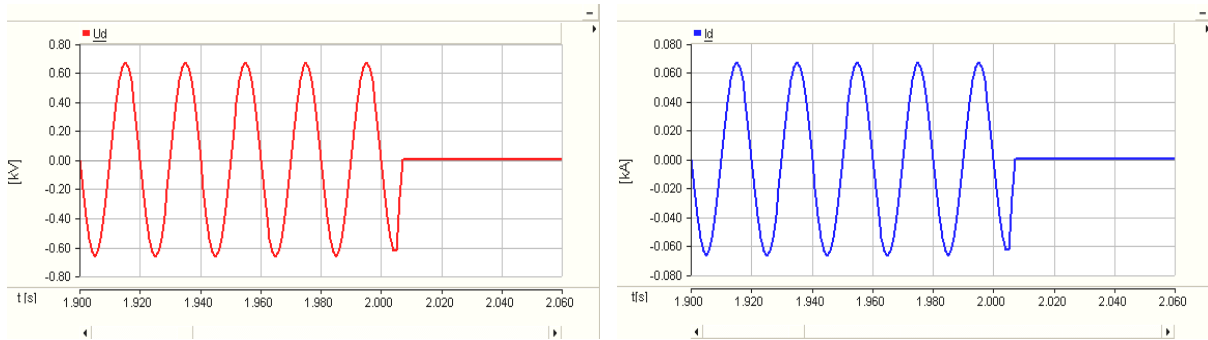


Figure 11. Neutral point displacement voltage and the neutral conductor current.

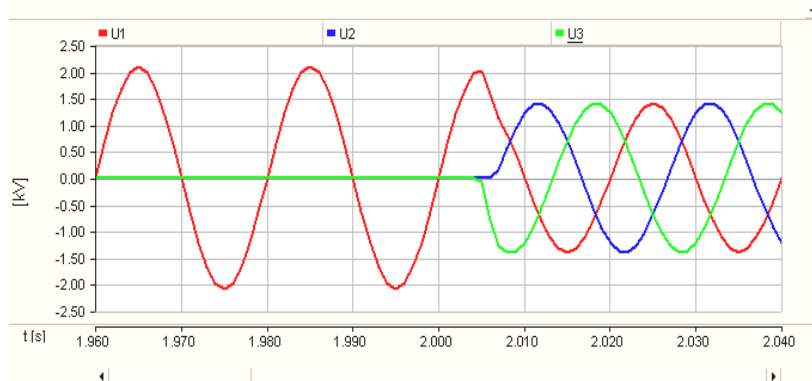


Figure 12. Voltages on receptor's phases.

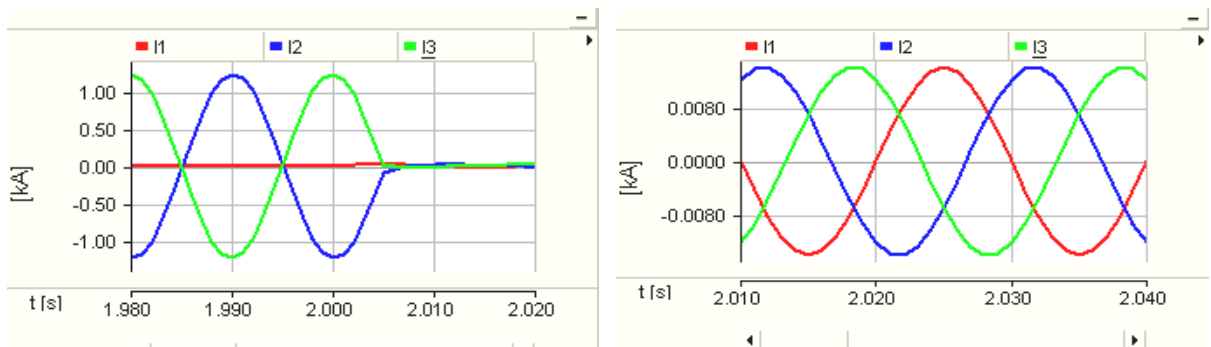


Figure 13. Currents absorbed from the grid.

During the fault the unbalance of system is very pronounced. Phase 1 voltage increases by 1,5 times compared to rated voltage. Current I_1 is null, but currents I_2 and I_3 are very high (increase by 80 times compared to rated currents) and in opposition on phase.

After 2 seconds, switch K_1 closes and switches K_2 and K_3 open. As consequence, the regime becomes symmetric.

3. CONCLUSIONS

Studying faults and abnormal operation regimes in three-phase electric systems has a special practical importance, because these operation regimes produce malfunctions or even failures of the electric installation, if they are not removed on time. Also, the study of faults and abnormal operation regimes are necessary for protection relay coordination.

In this work are analyzed few faults of three-phase electric systems by means of the PSCAD-EMTDC program.

PSCAD is a fast, accurate and easy-to-use simulator, being a very useful tool for analysis of asymmetrical faults.

A full library of advanced components allows to precisely modeling interactions between electrical networks and loads in various configurations. Users can easily interact with the components during the simulation because of the variety of control tools. The solution meters and the plotting traces are also visible and available during the simulation. Signals can be analyzed in real time.

The time steps interpolation technique combines accuracy and quickness; it allows the simulation to precisely represent the commutations of breakers and switches in the electrical model, for any model's size, up to extremely large models.

Fault analysis with PSCAD can be use for improving the system's performance and reliability.

REFERENCES

- [1] L. Hewitson, M. Brown, B. Ramesh, *Practical Power Systems Protection*, Elsevier Science&Technology Books, 2004.
- [2] M. Brown, J. Rawtani, D. Patil, *Troubleshooting of Electrical Equipment and Control Circuits*, Elsevier Science&Technology Books, 2005.
- [3] J. de Kock, C. Strauss, *Practical Power Distribution for Industry*, Elsevier Science&Technology Books, 2004.
- [4] K. R. Padiyar, *Power System Dynamics: Stability and Control*, John Wiley & Sons (Asia) Pte. Ltd. and Interline Publishing Pvt. Ltd., Singapore, 1995.
- [5] G. Ziegler, *Numerical Differential Protection: Principles and Applications*, Siemens, Berlin, 2005.
- [6] R. C. Dugan, M. F. McGranaghan, S. Santoso, H.W. Beaty, *Electrical power systems quality*, Second Edition, McGraw-Hill, 2004.
- [7] R. Al-Khannak, B. Bitzer, Developing Power Systems Reliability and Efficiency by Integrating Grid Computing Technology, *WSEAS TRANSACTIONS on POWER SYSTEMS*, Vol. 3, Issue 4, 2008, pp.226-236.
- [8] F. Muzi, Real-time Voltage Control to Improve Automation and Quality in Power Distribution, *WSEAS Transactions on Circuit and Systems*, Vol. 7, Issue 1, 2008, pp.173-183.
- [9] T. Miki, The Efficient Offline Search System for High Risk Events of Power Systems Caused by Natural Disasters, *WSEAS TRANSACTIONS on POWER SYSTEMS*, Vol. 3, Issue 5, 2008, pp.267-276.
- [10] H. M. Soliman, M. F. Morsi, M. F. Hassan, M. A Awadallah, Power System Reliable Stabilization with Actuator Failure, *Electric Power Components and Systems*, Volume 37, Number 1, January 2009, pp. 61-77.
- [11] *** PSCAD-EMTDC – *User's Manual*, Manitoba HVDC Research Centre, USA, 1999.



EXPERIMENTAL RESEARCH FOR IDENTIFYING INDUSTRIAL PROCESSES BY STATISTICAL METHODS

Stela RUSU-ANGHEL, Gelu Ovidiu TIRIAN

“Politehnica” University of Timisoara, Faculty of Engineering of Hunedoara,
Department of Electrical Engineering and Industrial Informatics, ROMANIA

Abstract:

This paper work refers to the results of an identification of the clinker furnace, by using statistic methods. We have obtained a mathematical model who describes the processes inside the furnace very accurately (more than 90%). Due to their complexity, the analytical shaping-up is impossible.

Keywords:

identification, clinker furnace, statistics, software.

1. INTRODUCTION

The analytical identification of the process during the fabrication of the concrete is difficult because this process is highly complex and they have helped us obtain some accurate mathematical methods who allow an effective conventional management.

According to the current evolution of the calculation techniques and of the process' management principles, the experimental identification based on statistic data is an alternative we should consider.

The most usual methods are the system, the linear, and the discrete models who enclose the effect of the random disturbance, such as in Figure no.1 [1].

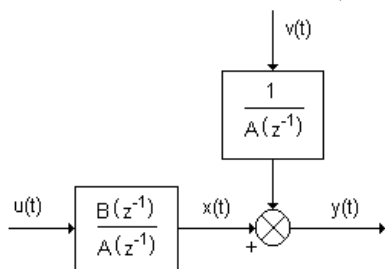


Figure no. 1

Synthetically speaking, $z(t)$ is uptaken to this process (the parameter is the discrete time t). Because $y(t)$ contains some noise (in addition), it is considered as such (it encloses a determination element $x(t)$). The statistic features of the output we have measured - $y(t)$ - are determined by the statistic features of the noise $z(t)$, or $v(t)$, according to Figure no. 4.1. Due to the fact that the identification experiment does not use - for economic and engineering reasons - all the accomplishment of the noise, and/or either of the $y(t)$ output, it does not acknowledge the identification methods of the output, because they need some statistic properties (hypothesis) which help them

identify the PFD pattern. This is not possible after only one significant experiment (for off-line identification methods) or after continuous process, but they have the same properties (for on-line identification methods).

2. PROCESS PATTERN

This process is described in Figure no. 2.

The reason of this experimental identification is represented by the pattern of the operator controlled-segment [2], [3], and [4].

The process inside the furnace is steady, but the relation between the cooling grating and the furnace causes some vacillations of the temperature (heat) inside the furnace. The only way to eliminate this is to keep up a constant temperature of the combustion gas, by adjusting the energy flow. Therefore, the temperature of the combustion gas could be considered a process output variable.

Besides that, one of the outputs should enclose information about the quality of the clinker. Because the quality of the clinker is measured (off-line) after the material gets out of the furnace, after a thorough analysis (for practical purposes) - after two hours -, it is difficult to use a quality control of the material.

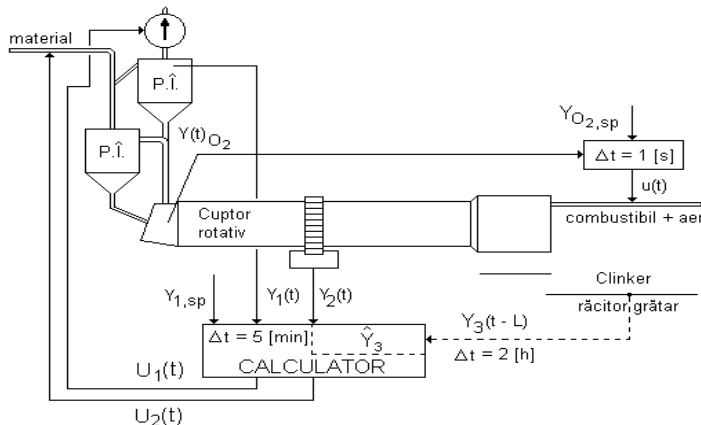


Figure no. 2

We have found out that the force of the motor that makes the furnace work is correlated to the temperature of the combustion area and the quality of the clinker. We could consider it is a second output for the process pattern we are about to identify.

An important effect of the temperature transfer and of the chemical reactions inside the furnace is the combustible matter flow. This is the first control variable. The material flow is the second control variable.

Table 1

DATA MEASURED AND CALCULATED

Speed oven nc [rot/min]	Engine speed nm [rot/min]	Computed Measuring		Temperature measured Y1	Power calculated Y2	Fuel flow X1	Material flow X2	Y1 centered yc1	Y2 centered yc2	X1 centered xc1	X2 centered xc2
		torque M [kNm]	motor m [%]								
1,7	626,316	17671,5	45	355	269,432773	14	210	7,458	31,78077	0,4625	-18,333
1,8	663,158	16493,4	42	350	237,5	13,75	225	2,458	-0,152	0,2125	-3,333
1,8	663,158	17278,8	44	347	248,809524	13,5	225	-0,542	11,15752	-0,0375	-3,333
1,8	663,158	17278,8	44	347	248,809524	13,5	225	-0,542	11,15752	-0,0375	-3,333
1,8	663,158	17278,8	44	347	248,809524	13,5	225	-0,542	11,15752	-0,0375	-3,333
1,8	663,158	16100,7	41	347	231,845238	13,5	230	-0,542	-5,80676	-0,0375	1,667
1,8	663,158	14529,9	37	350	209,22619	13,75	230	2,458	-28,4258	0,2125	1,667
1,8	663,158	15708	40	347	226,190476	13,5	230	-0,542	-11,4615	-0,0375	1,667
1,8	663,158	16100,7	41	347	231,845238	13,5	230	-0,542	-5,80676	-0,0375	1,667
1,8	663,158	15708	40	347	226,190476	13,5	230	-0,542	-11,4615	-0,0375	1,667
1,8	663,158	15708	40	347	226,190476	13,5	230	-0,542	-11,4615	-0,0375	1,667
1,8	663,158	15708	40	347	226,190476	13,5	230	-0,542	-11,4615	-0,0375	1,667
1,8	663,158	15708	40	348	226,190476	13,6	230	0,458	-11,4615	0,0625	1,667
1,8	663,158	15708	40	348	226,190476	13,6	230	0,458	-11,4615	0,0625	1,667
1,8	663,158	16100,7	41	348	231,845238	13,6	230	0,458	-5,80676	0,0625	1,667
1,8	663,158	15315,3	39	349	220,535714	13,7	230	1,458	-17,1163	0,1625	1,667
1,8	663,158	16100,7	41	347	231,845238	13,5	230	-0,542	-5,80676	-0,0375	1,667
1,8	663,158	16493,4	42	347	237,5	13,5	230	-0,542	-0,152	-0,0375	1,667
1,8	663,158	17671,5	45	346	254,464286	13,4	230	-1,542	16,81229	-0,1375	1,667
1,8	663,158	17671,5	45	345	254,464286	13,3	230	-2,542	16,81229	-0,2375	1,667
1,8	663,158	18064,2	46	345	260,119048	13,3	230	-2,542	22,46705	-0,2375	1,667
1,8	663,158	17671,5	45	345	254,464286	13,3	230	-2,542	16,81229	-0,2375	1,667
1,8	663,158	16493,4	42	348	237,5	13,6	230	0,458	-0,152	0,0625	1,667
1,8	663,158	16493,4	42	347	237,5	13,5	230	-0,542	-0,152	-0,0375	1,667

Arithmetic average

347,5417	237,6525	13,5375	228,3333
----------	----------	---------	----------

There are other possible variables, but the first two are the most important and the identification process sticks to them.

We have measured it every 5 minutes and we have found out 24 values of the following elements (Table no. 1):

- ✚ combustion gas temperature- $Y_1(t)$, in $^{\circ}\text{C}$;
- ✚ the coupling to the motor shaft - m [%] – is used for calculating the training force - $Y_2(t)$.

- to see the graphics of the sizes, according to two methods : PLOT and BAR;
 - to estimate the process by the method of the smallest squares, using two regress patterns : linear and non-linear II-type regress;
 - to use the data by two methods: interpolator cubic shift, where the insertion steps are: 1, 0.5, 0.4, 0.3, 0.2, 0.1 și 0.05, and the insertion based on the Fourier fast transformation method is valid for 30, 60, 90, 120, 150, 180 and 200 insertion points. We can see the insertion curves on the monitor.

The main software is called « ie.m » and is able to perform a graphic interface with buttons – selected optionally; we could use the calculation methods of the above mentioned functions.

Figure no. 3 and 4 refer to the results of the shaping-up by two methods. The continuous line describe the data we have measured, meanwhile the dotted line refers to the determined methods.

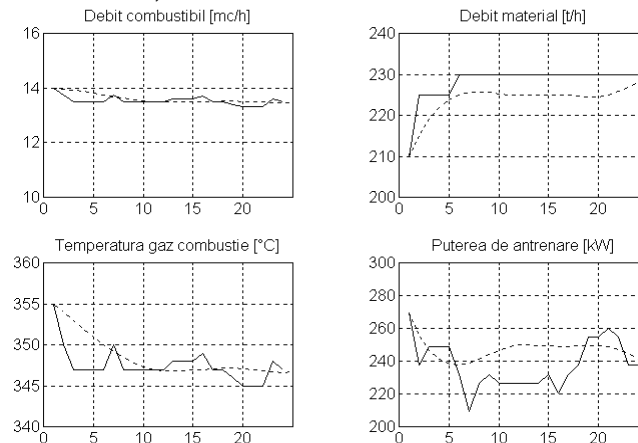


Figure no. 3 Cubic shift insertion of 0.2 step

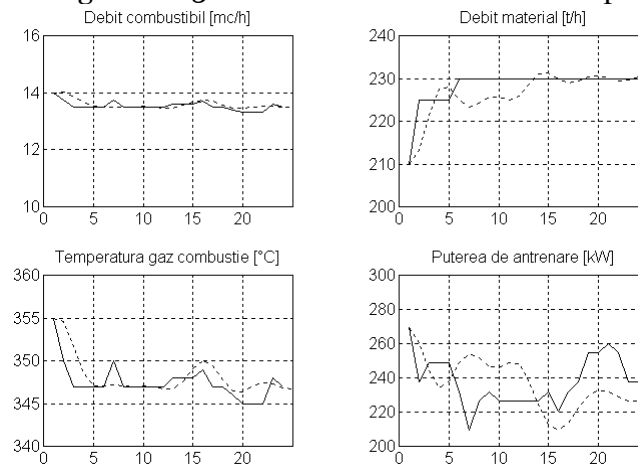


Figure no. 4 60-points FFT insertion

5. CONCLUSIONS

This paperwork describes the mathematical method based on statistic methods for a clinker furnace. The accuracy of the model is very high, as far as the statistic indicators have proved it. This method is relatively simple and it has been used in experiments. We have come up with the MATLAB calculation software, but we are not able to describe them in this paperwork for space reasons.

REFERENCES

- [1] Dumitrache, I. ș.a., Numerical adjustment of industrial goods, Technical Publishing House, Bucharest, 1984
- [2] Rehner, H., Mathematical methods and software management of the furnaces used in silicates industry, Construction materials magazine no.1/1990
- [3] Morris, L., Eaton-Linear statistical models, Institutes Mathematical Statistics, Beachwood, Ohio, USA, 2007



AUTOMATIC DETERMINATION OF THE MINERAL COMPOSITION OF THE PORTLAND CEMENT CLINKER

Stela RUSU-ANGHEL

“Politehnica” University of Timisoara, Faculty of Engineering Hunedoara,
Department of Electrical Engineering and Industrial Informatics, ROMANIA

Abstract:

This paperwork points out software for the automatic determination of the mineral composition of the cement clinker. Although they have rather similar oxide composition, the mineral structure may be rather different and it influences the quality of the cement. Therefore, the software we suggest allows the fast determination of the mineral composition and any method of improvement, according to the required properties of the Portland cement.

Keywords:

cement, mineral composition, clinker, software.

1. INTRODUCTION

According to the balance diagrams [1], we are able to calculate the basic composition of the clinkers. This calculation is possible if the cement turns solid in case of both termic-dynamic and non termic-dynamic balance.

In case of the complete balance solid state, the product does not turn glassy. In fact, there is no termic-dynamic balance in case of the solid state, and if we consider that possibility, the mineral composition we calculate according to that hypothesis is a potential composition – it is possible only if the chemical composition is not equal to the real mineral composition (of those minerals that make up the composition).

a) Presuming that the clinkers are situated in the termical balance sub-system $C_3S-C_2S-C_3A-C_4AF$ ($M_{Al} > 0,64$), Bogue has determined that we could calculate the mineral elements according to the following formula:

$$\begin{aligned} \%C_4AF &= 3,04\%Fe_2O_3 \\ \%C_3A &= 2,65\%Al_2O_3 - 1,69\%Fe_2O_3 \\ \%C_3S &= 4,07\%CaO - 7,60\%SiO_2 - 6,72\%Al_2O_3 - 1,42\%Fe_2O_3 \\ \%C_2S &= 8,60\%SiO_2 + 5,06\%Al_2O_3 + 1,07\%Fe_2O_3 - 3,05\%CaO \end{aligned} \tag{1}$$

b) For the clinkers in the termic balance sub-system $C_3S-C_2A-C_4AF-C_2F$ ($M_{Al} < 0,64$), the result is based on Bogue’s analogical argument. Thus:

$$\begin{aligned} \%C_4AF &= 4,76\%Al_2O_3 \\ \%C_2F &= 1,70\%Fe_2O_3 - 2,65\%Al_2O_3 \\ \%C_3S &= 4,07\%CaO - 7,60\%SiO_2 - 4,48\%Al_2O_3 - 2,84\%Fe_2O_3 \\ \%C_2S &= 8,60\%SiO_2 + 3,36\%Al_2O_3 + 2,14\%Fe_2O_3 - 3,05\%CaO \end{aligned} \tag{2}$$

c) For the intermediary case of the clinkers belonging to the $C_3S-C_2A-C_4AF$ ($M_{Al} = 0,64$), we have:

$$\begin{aligned} \%C_4AF &= 3,04\%Fe_2O_3 \\ \%C_3S &= 4,07\%CaO - 7,60\%SiO_2 - 5,70\%Fe_2O_3 \\ \%C_2S &= 8,60\%SiO_2 - 4,30\%Fe_2O_3 - 3,05\%CaO \end{aligned} \tag{3}$$

The relations according to Bogue are particular and they use some coefficients specific to the termical balance sub-systems:

$$\begin{aligned} C_3S-C_2S-C_3A-C_4AF &\text{ with } M_{Al} > 0,64 \\ C_3S-C_2A-C_4AF-C_2F &\text{ with } M_{Al} < 0,64 \end{aligned} \tag{4}$$

$C_3S - C_2A - C_4AF$ with $M_{Al} = 0,64$

These relations are not valid for other termic balance sub-systems. Considering all these facts, we have come up with software who determines the composition for each stage of the clinker, for both mineral composition of the dust and the termic balance sub-system. We made the software by generalizing the following example which was based on the weight survey. We are going to describe it in the following.

2. THE SO-CALLED SOFTWARE

software *CompClinker*;

uses *Crt, Graph, UApp*;

const $Mc = 56$; $Ma = 102$; $Ms = 60$; $Mf = 160$;

Var

$CaO, Al_2O_3, SiO_2, Fe_2O_3$: Real;

$SCaO, SAl_2O_3, SSiO_2, SFe_2O_3$: String;

Paragenesis : String;

M : array[1..4] of real; N : array[1..4,1..4] of Byte ; X : array[1..4] of real;

B : array[1..4] of real; A : array[1..4,1..4] of real;

procedure *Init*;

begin

Title('Determination of the portland cement clinker for each stage');

DefineBtn(0, 10, 55, 620, 393, 0, 0, "", Off);

{ define the main menu buttons }

DefineBtn(10, 10, 26, 60, 19, 2, 1, 'Info',

'General information about the software', Off);

DefineBtn(11, 75, 26, 60, 19, 2, 1, 'Calculation',

'Determination of the stage composition ', Off);

DefineBtn(12, 570, 26, 60, 19, 2, 5, 'Exit',

'Stop the software', Off);

SCaO:='';

DefineInp(1,100,100,320,30,50, '% CaO ',SCaO);

SAl2O3:='';

DefineInp(2,100,130,320,30,50, '% Al2O3 ',SAl2O3);

SSiO2:='';

DefineInp(3,100,160,320,30,50, '% SiO2 ',SSiO2);

SFe2O3:='';

DefineInp(4,100,190,320,30,50, '% Fe2O3 ',SFe2O3);

Paragenesis:='';

DefineInp(5,100,220,320,30,200, 'Paragenesis ',Paragenesis);

end;

procedure *Info*;

begin

end;

procedure *Calculation*;

Var I, J, K, L : Integer; S : String[10]; Code, MM, Poz : Integer; T : Real;

Sform : array[1..4] of string[15]; SS:string; Sf : array[1..4] of string[15];

begin

Drawinp(1); Drawinp(2); Drawinp(3); Drawinp(4); Drawinp(5);

Inp(1); Inp(2); Inp(3); Inp(4); Inp(5);

Val(SCaO, CaO, Code); Val(SAl2O3, Al2O3, Code); Val(SSiO2, SiO2, Code); Val(SFe2O3, Fe2O3, Code);

for i:=1 to 4 do

for j:=1 to 4 do

N[i,j]:=0;

Insert('-', Paragenesis, length(Paragenesis)+1);

K:=1;

for i:=1 to 4 do

begin

while (Paragenesis[k]<>' ') do

begin

if Paragenesis[k]='C' then

begin

Inc(k);

if (Paragenesis[k]>='A') and (Paragenesis[k]<='S') or (Paragenesis[k]=' ') then

N[i,1]:=1

else

begin

if (Paragenesis[k+1]='0') and (Paragenesis[k+1]<='9') then

begin

S:=Copy(Paragenesis, k, 2); Inc(K);

end

else

```

    S:=Copy(Paragenesis,k,1);
    Val(S,N[i,1],Code);
    Inc(K);
end;
end;
if Paragenesis[k]='A' then
begin
    Inc(k);
    if (Paragenesis[k]>='A') and (Paragenesis[k]<='S') or (Paragenesis[k]='.') then
        N[i,2]:=1
    else
        begin
            if (Paragenesis[k+1]>='0') and (Paragenesis[k+1]<='9') then
                begin
                    S:=Copy(Paragenesis,k,2); Inc(K);
                end
            else
                S:=Copy(Paragenesis,k,1);
                Val(S,N[i,2],Code);
                Inc(K);
            end;
        end;
    if Paragenesis[k]='S' then
        begin
            Inc(k);
            if (Paragenesis[k]>='A') and (Paragenesis[k]<='S') or (Paragenesis[k]='.') then
                N[i,3]:=1
            else
                begin
                    if (Paragenesis[k+1]>='0') and (Paragenesis[k+1]<='9') then
                        begin
                            S:=Copy(Paragenesis,k,2); Inc(K);
                        end
                    else
                        S:=Copy(Paragenesis,k,1);
                        Val(S,N[i,3],Code);
                        Inc(K);
                    end;
                end;
        end;
    if Paragenesis[k]='F' then
        begin
            Inc(k);
            if (Paragenesis[k]>='A') and (Paragenesis[k]<='S') or (Paragenesis[k]='.') then
                N[i,4]:=1
            else
                begin
                    if (Paragenesis[k+1]>='0') and (Paragenesis[k+1]<='9') then
                        begin
                            S:=Copy(Paragenesis,k,2); Inc(K);
                        end
                    else
                        S:=Copy(Paragenesis,k,1);
                        Val(S,N[i,4],Code);
                        Inc(K);
                    end;
                end;
            end;
            Inc(k);
        end;
end;
for I:=1 to 4 do
    M[I]:=N[I,1]*Mc+N[I,2]*Ma+N[I,3]*Ms+N[I,4]*Mf;
B[1]:= CaO/Mc;
B[2]:= Al2O3/Ma;
B[3]:= SiO2 /Ms;
B[4]:= Fe2O3 /Mf;
for I:=1 to 4 do
    begin
        A[i,1]:=N[i,1]/M[1]; A[i,2]:=N[i,2]/M[2]; A[i,3]:=N[i,3]/M[3]; A[i,4]:=N[i,4]/M[4];
    end;
Mm:=4;
for k:=1 to mm do
begin
    if a[k,k]=0 then
        begin
            j:=k+1;
            while (j<=mm) and (a[j,k]=0) do j:=j+1;
            if j<=mm then

```

```

begin
  for l:=k to mm do
    begin
      t:=a[k,l]; a[k,l]:=a[j,l]; a[j,l]:=t;
    end;
    t:=b[k];
    b[k]:=b[j];
    b[j]:=t;
  end
  else
    begin
      Outtextxy(100,500,'The system cannot be solved by Gauss' method');
      Halt;
    end;
  end;
  for i:=k+1 to mm do
    begin
      for j:=k+1 to mm do
        a[i,j]:=a[i,j]- a[k,j]*a[i,k]/a[k,k]; b[i]:=b[i]-b[k]*a[i,k]/a[k,k];
      end;
    end;
  x[mm]:=b[mm]/a[mm,mm];
  for k:=mm-1 downto 1 do
    begin
      t:=0;
      for j:=k+1 to mm do t:=t+a[k,j]*x[j];
      x[k]:=(b[k]-t) /a[k,k];
    end;
  j:=0;
  k:=1;
  poz:=1;
  for i:=1 to length(Paragenesis) do
    if Paragenesis[i] <>'-' then Inc(j)
    else
      begin
        Sform[k]:=copy(Paragenesis,poz,j);
        poz:=i+1;
        Inc(K);
        j:=0;
      end;
  Str(x[1]:6:3,Sf[1]);
  Str(x[2]:6:3,Sf[2]);
  Str(x[3]:6:3,Sf[3]);
  Str(x[4]:6:3,Sf[4]);
  SS:="";
  DefineInp(10,90,260,350,30,0,'The stage composition of the clinker is: ',SS);
  DrawInp(10);
  SS:=SF[1];
  DefineInp(6,100,300,320,30,100,'% '+Sform[1]+' ',SS);
  DrawInp(6);
  SS:=SF[2];
  DefineInp(7,100,330,320,30,100,'% '+Sform[2]+' ',SS);
  DrawInp(7);
  SS:=SF[3];
  DefineInp(8,100,360,320,30,100,'% '+Sform[3]+' ',SS);
  DrawInp(8);
  SS:=SF[4];
  DefineInp(9,100,390,320,30,100,'% '+Sform[4]+' ',SS);
  DrawInp(9);
  WaitEsc;
end;

procedure Run;
begin
  { Start main menu }
  MainSel := 10;
  repeat
    ClearClient;
    HMenu(10, 12, MainSel);
  case MainSel of
    10: Info;
    11: Calculation;
  end;
  until MainSel = 12;
end;

procedure Done;

```

```
begin
EndGraph;
DoneButtons;
end;
```

```
begin
Init;
Run;
Done;
end.
```

3. CALCULATION EXAMPLE

Considering a quaternary mix with the composition 66,7% CaO; 21,4% SiO₂; 6,9% Al₂O₃; 5% Fe₂O₃ and knowing that this mixture belongs to the paragenesis C₃S-C₂S-C₃A-C₄AF – in case it reaches a balance – we have to establish the stage composition of the clinker.

During the crystallizing processes, the weight of the mixture is constant. When we perform the weight survey for each of the four oxides, we have:

$$\begin{cases} m_{\text{CaO}_{\text{in}}\text{bial}} = m_{\text{CaO}_{\text{din}}\text{C}_3\text{S}} + m_{\text{CaO}_{\text{din}}\text{C}_2\text{S}} + m_{\text{CaO}_{\text{din}}\text{C}_3\text{A}} + m_{\text{CaO}_{\text{din}}\text{C}_4\text{AF}} \\ m_{\text{SiO}_2\text{in}}\text{bial} = m_{\text{SiO}_2\text{din}}\text{C}_3\text{S} + m_{\text{SiO}_2\text{din}}\text{C}_2\text{S} \\ m_{\text{Al}_2\text{O}_3\text{in}}\text{bial} = m_{\text{Al}_2\text{O}_3\text{din}}\text{C}_3\text{A} + m_{\text{Al}_2\text{O}_3\text{din}}\text{C}_4\text{AF} \\ m_{\text{Fe}_2\text{O}_3\text{in}}\text{bial} = m_{\text{Fe}_2\text{O}_3\text{din}}\text{C}_4\text{AF} \end{cases} \quad (5)$$

Considering that:

$$M_{\text{C}_3\text{S}} = 3 \cdot 56 + 60 = 228$$

$$M_{\text{C}_2\text{S}} = 2 \cdot 56 + 60 = 172$$

$$M_{\text{C}_3\text{A}} = 3 \cdot 56 + 102 = 270$$

$$M_{\text{C}_4\text{AF}} = 4 \cdot 56 + 102 + 160 = 486$$

And that: $x = \% \text{C}_3\text{S}$; $y = \% \text{C}_2\text{S}$; $z = \% \text{C}_3\text{A}$ și $u = \% \text{C}_4\text{AF}$, we have:

$$66,7 = x \frac{3 \cdot 56}{228} + y \frac{2 \cdot 56}{172} + z \frac{3 \cdot 56}{270} + u \frac{4 \cdot 56}{486}$$

$$21,4 = x \frac{60}{228} + y \frac{60}{172} \quad (7)$$

$$\left. \begin{aligned} 6,9 &= z \frac{102}{270} + u \frac{102}{486} \\ 5 &= u \frac{160}{486} \Rightarrow u \end{aligned} \right\} \Rightarrow z \quad (8)$$

$$x + y + z + u = 100$$

After the calculation, we have:

$$u = 15,19 \% \text{C}_4\text{AF}$$

$$z = 9,83 \% \text{C}_3\text{A}$$

$$(9)$$

If we replace the „u” and the „z” from the first equation, we have:

$$\begin{cases} x + y = 74,98 \\ \frac{60}{228}x + \frac{60}{172}y = 21,4 \end{cases} \text{ and we calculate:}$$

$$x = 55,56 \% \text{C}_3\text{S};$$

$$y = 19,42 \% \text{C}_2\text{S}$$

$$(10)$$

The software runs if we take the following steps:

Step 1. – *Open dialogue window* made of:

- ✚ the name of the software: “Determining the composition of the portland cement clinker for each stage”;
- ✚ the menu bar with the buttons: “Info”, “Calculation” și “Exit”;

✚ the windows for introducing the primary data: %CaO, %Al₂O₃, %SiO₂, %Fe₂O₃ and Paragenesis;

Step 2. – *Introduce data* – with the help of the keyboard;

Step 3. – *Data processing* – it begins when we press the “Calculation” key, by selecting the right key from the menu bar. The algorithm is based on the example we have already discussed about, and it turns it into a general rule. Thus, it should:

a) – identify the paragenesis we have used and make another matrix $N[i,j]$, $i = 1 \dots 4$, $j = 1 \dots 4$, where the coefficients of the oxides correspond to the mineral elements;

b) – calculate the molecular weight of each stage:

$$M[i] = N[i,1]*M_c + N[i,2]*M_a + N[i,3]*M_s + N[i,4]*M_f, \quad i = 1 \dots 4 \quad (11)$$

c) – calculate the free elements (%oxide/ oxides’ molecular weight) and the coefficients of the unknown quantities of the equation system:

$$B[i] = x[1]*A[i,1] + x[2]*A[i,2] + x[3]*A[i,3] + x[4]*A[i,4], \quad i = 1 \dots 4 \quad (12)$$

where:

$$A[i,1] = N[1,i]/M[1]; \quad A[i,2] = N[2,i]/M[2]; \quad A[i,3] = N[3,i]/M[3]; \quad A[i,4] = N[4,i]/M[4]; \quad (13)$$

d) – solving the equation system by Gauss’ method;

e) – posting the results;

Step 4. – *Closing the working window* by pressing the “Exit” key or introducing new data and performing a new calculation.

5. CONCLUSIONS

The method and the software we have discussed about in this paperwork allow us to determine the mineral composition of the Portland cement clinker faster. According to the properties of the cement we would like, we can get some useful information about the composition we need for the clinker. Therefore, we can get a finite good of a higher constant quality.

REFERENCES

- [1] CEPROCIM S.A. The book of the cement industry engineers, Technical Publishing House Bucharest, 1994
- [2] Emanuelson A.- Portland Cement Clinker, Lund Institute of Technology, Sweden 2002
- [3] www.CemNet.com/ The latest cement news and information, January 2009



MODELING OF THE ENERGY ENTITIES FUNCTIONING USING THE MARKOV CHAINS METHOD

ROB Raluca, IORDAN Anca, PANOIU Caius, PANOIU Manuela

Politechnical University of Timisoara, Faculty of Engineering Hunedoara, ROMANIA

Abstract:

In this paper the authors present a functioning of the energy entities modelling method using Markov chains. It is modelled the functioning of an electric supply loop for a 0.4kV voltage consumer by successive reducing of the electric supply scheme and taking into consideration the two possible states for each loop element: failure and repair rates.

Keywords:

Markov chains, state transition rates matrix, failure rate, repair rate

1. INTRODUCTION

The Markov processes represent a particular case of the stochastic processes, whose characteristic property is that they have no memory. The final states of the systems that are modelled by Markov chains are connected only with the transition probability from an i state (at t time) to a j state (at $t+1$ time) and they have no connection with the initial state. The evolution of a Markov process is influenced only by its current state. If a Markov process has a finite number of states, then it is a Markov chain.

In energy systems field this modelling method is used only when the independence of the containing elements assumption cannot be admitted.

In this paper the behaviour of the elements is modelled by an exponential distribution function of the stochastic variable, described by the relation:

$$f(t) = \lambda \cdot e^{-\lambda t} \quad , \quad (1)$$

The probability density is given by the relation:

$$F(t) = 1 - e^{-\lambda t} \quad , \quad (2)$$

2. PROBLEM FORMULATION

The evolution in time of an energy entity through the various states that can appear after the failure and repairing of the containing elements can be assimilated with a continuous time Markov chain [1]. The determining of the state probabilities for a given reference period is made by solving the differential equations system, written in the following matrix form:

$$P'(t) = P(t) \times Q \quad , \quad (3)$$

where

$P(t)$ represents the state transition functions matrix at t moment.

Q represents the state transition rates matrix.

The state transition functions p_{ij} are the elements of the state transition functions matrix. They depend only on the difference between two moments of time and they have the properties:

$$p_{ij} \in [0, 1] \quad , \quad (4)$$

$$\sum_{j=1}^m p_{ij} = 1 \quad , \quad (5)$$

The state transition functions are used in directly form very rarely. A continuous time Markov chain is usually characterized by the state transition rates [2, 6]. In functioning of the energy entity

modeling is using the state transition rates matrix $Q = [q_{ij}]$, $i, j = 1, 2, \dots$ with the following property:

$$\sum_{j=1}^m q_{ij} = 0 \quad , \quad (6)$$

The Q matrix form is given by the relation:

$$Q = \begin{pmatrix} q_{11} & q_{12} & \dots & q_{1n} \\ q_{21} & q_{22} & \dots & q_{2n} \\ \dots & \dots & \dots & \dots \\ q_{n1} & q_{n2} & \dots & q_{nn} \end{pmatrix} , \quad (7)$$

The elements $q_{ij} \geq 0$ of the state transition state matrix Q indicate the probabilities that the system to pass from i state in j state, $i, j = \overline{1, n}$, where n is the number of the possible states for the studied installation. As it is shown in [1], is using the following notations for the reliability parameters in energy installations:

- λ [h⁻¹] is the failure rate of an energy entity element
- μ [h⁻¹] is the repair rate of an energy entity element
- ν [h⁻¹] is the replacement rate of an energy entity element.

In situation when the system passing from i state in j state is made by failure of an element with λ failure rate, then $q_{ij} = \lambda$.

In situation when the system passing from i state in j state is made by repairing of an element with μ repair rate, then $q_{ij} = \mu$.

In situation when the system passing from i state in j state is made by repairing of an element with ν replacement rate, then $q_{ij} = \nu$.

Taking into consideration a system composed by n elements, each element having two possible states (failure and repairing), the total number of the possible states of the installation is 2^n . From here is resulting that to determine the state probabilities P_i , $i = \overline{1, n}$ is necessary to solve an 2^n equations system.

If the reference time is ample ($t \rightarrow \infty$), the (1) differential equations system becomes an algebraic equations system written in the following form:

$$P \times Q = 0 \quad , \quad (8)$$

The functioning of the electric supply scheme modelling implicates the reducing of its structure.

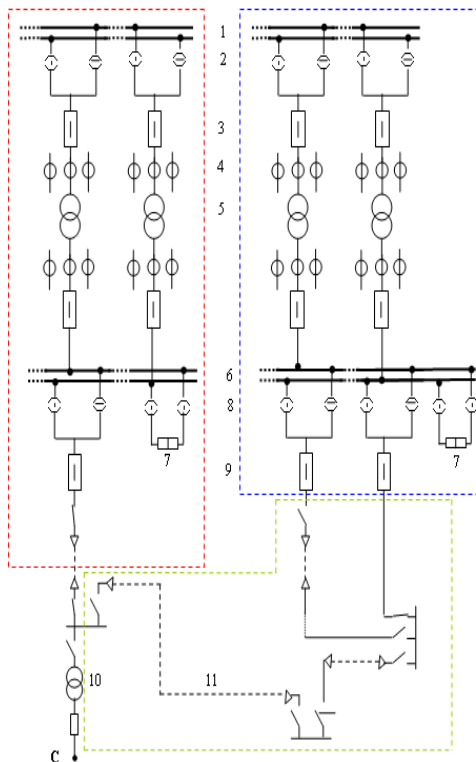


Fig.1. Electric supply scheme where C consumer is connected
 Legend fig. 1: 1-110kV electric line, 2-110kV disconnector, 3-110kV circuit breaker, 4-110kV current transformers, 5-110/20kV power transformers, 6-20kV electric bar 7-20kV transversal couple, 8-20kV disconnector 9-20kV circuit breaker, 10-20/0,4kV power transformer 11-20kV underground cable

After successive reducing of the scheme in fig.1, the authors obtained the block diagram in fig.2. The situation is analysed taking into consideration the followings:

- ✚ the containing elements of the scheme can be failed only when the entity is functioning.
- ✚ the state with all three failed elements is not existing, because the element no.3 cannot fail if the elements no.1 and no.2 are failed, and also, the elements no.1 and no.2 cannot fail if the elements no.3 is failed.

4. OBTAINED RESULTS

The solution of the equation system (11) is the probability state vector $P = [P_1 \dots P_7]$:

$$P_1 = 0.995 ; P_2 = 0.0048 ; P_3 = 0.0001135253 ; P_4 = 0.000064 ;$$

$$P_5 = 0.000000432 ; P_6 = 0.00000031 ; P_7 = 0.000000005 \quad (12)$$

The probability state vector serves in determining the reliability indicators:

- success probability

$$P = \sum_{i \in S} P_i = 0.995 \quad (13)$$

- unsuccessful probability

$$Q = \sum_{i \in R} P_i = 1 - P = 0.005 \quad (14)$$

- medium success duration in 1 year (8760 h)

$$M[\alpha(T)] = P \times T = 8716.2h \quad (15)$$

- medium unsuccessful duration in 1 year (8760 h)

$$M[\beta(T)] = Q \times T = 43.8h \quad (16)$$

- failure total number in 1 year (8760 h)

$$M[v(T)] = \left[\sum_{i \in S} P_i \times \sum_{j \in R} q_{ij} \right] \times T = 394,17 \quad (17)$$

- medium functioning time

$$M[T_f] = \frac{M[\alpha(T)]}{M[v(T)]} = 22222h \quad (18)$$

- medium unfunctioning time

$$M[T_d] = \frac{M[\beta(T)]}{M[v(T)]} = 14,28h \quad (19)$$

In relations (12)-(19) there were noted: S-success states set, $P_7 = 0.000000005$ and R- unsuccessful states set

5. CONCLUSION

The computing of the state probabilities based on solving the equation system (8) is useful in all cases when it's making a quantitative analysis of the energy installation reliability, indifferent if the containing elements of the system are dependent or independent. The advantages of the Markov chain modelling are:

- ✚ the energy system that is analysed can be modelled with dependent elements.
- ✚ It can be analysed each possible state of the system, using Markov chain transition graph, and the reliability parameters (λ , μ and ν)
- ✚ the resulting data, reliability indicators can give important informations about the system functioning.

This modelling method is limited in situations when implicates a lot of calculation, the reason for reducing the computing scheme. In situation when the results do not demand accuracy, it is indicated to use the binomial method, in witch the element can be considered independent.

REFERENCES:

- [1.] ENEL Distribuție Banat SA, „Lucrarea nr.216T/2002 – Alimentare cu energie electrică SC Alin Trans SRL Deva”, 2002.
- [2.] Iosifescu M., „Lanțuri Markov finite și aplicații”, Editura Tehnică București 1977.
- [3.] Osaci M., Panoiu M., Heput T., “Numerical Stochastic Model for the Magnetic Relaxation Time of the Fine Particle System with Dipolar Interaction”, *Applied Mathematical Modelling*, vol.30, 2006, pag.545-553.
- [4.] *** PE 013 „Prescripție energetică privind metodele și elementele de calcul al siguranței în funcționare a instalațiilor energetice”, ISPE Bucuresti 1994.
- [5.] Panoiu M., Panoiu C., Iordan A., Rob R., “Simulation Results Regarding High Power Loads Balancing”, 12th WSEAS International Conference of SYSTEMS, *New Aspects of SYSTEM*, 2008, pag.614-619.
- [6.] Petrișor E., „Simulare Monte Carlo”, Editura Politehnica Timișoara 2006.
- [7.] Rafiroiu M., „Modele de simulare în construcții”, Editura Facla Timișoara 1982.
- [8.] Săcuiu I., Zorilescu D., „Numere aleatoare”, Editura Academiei 1978.



DETERMINATION OF THE CURRENT HARMONICS INTRODUCED IN THE GRID BY THE D.C.-SUPPLIED CONSUMERS

Ioan BACIU, Corina Daniela CUNȚAN, Angela IAGĂR

Polytechnic University of Timișoara, University Politehnica Timișoara,
Faculty Engineering of Hunedoara, Electrical Engineering
& Industrial Informatics Department, ROMANIA

Abstract:

This work is presenting a determination mode of the current harmonics for a supply circuit of a d.c. motor, to which the loading is adjusted by another identical motor, connected as generator. Their determination is achieved by direct measurement with an energy analyzer CA8334.

Keywords:

current harmonics, single-phased power rectifier, distortion factor

1. WORK'S PRESENTATION

For the current harmonics' study it was achieved a circuit of relatively reduced power using a d.c. motor of 750 W coupled directly with another motor, identically with the first one, which is connected as generator, to which the loading can be adjusted by means of a slide rheostat. The electric circuit's diagram (fig. 1) allows the adjustment of the motor's supply voltage using a single-phased autotransformer.

Will be analyzed the current harmonics for three different loading situations of the generator, respectively three values for the slide potentiometer, at three different supply voltages. Determinations of the current harmonics, as well as the THD factor, are made with a three-phased energy analyzer CA8334 which allows the calculation of these parameters as follows:

1 sec RMS values for voltage and current

$$V_{rms}[i] = \sqrt{\frac{1}{NechSec} \cdot \sum_{n=0}^{NechSec-1} V[i,n]^2} \quad (1)$$

where: V_{rms} single rms voltage $i+1$ phase; $V_{avg}[i] = V_{rms}[i]$

$$U_{rms}[i] = \sqrt{\frac{1}{NechSec} \cdot \sum_{n=0}^{NechSec-1} U[i,n]^2} \quad (2)$$

where: U_{rms} compound rms voltage $i+1$ phase $U_{avg}[i] = U_{rms}[i]$

$$A_{rms}[i] = \sqrt{\frac{1}{NechSec} \cdot \sum_{n=0}^{NechSec} A[i,n]^2} \quad (3)$$

where: $A_{rms}[i]$ - Effective current phase $i+1$; $A_{avg}[i] = A_{rms}[i]$

Calculation of harmonic bins :

By FFT (16 bits) 1024 samples on 4 cycles without windowing (CEI 1000 -4-7). From real and imaginary parts, each bin calculated on each phase V_{harm} , U_{harm} and A_{harm} in proportion to the fundamental value and the angles V_{ph} , U_{ph} , and A_{ph} between each bin and the fundamental.

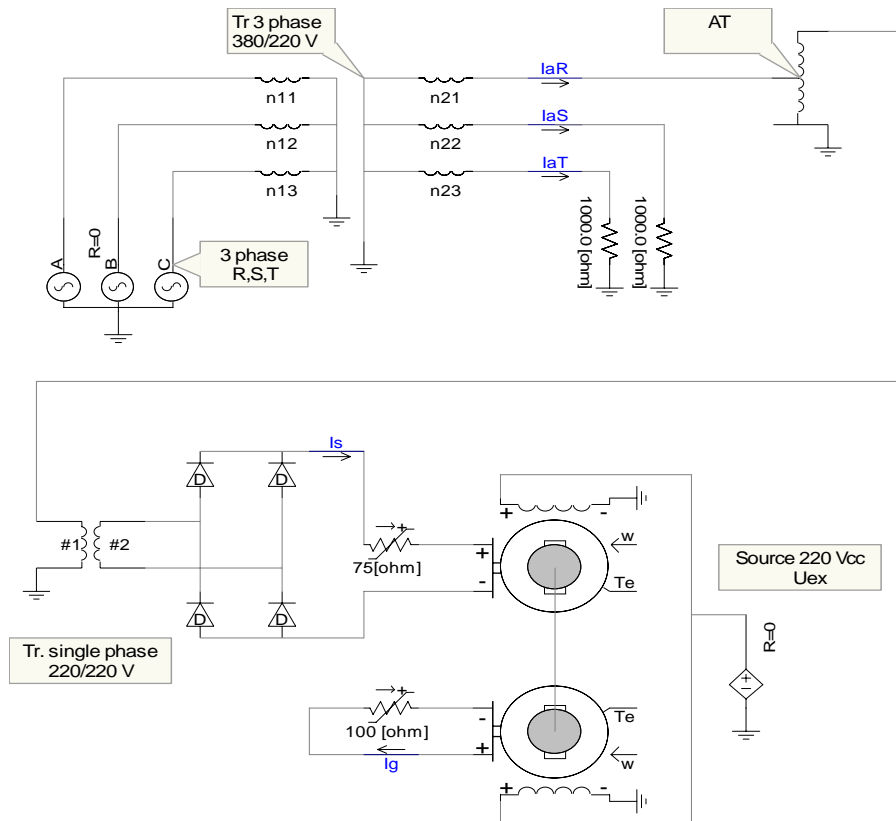


Figure 1 The d.c. motor's control circuit

This calculation is done with the following principle: Module in % : $\text{mod}_k = \frac{c_k}{c_1} \times 100$

angle in degree: $\varphi_k = \arctan\left(\frac{a_k}{b_1}\right)$

$$\text{With } \begin{cases} c_k = |b_k + ja_k| = \sqrt{a_k^2 + b_k^2} \\ b_k = \frac{1}{512} \sum_{s=0}^{1024} F_s \times \sin\left(\frac{k\pi}{512} s + \varphi_k\right) \\ a_k = \frac{1}{512} \sum_{s=0}^{1024} F_s \times \cos\left(\frac{k\pi}{512} s + \varphi_k\right) \\ c_0 = \frac{1}{1024} \sum_{s=0}^{1024} F_s \end{cases} \quad (4)$$

c_k is the amplitude of frequency $f_k = \frac{k}{4} f_1$, F_s is sampled signal, c_0 is the DC component,

k is the ordinal number (spectral bin).

Calculation of the distortion factor (DF):

There are calculated two global values which give the relative quantity of harmonics: total harmonic distortion (THD) against the fundamental and the distortion factor (DF) and DF against the effective value (RMS).

$$\begin{aligned} V_{thd}[i] &= \frac{\sqrt{\sum_{n=2}^{50} V_{harm}[i,n]^2}}{V_{harm}[i,1]} ; U_{thd}[i] = \frac{\sqrt{\sum_{n=2}^{50} U_{harm}[i,n]^2}}{U_{harm}[i,1]} \\ A_{thd}[i] &= \frac{\sqrt{\sum_{n=2}^{50} A_{harm}[i,n]^2}}{A_{harm}[i,1]} \end{aligned} \quad (5)$$

$$Vdf[i] = \frac{\sqrt{\frac{1}{2} \sum_{n=2}^{50} V_{harm}[i,n]^2}}{V_{rms}[i]} ; Udf[i] = \frac{\sqrt{\frac{1}{2} \sum_{n=2}^{50} U_{harm}[i,n]^2}}{U_{rms}[i]}$$

$$Adf[i] = \frac{\sqrt{\frac{1}{2} \sum_{n=2}^{50} A_{harm}[i,n]^2}}{A_{rms}[i]} \tag{6}$$

Multiplying the voltage’s harmonics factor with the current’s harmonics factor, results the power’s harmonics factor. Differentiating the voltage’s harmonic phase angle with the current’s harmonic phase angle, results the power’s phase angle.

- different ratios

$$PF[i] = \frac{W[i]}{VA[i]} \text{ power factor, phase } i+1$$

$$\cos(\phi[i]) = \frac{\sum_{n=0}^{N_{sec}-1} VF[i,n] \cdot AF[i,n]}{\sqrt{\sum_{n=0}^{N_{sec}-1} VF[i,n]^2} \cdot \sqrt{\sum_{n=0}^{N_{sec}-1} AF[i,n]^2}} \tag{7}$$

Cosinus angle between the voltage’s fundamental and the phase current $i+1$

$$PF3 = \frac{PF[0] + PF[1] + PF[2]}{3} \tag{8}$$

Total power factor various types of energy

$$Wh[o,i] = \sum_{T_{int}} \frac{W[i]}{3600} \text{ Active energy consumed } i+1 \text{ phase;}$$

$$VARhL[0,i] = \sum_{T_{int}} \frac{VAR[i]}{3600} \text{ for } VAR[i] \geq 0 \text{ Reactive inductive energy consumed } i+1 \text{ phase;}$$

$$VARhC[0,i] = \sum_{T_{int}} \frac{VAR[i]}{3600} \text{ for } VAR[i] \leq 0 \text{ Reactive capacitive energy consumed } i+1 \text{ phase.}$$

Motor loading	Is [A]	Ig [A]	IaR[A]	THD[%]
min	2.4	1.2	2.1	14.6
med	3.1	1.8	3	15.1
max	4.1	2.5	3.8	15.5

There are obtained the amplitude values of the harmonics of rank 3,5,7,9, 11..... and the THD factor calculated for there values of the harmonics. In the first stage, are determined the current harmonics and the THD for the situation when the insulation transformer is missing (Tr single-phase). The results will be written in a table (table 1) and, for exemplification, there are presented two graphics with the harmonics’ values and the THD’s value for a medium loading (fig. 2), respectively for a maximum loading (fig. 3).

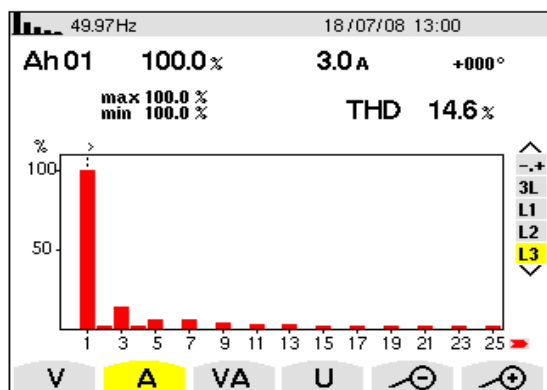


Fig. 2 Harmonics spectrum for a loading of 50%

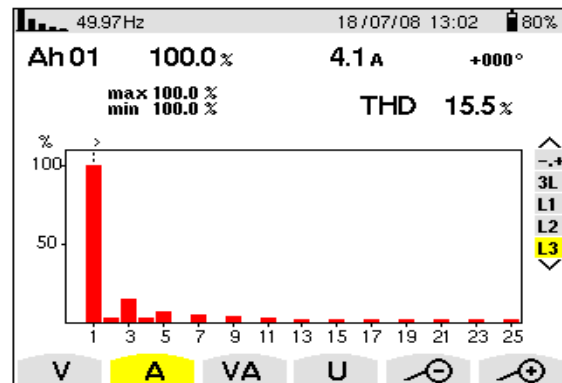


Fig. 3 Harmonics spectrum for a loading of 100%

Table 2

Voltage [V]	Motor loading	Is [A]	Ig [A]	THD [%]
50	min	0.8	0.5	13.2
	med	0.9	0.65	14.8
	max	1.1	1	16.3
100	min	5.9	1.5	6
	med	6.7	1.8	5.9
	max	7.9	2.75	3.5
150	min	8.4	1.55	4.8
	med	9	2	4.7
	max	10.4	2.7	4.6

In the circuit is introduced the insulation transformer (Tr single-phase), and are rerun the measurements for the supply voltages of the d.c. motor of 50 V, 100 V, 150 V at loading of the generator with minimum, medium and maximum load. The values are written in the table (table 2) and for the supply voltage of 100 V will be presented two distinct situations, at a medium loading of 50 % from the value of the generator's loading potentiometer (fig. 4) respectively maximum, 10% from 75 Ω (fig.5).

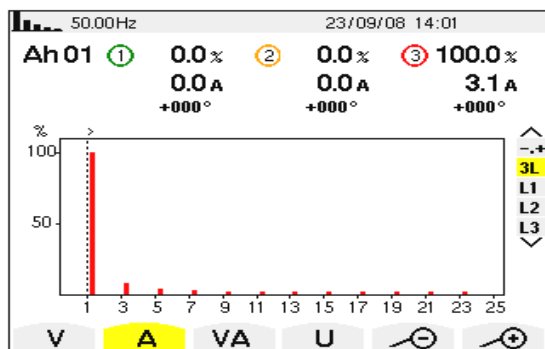


Fig. 4 Harmonics spectrum for a loading of 50% with insulation transformer

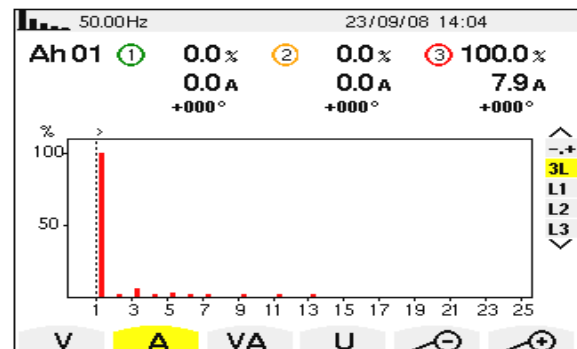


Fig. 5 Harmonics spectrum for a loading of 100% with insulation transformer

2. CONCLUSIONS

In case of the circuit without insulation transformer from fig. 2 and fig. 3 can be noticed a relatively small reduction of the distortion factor regarding the load currents at medium and maximum loading.

In case of the circuit with insulation transformer from fig. 4 and fig. 5, beside the pronounced THD's reduction, is noticed also a more pronounced reduction between the situation of medium loading and maximum loading of the d.c motor.

It can be easily noticed the reduction of the distortion factor in case of introducing the insulation transformer. Although the harmonics' values are relatively reduced related to the fundamental, is obtained a relatively high THD factor, especially at small load currents. By increasing the load current, the harmonics' effective value is not really reducing. The finding of the THD's reduction is due to the relative reduction of the ratio between the harmonics' values and fundamental. Reduction of THD is achieved by using of passive filters at small rank harmonics, completed by a power active filter.

REFERENCES

- [1] Manuela Panoiu, Caius Panoiu, Mihaela Osaci, Ionel Muscalagiu, *Simulation Result about Harmonics Filtering using Measurement of Some Electrical Items in Electrical Installation on uhp eaf*, WSEAS TRANSACTIONS on CIRCUITS and SYSTEMS, Volume 7, 2008, ISSN: 1109-2734, January 2008.
- [2] Angela Iagar, Gabriel Nicolae Popa, Ioan Șora, *Analysis of electromagnetic pollution produced by line frequency coreless induction furnaces*, WSEAS TRANSACTIONS on SYSTEMS, January 2009, volume 8, Issue 1 ISSN 1109-2777;
- [3] Dev Paul, *D.C. Traction Power System Grounding*, IEEE TRANSACTIONS on INDUSTRY APPLICATIONS, vol.38, no.3, May-June 2002;
- [4] Heinz W. van der Broeck, Hans-Christoph Skudelny, *Analytical Analysis of the Harmonic effects of a PWM A.C. DRIVE*, IEEE TRANSACTIONS on POWER ELECTRONICS, vol 3, no.2, April 1988;
- [5] Alan K. Wallace, Rene Spee, *The Effects of Motor Parameters on the Performance of Brushless D.C. Drives*, IEEE TRANSACTIONS on POWER ELECTRONICS, vol.5, no.1, January 1990.

ANALYSIS OF A DOUBLE-WAVE ACCURACY RECTIFIER'S OPERATION WITH OPERATIONAL AMPLIFIERS

Corina Daniela CUNȚAN, Ioan BACIU, Caius PĂNOIU, Corina DINIȘ

Polytechnic University of Timișoara, University Politehnica Timișoara, Faculty of Engineering of Hunedoara, Electrical Engineering and Industrial Informatics Department

Abstract:

In this work is studied the operation of a double-wave accuracy rectifier achieved with operational amplifiers LM741 at frequencies that exceed their cut-off frequency, using the Multisim simulation program. Is aimed the quality and accuracy of the obtained signal, having in view the damping introduced by the operational amplifiers' operation.

Keywords:

double-wave accuracy rectifier, operational amplifier.

1. WORK'S PRESENTATION

The double-wave rectifier can be obtained by serial connecting of a single-wave rectifier and a summation instrument. Diagram of a single-wave accuracy rectifier which rectifies the positive semi-periods of the input voltage is given in fig. 1. Because it's about small signals, the voltage between the two inputs of the operational amplifier is not neglected anymore, but

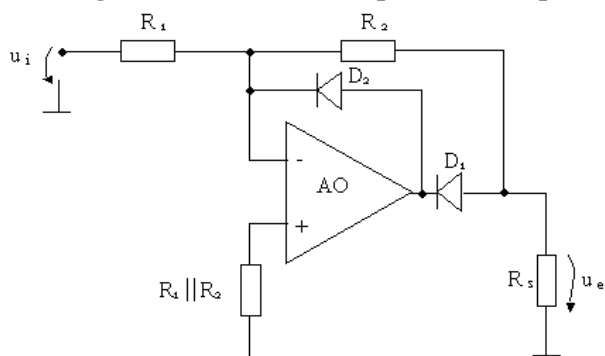


Figure 1. Operation diagram on positive alternance

instead are neglected the OA's input currents and the reverse current through the diode is blocking state.

Output voltage for the positive semi-period of the input voltage is:

$$u_e = -\frac{u_i \frac{R_2}{R_1} + \frac{u_{d1}}{R_1} A_u}{1 + \frac{1}{\frac{R_1}{R_1 + R_2} A_u}} \cong -u_i \frac{R_2}{R_1} \quad (1)$$

At the circuit's output is obtained an identical voltage as time-variation form, and reversed as phase. For the negative semi-period of the input voltage u_i diode D_1 is blocked and diode D_2 conducts all the current coming from the input (fig. 2). In this case, for the output voltage is obtained the relation:

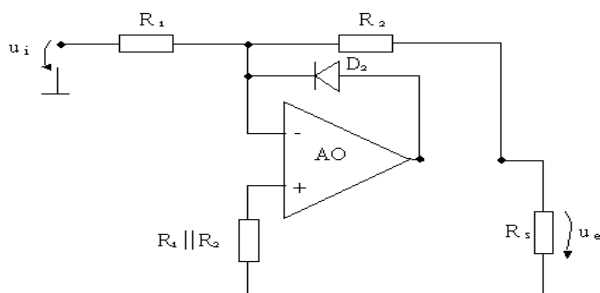


Figure2. Operation diagram on negative alternance

$$u_e = -u_i \frac{R_s}{R_2 + R_s} \cong \frac{u_{d2}}{A_u} \cdot \frac{R_s}{R_2 + R_s} \cong 0 \quad (2)$$

Is found that, during the negative semi-period of the input voltage, at output is obtained a voltage almost null.

The diagram of the double-wave rectifier is using such a rectifier, out of which outpt is connected a summation instrument with AO (fig. 3).

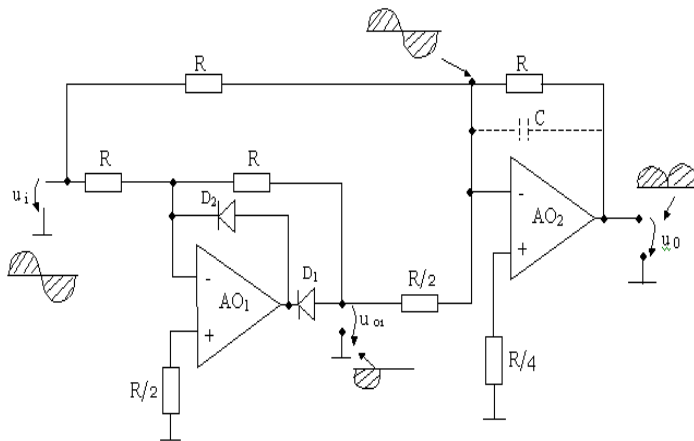


Figure 3. Diagram of the double-wave accuracy rectifier

For the first semi-period (positive) of the input signal, the voltage u_{e1} is negative and, in this case, at the summation device's inputs are brought voltages with equal amplitudes, one positive and one negative, amplified differently. The positive voltage has the amplification 1 and the negative one has the amplification 2, at the summation instrument's output being obtained the positive alternance of the signal u_i . For the negative alternance of the signal u_i is obtained $u_{e1} = 0$ and at the summation instrument's input is brought only the negative alternance of the signal u_i , for u_{e2} being obtained the alternance reversing and amplification 1.

As result, at output is obtained the input signal's rectification, this without being amplified. If it's desired its amplification, the resistances from the diagram will be modified in the ratio aimed to be obtained.

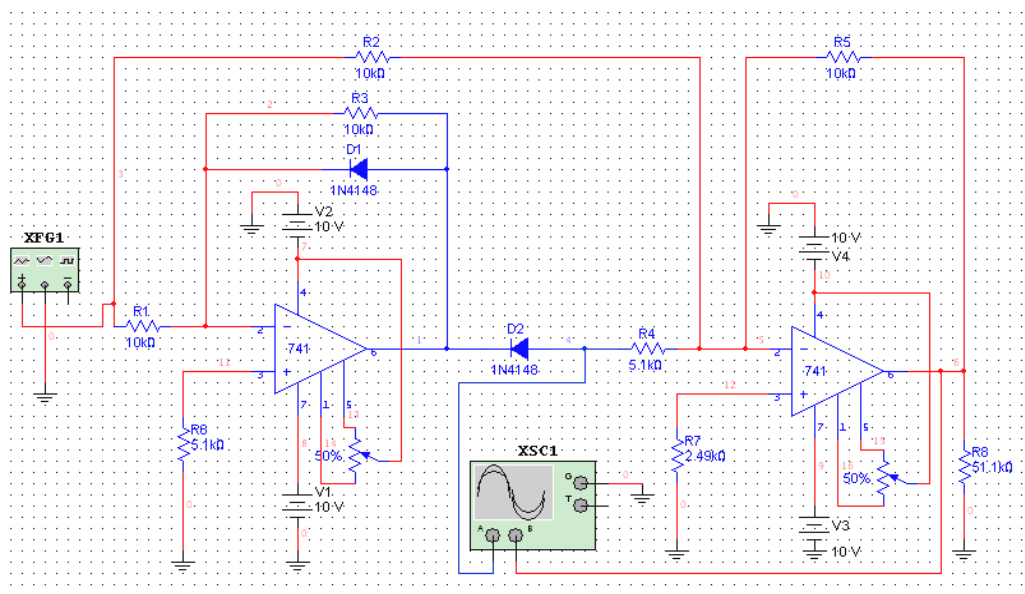


Figure 4. Electronic diagram of the accuracy rectifier

In order to check the rectifier's operation, it was used a generator of sinusoidal signal with amplitude of 275mV and adjustable frequency (fig. 4). The signal was recorded by means of a digital oscilloscope, which allowed the data acquisition in the memory of a PC system.

Are presented three distinct situations, corresponding to all frequencies of 1 KHz (fig. 5.a), 10KHz (fig. 6.a) and respectively 50KHz (fig. 7.a), with the wave forms related to each frequency in part. For each frequency in part are presented the parameters corresponding to the wave forms presented above (fig. 5b, fig. 6b, fig. 7b).

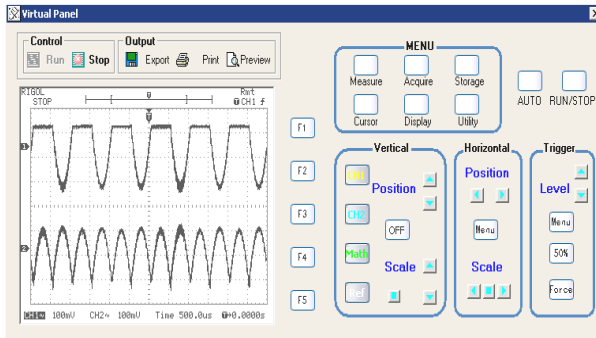


Figure 5.

- a) wave forms corresponding to frequencies of 1 kHz;
- b) parameters corresponding to the wave forms for 1kHz

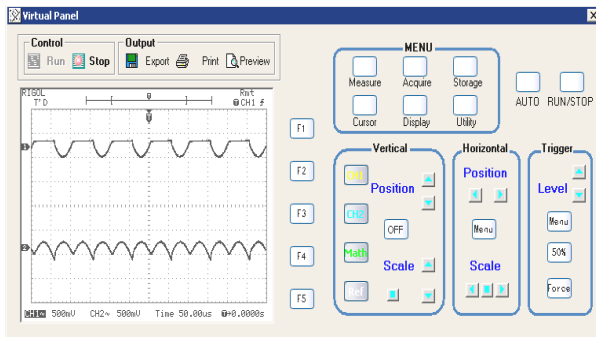


Figure 6.

- a) wave forms corresponding to frequencies of 10 kHz;
- b) parameters corresponding to the wave forms for 10kHz

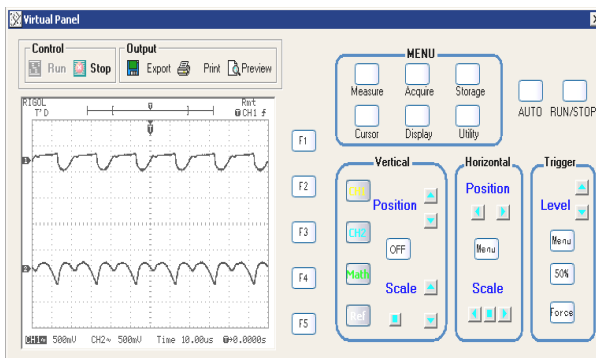


Figure 7.

- a) wave forms corresponding to frequencies of 50 kHz;
- b) parameters corresponding to the wave forms for 50kHz



2. CONCLUSIONS

Further the experimental verification of the double-wave rectifier, is found a correct operation within a relatively large frequency band, reaching to approximately 50KHz. One can notice that at the end of the negative semi-period is not reaching to zero, but to a value a

little superior, which cannot be compensated, because also the other value related to the positive alternance would be reduced identically. Once by increasing the frequency, is found a distortion of the output signal, especially due to the parasite capacities that occur in the circuit, which makes it to integrate the signal brought at input, reaching up to ramp-signal at very high frequencies.

REFERENCES

- [1] Adrian Sorin Mirea, Florin Domnel Grafu, *Analogue Integrated Circuits. Applications*, Blue Publishing House, Cluj-Napoca, 2006.
- [2] Thomas L. Floyd, *Dispozitive Electronice*, Editura Teora 2003.
- [3] Pașca S., Tomescu N., Sztojanov I., *Electronică analogică*, Editura Albastră 2004.
- [4] Oltean G., *Dispozitive și circuite Electronice*, Editura Risoprint 2003.
- [5] Ciugudean M., Tănase M.E., *Dispozitive și circuite Electronice*, IPTVT 1986.



VIBRATIONS INFLUENCE OVER THE METALLIC ALLOYS CRYSTALLIZATION

¹PIRVULESCU Crenguta Manuela, ²BRATU Constantin, ²MARGINEAN Ioan,
²VERDES Bogdan Alexandru, ²COCOLAS S. Adrian

¹Technical College “Media”, Bucuresti
²University Politehnica Bucuresti, ROMANIA

ABSTRACT:

Metal materials casting is influenced favorably under the mechanical vibrations influence applied over the liquid alloy bath. Vibrations producing methods may be different, by using mechanical vibrations, or pneumatic, hydraulic or electrical. The mechanical vibrations in the particular case we've studied are obtained by means of an element that is in translation for a wide range of forces and frequencies up to 75 Hz.

The aluminum-silicone and aluminum-copper alloys are among the most used nonferrous cast alloys. The present study (paper) presents the main phenomena occurring under the mechanical vibrations influence over the alloys especially the dendrites break and the superficial strain influence over the germinate particles.

1. INTRODUCTION

Crystallization, as any other process (chemical or physico- chemical) is studied from the static and kinematic point of view. The statics structures the balance relationships between the crystals, the solution they are formed from. The statics deals with the solubility of the phase that is pure, in the presence of other phases, with the kinds of crystals balance and their composition.

The kinematics is specific to the speed the process takes place at, it characterizes the speed taken by the process to deploy, respectively the mechanism of germination and solidification of the metallic alloys. In connection with this fact, you have to examine the main factors that influence the germination, the break of the dendritic branches, the influence of the superficial tensions of the germinated particles, all under the vibrations influence over the metallic alloys.

2. DOCUMENTARY STUDY

The process of crystallization from metallic melts has two stages: formation of crystallization germs and their growth.

The kinematics of the crystallization process may be characterized mainly by two ratings: speed of germs formation and speed of crystals growth. To have a clearer image over the process mechanism, each and every of these ratings have to be examined separately, as well as the influence of various factors over the speed needed by these process to deploy. The vibrations influence is a research factor. Further on we shall refer to the vibrations influence (mechanical vibrations) over the germination and crystallization of cast alloys.

The strong connection between the germs formation and their development, the impossibility to separate exactly these stages, makes difficult the study of the crystallization process. This explains the fact that neither of the theories proposed over the formation of crystallization germs and their growth cannot be considered complete for stating clear all the particularities of this heterogeneous process so complex.

A high oversaturation of the melt favors, evidently, also the occurrence of the forms of dendritic growth. Indeed, the inflow of the substance that crystallizes from the solution is achieved easiest towards the crystal peaks, that is why the growth speed of the crystal peaks supersedes by far the growth speed of the edges and sides, which finally leads to the formation of the dendritic crystal having arborescent shape. In the dendrites growth, the substance that crystallizes (gets solid) can fill gradually the clearance between the branches, that is why the final shapes of the dendritic growth can be of a great variety, from compact crystals to those resembling to a hedgehog, function of the nature of the

melt and of the growth conditions. Out of the conditions that favor the germination, besides the nature of the melt, a very significant influence is generated by the influence of the vibration with frequency (pulses) amplitude and acceleration as its main parameters. Lately, the acceleration is a working parameter since it can be measured and controlled easier. It is worth being mentioned that the connection between the frequency (f), pulsation (ω), amplitude (A), speed (v) are in well defined relationships, this is the reason why one can work unitarily with each of them. By vibrating the melt, a uniform affluence of the solution that crystallizes at various faces is ensured, by this annihilating the influence of the concentration currents, which favors the formation of crystals with a regular shape.

The action of accelerating the vibration over the germs formation becomes more and more efficient by increasing the crystals speed that gets lower gradually.

It is established that the mechanic erosion of the crystals, as a sequence of rubbing between each other, as well as to the molds (matrix) sides, increases with the mechanic vibration intensification. The crystals obtained thus have a round shape with rounded corners and edges, and finally increases sudden the quantity of the fine fractions.

3. ANALYSIS, INTERPRETATION - EXPERIMENTAL PART

The expression of the compact state by the density of the metallic material melt has a significant importance because it influences the structure and features of the material obtained. The discontinuities that may occur when the alloy gets solid are due to the phenomenon of contraction, characteristic to the majority of the alloys, together with a strong decrease of the solubility of the gases within the melt at the crystallization temperature.

Obtaining a compact metallic material is guaranteed if the penetration speed v of an alloy in the capillaries of the biphasic zone is equal to the contraction speed v_{contr} :

$$V_{\text{contr}} = \alpha \cdot m \cdot R \text{ [m/s]} \quad (1)$$

where: α - contraction coefficient of the alloy when it gets solid;

m - relationship between the volume at the liquid state within the biphasic zone and the volume of this zone;

Under common circumstances, the speed v is expressed thus:

$$v = \frac{r^2}{8\eta} \cdot \frac{P_e + P_m - P_g + \frac{2\sigma}{r} \cdot \cos \theta}{l} \text{ [m/s]} \quad (2)$$

r - radius of the capillary [m/s]; P_e - external pressure [Pa]; P_m - metal static pressure [Pa]; P_g - pressure of the gas in the capillary [Pa]; σ - alloy superficial tension [N/m]; θ - humectation (moistening) angle [rad]; η - alloy dynamic viscosity [Pa·s]; l - length of alloy penetration into the capillaries [m].

From the equality between the relations (1) and (2) it results:

$$\frac{r^2}{8\eta} \cdot \frac{P_e + P_m - P_g + \frac{2\sigma}{r} \cdot \cos \theta}{l} = \alpha \cdot m \cdot R \quad (3)$$

Where from:

$$l = \frac{r^2 \cdot \left(P_e + P_m - P_g + \frac{2\sigma}{r} \cdot \cos \theta \right)}{8\eta \cdot \alpha \cdot m \cdot R} \quad (4)$$

The mechanical oscillations decrease the superficial tension σ at the liquid solid interface, the humectation angle θ and renders to the alloy an initial speed $v_i = A \cdot \omega$.

Under the vibrations physical action, the biphasic zone gets fragmented, thus lowering the capillaries length that must be run by the liquid alloy in order to fill the clearances provoked by the contraction and increasing thus the flow speed of the liquid alloy in these clearances, improving the conditions of supplying the micro cavities. Thus the overall volume of the micro blisters (shrinkage cavities) and the macro blisters concentrate at the top (large opening angle and low penetration depth fig.1), reducing the volume of the liquid alloy for the crop ends, phenomena that can be explained if it is considered that the alloy solidification under the influence of the mechanical oscillations takes place according to the following mechanism:

- ✚ the inertial forces generated by the vibrations render into pieces the solid phase in course of getting constituted and disperses it into the liquid alloy placed in front of the solidification front;

- the liquid alloy penetrates between the broken and dislocated fragments; it determines a temperature rise in the crust of solidified alloy, thus improving the conditions of thermal transfer at the interface alloy mould;
- the descendent circulation of the solid phase fragments and their storage at the bottom of the mould leads to the concentration of the macro blisters and porosities diminishing.

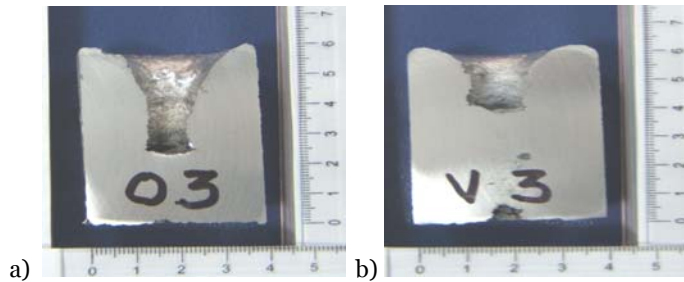


Fig. 1 Aspect of blisters without vibration and with vibration

blisters volume $O_3= 9,5\text{cm}^3$;
 $V_3=6,5\text{cm}^3$
 blisters height $h_{O_3}= 34\text{mm}$;
 $V_3=24\text{mm}$
 blisters diameter $d_{O_3}=22\text{mm}$;
 $V_3=24\text{mm}$
 relation $h/d_{O_3}=1,5$ $V_3=1$
 relation blisters volume /sample vol.;
 $O_3= 3,15$; $V_3=2,16$
 sample volume $301,44\text{cm}^3$;

Note: for the vibrated sample (V3) the blister height decreased versus the non vibrated sample (O3).

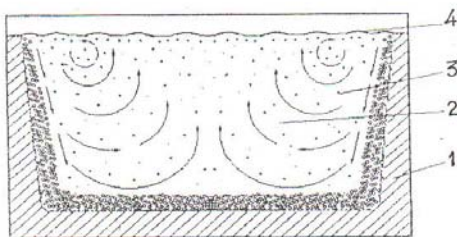


Fig. 2. Diagram of the movement of the fluxes in the liquid and solid phase in the solidification process

- 1 – crystallizer side walls, 2 - liquid phase, 3 - solid particles in the flux, 4 - crust

The general movement diagram of the liquid and solid phase flow in the conditions of applying the action of the mechanical vibration in the solidification procesus is shown in figure 2.

In the course of the observations it was established that oriented fluxes (circulation currents) are formed in the area next to the melted mass surface.

By means of these fluxes the most minute particles of the crystals that are broken are taken away within the volume of the melted mass, and the larger ones are precipitated at the bottom. The dendrites destruction mechanism, the diagram of the dendrite cell that develops in the solid- liquid area and temperatures distribution in it is shown in figure 2.

The growth of the thinnest branches of the second degree dendrite takes place in the surrounding liquid phase, figure 3.a, and between the peaks of these derivations the dendritic structure is sufficiently open for the liquid phase outlet. As long as the solidification advances, the dendritic cell derivations get thicker, and the liquid phase within it is in the state of small movement. The temperature along the length of each dendrite is modified from the liquid temperature T_{lic} (according to the axe of the clearance between the dendrites) up to the temperature of the solid mass T_{sol} at its basis. By applying vibrational force on the vibrant table on which the mould is mounted a phenomenon is produced: the liquid phase mixes and the dendrite branches are destroyed figure 3.b.

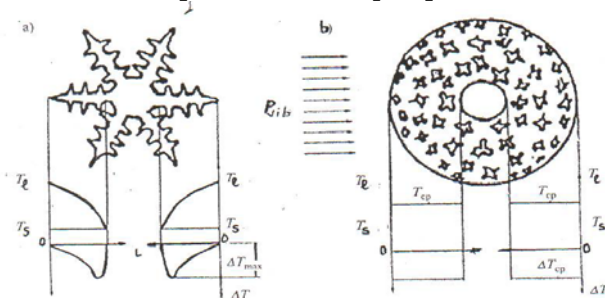


Fig.3. Conditions of growth of the dendrites axes in state of rest and in the conditions of pressure exertion P_{vib} over the melted mass.

- a) dendrite growth in the melted mass;
- b) breaking of the dendrite branches when applying the mechanical vibrations

The temperature within the solidification interval is established at the average values over the entire mould cross-section, and in the clearance available between the dendrites crystallization germs occur, that, afterwards, under the action of the mechanical vibrations, move within the volume of the unsolidified part of the alloy. Each one of these disintegrations (breakings) of dendrites is serving the crystallization centre in the melted mass volume. Thus, the under cooling around each breaking is considerably higher than within the surrounding liquid. The amount of this under cooling is equal to:

$$\Delta T_B = (\sigma_{l-s} \cdot T_{lic}) / r \cdot \rho \cdot q_{cris} \quad (5)$$

where: σ_{l-s} - superficial extend at the limit between phases $[\text{N}/\text{m}^2]$;

T_l - melted mass liquid temperature $[\text{°K}]$;

r - broken dendrite radius $[\text{m}]$;

ρ - melted mass density $[\text{kg}/\text{m}^3]$;

q_{cris} - crystallization temperature of the melted mass $[\text{°K}]$.

Out of the equation (5) it can be seen that the lower the radius of the broken dendrite is the higher the under cooling is around it. That is why, by increasing the vibration frequency, the destruction of the dendrite branches, the under cooled liquid volume and the melted mass crystallization speed increase incessantly.

The characteristic peculiarity of ingot forming under the mechanical vibrations action is the small constant thickness of the crust on the vertical, lateral sides (surfaces) of the ingot. This fact ensures the constant, intense exhaustion of the crystallization heat and the incessant growth of the horizontal area thickness of the crystals that fall down. After the solidification is finished, the even crystalline dispersed structure is obtained over the entire ingot cross-section that is characteristic for the crystallization of the alloys volume. In the research process the variant of the moulded part complete solidification duration has been studied function of the alloy overheating under usual circumstances and by applying the mechanical oscillations.

4. CONCLUSIONS

The solidified part of the dendrite represents a solid body and in it longitudinal waves occur (of strain/elongation and compression), that create variable pressures and that determine the elastic deformation, respectively the occurrence of fragmenting strains. The critical force at which the crystal gets fragmented is given by the relation:

$$F_{cr} = p_{max} \cdot \pi \cdot r^2, [N];$$

The break of the dendritic branches is possible, having in view their low withstand at high temperatures. Due to the vibrations, the speed the alloy moves with from the biphasic zone in front of the solidification front is much higher, which determines an intense fragmenting of the dendritic branches. The solid particles movement speed depends upon:

- ✚ solidified crust thickness;
- ✚ alloy kinematic viscosity;
- ✚ melting temperature;
- ✚ dimensions of the part;
- ✚ conditions of the heat exchange;
- ✚ oscillations energy, respectively the acceleration, their amplitude and frequency.

The physical-mechanical treatment, applied to the liquid state alloy intensifies the vibrations layers at the edges, which produce side currents, hydro-dynamic phenomena at the limit between the solidified layer and the mould side walls, the speed increases and the solidification time decreases. Among the most important technological effects of applying the mechanical vibrations within the solidification process we can list: homogenization and finishing of the structure, molded material getting compact, alloy degassing, segregations contraction, separation of the nonmetallic inclusions and growth of the capacity of achieving a high quality alloy as well as improving certain mecano-physical characteristics.

REFERENCES

- [1] Camui C. – Cercetării privind influența tratamentelor fizico-mecanice asupra solidificării pieselor turnate din aliaje neferoase, Teza de doctorat 1997
- [2] Efimov V.A. – Turnarea și cristalizarea oțelurilor, Ed.Teh. București 1980
- [3] Eldarhanov ș.a. – Processo cristallizatii v pole uprugih vole, Moscova 1996
- [4] Sofroni L., Bratu C., Brabie V.- Bazele teoretice ale turnării, E.D.P. București 1980
- [5] Soporan V., ș.a – Solidificarea aliajelor, Ed.Transilvania Press, Cluj-Napoca 1995
- [6] Stefanescu Fl. – Cercetări privind dirijarea proceselor de solidificare a aliajelor turnate în piese. Teza de doctorat.



FEW THEORETIC ELEMENTARY NOTIONS REQUIRED FOR CHARACTERIZATION OF METAL MELT AND APPRECIATION OF BEHAVIOR AT INTERFACE DURING CASTING

¹MARGINEAN Ioan, ¹VERDES Bogdan Alexandru,
¹COCOLAS S. Adrian, ²PIRVULESCU Crenguta Manuela, ³SUSU Catalin

¹ University Politehnica Bucuresti,
² Technical College "Media", Bucuresti
³ University Tehnica Cluj – Napoca, ROMANIA

ABSTRACT:

Surface tension is one of the properties of metal melt, which depends on two other properties, cohesion and adhesion. Atomic-scale phenomena can be regarded as if atoms or molecules within a substance are spaced sufficiently small, then each of them is surrounded by a field of forces, which form a system equivalent to zero. Forces are forces of cohesion, named "Van der Waals" forces.

1. INTRODUCTION

To separate atoms or molecules of the same type, some others must consume a mechanical work, it carry the name mechanical work of cohesion. The force that opposes atoms separation or molecules of that substance reported at length shall be known as surface tension (σ). Adhesion is the force of attraction between atoms or molecules that are in different phases. It is characterized by the work that needs to be done to separate the two phases in contact with the surface contact unit. The properties of surface flows have an important role, which include both surface tension and inter-phase and moistening phenomena.

2. DOCUMENTARY STUDY

Understanding the nature of surface tension in metals and alloys requires a profound study of this phenomenon. When two phases, for example liquid and gas are in direct contact, between them it forms a very thin separation layer, called the interface or inter-phase or phase separation. The interface properties differ from those of phases in contact. In this area the number of atoms and distribution functions of their energy is changing continuously, from the value which they have in melt, to the one which they have outside the melt. While atoms are leaving the surface, entering in liquid or evaporating outside the liquid, other atoms are replace. Stationary time of atoms at the liquid surface is very short, but it's longer than the remaining sibotaxis groups of atoms inside the liquid. At the melt surface occur a flux of collectivized electrons, which tend to get of the environment, but positive ions pull them back into the melt.

Metal melt surface are covered by a thin layer of liquid with negative loads, under which by a certain depth of atomic radius order, it's located a layer with compensating positive electrical loads. The two layers form a double layer with a thickness of interaction radius of an atom order. This double layer acts as a electrical condenser as a barrier, preventing, at least partially, the outgoing of electrons molten metal.

An atom in the melt, under the double layer, at a distance greater than the range of inter-atomic forces is surrounded by a field of forces, which together with its own forces form a system equivalent to zero. It has an effect of mutual annihilation of the forces of interaction between atoms, which allows free movement, as there is cohesion between them.

So the forces of interaction between atoms which belong to melt and the gas from the interface, will be much smaller than the forces of interaction between atoms on the surface of the liquid and the liquid inside.

If we consider a point particle (N) at a depth (X) less than the radius of the sphere of action of inter-atomic forces (r), figure 1, all atoms which are located in the EGF ABFE sector, will draw down N atom, while atoms in the ABCD and CHD sector, N atom will be attract upwards.

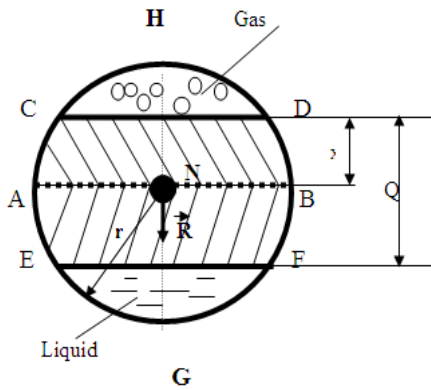


Figure 1. Schematic representation of double layer Q, between liquid and gas phases

change at constant temperature and pressure, reported to the surface between both phases shall be known as inter-facial surface tension or tension Gibbs.

Consequence that the attraction of atoms from metal melt surface, produces forces directed towards the inside, is that the surface free energy is greater than the one from inside. The absence of this excess energy, surface separation would not be stable, would degrade at the lowest energy state of fluctuation, the two phases in contact would disperse to another one.

To form a surface should be consumed a mechanical work needed to bring the atoms of the liquid on the surface, the same thing for the surface growth. Consuming a mechanical work it's decreasing the surface free energy.

3. ANALYSIS, INTERPRETATION - EXPERIMENTAL PART

If we note (σ) generalized force corresponding to the surface (S), then the mechanical work (dW) required for modification iso-thermic surface area will be:

$$dW = -\sigma \cdot dS \quad (1)$$

On the other hand this mechanical work is equal to the decrease of the surface free energy (dE, Gibbs energy change), so:

$$dE = \sigma \cdot dS \quad (2)$$

$$\text{or} \quad \sigma = \left(\frac{dE}{dS} \right)_{T, p, n_i} \quad [J / m^2] \quad (3)$$

If we express mechanical work used to increase the surface (dS), as the acting force (dF) or displacement (d ℓ), then:

$$dW = dF \cdot d\ell = -dE = -\sigma \cdot dS \quad (4)$$

This is another way of expression the surface tension, being force tangent to the surface, reported at length.

For a system being in energy balance, the free energy should be minimal. For a given volume which can have different values of the area, the lowest value being that of the spherical surface, because surface tension is constant, then the free energy will take different values, it will be minimal if the separation of the volume given will be minimal. This property explains why drops of liquid in a gas tend to form spherical, the surface having the smallest separation.

Pure liquids, composed of identical atoms or molecules, have generally a constant surface tension, which is established very quickly after the surface forming. For compound liquid, to reach equilibrium, it is necessary to pass a greater time interval.

Surface tension of a phase is defined as surface tension on the surface in the vacuum phase, while the surface tension of the interface phase in contact with those other phase voltage is inter-facial.

The inter-facial surface tension (σ_i), the limit of separation between a liquid and its vapour, in equilibrium is equal to the difference between the absolute surface tension liquid (σ_l) and its vapour (σ_v):

$$\sigma_i = \sigma_l - \sigma_v \quad (5)$$

Knowing the values of (σ_i) and (σ_l) we could determine the absolute surface tension liquid (σ_v).

The same can be said in general, when we have two phases in equilibrium, the contact A and B (solid - liquid, solid - gas, liquid - gas, liquid - liquid, solid - solid, gas - gas);

$$\sigma_{iAB} = \sigma_A - \sigma_B \quad (6)$$

At critical vaporization temperature of the liquid $\sigma_l = 0$, because the separation surface has disappeared and so $\sigma_l = \sigma_v$.

In the case of two liquids in contact, the interfacial liquid - liquid tension will not be immediately determined, because the equilibrium between the two liquids will be set only after the two saturated solution will be formed. In the case liquid - gas system, the interfacial surface tension will be stabilized only when the gas dissolution in liquid cease. The same phenomenon happens in the limit of separation between the crystals that is formed in the fusion.

The interfacial surface tension decreases with temperature, becoming zero at the critical temperature, when the separation surface disappears, like the relation of Eötvös shows:

$$\sigma_M = K_E (T_{cr}' - T) \quad (7)$$

The equation is thus derived from the graphical representation of the variation of pure metals surface tension with temperature, figure 2, starting from the melting temperature (T_{top}) which corresponds the surface tension (σ_{Top}), we can write the equation of the right from the figure.

$$\sigma = \sigma_{top} - \alpha(T - T_{top}) \quad (8)$$

$$\text{for } T = T_{cr}', \sigma = 0, \text{ so } \sigma_{top} - \alpha(T - T_{top}) = 0 \quad (9)$$

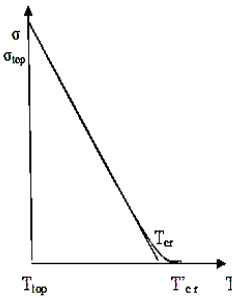


Figure 2. Variation of σ with temperature T for pure metals

and substituting the σ_{top} the relation (9) in relation (10) we obtain:

$$\sigma = \alpha(T_{cr}' - T) \quad (10)$$

where α is the angle of right: $\alpha = -\frac{d\sigma}{dT}$; T - absolute temperature of the

liquid; T_{cr}' - the critical absolute fluid temperature. Because T_{cr}' is constant for a pure metal, (σ) decreases with increasing temperature (T).

If we multiply the equation (10) with so-called "molar area" which is conventionally taken equal to $V^{2/3}$ (V being the molar volume of liquid) we obtain the free surface molar energy:

$$\sigma_M = \sigma \cdot V^{2/3} = \alpha(T_{cr}' - T) \cdot V^{2/3} \sigma_M \quad (11)$$

and noting $k_E = \alpha \cdot V^{2/3}$ is obtained the relation (7). The constant (k_E) is the change of entropy for increasing the molar area ($V^{2/3}$).

Beginning from temperatures from 4 ... 7 degrees below the absolute critical temperature (T_{cr}) the surface tension varies no longer linearly with temperature. Besides temperature, the surface tension is influenced by other factors, including: the degree of dispersion, the nature of the phases, pressure, density decreasing and curvature radius of the surface.

The surface tension varies with the degree of dispersion and the specific surface of dispersed phase. Under specific surface we understand the relation between the surface phase and its volume. When the dispersion exceeds a certain limit, the surface tension starts to decrease, and when you reach the molecular dispersion of surface, the tension tends to zero. We find a large specific surface by porous bodies which have a great importance in the phenomena of filtration of liquids. The surface tension depends on the nature of the phases in contact, by their molar volume, polarity of molecules, the nature of links between the liquid particles, the phase's density. The surface solutions tension differs from that of pure metal in that the superficial layer has a different composition from the inner layers of the solution. The influence of pressure and radius curvature can be explained as follows: it is considered two fluids at mechanical balance, separated by an interface. The separation area between two fluids may take any form, from flat surface to the spherical. The condition of mechanical equilibrium at every point of the surface is given by Laplace equation.

$$\Delta P = P_2 - P_1 = \pm \sigma \cdot \left(\frac{1}{R_1} + \frac{1}{R_2} \right) \quad (12)$$

Where: P_2 is the pressure from outside on the liquid; P_1 - pressure inside the liquid, R_1 and R_2 are the radius of curvature in normal section, taken through the separation area. For spherical surface $R_1 = R_2$

$$= R \text{ and } \Delta P = \pm \frac{\sigma}{R} \quad (13)$$

For flat surface $R_1 - R_2 = \infty$ and $\Delta P = 0$.

If the two phases in equilibrium are separated by an interface curvature $C = \frac{1}{R_1} + \frac{1}{R_2}$, ΔP can be considered as the difference of pressure which push over interface from phase A (P_A) and from phase B (P_B). Laplace's relation can be written as follows:

$$P_A - P_B = \pm \sigma_i \cdot \left(\frac{1}{R_1} + \frac{1}{R_2} \right) \quad (14)$$

where: σ_i is the interfacial surface tension. For spherical surfaces the relation (14) becomes:

$$P_A - P_B = \pm \frac{2\sigma_i}{R} \quad (15)$$

Besides the pressure difference (ΔP) determined by the surface curvature on each point of the surface separation of two phases, acts also the hydrostatic pressure. If in a particular point from the separation area is the pressure difference ΔP_0 , at another point at height h , the pressure difference will be:

$$\Delta P_h = \Delta P_0 + \gamma \cdot h = \Delta P_0 + g \cdot h (\rho_A - \rho_B) \quad (16)$$

where: γ is the specific weight of the phase at a point; ρ_A and ρ_B - density of both phases A and B.

Entering the relation (16) and (14) is obtained:

$$\Delta P_h = P_A - P_B + g \cdot h (\rho_A - \rho_B) = \sigma_i \left(\frac{1}{R_1} + \frac{1}{R_2} \right) \quad (17)$$

For linear system the surface tension can be expressed by the relation:

$$\sigma = \sigma_0 - D(p - p_0) + (p - p_0)^2 \quad (18)$$

where: σ_0 is the surface tension at pressure p_0 ; D - positive constant.

According to equation (18) at pressures not too high, the surface tension decreases linearly with increasing pressure.

If we consider three crossing areas and which separate three phases, in a point of intersection (M), acts interfacial surface tension, figure 3.

At equilibrium must be satisfied the condition:

$$\sigma_1 + \sigma_2 + \sigma_3 = 0 \quad (19)$$

An important practice presents special phenomena of moistening the surface of solid melt. If we put a drop of metal melt on a solid surface, this may take the form shown in figure 4 a, b, c.

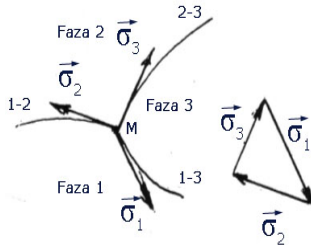
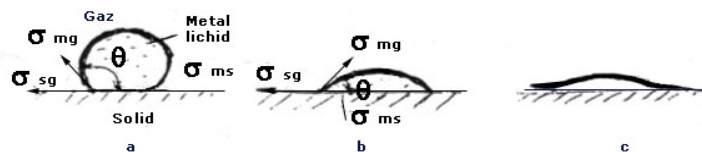


Figure 3. Way of action of inter-phasic tensions and of them composition

Figure 4. Shapes which could take the drop of metal liquid on the solid surface



In the meeting of the three-phase surface tension acting σ_{sg} , σ_{mg} , σ_{ms} who must satisfied at equilibrium the Neumann's law relation (19).

The angle between σ_{mg} and σ_{ms} bears the name of moistening angle θ . At mechanical equilibrium must have therefore:

$$\sigma_{sg} - \sigma_{ms} - \sigma_{mg} \cdot \cos\theta = 0 \quad (20)$$

4. CONCLUSIONS

Moistening angle θ does not depend on the size fluid drop, but on the nature of the surface separation. As much the superficial tension of flow is lower, better the oxide film moistening and thus better protects the melt from the oven atmosphere, and the ability moistening flow from melt which need to be minimum at discharge the alloy from furnace to ensure the best possible separation of the melt flow during casting. Getting a solid particles moistening from fusion by flow is possible if the inter-phasic tension at separation limit between flow and nonmetallic inclusions is reduced. A good moistening of solid inclusions particles allow their easy removal of fusion. We have complete moistening when $\theta = 0$ and a "good" moistening when $\theta < 90^\circ$; non moistening will occur when: $\sigma_{sg} > \sigma_{ms}$, $\cos\theta < 0$ și $\theta > 90^\circ$; total moistening will be incomplete when $\theta = 180^\circ$ and $\cos\theta = -1$.

REFERENCES

- [1] Moldovan, P., Panait, N., Mărginean, Șt. – Bazele tratării topiturilor neferoase,
- [2] Editura INTACT, București, 1998.
- [3] Sofroni, L. – Elaborarea și turnarea aliajelor, Editura Didactică și Pedagogică, București, 1975.
- [4] Teza de doctorat : “Contribuții la îmbunătățirea calității topiturilor unor aliaje de aluminiu destinate turnării pieselor” autor : Ing. Cătălin Șuşu
- [5] D. Emadi, J.E. Gruzleski and J.M Toguri, The effect of Na and Sr Modification on Surface Tension and Volumetric Shrinkage of 356 and Their Influence on Porosity Formation. Metall. Trans. B. 1993, 24 B.



STATISTICAL EXPERIMENTAL DESIGN OF THE REMOVAL OF DIFFERENT COMPOUNDS FROM SYNTHETIC WASTEWATER BY MICELLAR-ENHANCED ULTRAFILTRATION

Szabolcs KERTÉSZ^a, Junkal LANDABURU-AGUIRRE^b, Veronica GARCIA^b,
Cecilia HODÚR^c, Eva PONGRÁCZ^{b,d}, Riitta L. KEISKI^b

^A School of Environmental Sciences, University of Szeged, Szeged, HUNGARY

^B University of Oulu, Department of Process and Environmental Engineering,
Mass and Heat Transfer Process Laboratory, FINLAND

^C Department of Mechanical and Process Engineering, University of Szeged, HUNGARY

^D University of Oulu, Thule Institute, Nortech Oulu, FINLAND

Abstract

In this study, the removal of zinc ions (Zn^{2+}) and n-butanol (n-BuOH), including salt (NaCl) from model synthetic wastewater was investigated by micellar-enhanced ultrafiltration (MEUF) using sodium dodecyl sulfate (SDS). Statistical experimental design was used in order to analyze the effect of initial concentration of Zn^{2+} , n-BuOH, SDS, NaCl on the process performance. Further, the effect of Transmembrane Pressure (TMP) and membrane nominal molecular weight limit (NMWL) were also studied. It was found that n-butanol could not be removed by using MEUF. On the contrary, Zn^{2+} was successfully removed obtaining rejection coefficients up to 99% in the most favorable conditions.

Keywords

MEUF, SDS, Zinc, MODDE, Factorial Design

1. INTRODUCTION

Heavy metal ions such as zinc are detected in the waste streams of mining operations, tanneries, electronics, electroplating and petrochemical industries, as well as in textile mill products [1]. Heavy metals toxicity in air, soil and water is a global problem and a threat to the environment and human health. Therefore, removal of heavy metals is a technological challenge with respect to industrial and environmental applications. Furthermore, volatile organic compounds (VOCs) such as n-butanol are also commonly present in industrial wastewaters. VOCs have been proven to be carcinogens and mutagens [2]. MEUF is a viable membrane-based separation technology for the simultaneous removal of heavy metals and organic compounds [3]. The principle of the process is that the surfactant monomers are aggregated to form micelles at concentrations higher than its critical micelle concentration (CMC) [4]. The solutes can be retained after being trapped by the micelles, whereas the untrapped species readily pass through the UF membranes [5]. Organic compounds are solubilised in the micelle interior and the metal ions get trapped on the surface of the oppositely charged micelles by electrostatic interaction [6]. The advantages of MEUF are low energy consumption as compared to Reverse Osmosis or Nanofiltration, relatively high fluxes and high removal efficiency. There is very few published information on the application of factorial designs by MODDE in the study of MEUF [7]. Factorial design is an efficient technique that can be applied to determine the main effects and interactions of these factors on process performance. Results of factorial design can subsequently be used to optimize and decrease the number of experiments needed. Furthermore, the use of raw material, time and natural resources will be decreased improving the efficiency of the process. This paper reports the removal of zinc ions from aqueous solutions containing n-butanol and sodium chloride by MEUF. The micelles were formed by adding the anionic surfactant sodium dodecyl sulfate (SDS) to the solutions. The main purpose was to separate zinc ions from the aqueous solutions. Additionally, the removal of n-butanol was also expected. Another goal of the present study was to screen the effect of pressure, membrane nominal molecular weight limit, the feed concentration of zinc, n-butanol, sodium chloride and SDS on the process performance.

2. MATERIAL AND METHODS

2.1. Chemicals and equipments

All chemicals involved in the experiments were of analytical reagent grade. Zinc chloride (ZnCl₂ extra pure 99.99%) and sodium dodecyl sulfate (SDS, purity > 99%) from Fisher Scientific, UK were used without further purification. SDS has a molecular weight of MW = 288.38 g/mol and its CMC equal to 8.2mM (2.36 g l⁻¹) [8].

N-butanol (obtained from Kemfine Oy, Finland) was supplied by Aldrich. The distilled water used in this study was purified by a Milli-Q plus water purification system (Millipore, USA) and had an initial resistivity of 18.2 MΩ-cm. N-butanol was determined by gas chromatography with a flame ionized detector (Agilent, 6890N). Sodium chloride (Merk, pro-analysi) was quantified.

The concentration of zinc was determined by Atomic Absorption Spectroscopy (Perkin Elmer 4100 with 3047 and 3044 flame atomization methods). The SDS content was analyzed by Total organic carbon portable analyzer (Sievers 900 Portable).

2.2. Experimental design

A set of experiments was designed by Modde 8.0 (Umetrics) using a fractional factorial design (Table 1). The factors and their respective range to be studied were pressure (P, 20 and 70 psi), SDS feed concentration (C_{SDS}, 3.5 and 20 mM), Zinc feed concentration (C_{Zn²⁺}, 0.5 and 3mM), Sodium Chloride feed concentration (C_{NaCl} 0 and 1w%), butanol feed concentration (C_{BuOH} 1 and 13 mM) and membrane nominal molecular weight limit (NMWL 3 and 10 kDa). Three centre points were included to analyze the reproducibility of the experiments.

Table 1. Experiments conducted using fractional factorial design and their respective results.

Experimental Number	Screening Part						Responses	
	Factors							
	C _{SDS} [mM]	C _{BuOH} [mM]	C _{Zn²⁺} [mM]	C _{NaCl} [mM]	Pres. [psi]	NMWL [kDa]	J [Lm ⁻² h ⁻¹]	R _{Zn²⁺} [%]
1	3.5	1	0.5	0	20	3	3.26	73.38
2	20	1	0.5	0	70	3	17.51	99.22
3	3.5	13	0.5	0	70	10	69.51	53.70
4	20	13	0.5	0	20	10	13.15	95.98
5	3.5	1	3	0	70	10	60.81	37.83
6	20	1	3	0	20	10	11.36	96.86
7	3.5	13	3	0	20	3	3.46	36.98
8	20	13	3	0	70	3	20.15	90.02
9	3.5	1	0.5	1	20	10	10.34	17.52
10	20	1	0.5	1	70	10	63.31	57.70
11	3.5	13	0.5	1	70	3	18.60	23.19
12	20	13	0.5	1	20	3	2.64	56.75
13	3.5	1	3	1	70	3	34.10	9.91
14	20	1	3	1	20	3	4.17	42.29
15	3.5	13	3	1	20	10	12.88	13.42
16	20	13	3	1	70	10	54.30	54.87
17	11.75	7	1.75	0.5	45	5	12.21	65.36
18	11.75	7	1.75	0.5	45	5	12.88	65.68
19	11.75	7	1.75	0.5	45	5	12.76	65.05

The measured responses were the rejection coefficients for zinc (R_{Zn}) and butanol (R_{BuOH}) and the absolute permeate flux (J_v), which were calculated with the following equations:

$$R = 1 - \frac{C_p}{C_r}, \quad (1)$$

where C_p and C_r are the zinc or n-butanol concentration in the permeate and retentate, respectively.

$$J_v = \frac{V}{t \times A}, \quad (2)$$

where J_v is the absolute permeate flux, V is the volume of the permeate sample collected, t is the time needed for collecting the permeate sample and A is the membrane effective area. The validity of the empirical models fitted with multiple linear regression (MLR) was tested with analysis of variance (ANOVA). The confidence level used was 95 %.

2.3. Dead-end micellar-enhanced UF experiments

All UF experiments were carried out in batch solvent resistant stirred cell (Millipore, Model 8400) with a capacity of 400 cm³. In all MEUF tests the TMP was controlled and adjusted with pressurized N₂ gas by means of a transducer. The operating temperature was 25 ± 1°C controlled by an air conditioner. The solution in the reservoir was agitated using a magnetic stirrer to provide efficient mixing at 500 rpm. This stirring speed was selected because it could lead a sufficient agitation to result

a homogenic solution without excessive vortex formation. The permeate flux was determined by measuring the first 100 cm³ (five times 20 cm³) of the feed solutions. In each experiment the first, second and the fifth permeate sample was analyzed and then integrally averaged because the compositions of the permeate varied during the experiments.

In the dead-end ultrafiltration (UF) experiments, UF flat sheet membranes of Amicon regenerated cellulose (PL series, Millipore) of different nominal molecular weight limits were used. Each membrane has a membrane effective area of 0.004m². Only the membranes with a deviation of the pure water flux, measured before and after MEUF tests, smaller than 5 % were repeatedly used. Ultra distilled water was used after each experiment test for membrane cleanings.

2.4. Experimental procedures

The initial feed volume was 200 cm³. The average permeate flux was calculated by measuring the time needed for collecting permeate samples of 20 cm³. The ultrafiltration experiments were carried out until 100 cm³ of the total sample was filtered (VCF = 2). The VCF is defined in Eq. (3):

$$VCF = V_b / V_e \quad (3)$$

where V_b and V_e are the volumes of solutions in the MEUF device at the beginning and at the end of the test, respectively. The membrane was submerged before the concentration tests for 1 h to reach equilibrium with the solution.

3. RESULTS AND DISCUSSIONS

The main purpose was the simultaneous removal of Zn²⁺ and n-BuOH by MEUF. From table 1 can be observed that butanol was not removed using micellar-enhanced ultrafiltration. The reason why the R_{BuOH} is not included in Table 1 is that, in all cases, the rejection coefficients of BuOH were very low (average 5 ± 2 %). Therefore, the research was continued in order to see the effect of the mixture of butanol and salt in the removal of zinc by micellar-enhanced ultrafiltration. In this way, the responses included in the experimental design were R_{Zn} and J_v .

3.1. Effects of factors on the absolute permeate flux

The effect of single factors on the permeate is illustrated in Fig. 1, displaying the change in the response when a factor varies from its low level to its high level while all other factors are kept at their averages. Negligible effects are those where the confidence interval includes zero.

As it can be observed from Fig. 1, pressure has a positive effect on the absolute permeate flux as expected. This means that increasing the pressure, higher permeate flux will be achieved. When pressure is increased the driving force is also increased obtaining a higher flux. NMWL has also a positive effect. Consequently, using a higher pore size membrane higher flux will be observed. Further, concentrations of SDS, BuOH, Zn²⁺ and NaCl show a negligible effect on the absolute permeate flux.

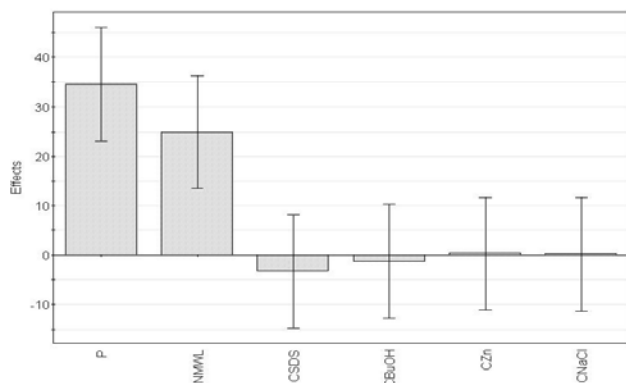


Figure 1. Effect of main factors on the absolute permeate flux varies from its low level to its high level while all other factors are kept at their averages. Negligible effects are those where the confidence interval includes zero.

As it can be observed from Fig. 2, the concentration of SDS, NaCl and the Zn²⁺ have the major effect on the rejection coefficient. Concentration of SDS has a most significant positive effect, thus, when increasing the SDS feed concentration, the rejection coefficient is also increased. This is because at higher SDS concentration, more SDS is present in micellar form. NaCl concentration of the feed has a negative effect on the rejection coefficient, therefore, increasing it will decrease rejection. This result complies with earlier study [9] reported in the literature. Since Na⁺ is a monovalent ion, it can readily bind with the negative charge head of the micelle competing with the heavy metal cations. Therefore, rejection coefficient decreases with an increase in the salt concentration. Further, zinc feed concentration also shows a negative effect on the rejection coefficient. Consequently, when increasing the zinc feed concentration rejection coefficient decreases. This shows that MEUF is more efficient for

When evaluating the validity of the fitted model with ANOVA, the regression model is statistically significant with a 95% confidence level in the range studied. The response variation percentage explained by the model, R^2 , for the permeate flux is 0.85. The response variation percentage predicted by the model, Q^2 , is 0.60. The reproducibility of the experiments is good.

3.2. Effect of factors on the rejection coefficient

The effect of single factors on the permeate is illustrated in Fig. 2, displaying the change in the response when a factor varies from its low level to its high level while all other factors are kept at their averages. Negligible effects are those where the confidence interval includes zero.

diluted heavy metal streams. Further, concentrations of NMWL, BuOH and pressure show a negligible effect on the rejection coefficient.

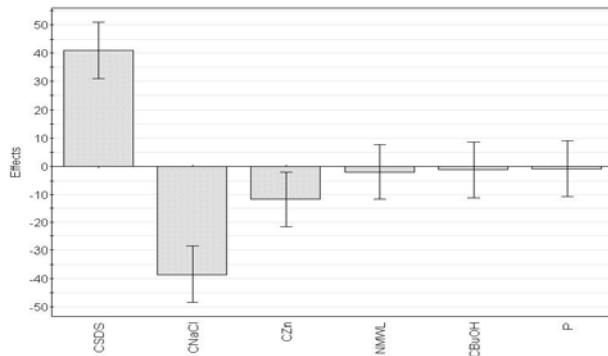


Figure 2. Effect of factors on the rejection coefficient of zinc

salt (NaCl) from model synthetic wastewater was investigated by micellar-enhanced ultrafiltration (MEUF) using an anionic surfactant agent, sodium dodecyl sulfate (SDS).

It was found that n-butanol could not be removed by using MEUF. On the contrary, Zn^{2+} was successfully removed obtaining rejection coefficients up to 99% in the most favorable experimental conditions.

A statistical experimental design (including Screening Part, SP) was used in order to analyze the effect of initial concentration of Zn^{2+} , n-BuOH, SDS, NaCl on the process performance. Further, the effect of Transmembrane Pressure (TMP) and membrane nominal molecular weight limit (NMWL) were also studied.

Pressure and NMWL have the most significant positive effects on the absolute permeate flux. Concentration of SDS has the most important positive effect, while NaCl has the most important negative effect on the rejection coefficient. Further, Zn^{2+} feed concentration has the major negative effect on the rejection coefficient.

By using fractional factorial design, the effects of 6 different factors on the MEUF process performance were evaluated in only 19 experiments. This shows the high effectiveness of experimental design for screening experiments. Further, experimental designs can now be developed as the factors with statistically no significant effect are identified.

ACKNOWLEDGMENTS

The authors gratefully acknowledge the financial support provided by KNRETo7/2005 Hungarian project and the Maj and Tor Nessling Foundation, the Academy of Finland and the Global Change Programme of the Thule Institute at the University of Oulu.

REFERENCES

- [1] T.G. Chuah, A. Jumariah, I. Azni, S. Katayon, S.Y.T. Choong, Rice husk as a potentially low-cost biosorbent for heavy metal and dye removal: an overview, *Desalination* 175, 305–316, (2005)
- [2] Y. Kuo-Pin, W.M. L. Grace, W.M. Huang, W. Chihcheng, Y. Shinhao, The correlation between photocatalytic oxidation performance and chemical/physical properties of indoor volatile organic compounds, *Atmospheric Environment* 40 (2), 375-385, (2006)
- [3] D. Chandan, D. Sunando and D. Sirshendu, Prediction of permeate flux and counterion binding during cross-flow micellar-enhanced ultrafiltration, *Colloids and Surfaces A: Physicochem. Eng. Aspects* 318, 125–133, (2008)
- [4] L. Chi-Wang, L. Chuan-Kun and Y. Wei-Shuen, Micellar-enhanced ultrafiltration (MEUF) with mixed surfactants for removing Cu (II) ions, *Chemosphere* 63, 353–358, (2006)
- [5] B.R. Fillipi, L.W. Brant, J.F. Scamehorn and S.D. Christian., Use of Micellar-Enhanced Ultrafiltration at Low Surfactant Concentrations and with Anionic–Nonionic Surfactant Mixtures, *J. Colloid Interface Sci.* 213, 68-80, (1999)
- [6] J. Lee, J.-S. Yang, H.-J. Kim, K. Baek and J.-W. Yang, Simultaneous removal of organic and inorganic contaminants by micellar enhanced ultrafiltration with mixed surfactant, *Desalination* 184, 395–407, (2005)
- [7] X. Ioannis, J. Agnieszka and Z.-T. Grażyna, Response surface methodology for the modelling of copper removal from aqueous solutions using micellar-enhanced ultrafiltration, *J. Membr. Sci.* 321 (2), 222-231, (2008)
- [8] M. Rosen, *Micelle Formation by Surfactants*, in *Surfactants and Interfacial Phenomena*, 2nd edition, John Wiley & Sons, Inc. 122, (1989)
- [9] V.D. Karate and K.V. Marathe, Simultaneous removal of nickel and cobalt from aqueous stream by cross flow micellar enhanced ultrafiltration, *J. Hazard. Mater.* 157 (2-3), 464-471, (2008)



FATIGUE TESTS AT HYBRID ALUMINUM ALLOY JOINTS

Dinu DRĂGAN, Mircea Cristian ARNĂUTU,
Ion SIMION, Nicușor Laurențiu ZAHARIA

¹ Romanian Railway Authority – AFER, București, ROMÂNIA

Abstract:

This paper presents a study on fatigue performance of adhesive/rivets joints in an aluminum structures. Hybrid joints were shown to have greater strength, stiffness and fatigue life in comparison to adhesive joints. The results from fatigue tests confirm the static tests made on the same type of test samples.

Keywords:

Aluminum, Adenit, Si-Plane, joints

1. INTRODUCTION

Aluminum alloy joints are used in aircraft construction, some cars, railway vehicles etc. The joints can be assembling by welding, gluing, rivets etc.

In this paper it will be presented joints assembled hybrid (gluing and rivets).

The tests were performed in the CEEEX program named “Adhesives, Rivets and Hybrid Aluminum Alloy and Composite Materials Joints”.

2. MEASUREMENT DEVICES AND JOINT TYPES

The tensile fatigue tests were performed at Romanian Railway Authority – AFER on universal testing machine SI-PLANE 942-1 type (fig. 1). The testing machine was designed and manufactured by British Company Si-Plan Electronics Research Limited in the year 2005.

The machine is hydraulically manipulated from a computer and can perform tests with tensile or compressive forces (static and dynamic) and it has the next characteristics:

- ✚ Maximum force for static tests: $\pm 350\text{kN}$;
- ✚ Maximum force for dynamic tests: $\pm 250\text{kN}$;
- ✚ Maximum high for the vertical tests: 400mm;
- ✚ Frequency for dynamic tests: $\leq 40\text{Hz}$.

All the preparing operations and the test are performed by the hydraulic installation of the machine. He steps for performing the tests were:

1. Each type of joint was named **N^{tip}n**, where „**tip**” means the joint type of the aluminum alloy (nit – rivet joint, hib – hybrid joint or adz – adhesive joint), **N** is given by the thickness of the material or the joint geometry and **n** is the identification number for the same type of joint.
2. For each of joint a reference tensile force was calculated based on static tests which were performed on other stage of the project.
3. Based on reference tensile force, the maximum and minimum dynamic tensile forces were calculated for five value domains as following: 80%, 70%, 60%, 50% and 40% from the reference tensile force and the minimum values were 10% from the maximum values (the 1/10 value was used for each fatigue cycle).
4. A 5Hz frequency was used for all fatigue tests. During the test it was cases when the joints break it after hundreds of cycles before to reach the stability of the dynamic regime at 5Hz frequency (the test was repeated if it was possible on another same type joint) or the joint doesn't break it not even after 500.000 cycles.

5. For each joint it was recorded the number of cycles when the joint was break it and the type of joint break (adhesive, cohesive or adhesive-cohesive).
6. Photos were made on each joint before, during and after the tests. Also a print screen on Si-Plane machine computer for each joint was made. In this print screen it is shown the minim and maximum of force cycle, frequency and number of cycles.
7. Based on values recorded at step number 6, the normalized curve $S-N$ (Wöhler curve) was draw by quasi-linearity interpolation which crosses the horizontal axis in the point which has the coordinates (0; 1).

$$\frac{F_M}{F_R} = 1 - k \cdot \lg(N) \quad (1)$$

which mean that the ratio between maximum force of the cycle and the reference force depending on decimal logarithm of breaking number of cycles.

8. The tests were performed at 21 degree Celsius temperature and 55% relative humidity.



Figure 1 The Universal Testing Machine SI-PLAN 942-1 type

Many types of joints were tested. The aluminum pieces were jointed in different shapes: end to end, one above other, angle joint etc. as follows:

- ✚ Adhesive joints;
- ✚ Hybrid joints (adhesive+rivet).

In fig. 2÷3 are shown the types of joints were the value of ratio $1/K$ had the highest value.

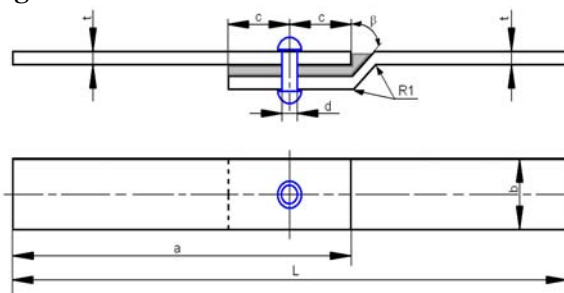


Figure 2 4hib joint type

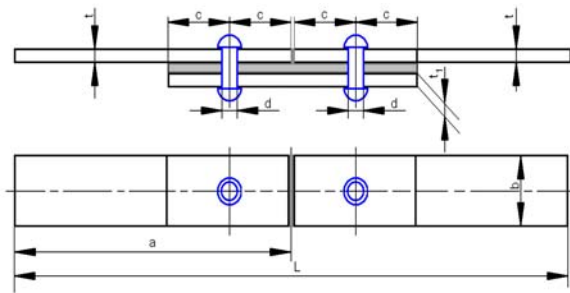


Figure 3 5hib joint type

3. RESULTS

3.1. 4hib joint type

In table number 1 are presented the results for 4hib joint type.

Regarding to this table the following explanation are necessary:

- ✚ F_{max} and F_{min} measured in daN units are maximum and minimum value for a pulsate cycle at 5Hz frequency;
- ✚ The value $F_{max}=170daN$, is represent 60% from tensile reference force;

Table 1. Results for 4hib joint type.

Proof sample	F _{max}	F _{min}	N	Lg(N)
4hib_3	170	17	59844	4,78
4hib_4	200	20	184432	5,27
4hib_5	200	20	2579	3,40
4hib_6	230	23	68413	4,84
4hib_7	230	23	2583	3,41

- ✚ The value F_{max}=200daN, is represent 70% from tensile reference force;
- ✚ The value F_{max}=230daN, is represent 80% from tensile reference force;
- ✚ N is the number of cycles when the joint break it.

In fig. 4 is shown the normalized Wöhler curve draw by quasi-linearity interpolation.

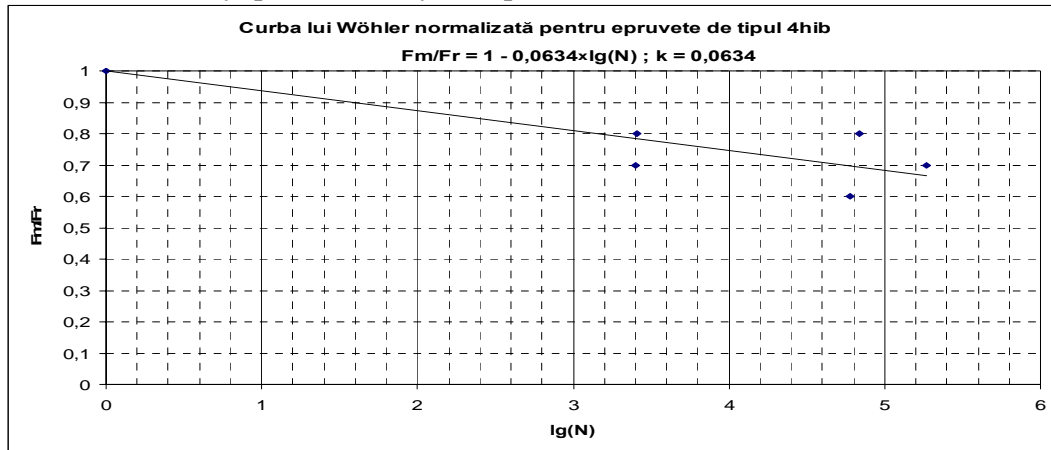


Figure 4 Wöhler curve for 4hib joint type



Figure 5. Adhesive break



Figure 6. Metal break

The proof sample 4hib_3, 4hib_4 and 4hib_6 were break it in the metal and the proof sample 4hib_5 and 4hib_7 were break it in the adhesive.

In fig. 5 it is presented an adhesive break and in fig. 6 it is presented a metal break.

3.2. 5hib joint type

In table number 2 are presented the results for 5hib joint type.

Regarding to this table the following explanation are necessary:

- ✚ F_{max} and F_{min} measured in daN units are maximum and minimum value for a pulsate cycle at 5Hz frequency;
- ✚ The value F_{max}=190daN, is represent 60% from tensile reference force;
- ✚ The value F_{max}=220daN, is represent 70% from tensile reference force;
- ✚ The value F_{max}=260daN, is represent 80% from tensile reference force;
- ✚ N is the number of cycles when the joint break it.

Table 1. Results for 5hib joint type.

Proof sample	F _{max}	F _{min}	N	Lg(N)
5hib_6	190	19	240037	5,38
5hib_4	220	22	103031	5,01
5hib_7	220	22	120806	5,08
5hib_8	220	22	40100	4,60
5hib_5	260	26	605	2,78
5hib_9	260	26	1939	3,29
5hib_10	260	26	5537	3,74

In fig. 4 is shown the normalized Wöhler curve draw by quasi-linearity interpolation.

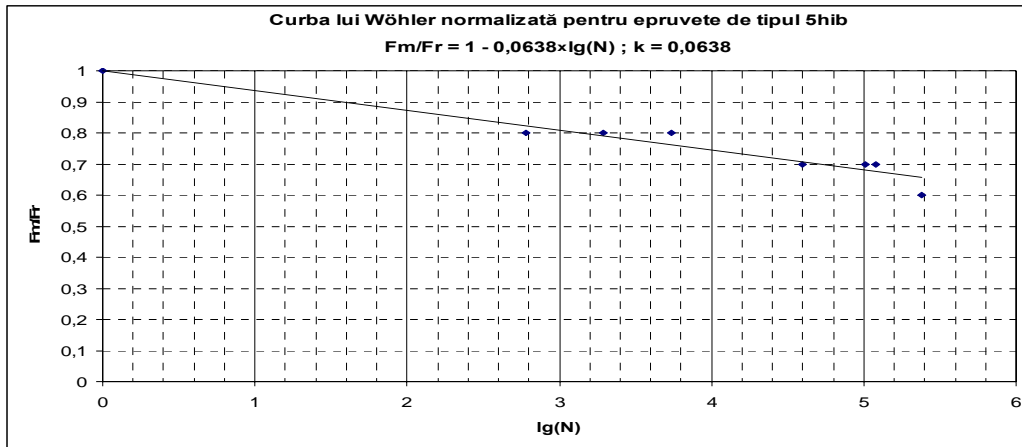


Figure 7 Wöhler curve for 5hib joint type



Figure 8 5hib_6 proof sample



Figure 9 5hib_9 proof sample

The proof sample 5hib_6 has an adhesive break but not a rivet break. The proof sample 5hib_4 has an adhesive-cohesive break and the other proof sample had an adhesive break.

In fig. 8 it is presented an adhesive break and in figure 9 it is presented an metal break.

4. CONCLUSION

In fig. 10 the different types of joints had been arranged from the point of view of 1/K ratio (the inverted of normalized Wöhler curve) which significance is the fatigue lastingness of the proof sample.

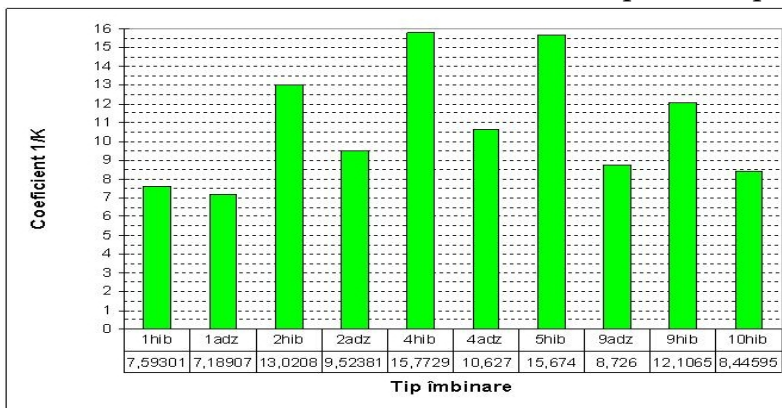


Figure 10. 1/K ratio histogram

From fig. 10, it can be seen that the hybrid proof sample number had a higher lastingness but we must remember that the tensile reference forces are different from one type of joint to other (the tensile reference forces are higher at adhesive joints).

REFERENCES

- [1] Hoffman, K. – *An Introduction to Measurement using Strain Gages*, HBM GmbH Darmstadt, 2005
- [2] Mănescu T.Ș., Copaci I., Olaru S., Creangă F. – *Tensometria electrică în cercetarea experimentală*, Ed. Mirton Timișoara, 2006
- [3] ***** – *Catman 4.5 User's Guide*, HBM GmbH, 2004
- [4] ***** – *Spider8 Operating Manual*, HBM GmbH, 2004
- [5] Zaharia N.L., Simion I, Costescu D. M., – *Fatigue Tests At Hybrid Adhesives And Rivets Joints For Composite And Aluminum Structures*, The Annals of “Dunărea de Jos” University Of Galați 2008.

ROTORS CASTING FOR AVIATION TURBOCOMPRESSORS

CHIRA Ion, VERDEȘ Bogdan Alexandru

Politehnica University of Bucharest, ROMANIA

ABSTRACT

Choosing the best casting technology is made considering the quality indices (I.C.) of the casted part, in the status of FINISHED PART. Each phase of the technological process has several possibilities with advantages and disadvantages of techno-technological nature, efficiency, production or the domain in which the part is used.

The projection of the casting technology is realized taking into consideration several imposed parameters – which much be applied and included in the technology which is used and various operations, phases, materials, SDV and technologic equipments, which support optimization processes in order to assure total quality to the casted part.

The current paper intends to present the methodology for choosing the optimum casting technology for a turbo compressor rotor used in the aviation, part which must be assimilated in the national industry.

Key words:

casted turbo compressor rotors used in the aviation industry; precise casting thru special procedures, non-conventional

1. INTRODUCTION

In a flying aircraft is activating four forces which have to be in equilibrium; these forces are weight, traction, resistance and portanta (fig. 1).



Fig 1 Force systems which operate on an airplane

The traction is assured by the propulsion system; considering the propulsion system the airplanes can be classified in:

- ✚ Propeller solutions – equipped with classic engines with pistons (AN-2, Cessna 172, ZLIN Z-142);
- ✚ Reaction airplanes – equipped with turbo reaction engines (Boeing 747, A340, MIG-21, F-16, AN-124, Concorde);
- ✚ Constructions with propeller and reaction – equipped with turbo propulsion engines (ATR-42, C-130 Hercules).

An engine with reaction produces traction in a similar way as the engine-propeller combination, but while the propeller gives a small acceleration to a high quantity of air, the engine with reaction gives a high acceleration to a small quantity of air.

Currently, there is a large diversification for the aviation engines; if we refer strictly to engines with reaction as aero-reactors, these are developed as:

- ✚ Turbo-reactor engine
- ✚ Sato-reactor engine: with subsonic burn – ramjet type; with supersonic – scramjet type;
- ✚ Pulsoreactor engine;
- ✚ Motoreactor engine.

SIMPLE ENGINE REACTOR - MTR is currently equipping the aircrafts flying at high altitudes and speeds over Mach 0.6. Its operating principle is as follows: air entering through the inlet is compressed by the compressor, enters in the combustion chamber where together with fuel injected mixture of combustion gases takes place the actual combustion. The burned gases then pass through the turbine, where the partial retaining thru their rotation, and then pass through the nozzle side and leaving the system with a kinetic energy much higher than the input, thus is providing the traction of the plane. Eventually, at supersonic airplanes we can meet the post-combustion; it is incorporated into

the exhaust system and has the role to inject a fuel mixture dose in the combusted gas from the combustion chamber.

We have to remember that the double flow turboreactor engines - called generically turboventilator - are actually turboreactor modified. They are characterized by the existence of two streams flowing parallel: one secondary, trained by a fan mounted on the compressor shaft with a low-pressure turbine, which takes the flow of primary air (inside) made from waste gases. The traction of the dual-stream engine is the thrust of the two resulting streams. Do not forget that the fan has the role of propulsion, operating as a propeller. The double flux turboreactor engine - MTR + DF are the most widespread types of aviation engines, which is equipping most of the civilian aircraft and a good part of military aircraft (see tab. 1).

Tabel 1. Types of reaction engines and airplanes equipaded with such systems

LICENCE – PRODUCTION	AIRPLANE MODELS
CIVIL AIRPLANES	
<u>SNECMA-GE CFM-56</u>	Boeing 737, Airbus A318, A319, A320, A321
<u>General Electric GE90</u>	Boeing 777
<u>CF6</u>	A300, A310, A330, Boeing 747
<u>Pratt & Whitney JT9D</u>	B747, Boeing 767, A300, A310
<u>W4000</u>	B777, A330
<u>PW6000</u>	A 380
<u>Rolls-Royce Trent 500-900</u>	For almost all types of Boeing and Airbus
MILITARY AIRPLANES	
<u>General Electric F110</u>	F14, F15, F16
<u>F103/CF6</u>	Air Force One, B767 AWACS
<u>F404</u>	F/A-18, F117, A-4 Skyhawk
<u>Rolls-Royce EJ200</u>	Eurofighter Typhoon
<u>Pegasus</u>	Boeing-BAe Harrier
<u>Snecma M53</u>	Mirage 2000
<u>M88</u>	Rafale

A turbine which functions on gas is a thermo one, which uses the fall of the enthalpy of a gas or a mixture of gases to produce through the spinning blades a quantity of mechanical energy available for the turbine; the gas turbine is also known as GAS TURBINE INSTALLATION – ITG.

For the thermodynamics point of view a gas turbine works rather like a car engine. Atmospheric air is admitted in a blades compressor, where is compressed, follows the introduction of a fuel's ignition and its ignition in a combustion chamber. The combustion gases are then discharged into the atmosphere. The process is continuous, and the parts execute only rotation movements, which for a period of time might lead to smaller total mass; as a result, gas turbines were developed especially as reaction engines: turboreactor, turbo propeller, turboventilator and turbines to engage the helicopter propellers (see tab. 2).

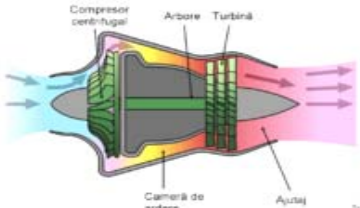
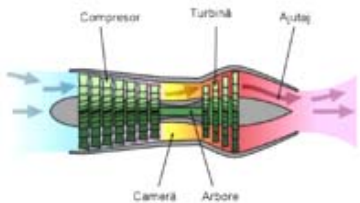
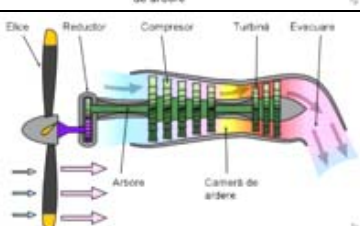
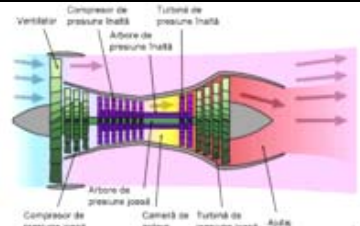
The most prevalent type of jet aviation is the turbojet, the main constructive elements: the speaker, compressor, combustion chamber, gas turbine and effuse component.

THE COMPONENTS OF A COMPRESSOR - Compressors are labor consuming machine through which gas pressure is raised. After operation principle, compressors can be classified into two main groups namely:

- ✚ Volumetric compressor (pressure at which gas lifting is done by closing it within a certain volume, decrease the volume until the lifting of the gas discharge pressure and gas evacuation). In this group can be piston compressors, which have a cylinder moves linearly and rotary compressors, which also have a cylinder in which we can find a piston with rotary motion. These compressors are used for high and very high pressures (1000 bar), with relatively small gas flows (450 cm³/min);
- ✚ Dynamic compressor (to increase pressure is done by transferring kinetic energy to the gas, through a large propeller rotor, followed by its conversion into potential pressure energy, the process taking place continuously; in this group we can include the centrifugal compressors and the axial compressors) .

At centrifugal compressors the energy transformation is done through centrifugal force on gas molecules, brought in a circle movement with a propeller rotor. Depending on the ratio of the pressure p_r and suction pressure p_a , we can identify: - turbo-compressor if $p_r / p_a > 2.5$; turbo-ventilator if $1.1 < p_r / p_a < 2.5$; ventilator if $p_r / p_a < 1.1$.

Tabel 2. Typical construction, principle, for turbine with aviatic gaz and typical solutions for jet engines

Constructive types of turbines	Reactive engines
Turboreactor with centrifugal compressor	
Turboreactor with axial compressor	
Turbopropulsor	
Turboventilator	

In axial compressors the transformation of energy is through done through a gas dynamic forces acting on gas molecules, caused by a large rotor. Are used for pressures of 5 - 6 bar and flow rates that can exceed 10,000 m³/min.

2. THE STUDY

High flow centrifugal compressors have a simple rotor or a double sided one, and occasionally is used the two-tier version, simple as building the Rolls-Royce Lance (Dart) engine. Rotor is supported in a housing which also contains a ring of the speaker. If using a rotor with double-entry, the air flow towards the rear is reversed in the opposite direction and requires an intermediary room.

Rotor is whirled at high speed by the turbine and the air is controlled permanently by the rotor. Centrifugal force makes the air flow to propagate to the outside, over to cavil (wall profile) so that accelerating mass will cause an increase in air pressure. Inlet pipe of the engine can be imperfect, which can cause an initial turbulence of the air at its entrance into the compressor.

To maximize air flow and increased pressure by the compressor is necessary that the rotor is rotated at high speeds; thus rotors are designed to work on the peripheral speeds of about 500 m / s.

Aviation turbo compressor rotors are made with different construction solutions, with advantages and disadvantages -

aerodynamic efficiency, endurance and reliability, economic efficiency and maintenance:

1. Disk blades, mono-block (similar rotor Platan from dense liquid pumps), active on one part or both sides (see fig. 2);
2. Blocks, embedded in pallets (combined with a type of swallow tail), which on the outside may or may not be additional reinforced with a circular fitting (as classic steam turbines);
3. Sandwich, with two lateral discs, which are disposed profiled palettes (like the suction fan).

The designer and the company which obtains the manufacturing license is the owner of technical solutions found, they provide and require a number of features and performance of these rotors, which must be accomplished by the casted part, realized by the technologist: shape, configuration and stability during operation; nominal dimensions and admissible tolerances; speed, peripheral speed, temperature and duration of continuous operation to achieve necessary thermodynamic efficiency; flatness of the surfaces, cost limits for part assimilation and production etc.



Fig. 2 Specific constructions of rotors of centrifugal compressors in aviation

3. ANALISES, DISCUSIONS, APPROACHES, INTERPRETATIONS

The design technical work linked with computer applications is defined as COMPUTER AIDED DESIGN - CAD.

CAD applications, with systems for designing assistance are the most known and consist of the following:

1. a field of communication organizes data entry and exit to and from the design department;
2. a range of methods includes modules for modeling work, information and calculations;

3. a field of administration and management of data and a system of integrated data bank organizes all storage and transfer of data between algorithms and methods of communication on the one hand, and networks of data banks or specialized individual files or standardized on the other; database of design contains all the geometric data and stored non-geometric that both methods are needed to design and communication between the operator and the CAD designer.

A fundamental feature of CAD systems is constituted by the concept RID = internal representation of geometric objects. This system is based on the real object; abstraction is achieved by a virtual mental model, in which the formalization and multiple filtering in specific languages leads to the INFORMATION MODEL. Through a series of transformations and transpositions based on the binary code, it is formed an internal model in the computer memory - RIM type configuration.

Chaining programs with systems engineering data processing, in the engineering sciences field, is abbreviated CAE = COMPUTER AIDED ENGINEERING.

The integration of a firm in a complex and comprehensive system of monitoring, processing and managing data is known as COMPUTER INTEGRATED MANUFACTURING - CIM.

In the specific area of design technology of casting systems are used systems as COMPUTER ASSISTED CONCEPTION AND MANUFACTURING - CFAO, and sub-programs: COMPUTER ASSISTED DESIGN - DAO, COMPUTER ASSISTED MANUFACTURING - FAO, COMPUTER ASSISTED CONCEPTION - CAO.

Using computer graphics reduce the period of conception and design; starting from the establishment, development and multiplication of simple design drawing by 3D techniques there have been realized programs that allow complex projections for simple parts or complex parts, rapid completion of drawings by the importation of printed standardized elements (screws, axles, rolling bearings, gears, etc..), the production of prototypes to test the functionality of products for approval and launch phases in the series of casting technologies assimilated.

It has the following special procedures for casting accuracy:

- ✚ Static casting in metal shape - shell;
- ✚ Casting under high pressure (ICTY) - in the mold;
- ✚ Casting at low pressure (TJP) - in the form of mixture or matrix;
- ✚ Casting static forms with binder strip thermo-reactive (bakelite; Croning process or Shell);
- ✚ Static casting oven by tilting forms multi-layer type crust or rind ceramic form casting, packaged or not: MUF model type, the request - made by injecting mold; MGP model type made by injection or expand in the mold -- REPLICAST process, models of resin made by SLA (see Fig. 3 and 4);
- ✚ Casting forms ceramic monolith, Shaw type: metallic, processed on modeling (tool-room) the model consumable - MUF, MGP = injection / expand; of resin, paper.

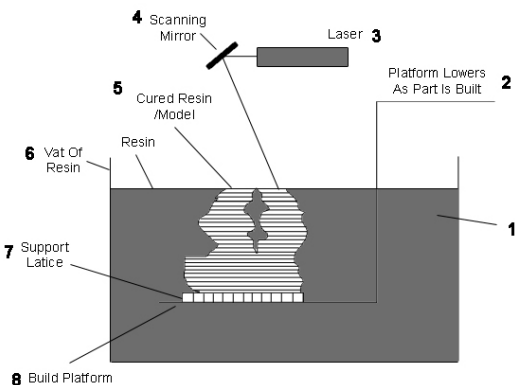


Fig. 3 Stereo lithography SLA: 1- liquid resin; 2 - model support; 3 - laser scanning system; 4 - mirror; 5 - solid model realized by polymerizing the resin; 6- compartment with liquid resin; 7- support for this model; 8 - system with vertical movement.

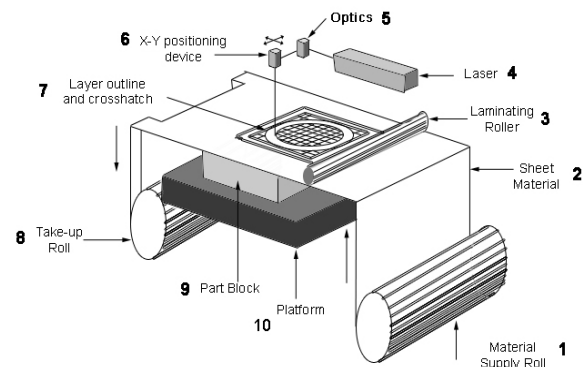


Fig. 4 Scheme to achieve prototypes through LOM technology : 1- material supply role; 2 – sheet material; 3 – laminating roller; 4 –laser scanning system; 5 - optics; 6 – positioning device; 7 – layer outline and crosshatch; 8 – take-up roll; 9 – part block; 10 – platform and system with vertical movement.

The stereo-lithography technique (variants RAPID PROTOTYPING, SLA, LOM) permits to fabricate photo-sensitive resin prototypes (MODELS) by selective and controlled strengthening with laser beams and computer assisted control panel; is a current CAD application.

In Table 2 are listed the main indices of quality of casted parts by special casting processes, technologies by which are casted the rotors for turbo-compressors for aviation.

Tabel 2. The main quality indices of casted parts, casted by special procedures

QUALITY INDICES	SPECIAL CASTING PROCEDURES						
	CRONING or SHELL	Shaw	MUF ceramic shell	MGP ceramic shell Replicast	Static metallic forms	Casting at high pressure	Casting in liquid form
1	2	3	4	5	6	7	8
Material often cast	cast iron, steel, ferrous super alloy	steel, cast iron, super alloy, nonferrous	special steel, iron, super alloy	special steel, iron, super alloy	non-ferrous, steel, iron, super alloy	non-ferrous (Al, Mg, Zn, Sn, Sb, Pb-Alloy, brasses, bronzes)	special steel, non-ferrous (silumins, brasses, bronzes)
Complexity of cast part	large, with cores, straight separation	large, with cores, without separation	Large, with cores, without separation	large, with cores, without separation	big, metallic and un-metallic cores, straight separation	large, with metallic cores, straight separation	small and medium, without cores
Parts size min., kg/pc. Min. sizes, mm	0.02 3.0	0.03 1.5	0.01 0.3	0.01 3.0	0.03 1.5	0.01 0.2	0.04 5.0
Parts size max./usual, kg Max. sizes, mm	150 / 5.0 800	250 / 25 1200	40 / 0.8 600	80 / 15,0 700	130 / 10 800	50 / 5.0 700	60 / 10 300
Dimensional precision, % Dimensional tolerances, ± mm / la 100 mm	10.5 ± 1.5	3.5 ± 0.4	2.0 ± 0.3	3.0 ± 0.4	11.5 ± 0.8	1.5 ± 0.2	12.0 ± 2.0
Usual rugosities, µm	12.5 - 25	1.6; 3.2; 6.3; 12.5	1.6; 3.2; 6.3; 12.5	3.2; 6.3; 12.5; 25	3.2; 6.3; 12.5; 25	1.6; 3.2; 6.3; 12.5	25 - 50 steel; 3.2 – 6.3 nonferrous
Special properties registered for casted parts	for permanent magnets, refractory and anticorrosive steels, big productivity for iron	for steel-mold for forge and rubber and plastic industry	finless parts, threads from M5 casting parts without pulp, high productivity	Steel parts, big dimensions like by MUF	armed with inserts parts, parts of cast iron with hard crust, nonferrous with fine structure	finless parts, threads from M2 casting, with micro-porosity, volumetric solidification, armed pieces	structure-oriented material, fibrous, very compacted, special steel and nonferrous
SDV durability, max. no. pc. casting parts	100000	25000	100000	1000000	10000	50000	5000
Efficient lots/ production series, min. pc.	10000 / 1000000	1000 / 15000	1000 / 100000	1000 / 100000	500 / 10000	20000 / 1000000	1000 / 10000

4. CONCLUSIONS

As it is known, the mixture forms – ceramics, used exclusively preheating, ensure moderate rates of cooling; on the one hand it fosters a directed and successive solidification, but the gross cast part has a rough appearance, with impurities, which complicates the thermo treatment.

Possibly to increase the wall capacity and its fluidity, either will be used the tipping of the oven when crust shape or form will spin Shaw (see fig. 5, where a rotor with Ø 300 mm and H 60 mm - the horizontal position, with the blade down and blocking the top; for calculation is considered the highest point at the top of the blade).

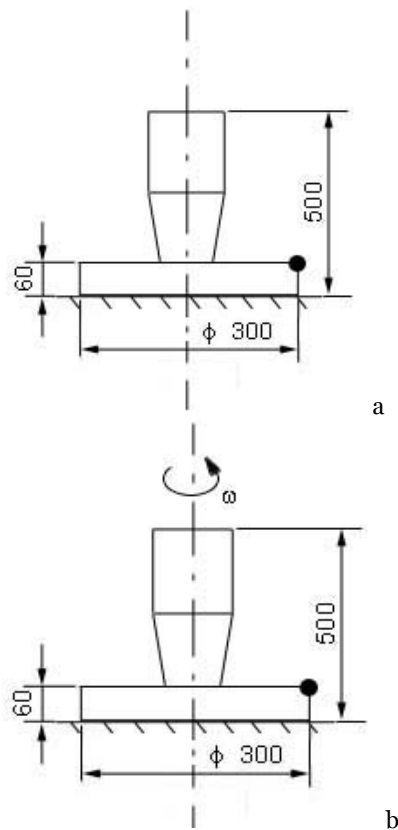


Fig. 5 Calculation scheme for the metal-static pressure: a – for static casting; b – for centrifugal casting, with vertical ax.

$$P = \gamma \cdot H$$

$$H = 440 \text{ mm}$$

$$\gamma = 7.8 \text{ daN/dm}^3$$

$$\Rightarrow P = 7.8 \text{ daN/dm}^3 \cdot 4.4 \text{ dm} =$$

$$P = 34.32 \text{ daN/dm}^2$$

$$P = \rho \cdot \left(\frac{\omega^2 \cdot r^2}{2} - g \cdot z \right) + C \Leftrightarrow$$

$$P = \gamma \cdot \left(\frac{\omega^2 \cdot r^2}{2g} + z_0 - z \right)$$

$$H = 440 \text{ mm}$$

$$\gamma = 7.8 \text{ daN/dm}^3$$

$$n = 600 \text{ rot/min}$$

$$\omega = \pi \cdot n / 30 = 3.14 \cdot 600 / 30 = 62.80 \text{ rad/s}$$

$$\Rightarrow P = 7.8 \cdot \left(\frac{62.8^2 \cdot 15^2}{2 \cdot 980} + 44 \right) =$$

$$= 7.8 \text{ daN/dm}^3 (452.74 \text{ cm} + 44 \text{ cm}) =$$

$$= 7.8 \cdot 496.74 \cdot 10^{-1} \text{ daN/dm}^2 =$$

$$P = 387.45 \text{ daN/dm}^2$$

REFERENCES

- [1] * * * - Rapid Prototyping. Rapid Tooling. Rapid Manufacturing. În: Giesserei-Praxis, nr. 11, 2003, p. 462.
- [2] CHIRA I. - Bazele teoretice ale proiectării și turnării pieselor. Curs universitar pe suport magnetic – CD (reeditat). Edit. Samizdat, București, 2005.
- [3] CHIRA I. - Calitatea pieselor turnate. Curs universitar pe suport magnetic – CD (pentru realizarea paginii web. p. 76. Format jpg/MFP7.0/r14). Edit. Samizdat, București, 2006.
- [4] CHIRA I. - Realizarea pieselor prin turnare. Curs universitar pe suport magnetic – CD (pentru realizarea paginii web. p. 116. Format jpg/MFP7.0/r14). Edit. Samizdat, București, 2006.
- [5] CHIRA I. ș.a. - Informare și documentare în cercetarea metalurgică. Edit. Litografia IPB, București, 1989, p. 218.
- [6] CHIRA I. și Ioniță Gh. - Fundamentele inginerului metalurg - turnător. Calitatea pieselor turnate. Edit. Științifică „Fundația Metalurgia Română”, București, 1998, 408 p., (ISBN 973-98904-0-7).
- [7] PHAM D. T. și DIMOV S. S. - Rapid manufacturing. Edit. Springer-Verlag, Berlin, 2001, (ISBN 1-85233-360-X)



THE PROMOTING, THE PARTNERSHIP AND REGIONAL COLLABORATION OF FOUNDRIES

CHIRA Ion, VERDES Bogdan Alexandru

Politehnica University of Bucharest, ROMANIA

ABSTRACT

The Information Society (I.S.) realized the salt from QUALITY stage (TECHNICAL QUALITY CONTROL – T.Q.C.) to the philosophy and the concepts of TOTAL QUALITY (T.Q.) and TOTAL QUALITY MANAGEMENT (T.Q.M.), with all their particularities and technical and economical consequences.

The activities and processes globalization involves new ways to realize and approach the PROMOTION, PARTNERSHIP and COLLABORATION concepts.

On the other hand, the IT&C field (INFORMATION TECHNOLOGY – IT; TELECOMMUNICATIONS - IT&T; COMPUTERS - IT&C) with its software and hardware elements, as fundamental support of the information society has become omnipresent and the INTERNET – a global way to communicate and an infinite data-base.

The current paper plans only to initiate some discussions in this vast area, which is continuing developing as fund and sophisticated in form.

1. INTRODUCTION

In short, is an online strategy to promote websites. More exactly, it is a plan to promote one's website through exclusively online tools, mainly aiming to attract as many new customers, following the strategy: minimum cost - maximum sales profits.

Essential stage of any marketing plan on the Internet is optimization of websites for their identification by search engines, and the insertion of domain and subdomains in web directories.

A modern business, no matter how big or small, is without a marketing plan on the Internet either only a local business or a simple business implemented without much perspective in time and space.

From my own experience, I concluded that any person, activity, achievement, etc., as valuable as it would be in theory, if it is not posted and promoted over the internet, is equivalent with the absence of it. Everything is evaluated and compared with "something", which now the internet makes it accessible to us [2].

For a website to be accessed and seen by as many visitors, it must be designed and implemented a promotion campaign. Neither the best designed website doesn't worth anything, if it isn't brought to the attention of field specialists, the public opinion, which is becoming increasingly informed.

To watch how it is achieved this step can create a database that includes all actions to promote. For instance, for the promotion with the aid of search engines you can create a table includes the following information: name of search engine / directory, date of registration, the time required for registration; keywords used. After you complete the online form registration one must wait several days or several weeks (depending on the chosen search engine) until it is registered.

2. THE STUDY

An organization can absorb information from other organizations that are considered market leaders in this field based on the results achieved, aiming at continuously improve them [3.7].

To achieve this goal can be used benchmarking as a source of acceleration of organization's progress.

The essence of benchmarking is to choose what is best in a business, to adapt what is best from a company and to continuously improve your operations, by appropriate and specific strategies to ensure success.

Benchmarking is a tool used in management quality, appeared in early 1980 and first time was used by the US company Xerox, following the sudden decline of its market share.

As underlined in a report, the Committee on Industrial Productivity in the Institute of Technology in Massachusetts, benchmarking has been in recent years, an essential factor for success of the biggest known organizations in all areas of the economy.

Currently, the rapid development of the benchmarking lead to including it in the tools to improve the quality standard "ISO 9004-4: Quality management and quality system elements - Part 4. Guidelines for the increase of quality."

Specialists have brought a relatively high number of definitions of the new tool used in quality management and marketing. Among the most significant set of definitions are the following:

- ✚ In business, benchmarking is a process in which a company compares its products and methods with those of the most successful companies in its field, in order to try to improve its own performance;
- ✚ Benchmarking is the process of comparing the cost, time or quality of what one organization does against what another organization does. The result is often a business case for making changes in order to make improvements;
- ✚ Also referred to as "best practice benchmarking" or "process benchmarking", it is a process used in management and particularly strategic management, in which organizations evaluate various aspects of their processes in relation to best practice, usually within their own sector. This then allows organizations to develop plans on how to make improvements or adopt best practice, usually with the aim of increasing some aspect of performance. Benchmarking may be a one-off event, but is often treated as a continuous process in which organizations continually seek to challenge their practices;
- ✚ Benchmarking is the process of identifying, understanding and adopting the methods and processes of any outstanding world organization, in order to increase the organization's performance (the American Center for Quality and Productivity);
- ✚ Benchmarking represents the research of the best processes, procedures or results relevant to achieve the business targets. Therefore, the goal is to learn to improve ones performance (D.T. Kearns – Xerox GM);

In 2008, a comprehensive survey on benchmarking was commissioned by the Global Benchmarking Network (a network of benchmarking centers representing 22 countries - and for which the founder of benchmarking, Dr Robert Camp, is the honorary president). Over 450 organizations responded from over 40 countries. The results showed that:

1. Mission and Vision Statements and Customer (Client) Surveys are the most used (by 77 % of organizations) of 20 improvement tools, followed by Strengths, Weaknesses, Opportunities, and Threats SWOT (72 %), and Informal Benchmarking (68 %). Performance Benchmarking was used by (49 %) and Best Practice Benchmarking by (39 %);
2. The tools that are likely to increase in popularity the most over the next three years are Performance Benchmarking, Informal Benchmarking, SWOT, and Best Practice Benchmarking. Over 60 % of organizations that are not currently using these tools indicated they are likely to use them in the next three years;
3. When Best Practice Benchmarking is done well significant benefits are obtained with 20 % of projects resulting in benefits worth US\$ 250,000.

4. ANALISES, DISCUSSIONS, APPROACHES, INTERPRETATIONS

- ✚ Process benchmarking - the initiating firm focuses its observation and investigation of business processes with a goal of identifying and observing the best practices from one or more benchmark firms. Activity analysis will be required where the objective is to benchmark cost and efficiency; increasingly applied to back-office processes where outsourcing may be a consideration.
- ✚ Financial benchmarking - performing a financial analysis and comparing the results in an effort to assess your overall competitiveness.
- ✚ Performance benchmarking - allows the initiator firm to assess their competitive position by comparing products and services with those of target firms.
- ✚ Product benchmarking - the process of designing new products or upgrades to current ones. This process can sometimes involve reverse engineering which is taking apart competitors products to find strengths and weaknesses.
- ✚ Strategic benchmarking - involves observing how others compete. This type is usually not industry specific meaning it is best to look at other industries.
- ✚ Functional benchmarking - a company will focus its benchmarking on a single function in order to improve the operation of that particular function. Complex functions such as Human Resources, Finance and Accounting and Information and Communication Technology are unlikely to be directly comparable in cost and efficiency terms and may need to be disaggregated into processes to make valid comparison.

For a department, industry, foundry in Romania or for an European regional cooperation can use concepts such as:

- ✚ "Horizontal benchmarking" - aimed at identifying best practices in the function of processes in referential organizations that are recognized as market leaders, but are not direct competitors of the organization conducting the benchmarking;
- ✚ "External benchmarking" - is similar to the horizontal one, but aimed directly competing organizations (in the same activity area);
- ✚ "Functional benchmarking" - aimed at comparing the functions of the organization conducting the benchmarking with a similar function in a given referential profitable organization;
- ✚ "Internal benchmarking" - aimed to analysis comparatively the processes of two departments of the same organization (one of them being considered as reference) [4.5].

There is no single benchmarking process that has been universally adopted. The wide appeal and acceptance of benchmarking has led to various benchmarking methodologies emerging. The most prominent methodology is the 12 stage methodology by Robert Camp (who wrote the first book on benchmarking in 1989): 1. Select subject ahead; 2. Define the process; 3. Identify potential partners; 4. Identify data sources; 5. Collect data and select partners; 6. Determine the gap; 7. Establish process differences; 8. Target future performance; 9. Communicate; 10. Adjust goal; 11. Implement; 12. Review / recalibrate. There are organizations which use other benchmarks models tailored to their needs (see fig. 1) [7]:

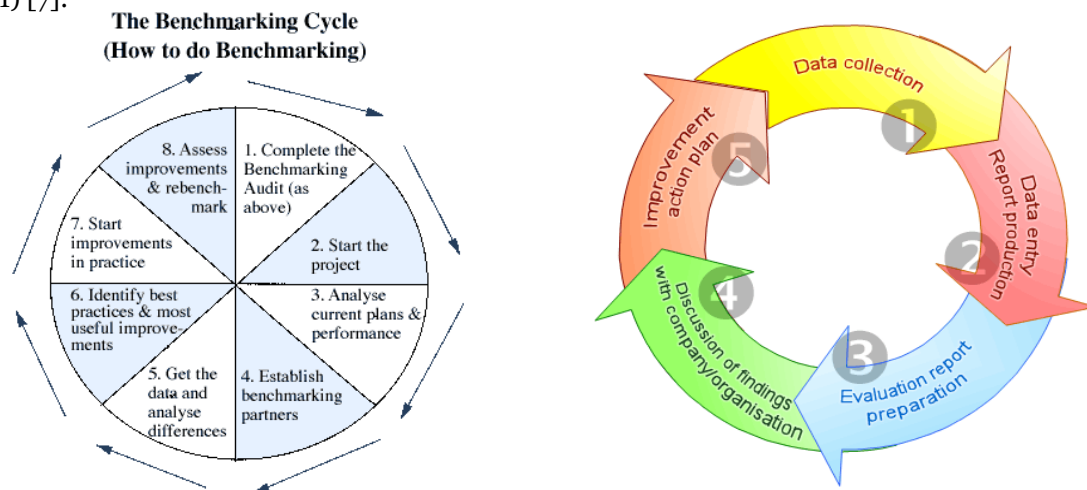


Fig. 1 Different benchmarking models

The following is an example of a typical shorter version of the methodology:

1. Identify your problem areas - Because benchmarking can be applied to any business process or function, a range of research techniques may be required. They include: informal conversations with customers, employees, or suppliers; exploratory research techniques such as focus groups; or in-depth marketing research, quantitative research, surveys, questionnaires, re-engineering analysis, process mapping, quality control variance reports, or financial ratio analysis. Before embarking on comparison with other organizations it is essential that you know your own organization's function, processes; base lining performance provides a point against which improvement effort can be measured.
2. Identify other industries that have similar processes - For instance if one were interested in improving hand offs in addiction treatment he/she would try to identify other fields that also have hand off challenges. These could include air traffic control, cell phone switching between towers, transfer of patients from surgery to recovery rooms.
3. Identify organizations that are leaders in these areas - Look for the very best in any industry and in any country. Consult customers, suppliers, financial analysts, trade associations, and magazines to determine which companies are worthy of study.
4. Survey companies for measures and practices - Companies target specific business processes using detailed surveys of measures and practices used to identify business process alternatives and leading companies. Surveys are typically masked to protect confidential data by neutral associations and consultants.
5. Visit the „best practice” companies to identify leading edge practices - Companies typically agree to mutually exchange information beneficial to all parties in a benchmarking group and share the results within the group.

6. Implement new and improved business practices - Take the leading edge practices and develop implementation plans which include identification of specific opportunities, funding the project and selling the ideas to the organization for the purpose of gaining demonstrated value from the process.

The technique initially used to compare existing corporate strategies with a view to achieving the best possible performance in new situations (see above), has recently been extended to the comparison of technical products. This process is usually referred to as „Technical Benchmarking” or „Product Benchmarking”. Its use is particularly well developed within the automotive industry („Automotive Benchmarking”), where it is vital to design products that match precise user expectations, at minimum possible cost, by applying the best technologies available worldwide.

Many data are obtained by fully disassembling existing cars and their systems. Such analyses were initially carried out in-house by car makers and their suppliers. However, as they are expensive, they are increasingly outsourced to companies specialized in this area. Indeed, outsourcing has enabled a drastic decrease in costs for each company (by cost sharing) and the development of very efficient tools (standards, software).

Since the new trend in benchmarking practice establishes a partnership between organizations, before any activity, they are obliged to sign a statement by which each party undertakes to comply with the Code of Conduct for the benchmarking practice.

In the U.S., members of the American Center for Quality and Productivity (APOQ) must, if they practice benchmarking in partnership, apply 8 principles of the Code created by this institution (see tab. 1) [7.8].

Another approach to making comparisons involves using more aggregative cost or production information to identify strong and weak performing units. The two most common forms of quantitative analysis used in metric benchmarking are data envelope analysis (DEA) and regression analysis (RA).

DEA estimates the cost level an efficient firm should be able to achieve in a particular market. In infrastructure regulation, DEA can be used to reward companies/operators whose costs are near the efficient frontier with additional profits.

Table 1 Principles of A.P.O.Q. code in the benchmark partnership

PRINCIPLE	RECOMANDATIONS
1. Legality principle	<ul style="list-style-type: none"> • There is no discussion about costs • One mustn't offer data and studies to other companies
2. Mutual exchange principle	<ul style="list-style-type: none"> • The same kind of information is exchanged between partners • All communication channels between partners are active
3. Confidentiality principle	<ul style="list-style-type: none"> • It is forbidden to trade information with others without the partner's consent
4. Using principle	<ul style="list-style-type: none"> • The obtained information can be used only in the initial purpose established between partners
5. Contacting principle	<ul style="list-style-type: none"> • Must be respected the partner's company structure • There will be contacted only the persons indicated by the partner • Must be established communication procedures and responsibilities • The names of the contact persons will be used, no matter the situation, only with their approval
6. Activity preparation principle	<ul style="list-style-type: none"> • Must be set priorities in the initial contact with the partner • Must be prepared carefully the information exchange between partners • Mutual establishing of the activities and visits calendar
7. The continuous improvement of the activity principle	<ul style="list-style-type: none"> • Following-up the manner in which is respected the activities calendar previously established • Continuous recording of feed-back
8. The principle of establishing mutual relations with the partner	<ul style="list-style-type: none"> • Delivery of information in the form and manner requested by the partner

RA estimates what the average firm should be able to achieve. With regression analysis firms that performed better than average can be rewarded while firms that performed worse than average can be penalized. Such benchmarking studies are used to create yardstick comparisons, allowing outsiders to evaluate the performance of operators in an industry. A variety of advanced statistical techniques, including stochastic frontier analysis, have been utilized to identify high performers and weak performers in a number of industries

The London Benchmarking Group (LBG) is a group of over 100 companies working together to measure Corporate Community Investment (CCI).

It is a member-driven organization where companies have been working collectively since 1994 to:

- ✚ Continue development of a global measurement standard - the LBG model;
- ✚ Benchmark and share best practice;
- ✚ Develop and refine measurement tools;
- ✚ Improve management and implementation of CCI projects;
- ✚ Better communicate CCI results to stakeholders with LBG centers;

The model is used by hundreds of leading businesses around the world and LBG has centers in a number of key world markets including Australia, Canada, the Czech Republic, Germany and the US. Members include multinationals such as HSBC, Vodafone and Unilever, as well as major UK companies such as Marks and Spencer and BSKyB.

The LBG model provides a comprehensive and consistent set of measures for CCI professionals to determine their company's contribution to the community, including cash, time and in-kind donations, as well as management costs. The model also captures the outputs and longer-term impacts of CCI projects on society and the business itself.

Starting with September 2008, London Benchmarking Group (LBG) has a local branch. The organization provides to its members the LBG Model, a tool for collecting and analyzing data, related to programs. The Association for *Community* Relations (ARC) is the only organization in Romania authorized to manage the LBG model.

For our country it is mandatory to create a benchmarking network in order to use strategic, performance and process benchmarking to support economic reform, commerce for small and medium Enterprises, as Foundries for instance.

What is evident in the production - optimization of the capacity and reduced production costs - can be done successfully and in services. With the design of the Horvath & Partners program to improve the performance of services, indirect costs may be deducted up to 40 %. In light of the current situation and the location chosen for the deployment of services [8]; to be consulted as well the web page <http://www.horvath-partners.com>.

How can be optimized accounting services, human resources, IT, procurement and facility management? In a first of the services of a company does not appear to fall within the scope of optimization. There is no benchmarking of the „market price” and last but not least, domestic suppliers companies have a real monopoly. However: the implementation of a program to improve the performance of services in certain trees, not only for the purpose of lowering indirect costs - which make it possible depreciation costs of implementation in a very short time, but for better control of costs and greater transparency. Initiative is such a culture of service, bureaucratic structures are replaced with partnerships based on value creation and ensure a standardization processes and systems in the company.

A positive aid for promoting national and foundries business partnership and collaboration was produced by the appearance of the Technical Association of Romanian Foundries (ATTR) and by the profile publication Casting Magazine (RT).

For example in April, May, July and October 2007 were sent questionnaires towards 192 companies from national castings industry for the purpose of drawing up the analysis of production of castings in 2006, unfortunately to this project replied only 121 firms (see tab. 2) [1].

4. CONCLUSIONS

We suggest creating a portal about foundries – the casting of foundered products and a discussion topic for the forum on the opportunity and ways of:

- ✚ initiating benchmarking program for each company / foundry; - forming a national network of benchmarks in this area; - the training of specialists in initiating, conducting, developing and implementing benchmarking projects;
- ✚ identifying the areas of interest and developing a database; - affiliation with European and international benchmarking networks; - organizing international symposiums with international participation; - supporting publishing books, magazines, articles with this theme.

Table 2 Summary of the national production of castings in 2006

PARAMETER	COMPANY	RANKING
1 – Total Production, t	- position 1 / SATURN S.A. Alba Iulia = 15,170.00	
	- position 121 / FORJA Cugir SRL = 6.20	
2 – Cast iron products, t	- position 1 / SATURN S.A. Alba Iulia = 15,170.00	
	- position 72 / FORJA Cugir SRL = 1.50	
3 – Steel products, t	- position 1 / DOOSAN – IMGB S.A. Bucuresti = 4,750.00	
	- position 54 / MECANEX S.A. Botosani = 3.50	
4 – Non-ferrous alloys products, t	- position 1 / PIERREPI PRESSOFUSIONI Bucuresti = 7,686.00	
	- position 84 / ARIS S.A. Arad = 0.51	

The expected results and the estimated effects are: - promoting the concept, techniques and tools of benchmarking in Romania and creating a portal on the Internet in the mentioned field; - forming benchmarking organizations and benchmarking network; - offering a new benchmarking service to SMEs, such as and other governmental or nongovernmental organizations; - creating the premises of continuously improving the performance by identifying and implementing the best technologies and processes for casting, along with the consolidation of a market-specific sales and marketing activities of castings.

These data, and each site / web page of a company represents a database with known valences and opportunities.

The mutual beneficial exchange of technical information and documents of the type of technologies and processes for casting, sales opportunities and sales (raw materials, metal and nonmetallic materials ancillary foundry, SDV technologies, equipment technology, casting), can be achieved by the methodology "SHARED", specify the exchange of multimedia on the Internet (and audio products, video), process the day to day, take a scale difficult to impossible to forecast and counting.

"SHARED" is the past and / or past part. Of the "share" noun with the meaning of: part, quota, exchange (give and receive something else similar).

Intransitive verb has the meaning of: "a share, to take part, to participate". In English, in this sense, are usually present the expressions: "to share in, to share out, a share in doing something, Founder's share, share in profits, to pay one's share, to share something with somebody."

Currently, the Internet with such specialized web-pages regarding local or worldwide foundries, keeps a constant discussion in shared regime. Thru these web-pages and by a good benchmark policy lead to effective promoting, partnerships and collaboration activities between national foundries and the ones from neighbor countries: West – Hungary, Serbia, South – Bulgaria, Turkey, and East – Republica Moldova, Ukraine and Russia.

REFERENCES

- [1.] BĂCANU I. A. – Producția de piese turnate a României în anul 2006. În: Revista de Turnătorie, nr. 11, 2007, p. 8 - 16.
- [2.] CHIRA I. - Calitatea pieselor turnate. Curs universitar pe suport magnetic – CD (pentru realizarea paginii web; 76 p.; Format jpg/MFP7.0/r14). Edit. Samizdat, București, 2006.
- [3.] CHIRA I. - Fundamentele universitarului. Elaborarea lucrărilor științifice. Edit. Nawa, București, 1999, 412 p., (ISBN 973-99080-4-2).
- [4.] CHIRA I. - Managementul calității. Curs universitar pe suport magnetic – CD. Edit. Samizdat, București, 2005.
- [5.] CHIRA I. - Managementul calității totale. Curs universitar pe suport magnetic – CD (pentru realizarea paginii web; 54 p.; Format jpg/MFP7.0/r14). Edit. Samizdat, București, 2006.
- [6.] CHIRA I. și IONIȚĂ Gh. - Fundamentele inginerului metalurg - turnător. Calitatea pieselor turnate. Edit. Științifică „Fundația Metalurgia Română”, București, 1998, 408 p., (ISBN 973-98904-0-7).
- [7.] EVANS R. J. - The management and Control of Quality. Edit. West Publishing Company, U.S.A., 1996.
- [8.] HORVATH & Partners - Controlling. Sisteme eficiente de creștere a performanței firmei. Edit. CH Beck, 2007, (ISBN 978-973-115-115-1).



ANALYSIS OF THE TECHNOLOGY OF STEEL ELABORATION *T 35 Mn 14* INTENDED FOR CASTING THE PIECES

Ana JOSAN, Vasile PUȚAN, Sorin RAȚIU

„Politehnica” University of Timișoara, Engineering Faculty of Hunedoara, ROMÂNIA

Abstract:

In this work it is made a critical analysis of the technology of elaboration of the alloy intended for the obtainment of *Driving spindle wheel*, respectively slightly allied steel *T35Mn14*. There are presented the two types of charges used for the elaboration of steel, respectively the chemical compositions of the charges elaborated. With the help of these data there are made a series of correlations in order to emphasize the variation of the contents of the elements for the 14 bathes elaborated and studied.

Keywords:

slightly allied steel, casting pieces, metallic charge, chemical composition

1. INTRODUCTION

Steel *T 35 Mn 14* is part of the category of slightly allied steels. The slightly allied steel contain the main alloy element below 2% and the sum of all the alloy elements does not exceed 5%. The slightly allied steel s are part of the perlitic class [1,3].

The chemical composition of steel *T 35 Mn 14*, as per STAS 1773-76 is presented in table 1.

Table 1. The chemical composition of steel T 35 Mn 14 [STAS 1773-76].

Steel mark	Chemical composition, %					
	C	Mn	Si	P max.	S max.	Cr
T 35 Mn 14	0,33...0,38	1,30...1,50	0,30...0,50	0,035	0,035	0,50...0,70

The mechanical characteristics of steel T 35 Mn 14 are presented in table 2.

Table 2. The mechanical characteristics of steel T 35 Mn 14 [STAS 1773-76].

Steel mark	Mechanical characteristics				
	Flow limit, $R_{p0,2}$ N/mm ²	Traction resistance, R_m N/mm ²	Extension at breakage, A %	Swage at breakage Z, %	Hardness, HB
T 35 Mn 14	295	540...780	12	25	160

2. ANALYSIS OF THE CHARGES ELABORATED IN VIEW OF CASTING THE PIECE ANALYSED

The elaboration of the slightly allied steel *T 35 Mn 14*, out of which it is made the *Driving spindle wheel* is made in electric furnace of the type DSN-3, with basic casing, with a nominal capacity of 3000 kg.

For the elaboration of the batches intended for casting these pieces there have been used charges of the type [3]:

A). Type I:

- Scrap iron

- Proper waste, respectively lost heads, casting networks etc. charged from the steel cast pieces T 35 Mn 14
- Scrap cast iron

B). Type II:

- Scrap iron
- Proper waste, respectively lost heads, casting networks etc. charged from the steel cast pieces T 35 Mn 14

For the alloy there are used:

- FeSi 66...50
- FeMn 75 or 79
- Gross electrodes
- CaF₂

In table 3 there are presented the chemical compositions and the casting temperatures for 14 charges elaborated made of steel *T 35 Mn 14*, out of which there have been cast the pieces studies, respectively *driving spindle wheel*.

Table 3. The chemical compositions for charges elaborated

No.	No. charge	Chemical composition, in %						Evacuation temperature, °C
		C	Mn	Si	P	S	Cr	
1	6423	0,35	1,33	0,59	0,069	0,028	0,68	1580
2	6424	0,31	1,5	0,32	0,055	0,033	0,51	1610
3	6425	0,36	1,3	0,3	0,059	0,035	0,52	1585
4	6427	0,36	1,5	0,59	0,061	0,034	0,74	1580
5	6428	0,33	1,32	0,38	0,045	0,035	0,5	1610
6	6430	0,36	1,44	0,23	0,045	0,029	0,63	1615
7	6435	0,3	1,6	0,27	0,068	0,035	0,7	1610
8	6438	0,34	1,3	0,49	0,054	0,036	0,69	1610
9	6439	0,35	1,46	0,4	0,045	0,034	0,7	1585
10	6441	0,32	1,29	0,42	0,059	0,035	0,62	1610
11	6442	0,35	1,37	0,28	0,056	0,03	0,63	1590
12	6455	0,34	1,17	0,53	0,03	0,037	0,37	1600
13	6456	0,34	1,5	0,38	0,033	0,035	0,55	1590
14	6459	0,33	1,25	0,41	0,04	0,033	0,52	1600

3. CONCLSIONS

With the help of the data presented in table 3, there have been made a series of correlations in order to emphasize the variation of the contents of the elements for the 14 bathes elaborated and studied.

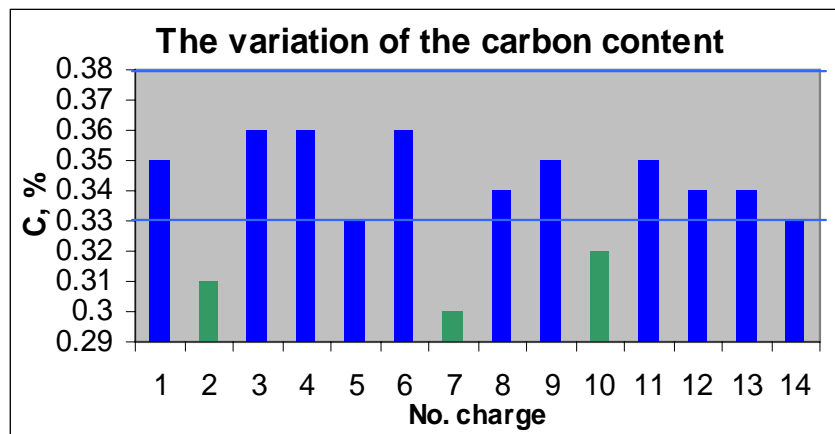


Figure 1. The histogram of the variation of the carbon content of the charges elaborated

Thus, in figure 1 it is presented the variation of the carbon content for the charges elaborated. From the analysis of this histogram there can be noticed that only three charges (6424, 6435, 6441) have a carbon content below the limit provided in the STAS, the other three charges having a carbon content lower than 0,33%.

Similarly, there are executed, with the help of the program EXCEL, the histograms for the contents of manganese and chrome. They are presented in fig. 2, 3.

It results the following:

- ✚ the manganese content, for the charge nr.6430, exceeds the value provided in STAS, and charges 6455 and 6459 have a manganese content below the limit allowed;
- ✚ the chrome content is lower for charge 6456 only.

In figure 4 there is presented the histogram of the casting temperatures registered. There can be noticed that the casting temperatures are contained in the interval 1585-1615 °C. Most of the values are registered in the interval 1605-1615°C.

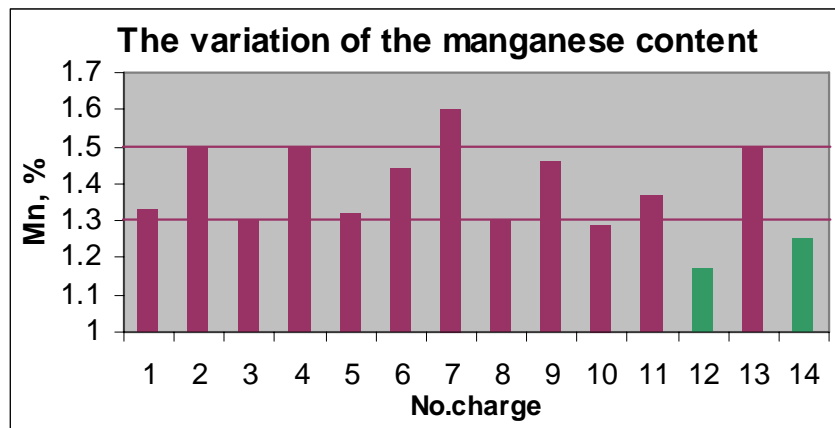


Figure 2. The histogram of the variation of the manganese content of the charges elaborated.

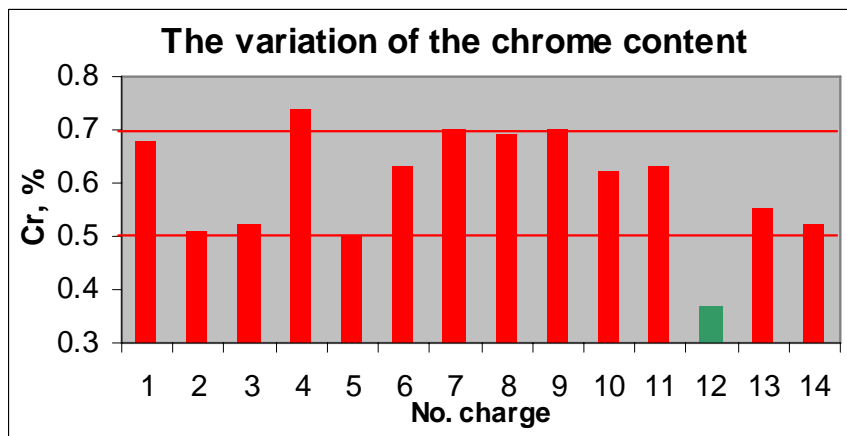


Figure 3. The histogram of the variation of the chrome content of the charges elaborated

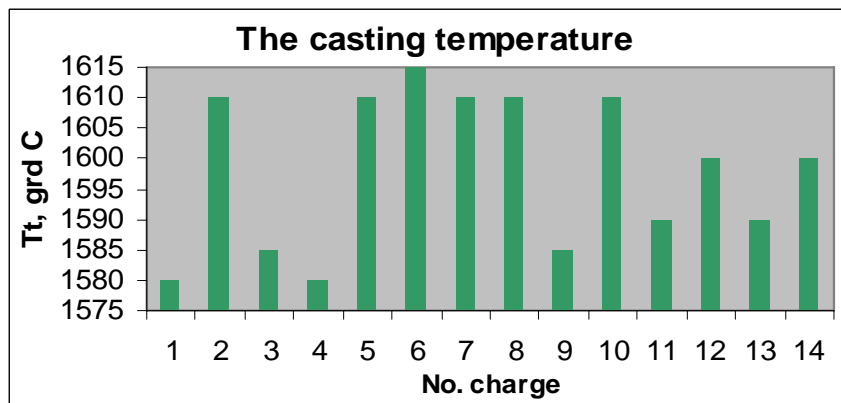


Figure 4. The histogram of the variation of the casting temperatures of the charges elaborated

In general, the elaboration of steel *T35Mn14*, intended for casting the studied piece within a metallurgical enterprise does not raise particular problems, but there must be made a critical control of the process of elaboration of the alloy in view of obtaining quality castings.

REFERENCES:

- [1] Cheșa, I. ș.a., Alegerea și utilizarea oțelurilor, Ed. Tehnică, București, 1984
- [2] Socalici, A., Ardelean, E., Ardelean, M., Hepuț, T., Josan, A., Turnarea și solidificarea oțelului, Ed. CERMI Iași, 2007
- [3] Ștefănescu, Cl. ș.a., Tehnologii de executare a pieselor prin turnare, Ed. Tehnică, 1980



MATHEMATICAL MODELLING OF THERMAL STRATIFICATION PHENOMENA IN STEEL LADLES

Vasile PUTAN, Ana JOSAN, Lucia VILCEANU

“POLITEHNICA” University of Timisoara, Faculty of Engineering – Hunedoara, ROMANIA

Abstract

This paper presents a three-dimensional numerical model simulating fluid flow and heat transfer in 105 t steel ladles before and during the casting process. The model was developed by combined implementation of a numerical simulation package, TEMPSIM, and a computational fluid dynamics (CFD), simulation package, ADINA (Automatic Dynamic Incremental Nonlinear Analysis). In this study, TEMPSIM was used to calculate the heat transfer in ladle linings and predict the heat losses from the steel melt to the linings. These data were used as input into ADINA for 3-D CFD modeling of fluid flow and heat transfer.

Key Words:

Model, numerical simulation, CFD, steel ladle, fluid flow, heat transfer, stratification.

1. INTRODUCTION

The melt stratification phenomenon, which results from the natural convection in ladles holding molten steel, is of fundamental importance for the temperature control in continuous casting process. The progressively increasing stress on the quality of continuously cast products necessitates much tighter tundish temperature control, which in turn will require a more precise definition of the extent of melt temperature stratification in ladle.

According to the data to be found in the reference literature, the hydrodynamics of the fluid alloy in the casting ladle during the casting process has been studied by means of 2-D, symmetric - axial simulations of a ladle with the central tapping [3] and by means of 3-D symmetric - axial simulations of an eccentric tapping ladle [4]. The results of such simulations have been compared to those obtained by means of physical models using water [7], or by temperature measurements [1, 2, 3, 5].

The objective of the present study is to establish, under more precisely defined conditions, a 3-D CFD model for simulating stratification and fluid flow in steel ladles during both the holding period and the casting period. The transient and ladle configuration dependent heat losses from steel ladle linings were more accurately predicted by using a numerical simulation package, TEMPSIM. These data were used as boundary conditions for further simulation on the fluid flow and heat transfer, by using a commercial CFD simulation package, ADINA.

2. SIMULATIONS CONDITIONS

Considering these aspects, we simulated the hydrodynamics of the fluid alloy in the 105-t ladle used by S.C. Mittal Steel S.A. Hunedoara, before and during the casting process by means of CFD-3D model. This is also due to the fact that the ladle, whose configuration and geometrical dimensions are given in figure 1, has an eccentric tapping.

At first, a geometrical sketch of the ladle was made (fig.2), starting from the configuration and geometrical dimensions of the industrial casting ladle (fig.1). As it can be noticed, in order to simplify the modeling, we neglected the fact that the ladle has a conical shape, it being considered cylindrical.

In order to achieve a closest simulation of the hydrodynamics and temperature of the fluid alloy in the ladle during tapping, we considered it necessary to take into consideration the fact that the metal bath in the ladle is thermally stratified at the moment of tapping. The consideration given above is mandatory, as in the secondary refining station (LF), the metal bath is homogeneous from the thermal point of view, but during the ladle transportation from the LF station to the tundish a thermal stratification of the metal bath takes place because of natural convection.

Considering this, the simulation will be done in two stages: the first will simulate the 10 minute-station of the ladle, when the metal bath will be thermally stratified, and the second will simulate the ladle emptying during the casting process.

The emptying stage also involves two periods:

- ❑ the first period, which lasts about 3 minutes, represents the filling of the 15-t tundish;
- ❑ the second period, which lasts about 40 minutes, corresponds to the normal casting rate.

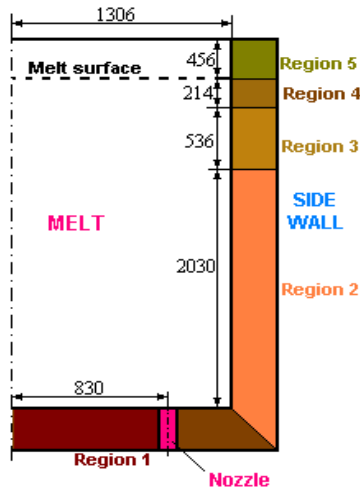


Fig.2. The geometry of the ladle used in the CFD-3D simulation

According to the reference information and also considering the practice of continuous casting (TC) at S.C. Mittal Steel S.A. Hunedoara, in the simulations we considered constant casting flow rates of 77,8 kg/s for the first period of emptying, respectively 36,1 kg/s for the second period.

Using two custom softwares, we simulated the hydrodynamics and the temperature of the fluid alloy in the ladle during the period of its emptying.

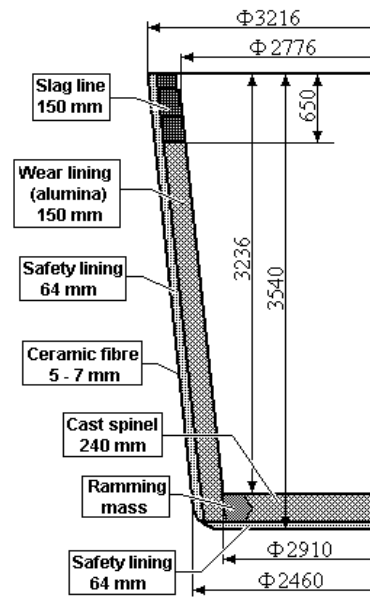


Fig.1. Geometric dimensions and configuration of the refractory masonry of the ladle under study

3. RESULTS OF NUMERICAL SIMULATIONS

After having simulated the thermal stratification of the metal bath, for a 10-minute period of stationing, we obtained the rate field (fig.3) and the distribution of temperature (fig.4). These data shall be further used as initial conditions in the stage of ladle emptying. In order to better emphasize the temperature differences arising in the thermally stratified metal bath, because of the phenomenon of thermal convection, we gave the distribution of temperature field for different planes of the field of analysis (fig.5). Further on, we gave the results of the simulations after 10, 25, and 39 minutes from the opening of the tap.

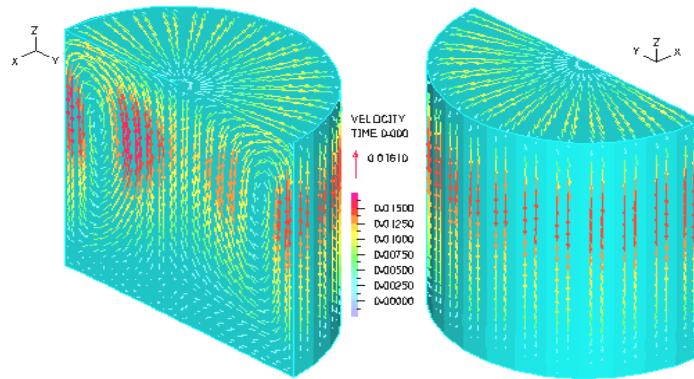


Fig.3. The rate field after 10 minutes of thermal stratification simulation

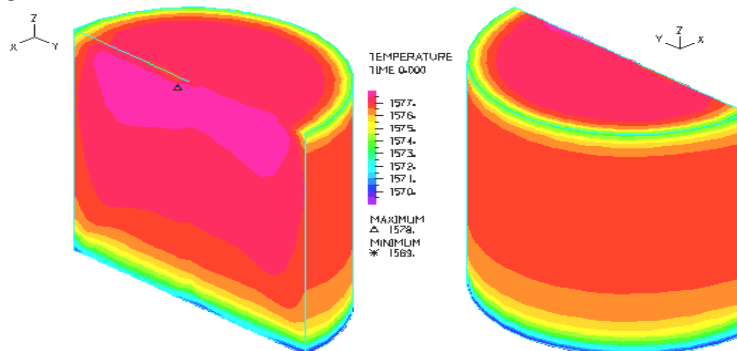


Fig.4. The rate field after 10 minutes of thermal stratification simulation

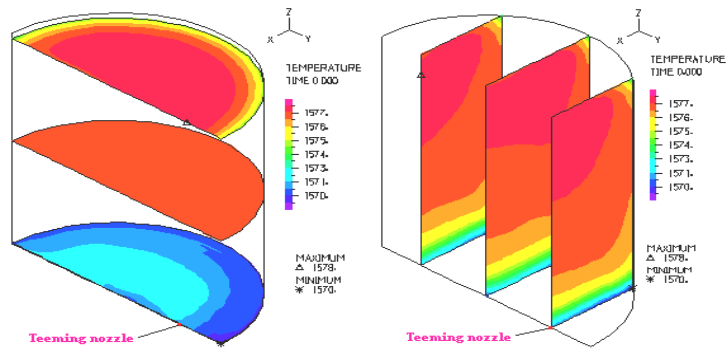


Fig.5. The temperature of the metal bath in different horizontal and vertical planes, after 10 minutes of thermal stratification

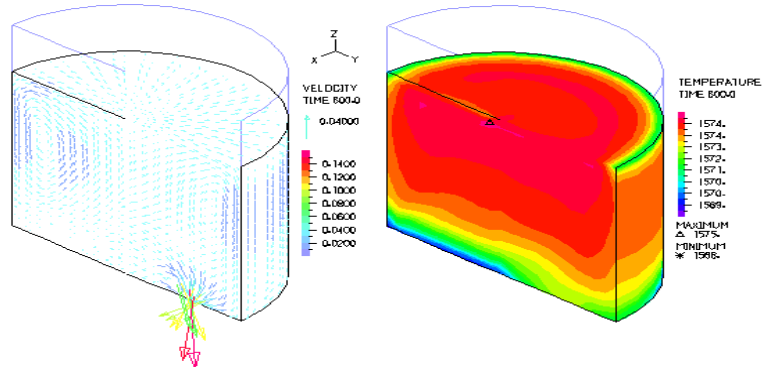


Fig.6. The field of rates and temperatures of the metal bath after 10 minutes from the opening of the tap.

4. ANALYSIS OF THE SIMULATION RESULTS

Figure 6 gives the field of rates and the distribution of temperature in the metal bath after 10 minutes from the opening of the tap. One can notice that the movement of the alloy in the ladle is further due to the phenomenon of natural convection, the rate field having the same profile as in the initial stage (fig.3).

Continuing the analysis of the rate field evolution, one can notice that it starts being influenced increasingly by the fact that a movement of the alloy arises from its flowing out through the tap. After about 25 minutes from the opening of the tap (fig.7), this movement starts to prevail over the one due to natural convection.

This tendency is also revealed by the evolution of the temperature field inside the metal bath. Thus, at the beginning of tapping, the phenomenon of thermal stratification is still present because the metal bath keeps losing heat to the environment and natural convection is still present. In the latter half of the tapping period (after about 25 minutes from the opening of the tap), because of the low level of the metal bath in the ladle, the heat lost to the exterior is diminished and the phenomenon of thermal stratification comes to an end. At the same time, the movement of the fluid alloy through the tap determines the mixing of the metal bath, which leads to diminishing the thermal stratification already existent.

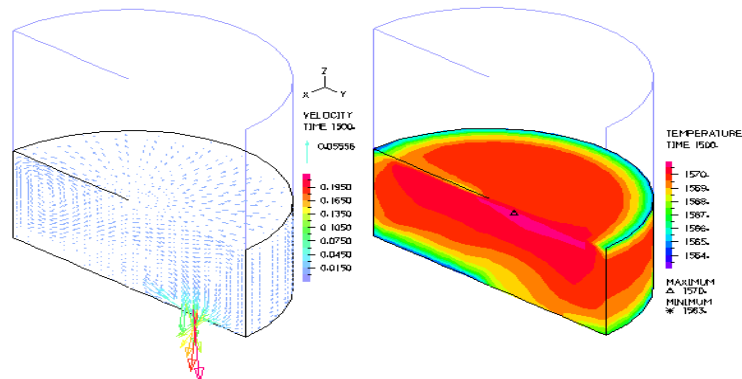


Fig.7. The field of rates and temperatures of the metal bath after 25 minutes from the opening of the tap

One very important result to be noticed when simulating the hydrodynamics and temperature of the fluid alloy from the ladle during its emptying is the fact that we know the temperature of the fluid alloy at the knots of the domain of analysis, corresponding to the entrance of the ladle tap. Taking into consideration the fact that, on leaving the tap, the alloy flows through a protection ceramic tube, up to the tundish of the continuous casting machine, and the loss of heat to the walls of this ceramic tube is very low (corresponding to a decrease of under 0,1 °C of the temperature of the fluid alloy [6]), we can consider that this is the temperature at which the fluid alloy enters the tundish and we shall further call it *the temperature of the alloy flow*.

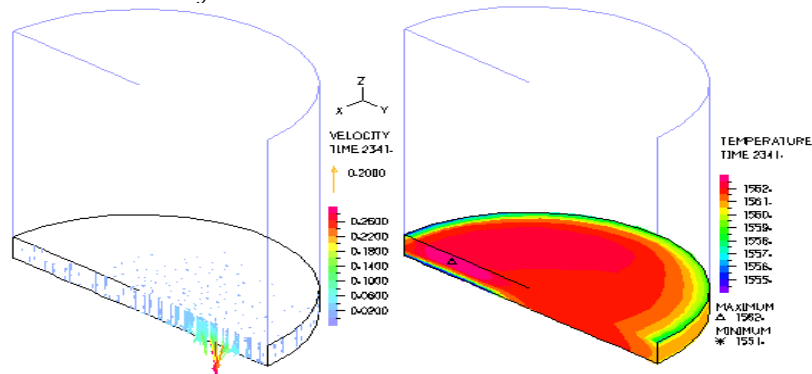


Fig.8. The field of rates and temperatures of the metal bath after 39 minutes from the opening of the tap.

5. CONCLUSIONS

The results obtained by modeling and simulating the hydrodynamics and temperature of the fluid alloy in the ladle during its emptying stage can lead to the following conclusions:

- the three-dimensional model developed in order to simulate the phenomena occurring in the ladle before and during its emptying stage is valid if one considers the results obtained. This model has been developed starting from the one-dimensional model of thermal conduction (1-D), which simulates the non-stationary heat transfer through the refractory masonry of the ladle, and also using the CFD-3D model, which simulates both the thermal stratification of the fluid alloy in the ladle during its stationary period and the hydrodynamics and heat transfer occurring in the fluid alloy during the emptying of the ladle.
- at the beginning of the emptying period, the phenomenon of thermal stratification is still present, as the metal bath keeps losing heat to the environment by natural convection. In the second period of emptying (after about 25 minutes from the opening of the tap), because of the fact the level of the metal bath in the ladle is low, the amount of heat lost to the environment diminishes, and the phenomenon of thermal stratification halts. At the same time, the movement of the fluid alloy due to its flowing out through the tap triggers a mixing process of the metal bath, which leads to the diminishing of the existent stratification.
- once we know the variation of the alloy flow temperature into the ladle, we can take technological steps in the sense of increasing, respectively decreasing the temperature inside the tundish in order to range it within the limits required by the continuous casting technology.

BIBLIOGRAPHY

- [1] Ilegbusi, O. J., Szekely, J., *Melt Stratification in Ladles*, Transactions Iron Steel Inst. Jpn., Vol. 27, 1987 p. 563-569.
- [2] Austin, P. R., Camplin, J. M., Herbertson J., Taggart, I. J., *Mathematical Modelling of Thermal Stratification and Drainage of Steel Ladles*, ISIJ Int., Vol. 32, Nr.2, 1992, p. 196-200.
- [3] Chakraborty, S., Sahai, Y., *Effect of Slag Cover on Heat Loss and Liquid Steel Flow in Ladles before and during Teeming to a Continuous Casting Tundish*, Metallurgical Transaction B, Vol. 23B, April, 1992, p. 135-167.
- [4] Grip, C.E., ș.a., *Prediction of Emptying Flows in Ladles and Verification with Data from Trace Element Plant Trials*, ISIJ International, Vol. 37, Nr. 11, 1997, p. 1081-1090.
- [5] Bekele, O., Yahua, P., ș.a., *Numerical Simulation and Industrial Investigation on the Melt Stratification Phenomena in Ladles Holding Molten Steel*, Scandinavian Journal of Metallurgy, Vol.25, 1999, p. 18-26.
- [6] Grip, C.E., Osterberg, A.K., *Prediction Model for Temperature Behavior in a Tundish: a practical Approach Using an Expert System*, SCANINJECT VII Proceedings (Part II), 1995, Lulea, Sueden, p. 147-170



DETERMINATION OF TEMPERATURE VARIATION IN THE METALLIC WALL FORMS AT THE STATIC CASTING OF BIMETALLIC MILLING ROLLS

Gabriela MIHUȚ, Erika POPA

University "Politehnica" Timisoara, Faculty of Engineering Hunedoara, ROMANIA

Abstract:

In the paper it's proposes, in main, to obtain of a model of numerical simulation, valid general and applicable the whole peculiars cases of bimetal casting, model with which help can be studied through the computer, the optimization possibility of flowing working condition of liquid alloy of the distribution of temperatures field, of the liquid phase and contraction during the solidification, with the minimum price (necessary reimbursement of the software and calculus equipment) in very short time etc.

Key words:

bimetal casting, milling rolls, temperature

1. INTRODUCTION

Bimetals cylinders rolling destination are make, in Romania, by casting of a two alloys types into a shape from making (for inferiors axels and maselete) combined with metallic one (for pane), this casting could be made static (S.C. "Cilindrul" S.A. Călan) or dynamic (S:C: Fortus" S.A. Iași).

Static casting presume the casting of an alloy named "primary", alloy whit who it is wanted to obtain of an hard crust, and an alloy named "secondary", who is whicker alloyed and leads to the obtain of a middle and a inferiors axels with mechanical characteristics of an lower resistance, but tenacious. This variant of casting presume more stage: primary alloy casting trough the casting net, until the filling of a certain part of casting shape (over the chill mould level); after this operation, it is stay a time part to realization the hard crust solidification, from the chill mould thru the shape center, next moment a refer to beginning of gradually washing of the middle with secondary alloy, and then the finale stage – continuous washing, until the axels and middle obtaining.

In this paper has as purpose the technology optimization of bimetal casting, in static variant, as a result of economic technical analysis of the current technology from S.C. Cilindrul S.A. Călan, on a 78 cylinders ϕ 750x1740 mm and ϕ 928x3300 mm lot, and also, by originals contributions bringed casting ensemble, by numerical modeled and simulation of the shape filling processes and alloys solidification. In sequel, under surname "*communication vessels system*", it is will be present the purposed bimetal casting technology.

2. STUDIES AND RESEARCHS

The establish of the bimetal casting technology (of a communication vessels), in porous metal consumption reduction and taking out index increasing. The presented proceeding in figure 1 remove the classical method short comings, anterior remembered, by using of un exact quantity of an secondary and primary alloys, realization an hard crust and passing stratum dimension well checked, removing of cracks appearance to warm or/and to could and the cylinder relating, on base internal tension decreasing.

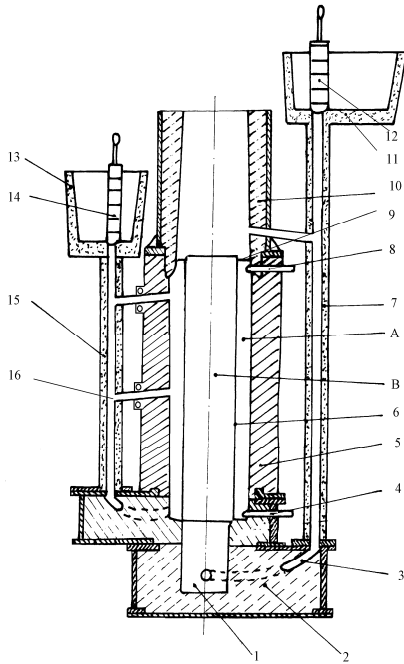


Fig.1. Proceeding and plant for casting of bimetals rolling cylinders, with the possibility of primary alloy casting on ranged net: 1 – inferior axle shape; 2 – inferior frame; 3 – alimentary channel; 4 and 8 – level signaling device; 5 – metallic shape (chill mould); 6 - dissolvable membrane; 7 and 15 the foot of casting net; 9 – membrane supports; 10 – superior frame (for making of superior axle); 11 and 13 – casting reservoir; 12 and 14 - stopper; 16 – the alimentary of ranged net.

The installation for the proceeding realization it is composed from an inferior frame 2, provided with an alimentary channel 3 which is in relation with an alimentary net 7 (in cascade, with two alimentary). This from behind distribute secondary liquid alloy from casting reservoir 11, assured with an stopper 12, which role is to begin and interrupt the shape supply and, also, retain the slag in reservoir 11.

Over inferior axle shape 2 it is set the metallic shape 5, having vertical separation surface to allowed the making out and extract casted raw cylinder. In her interior is dispose cooling membrane dissolvable of cylinder shape 6, which symmetrical axe correspond to with the chill mould one, her role being the one of a separate this space in two compartments: exterior compartment **A** destined primary alloy casting, for making hard crust of the pane, and interior compartment **B** is destined secondary alloy casting, which will make the cylinder middle. Separating membrane is centered at superior part of the chill mould by three supports 9 (manufactured from the same material as the membrane) fixed in shape wall, which have also the role to stop membrane raising during shape alimentation with the two alloy. Separating membrane and fixing supports it is realized from alloys with thermo-physical characteristics of well-determined material, will alled the dissolved during the solidification of two types of pig iron (with which comes in contact), having measured thickness from the condition of thermic balance.

To the inferior part of the chill mould it is dispose a second casting net (in cascade, with three supply, vertically set) mint to the primary alloy casting, adequate dimensioned, from the shape filling condition, in compartments **A** and **B** of the chill mould 5, with the same speed:

$$S_{alloyI} \cong S_{alloyII},$$

in which S_{alloyI} and $S_{alloyII}$ are increasing speeds in the shape of the two alloys, primary and secondary. Casting reservoir 13, with who are connected the net 15, is assured with stopper 14, having the same role as the one in the position 12.

Presented proceeding allowed concomitant casting of the liquid alloys, by different ways, for the liquid alloy, which will make the axles and the cylinder middle, to rise in shape at the same level, with the alloy which will make hard crust or active part of the cylinder.

After the both casting reservoirs are supplied with adequate alloys, at the optimum temperatures of casting, it is rise de stopper 12, beginning filling sequence of the supply net 7 with secondary alloy, followed by the inferior shape filling 1. When liquid alloy touched the inferior level of the cylinder pane, begin also the casting sequence of the primary alloy, by the second net of casting 15. This sequence it is initiated by rising de stopper 14, in the moment of touching realization between the secondary liquid alloy and level signaling device 4.

Departing membrane it is dimensioning in such way the not dissolve her self, on her height, before the chill mould filling with the both liquid alloys. Because of the alloys temperature, still in liquid phase, with which comes in contact, the membrane it is dissolve, taking place a miscibilitate a tho two alloys, realizing the passing zone between the hard crust and the tenacious middle of the cylinder, on a thickness not bigger then 20 ... 40 mm, because of the solidification, in species by meeting of the two crystallization fronts (from the chill mould 5 to the cylinder axe and from the cylinder axe to the cavity periphery **A**).

Next sequence of the proceeding it is refer to the stopping of the primary alloy casting, when this level is in the right of the second signaling device 8, identical from building point of

view with the signaling device 4, established in the superior frame, at the superior quote of the cylinder pane. The casting stopping it is realizes by obturating supplies net 15, by descending of the stopper 14. In this time, the secondary alloy casting continues, until the filling of the superior shape, when it is descending also the stopper 12, and the supply net 7 are so obdurate.

If the alimentation net with primary alloy would have the alimentary disposed ranged, differenced, no in the same vertical plane, the rotation move imparted to the liquid alloy will be accelerated, then eventual impurity attracted in the time of casting processes will be decanted in the exterior stratum of the pane and in the superior part of the cylinder maselot, parts which, any way, are removed by mechanical processing (of the ulterior unthicken).

3. BIDIMENSIONAL NUMERICAL MODEL (WITH FINISHED DIFFERENCES) OF TEMPERATURE VARIATION IN THE METALLIC WALL FORMS OF BIMETAL MILLING ROLLS

It is purpose a model of numerical simulation using the method of finished differences, of the solidification phenomenon of the bimetal cylinders rolling. In this purpose, the analysis field, represented by a continuous medium is transformed in a discontinuous medium (discreet), formed by a points net (discretionary net), of which density is given by the chooses steps for each coordinates axe (fig. 2). The temperature in each knot represents the medium temperature of the knot adjacent surface. In those knots it is written the differential equations of the transforming heat transition in equations with finished differences.

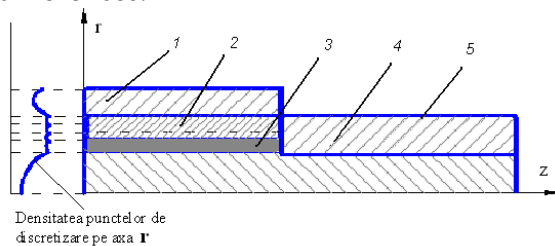


Fig. 2. Quality schem of thermic system used in simulation: 1 – chill mould; 2 – hard crust; 3- cooling membrane; 4 – middle and cylinder axle; 5 – axle shape

Differential equation of the heat transmittion after the three axes has the form:

$$\frac{\partial t}{\partial \tau} = a \cdot \nabla^2 t,$$

where: t - themperatura, [$^{\circ}\text{C}$];

τ - time, [s];

a - thermic difuzivity, [m^2/s];

∇^2 - Laplace operator (laplacian).

The realization of numerical model imposes the establishment of the simplifications ipotesis:

1. It is considering that the system has perfect axial symmetry (after z axe). As a result would not be transmitted heat only radial and vertical.
2. Because the cylinder has a complex shape, this will be simplified, removing the conics and connection rays.
3. It is neglecting the density variation, so of volume of the materials which form the system.
4. The heat transmittion to the chill mould surface and the frames to the ambient medium take place by convection and radium.
5. It is neglecting the heat release by the superior surface of the maselot and the inferior one of the inferior axle frame of the cylinder.
6. The hit transmittions by removing surfaces (middle – membrane – hard crust – chill mould) take place by conduction.
7. The latent heat release of melting. It is make during liquidus – solidus, proportional with the themperature.

4. THE DESCRIPTION AND PROGRAM FUNCTION FOR THERMIC FIELD SIMULATION. THE RESULTS PRESENTATION

The simulation was realized for the casting ansamble (the casting shape and casting raw cylinder), which geometrical dimensions are $\phi 1440 \times 8200$ mm. As the number of discretisation knots are bigger (for the casting shapes, as for the bimetal cylinder), respective enthalpy variation maximum in a smaller iteration, so as the real time of simulation is bigger.

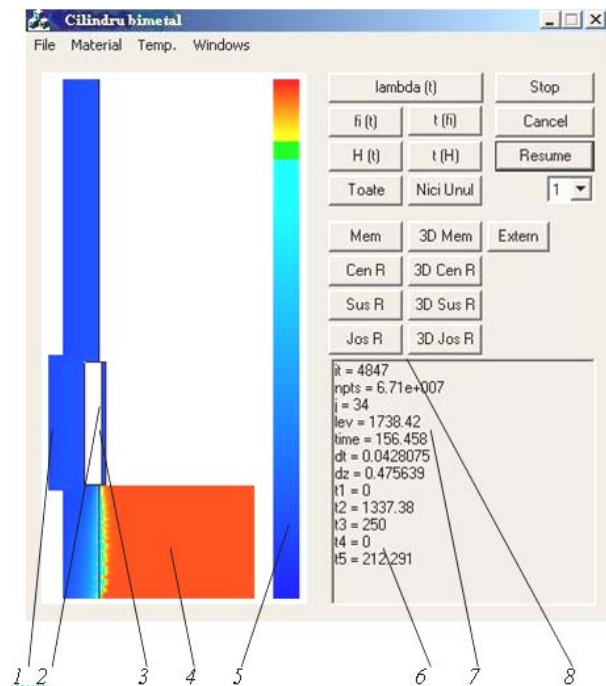
In the case of presented data, de simulation time was of 20 minutes for a real time of flowing process, solidification and cooling of 500 minutes.

The realized program allowds the quality seeing of the thermic field, for differentious time moments, in planes section of the cylinders $\phi 928 \times 3300$ mm, perpendiculars on z axe of the choosen reference system (in cylindrical coordinates). z axe is identical with symmetry axe of the bimetal cylinder, and the section are situated at the differentious heights face to the base plan, with whom those are parallels (for example $z = 0$, the plan is situated at the inferior axle base of the rolling cylinder).

In 1 table are presented the planes quotes of the discretonary net section from numerical model field with finished diferentious, those having correspondent with de planes from real field.

Table 1. The coordinates of sections planes and points in discretonary net

Quote on z axe	Mesuring points from cylinder inside	Mesuring plan from discretonary net inside of cylinder
$z_1=1750$	1 ($r_1=0$; $z_2/2=2675$), placed in cylinder axe	
$z_2=5350$	2 ($r_2=455$; $z_2/2=2675$), placed in cylinder crust	
$z_3=8000$	3 ($r_3=415$; $z_2/2=2675$), placed in membrane	
	4 ($r_4=500$; $z_2/2=2675$), placed to the interface of chill mould - crust	
	5 ($r_5=700$; $z_2/2=2675$), placed to the interface ambient field – chill mould	



In the very next moment, the obtained image allowd the seeing of the discretonary net (fig. 3), of the simulation time and of the temperatures from diferentious zones of bimetal cylinder, as also the level to which are arrived the alloys in shape. The temperatures are showed trough color gradient, with the values: red for casting temperature, blue for ambient thermic temperature and green for their mediate. Any intermediate temperature is a combination of those.

Fig.3. Seeing the simulation steps of the solidification and filling processes of bimetal cylinder: 1 – chill mould; 2- hard crust; 3 – dissolvable cooling membrane; 4 – inferior axle; 6 – touche temperatures in differentious zones of the casting ansamble; 7 – simulated time; 8 – iteration (simulation step).

In 3 figure, the 5 color gradient allows a quality analysis of the solidification in time. So, the coloured zones in red are liquidus, tone in blue are solids, and the zone in green shades show the distribution of biphasic zones (liquid and solid), with other words liquidus – solidus interval.

From 3 figure it is could be observe that at the 4848 iteration (mining 156,458 seconds simulated time) secondary alloy, arrived to the table level. Next step, to 158,08 seconds from the simulation beginning, mentions the beginning of 2 crust alimentation with primary alloy, to the temperatur of $t_4 = 1370^{\circ}\text{C}$ (in figure 3, indication $t_4 = 0$ show that still it is not begin the primary alloy casting).

The membrane temperature is introduced in simulation with initial value $t_3 = 250^{\circ}\text{C}$, so as the one of the chill mould $t_5 = 250^{\circ}\text{C}$. The temperature t_1 is measured to the superior part of the cylinder superior axle, and the indication $t_1 = 0$, from 3 figure, is refers to the fact that, at this moment of simulation, the liquid alloy have not arrived to the respective level.

From the tridimensional representations of the thermic field it is could be made the conexions between the level (z quote) to which had increase the alloys in shape, the temperatures and the simulated time (fig. 4). This imagines tipes are obtained by activating the dialog window Metal3DGraph, or of the butons from main window (3D Cem R etc).

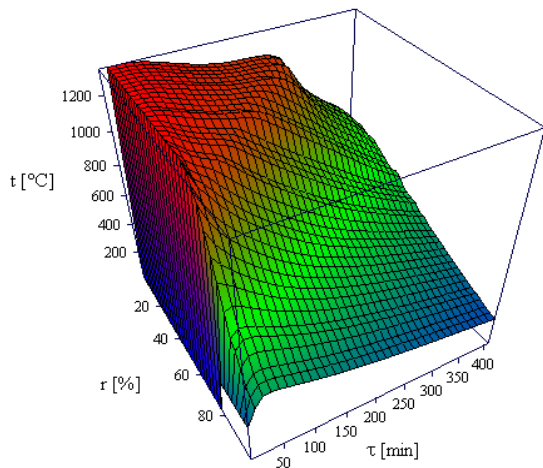


Fig.4. The temperature variation in time, determinated at the quotation $z_2/2 = 2675$, after 400 minutes from the simulation beginning

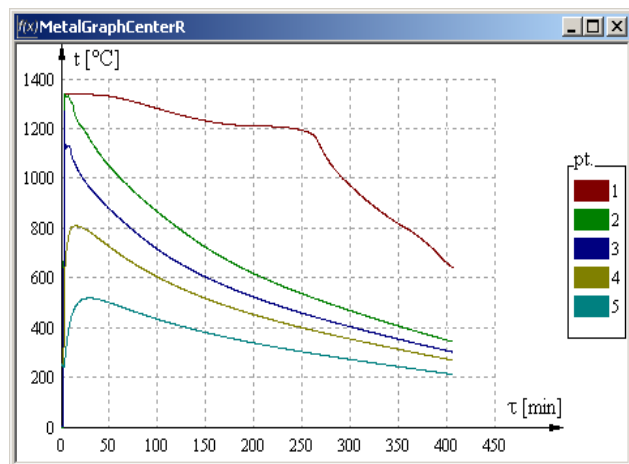


Fig.5. The graphic presentation of temperature evolution at the chill mould middle ($z_2/2 = 2675$), after 400 minutes from the simulation beginning

Observation: The variation graphics of the time, temperature, at the differentious planes of the section in long axes r and z , use the procentual expression of the coordinates.

The evolution in time of the 1, 2, 3, 4 and 5 points themperature (table 1) may be followed by activating the window **MetalGraph**, or directly, pushing the main window buttons (Cen R, Sus R etc), presented in figure 5.

The obtained data can be exported in purpose of their comparison with the obtained values by casuals experimental measures, realized with the helps of immersion thermocouples (plased in points of real field corresponding to the points of definite measure in discretionary net, simulated with the helps of finished differentious method).

5. CONCLUSION

As a result of critical analysis of actual technology of bimetal casting, in static regime, of the big diameters cylinders, destinedated pane rolling, it were proposed three variants (author own conception) of technology improving, final, establishing as optimum the vessels communication, which use a dissolvable micro-cooler membrane and of ranged casting nets. Beginning from filling up principle of the two cavity of chill mould (**A** – destinedated to the tenacious middle obtaining of the cylinder pane and **B** – destinedated the hard crust realization, of equal thickness on pane generatrix) at the same level, on filling up whole way, it was dimensioned casting system, compose from the independent alimentary two nets.

Taking account of micro-cooler effect played by the dissolvable membrane, introduced in chill mould, was effectuated a moulding study of solidification process of bimetal cylinders (casting from A and B fusions), in this ipohesis.

The numerical and analytic moulding of the flowing processes solidification and cooling constitute a base instrument, useful as in conception phase such as in the analysis one of the metallurgical processes, which, combined with computers use, allowds the establish of the optimums regims of those development.

The results and the obtained conclusions after numerical moulding with the help of finite differences method can be extrapolated with a high veracity at the industrial processes which take place at the solidification conduction of bimetal cylinders of big diameters, in porous of their quality improving in exploitation.

In the presented context, one of the main objectives of this thesis (the quality improving of big diameters bimetal cylinders) was realized by solidification research and the links establishment regarding to technologic parameters various (casting temperature, specific consume of micro-coolers and those dimensions) depending on operational variables specific of solidification processes, to determinate the influence modalities of those in view of obtaining of some pieces (bimetals rolling cylinders) of superior quality, reproducibility conditions and maximum economic – technical efficiency.

REFERENCES

- [1] DRAGOTĂ, I., PETREHUȘ, V. – *Metode numerice pentru ecuații diferențiale*, Editura Orizonturi Universitare, Timișoara, 2002
- [2] MINKOWYCS, W.J. – *Advances in Numerical Heat Transfer*, Volume I, Taylor&Francis, 1996
- [3] MIHUȚ, G. - *Studyes and researches on the replacing of carbide rolls for wire rolling with bimettalics rolls*, Simpozionul Internațional Universitaria ROPET 2000, Univ. din Petroșani, pg.165-170
- [4] MIHUȚ, G., PREJBAN, I., MAKSAY, ȘT. - *The influence of the elements C, Cr and Mo upon the hardness of the bimetallic casted iron pig milling rolls*, 7th International Symposium Interdisciplinary Regional Research Hunedoara – 2003, Romania, pg.634-639
- [5] MIHUȚ, G., PREJBAN, I., MAKSAY, ȘT. – *The influence of the alloy elements C, Mo and V over the resistance of steel type 15VmoCr14X*, Zbornik radova sa naucno strucnog skupa istrazivanje i raynoj mašinskih elementa i sistema, Jahorina – Irmes – 2002, pg. 361-366



SOLIDIFICATION AND COOLING PHENOMENON IN THE AREA OF STEEL CONTINUOUS CASTING

Erika Monika POPA, Imre KISS, Gabriela MIHUT

University Politehnica Timisoara, Faculty of Engineering Hunedoara, ROMANIA

Abstract

The mathematical modeling of the solidification and cooling phenomenon of continuously cast semi-products, presented in afterwards, is based on the mathematical description of phenomenon. This solution problem is, practically, the heat solving equation in of non-steady regime. For defined the heat conduction between semi-product and crystallizer is necessary the cognition of initial conditions, the variation law of the heat flux between semi-product – crystallizer and the heat flux between crystallizer – cooling water.

Primordial method for the decrease of the superheat of the steel of the in of the crystallizer, consist in the introduction of consumable micro-coolers, which can be exterior or internal. In this paper is presented simulation solidification model of steel continuous casting, using finite element model. For this is considered a section in mould-continuous casting system. This section is divided with discreet element structure. Using these experiments is made graphical dependents of temperature in some different point from surface crust to center of semi-product, and also solidification speed for S235 (OL37) steel.

Keywords

continuous casting, steel quality, semi-product, crystallizer, mathematical modeling, solidification and cooling phenomenon

1. INTRODUCTION

The main task of the continuous cast is improved of continuous cast steel quality. In order to assured the solidification conditions imposed by the steel chemical composition must be synchronize a numerous technological factors, the most important be the steel chemical composition, the casting temperature and speed of drawing.

Primordial method for the decrease of the superheat of the steel of the in of the crystallizer, consist in the introduction of consumable micro-coolers, which can be exterior or internal. The exterior micro-coolers can be prepared out of the system and entered the crystallizer, and the internal micro-coolers are constituted from steels crusts, immediate format in the core of the semi-products, on the water cooled surfaces. The outside micro-coolers can be entered in the liquid steel below different forms: small shots, granules or particles, draw-bars, wire, tube, etc. The addition of micro-coolers in crystallizer drives to the growth of the zone of the echi-axial crystals, diminish the degree of superheat and reduce the axial porosity.

The mathematical modeling of the solidification and cooling phenomenon of continuously cast semi-products, presented in afterwards, is based on the mathematical description of phenomenon. This solution problem is, practically, the heat solving equation in of non-steady regime. For defined the heat conduction between semi-product and crystallizer is necessary the cognition of initial conditions, the variation law of the heat flux between semi-product – crystallizer and the heat flux between crystallizer – cooling water. Some conditions are can easy schematized, other only that drive to systems of which equations can be solved on analytic path.

2. IMPLEMENTATION OF THE ALGORITHM

The computer program is written in C++ and works under Win32 (i.e. Windows 95, 98, Me, NT4, 2000, XP – with Intel processor). For the graphic interface, the program uses MFC (Microsoft Foundation Classes), a class library that encloses the functional character of the standard programming interface Windows API – Application Program Interface. The 3D graphs are realized with the Windows implementation of OpenGL specification (Open Graphics Library).

For implementation of an algorithm of the above described model we need the following initial data: ambient temperature, casting temperature, initial temperature of the crystallizer, number of nodes from half-finished product and from crystallizer with respect to both axes, values of thermal conductivity for steel and copper function of temperature, values of enthalpy for steel and copper function of temperature. In case of steel this functional dependence need to include fusion latent heat; tapping condition of half-finished product from equipment; stopping condition of the algorithm. This could be: manual stopping, after a given time period, at a specified minimum, average, or maximum temperature of the half-finished product, maximum variation of enthalpy at an iteration.

3. THE SIMULATION OF THE CONTINUOUSLY CAST SEMI-PRODUCTS

The simulation is realized for a half-finished product (bloom), having the cross-section 240x270 mm, made of steel OL37-2K, according to the SR EN 10025 standard. The data are: the ambient temperature 20°C, the casting temperature 1550°C, the convection constant $K = 15$. The simulation of the continuously cast semi-products is effectuated in the case of 5% consumable micro-coolers introduced in crystallizer. The simulation is effectuated just for the primary and secondary cooling and not for the entire line of cast installation. Thus is explained the great values of the temperature of steel in the interior of the semi-products (the middle layers) but which we diminish the feather below the value of the temperature solidus up to the moment which in the semi-product is uttered.

With the number of knots of digitization is major (both the crystallizer and the semi-product) and the maximum the variation of in an enthalpy in single iteration is less, the real time of simulation is major. In this case, the real time is 9h 8 min 44 s corresponding to the 13 min 21 s, in simulated time. The run of the program can be interrupted all moments, but with the mention as be start from same moment of time but must run the program from beginning. For illustrate the operation of the program, we accomplished captures of the screen to different moments of times, from which can obtain some information concerning the temperatures in the cast equipment, the real and simulated times.

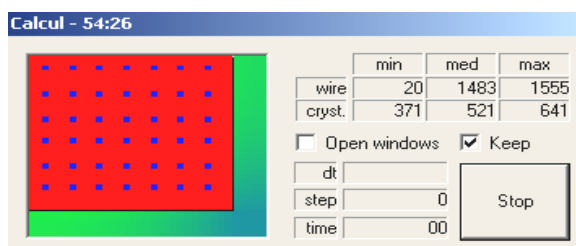


Fig. 3. The dialog window at 54 min 26 s (real time), respectively 0 s (simulated time) (at the moment of the micro-coolers introduces)

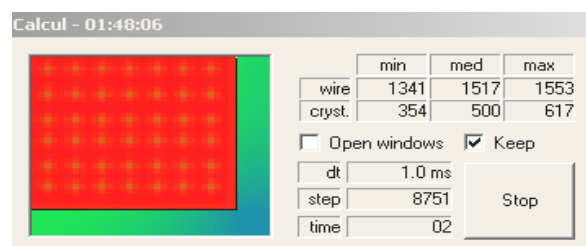


Fig. 4. The dialog window at 1h 48 min 06 s (real time), respectively 2 s (simulated time)

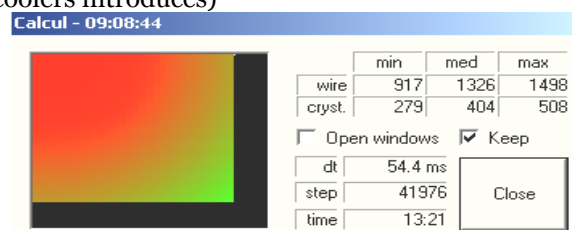


Fig. 5. The dialog window at 9 h 8 min 25 s (real time), respectively 13 min 21 s (simulated time) (at the end of program simulation)

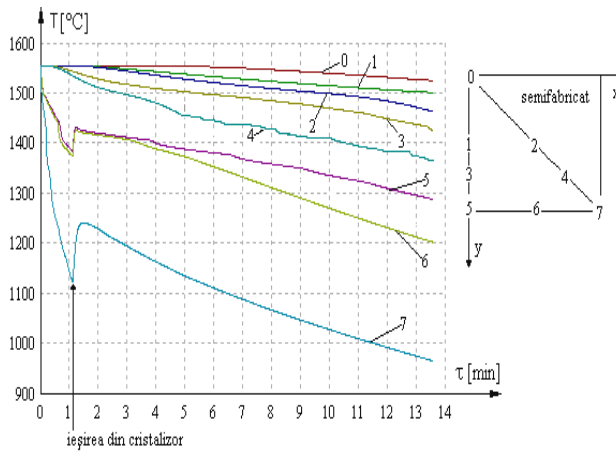


Fig.6. Temperature variation function of time

increasing of temperature in the superior layers of the half-finished product (with approximately 100°C in the corner and with 35...50°C in points 5 and 6 of the surface).

This increasing of the temperature is due to the lack of cooling of the wire immediately after the driving out from crystallizer to the first ring of secondary cooling. After this moment the cooling and the solidification of the wire took place normally, the recorded temperatures corresponding to the measured ones.

It needs to be specified that the simulation was realized just for primary and secondary cooling, not for the entire running of the wire in the equipment. This explains steel's high temperature values in the interior of the half-finished product (middle layers), but they are decreasing under the solidus temperature value until the cutting of the half-finished product.

As regards the temperatures distribution in the crystallizer (which take over the heat transferred by the half-finished product and transfer it to the cooling water), it is presented in fig.7. In this case to it is presented also the position of the discredited points.

In the moment of the cast process beginning, in crystallizer (in discretized points), the temperatures are relative high. At 10s (simulated time) the temperature is between 350-600°C, and it is observed a slowly decreasing of the temperature of points placed near the center of the half-finished product, but also the variation mode of the temperature from layers closer to wire surface (320...550°C at 30s, 275...520°C at 1 min 7s, in final moment of simulation).

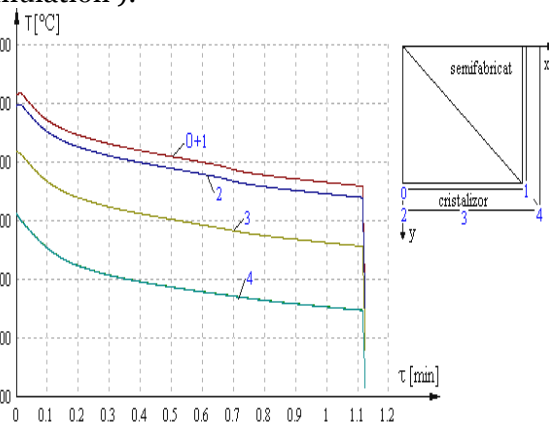


Fig.7. The temperature variation in the crystallizer, function of time

The temperatures are indicated by the mean of a colored gradient, having the values: red for casting temperature, blue for ambient temperature and green for their average. Any intermediary temperature is a combination of these.

A first obtained dependence is represented by temperature variation of the half-finished product function of time (fig.6.). The distribution of the discredited points is also presented.

At a time moment (in the presented case equal with 1 min 7s), when it took place the driving out of considered surface from crystallizer, it took place an

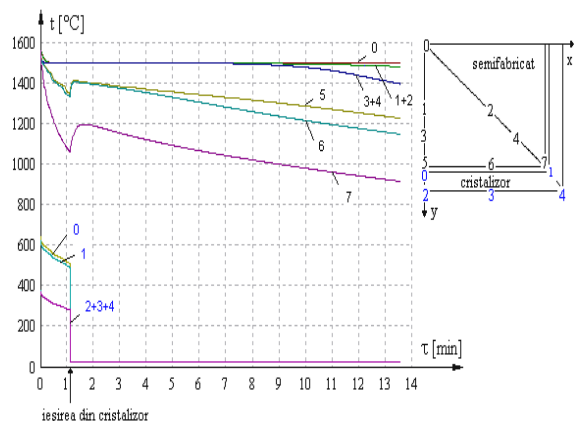


Fig. 8. The temperature variation in crystallizer and the cast line

In fig. 8 the cumulate diagramme of the temperature are presented. It is observed the two cooling zone, respectively the primary cooling (when varied both the temperature in crystallizer and the cast line), and the secondary cooling (when only the cast line temperature is present). It was obtained variation type for the solidification speed, function of time. It refers to a solidification speed calculated between two consecutive iterations, fact that partially explain the oscillating aspect of the curves.

Another type of temperature distribution, when the half-finished product is droved out from secondary cooling zone, it is presented in fig. 9...fig.13, at 3s, 9s, 24s, 30s and 60s, after introduced the micro-coolers.

The fig. 14 presents the thermal field in the semi-product in the moment of the 13 min 21s (simulated time). The obtained regression surfaces corresponded from a quarter from the semi-product section is like similarly of the other parts of the section. From the point of view of the temperature values, the semi-product corner is the first cooled section, and the core is the most slowly cooled part.

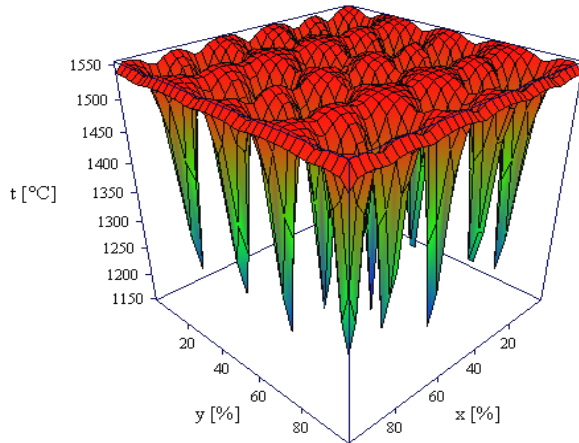


Fig. 9. The thermal field at 3s after the micro-coolers addition

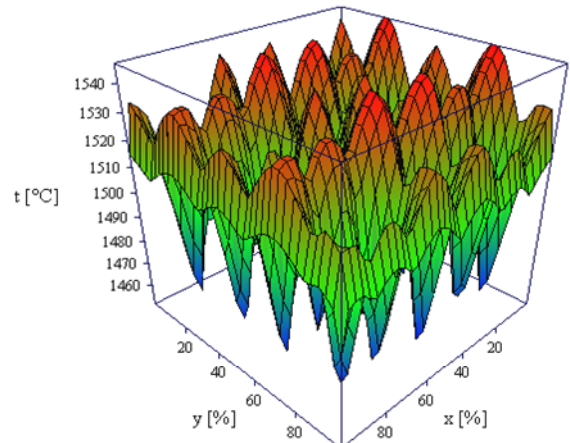


Fig. 10. The thermal field at 9s after the micro-coolers addition

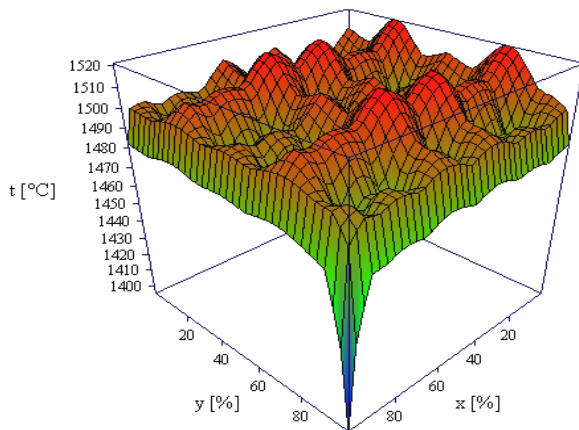


Fig. 11. The thermal field at 24s after the micro-coolers addition

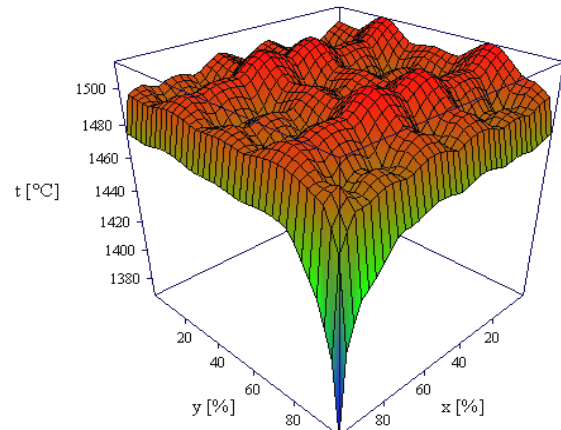


Fig. 12. The thermal field at 30s after the micro-coolers addition

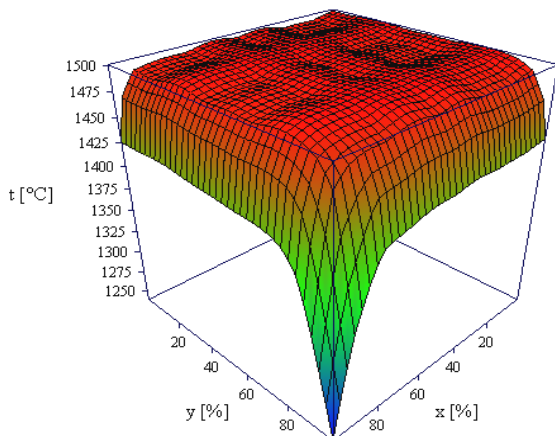


Fig. 13. The thermal field at 60s after the micro-coolers addition

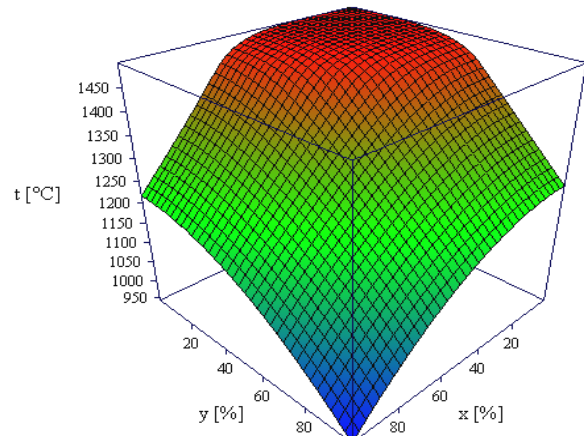


Fig. 14. The thermal field in semi-product (with section 240x270mm) at 13 min 21s (simulated time)

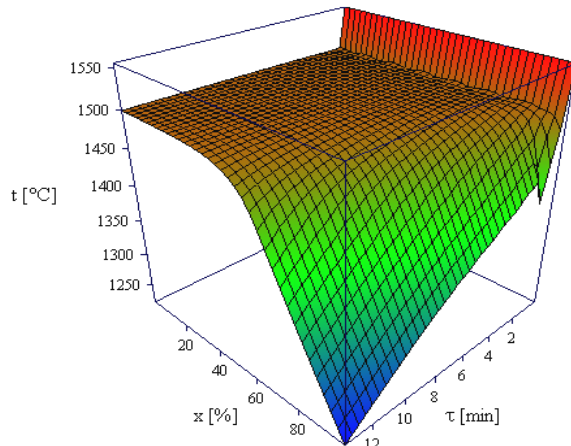


Fig. 17. The thermal field in semi-product (240x270mm) across the axe x for $y = 0$, depending in time

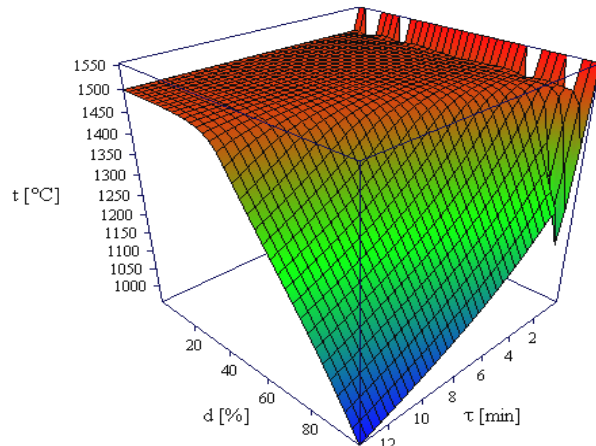


Fig. 18. The thermal field in semi-product (section 240x270mm) across the diagonal, depending in time

In order to realize a bi-dimensional mathematical modeling of a semi-finished product it is considered a section of half-finished product-crystallizer assembly, which is divided using a discretisation network. As results of the considered hypothesis, the half-finished product-crystallizer assembly is symmetric with respect to longitudinal axis of the half-finished product. The origin of the system of coordinates will be in the center of the half-finished product and the calculus will be made just for positive x and y .

The temperature of every node represents the mean temperature of node adjacent surface. In these nodes are written the finite differential equations presented above.

The model is realized based on the following simplifying assumptions:

- ✚ the heat transfer on longitudinal axis is neglected, considering that heat transfer take place just in horizontal section of the half-finished product
- ✚ the density variation is neglected
- ✚ the crystallizer section is consider to be a equivalent rectangular section
- ✚ it is consider that the crystallizer loose heat uniformly on each surface
- ✚ it is consider that at zero moment the temperature of steel mass is uniform. For the surface nodes it is correct to assume that at the casting moment it took place the formation of a thin solidified steel layer, and the loosed heat by this layer is transmitted instantaneously to the nodes from the interior surface of the crystallizer.
- ✚ the evolving of fusion latent heat it is produced in liquidus-solidus interval, direct proportional with the temperature

3. CONCLUSIONS

Analyzing the graphical dependences from the performed researches, based on literature review data and from own experimental work it results the following conclusions:

- ✚ The results obtained by simulation with presented program being similar with practical data;
- ✚ In every diagram there are observed a temperature leap or a solidification speed leap after approximately 1 min 7 s from the beginning of the casting, respectively immediately after the driving out from the crystallizer of the considered section, leap caused by the impossibility of elimination of a heat flux from the half-finished product interior;
- ✚ It is observed a numerous crystallizing centers, uniform distributed;
- ✚ Also, it is observed an appreciate difference between the liquid steel temperature and the steel temperature from immediate proximity of micro-coolers
- ✚ The indurations advances consisted standardized it a temperatures of first in of the minute after the administration of micro-coolers
- ✚ Through the addition of micro-coolers is obtained adjustment of the a temperature of the in of the crystallizer depending on the quality and the quantity of micro-coolers

- ✚ After precinct a minute from the administration micro-coolers don't else notices significant differences what in looks the variation of the temperature of the in mass of steel
- ✚ Modifying a series of parameters (number of discretized points, dissipated heat in crystallizer and in secondary cooling, data of steel grade) it could be obtained more correct values, applicable to other steel grades.

The number of nodes is established starting with the necessity of finding a solution for the following contradiction: the use of a high number of nodes increases the precision of the model (the error introduced by the hypothesis that the adjacent surface of every node has the same temperature as the node is decreases with the decrease of node area); on the other hand a high number of nodes lead to an increasing of processing time due to the increasing of nodes number and due to decreasing of time intervals between iterations imposed by stability conditions of the solutions.

The chosen time interval represent the time in which the unsteady heat transfer process is approximate with a steady process. From this reasons as well as the characteristics of the real process are far from that of a steady one, the iteration period should be smaller.

In order to realize a bi-dimensional mathematical modeling of a semi-finished product it is considered a section of half-finished product-crystallizer assembly, which is divided using a discretisation network. The temperature of every node represents the mean temperature of node adjacent surface.

REFERENCES

- [1.] BUTNARIU I., s.a. – Turnarea continua a semifabricatelor de otel, Ed. Tehnica, Bucuresti, 2000
- [2.] ARDELEAN, E, ș.a. – Turnarea continuă a oțelului, Ed. Politehnica Timisoara, 2001
- [3.] POPA Erika, KISS Imre – Mathematical modeling of the thermal regime in the continuous casting process, VIIth International Symposium, Resita, 2005
- [4.] POPA Erika, KISS Imre, DANCIU Adrian – Research and experiments the influence of casting parameters upon the surface temperature of the continuous cast semi-products, Annals of the Oradea University, 2005
- [5.] POPA Erika, KISS Imre – Mathematical modeling of the thermal regime in the continuous casting process, Analele Universitatii “Eftimie Murgu”, Resita, 2005



MULTIDISCIPLINARY APPROACHES IN THE FIELD OF THE CAST IRON ROLLING ROLLS MANUFACTURING

Imre KISS, Stefan MAKSAJ, Vasile ALEXA

University Politehnica Timisoara, Faculty of Engineering Hunedoara, ROMANIA

Abstract

The irons destined to these cast rolls belong to the class of low-alloyed irons, with reduced content of chrome, nickel and molybdenum. The technological instructions firmly state the elements required raising the quality of rolls, but the limits can be extensive or limited. Depending on the number of the technological parameters, it was chosen the analysis of multiple regressions studying the influence of the chemical composition upon the hardness, through the mathematical modeling.

The technical conditions, which are imposed to the cast iron rolls in the exploitation period, are very different and often contradictory. The obtaining of various physical and mechanical properties in the different points of the rolls meets difficult technological problems in the industrial condition. This supposes us to know many technological factors, which lead to the exploitation of this deformation equipment.

The experimented researches, as well as the optimization of the manufacturing technology, allow the conclusion of direct results for the rolls. The beneficiaries of these results are the unit in which the rolls are manufactured, as well as the unit that exploits them.

Keywords:

cast iron rolls, alloying elements, mathematical interpretations

1. INTRODUCTION

Poverty of detailed researches, theoretical and experimental, about the thermo-mechanical processes take place during the plastic deformations between the rolling mills rolls, represents a factor that reduces the possibility of rational exploitation of rolling mills. In the context of market economy is necessary a new evolution in the area of scientific researches, in the purpose of modernization of the equipments and metallurgical plants, using the most efficient solutions for obtaining aggregates with performances to the level of world technique. The technological processes of the rolls manufacture, as well as the quality of used materials have a quick extension, materialized in worldwide market competition, through exceptional qualities of rolls.

The technological manufacturing process of the rolling mills rolls, as well as the quality of material used in manufacturing them, can have a different influence upon the quality and the safety in the exploitation. Our proposal approaches the issue of quality assurance of the rolling mills rolls, from the viewpoint of the quality of materials, which feature can cause duration and safety in exploitation.

In these sense, our researches propose, on aside, to analyze the technological field of the rolling rolls manufacturing process – analysis materialized from prism of the foundry experiments, including the metallurgical and mechanical aspects (casting process, moulding, iron melting, nodularization of graphite, hardness, durability and so others), and on another side, the optimization of the manufacturing technology of the cast rolls, especially those from cast-iron – using electronic calculus technique as the molding phenomenon and mathematical interpretation of the technological processes.

The research on rolling mills rolls quality experimentally and teoretically defines an important chapter from the metallurgical, mechanical and mathematical aspects of these machines organs in the movement of rotation, in variable temperature mediums. Also, the

mathematical modeling establishes a methodology for the determination of the technological parameters values, for which a mechanical characteristic (the hardness) has the desirable values. Because is disposed of real data, the optimization model is based on industrial data, obtained from cast-iron rolling rolls. Their analysis shall lead to the optimization pattern, through the prism of the multicomponent correlations, enounced by mathematical formulae.

Starting from the principle of molding process, used as necessary basic instrument, both in phase of conception, as well as in the industrial technologies analysis, is determined the optimum regimes of the cast rolls, from the view from chemical composition, as one as the most important parameters of disturbance of the manufacturing process. The enunciation of some mathematically molding results, described through a number of multicomponent equations determined for the spaces with 3 the and 4 dimensions, as well as the generation of some regression surfaces, of some curves of levels, of the volumes of variation, of the lines of outlines of the volumes of variation of surfaces and the areas of variation of these, can be represented and interpreted by technologists and can be considerate diagrams of correlation between the analyzed variables. From this point of view the project is inscribes in context of scientific capitalization of the process and the industrial technologies optimizations, on the way of the analysis and the mathematical experiment.

2. THE TECHNOLOGICAL APPROACHES

The nodular graphite cast iron is considered as one of the most versatile roll materials nowadays. This type of material may be used to produce large scale rolls in double pouring process, the barrel of rolls has high hardness while the neck has high toughness, so this type of rolls exhibits the properties of high thermal stability and resistance to wear. As the characteristics of any casting are influenced by the microstructure that is formed during the solidification in the cast form, and under the influence of the cooling speed, the main criteria, which determines the mechanical properties of the rolls is the structure. All structural components can be found in cast iron rolls, each of the components having its own well-determined hardness. One of the parameters, which are determined the structure of the irons destined for rolls casting, is the chemical composition. If we do not respect this composition, which are guarantied by the exploitation properties of the each roll in the stand of rolling mill, this leads to rejection. All FNS type rolls are alloyed especially with chrome, nickel and molybdenum, in different percentages. The irons destined to these cast rolls belong to the class of low-alloyed irons, with reduced content of these elements. The technological instructions firmly state the elements required to raise the quality of rolls.

The recommended hardness's for the working surfaces of the half-hard rolls are presented in Table 1, according with the hardness classes adopted by the Romanian Standard Regulations. Also, the recommended hardness for the rolls necks and the core are presented in same Table 1. The usual chemical composition of the irons destined for casting the half-hard rolls is presented in Table 2.

TABLE 1. The recommended hardness's of the half-hard rolls for the rolls working surfaces (body), the necks and the core

Rolls Type	Hardness Classes	Hardness			
		on the rolls working surface		on the necks and in the core	
		[HS]	[HB]	[HS]	[HB]
FNS	0	33...42	218...286	30...40	195...271
FNS	1	43...59	294...347	30...40	195...271
FNS	2	69...75	499...550	35...45	218...309

TABLE 2. The usual chemical composition of the irons destined for casting the half-hard rolls

Rolls Type	Chemical Composition, [%]								
	C	Si	Mn	P	S	Ni	Cr	Mo	Mg
FNS	3,0..3,5	1,2..2,5	0,1..0,7	max. 0,15	max. 0,02	1,5..2,5	max. 0,8	0,3...0,5	0,02... 0,04

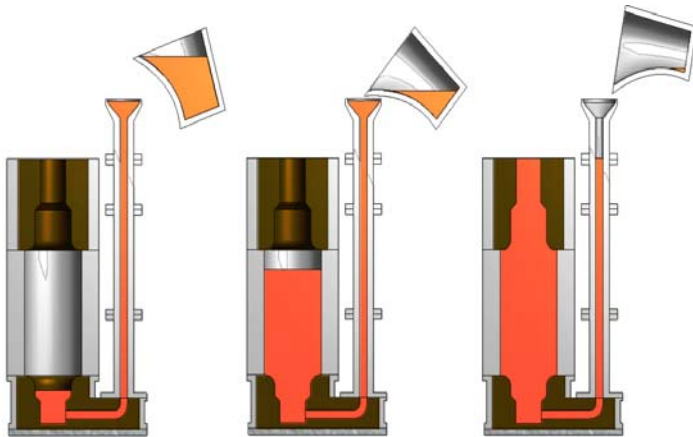


Fig. 1. The casting process of the half-hard iron rolls

as well as in usage. These requirements can't be completely fulfilled, compelling to the granting of priorities depending on the type of laminates, therefore to compromises. At large, the problem is reduced to the correct material choice, eased by the rich available experience in the current conditions of manufactured and burdened, in the same time, by the large diversity of material used.

Although the manufacture of rolls is in continuously perfecting, the requirements for superior quality rolls are not yet completely satisfied, in many cases, the absence of quality rolls preventing the realization of quality laminates or the realization of productivities of which rolling mills are capable.

To the selection of materials is considered the type of rolling mill, the sizes of rolls (in specially this diameter), the speeds of lamination, the stands from the train of lamination for which is achieved rolls, the working temperature in the lamination process, the module of cooling during work, the size caliber, the pressure on rolls, the rolled material hardness, etc.

The choice of material for rolls is the operation which takes into consideration the own solicitations of the lamination process afferent to the type of laminates (semiproduct or the finite laminate), and the features of different materials considerate optimum in the fabrication of different typo-dimensions of rolls.

Having abrading and dry friction wear resistance, as well as another mechanical characteristic superior to cast irons with lamellar graphite, the cast-irons with nodular graphite are successfully used to the cast of types of rolls. The main structural constituent of the cast-iron is the graphite, of the amount, form, sizes and module of allocation in basic metallic mass depends the physical and mechanical property of the cast-iron, inclusively of the rolls, as well as the wear resistance. For this reason, the amount and the module of distribution of the graphite separation in working surface of rolls it can be considered as main criterion of classification. The presents of graphite in working surface (body of rolls) assures the friction coefficient necessary to obtain quality laminate. From this point of view, the cast irons with nodular graphite is used to manufacture large types of rolls.

Having in view the complex solicitations in exploitation, another important characteristic imposed to the rolling mills rolls is the thermal shock resistance. The main cause of wear is the appearance of fissures on the working surface, due to thermal fatigue. The thermal wear, in principle, can be explained through the different behavior of the constituents that compose the basic metallic mass, in variations of temperature. The thermo-mechanical wear, due the crossing among the rolls of the laminates, warmed in the austenitic area, is direct influenced by the fineness of the basic metallic mass structure, as well as the form and size of graphite disjunctions. In order to obtained a good durability, it is needed a fine homogeneous structure, with a great degree of dispersion of the pearlite.

3. THE MATHEMATICAL APPROACH

The statistical methods of the analysis do not solve a whole series of appearances regarding to the decisions model to establish the management of the process. For this reason, in parallel with the statistical methods, was developed the methods of optimization.

As part as the basic experiment, through the regression analysis, it was aimed the determination of the mathematical functions form which connect the dependent variables u of the technological process with the free variables (the technological parameters) x, y, z, \dots , meaning $u = f(x, y, z, \dots)$, on the strength of some experimental determinations, this after it accomplished a dispersion analysis of these correlation data. The determination of what real coefficients enter into the expression $u = f(x, y, z, \dots)$ is done, in the vast majority of the cases, through the method of the smallest squares.

Depending on the number of free variables (the technological parameters) that we consider, it was chosen the analysis of multiple regressions studying the influence of free variables x, y, z, \dots upon the dependent variable u . In this sense, it was aimed to establish calculus methodologies of values for the technological parameters in the manufacturing process of the semihard rolling mill rolls, obtained through the simplex classical cast of the iron with nodular graphite, for which the mechanical features of rolling mill rolls have the required values.

Having "n" experimental points, respectively $(x_1, y_1, u_1)_1, (x_1, y_1, u_1)_2, \dots, (x_1, y_1, u_1)_n$, we need to determine the real coefficients c_0, c_1 and c_2 in the equation of the plan. This is accomplished through the method of the smallest squares, which leads to finding them through the following system of three equations with three unknown variables (a_0, a_1, a_2) :

$$\begin{cases} n \cdot c_0 + \left(\sum_{i=1}^n (x)_i \right) \cdot c_1 + \left(\sum_{i=1}^n (y)_i \right) \cdot c_2 = \sum_{i=1}^n u_i \\ \left(\sum_{i=1}^n (x)_i \right) \cdot a_0 + \left(\sum_{i=1}^n (x)_i^2 \right) \cdot a_1 + \left(\sum_{i=1}^n (x)_i \cdot (y)_i \right) \cdot a_2 = \sum_{i=1}^n (x)_i \cdot u_i \\ \left(\sum_{i=1}^n (y)_i \right) \cdot a_0 + \left(\sum_{i=1}^n (x)_i \cdot (y)_i \right) \cdot a_1 + \left(\sum_{i=1}^n (y)_i^2 \right) \cdot a_2 = \sum_{i=1}^n (y)_i^2 \cdot u_i \end{cases} \quad (1)$$

where the real coefficients (the sums from parentheses) are calculated tabularly. The solution of the system is done through the Cramer rule, using the determinants of the system.

Departing from the experimental results, in a first phase the stage are determined the mathematical models of dependencies for optimized parameters (the mechanical features the materials) with the technological parameters in the influences of the process, in the form of equation (2). In mathematical model it is reduced to complex mathematical processing of dependences in the features analyzed depending on two or three chemical elements, grouped depending on the influence upon them. Thus we can analyze dependences type (3).

$$\begin{array}{ll} \text{HB}_{(\text{infneck})} = f(\text{basic chemical elements}) & \text{HB}_{(\text{infneck})} = f(\text{alloying chemical elements}) \\ \text{HB}_{(\text{supneck})} = f(\text{basic chemical elements}) & \text{HB}_{(\text{supneck})} = f(\text{alloying chemical elements}) \\ \text{HB}_{(\text{body})} = f(\text{basic chemical elements}) & \text{HB}_{(\text{body})} = f(\text{alloying chemical elements}) \end{array} \quad (2)$$

$$\begin{array}{lll} \text{HB}_{(\text{infneck})} = f(\text{C, Si, Mn}); & \text{HB}_{(\text{supneck})} = f(\text{C, Si, Mn}); & \text{HB}_{(\text{body})} = f(\text{C, Si, Mn}); \\ \text{HB}_{(\text{infneck})} = f(\text{Ni, Cr, Mo}); & \text{HB}_{(\text{supneck})} = f(\text{Ni, Cr, Mo}); & \text{HB}_{(\text{body})} = f(\text{Ni, Cr, Mo}); \end{array} \quad (3)$$

Following the experiments we determine the mechanical features according to the technological parameters of influences in the process. Because we dispose of real data, afterwards it is required to present the model of optimization on industrial data, sampled from rolling mills rolls. As parameters for optimization we selected:

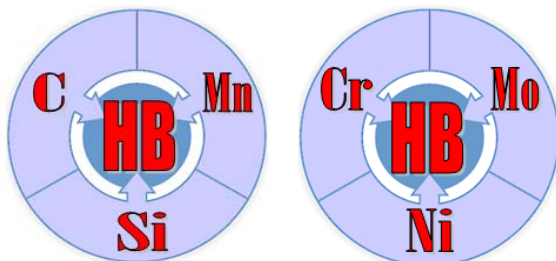


Figure 2. The influence of the basic and the alloyed elements upon the brinell hardness, in mathematical perspective

- ✚ the Brinell hardness, measured on the body of rolls, $\text{HB}_{(\text{body})}$;
- ✚ the Brinell hardness, measured on the necks of rolls, $\text{HB}_{(\text{infnecks})}$ and $\text{HB}_{(\text{supnecks})}$.

In order to reduce the experiments number and to simplify the optimization calculi, among the parameters of influence,

we chose the chemical composition of the cast irons with nodular graphite. These hypotheses lead the optimization model through the prism of the multi-component correlations in formula (II).

The industrial data are modeled in the form of equation (4). We consider the variations limits of the variables (x, y, z), as well as the variation limits of the analyzed features. Also, in the limits of graphical representation ($\lim x_{inf}, \lim x_{sup}, \lim y_{inf}, \lim y_{sup}, \lim z_{inf}, \lim z_{sup}$), as well as the average values of the variables and of the analyzed features ($x_{med}, y_{med}, z_{med}, u_{med}$) are stated.

$$u(x, y, z) = C_1 x^2 + C_2 y^2 + C_3 z^2 + C_4 yz + C_5 xz + C_6 yx + C_7 x + C_8 y + C_9 z + C_{10} \quad (4)$$

At that rate, the equations of the regression hyper-surfaces are in equation (3), for which there is a correlation coefficient (r_f) and a deviation from the regression surface (s_f).

4. THE PRESENTATION OF GRAPHICAL ADDENDA

Figure 3 presents the screen which generates the regression surfaces of the variable ($HB_{(body)}, HB_{(infnecks)}, HB_{(supnecks)}$) for the cases $x = x_{med}, y = y_{med}$ and $z = z_{med}$, waves x, y, z represent combination of chemical elements depending on the mathematical model under study.

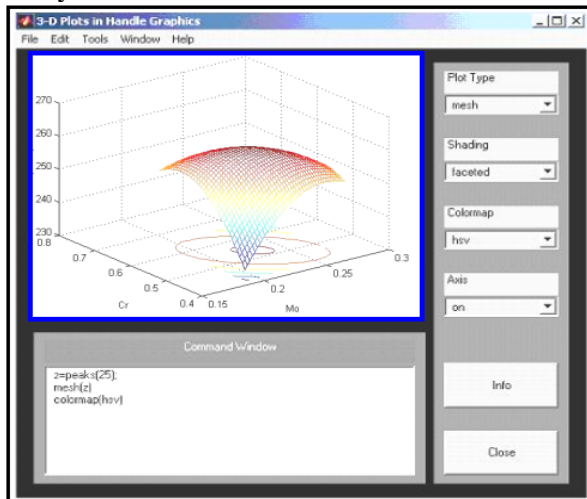


Figure 3. Regression surface of the variable u ($HB_{(body)}, HB_{(infnecks)}, HB_{(supnecks)}$) for the cases $x = x_{med}, y = y_{med}$ and $z = z_{med}$

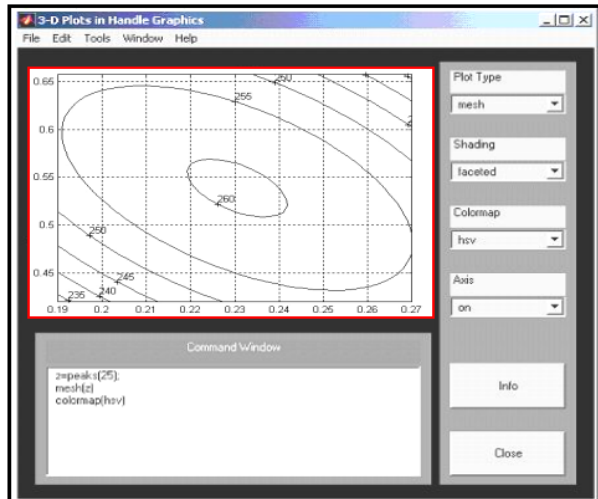


Figure 4. The level curves generation for the dependences $u = f(x, y, z)$, formally $u = f(x_{med}, y, z)$, $u = f(x, y_{med}, z)$ and $u = f(x, y, z_{med})$

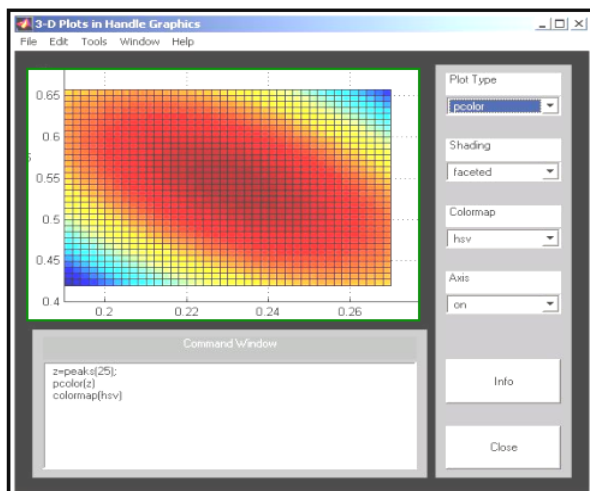


Figure 5. Screen for the variation domain generation of the dependences $u = f(x, y, z)$, formally $u = f(x_{med}, y, z)$, $u = f(x, y_{med}, z)$ and $u = f(x, y, z_{med})$

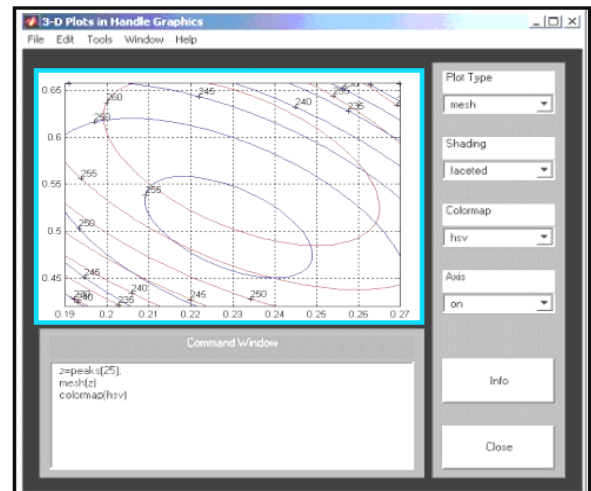


Figure 6. Screen for the adjusting diagrams generation built for the average values ale parameters ($x_{med}, y_{med}, z_{med}$)

Figure 4 presents the program screen capture which generates the level curves of the dependence $u = f(x, y, z)$, formally $u = f(x_{med}, y, z)$, $u = f(x, y_{med}, z)$ and $u = f(x, y, z_{med})$ for the cases $x = x_{med}$, $y = y_{med}$ and $z = z_{med}$. This level curves represents the projection in the two-dimensional plan of the regression surfaces presented in the Figure 3. Figure 5 presents the screen which generates the variation domain of the characteristics $u = f(x, y, z)$, formally $u = f(x_{med}, y, z)$, $u = f(x, y_{med}, z)$ and $u = f(x, y, z_{med})$ for the cases $x = x_{med}$, $y = y_{med}$ and $z = z_{med}$. This geometrical areas represents level curves variations in the two-dimensional plan.

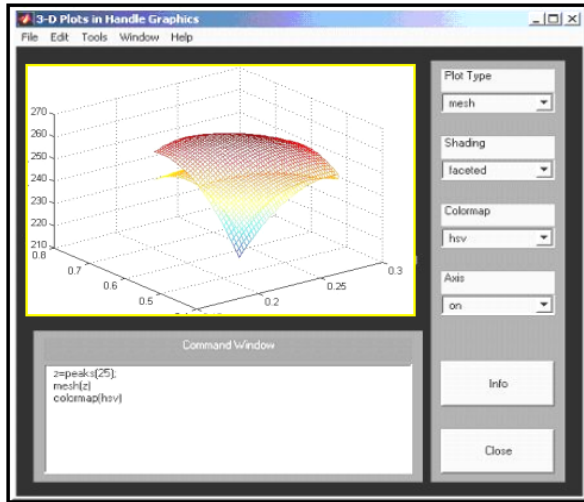


Figure 7. Screen for the regression surface volume variation generation for the average values $x = x_{med}$, $y = y_{med}$ and $z = z_{med}$

These diagrams are built for the average values of the parameters (x_{med} , y_{med} , z_{med}), only that through the representation of the diagrams for parameters values contained in the variations limits we can obtain adjusting diagrams (Figure 6), with which we can completely controlled the process. Figure 7 presents the screen, which generates the correlation surfaces, meaning the projection in the two-dimensional plan of the variation volumes of the regression surfaces. These are obtained through superposing of the $u = f(x_{med}, y_{med}, z_{med})$ and one of surfaces corresponding for the average values $x = x_{med}$, $y = y_{med}$ and $z = z_{med}$, meaning $u = f(x_{med}, y, z)$, $u = f(x, y_{med}, z)$ and $u = f(x, y, z_{med})$.

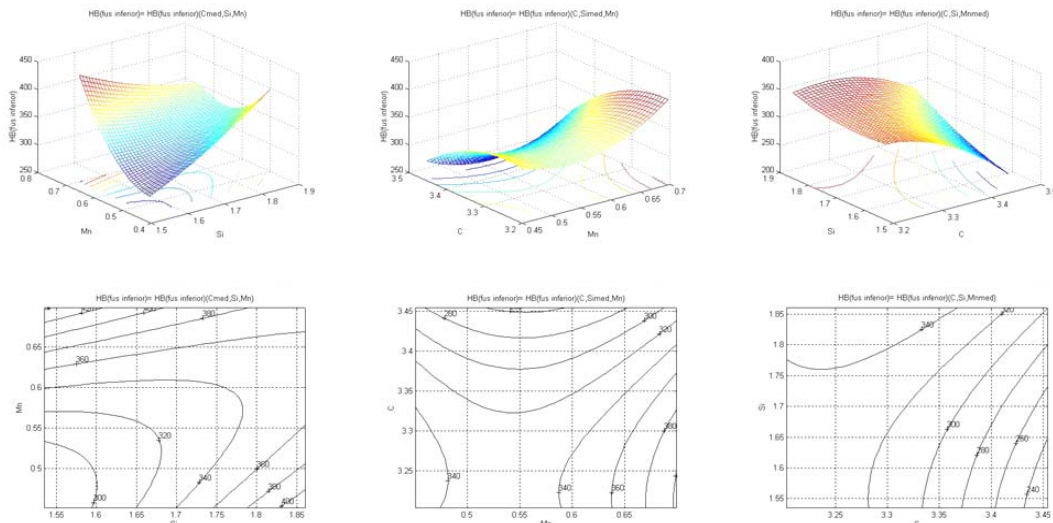


Figure 8. The regression surface and the level curves generated by the program for the dependences between hardness and chemical composition [presented example for the variation of the parameter $HB_{(Fusinf)}$ in the cases $C = C_{med}$, $Si = Si_{med}$ and $Mn = Mn_{med}$, in the $HB_{(Fusinf)} = f(C_{med}, Si, Mn)$, $HB_{(Fusinf)} = f(C, Si_{med}, Mn)$ and $HB_{(Fusinf)} = f(C, Si, Mn_{med})$ dependences]

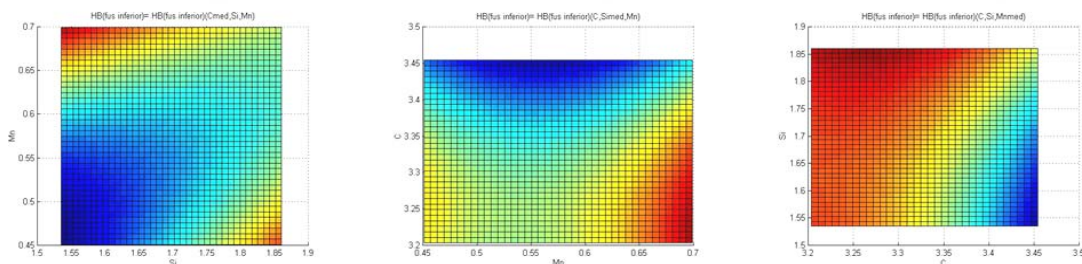


Figure 9. The variation domain in color panel presentation for the dependences between hardness and chemical composition [same case]

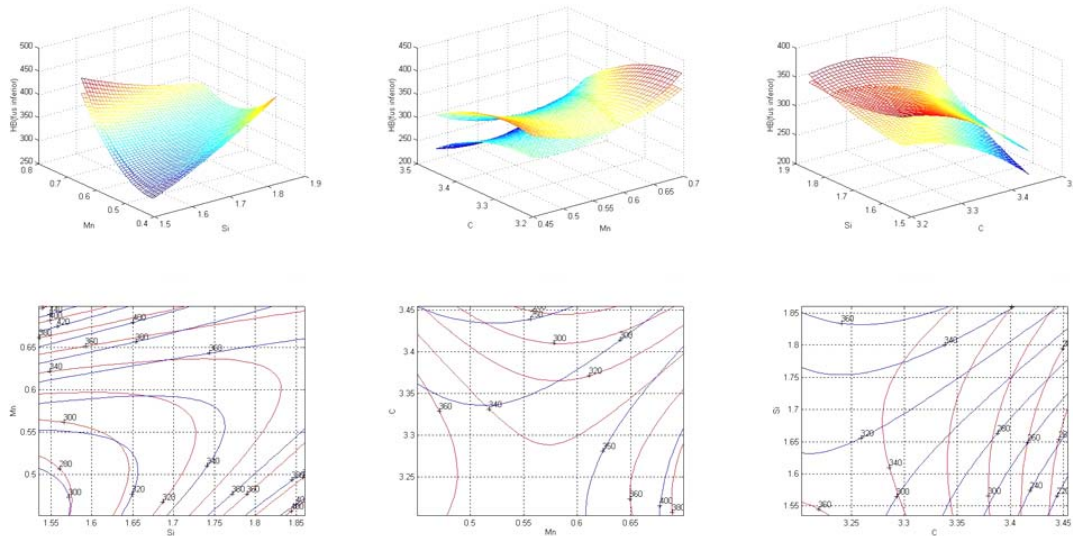


Figure 10. The regression surface volume variation domain and the adjusting diagrams for the dependences between hardness and chemical composition [same case]

7. CONCLUSIONS

The performed study had in view to obtain correlations between the hardness of the cast iron rolls (on the necks and on the working surface) and its chemical composition, defined by basic and the representative alloying elements. Analyzing the graphical dependences from the performed researches, based on literature review data and from own experimental work it results the following conclusions:

- ✚ the values processed were made using Matlab calculation program. Using this calculation program we determine some mathematical correlation, correlation coefficient and the deviation from the regression surface. This surface in the four-dimensional space (described by the equation) admits a saddle point to which the corresponding value of hardness is an optimal value of alloying elements.
- ✚ the existence of a saddle point inside the technological domain has a particular importance as it ensures stability to the process in the vicinity of this point, stability which can be either preferable or avoidable.
- ✚ the behavior of this hyper-surface in the vicinity of the stationary point (when this point belongs to the technological domain) or in the vicinity of the point where the three independent variables have their respective average value, or in a point where the dependent function reaches its extreme value in the technological domain (but not being a saddle point) can be rendered only as a table, namely, assigning values to the independent variables on spheres which are concentric to the point under study.
- ✚ as this surface cannot be represented in the three-dimensional space, we resorted to replacing successively one independent variable by its mean value. These surfaces (described by the equation), belonging to the three-dimensional space can be reproduced and therefore interpreted by technological engineers.
- ✚ knowing these level curves allows the correlation of the values of the two independent variables so that we can obtain a viscosity within the required limits.

The realization of a mathematical model starting from industrial data, gathered at the rolls hardness measurement, and at the national standards regulations, which recommends the hardness, for different chemical compositions, also determines the degree of originality of the research. The determination of the equations of regression hyperplanes, which describe the mathematical dependency between the chemical composition and the hardness, the determination of the multicomponent relations and the realization of the graphic interfaces for the representations variation areas of the cast-irons chemical composition, completes this area of preoccupations within a processing mathematical of molding and optimization.

The realization of an optimal chemical composition can constitute a technical efficient mode to assure the exploitation properties, the material from which the rolling mills rolls are manufactured having an important role in this sense. From this point of view is applied the mathematical molding, which is achieved starting from the differentiation on rolls component parts, taking into consideration the industrial data obtained from the hardness measurement on rolls, as well as the national standards regulations, which recommends the hardness, for different chemical compositions.

The optimum solution is determined through some mathematical restrictions to the input values that the mathematical molding is started. As a work method is chosen the way of the constraint of average successive values to some of the elements of chemical composition, leaving free the variation of a number of variables submitted to optimization. Is searched to constraint average values, inclusively to dependent variables, desired to achieve through the chemical optimum composition. It will be determined the equations of regression hiperplanes, which describe the mathematical dependency between the chemical composition and the hardness, and is searched a solution which can determine the optimum chemical composition for hardness desirable values.

REFERENCES

- [1] *I. Ripoșan*: “Nodular graphite iron for the cast iron rolls”, in: Bulletin of University Politehnica București, 1980/3
- [2] *I. Kiss, T., Hepuț*: “Mechanical properties of the cast iron rolls, assured by the chemical composition”, Scientific Bulletin of University Politehnica Timișoara, 2002
- [3] *I. Kiss, St. Maksay*: “Model de optimizare a compoziției chimice a fontelor cu grafit nodular (Cr, Ni, Mo) destinate turnării cilindrilor de laminor”, în: Analele Facultății de Inginerie din Hunedoara, 2002, Fascicola 4, pag. 159...168
- [4] *I. Kiss, S. Rațiu, Ana Josan, Maria Scurtu*: “Alloyed elements for the nodular cast iron semihard rolls”, The VIIth International Symposium Interdisciplinary Regional Research – ISIRR 2003, Hunedoara, pag. 749...754
- [5] *I. Kiss, V. Cioată, V. Alexa, Maria Scurtu*: “Industrial study upon the basic chemical composition of the nodular cast iron rolls”, at The VIIth International Symposium Interdisciplinary Regional Research – ISIRR 2003, Hunedoara, pag. 741...748
- [6] *I. Kiss, St. Maksay*: “Model de optimizare a compoziției chimice a fontelor cu grafit nodular (C, Si, Mn) destinate turnării cilindrilor de laminor”, în: Analele Facultății de Inginerie din Hunedoara, 2002, Fascicola 4, pag. 169...176
- [7] *I. Kiss, St. Maksay*: “Model de optimizare a compoziției chimice a fontelor cu grafit nodular (S, P, Mg) destinate turnării cilindrilor de laminor”, în: Analele Facultății de Inginerie din Hunedoara, 2002, Fascicola 4, pag. 183...190
- [8] *I. Kiss, St. Maksay*: “The mechanical properties of the nodular cast iron rolls assured by the alloyed elements and the Ni-Cr-Mo optimal correlation”, The 6th International Symposium Young People Interdisciplinary Research, Timișoara, 2004, pag. 176...185
- [9] *I. Kiss, St. Maksay, S. Rațiu*: “Triple correlation between the rolls hardness and the cast irons main alloyed elements”, în: Annals of the Faculty of Engineering – Hunedoara, 2003/3, pag. 91...96
- [10] *I. Kiss, St. Maksay, S. Rațiu*: “The hardness of the nodular cast iron rolls assured by the Ni-Cr-Mo optimal correlation”, în: Annals of the Faculty of Engineering – Hunedoara, 2003/3, pag. 97...102
- [11] *I. Kiss, St. Maksay*: “Triple correlation between the semihard cast nodular iron rolls hardness’s and the main alloyed elements (Cr, Ni, Mo) presented in the Matlab area”, în: Masinstvo – Journal of Mechanical Engineering, No.4/2004, Zenica, Bosnia & Herzegovina, pag. 217...224
- [12] *I. Kiss, St. Maksay, S. Rațiu*: “The triple correlation theory and the optimal form of molding in the case of the semihard cast iron rolls hardness’s”, în: Metalurgia International, No.2/2005, pag.14...21
- [13] *I. Kiss, St. Maksay*: “Optimization model and mathematical modeling in Matlab area in the case of ductile cast irons”, în: Metalurgia International, No.3/2005, pag.28...34
- [14] *I. Kiss, St. Maksay*: “The optimal form of molding in the case of the semihard cast nodular iron rolls hardness’s”, în: Masinstvo – Journal of Mechanical Engineering, No.1/2005, Zenica, Bosnia & Herzegovina, pag. 17...22



STUDY OF THE MACHINING ERROR DUE TO CONTACT DEFORMATION OF WORKPIECE-FIXTURE SYSTEM

CIOATĂ Vasile George, KISS Imre

University "POLITEHNICA" of Timișoara, Faculty of Engineering Hunedoara, ROMANIA

Abstract

In this paper work there are described the error's sources due to workpiece-fixture compliance which appear while the workpieces are clamped, is presented the analytic models of calculus of the errors due to contact deformation between locators and workpiece and an example of using the finite element method in order to determine the contact deformation for a practical example. The differences between the results obtained using the finite element method and the results obtained using analytical relations are very small, which demonstrates that the finite element method can be used for determining the machining error due to contact deformation.

Keywords:

Workpiece, fixture, deformation, machining error

1. INTRODUCTION

In the machining process the fixtures are used for the orientation and clamping, for the workpiece to be machined through various methods, assembling and controlling. Once the workpiece is orientated and clamped with locators and clamping devices the workpiece can be machined in order to accomplish the imposed accuracy conditions.

The errors due to fixtures are major ones and influence the workpiece's machining accuracy; the errors can amount to 20-60% of the overall machining error. Therefore, performance evaluations of the workpiece-fixture system constitute a significant task for fixture design optimization and control of the machining error before manufacturing and the application in production.

The errors due to the workpiece-fixture system can be classified in two categories: errors due to orientation of the workpiece in the fixture and errors due to deformations of the workpiece-fixture system during clamping and machining.

During clamping and machining the workpiece, for a point P situated on the machined feature, the force assembly which acts on the workpiece-fixture system determines the appearance of three types of errors: errors due to contact deformation, errors due to locator's deformation and errors due to workpiece deformation.

2. ANALYTIC CALCULUS OF THE ERRORS DUE TO CONTACT DEFORMATION

In many different situations, in device design practice, the contact geometry between surfaces of workpieces and locators or clamping elements of fixture can be a point (sphere-sphere contact), a line (cylinder - plane contact) and a plane surface (plane - plane contact).

The contact deformation between workpiece and locators and clamping elements of fixtures can be characterized with Hertz's model of contact stress. The hertzian theory of contact is based on the following simplifying assumptions [1]:

- ✚ the materials in contact are homogeneous and the yield stress is not exceeded;
- ✚ contact stress is caused by the load which is normal to the contact tangent plane which effectively means that there are no tangential forces acting between the solids;
- ✚ the contact area is very small compared with the dimensions of the contacting solids;
- ✚ the contacting solids are at rest and in equilibrium;
- ✚ the effect of surface roughness is negligible.

2.1. Contact between a sphere and a plane surface

The contact area between a sphere and a plane surface, as shown in Figure 1, is circular.

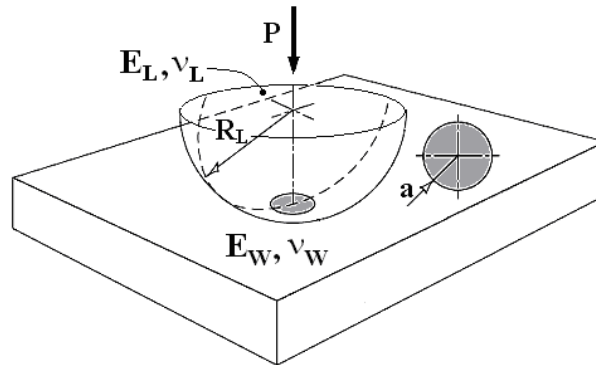


Figure 1. Contact between a sphere and a flat surface

The contact parameters for this configuration can be calculated according to the next formulae:

- contact area dimensions: $a = \left(\frac{3PR'}{E'} \right)^{1/3}$ (1)

- maximum contact pressure: $p_{\max} = \frac{3P}{2\pi a^2}$ (2)

- average contact pressure: $p_m = \frac{P}{\pi a^2}$ (3)

- maximum contact deformation: $\delta = 1.0397 \left(\frac{P^2}{E'^2 R'} \right)^{1/3}$ (4)

- maximum shear stress: $\tau_{\max} = \frac{1}{3} p_{\max}$ at a depth of $z = 0.638a$ (5)

where a is the radius of the contact area [m]; P is the normal load [N]; p is the contact pressure (Hertzian stress) [Pa]; δ is the contact deformation (total deflection at the centre of the contact $\delta = \delta_A + \delta_B$, where δ_A and δ_B are the maximum deflections of body A and B respectively) [m]; τ_{\max} is the shear stress [Pa]; z is the depth under the surface where the maximum shear stress acts [m]; E' is the reduced Young's modulus [Pa] and R' is the reduced radius of curvature [m] ($R' = R_L$).

The reduced Young's modulus is defined as:

$$\frac{1}{E'} = \frac{1}{2} \left(\frac{1 - \nu_L^2}{E_L} + \frac{1 - \nu_W^2}{E_W} \right) \quad (6)$$

where ν_L and ν_W are the Poisson's ratios of the locator and workpiece, respectively and E_L and E_W are the Young's moduli of the locator and workpiece, respectively.

2.2. Contact between a cylinder and a plane surface

According to the Hertz theory for the contact of cylindrical locator, when one of the contact bodies roughly takes the form of a rectangular block of thickness t , as shown in figure 2, then the deformation of the block through its thickness may be obtained with reasonable approximation, provided that the thickness of the block is large compared with the contact width ($t \gg a$), then the deformation of the block through its thickness is

$$\delta = P \frac{1 - \nu_L^2}{\pi E_L} \left[2 \ln \left(\frac{2t}{a} \right) - \frac{\nu_L}{1 - \nu_L} \right], \quad (7)$$

where t is the thickness of the block; ν_L is Poisson's ratio of the cylindrical locator; E_L is Young's modulus of the cylindrical locator; $a = \left(\frac{4PR_L}{\pi E'} \right)^{1/2}$ (8) is the contact width.

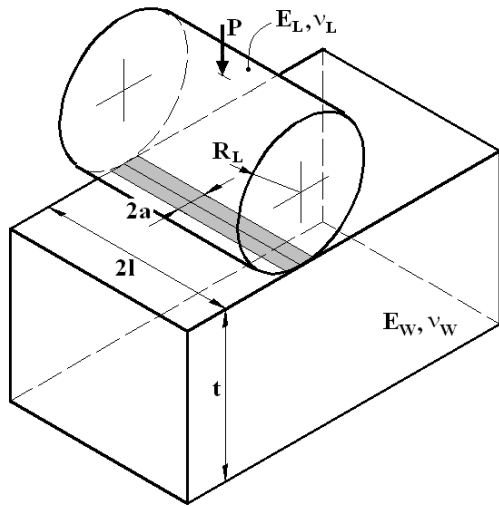


Figure 2. Contact between a cylindrical locator and a rectangular workpiece

3. EVALUATION OF THE MACHINING ERROR DUE TO CONTACT DEFORMATION WITH THE FINITE ELEMENT METHOD

A quick and efficient evaluation of the machining errors due to contact deformation which appear during clamping of workpieces can be realized with the finite element method. Forwards it is presented an example of application of this method for contact between a cylindrical locator and a rectangular workpiece.

An elastic cylindrical locator of steel with a radius of $R=10$ mm pressed against a flat surface of a workpiece of the same material by a pressure $P=0,20$ MPa. Geometry of the rectangular workpiece: length 25 mm, width 25 mm and height 20 mm. Materials for cylindrical locator and rectangular workpiece: steel having Young's modulus $E = 205$ GPa and Poisson's ratio $\nu=0.29$. The clamp-workpiece contact was modeled using surface to surface contact elements.

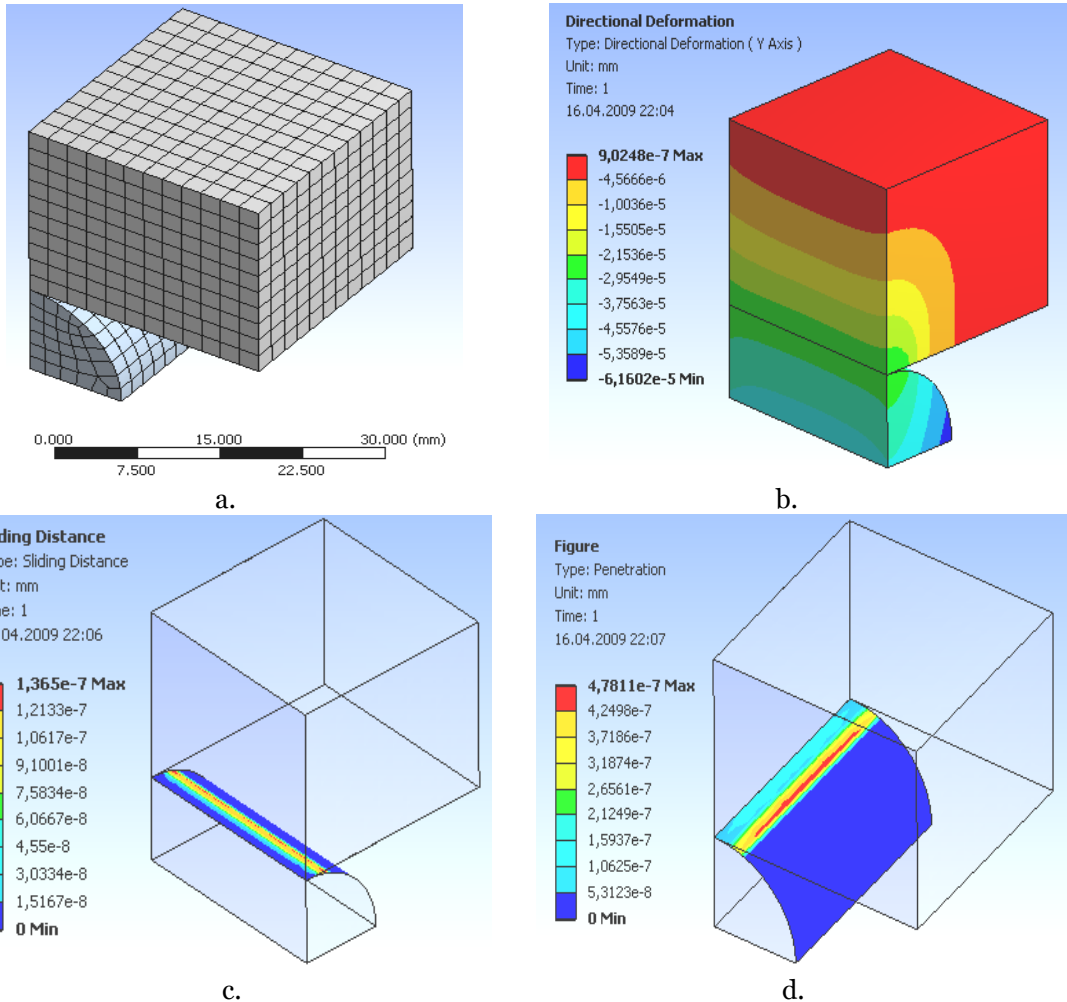


Figure 3. FEA analysis of the workpiece-locator system

The results are presented in figure 3. The contact deformation in contact zone are evaluated in figure 4, b.

3. CONCLUSION

The maximum contact deformation calculated with relation (7) is 0,388 μm . The contact deformation evaluated with the finite element method in middle point of contact line is 0,357 μm . These results demonstrate that the finite elements method permits a quick and efficient evaluation of the contact deformation due to workpiece-fixture system and the machining error due the contact deformation.

REFERENCES

- [1] K.L. Johnson, Contact Mechanics, Cambridge University Press, Cambridge, 1985
- [2] Li, B., Melkote, S. N., Fixture clamping force optimization and its impact on workpiece location accuracy. *Int. J. Adv. Manuf. Technol.*, Vol. 17, No. 2, (January 2001), 104–113, ISSN 0268-3768, 2001
- [3] Raghu, A., Melkote, S. N., Modeling of workpiece location error due to fixture geometric error and fixture-workpiece compliance. *J. Manuf. Sci. Eng.*, Vol. 127, No. 1, 75–83, ISSN 1087-1357, 2005
- [4] Rong, Y. M., Zhu, Y. X., *Computer Aided Fixture Design*, Marcel Dekker, ISBN 0-8247-9961-5, New York 1999



MULTIDISCIPLINARY RESEARCH AREAS FOR INCREASING THE ROLLING-MILL ROLLS QUALITY

KISS Imre, CIOATA Vasile George

Department of Engineering and Management, Faculty of Engineering Hunedoara,
University Politehnica Timisoara, ROMANIA

Abstract:

Quality assurance is the activity of providing evidence needed to establish quality in work, and that activities that require good quality are being performed effectively. All those planned or systematic actions necessary to provide enough confidence that a product or service will satisfy the given requirements for quality. Quality assurance covers all activities from design, development, production, installation, servicing and documentation. It includes the regulation of the quality of raw materials, assemblies, products and components, services related to production, and management, production, and inspection processes.

Our approaches the issue of quality assurance of the rolling mills rolls, from the viewpoint of the quality of materials, which feature can cause duration and safety in exploitation. The experimented durability research, as well as the optimization of the manufacturing technology, allows the conclusion of direct results for the rolls. The beneficiaries of these results are the unit in which the rolls are manufactured, as well as the unit that exploits them. The technological manufacturing process of the rolling mills rolls, as well as the quality of material used in manufacturing them, can have a different influence upon the quality and the safety in the exploitation.

Keywords:

quality assurance, cast-iron rolls, manufacturing, laboratory research, mathematical modeling

1. INTRODUCTORY NOTES

Roll makers always ask about rolling conditions and the necessity to choose the right grade of roll material and roll users always ask about the mechanical and physical properties of roll material. Sometimes they feed these figures into their rolling model, but sometimes they also need them for unknown reasons. This information is very rarely useful for selecting the right supplier. Roll makers and roll users frequently have to discuss experiences, performance results, special requirements of the mill. Roll failure problems can be solved by good co-operation. In engineering and manufacturing, quality control and quality engineering are involved in developing systems to ensure products or services are designed and produced to meet or exceed customer requirements. These systems are often developed in conjunction with other business and engineering disciplines using a cross-functional approach. By collecting data from samples at various points within the process, variations in the process that may affect the quality of the end product can be detected and corrected, thus reducing waste as well as the likelihood that problems will be passed on to the customer.

Quality assurance covers all activities from design, development, production, installation, servicing and documentation. It includes the regulation of the quality of raw materials, assemblies, products and components, services related to production and inspection processes. Production logistics is the term used for describing logistic processes within an industry. Also, the purpose of production logistics is to ensure that each equipment and technologies is being fed with the right product in the right quantity and quality at the right point in time.

What materials, products, or information come into the activity? What materials, products, or information flow out of the activity? Quality engineers use the D-M-A-I-C model (define, measure, analyze, improve, and control) to document processes before beginning process improvement. If processes are documented, another series of logical questions apply: Are the processes being followed? Are they within acceptable control and performance parameters? Are they outdated? Can they be improved? Those are the questions which determine the correlations between the logistics process and the quality assurance.

2. QUALITY ASSURANCE IN THE ROLL INDUSTRY

The manufacture of rolls (see Figure 1) is in continuously perfecting, the requirements for superior quality rolls are not yet completely satisfied, in many cases, the absence of quality rolls preventing the realization of quality laminates or the realization of productivities of which rolling mills are capable. Basic properties of rolls and properties of the material are two totally different sides of a problem and very often this difference is ignored. However, when we start to discuss about the rolls mechanical properties, we have to analyze the rolls material or the roll-properties.

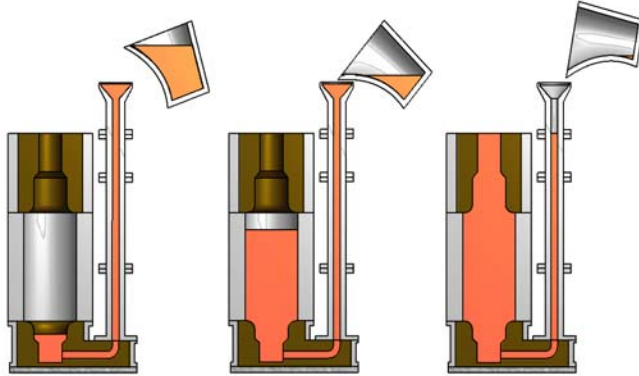


Figure 1. Casting technology of the iron rolls

modern calculation programmes, optimization technologies and the better capitalization of the manufacturing data (see Figure 2).

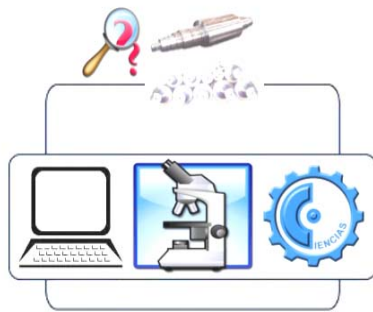


Figure 2. Quality assurance research fields



Figure 3. Quality assurance in rolling industry

In the rolling industry, the quality of the rolls is in directly accordance with the quality of technologies (defined by the casting equipments, materials, applied procedures, etc), and also, by the quality of the manufacturing process (charging, melting, inoculation, ladle treatment, casting, cleaning, etc), which are presented in Figure 3.

3. QUALITY OF ROLLS ASSURED BY MODELLING OF MANUFACTURING

Industrial engineering is also operations management, systems engineering, production engineering, manufacturing engineering or manufacturing systems engineering. Where as most engineering disciplines apply skills to very specific areas, industrial engineering is applied in every industry. Industrial engineers typically use computer simulation, especially discrete event simulation, for system analysis and evaluation. The computer is used to generate a numerical model of reality for the purposes of describing complex interaction among components of a system.

Starting from the principle of modelling process, used as necessary basic instrument, both in phase of conception, as well as in the industrial technologies analysis, is determined the optimum regimes of the cast rolls, from the view from chemical composition, as one as the most important parameters of disturbance of the manufacturing process. The enunciation of some mathematically modelling results, described through a number of multicomponent equations determined for the spaces with 3 the and 4 dimensions, as well as the generation of some regression surfaces, of some curves of levels, of the volumes of variation, of the lines of outlines of the volumes of variation of surfaces and the areas of variation of these, can be represented and interpreted by technologists and can be considerate diagrams of correlation between the analyzed variables. From this point of view the project is inscribes in context of scientific capitalization of the process and the industrial technologies

optimizations, on the way of the analysis and the mathematical experiment. The quality assurance through the modeling phenomenon is presented in Figure 4.

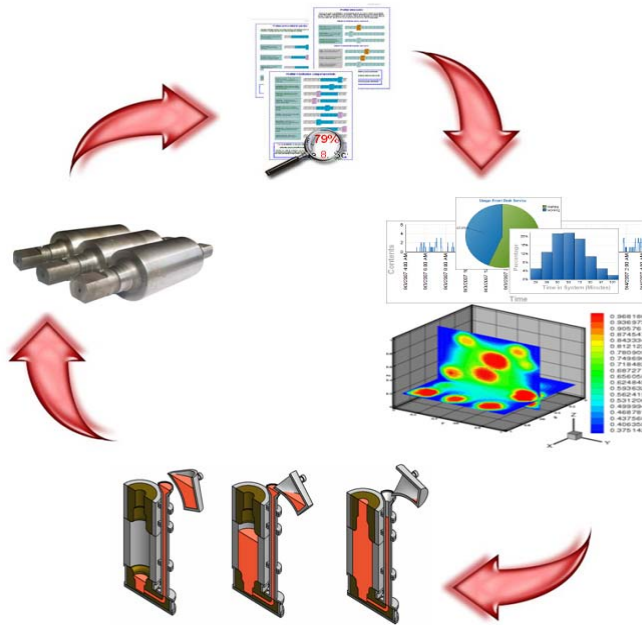


Figure 4. Quality assurance through the modeling phenomenon

The optimization of any technological process has, as a base, a mathematical model. The search for the best solution, for the truth, requests either to find, on the way of a study, definitive truths, or of relative valid truths, valid only in certain conditions, and which, in relation with the definitive truths, include implications and errors.

4. QUALITY OF ROLLS ASSURED BY THE LABORATORY EXPERIMENTS

The researches of durability in the exploitation of cast from cast-iron rolls, constitute a scientifically novelty, and experimentally define an important chapter from the thermal fatigue of the organs of machines in the movement of rotation, in variable temperature mediums. Hot rolling mills rolls work the in the variable compound solicitations, due to lamination process and which repeated to regular intervals of time.

All these phenomena, which are more or less emphases depending on the type and typical of rolling mills, are not taking into consideration in the classic calculus of rolls. If the study of the rolls resistance is extended upon their durability, we must consider the whole complex of tensions with

mechano-thermic influences. The research on durability in exploitation of hot rolling mills rolls assures relevant conditions for the appropriation of the research methods of the thermal regimes that are submitted the rolls or other organs of machines, that works in constant (symmetrical) or variables (asymmetrical) thermal solicitation conditions.

The recommendations for the increase of the duration of exploitation and remove of the damages through the accidental rupture of rolls from the stands of lamination, the attenuation of rolls thermal fatigue, the avoiding of thermal shock and their rational exploitation are actuality issues that must be continuously researched.

In this trend is situated the research of the thermal fatigue phenomena, materialized in technical reports, whose

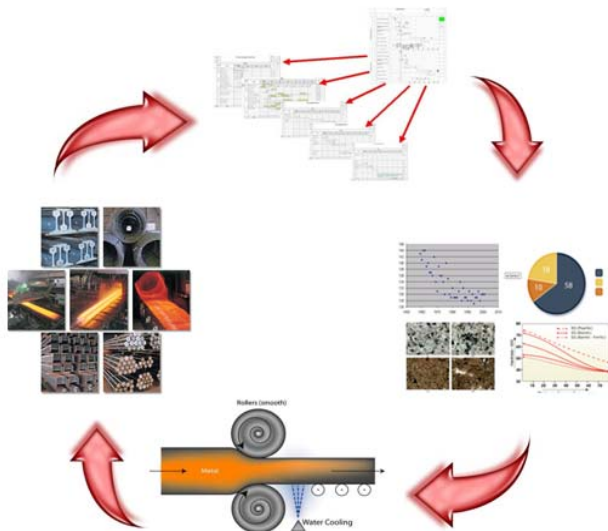


Figure 5. Quality assurance through the laboratory and industrial experiments

beneficiary is the unit in which the rolls are exploited, as well as through scientific papers, that can develop the framework of scientific research. These researches results lead to direct conclusions about the cast-iron rolls, and permit their comparison with data about steel rolls, area studied thoroughly researched of specialists. The quality assurance through the laboratory and industrial experiments is presented in Figure 5.

The work is of practical immediate utility, inscribing itself in the context of technical capitalization of the manufacturing technologies and of exploitation of cast-iron rolling mill rolls, for which exists an attentive preoccupation both from foundry sectors, as well as from lamination sectors, having as determinate aim the quality assurance and increase the durability in exploitation.

5. CONCLUSION

The aim of the propose research is to answer to as many questions possible regarding the quality of rolls. In this sense, durability in exploitation is extremely current, both for immediate practice, and for the scientific research attributed to the cast-iron. Also, the realization of optimum chemical compositions of the cast-iron can constitute a technical efficient way to assure the exploitation properties, the material from which the rolling mills rolls are manufactured having an important role in this sense.

In these sense, our researches propose, on aside, to analyze the durability in industrial exploitation of rolling mills rolls – analysis materialized from prism of the laboratory experiment (Figure 8), and on another side, the optimization of manufacturing technology of the cast rolls, especially those from cast-iron – using electronic calculus technique as the modelling phenomenon (Figure 7) and mathematical interpretation of the technological processes. The research on durability in exploitation of hot rolling mills rolls assures relevant conditions for the appropriation of the research methods of the thermal regimes that are submitted the rolls or other organs of machines, that works in constant (symmetrical) or variables (asymmetrical) thermal sollicitation conditions. Also, it can be emphasized the thermal shock, phenomenon that constitutes a permanent danger, which leads to rupture, specific to rolling mills rolls. On another hand, the realization of an optimal chemical composition can constitute a technical efficient mode to assure the exploitation properties, the material from which the rolling mills rolls are manufactured having an important role in this sense. From this point of view is applied the mathematical modelling, witch is achieved starting from the differentiation on rolls component parts, taking into consideration the industrial data obtained from the hardness mensuration on rolls, as well as the national standards reglementations, which recommends the hardness, for different chemical compositions.

Through the original aimed elements mentioned above, the suggested researches allows the enunciation of new approaches in the area afferent to the theme. The best way for roll makers to achieve better rolls is to ensure that better materials and improved manufacturing processes are used and that roll users take account of rolling conditions and improved rolling processes. When we start to discuss about the rolls mechanical properties, we have to analyze the rolls material or the roll-properties. In conclusion, the rolls quality problems can be solved by good co-operation between the rolls manufacturers and roll users.

REFERENCES

- [1] Kerr, E.J., Webber, R. 2003. Roll performance - present overview and look to the future, at: International Symposium “Rolls 2003” - International Convention Centre, Birmingham
- [2] Kiss, I. 2005. The quality of rolling mills cylinders cast by iron with nodular graphite, Mirton, Timisoara
- [3] Kiss, I. 2005. Researches regarding the quality assurance of the rolling mills cast-iron cylinders through mathematical molding of the manufacturing process and the experimental study of durability in exploitation, National contract No 5889/2005, Bucuresti
- [4] Kiss, I., Cioată, V.G., Alexa, V. 2003. The main alloyed elements influences upon the nodular cast iron semihard rolls hardness, Annals of the Faculty of Engineering Hunedoara, Fasc. 2, pp. 145...150
- [5] Kiss, I., 2008, Rolling Rolls – Approaches of quality in the multidisciplinary research, Mirton Publishing House, Timisoara
- [6] Pellizzari, M., Molinari, A., Biggi, A. 2002. Optimization of the hot roll performances through microstructural tailoring, at Conference of University Trento, Brescia
- [7] Schroder, K. H.1988. Rolling conditions in hot strip mills and their influence on the performance of work rolls, Metallurgical Plant and Technology, no.4/88, 44-56, Dusseldorf
- [8] Schroder, K. H. 2000. Questions, answers, more questions – Twenty-five years of experience in discussing rolls and rolling technology, 42nd Mechanical Working and Steel Processing Conference Proceedings, Toronto
- [9] Stevens-Oost, B. 2003. Roll quality and roll cost development: where do we come from and where are we going?, at International Symposium “Rolls 2003” - International Convention Centre, Birmingham



EXPERIMENTAL RESEARCH IN PILOT PHASES REGARDING THE SEMISOLID STATE PROCESSING OF STEEL

MILOSTEAN Daniela-Cătălina, FLORI Mihaela-Corina

University „Politehnica” Timisoara, Faculty of Engineering Hunedoara, ROMANIA

Abstract

The work presents the results obtained through laboratory stage experiments regarding the semisolid state die forging of steel. The studied steel is submitted to semisolid state die forging in the presence of mechanical vibration with frequencies of 15, 25 and 40 Hz. The use of mechanical vibrations is very important as they play the role of modifying the microstructure and decreasing the quantity of defects. Also through this process the mechanical characteristics of the part are changed.

Key words:

semisolid, steel, die forging, mechanical vibration, frequency, microstructure

1. INTRODUCTION

The early 1970's represents the appearance period of a new material processing technology, currently known as semisolid metal forming (SSF) [1]. This technology was discovered by a student from MIT (Massachusetts Institute of Technology) which obtained for the first time a semisolid suspension with thixotropic characteristics by mechanical stirring [2]. Due to the observed advantages, the researches continued on low melting point alloys. Currently, in the world are many companies which implemented this new technology and commercialized parts, mainly from aluminum and magnesium alloys [3-5]. Simultaneous with the research of the low melting point alloys were studied and the high melting points alloys like steels, cobalt alloys, etc [6].

Semisolid state processing consists in obtaining of a semisolid suspension formed of spherical solid particles included in a liquid matrix. This suspension has a thixotropic behavior i.e. to behave like a fluid when it's agitated and like a gel when it's at rest. The investigations carried out on Sn-15Pb semisolid suspension with the viscometer, showed that the apparent viscosity of the suspension decreases with increasing shearing rate [7]. Hence are resulted the main advantages of this technology namely: improved flow properties, reduced processing forces, obtaining parts in a finished and complex shape, etc. [8]. In the main there are two options for obtaining parts by semisolid state processing namely: rheocasting and thixoforming. If the liquid metal is intensively agitated in the solidification range the dendrites are broken and thus spherical particles are formed which float in the liquid mass. If this semisolid suspension is used to produce parts directly by casting the process is called rheocasting, and if it's used to obtain semi-finished products which are subsequent heated in the semisolid range and used to produce parts, the process is called thixoforming [9]. The methods used to obtain the precursory alloy with globular structure for thixoforming are: electromagnetic stirring, low superheat casting, SIMA method, etc.

The experimental process presented in this paper use mechanical vibration in order to stir the melt. Experiments were conducted on 200-400 steel in order to obtain glass shape parts. Throughout the die forging process the melt was mechanically agitated with an eccentric vibrating motor powered by a frequency converter. Thus the frequency varied in the range 0Hz - 40Hz.

2. EXPERIMENTAL PROCEDURE

2.1. Obtaining the pieces by die forging

Experiments were conducted on the laboratory hydraulic press shown in the photo from Figure 1. The material used for experimentation, 200-400 steel (in correspondence with the OT400 steel, STAS 600-82), has the following chemical composition: 0.18% C, 0.40% Mn, 0.25% Si, 0.011% S, 0.016% P, 0.12% Ni, 0.03% Mo.



Figure1. Photo of the experimental set-up

The steel was melted in the 100kg induction furnace. The melt reached to the desired temperature has been cast in to the mold through a chute (Figure 2). The die, the punch, the counter-punch and the chute were lubricated with refractory paint to avoid melt sticking. When the melt in the die reached the semisolid temperature range corresponding to a solid fraction between 40-60%, the punch was lowered and the material took the form of the gap between die and punch.



Figure2. Casting of the melt in the die

We have obtained four pieces in glass shape through experiments conducted in different conditions given in Table 1. The first piece (denoted A) was obtained without the use of vibrations at a temperature above the liquidus line. The other three pieces (denoted C, D, E) were obtained in a field of mechanical vibration at different frequencies and amplitudes (see Table 1), in the semisolid temperature range. The vibration frequency was changed by supplying the three-phase vibrating engine with a static frequency converter.

Table1. Conditions used for die forging of the pieces

Piece	A	B	C	D
Vibration frequency, f [Hz]	0	15	25	40
Vibration amplitude, a [mm]	0	1	0.7	0.4

The temperature range of the semisolid state processing (40-60% solid fraction, f_s) was determined both by the calculations (based on the Fe-C equilibrium diagram) and by the Thermocalc soft [10]. Due to the small differences between temperature results obtained by calculations and by the Thermocalc soft (1-3 degrees), for further experiments we have considered the processing temperature range of 1504-1514 °C, corresponding to 40-60% f_s .

The piece A (Figure 3, a) was longitudinal cut into four equal parts noted A1, A2, A3, A4 as seeing in Figure 3, b. These samples were used for different analysis as: metallographic observations, impact tests and Brinell hardness tests. For metallographic observations and Brinell hardness tests, A1 and A2 samples were transversal sectioned in pieces of 10 mm size. Samples A3 and A4 as-obtained were used for impact tests.

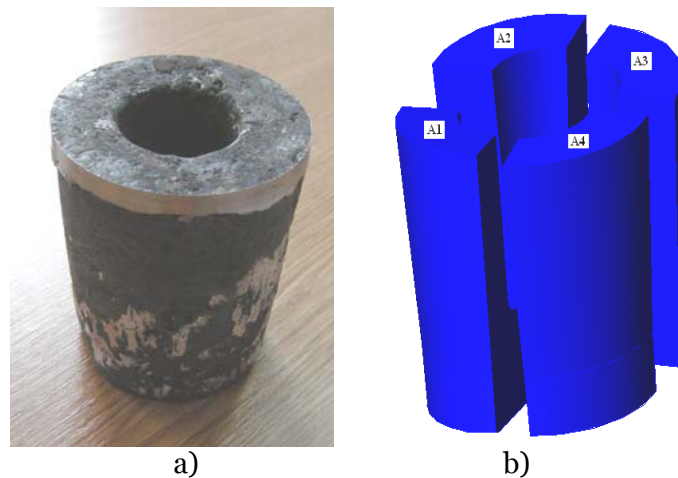


Figure3. Piece A (a) and the cutting way of the samples notated A1-A4 (b)

The pieces B, C and D were sectioned in the same way as the piece A and submitted to the same analysis.

2.2. Sample preparation and analysis details

The sample preparation for microstructure observations was made in accordance with the standard procedure. For preliminary polishing we have used seven different metallographic papers with SiC fine abrasive particles (200, 280, 360, 400, 600, 800 and 1000). The final polishing was made on a felt disk impregnated with alumina suspension (Al_2O_3) of 0.3 μm granulation. Then, the samples were etched with 3% Nital reagent and observed by means of a Kruss optical microscope.

The impact test (at room temperature) was performed on U notch samples. From each piece (denoted A-D) were tested two samples of 55x10x8 mm size. The experimental values represent the arithmetic mean of two tests conducted on each piece.

The Brinell hardness test was performed with a Brinell instrument on three transversal cut samples from each piece, having about 20x20x10 mm size. So, the experimental values represent the arithmetic mean of three tests conducted on each piece. The Brinell ball has 10 mm diameter and the static force applied for 10-15s was of 3000 daN.

3. RESULTS AND DISCUSSIONS

3.1. Microstructural study

The samples were studied with the microscope before and after the 3% Nital etching. On the un-etched samples obtained without mechanical stirring was reveal defects like: shrinkage cavity, cracks and inclusions. A micrograph of this structure is shown in Figure 4,

a. The samples obtained by mechanical stirring reveal a reduction of defects quantity, as shown in micrograph from Figure 4, b.

The microstructure of the steel samples consists of ferrite and pearlite, which was revealed after 3% Nital etching (Figure 5). The dark areas represent pearlite and the bright areas represent ferrite. It's also noted that the grain boundary are represented by the thin dark lines. In the micrograph of piece A (see Figure 5) is observed an acicular structure (Widmannstätten), specific to cast steels [11]. This structure is formed due to that, at fast cooling rate it's not possible the complete separation of ferrite at the large austenite grain boundaries. Another feature of this structure is that it has low impact values and percentage elongation, so in generally must be avoided.

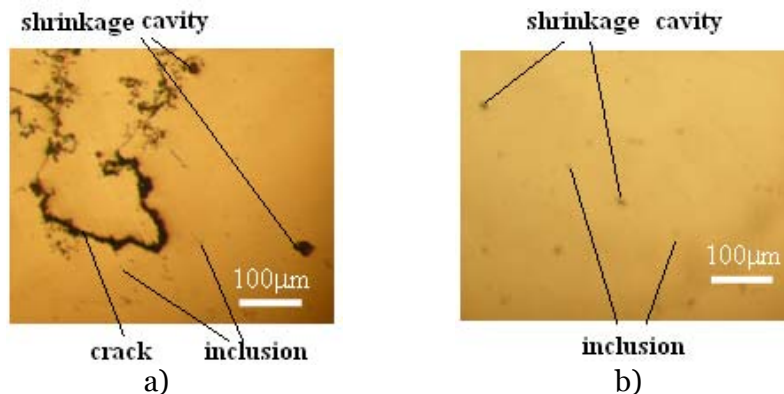
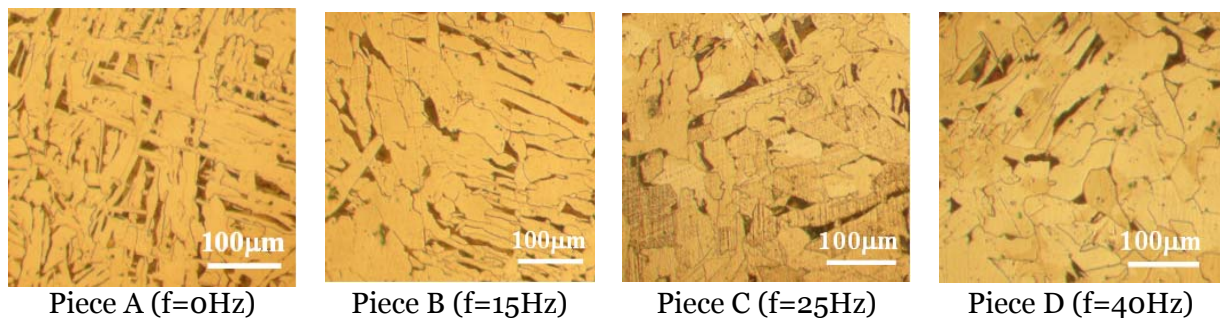


Figure4. Micrographs of the un-etched samples: a) Piece A and b) Piece D



Piece A (f=0Hz)

Piece B (f=15Hz)

Piece C (f=25Hz)

Piece D (f=40Hz)

Figure5. Micrographs of A, B, C and D pieces, etched with 3% Nital

Low frequency vibrations, applied to the semisolid melt lead to the formation of spherical particles in the semisolid suspension [12]. It is well known that by mechanical stirring the dendrite arms are broken (which usually are formed by classical casting), thus results solid spherical particles dispersed in the melt [13]. These solid particles represents new crystallization nucleus which lead to obtaining of a semisolid suspension with thixotropic features. As can be seen in Figure 5, there is a difference between piece A and B, C and D pieces obtained by semisolid die casting in the mechanical vibration field. This is because with increasing the vibration frequency of the die, the structure becomes more globular, with a direct proportional dependency.

3.2. Impact and Brinell hardness tests

The variation of the energy absorbed trough tearing (KU) with the die vibration frequency is shown in Figure 6.

The results show an increase of the energy absorbed trough tearing (KU) with increasing vibration frequency up to 40 Hz. So, due to the application of low frequency mechanical vibration during solidification, the alloy no longer has a typical casting structure, but a globular structure with fewer defects (inclusions, shrinkage cavities). This leads to an increase of the energy absorbed trough tearing. One can see that the highest value of KU corresponds to the highest vibration frequency, i.e. 40 Hz. Hence, the vibration applied during solidification makes the steel to be more tenacious.

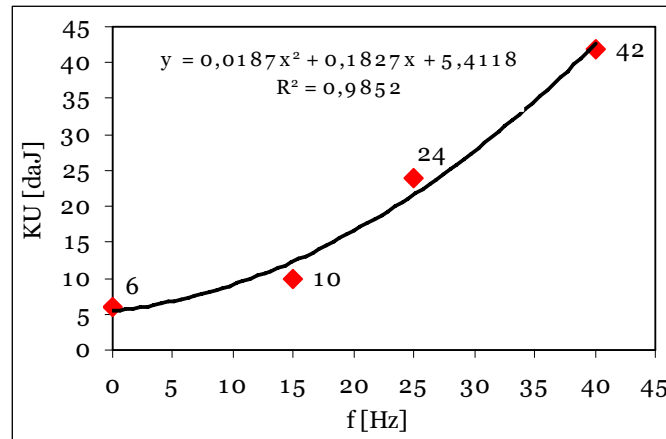


Figure 6. Variation of the energy absorbed trough tearing (KU) with the die vibration frequency (f)

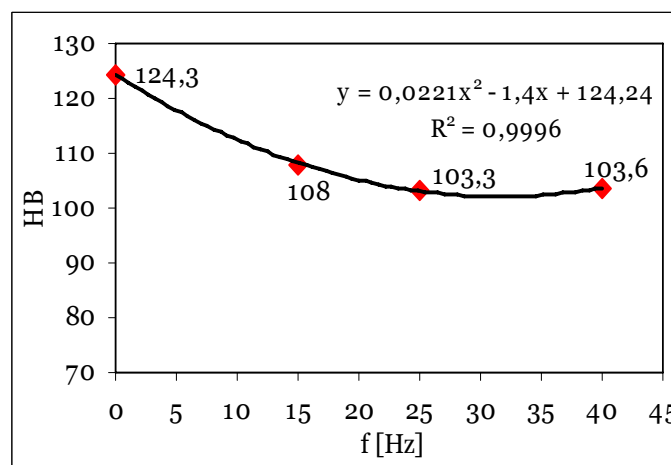


Figure 7. Brinell hardness variation (HB) with the vibration frequency (f) of the die

In Figure 7 is presented the Brinell hardness variation (HB) with the vibration frequency of the die. It is noted a decrease of hardness experimental values with the increase of the vibration frequency. This is because a lamellar structure (obtained in this case by liquid state die forging- Figure 5, piece A) is harder than a globular structure (obtained by semisolid state die forging- Figure 5, piece B, C and D). It may be seen that for vibration frequencies of 25 and 40Hz, the hardness values are approximately the same (about 103 HB). Also, for small vibration frequencies the Brinell hardness have the biggest values.

4. CONCLUSION

The interpretation of the obtained results led to the following conclusions:

- ✚ Application of the mechanical vibration of low frequency at semisolid die forging reduces defects as: shrinkage cavity, cracks and inclusions. This improves the quality of the obtained pieces.
- ✚ It was remarked that the microstructure of the pieces subjected to mechanical stirring by vibration have a spherical grain structure, which favors the thixotropic behavior. This feature is best observed in the C and D pieces structure obtained at 25 and 40 Hz frequencies.
- ✚ The energy absorbed trough tearing (KU) increases with increasing the vibration frequency for the semisolid die forged pieces compared to those die forged in liquid state.
- ✚ It was observed that the Brinell hardness depends on the microstructure features.

REFERENCES

- [1] R. Song, K. Yonglin, Z. Aimin, *Semi-solid rolling process of steel strips*, Journal of Materials Processing Technology, 198 (2008) 291-299.
- [2] M.C. Flemings, *Semi-solid forming: the process and the path forward*, Metallurgical Science and Technology, 18/2 (2000) 3-4.
- [3] D. Apelian, *Advanced casting technologies in Japan and Europe, Chapter 2: Melting and handling*, World Technology Evaluation Center Panel Report, 1997.
- [4] G. Govender, L. Ivanchev, *Near Net Shape Forming Using semi-Solid Metal Forming*, International Conference on Competitive Manufacturing, 2004.
- [5] ***www.sag.at
- [6] P. Kapranos, D.H. Kirkwood, C.M. Sellars, *Semi-solid processing of tool steel*, Journal de physique IV, 3 (1993) 835-840.
- [7] C. Rouff, *Contribution a la caractérisation et la modélisation du comportement d'un acier a l'état semi-solide application au thixoforgeage*, L'école Nationale Supérieure d'arts et Métiers, PhD These, 2003.
- [8] Z. Fan, *Semisolid metal processing*, International Materials Review, 47/2 (1991) 30-32.
- [9] X. Pan, H. Zhang, A. Wang, B. Ding, K. Qiu, Z. Hu, *Trend and development of semi-solid metal processing*, J. Mater. Sci. Technol., 16/5 (2000) 453-460.
- [10] ***www.thermocalc.com
- [11] H. Protopopescu, *Metalografie și tratamente termice*, Editura Didactică și Pedagogică, București, 1983.
- [12] S. Wu, L. Xie, J. Zhao, H. Nakae, *Formation of non-dendritic microstructure of semi-solid aluminum alloy under vibration*, Scripta Materialia, 58 (2008) 556-559.
- [13] S. Ji, *The fragmentation of primary dendrites during shearing in semisolid processing*, Journal of Materials Science, 38 (2003) 1559-1564.



VIEWING PERIODICAL SYSTEM WITH THE HELP OF MICROSOFT ACCESS DATA BASE

Sorina SERBAN

Universitya Politehnica Timisoara, Faculty of Engineering Hunedoara, ROMANIA

Abstract:

The aim of this paper is to use a Microsoft Access study program for teaching purposes. This application is intended for high school pupils and for 1st and 2nd year college students as well, thus they will enlarge the perspective upon physical and chemical properties and electronic configuration of elements in periodical system.

Keywords:

periodical system, nonperiodic properties, atomic numbers, data base

1. THEORETICAL CONSIDERATIONS

As an expression of periodic law, the structure of periodical system created by Mendeleev embodied many forms in time. For the present form of the periodic table, knowing the electronic configuration of each element and of outermost electrons in particular is of great importance.

This explains the periodicity of specific properties in terms of atomic number Z (atomic and ionic radius, ionization energy, electron affinity, melting and boiling points). There are also certain properties, called *nonperiodic properties* that vary constantly (atomic mass, for example). Nonperiodic properties of elements are given by atomic nuclei, as the periodic properties are given by their electron shells.

The periodic table contains 110 elements organized in groups and periods, and recently elements with atomic numbers 111, 112, 114, 116, 118 have been discovered.

The most important properties are presented for each element (discovery, natural state, source, use and biological role), physical properties (atomic number, atomic weight, melting and boiling point, density, electron configuration, electron affinity), information on isotopes (nuclei, atomic mass, range, life duration), ionization energy.

2. APPLICATION PRESENTATION

To study the periodic table, a data base called *Periodical System* was created. The data base is designed to align all the elements with all their physical and chemical properties. Autoexec will open the form *Introduction* which is active for 8 seconds and then the main menu opens automatically. This form appears as:

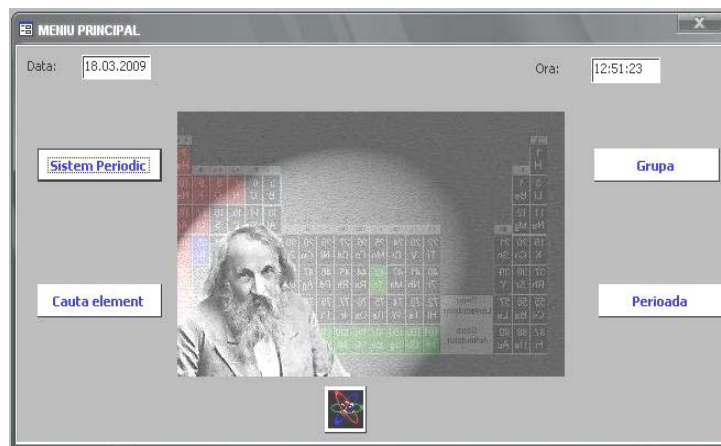


For the form to work properly, the event Timer was programmed (with an 8000 millisecond interspace)

```
Private Sub Form_Timer()
    DoCmd.Close
    DoCmd.OpenForm "menu"
End Sub
```

Thus, after 8 seconds this window will close automatically and it will open MAIN MENU; which is for us the main form. The main menu contains two text boxes that inform us on date and time, events programmed with Timer property at a 1000 mseconds interspace. The code is:

```
Private Sub Form_Timer()
    Me!Data_txt.Value = Date
    Me!Ora_txt.Value = Time
End Sub
```



As for the rest, when pressing the buttons, the work forms will open, except for the button “close application”. The code for the 4 open buttons is similar, so we will present only one

```
Private Sub sisp_btn_Click()
On Error GoTo Err_sisp_btn_Click
    Dim stDocName As String
    Dim stLinkCriteria As String
    stDocName = "SIS_P"
    DoCmd.OpenForm stDocName, , stLinkCriteria
Exit_sisp_btn_Click:
    Exit Sub
```

```
Err_sisp_btn_Click:
    MsgBox Err.Description
    Resume Exit_sisp_btn_Click
End Sub
```

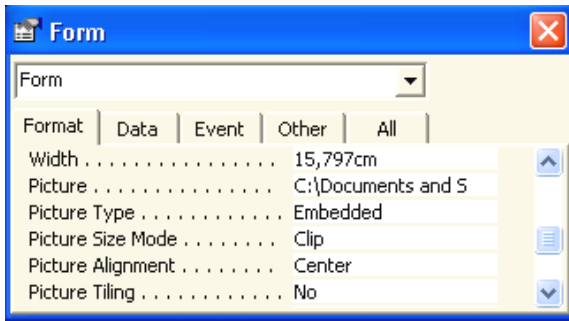
The code for closing application:

```
Private Sub STOP_Click()
On Error GoTo Err_STOP_Click
    DoCmd.Quit
```

```
Exit_STOP_Click:
    Exit Sub
```

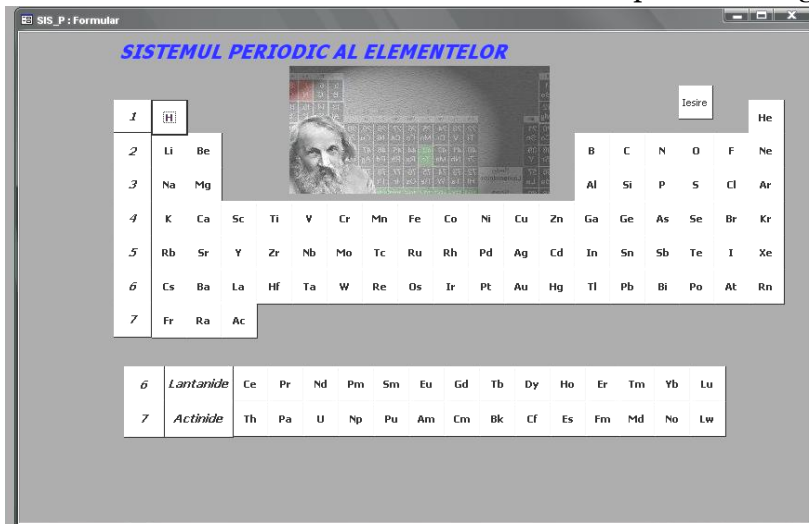
```
Err_STOP_Click:
    MsgBox Err.Description
    Resume Exit_STOP_Click
```

```
End Sub
```



For most of the forms we used background images which can be added by opening the **Properties** window.

Thus, for **Pictures** property we choose the background file, **Embedded** type, in order to differentiate it from the image on the hard disk of the computer, and to embed it in our data base. For the forms that are bigger than the image we choose Stretch option instead of Clip for the image to cover the entire form.



When pressing the *Periodical System* button, the form with the same name will open. The form contains numerous buttons with the name of each element in periodic table. By pressing one button a form will open, the same for all buttons, Element form, which will post all elements' properties.

We realized the capture of this form in DESIGN mode to highlight the text box, Texto, which is

a hidden box, and in this box the symbol of each element will appear when pressing the drawn buttons. We realized this to open the form Element, for the element which corresponds to each button. The form Element is generated when querying Element, and it will make a selection based on the content in the text box hidden in our form.

```
Private Sub H_Click()
    On Error GoTo Err_H_Click
```

```
Me!Text0.Value = "0"
```

```
Dim stDocName As String
Dim stLinkCriteria As String
```

```
stDocName = "ELEMENT"
DoCmd.OpenForm stDocName, , stLinkCriteria
```

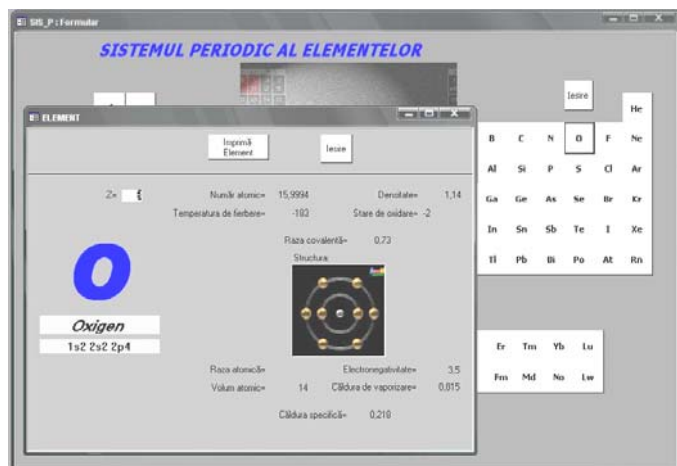
```
Exit_H_Click:
Exit Sub
```

```
Err_H_Click:
MsgBox Err.Description
Resume Exit_H_Click
```

```
End Sub
```

The Element form appears as:

We can observe The Structure image, which is an OLE type object in our data base. A second button, Search element in main menu, opens a form where we can search a chemical element using three criteria: name, symbol, atomic number.



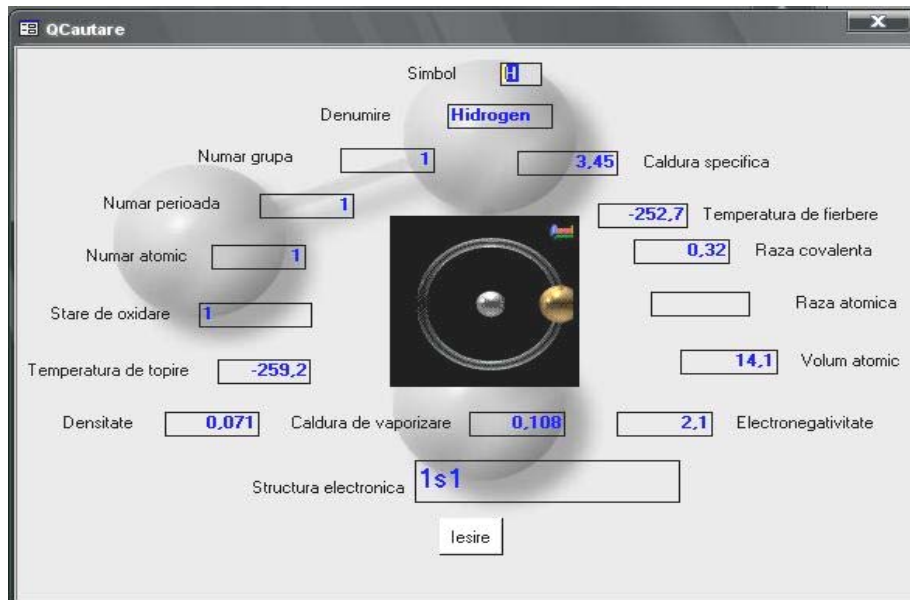
Apart from the filled in text box, when pressing the Search button a new form will open and it will contain the element we searched for with all its properties. Behind this form there is a query which will have as a selection criterion all the 3 text boxes, and only one of them needs to be filled in.

Field:	SYMBOL	NUME	NUMAR_ATOMIC	IMAGINE	Nr_grupa
Table:	ELEMENTE	ELEMENTE	ELEMENTE	ELEMENTE	ELEMENTE
Sort:					
Show:	<input checked="" type="checkbox"/>	<input checked="" type="checkbox"/>	<input checked="" type="checkbox"/>	<input checked="" type="checkbox"/>	<input checked="" type="checkbox"/>
Criteria:	Nz([Forms][Cautare][Text19];[ELEMENTE])[SYMBOL] Nz([Forms][Cautare][Text19];[ELEMENTE])[NUMAR_ATOMIC] Nz([Forms][Cautare][Text19];[ELEMENTE])[IMAGINE] Nz([Forms][Cautare][Text19];[ELEMENTE])[Nr_grupa]				
or:					

Thus, as a selection criterion, we will use a function:

$Nz([Forms]![Cautare]![Text19];[ELEMENTE]![SIMBOL])$

This will search in the text box corresponding to our Search form for any text, and if there is a text inside, the value in the text box will be the criterion, and if there is no text, it will select all values in Elements table, then it will pass to the next column to continue the criterion. The generated form will have a structure that differs from Element form shown above.



Simbol:

Denumire:

Numar grupa: Caldura specifica

Numar perioada: Temperatura de fierbere

Numar atomic: Raza covalenta

Stare de oxidare: Raza atomica

Temperatura de topire: Volum atomic

Densitate: Caldura de vaporizare: Electronegativitate

Structura electronica:

On the main interface there are two more buttons; when pressing them we can see the position of chemical elements in group and period.



Grupa:

NUMAR_ATOMIC	SIMBOL	Nr_grupa	NUME
1	H	1	Hidrogen
3	Li	1	Litiu
11	Na	1	Natriu
19	K	1	Potasiu
37	Rb	1	Rubidiu



Perioada:

NUMAR	SIMBOL	Nr_grupa	NUME
3	Li	1	Litiu
4	Be	2	Beriliu
5	B	3	Bor
6	C	4	Carbon
7	N	5	Azot

Groups are considered the most common way to classify the items. In some groups, the elements have properties similar or identical property whole group - these groups are given names that are used quite often, eg. alkali metals, alkaline-earth metals, transitional metals, etc.

A period is a horizontal row of the periodic table. Although groups are the most common way to group elements are regions of the periodic system where the similarities are

more significant horizontal than vertical. The number shows the number of layers occupied by electrons.

The problems encountered when using the periodic table for teaching purposes are: the complexity of properties that characterize each and every element and the multitude of elements.

3. CONCLUSIONS

The usage of educational soft will increase the students' proficiency and creativity, the level of medium and superior training, the amount of knowledge and it will lead subsequently to a better usage of Informatics in various fields of activity.

Bibliography

- [1] Florescu Vasile – „Database - fundamental theoretical and practical”, Publishing Infomega, Bucharest 2002
- [2] Eduard Koller – „Programming in Access 97”, Teora, Buharesti 2002
- [3] C.D. Nenițescu – „General Chemistry”, Didactic and Pedagogic Publishing House Bucharest.



INFLUENCE OF THERMAL REGIME IN THE CALCULUS OF THE THERMAL STRESSES UPON WARM CYLINDERS

Camelia B. PINCA

University "POLITEHNICA" of Timișoara
Faculty of Engineering Hunedoara, ROMANIA

Abstract

The research of the thermal stress that action in the rolling cylinders is impetuously necessary not only to diminish the fissures caused by thermal fatigue, to increase the exploitation duration, but also to avoid thermal shocks, which are very dangerous in the exploitation process and produced by large variations, temperature snapshot that lead to shearing of caliber beads in cylinders.

The present work proposes to determine the influence of thermal regime in the calculus of the thermal tension upon warm cylinders.
